LARGE SAILING SHIPS -
A FLUID DYNAMIC INVESTIGATION

by

William Michael Spenser Bradbury

Thesis submitted for the degrees of
Doctor of Philosophy of the University of London
and Diploma of Imperial College.

Department of Aeronautics
Imperial College of Science and Technology
Prince Consort Road, London S.W.7.

- October 1983 -

GRIMBLEDON DOWN

Bill Tidy

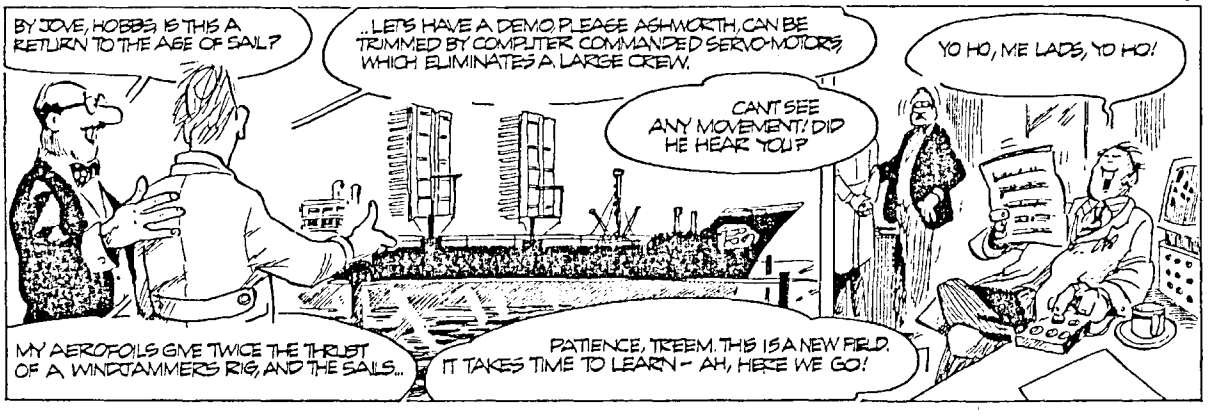

TIDY (1983)

Abstract

Wind energy is one resource available to supplement dwindling world fuel supplies. Past ships were wind driven and it seems increasingly likely that some future commercial ships will be wind-assisted or wind-powered.

When a ship is sailing the hull moves obliquely through the water at a greater angle of leeway than when under power. A wind tunnel is used to investigate the flow past a Mariner type hull for the range of leeway angles expected when sailing. Flow visualisation experiments are conducted, and the non-wave-making components of hydrodynamic hull forces are measured. A systematic series of hull-like blocks is similarly tested to investigate the influence of certain parameters such as beam, draft and trim. An important feature of the flow about a hull at leeway is the longitudinal vortices shed from the bilges. A slender-body, line-vortex calculation is used to model this feature for a hull-like block.

Practical considerations suggest that modern sailing ships are likely to have arrays of sails. A model with the important features of the above-water part of a sailing ship is tested in a wind tunnel. Various simplified sail-like aerofoils are compared singly and as arrays of sails. The effects of heel, mast-number and end-plates are investigated, and various strategies for trimming and reefing sails are compared. The flow through an array of sails has aerodynamic similarities to both cascade flow and the flow through multicomponent aerofoils. Distances between aerofoils are small compared with their length, so the flow is expected to be approximately two-dimensional away from their

ends. A two-dimensional potential flow calculation is used to predict sail trim geometries, which are expected to have favourable aerodynamic characteristics.

In steady sailing conditions, the total forces and moments on hull and sails are in equilibrium. These conditions form the basis of various approximate performance models. A new performance model is derived, which is suitable for comparative analysis of various sailing ship design features.

CONTENTS

Page

Page

A7 : APPENDIX TO CHAPTER 7

LIST OF TABLES

LIST OF ILLUSTRATIONS

Acknowledgements

The author would like to express his gratitude to his supervisor, Dr. John Harvey, for his very generous guidance and support.

He would also like to thank Dr. Peter Bearman, Dr. Mike Graham and Dr. Martin Downie for their suggestions and ideas; and Jack Beazley, John Coles, "Mac" McCara, John O'Leary, Alan Maynor, Deanne Eastwood, Pauline Harrison, Liz Bradbury, Mary Bradbury and Joy Richardson for their various practical contributions.

The author was supported by a Science and Engineering Research Council grant for the first three years of this work.

1. INTRODUCTION

1.1 Background

For most of man's recorded history the majority of sea-going ships have been sailing ships. It was only in the last hundred years that sailing vessels were largely replaced by coal-, then oil- powered ships. These latter ships burnt cheap abundant fossil fuels and had the significant advantages of increased reliable speeds and reduced manpower requirements. Large sailing ships became completely obsolete, and the use of sails on smaller commercial vessels was restricted to some fishing vessels and to third world coastal trading vessels.

More recently, it has become apparent that the world's fuel supplies are finite, and extraction costs have risen as the easiest supplies have been exhausted. In the early 1970s a number of previously exploited oil producing nations formed a powerful cartel: their efforts at husbandry and price control led to sudden severe price rises and shortages. Despite subsequent price reductions the world economy has still not recovered from this "oil crisis". As supplies are further depleted, the cost of oil will inevitably rise, and the world will become more vulnerable to possible future oil crises. This situation justifies interest in alternative supplies of energy. One alternative supply is the wind, and history shows that ships are well suited to wind propulsion.

There is a growing range of situations for which sail is economically justified. It is interesting to note that this resurgence of sail is occurring in two distinct ways. Firstly, there are changes in the economic merits of low-

technology sailing or motor-sailing craft compared with similar powered craft in marginal situations where the use of sail has declined but not ceased. This will lead to an increase in the use of fairly conventional sails for fishing vessels and for small third world trading vessels. Secondly, it appears that high-technology sail-powered or wind-assisted ships will become increasingly competitive with conventional ocean-going powered ships. This will lead to the production of fast, and sometimes large, sail equipped vessels which are quite unlike anything known in the past.

This decline and subsequent resurgence of sail was predicted more than seventy years ago by Laas (1912). He wrote "For the present, sailships will hold their own in coastwise transportation and for fishermen. But the sail sport will endure forever, being one of the most vigorous and beautiful sports in existence. Perhaps its mission will be to preserve and further the knowledge of mastering the wind and finally, after long, long years when oil and coal shall have become too costly, to revive to new splendour the grand art of sailing, in modified form perhaps, and based upon further progress in aviation and meteorology, as well as upon other advances in the engineering art."

Numerous commercial sailing ship projects are reviewed in Chapter 2. A small number of coastal vessels have already been built or "retrofitted" with auxiliary sails, and a wide range of sizes and types of sailing vessels are being considered. Sail propulsion has been proposed for vessels as large as 60,000 dwt and a vessel of 14,400 dwt is already under construction (Anon. 1980e). The technology of proposed ships varies between the traditional barque

(Willoughby, 1979) to the high speed surface effect vessel (Wynne, 1979). High-technology wind propulsion systems proposed include the rotor, first suggested by Flettner (1926), the wind turbine (Rainey, 1980) and the kite (Schaeffer and Allsop, 1980). Many proposals are for vessels rigged with some kind of aerofoil sail (Priebe, 1981; Watanabe, Endo, Nakanishi and Takeda, 1982; Armand, Marol and Saint-Blancat, 1982; Anon., 1983a; and Cross, 1983). A particularly well researched proposal is for the "Dynarig", which consists of roller-furled square sails mounted on cantilever masts.

The first economic reevaluation of commercial sail was conducted by Miles (1973). Many other economic calculations have subsequently been published (Woodward, Beck, Scher and Cary (1975); Warner and Hood (1975); Wynne (1975); Herbert (1976); Couper (1977); Couper, King and Marlow (1979); Hood (1980); Rainey (1980); and Sorensen-Viale (1981). All of these have been cost-benefit analyses of example ships and have sometimes been made with questionable basic assumptions. Most of these have concluded that sail is, or will shortly become, economically justified for certain routes and trades. More general principles of sail economics are discussed by Herbert (1980) and Crowdy (1980). Croudy's work is undoubtedly the most important economic investigation of sail.

Croudy (1980) concludes, "The economic speed of low cost ships carrying low cost cargoes is today little higher than the port-to-port speeds achieved by sailing ships at the turn of the last century. Composite sail/power ships could be designed today for such trades, which would out-perform many of the pure motor ships currently building.

If coal prices reduce in real terms, coal fired steam ships will certainly attract growing attention. If the oil/coal price ratio widens and supplies of crude oil become unreliable, investment in coal liquefaction plant will ensure the continuation of diesel fuel supplies. The almost inevitable increase in the price of fossil fuels that will accompany diminishing reserves will enhance the attraction of nuclear propulsion - and less controversially, the attraction of sail."

Surprisingly few experimental investigations of commercial sailing ships have been conducted. The first reported series of tests were those conducted by Flettner (1926); various wind tunnel tests were made before rerigging the former barquentine "Buckau" as a rotor ship. The most comprehensive series of tests were the "Dynaship" experiments conducted by Wagner (1967); these included many wind tunnel tests and limited towing tank tests. NKK (1979) report wind tunnel tests conducted before they built the "Shin Aitoku Maru"; these included tests of the sails individually, and mounted on a model ship. Armand, Marol and Saint-Blancat (1982) report initial wind tunnel tests of their proposed aerofoil ship. Several other commercial groups have conducted experiments but apparently not published any results.

1.2 This investigation

The propulsive equipment for a sailing vessel consists of two force-producing elements immersed in two fluids with mutual relative motion: the force-producing devices are the sails and hull; and of course, the fluids are the air and the sea. The devices deflect flow and develop fluid dynamic forces. If the combined forces acting on the vessel are not in equilibrium, the resultant force accelerates or decelerates the vessel until it takes up a velocity so that all forces are in equilibrium. Usually the angle between the ship centre-line and direction of motion through the sea is small; and for this reason the convention has been to regard the velocity relative to the sea as the speed of the vessel and the velocity relative to the air as (minus) the relative wind. This implies that the propulsive mechanism is asymmetric; in fact, the mechanism is mathematically symmetric, and a sailing vessel's performance is determined by both its hydrodynamic and aerodynamic characteristics.

The work presented in this thesis describes both hydrodynamic and aerodynamic investigations of large sailing ships. Experimental and theoretical hydrodynamic investigations of the flow past the underwater hull are described in Chapters 3 and 4; experimental and theoretical aerodynamic investigations of the flow through multi-mast arrays of sails are described in Chapters 5 and 6; and finally the estimation of sailing ship performance from field dynamic characteristics is discussed in Chapter 7.

Hydrodynamic hull-flow investigations. When a ship is sailing the hull moves obliquely through the water at an angle of leeway. It develops a sideforce and additional induced drag. This thesis reports a wind tunnel

investigation of the flow past a Mariner type hull for the range of leeway angles normally encountered when sailing. Flow visualisation experiments are conducted, and the non-wave-making components of hydrodynamic hull forces are measured. A systematic series of hull-like blocks is similarly tested to investigate the influence of certain parameters such as beam, draft, cross-sectional area, trim, heel, rounding the bilge and rounding the bow planform. Force measurements are made in all cases.

An important feature of the flow about a hull at leeway is the longitudinal vortices shed from the bilges. A slender-body, Brown and Michael line-vortex model is used in a theoretical study of the flow past a hull-like block at leeway. This method is used to predict the evolution and shedding of bilge vortices and to determine the associated hull surface pressure distribution and forces. The effects of varying leeway and beam are investigated. Comparisons are made with experimental results.

Aerodynamic sail-flow investigations. Practical considerations suggest that modern sail-powered ships are likely to have arrays of sails. This thesis reports wind tunnel tests of a model with the important features of the above water part of a sailing ship. Various simplified sail-like aerofoils are compared individually and combined as sailing rigs; the effects of heel, mast-number and end-plates are investigated, and various strategies for trimming and reefing sails are compared.

In a multi-mast array of sails the local flow conditions at each sail are influenced by the induced flow of its neighbours; to obtain advantageous individual local flow conditions at all sails a graduated array of trim

angles is required. An iterative two-dimensional thin wing model is used to predict possibly advantageous graduated trim arrays for sails of any slender aerofoil section. The model is for attached two-dimensional flow, and hence is only applicable to low angles of inflow for which individual aerofoil-sails are set so that they are not stalled and so that the gaps between aerofoil-sails are small compared with their heights. Various graduated trim arrays are calculated and these are tested in the wind tunnel to determine whether they are, in fact, advantageous.

Performance calculations. A new mathematical model is derived which can estimate sailing performance according to various engine-use strategies. This model considers the trigonometry of velocity components, the equilibrium of horizontal forces, and the equilibrium of yawing and heeling moments. It also includes consideration of the following features; hull wave-making resistance, hull roughness and fouling resistance, rough water effects, variable propeller thrust, effect of heel on sail forces, and the wind profile. Various example performance calculations are conducted.

1.3 Note on terminology

The nature of this work makes the use of both nautical and aerodynamic technical terms inevitable. It is hoped that this work will be read by some people who are not familiar with both technical vocabularies; and as far as possible, obscure terms are avoided unless their meanings are indicated at first use. Nevertheless, many technical words are used freely because of their obvious or well-known meaning, because of their conciseness, or simply because they are part of the author's normal vocabulary. If any nautical terms need explanation, there are many good nautical dictionaries, such as Smyth (1897). It is more difficult to recommend a good aerodynamic dictionary; Adams (1959) is one possibility: a non-aerodynamic reader is probably better advised to follow up unfamiliar terms in an aerodynamic text book such as Batchelor (1967).

2. A REVIEW OF SOME COMMERCIAL WIND PROPULSION PROJECTS

2.1 Introduction

In 1980 the Times printed an article on its front page under the headline, "Oil prices put sails back on the horizon" (Baily, 1980). This article must have surprised many people. It reflected a growing awareness and interest in the idea of wind propulsion for commercial ships. A better indication of this interest may be the number of related symposia held since the oil crisis; the Royal Institution of Naval Architects (1975 and 1980), Liverpool Polytechnic (1976), the Royal Institute of Navigation (1977) and the Department of Industry (1979) have all organised meetings on the subject in this country alone.

This work was started when there was a shortage of oil and prices were high: there is now a glut and prices are low. It is inevitable that oil will eventually become scarce and expensive: it is not, however, inevitable that sailing ships will eventually replace diesel ships. Various alternative fuels are being developed, and wind energy must compete with these. Shipowners will only invest in wind-powered or wind-assisted ships for sound economic reasons. Objective consideration of the commercial use of sail power is hindered by a widely held romantic and nostalgic love of sailing ships, and some advocates are undoubtedly idealistic dreamers. Nevertheless, this review does show that a number of people are investing money in wind powered ships, and this must be a clear indication of their serious interest - if not always of their wisdom.

2.2 Various sail projects

Third world sail. The idea that sailing vessels are no longer used to carry cargo is Eurocentric. Couper and King (1980) comment, "In inter-island and some other trades of developing countries the extent to which sailing vessels have continued to operate is appreciable." They describe the importance of sailing vessels in Indonesia, Malacca, Southern Philippines and the Indian Ocean. They comment on the existence of some auxiliary schooners in the Pacific Islands and the Caribbean islands. Irani (1980) describes the various traditional sailing craft used in India and the modernised auxiliary vessels which are gradually replacing them. The Indian government has played a major part in developing these modernised vessels of 150 or 300 tons fitted with the traditional lateen rig. They have also made the necessary provisions to control and regulate this sailing traffic which carries about one million tons of cargo per year.

Rotor ships. Early in the 1920s Flettner (1926) was trying to find an alternative to traditional sails. At this time Prandtl was conducting experiments at Göttingen on rotating cylinders in a fluid flow. These rotating cylinders deflect the incoming flow and experience a fluid dynamic lift force as described below. The effect is named after Magnus. Flettner realised that this effect could provide a solution to his problem.

In 1924, after various tests, and as a demonstration, the 50 m, 200 hp auxiliary barquentine "Buckau" was rerigged as a two stack rotor ship (Figure 2.1). A sail area of about 850 m^2 was replaced by a rotor area of about 85 m^2. Each rotor was turned by an 11 Kw electric motor. This

demonstration vessel, renamed "Baden Baden", successfully sailed both ways across the Atlantic.

Following this success, the German Navy Transportation Department ordered a larger auxiliary rotor ship. This vessel, the "Barbara", was a 2077 grt, 91 m vessel, capable of a maximum speed of 22 kt. She was fitted with three 17 m rotors rotated by 35 hp electric motors. She was provided with a total available power of 1,060 hp to drive the propeller and generators. She apparently traded for some time in the Mediterranean fruit trade (Anon., 1978b) and also for several years between Hamburg and the River Plate (Rocca, 1980). In the economic conditions of the early 1930s she was stripped of her rotors and the concept was largely forgotten.

Recently the rotor system has been considered in a number of surveys of possible modern wind propulsion systems (Wellicome, 1975; King, 1976; Mudie, 1977a; and Anon., 1979b). It is reported that Esso had some interest in reviving the concept (Anon., 1978b). The Department of Industry (1979) favoured the study of several wind assistance systems, including the Flettner rotor. Willoughby, director of Windrose Ships Limited, is reported to believe that the rotor ship has great possibilities in the future (Green, 1980).

One way of understanding the Magnus effect is to consider the momentum exchange perpendicular to the inflow direction. See figure 2.2. The flow about a spinning cylinder is asymmetric with flow separation occurring at different positions from the upper and lower surfaces and different pressure distributions existing on the two surfaces. This asymmetric flow is associated with a wake

flow which is deflected at an angle to the inflow. This represents the creation of a component of momentum perpendicular to the inflow. Newton's second law relates this rate of creation of momentum component to the lift force on the spinning cylinder. This lift force is experienced by the cylinder as the integral of the pressure force component perpendicular to the inflow. The lift force is used to drive a ship in the same way as is the lift force on a conventional sail ("lift force" is used here to denote the horizontal force acting perpendicular to the relative wind).

This propulsive system has caused some confusion in the shipping world. Crowdy (1980) makes unjustified technical criticisms of the system. One author attempts to explain the mechanism of propulsion as follows: "... the tall cylinders, spinning by means of electric motors, threw off the air from their front surfaces, so lowering the pressure and, of course, accumulating higher pressure against their after surfaces. The combined effect of a partial vacuum before and increased pressure behind 'sucked' the vessel forward." (Anon., 1980e).

It is interesting to note that a Magnus effect device has recently been proposed as a rudder (Pike, 1980). A 3,700 hp twin screw river push tug is being fitted with such a device in the United States.

Wind turbine vessels. The windmill ship has a long history, as described by Flettner (1926) and Rainey (1980). As early as 1712, Du Quet proposed using a windmill to power a paddlewheel vessel. During the last hundred years a number of small windmill craft have been successfully built and sailed. Recently the possibilities of wind

turbines have been considered by Wellicome (1975), Mudie (1977a), Nance (1979), Anon. (1979b), Crowdy (1980) and Herbert (1980).

The Department of Industry (1979) expressed interest in this concept and subsequently sponsored a feasibility study. Rainey (1980) describes this study. Achievable performance was calculated using a graphical procedure which compares aerodynamic and hydrodynamic power surfaces. Economic analysis, using government forecasts, predicted that a 4,000 tonne auxiliary vertical axis turbine vessel, trading between Cape Town and Ascension, should pay back her additional rig first cost in 5 to 7 years. Rainey concluded, "further work on the wind turbine rig is therefore justified".

Kite sails. Shaefer and Allsop (1980) report a number of historic successful attempts at kite sailing. They describe their mathematical and experimental investigations of kite sailing. They consider advantages of kite sails over fixed sails to include the greater energy available aloft and reduced problems of ship stability. They describe the considerable problems to be overcome, but are optimistic about the future of the kite sail.

British Petroleum are considering auxiliary kites for wind assisted oil tankers. They are reported to have patented a kite sail and a method for launching such a sail (Anon., 1983b).

Aerofoil ships. In the early 1920s Flettner (1926) persuaded the Germania Werft to assist with a project to fit aerofoil sails on the 50 m barquentine "Buckau" (Figure 2.1). She was to be fitted with two triplane units of three aerofoils. Each unit would consist of symmetric section

aerofoils set side by side. The aerofoils would have 1/3 flaps and the units would be passively controlled by tail fins on a long tail shaft. Flettner intended using the wind to provide main propulsion and determined that a sufficiently powerful rig would be very large. He eventually decided that the rotor was a more attractive wind propulsion system and the "Buckau" was fitted with twin rotor stacks, as already mentioned.

Barkla (1951) proposed a high speed, light displacement craft fitted with an aerofoil rig similar to Flettner's rig. He analysed the possible performance of light displacement craft and commented, "The scientific sailing vessel may never be adopted, but its potential performance deserves to be recognised." Shortly before the fuel crisis Greenhill (1972) considered the role of the sailing ship in a world with dwindling fuel supplies. He foresaw high technology ships rigged with arrays of aerofoils "rather like vertical airliner wings with a flap system designed to extend and contract their area." Subsequently Wellicome (1975) attempted to compare various possible rigs for wind driven ships. He considered single symmetric aerofoils and "high-lift" aerofoils. The "high-lift" aerofoils consisted of three symmetric aerofoils set nose to tail with facilities to alter overall camber. Figure 2.3 shows such an arrangement tested by Otto Scherer (1974). This double slotted aerofoil sail achieved a very high lift coefficient. This was attributed to the flow through the two slots increasing the kinetic energy of the boundary layer over the trailing part of the aerofoil and thus delaying trailing edge stall (this explanation is criticised in section 5.2(c)). Recently, the French Government have sponsored a fairly

primitive feasibility study for a 91 m vessel fitted with two similar "high-lift" aerofoil sails (Armand, Marol and Saint-Blancat, 1982).

Mudie (1977a) considered multiple aerofoil units as one possible way of providing wind assistance. Wynne (1979) considered the factors limiting the performance of light displacement sailing craft. He discusses the theoretical possibilities of building a 200 dwt vessel with a maximum sailing speed of over 100 kt (Figure 2.4). This vessel would use supercavitating hydrofoils, aircraft wing type sails and would support its weight, at relative wind speeds over 61 kt, using ground effect. It would require retractable turbo fans to propel it up to flying speed. Herbert (1980) considered the economics of wind propulsion. He concluded that wind powered ships must be designed to sail at relatively high speeds to compete with fuel powered ships. He outlined various high technology aerofoil ships which he thought might become viable. Recently, the Windship Development Corporation has conducted experiments with a rigid aerofoil rig (Anon., 1983a). Bradbury (1980a and b) has conducted wind tunnel tests of arrays of aerofoil sails.

In 1968 Walker designed and built an aerofoil yacht (Stoeckert, 1968). This was fitted with a five-aerofoil unit passively controlled by a tail fin much like Flettner's proposal of 1922. Very recently, his company, Walker Wingsail, has obtained £125,000 from Prutech to investigate wind powered cargo ships (Cross, 1983). Walker proposes fitting a vessel with two triplane aerofoil units actively controlled by microcomputer.

The "Dynaship". Thieme (1955) from Hamburg University published a wide ranging and thorough analysis of the

mechanics of sailing. This started a programme of research at Hamburg, which led to the design and analysis of a possible high technology sailing ship. Prölss (1967) proposed the "Dynaship" (Figure 2.5). This vessel was to be rigged with a modern interpretation of the traditional square rig. The masts would be unsupported, cantilever beams mounted on turntables so that they could be rotated according to the angle of the relative wind. The yards would be curved and fitted with tracks so that the sails, which would be stretched between pairs of yards, could be set and furled without men having to go aloft. A vessel of about 15,000 dwt to 20,000 dwt was originally envisaged. Wagner (1966 and 1967b and c) published a series of reports on wind tunnel experiments associated with the Dynaship project. Wagner (1967a) developed a method to estimate the performance of sailing ships which was subsequently improved by Schenzle (1976). The Hamburg sailing ship research project was summarised and reviewed by Wagner (1976).

Following the fuel crisis, companies were set up in Copenhagen and California to market the Dynaship idea (Dynaship Corporation, 1975). King (1975 and 1976) described the Dynaship and comments on its possible performance. Wellicome (1975) compared the Dynaship with various other possible wind driven ships. Articles about the Dynaship appeared in a number of papers (Anon., 1975a and b; Lemon, 1975; Nance, 1976b; and Rocca, 1980). Nance (1976a) reports trials with a model Dynaship rig on a yacht hull. Recently Azad (1980) and Hogben (1982b) report that the EEC may give financial backing to a joint venture, involving the Dynaship Corporation of Sweden and Cockerill Shipyard of

Belgium, to design and build a 30,000 dwt sailing vessel.

Illies (1977) considered future sources of energy for the propulsion of ships. He considered wind energy as one of six possible sources. He noted that wind propulsion is suited to the bulk trade, requiring ships such as the Dynaship.

Windrose Ships Ltd. Shortly after the fuel crisis a company was formed to develop a conventional 12,000 dwt auxiliary barque as an economic proposition (Anon., 1978a and 1980a; Azad, 1978; Hogben, 1978; Scantling, 1978b; and Windrose, 1978). The directors of this company, "Windrose Ships Limited", are Willoughby, Drummond, Lord Strathcona and Mount Royal, Pochna and Miles. Adoption of an historic but well tried rig was justified by claims that it would not incur the high development costs attributed to more modern rigs. Willoughby (1979) reviewed the impressive performance of many past sailing ships to justify the speed claimed for the new vessel. A feasibility study was partly financed by the Department of Industry (North, 1979). One conclusion was that in certain circumstances a sailing ship could become competitive once oil prices rose above $115 per ton. Prices had reached $180 per ton in 1980 but Windrose were still unable to attract financial backing (Rocca, 1980). Willoughby and Corlett (1980) describe the particular design problems of large sailing ships. They also give the most recent designs of the Windrose "Sailiner". She would be a 137 m, 15,000 dwt, 5 masted auxiliary barque. She would carry 6,200 m^2 of sail and be fitted with a 3,900 shp main engine (Figure 2.6).

Other bulk carriers. The Russians are reported to

have taken a decision at a symposium held in 1979 to design a 60,000 dwt cargo vessel (Nance, 1980). This bulk ore carrier, "The Fatum", is apparently being designed by Kryuchkov at the University of Nikolayev. It is to have 15,000 m^2 of computer controlled sails set on seven masts with curved yard arms (Azad, 1980 and Hogben, 1980a).

Hood (1980) considered a similar sized bulk carrier. He investigated a Southern Ocean 60,000 dwt bulk grain carrier. This was to be a pure sailing vessel circumnavigating Antarctica, running with the prevailing winds. It was to take grain from Sydney to Capetown for transhipment to Europe and to sail on to Sydney in ballast. Hood proposed a seven masted Bermudan type rig with facilities to goosewing twin sails when running. He concluded that the project was technically feasible, but the complications of transhipment made it economically unjustified.

Recently it was reported that the Deutscher Foerderverein Segelschiffahrt had been formed to design and put to sea a smaller grain vessel (Anon., 1982a). This proposal is for a 160 m, 12,000 dwt bulk carrier. She would be a five masted barque with 8,000 m^2 of sail and a 2,500 Kw Schottel propulsion unit. The vessel would require 25 crew.

Japanese wind assisted ships. In 1977 NKK obtained sponsorship from the Japan Marine Machinery Development Association to study commercial sailing ships (Azad, 1978 and 1980; Anon., 1979a and c; and Green, 1980). Initially various possible sail designs were tested in a wind tunnel. Three of the best sails were fitted to the 25 m, 77 grt scale model tanker "Daioh", and sea trials were carried out from May to July 1979. One of Daioh's sails, a rigid folding sail of canvas and iron, was subsequently tested

ashore. NKK (1979) concluded, "we can expect the realisation of sail equipped motor ships in the near future."

The sail assisted motor tanker, "Shin Aitoku Maru", was launched in August 1980 (Anon., 1980d; Cullinson, 1980; and Rocca, 1980). This 66 m, 1,600 dwt vessel is fitted with two 97 m^2 NKK folding sails and a 1,600 bhp diesel engine (Figure 2.7). The sails were expected to reduce fuel consumption by 10-15%. Other fuel saving design features were expected to further reduce consumption to 50%. A microcomputer controls all propulsive devices and no extra crew are required (Anon., 1980c and Bowbee, 1980). After several years it was reported that the vessel continued to perform satisfactorily, and that all expected fuel savings had been achieved (Hogben, 1982c).

A sister ship, the "Aitoku Maru", was fitted with a single 85 m^2 sail located near the bow (Anon., 1982c). A similar 72 m, 2,100 dwt coastal steel vessel has been ordered for completion in March 1983 (Anon., 1982). This vessel will be fitted with two 138 m^2 sails. A 73 m, 2,100 dwt coastal coal vessel is also being considered. This coal vessel may be fitted with three sails (Hogben, 1982c).

Mitsui, advised by NKK and the Marine Machinery Development Association, are building an 87 m, 14,400 dwt wind assisted low speed towed barge. This unmanned vessel has four masts and a total sail area of 2,500 m^2 (Anon., 1980e). A similar 18,000 dwt vessel is being considered (Anon., 1980b). NKK are also considering wind assistance for the 37,000 dwt car/bulk carrier, "Global Wing". A recent survey of the NKK project is provided by Watanabe, Endo, Nakanishi and Takeda (1982).

Ocean Carriers Corporation. In 1972 Lawrence (1975) acquired the steel hull of the 4 masted barque, "Fennia", with the intention of returning her to sea in commercial service. However, hull corrosion was found to be excessive. He subsequently designed a ship with very similar hull lines to the "Fennia" (Anon., 1976 and Nance, 1976c). This vessel, the "Western Flyer", was to be a 96 m, 4,500 dwt, 4 masted auxiliary schooner. She was to be fitted with bermudan sails on bipod masts and a 600 hp diesel engine. In 1978 Lawrence obtained the hull of the 460 dwt, 3 masted schooner, "Aar", which had been built in 1932. This vessel was to be repaired in Harrison's Tyne shipyard under the supervision of Wynne. It was to be rerigged as a 3 masted auxiliary schooner and fitted with a 300 bhp Cummins engine (Azad, 1978; Hogben, 1979a; and Anon., 1979a). The vessel was intended to trade between Miami, Nevis and St. Kitts. The conversion was originally expected to be completed during 1979 (Azad, 1978). There are still no reports of completion.

Windship Development Corporation. Woodward, Beck, Scher and Cary (1975) reported on the possible use of sailing cargo ships for the American merchant navy. This feasibility study had been financed by the U.S. Department of Commerce. They considered large bulk carriers in the range 15,000 dwt to 45,000 dwt. These would be fitted with a modernised square rig and sufficient power to give 6 kt in still conditions. The sailing ships were compared with similar sized powered ships on long routes from North American ports. It was concluded that "an immediate move to build sailing ships is not justified", although sailing ships were on "close to equal footing with powered ships."

Some years later, the Department of Commerce (1979) announced that an $138,000 contract for a follow-up study had been awarded to the Windship Development Corporation. This was apparently one of a number of syndicates formed to tender for this contract. The group consisted of Bergeson, Maclear, Marcus, Mays, Bates, Spierings and Anderson. Rocca (1980) reported that the Bergeson group favoured schooner type rigs and intended scaling up a yacht system which uses leading edge rollers for sail stowage. Green (1980) reported that they favoured the use of sailing ships to carry cargo on an unscheduled basis!

The study concluded that sail assisted ships offered fuel savings of 20 to 30 per cent, and total operating cost savings of 5 to 15 per cent (Anon., 1981). Simple conventional triangular sails and rigid aerofoil sails were both considered suitable for commercial application (Anon., 1983a).

In August 1981 the 65 m, 3,000 dwt, Greek general purpose cargo vessel, "Mini Lace", was retrofitted with a cat style rig (Pike, 1982). The rig is a 250 m^2 triangular sail on an unstayed roller-furl mast (Figure 2.7). The vessel has a 1,000 hp diesel and maintains a service speed of 7 kt. After 13 months of service in the Caribbean fuel savings of more than 20% were reported. Similar retrofits were being prepared for the conservation vessel, "Rainbow Warrior" and for the U.S. Navy's AGOR 14 class research vessels.

The Windship group were recently experimenting with a rigid aerofoil sail. The 28 m^2 prototype had a symmetric section and a 20% flap. Following tests they hoped to scale

the sail up to 300 m^2 or 550 m^2 for application to coastal tankers or cargoships (Anon., 1983a).

Other wind assistance experiments. In 1978 twin roller furled, loose footed sails were fitted on the jack-up drilling rig, "Rowan Louisiana". This rig was being towed from Galveston, Texas, to the Bay of Campeche, near Mexico. Its leading leg was fitted with two 630 m^2 triangular sails with 55 m luff lengths. The objectives were to identify problems associated with such sails and to establish performance. It was deduced that a 31.5 kt wind provided more thrust than a 1,000 hp tug and that an increase in towing speed of 0.5 kt represented a saving of $2,400 per day (Hood, 1979 and 1980; Anon., 1980; and Morin Scott, 1980).

Morin Scott (1980) and Metcalf Shipping Ltd. planned an experiment with the 67 m, 1,310 dwt coaster, "Firethorn". She was to be fitted with a simple low aspect ratio bermudan rig, giving a sail area of 500 m^2. Investment was to be kept low by avoiding untried technology. Returns may also have been low as squat rigs tend to give poor performance. At one stage a government body expressed interest in the project. However, cutbacks in government expenditure prevented the scheme from proceeding.

A more successful project is reported by Hogben (1982c). A triangular sail is in use on the Singapore vessel, "Wild Rover". This is a 1,250 dwt vessel trading regularly to Western Australia. This is apparently a wind assistance project similar to the Windship Development Corporation's "Mini Lace" project.

Hogben (1983) also reports that the Oost Atlantic Line have fitted a 130 m^2 square sail to the 3,000 dwt

"Atlantic Coast". He describes the sail as looking like a Tudor square topsail!

Rebel Marine Services U.S.A. Following trials with a smaller vessel, the building of a 16 m auxiliary tug was announced (Hogben, 1982a). This tug has a gaff schooner rig with a normal sail area of 78 m^2. The main engine is a 320 shp diesel. There are 5 crew. The objectives of the project were to reduce fuel consumption and, when possible, increase speed on medium or long distance tows (Scantling, 1979). Fuel savings of 40% were anticipated (Anon., 1980e). The vessel was launched on 22 May, 1980 (Bowbee, 1980). Performance curves for the tug were established by the Virginia Institute of Marine Sciences. In 1982 fuel savings of "up to 40%" were reported by Briggs of Rebel Marine (Scantling, 1982a).

Two South Pacific projects. Hood (1979) was contacted in 1974 about a possible sailing ship for a Tongan shipping line. This vessel was to operate in the area of New Zealand, Fiji, Tonga and Western Samoa. Easterly winds prevail in this region for 11 months of the year and would favour certain North/South sailing routes. Warner and Hood (1975) designed an auxiliary 4 masted schooner as an alternative to an existing motor ship. The proposed 2,200 dwt vessel was to be 73 m long. It was to be fitted with sufficient power to make 6½ kt without wind. Economic calculations found such a vessel to be commercially profitable. However, Warner reported that his bankers were unwilling to invest in the vessel until experience had been gained with a smaller prototype (Scantling, 1978a). He was hoping that the World Council of Churches would finance a suitable vessel for another inter-island sail project.

Nance (1978b) stated that the Tongan vessel was not built because of a glut of ships of that size in the area.

The Australian government, on behalf of the government of Tuvalu, financed another study by Hood of a possible sailing vessel (Nance, 1980). This vessel was to replace an island supply vessel, the "Nivanga". Hood was to investigate a pure sailing ship and a wind assisted motor ship. In 1978 Hood reported adversely on the sailing vessels. Economic analysis showed that the vessel must spend more than a third of the time sailing to be profitable. Analysis of the region's winds showed this not to be possible (Hood, 1979). An additional important problem for a sailing vessel was that many of the island lagoons could only be entered at daylight highwater. This would impose a very rigid schedule (Nance, 1978a).

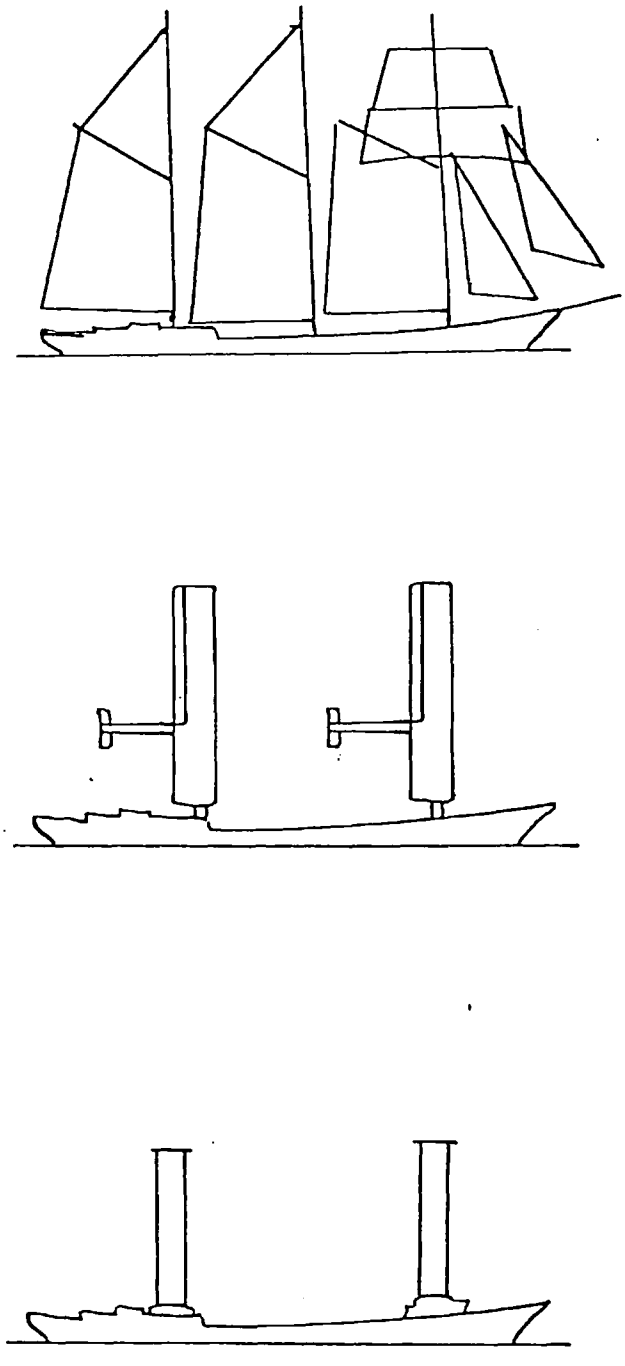

Figure 2.1

The "Buckau"; as a barquentine (top),
with proposed aerofoil rig (middle),
and converted to a rotor ship (bottom).

Flettner (1926)

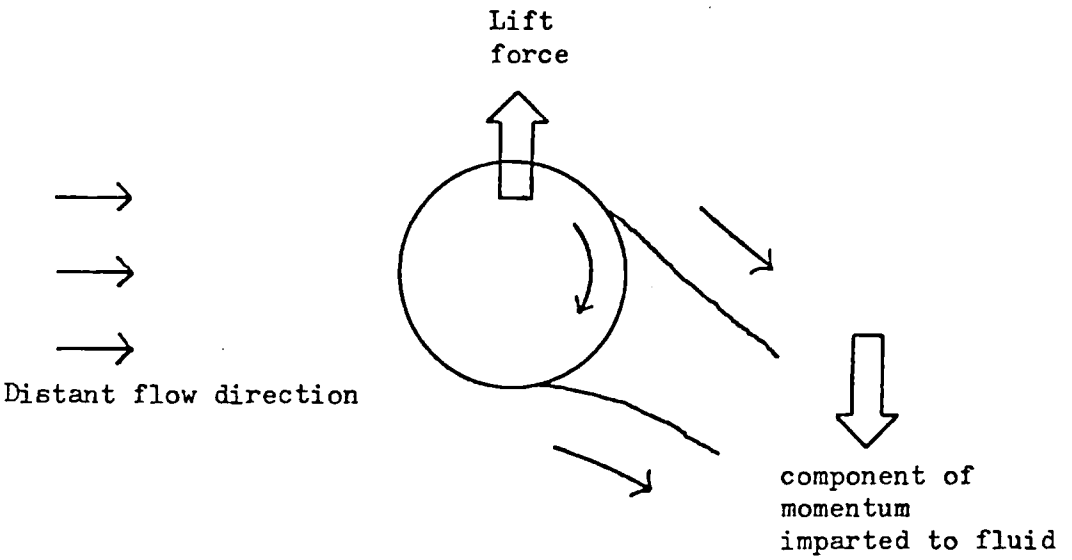

Figure 2.2; Magnus effect

Schematic flow past a spinning cylinder indicating the asymmetric separation and deflected wake.

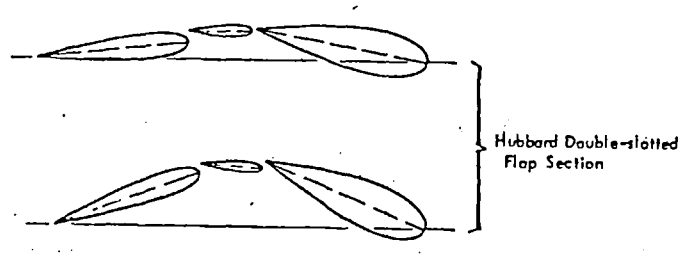

Figure 2.3

Multi-component aerofoil-sail: Otto Scherer (1974)

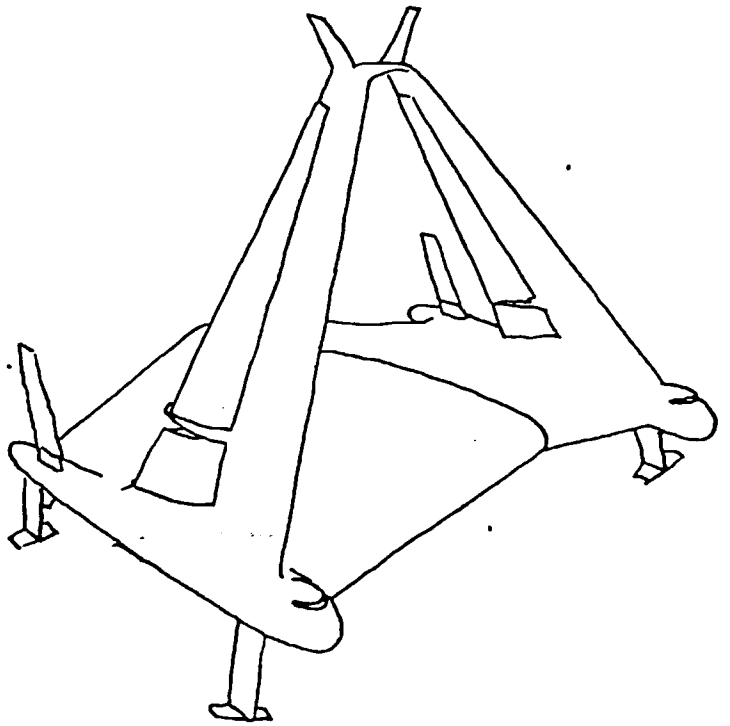

Figure 2.4

High technology aerofoil vessel: Wynne (1979)

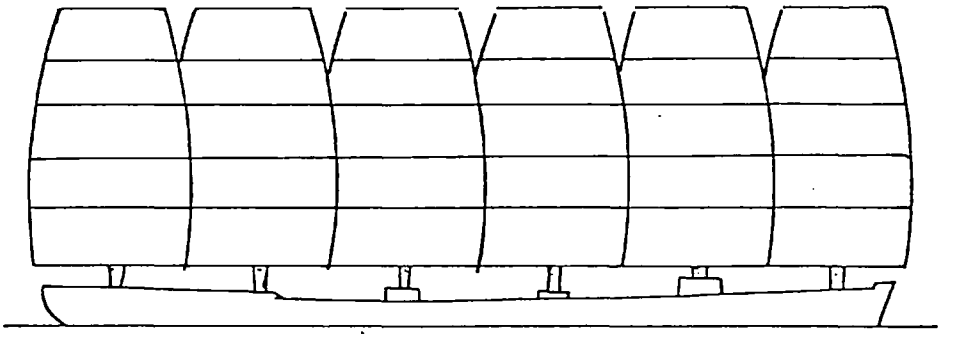

Figure 2.5

The "Dynaship" style rig: King (1975)

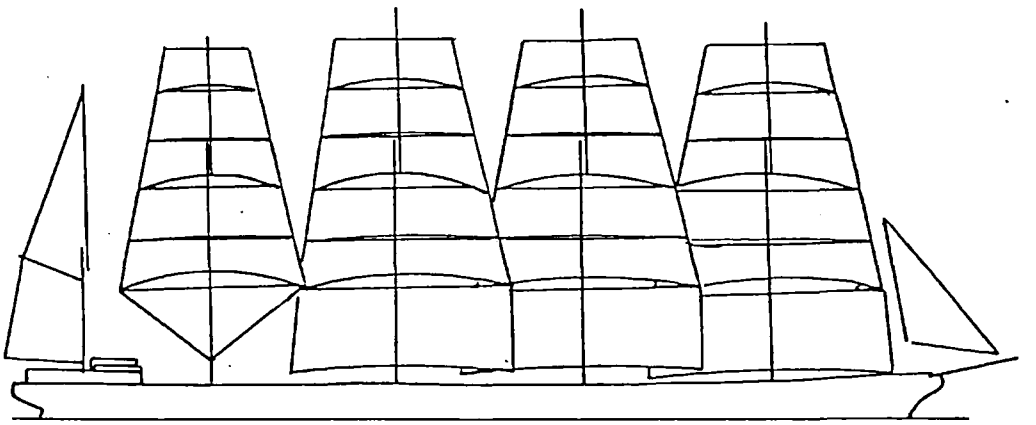

Figure 2.6

The "Windrose" style rig: Willoughby and Corlett (1980)

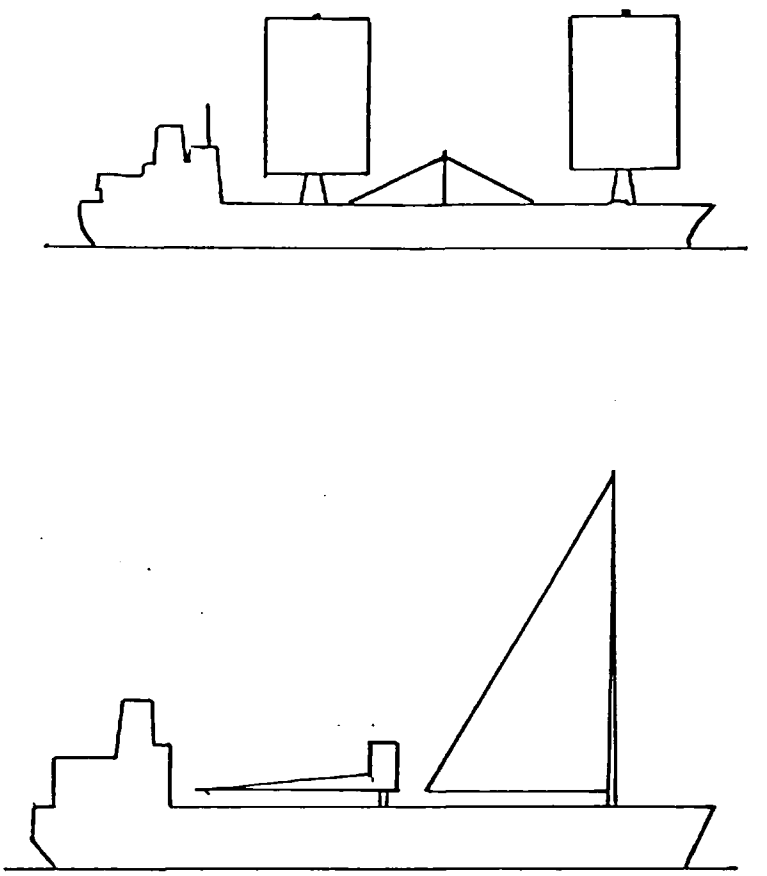

Figure 2.7

Wind assisted ships: NKK style rig (top) and

Cat style rig (bottom).

2.3 Conclusion

This review has mostly surveyed sailing ship projects concerning reasonably large ships or unusual rigs. Sail is perhaps particularly suited to smaller vessels, and there are a number of projects to put sails on small trading vessels or fishing vessels. Some of these are reported by Anon., (1980d), Arnold (1982), Azad (1980), Hasler (1977), Hogben (1979b, 1980a, 1982b and 1983), Jacquemin (1980), Nance (1980) and Scantling (1982a and b).

Despite the shipping slump and present low fuel prices, this review does suggest that there is an increasing interest in commercial sail. It seems more and more possible that sail will once again have a role in our merchant trade. Sail has its costs and disadvantages, but, as Mudie comments: "oil fuel is valuable and the wind is free."

It will not all be plain sailing, however, as was discovered recently in Fiji. Cornell (1979) reported the launching of a 33 m auxiliary trading schooner. The vessel was named "Cagidonu", which means "Fair wind" in Fijian. The owners hoped "that she will not be too dependent on her auxiliary engine." Eighteen months later Cornell (1980) wrote, "The 'Cagidonu' is in every respect a compromise, being neither sailing vessel nor motor vessel. Her masts serve mainly as a decoration, since the master and his crew do not know how to sail ... even if sails were made available to them."

3 : AN EXPERIMENTAL INVESTIGATION OF THE FLOW PAST HULLS AT LEEWAY

3.1 Introduction

When a ship is sailing, its underwater hull must develop a sideforce to balance the sideforce acting on the above-water part of the ship ("sideforce" is used here to denote the horizontal force perpendicular to the ship's centre-line). One way of developing this sideforce would be to fit high aspect ratio keels. These could either be fixed or adjustable in orientation; in the latter case it would be possible to orientate the keels to give the desired sideforce while the hull is sailed without leeway. In either case, these keels would pose considerable engineering and other practical problems. It is thought likely that future sailing ships will be designed to develop sideforce in the traditional way: they will sail with the hull at an angle of leeway to the relative flow direction so that the hull itself will develop hydrodynamic lift ("lift" is used in this discussion of sailing ships to denote the horizontal force perpendicular to the relative flow direction; this definition is normal in fluid dynamic discussions of sailing - see Marchaj (1979) - and arises because of the analogy between this hydrodynamic force and the lifting aerodynamic force experienced by aircraft flying at an angle of attack).

There has been little research concerning the flow past ships' hulls at leeway. Wagner (1967a) reports one of the few tests motivated by interest in large sailing

ships; oblique towing tests were conducted with a modern Mariner type hull and a traditional sailing ship hull. Recently a new wind propulsion dynamometer has been developed at the Netherlands Maritime Research Institute (Anon., 1982d). This allows the measurement of hydrodynamic forces experienced by an appropriately ballasted model, which is propelled by a force applied at a position corresponding to the centre of effort of the (sail and above-water-hull) aerodynamic forces.

Useful information on the behaviour of hulls at leeway is available from three related fields. These are; investigations into the manoeuvring characteristics of ships, investigations of the flow past sailing yacht hulls, and research into oblique flow past slender bodies of revolution (such as airships and missiles). Some results of the ship manoeuvring research are directly applicable to large sailing ships. However, little attempt has been made to investigate the hydrodynamic features of the flow past hulls at leeway, or to systematically investigate the effect of hull shape or appendages. The yacht research generally considers bodies of a considerably different shape to a ship's hull. These are usually fitted with high aspect ratio keels which develop much of the sideforce. More effort has, however, been made to investigate the nature of the flow past these hulls. The oblique flow past a missile is similar to the flow past a reflex model hull at leeway (a reflex model hull is a model of the underwater part of a hull and its image in the waterplane; the use of such models for testing is justified in section 3.2(e)). Considerable efforts have been made to understand the fluid dynamics

of these missile flows. Another similar slender-body flow is that past a train in a cross wind: aerodynamic investigations of high speed trains are reported by Howell (1979) and Howell, Rhodes and Everitt (1980).

The objectives of this series of experiments were; to investigate the flow past hulls at a range of angles of leeway, to measure additional hull forces associated with leeway, and to investigate the effects of various changes in hull proportion on these flows and forces.

Experiments were conducted to investigate the flow past a Mariner type hull and a Mariner waterplane block at leeway. A series of experiments were conducted with hull-like blocks with varying proportions to investigate the influence of beam, draft, cross sectional area, trim, heel, rounding the bilges and rounding the bow planform. Force measurements were also made in all cases.

3.2(a) Review: ship manoeuvrability investigations

Considerable efforts have been made to mathematically model the manoeuvring behaviour of ships. These models require information on the dependence of forces and moments on variables such as incidence angles, velocities and accelerations. Some such information can be inferred by analysis of carefully planned full scale trial manoeuvres. Detailed mathematical models require more information which can only be obtained from model tests.

Burcher (1972) and Gill (1979) describe the four usual experimental techniques. These are:

(1) straight line towing tests, often referred to as oblique towing tests, where a captive model is towed along a straight path at various angles of leeway, heel, etc;

(2) rotating arm tests, which are similar in principle to the straight line towing tests, except that the model is constrained to follow a circular path;

(3) planar motion mechanism tests which are similar to the straight line tests, except that the model can be continuously manoeuvred during the test to investigate, for example, acceleration effects; and

(4) free model tests where a self propelled model is accurately tracked while being manoeuvred by radio control, and functional relationships are inferred analytically.

The first three of these techniques can easily be used to provide information on how hull forces and moments depend on leeway. For example, Eda and Lincoln Crane (1965) used rotating arm tests, Eda and Savitsky (1969) used straight line tests, and Smitt and Chislett (1974) used planar motion mechanism tests.

Gertler (1966 and 1969) describes the ITTC standard captive-model-test programme. This was an international co-operative project which compared the results obtained by ten different establishments using these three techniques to test a Mariner type hull. Figure 3.1 shows results of moment and force tests at leeway. These test results show considerable scatter which is only partly explained by differences in propeller speeds and test Froude numbers.

Wise and English (1975) report oblique towing tests motivated by a slightly different interest. They conducted experiments to determine coefficients for a mathematical model of a drilling ship's dynamic positioning system.

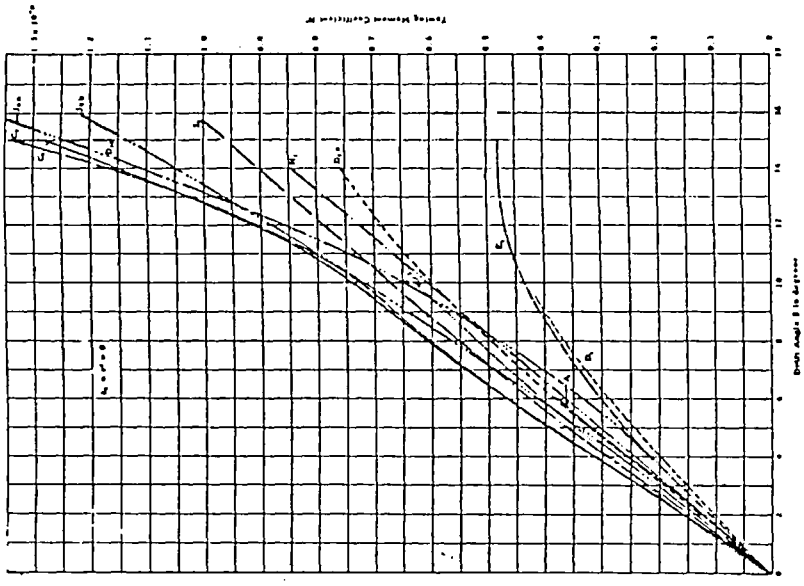

Comparison of yawing moment coefficients as functions of drift angle (The comparison is made for a nominal full-scale speed of 20 knots (F_n = 0.259); however the speed values for the individual organizations vary from F_n = 0.194 to 0.285)

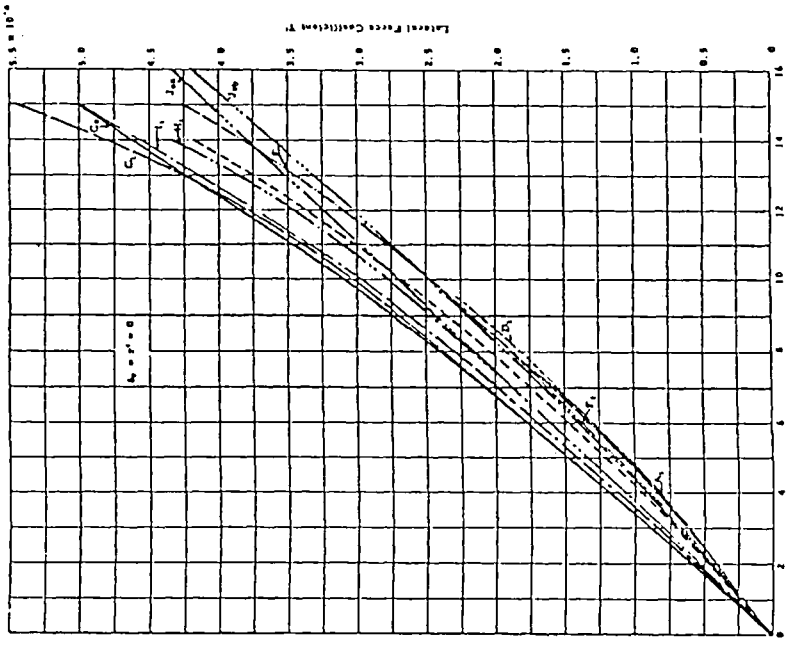

Comparison of lateral force coefficients as functions of drift angle (The comparison is made for a nominal full-scale speed of 20 knots (F_n = 0.259); however the speed values for the individual organizations vary from F_n = 0.194 to 0.285)

Figure 3.1

Dependence of forces and moments on leeway for a Mariner hull: Gertler (1969)

3.2(b) Review: yacht oblique towing tests

A great deal of money and enthusiasm is invested in racing sailing yachts. These yachts are often highly refined, and great efforts are made to produce marginal improvements in performance. In consequence, techniques of yacht testing have been more carefully developed than might be expected from their recreational motivation.

Davidson (1936) conducted oblique towing tests of yacht hulls at various heel and trim angles. He argues that the induced drag of a yacht hull at leeway "can be considered to be practically independent of the wave making resistance". Von Kármán (1936) disagrees and notes that there is circulatory flow at the sea surface as well as at the keel. At the surface, this is manifest as an elevation and depression of the sea either side of the hull; while at the keel, it is manifest as flow round the end of the keel. These flows produce, respectively, an asymmetric wave train and a trailing vortex. Both represent stores of kinetic energy, and both contribute to the induced drag.

Allan, Doust and Ware (1957) and Herreshoff (1964) discuss the practical details of yacht hull testing. Tanner (1962) comments that most yacht tank tests have "been of an ad hoc nature so that the basic hydrodynamic principles remain obscure".

Herreshoff (1964) notes that, for relatively deep keel boats, it is reasonable to assume that lift is developed primarily over the keel. He reports that full scale yacht performance suggests that model tests underestimate the sideforce. Yachts normally sail with the rudder at a greater angle of incidence to the relative

flow than the hull. The models were apparently tested with the rudder amidships, which might have been responsible for this underestimation. Herreshoff, however, attributes quite large differences, in lift coefficients, to the Reynolds number effect. De Saix (1964) notes that the Reynolds number effect on lift coefficients, for keel-like aerofoils, is small in the range of Reynolds numbers considered and range of incidence angles normally encountered by yacht keels. Herreshoff and Newman (1966) report full size tank towing tests of a 31ft yacht, the "Antiope". The results are compared with model tests of similar yacht hulls. They report that "preliminary comparison shows no sign of drastic scale effects on either the resistance or the sideways force." Letcher (1975) reanalysed this data. He notes that residual trailing keel vortices from previous runs probably caused the greatest experimental errors. He finds that "most force and moment coefficients have little variation with forward speed". Kirkman and Pedrich (1974) review investigations of scale effects in yacht hull testing. They find that there are significant unpredictable scale effects on both lift and drag, although these are less severe for the lift.

Marchaj (1979) gives a useful general discussion of yacht hull hydrodynamics. He reports various wind tunnel and tank tests of yacht hulls.

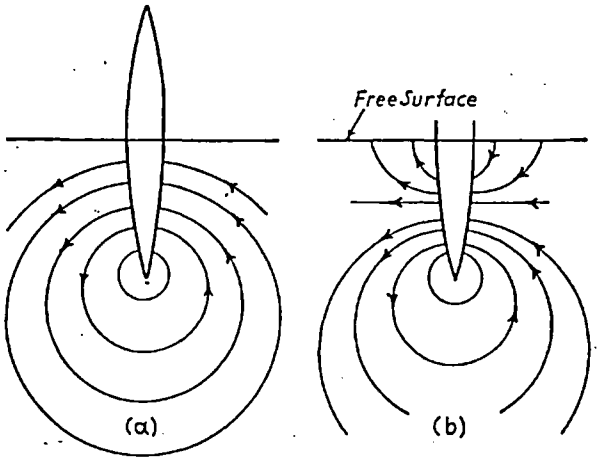

Figure 3.2

Schematic hull circulatory flow: Von Karman (1936)

3.2(c) Review: inclined slender bodies of revolution

At low angles of incidence, and at low Mach numbers, either half of the symmetric flow past airships or missiles is similar to the flow past a hull (the plane of symmetry representing the sea surface provided that this is approximately flat). This similarity breaks down in conditions where these flows become asymmetric. The main difference is that the missiles are generally circular in cross section, while merchant ship hulls are nearer rectangular for part of their length. The high curvature in the cross sectional profile at the hull's bilges can produce strong adverse pressure gradients which tend to induce separation close to the bilges. This constraint on the position of separation may well delay the onset of asymmetric vortex shedding. There will generally be primary separation near both bilges of a hull, while primary separation generally only occurs along a single line on each side of a missile-like body. Stronger vortices are likely to exist near a hull's bilges than are found near a similarly proportioned body of revolution.

Munk (1924) derives the mathematical equations governing potential flow past a slender body. He describes, in a general way, the flow past an inclined slender body such as an airship. Freeman (1933) conducted experiments with a 1/40 scale model of an airship. He measured the pressure distribution, forces and pitching moment at various angles of incidence. Figure 3.3 shows the dependence of lift on incidence. He finds that the integrated transverse pressure forces are in good agreement with the directly measured forces. Allen and Perkins (1951)

reanalyse Freeman's data and show that the flow separates towards the stern on the leeside of the airship. They conducted flow visualisation experiments with a fine missile-like body at incidence. They find that a pair of symmetric vortices are formed near the bow which become irregular and asymmetric at stations far removed from the bow. Letko (1953) measured the forces on a slender body of revolution with a fineness ratio of about 10 at a large range of incidence angles. Figure 3.4 shows the dependence of lift on incidence. He reports that the vortex disposition on this body becomes asymmetric for angles of incidence greater than about 15°.

Tinling and Allen (1962) measured forces and pressures on a missile-like body and also investigated the vortex positions using a 5 hole directional probe. Figure 3.5 shows positions of vortex cores at 3 moderate angles of incidence. Grosche (1971) used a 9 hole automatically aligning probe to conduct similar experiments. Peake, Rainbird and Atraghji (1972) review flow separation from slender and not-so-slender bodies. They report tests of a 6:1 fineness ratio ellipsoid. One interesting result is that the contribution to the lift of reduced surface pressure near the vortices is small at 10° incidence, but substantial at 25° incidence. They also investigate conditions influencing the onset of flow asymmetry for missile-like bodies. Fiddler, Schwind and Nielsen (1977) used a laser anemometer to investigate the flow field on the leeside of a missile. Peake, Owen and Higuchi (1978) investigated the flow near a slender cone at incidence. They used a number of experimental techniques, including laser/vapour screen flow visualisation. They also used a laser velocimeter to measure fluctuating velocities near an ogive-cylinder.

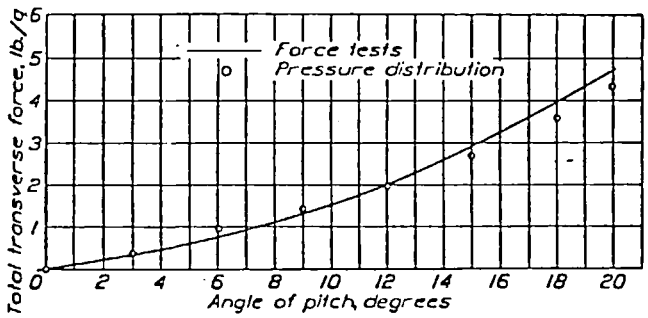

Comparison of total transverse forces obtained from pressure distribution and from force tests on the bare hull of 1/40-scale model *Akron*

Figure 3.3; lift on an airship at incidence:

Freeman (1933)

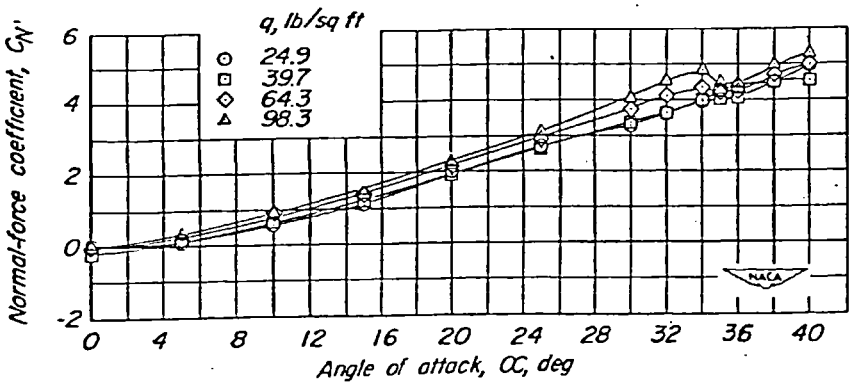

- Effect of dynamic pressure on the variation of fuselage normal-force coefficient with angle of attack. $\beta = 0^{\circ}$.

Figure 3.4; lift on a sharp nosed fuselage at incidence:

Letko (1953)

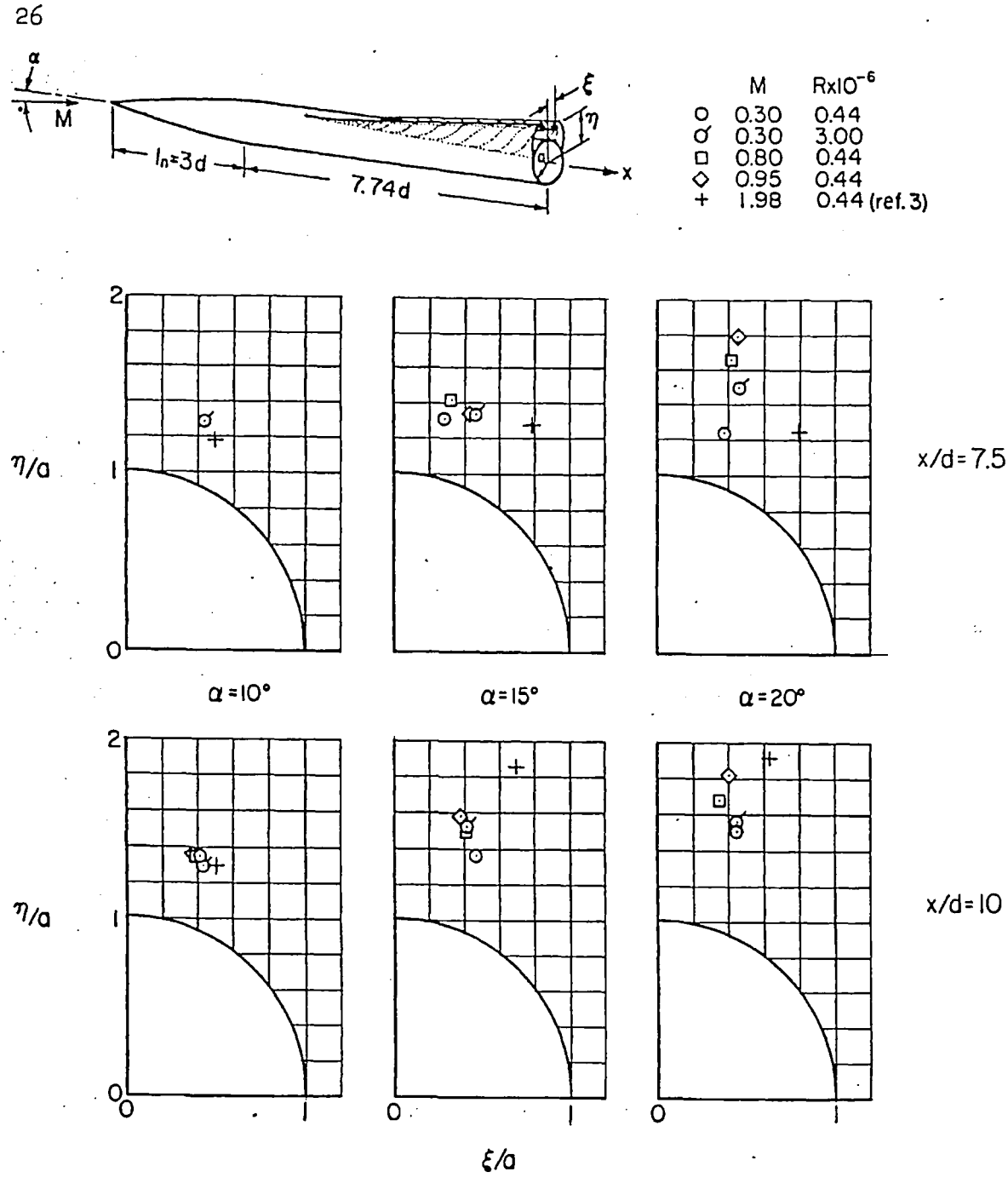

- Vortex core positions (average of right and left vortices) at two axial stations for several angles of attack.

Figure 3.5; missile vortices: Tinling and Allen (1962)

3.2(d) Review: Components of resistance

Todd (1957) describes the usual device of considering hull forces as the sum of attributable components. This was first proposed by Froude, who divided the total resistance into two parts; one associated with wave making (and scaling as a function of Froude number $V/\sqrt{gL}$), the other associated with viscous friction (and scaling as a function of Reynolds number pVL/μ). He assumed that this latter part was equal to the frictional resistance of a smooth plank having the same length and wetted area.

Todd takes the analysis a step further, writing the total force $\underline{C}_T$ as the sum of three components:

$$\underline{C}_T = \underline{C}_F + \underline{C}_V + \underline{C}_W$$

where $\underline{C}_F$ is the resistance of an equivalent plank, $\underline{C}_V$ is the form drag due to shape of hull, and $\underline{C}_W$ is the wave making resistance. Clearly the waveform does have some effect on the frictional resistance and the skin friction does have some effect on the waveform; however, C_F is assumed to be a function of Reynolds number, and C_W a function of Froude number. The form drag, C_V, can not be scaled so simply: it is made up of components associated with additional skin friction caused by curvature effects, separation of the flow and eddy-making. These components cannot be separated in any clear cut way, particularly since the position of separation lines may well change in a complicated manner with Reynolds number. Despite all its shortcomings, the above assumptions, known as the "Froude assumptions", form the basis of most methods of predicting full size ship resistance from model tests.

These experiments concern ships sailing at leeway.

The total force on such a ship can be written:

$$\underline{C}_T = \underline{C}_F + \underline{C}_V + \underline{C}_W + \underline{C}_\lambda$$

where $\underline{C}_\lambda$ is the additional force associated with leeway. This component will show some dependency on both Reynolds number and Froude number. If the flow separation position changes with Reynolds number this component can be expected to show a Reynolds number scale effect: this is likely to be small over a range of Reynolds number if, either the flow separation patterns can be shown to be virtually unchanged over this range, or the flow separation positions can be contrived to remain unchanged over this range. This component can also be expected to show a Froude number dependency, as there will be asymmetric pressure forces associated with the asymmetric surface wave pattern. The wind tunnel experiments described subsequently only measure the non-wave-making part of the forces associated with leeway. The relative importance of wave making forces and the Froude number dependency are therefore of particular interest.

Sharma and Bellows (1976) conducted oblique towing tests of a series 60 model to study the wave-making of a ship at leeway. They concluded, "Analysis of directly measured horizontal forces on an obliquely towed model verified the common assumption that these vary nearly with speed squared over the range of moderate Froude numbers. Analysis of measured wave cuts revealed that while the wave pattern can account for up to 15% of total cross force, it does not seem to contribute at all to the extra drag at non zero drift angles." Wagner (1967a) conducted oblique towing tests and reported, "die Froude-Zahlabhängigheit ist jedoch

nicht sehr gross". (However, the Froude number dependency is not very strong). Gill (1979) conducted oblique towing tests of a container ship model at Froude numbers of 0.114 and 0.164. It is interesting to note that the forces are apparently not affected by Froude number in this range for angles of leeway up to 15°. Treshchevsky and Korotkin (1976) quote work by Goffman indicating that the effect of wave making on hydrodynamic flow characteristics is insignificant at Froude numbers below 0.2 (about 15 kts for a 160m ship).

Treshchevsky and Korotkin (1976) used reflex models to investigate the characteristics of flow around ships at leeway in shallow water. They find that at large angles of leeway the flow separation positions become significantly dependent on Reynolds number, particularly in the "critical" range of Reynolds number. The mechanism for this dependence is discussed in section 5.2(e): the position of boundary layer separation depends on the boundary layer characteristics which vary with Reynolds number. They reduced the dependence of flow separation on Reynolds number by artificially tripping the flow; this was achieved by giving the models rough surfaces. They estimate that the additional frictional resistance is no more than 3% of the total resistance at a Reynolds number of 10^5. (Note that full-scale hull Reynolds numbers are of the order of 10^9). They find that coefficients obtained using a model with tripped flow "correlate fairly well" with the results of a full-scale ship experiment. Flow tripping tests conducted as part of this investigation are reported in appendix A3.2.

3.2(e) Review: modelling the sea surface

It is possible to study the underwater flow about a hull using a wind tunnel with an appropriate representation of the free surface. A flat sea surface can be considered as a plane of symmetry with the real flow below and an image flow above; this concept is similar to that used in potential flow theory to represent an infinite solid boundary. It is exploited by testing a reflex model (consisting of the underwater hull together with its image in the waterplane) near the middle of the wind tunnel. This method only provides a realistic model if the mirror plane is indeed a stream surface: for very bluff bodies, this would be unlikely (due to possible periodic or random vortex shedding in the wake); and even for slender reflex model hulls, it is important that this is confirmed (as reported in appendix A3.3). There are inevitably slight violations of this condition due to the upstream influence of the periodic fluctuations of the wake.

The problem of experimentally modelling an assumed flat sea surface is similar, but not identical, to that of modelling the road near to a car. The latter has been discussed extensively, for example, by Davis (1982); he lists 7 ways of modelling the solid ground plane near to a car. The boundary condition at the sea surface (an interface between two fluids) is not the same as that at the road (an interface between a fluid and a solid). The reflex model method adopted (and described above) is the method Davis refers to as the "image method". This method avoids problems associated with the boundary layer on the

tunnel wall when this is used to simulate the sea surface, but neglects real wave phenomena at the real sea surface.

Okada and Tsuda (1966) report wind tunnel tests of a reflex super-tanker model which were made to determine the viscous component of its resistance. Joubert and Matheson (1970 and 1973) and Joubert and Hoffman (1979) conducted similar wind tunnel tests with reflex models in comparisons of three different hull forms. Aertssen, Gadd and Colin (1980) report wind tunnel tests with four reflex models and one single model. In the single model test the tunnel wall was used to model the sea surface. Colin comments on the adverse effects of the wall boundary layer in this test.

Treshchevsky and Korotkin (1976) used a wind tunnel to investigate the forces on a ship at an angle of drift in a shallow channel. A triple array of reflex model hulls was used: the hull plane of symmetry modelled the water surface; the plane bisecting the flow between hulls modelled the channel bottom.

3.3(a) Method: the models

Tests were carried out with a reflex model of a Mariner type hull and a series of hull-like blocks with varying proportions. The reflex Mariner hull was carved in jelutong by the Aerodynamic Department's carpenter, Mr. Beazley. It was decided to use block models for the systematic series of tests as carving a hull is a time consuming affair and the cost of carving a large series of hulls was considered prohibitive. These block models have a rectangular cross section. Tagori (1966) used block models, as well as realistic hull shapes, in flow visualisation investigations of the vortices shed at the bilge of a ship at zero leeway.

Figure 3.6 is taken from Tagori's results. These were taken from photographs of a wool tuft grid, attached to the block model in a recirculating water channel. Joubert and Matheson (1973) also report the existence of these longitudinal vortices. Figure 3.7 indicates the positions of these vortices.

Longitudinal vortices were expected to be an important feature of flow about hulls at leeway. Although the flow about a block hull is different from the flow about a realistic hull, the flows have important similarities, including some major flow features such as these longitudinal vortices; on the other hand, in some circumstances the flows may be significantly different if a sharp bilge induces separation where there is no corresponding separation from the rounded bilge. It was thought that an investigation of the influence of proportion on the flow about block hulls gives insight into mechanisms which are also important when

considering the effect of proportion on the flow about realistic hulls. Additional advantages of block models are: sharp edges tend to trip turbulent flow, this reduces possible problems with laminar flow; sharp bilges define separation lines and reduce the uncertainties and Reynolds number effects associated with smooth surface separation; and the mathematical modelling of the flow about a rectangular hull is a more tractable problem than for a realistic hull, and has been attempted (Chapter 4).

The model hulls are listed and described in table 3.1. Figure 3.8 indicates their plan forms. The area ratio of model cross section to tunnel cross section is about 1/270 for the parent model.

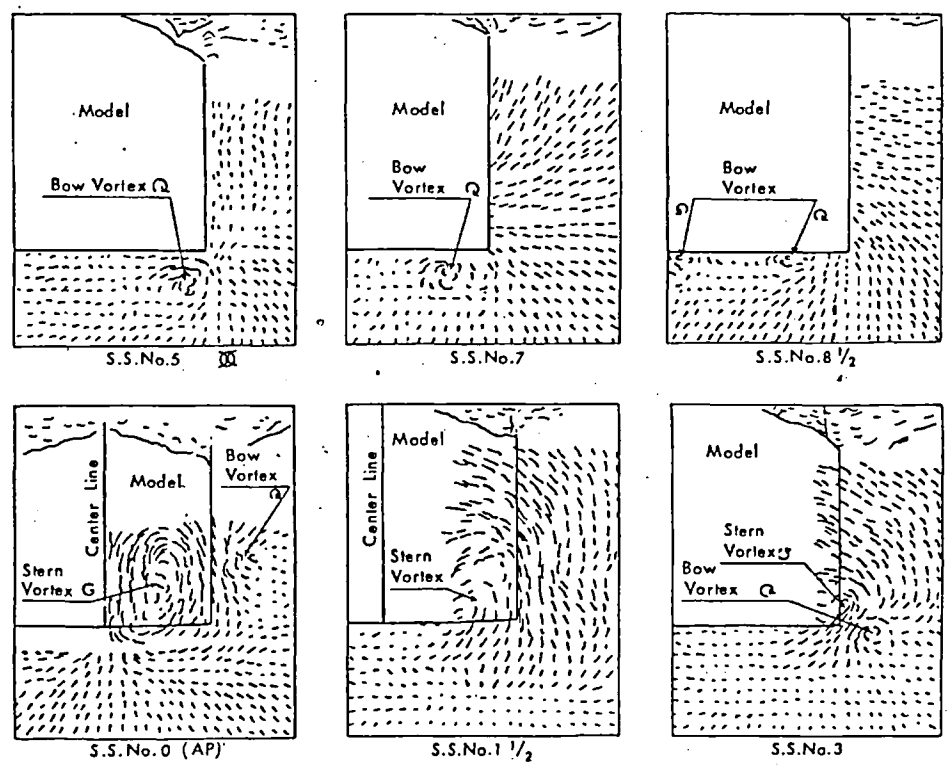

Results of flow observation with two-dimensional model WM-4 by means of tuft grid, F_n=0.25

Figure 3.6

Stern view of hull vortices: Tagori (1966)

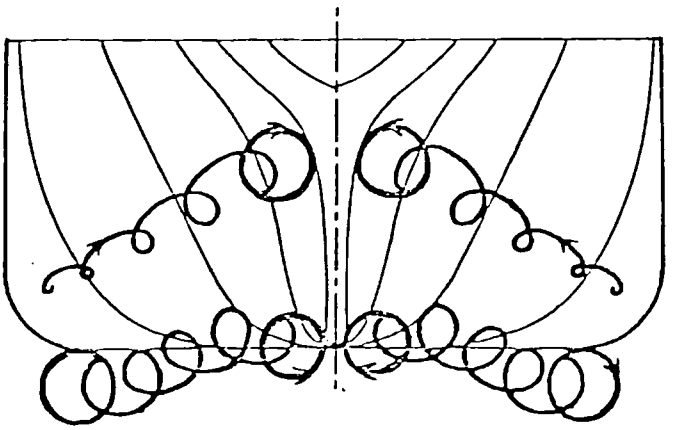

Figure 3.7

Stern view of hull vortices: Joubert and Matheson (1973)

TABLE 3.1 MODEL HULL CHARACTERISTICS.

MODEL	DESCRIPTION	LENGTH (MM)	BEAM (MM)	MID-DRAFT (MM)	TRIM	HEEL (O)
A1	PARENT MODEL	640	96	32	0	0
	ALL A,B,C&D MODEL.S ARE BASED ON THIS PARENT MODEL. THE PLANFORM IS THAT OF A MARINER HULLS MID-DEPTH PLAN.					
A2	SHALLOW DRAFT	"	"	24	"	"
A3	DEEP DRAFT	"	"	48	"	"
A4	TRIMMED 1/20 BY BOW	"	"	32	-1/20	"
A5	TRIMMED 1/20 BY STERN	"	"	"	+1/20	"
A6	HEELED 15 DEG	"	"	"	0	15
A7	HEELED 30 DEG	"	"	"	"	30
A8	ROUNDED BILGE	"	"	"	"	0
	BILGES ROUNDED WITH A RADIUS OF 16MM.					
B9	ROUNDED BOW	"	"	"	"	"
	A ROUNDED BOW PLANFORM (RADIUS 16MM) REPLACES THE NORMAL FINE BOW.					
C10	NARROW BEAM	"	64	"	"	"
D11	WIDE BEAM	"	128	"	"	"
A12	TRIMMED 1/40 BY STERN	"	96	"	+1/40	"
E12	BLOCK MARINER	632	92	61	+1/57	"
	THIS PLANFORM IS THE WATERPLANE PLAN OF THE MARINER HULL.					
F13	MARINER TYPE HULL	"	"	"	"	"
	THIS IS A MODEL OF THE UNDERWATER PART OF A MARINER HULL. IT IS NOT FITTED WITH A RUDDER OR A PROPELLER AND THE LINES ARE SLIGHTLY MODIFIED IN THE VICINITY OF THE RUDDER STOCK AND PROPELLER BOSS.					

/

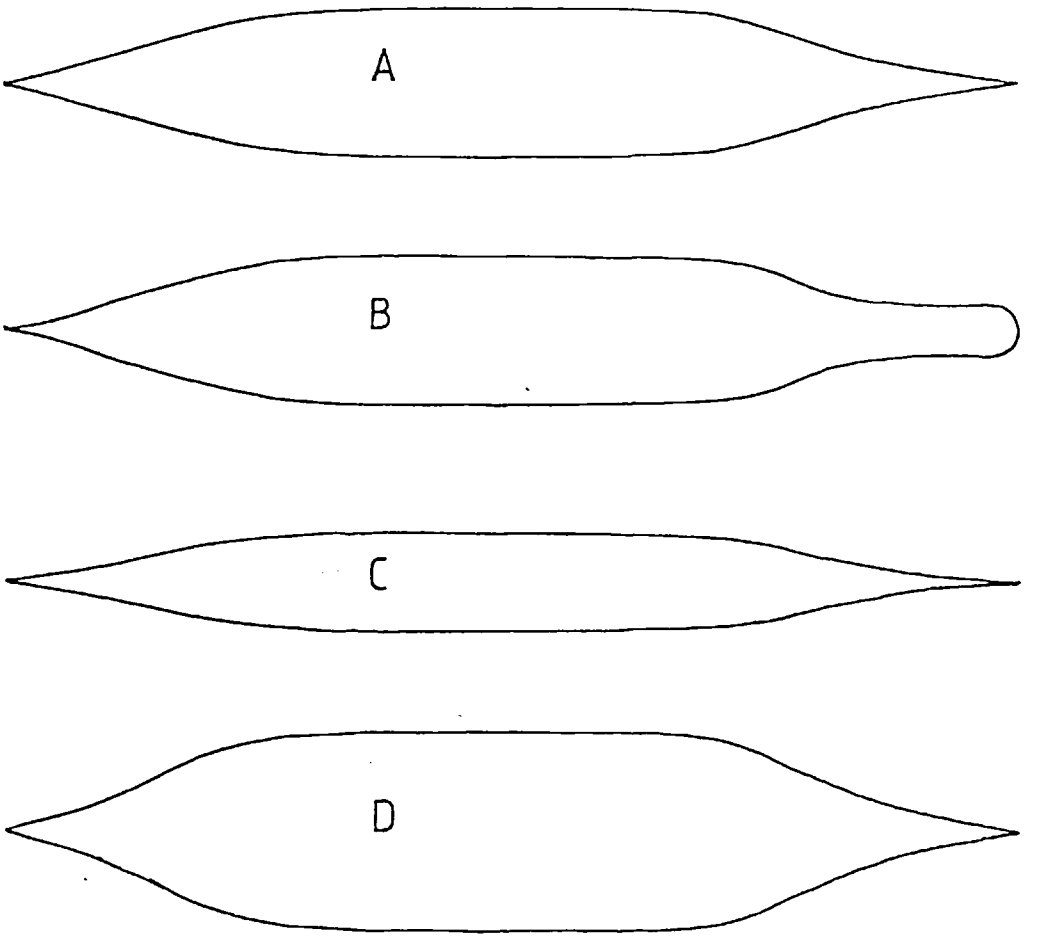

Figure 3.8

Model hull planforms.

3.3(b) Method: the wind tunnel

The tests were conducted in the Donald Campbell Low Speed Wind Tunnel in the Imperial College Aeronautics Department. This is a closed return circuit tunnel. The working section is 4.5ft wide, 4ft high and 10ft long. Breather slots at the downstream end of the working section help to maintain static pressure close to atmospheric pressure within the test section. The flow ahead of the contraction is smoothed by passing through a small cell honeycomb and a screen which reduce the turbulence level to 0.2% in the working section. Calibration and details are given by Bearman, Harvey and Gardner (1976).

Tunnel speed measurement. To infer with minimum error the wind speed, the difference in static pressure upstream and downstream of the contraction is measured using a Betz manometer with a resolution of 0.1mm H_2O. The relationship between pressure difference and speed, for the empty tunnel, is known from previous calibrations. This method of determining wind speed is described by Pope and Harper (1966). Most hull experiments were run at a speed of about 23 m/s, giving a Reynolds number ($\rho VL/\mu$) of about 10^6.

Force measurements. The wind tunnel is equipped with a three component balance mounted above the working section which can measure lift, drag and pitching moment. The balance is of moving weight weighbeam type. The mechanism is shown in figure 3.9. The resolution of the balance is 0.01 lbf lift, 0.001 lbf drag and 0.001 ftlbf pitching moment. The weighbeam controls are interfaced to a computer. A computer routine developed by Davis is

used to balance the weighbeam automatically. During the experiment force coefficients were calculated and plotted immediately so that errors and interesting features were identified during the test. The forces are non-dimensionalised by $\left(\frac{1}{2}\rho_A V^2\right)\times\left(\frac{\rho_A}{\rho_H} L^2\right)$. The reference area of density ratio times length squared is unusual but convenient as it simplifies the mathematics of performance calculations: this reference area is used by Hafner (1980).

Incidence control. The model's incidence is adjusted by a servo-motor, with digital read-out, controlled manually at the tunnel console. The minimum resolution is 0.01°.

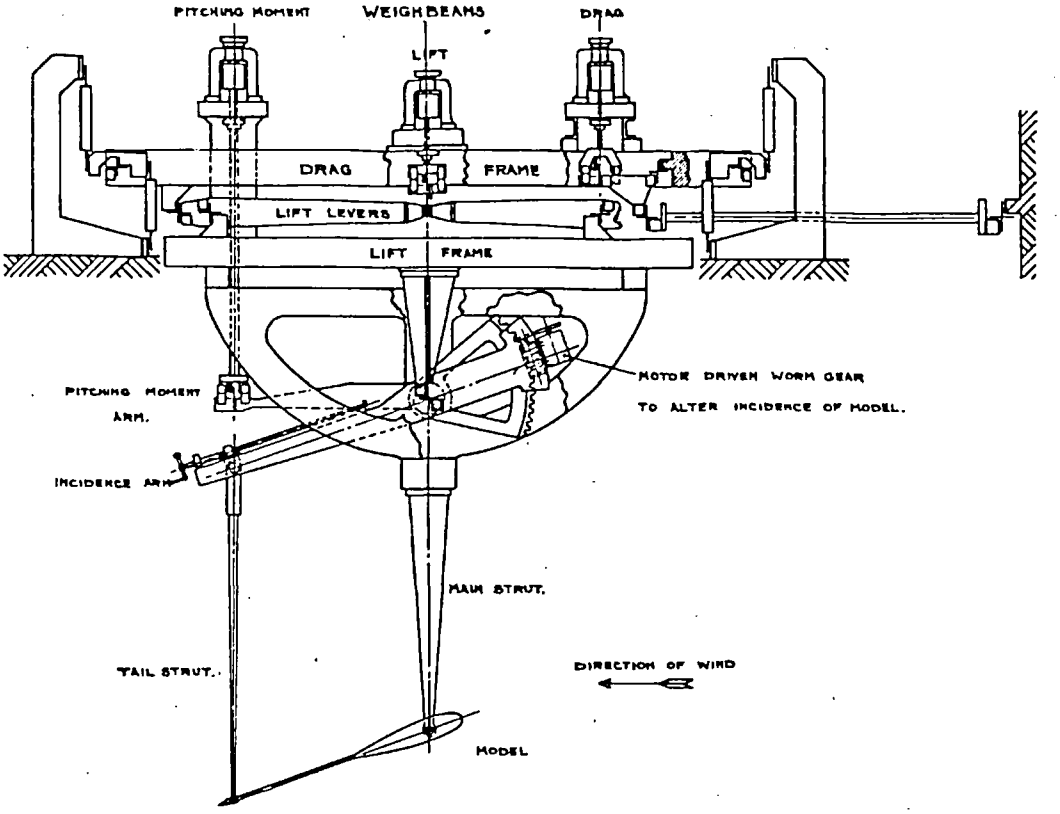

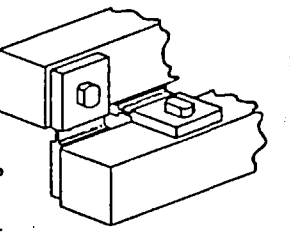

ARRANGEMENT OF CROSSED
FLEXURE PIVOTS.
SHOWN IN DIAGRAM THUS +

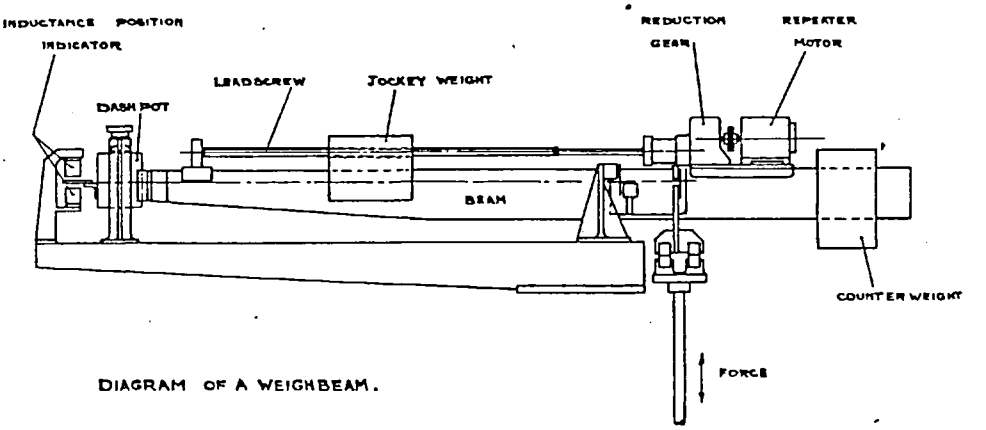

DIAGRAM OF A WEIGHBEAM.

Figure 3.9

Balance mechanism

3.3(c) Method: the self aligning probe

Wake surveys were accomplished using an ingenious self-aligning probe and traverse package developed by Davis (1982). Comparison of conventional directional probe systems and Davis's system makes the advantages of the latter apparent. The local flow direction can be determined using a directional probe which remains aligned with the distant free stream direction; one disadvantage is that a probe not aligned with the local free stream direction is likely to distort the local flow field; a second disadvantage is that the flow direction must be calculated from calibration information (relating angles of incidence to pressure differences) rather than measured directly. Both these disadvantages can be overcome by using a probe which is aligned with the local flow direction; the flow is far less distorted, and the calibration information is only used during the iterative alignment of the probe, but not in the final measurement of direction. Probe alignment is usually achieved by yaw-pitch heads which are mounted on a carriage so designed that the head can be rotated in two planes with the centres of rotation at the probe's tip: such devices tend to be bulky and to cause considerable distortion to the flow. Davis's package controls a probe and traverse together, so that the probe is iteratively adjusted until it is aligned with the time averaged local free stream, while simultaneously, the traverse carriage position is adjusted so that the probe's tip is returned to the desired position after each change in probe angles; a computer performs the necessary calculations and controls the probe and traverse:

this system allows the use of a much more slender probe and carriage, which causes less distortion to the flow (see figure 3.11).

The survey marches through a grid of positions, in a plane perpendicular to the flow, and records probe angles and positions at each. (The position of the plane is indicated in figure 3.12). This information is used to produce various flow visualisation plots: general features of the flow are indicated by plotting vectors representing cross flow velocity components at grid points; more details of the cross flow can be shown by plotting vorticity contours or total head contours (the vector and vorticity contour flow visualisations are used in this investigation). The wake survey data can also be used to determine the vortex strengths (or "circulations") by either a contour integration of velocity or an areal integration of vorticity: the latter method is used here. The data also allows estimates of the forces on the body to be calculated from the wake characteristics; Davis made such estimates for a car-like body; no attempt has been made to perform such calculations as part of this investigation. The interpretation of wake survey data is discussed in appendix A3.1(b).

Figure 3.11 shows the probe mounted on the traverse behind a reflex model Mariner hull. Figure 3.10 indicates the alignment and pressure tappings.

The probe is aligned by means of two perpendicular pairs of pressure tappings on the probe's conical end. The pressures detected by a diametric pair are compared. The difference in pressure is related to the local angle of

flow incidence. In fact, the relationship between local angle of incidence and pressure difference is linear for angles of up to about 15°. The pressure difference is used to calculate angle changes required to more nearly align the probe with the local flow.

The computer calculates the desired change in angle and also the changes in probe position which are associated with these changes in angles. It then simultaneously drives five stepper motors controlling the angles of yaw and pitch and x, y and z positions of the traverse so that the probe alignment is improved and its tip remains in the correct position. This procedure is repeated until the probe is aligned to within specified limits.

In addition to the 4 alignment tappings the probe is provided with a tapping on its forward end which measures total pressure and 4 tappings around its side, which can be calibrated to give the static pressure. All pressures are taken as the average of 100 samples taken in about 5 seconds.

Angular errors: as described above, the computer aligns the probe so that the pressure difference between opposite alignment tappings is within preset limits. Davis identifies and estimates two main sources of error; these are the minimum resolution associated with these preset limits, and an error associated with the pressure-gradient perpendicular to the probe. The resolution and pressure-gradient error are given by the following equations (although Davis notes that there is some evidence that the pressure gradient error is underestimated);

minimum resolution = $C_1 C_3 \max\left(\frac{\Delta p}{\beta}\right)$

maximum p-g error = $C_1 C_2 C_3 \max\left(\frac{\partial p}{\partial z}\right)$ where;

C_1 (= 0.55) is a constant dependent on the probe geometry,

C_2 (= 1.7mm) is the distance between alignment tapping centres, C_3 (= 20.4 $^{o}/C_p$) is the probe alignment calibration, max $(\Delta_p/\square)$ is the preset limit on C_p difference across a pair of alignment tappings, and max $(\partial P/\partial z)$ is the maximum pressure-gradient perpendicular to the probe.

For the wake surveys conducted, typical values of the minimum resolution and maximum pressure-gradient error are, for example; 0.11° and 0.58° for the Mariner water plane block, and 0.22° and 0.92° for the Mariner type hull.

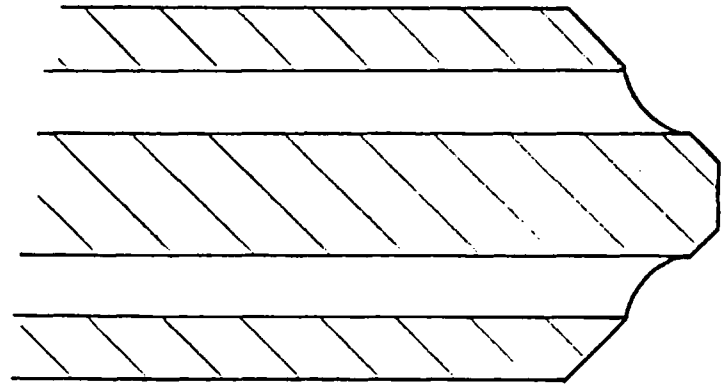

Probe - alignment tappings

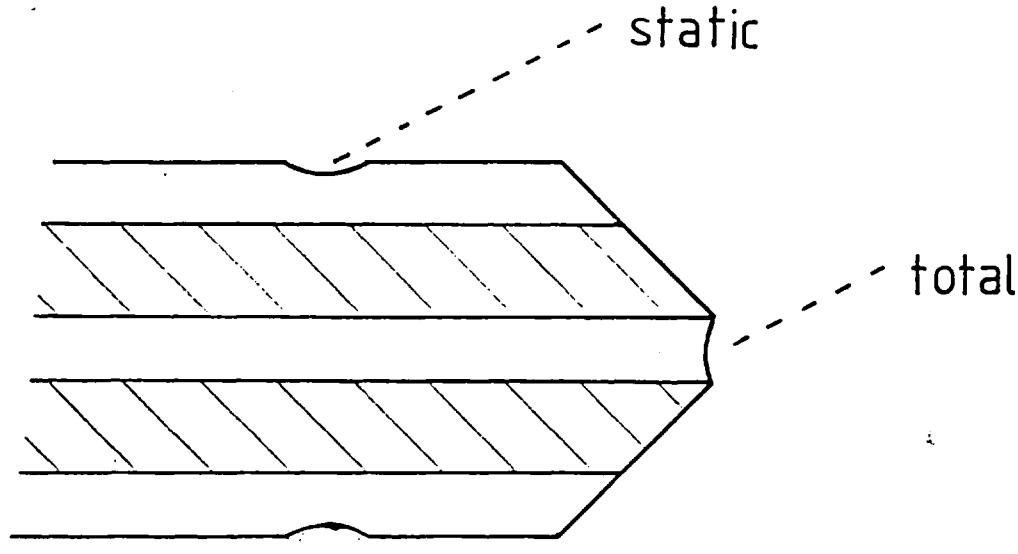

Probe - pressure tappings

Figure 3.10

Schematic cross sections through probe tip

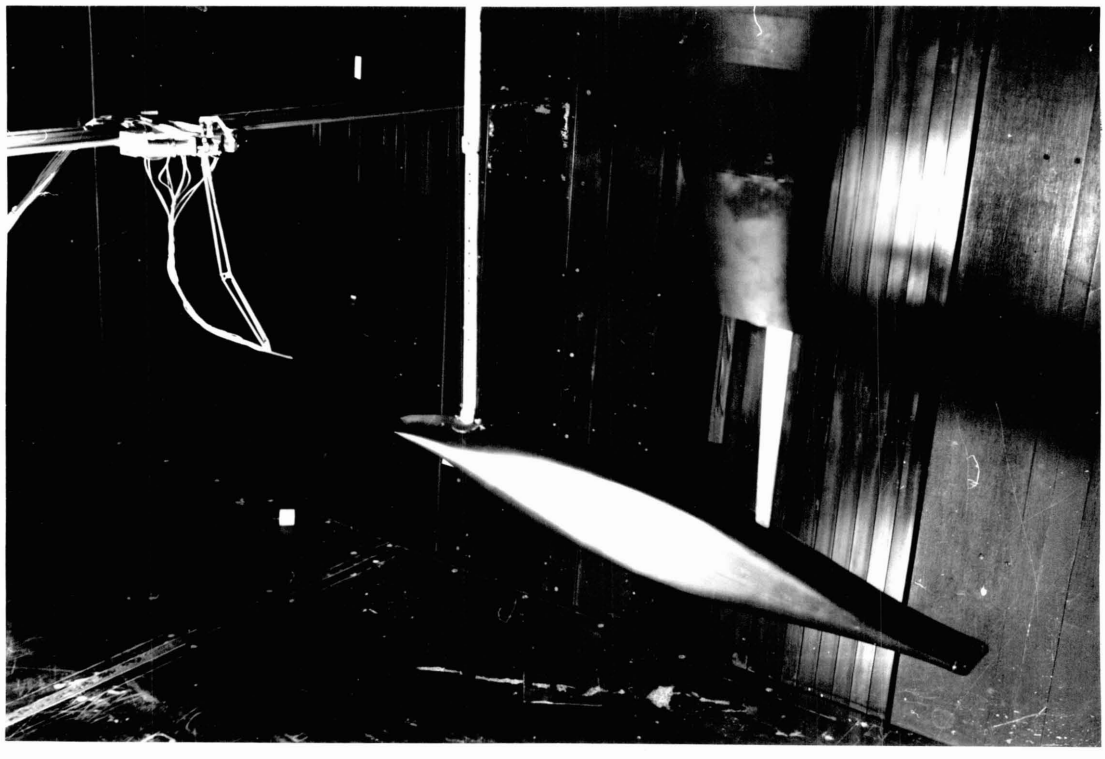

Figure 3.11

Probe and traverse behind reflex model Mariner hull.

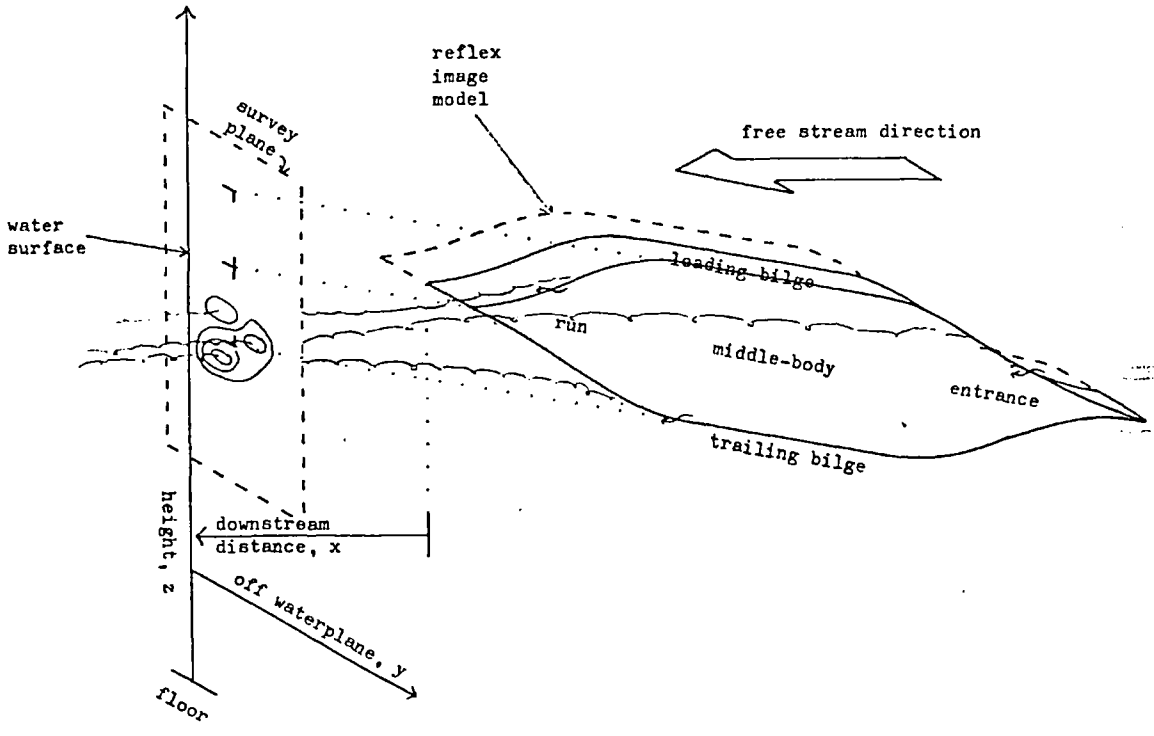

Figure 3.12

Indication of flow axes, orientation of wake survey plane,

and terms used in describing vortex positions.

3.3(d) Method: flow visualisation techniques

The oil flow experimental technique is well described by Maltby and Keating (1962). In this experiment matt black models were used. They were painted with a suspension of french chalk powder in white spirit and oleic acid. The wind tunnel was then run which dried the french chalk in a pattern which indicated features of the surface flow. These patterns were photographed on black and white film.

The patterns are often complicated and require care in interpretation. Squire (1962) develops the mathematics of the technique. He shows that the oil streamlines closely follow the surface streamlines, which would exist in the absence of the oil. Maskell (1955) considers separation in terms of "limiting streamlines" on the body surface. He shows that separation occurs at a point only when two distinct limiting streamlines converge and meet at that point, then combine and depart from the surface as a single "separation streamline". A converse description defines attachment. Lighthill (1963) and Hunt, Abell, Peterka and Woo (1978) develop the topological concepts of nodal and saddle points of separation and attachment. A separation line can then be defined as a skin friction line which issues from both sides of a saddle point of separation and disappears into a nodal point of separation. A converse description defines an attachment line. Two example interpretations of oil-flow patterns are discussed in appendix A3.1(a).

A tuft probe was used to indicate local flow direction, large scale turbulence, areas of recirculating flow, and vortex positions. This tuft probe consisted of

a piece of fine wool at the end of a long rigid wire.

A stethoscope was used to listen to the flow in an attempt to identify regions of turbulent flow. This is particularly useful when investigating the boundary layer. The working end of the stethoscope consists of fine pressure tubing supported at the end of a long rigid wire.

3.4(a) Results: the flow past a Mariner hull

The approximate positions of flow features observed by the wool tuft and stethoscope are represented in figure 3.13. The surface oil flow pattern is shown in figures 3.14 to 3.17. The results of the wake survey are plotted in figure 3.18. These features are described below at four angles of incidence (the meanings of terms used to describe vortex positions are indicated in figure 3.12). Note that the model was fitted with a trip wire about 1cm from the bow for this test.

0° incidence: A pair of very weak vortices appear to be shed along the hull entrance; this is deduced from the dark separation lines (1), and from the attachment line (indicated by the oil flow pattern) along the keel line. These vortices are not discernible by the wool tuft or by the wake survey. A stronger pair of longitudinal bilge vortices are shed at the run (2) near the separation lines indicated; these are the vortices shown by the wake survey. The flow is turbulent aft of the trip wire.

5° incidence: The wool tuft detects a weak vortex (1) near the leading entrance bilge; this is about 1/5 draft inboard of the dark separation line and about 1/10 draft off the body; it cannot be identified at the wake survey plane, but probably contributes to the large area of negative vorticity. Most of this vorticity is traced to the vortex shed at the trailing run bilge (2); this vortex is detected just outboard of the dark separation line indicated. A weak positive vortex is indicated by the wake survey which is shed at the leading run bilge and then swept round by the dominant trailing run bilge vortex. The flow is

turbulent aft of the trip wire.

10° incidence. A well defined vortex (1) is detected near the separation line at the forward part of the leading entrance bilge. At the start of the middle body (2) this becomes less strong and a number of weak poorly defined vortices are shed across the body. At the wake survey plane, these can be detected as a thin region of diffuse vorticity extending from the trailing side of the wake near the waterplane (that is, the modelled sea surface). Another vortex (3) is observed near the separation line along the trailing middle body and run bilges. At the start of the run it is about 4/5 draft from the modelled waterplane and about 1/5 draft off the body. This is the dominant vortex shown by the wake survey. A very weak vortex is shed from the leading run bilge which is swept round by the dominant trailing run bilge vortex. The flow is turbulent aft of the trip wire. Various other comments on the flow plast a Mariner hull at 10° leeway are made in appendix A3.

15° incidence. A vortex (1) is shed from the leading entrance bilge; at the start of the middle body (2) this becomes less strong and a number of weak, poorly defined vortices are shed across the body; and at the wake survey plane these can be detected as a diffuse negative vortex on the trailing side of the wake near the waterplane. A vortex is shed from the whole length of the trailing bilge; at the entrance (3) it is very weak, but it becomes strong at the run (4); and this is the dominant vortex shown by the wake survey. The flow is turbulent aft of the trip

wire. Separation occurs at the bow and a region of very turbulent recirculating flow extends about 1/20 length along the trailing side.

Force measurements. The graphs in figure 3.19 represent the results of the force measurements made on a Mariner hull model at angles of leeway of up to 15°. The top left hand graph is a conventional plot of lift coefficient against drag coefficient. The graph below it is a plot of the distance of the centre of effort from the bows (L_H) against incidence (or leeway, λ_H). The graph on the right is an alternative representation of lift and drag coefficients. Here they are plotted against incidence (λ_H).

The Mariner hull, which is a fairly streamline body, has its highest lift/drag ratio of nearly 3 at an angle of incidence of about 10°. At 15° the rate of increase of lift with incidence is still positive, but the associated drag penalty is becoming more severe. The apparent centre of effort is near the bows for low angles of incidence but has moved aft to about L_H = 0.4 for an incidence angle of 15°.

Comparison of wind tunnel and towing tank forces. The coefficients, obtained from these wind tunnel tests of the 0.64m Mariner type hull, were compared in figure 3.20 with those Wagner (1967a) obtained from towing tank tests of a 2m similar hull. There are a number of reasons why differences might be expected in these results: the tests are conducted at different Reynolds numbers; the tank tests include free surface wave making effects which are excluded from the wind tunnel tests; and there are intrinsic experimental dissimilarities. These dissimilarities include differences in the flow tripping techniques, the blockage effects and the interference of the wind tunnel model support.

However, probably the most important reason for the lower forces obtained in the wind tunnel is that the hull for this test was not fitted with bilge keels. Wagner (1967a) does not state whether bilge heels were fitted for the tank test but the forces he obtained are close to the upper values reported by Gertler (1969) for Mariner hulls fitted with bilge keels.

F13 MARINER TYPE HULL

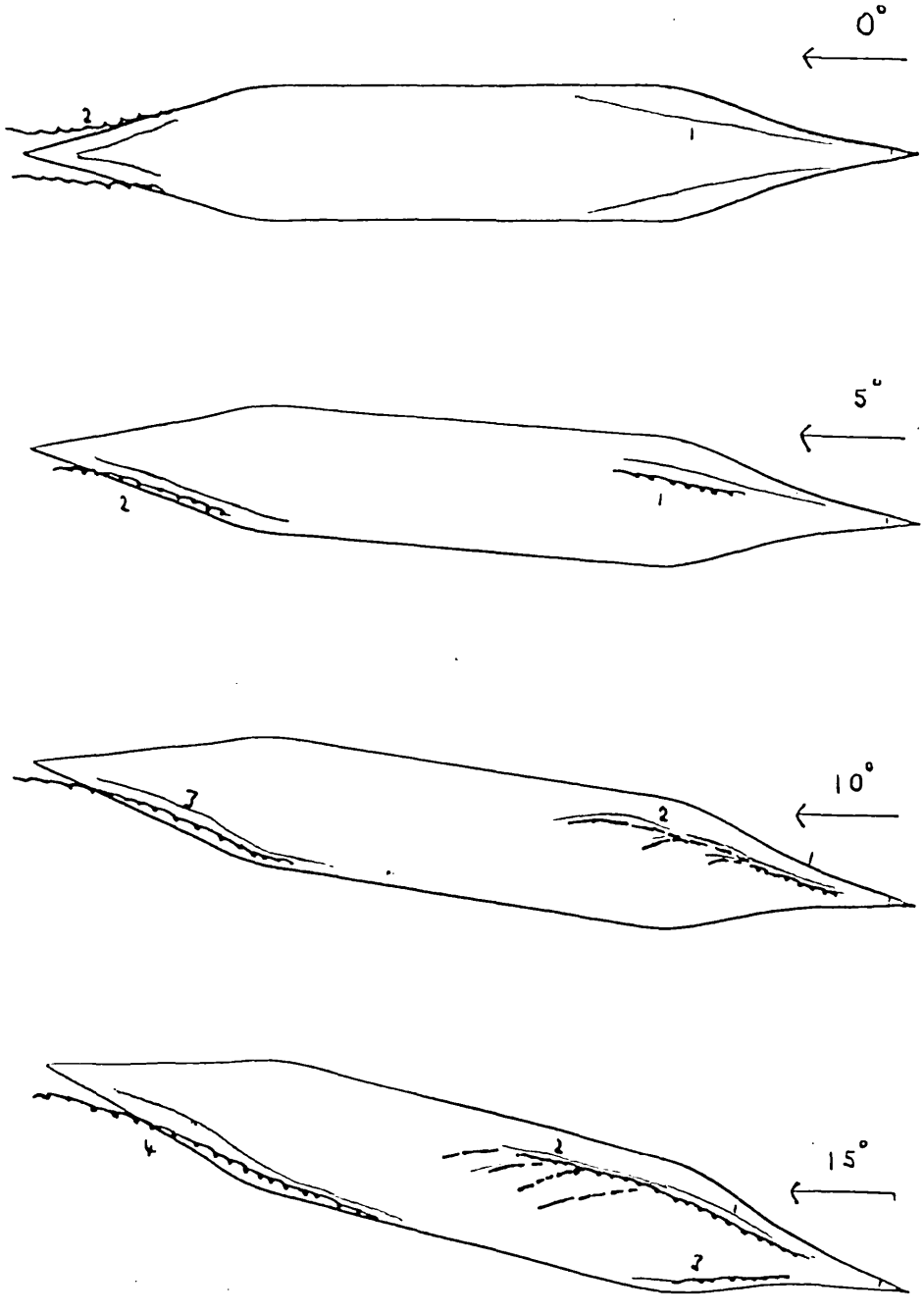

Figure 3.13

Vortices identified by the wool tuft; Mariner type hull

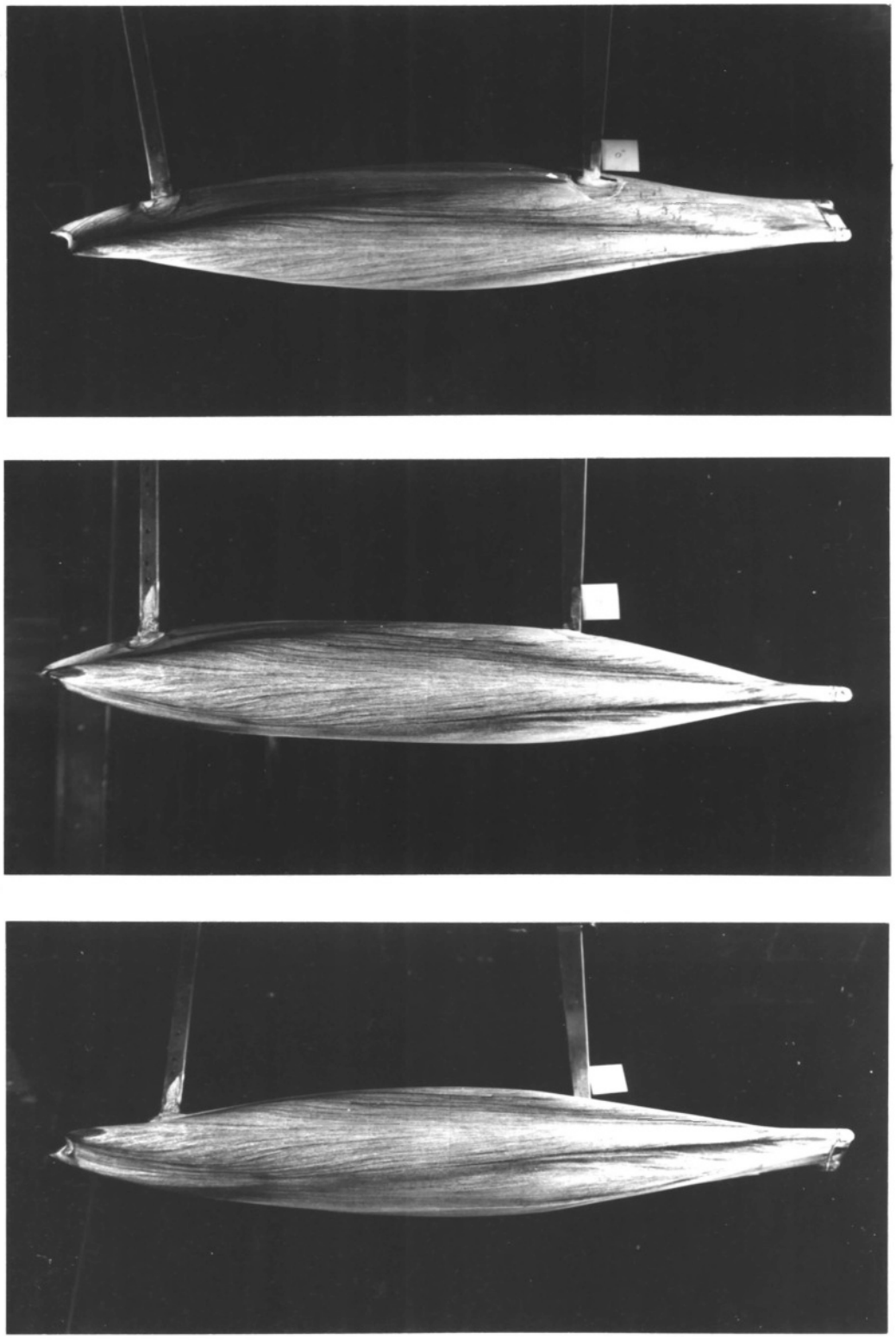

Figure 3.14

Oil flow pattern: Mariner type hull at 0^{c} incidence

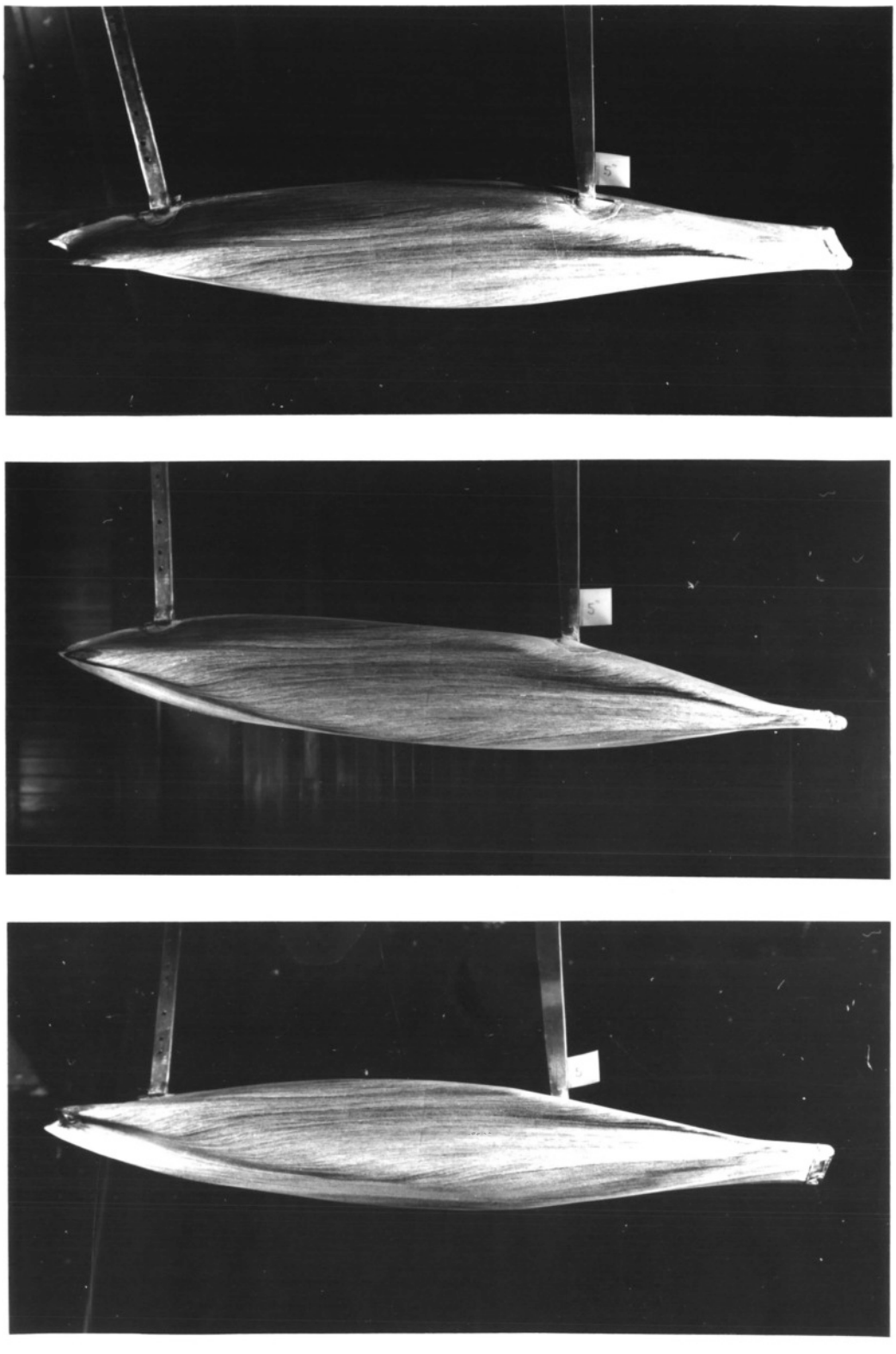

Figure 3.15

Oil flow pattern: Mariner type hull at 5° incidence

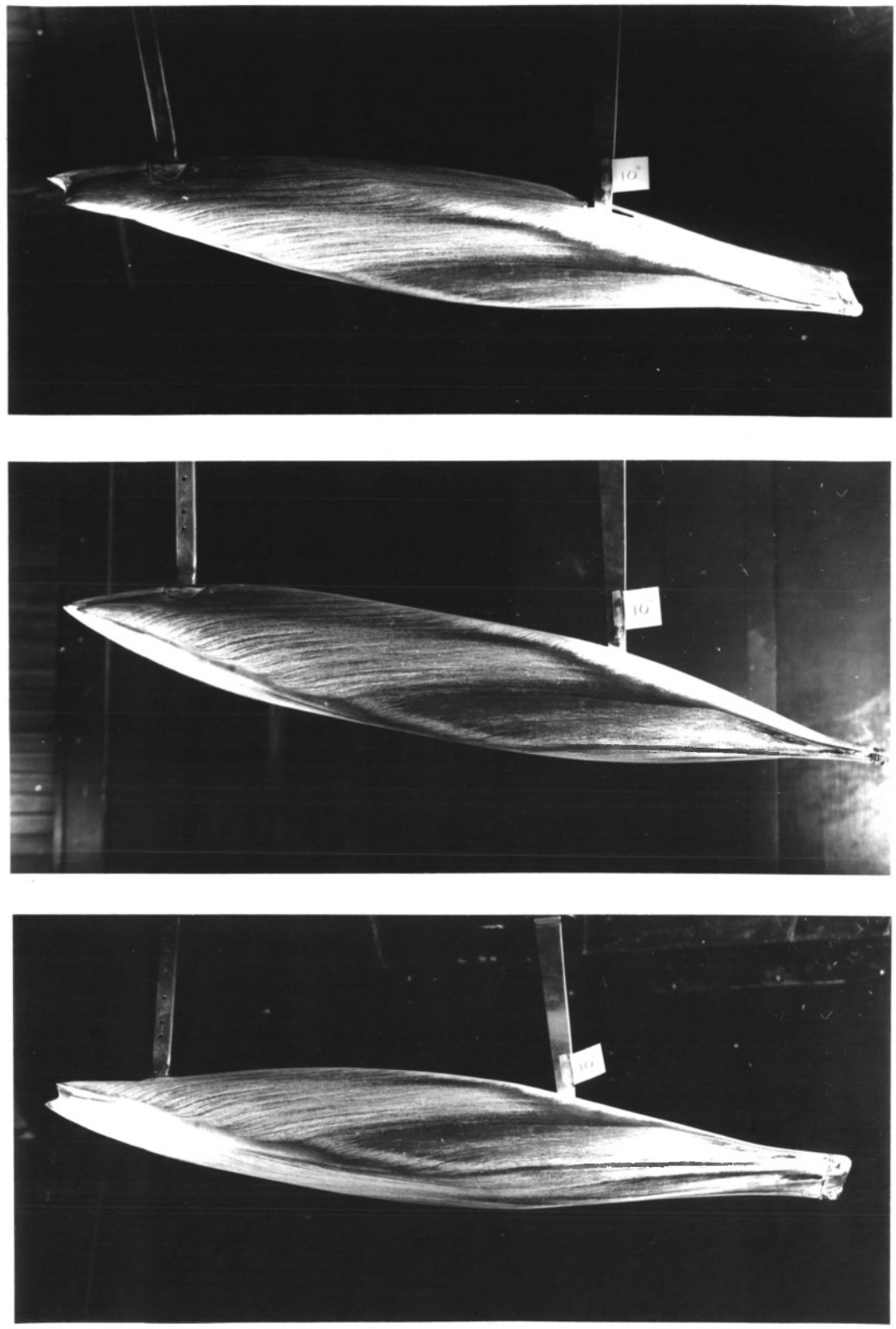

Figure 3.16

Oil flow pattern: Mariner type hull at 10^{c} incidence

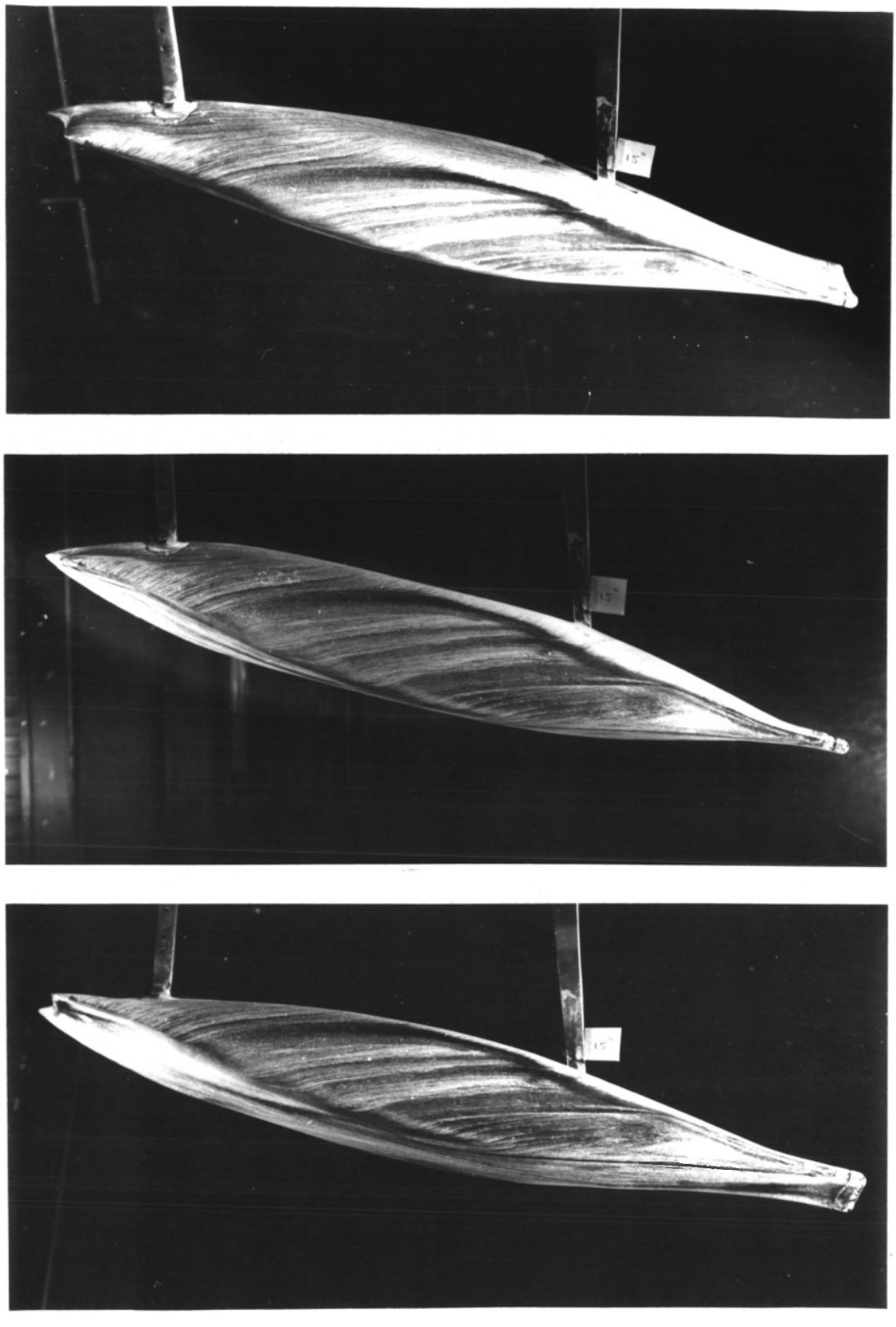

Figure 3.17

Oil flow pattern: Mariner type hull at 15° incidence

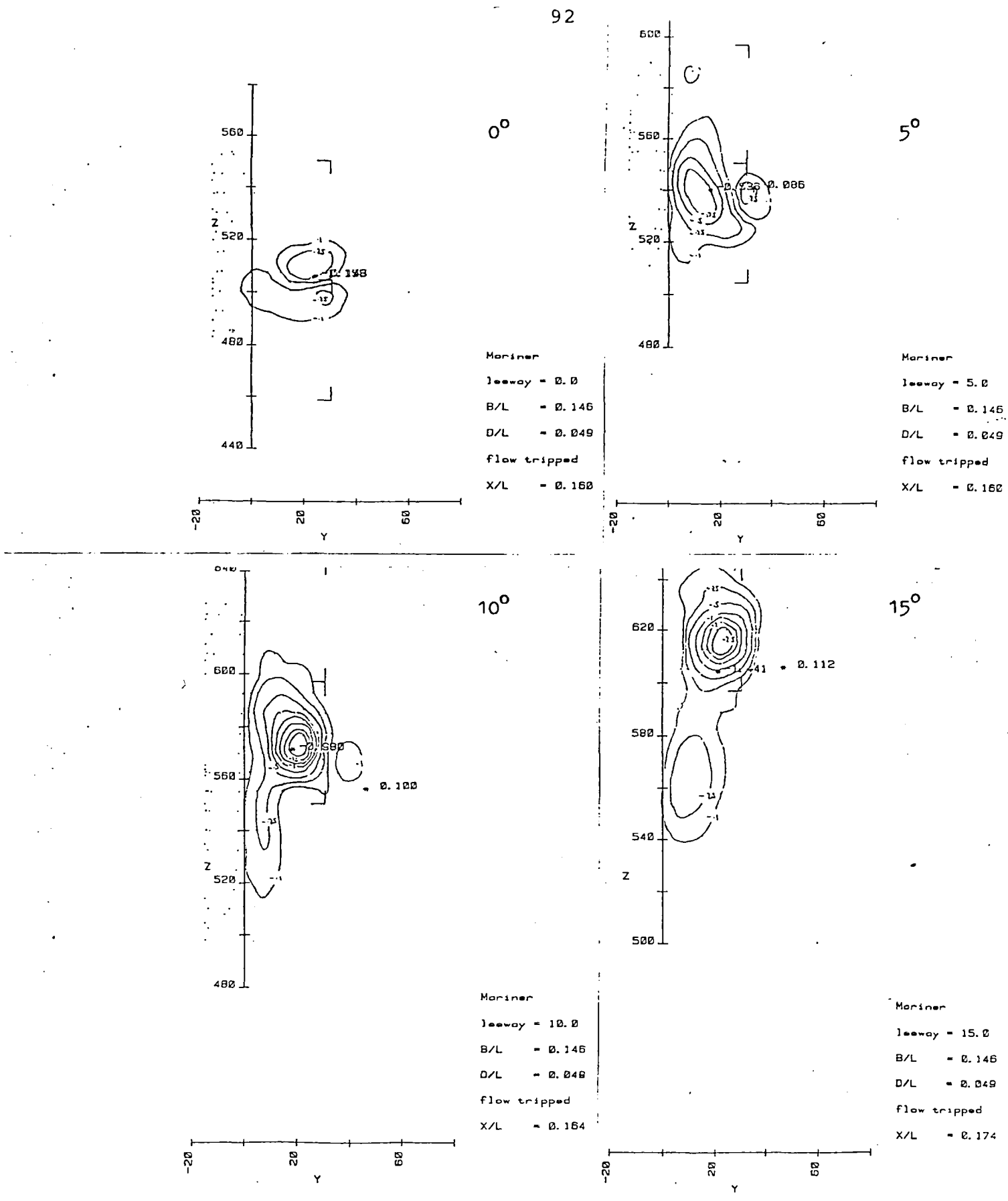

Figure 3.18

Vorticity plots: flow behind a Mariner type hull.

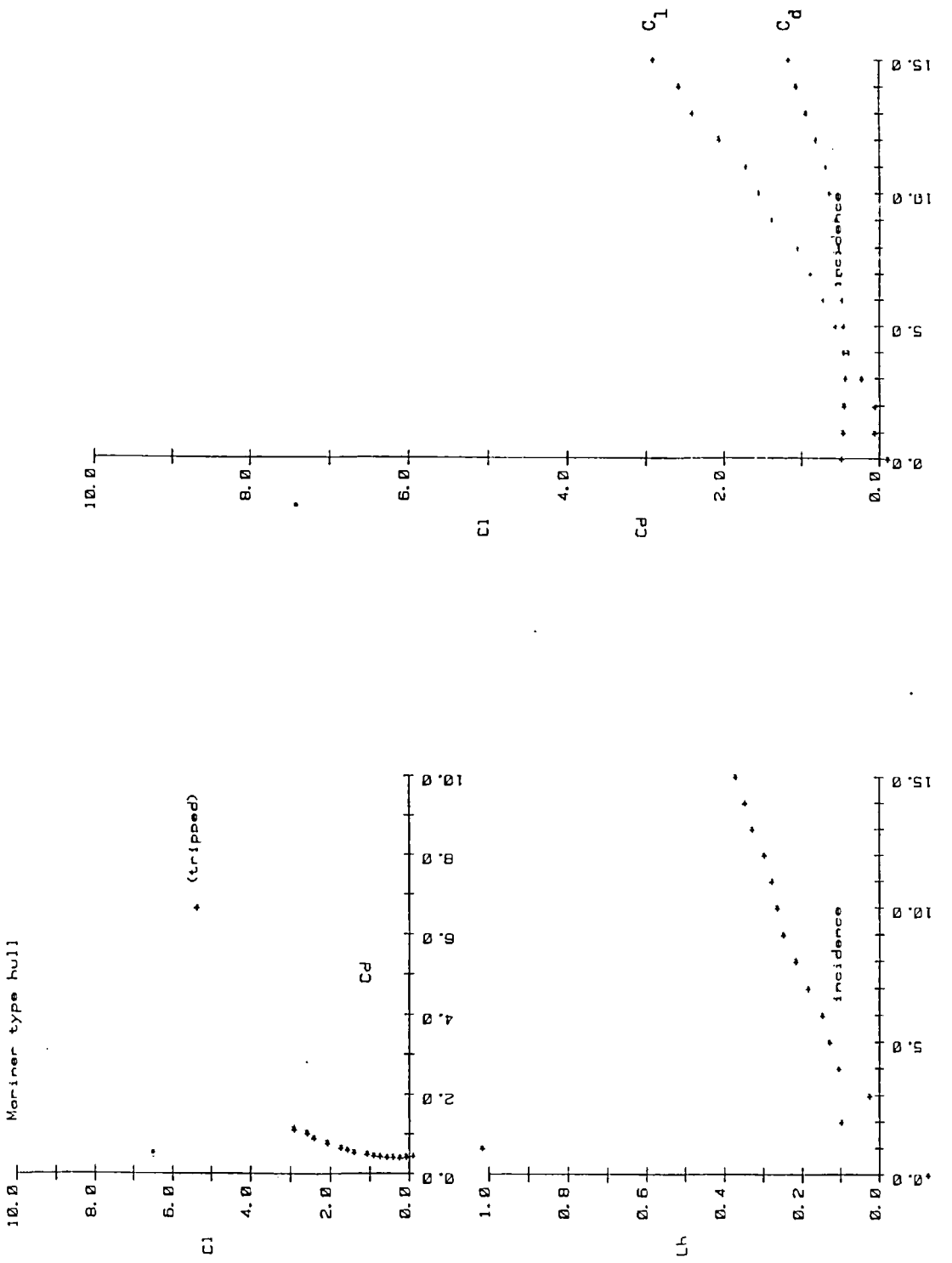

Figure 3.19

Mariner type hull force curves

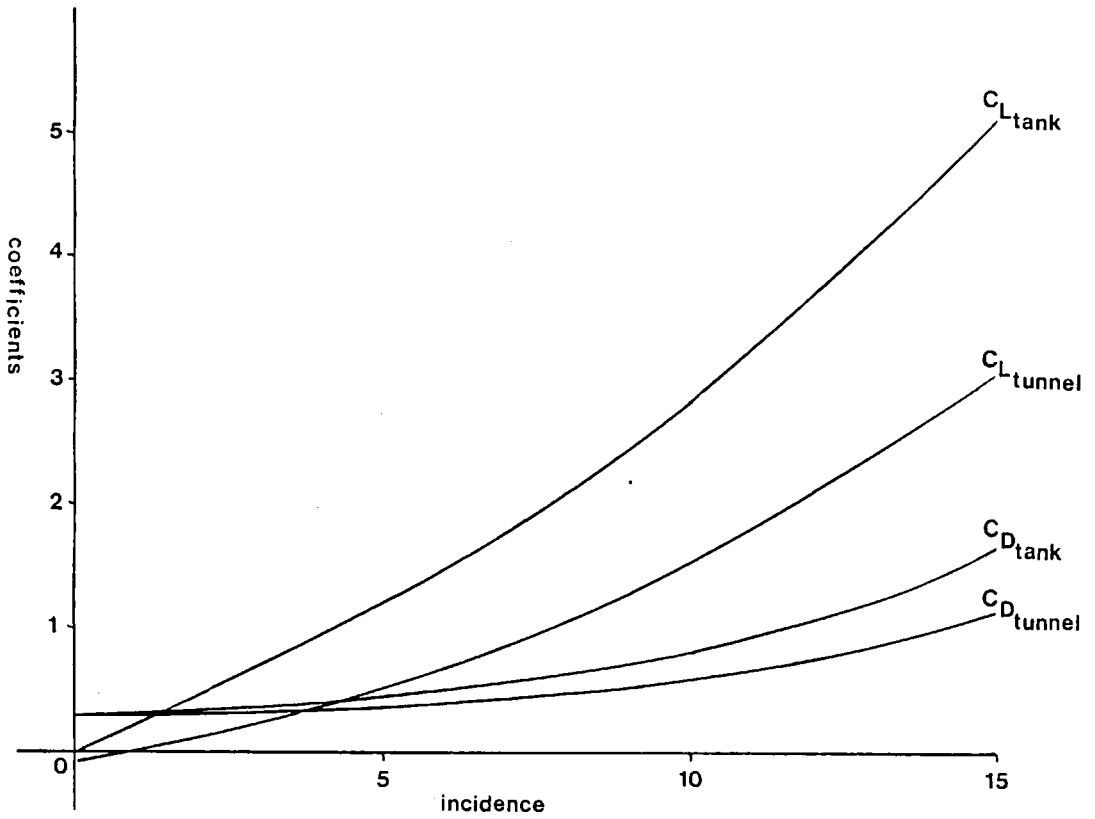

Figure 3.20

Mariner force curves; comparing tank and tunnel results

3.4(b) Results: the flow past a Mariner waterplane block

Flow visualisation observations. The approximate positions of flow features observed by the wool tuft and stethoscope are represented in figure 3.21. The surface oil flow pattern is shown in figures 3.22 to 3.25. The wake survey plots are shown in figure 3.26. The flow features at four angles of incidence are described below.

0° incidence: Intense vortices (1) are shed from the entrance bilges. These lie just inboard of the dark secondary separation line and are about 1/10 draft off the body near the forward end of the middlebody. They are detectable by wool tuft until about 3/4 length from the bow. No secondary vortices could be detected by the wool tuft. Towards the stern these entrance vortices are swept towards the waterplane by the run bilges. They are the outside pair of weak vortices indicated by the wake survey. A strong pair of vortices (2) are shed from the run bilges. These are the dominant pair of vortices indicated by the wake survey. The flow is turbulent everywhere except on the forward parts of the hull sides. The limits of laminar flow are indicated (3 & 4). The support trips the flow slightly earlier than would otherwise be the case. The flow indicated by the wool tuft is approximately parallel to the free stream near the transition region at 4.

5° incidence: A strong vortex (1) is shed from the leading entrance and middle body bilge. Where this can first be detected by wool tuft, it is about 1/10 draft off the dark secondary separation oil flow line. It gradually moves inboard and away from the hull bottom. It

crosses the stern on the leading side of the run and is detected as the weaker negative vortex at the wake survey. The wool tuft does not detect the secondary vortex near vortex (1). Another, strong negative vortex (3) is shed at the trailing run bilge. This is the dominant vortex at the wake survey plane. Weaker positive vortices are detected by wool tuft at the trailing entrance (2) and the leading run (4). Only the latter can be identified at the wake survey. The flow is turbulent everywhere except forward of the support on the leading side (5).

10° incidence: A strong vortex (1) is shed from the leading entrance and middle body. This is about 1/10 draft off the dark secondary separation line where it can first be detected. It gradually moves away from the body and across it, leaving the stern on the trailing side. It is swept round the strong trailing run and middle body bilge vortex and can be detected at the wake survey as the weaker peak of negative vorticity. No secondary vortex was detected by the wool tuft. The trailing run and middle body bilge (3) is initially close to the bilge but moves away from the hull and towards the waterplane. This vortex becomes very strong at the run and is the dominant negative vortex at the wake survey. A weaker vortex (2) of the opposite sense is shed from the leading run bilge. Flow is turbulent everywhere except forward of the support on the leading side. Various other comments on the flow past a hull-like block at 10° leeway are made in appendix A3.

15° incidence: A strong vortex (1) is shed from the leading bilge. This is about 1/5 draft off the body and inboard of the dark separation line where it can first be

detected. It gradually moves away from the surface and across the body as indicated. At the stern it is swept round the dominant trailing bilge vortex. It appears to be manifest at the wake survey as the thin region of diffuse negative vorticity, extending to the trailing side of the wake, near the waterplane. No secondary vortex can be detected by the wool tuft. The dominant vortex (2) is shed from the trailing bilge; it is initially weak and close to the bilge; towards the stern it becomes very strong and moves away from the body and towards the waterplane. At the aft end of the middle body it is about 1/3 draft off the body and 2/3 draft from the waterplane. The flow is turbulent everywhere except forward of the support on the leading side (3).

Force measurements. The rectangular cross section hull develops considerably larger forces than the Mariner hull. At all angles of incidence the lift and drag of the block Mariner are about twice those of the Mariner. The maximum lift/drag ratios of the models are very similar.

There are two reasons why the sharp bilged hull develops greater sideforce. Firstly, there is a pressure difference between the two sides of a hull developing lift; the pressure gradient across the bottom of the hull encourages flow from the high pressure to low pressure side; and this flow tends to reduce the pressure difference. This flow is inhibited by the sharp bilges and their associated local flows, and so the sharp bilged hull can sustain a greater pressure difference between the two sides. Secondly, strong vortices are formed near the sharp bilges, and there are regions of reduced pressure

on the hull surface near these vortices; reduced pressure near the trailing vortex results in a contribution to the lift. This experiment gives no indication of the relative importance of these two mechanisms: the mathematical model described in the next chapter suggests that the first is at least as important as the second.

The strong vortices largely explain the higher drag of the block hull: firstly, they lead to increased vortex drag; and secondly, the reduced surface pressure near the trailing bilge results in a suction force roughly perpendicular to the ship's centre-line which has a drag component. A third contribution to the increased drag is the increased skin friction on this hull's larger surface area.

The block Mariner's centre of effort remains at about $L_h = 0.4$ for all angles of incidence: the Mariner's centre of effort moves much further forward at low angles of incidence. This indicates important differences in the flows at low angles of incidence.

EIR BLOCK MARINER

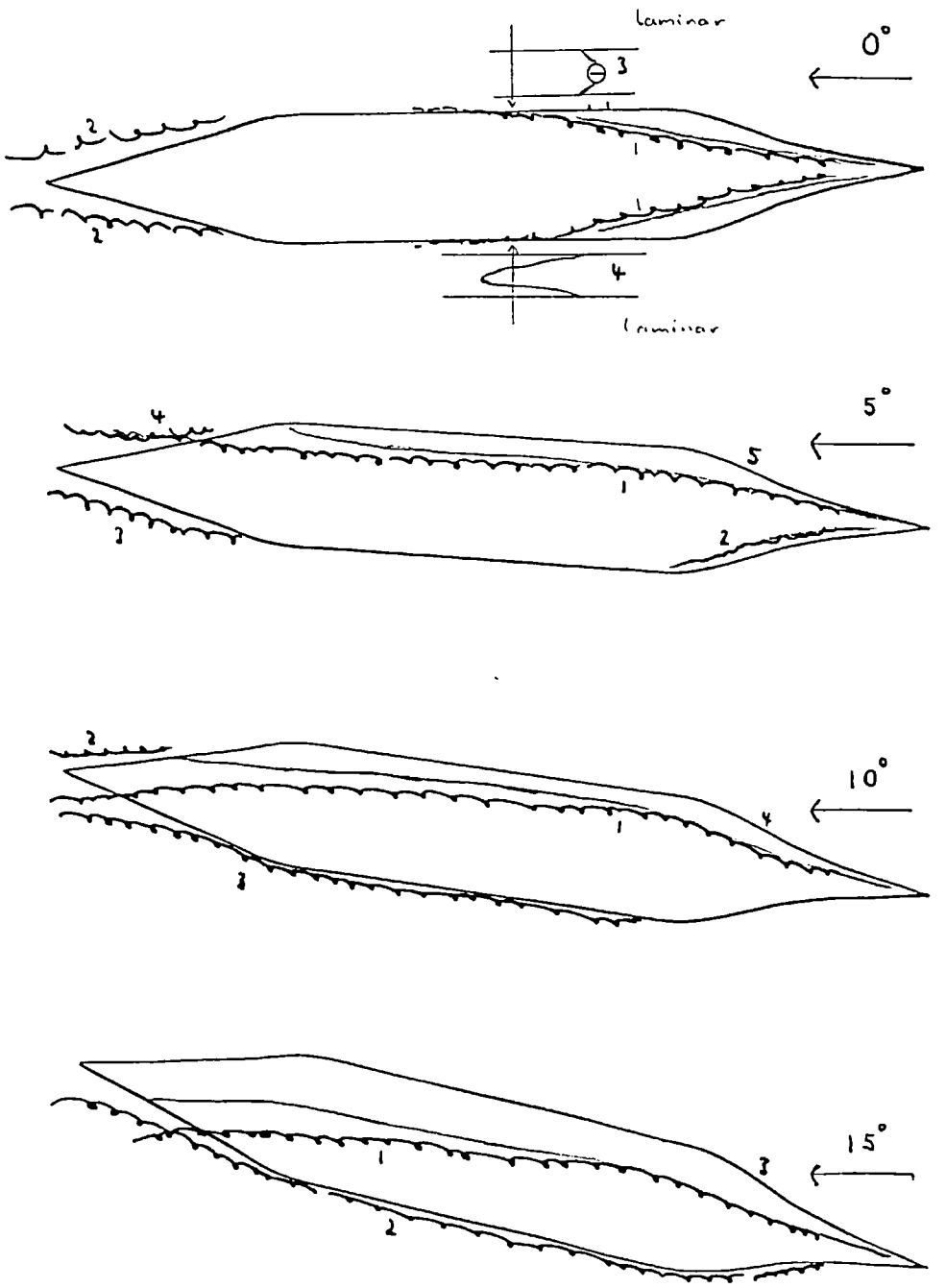

Figure 3.21

Vortices identified by the wool tuft; block Mariner hull.

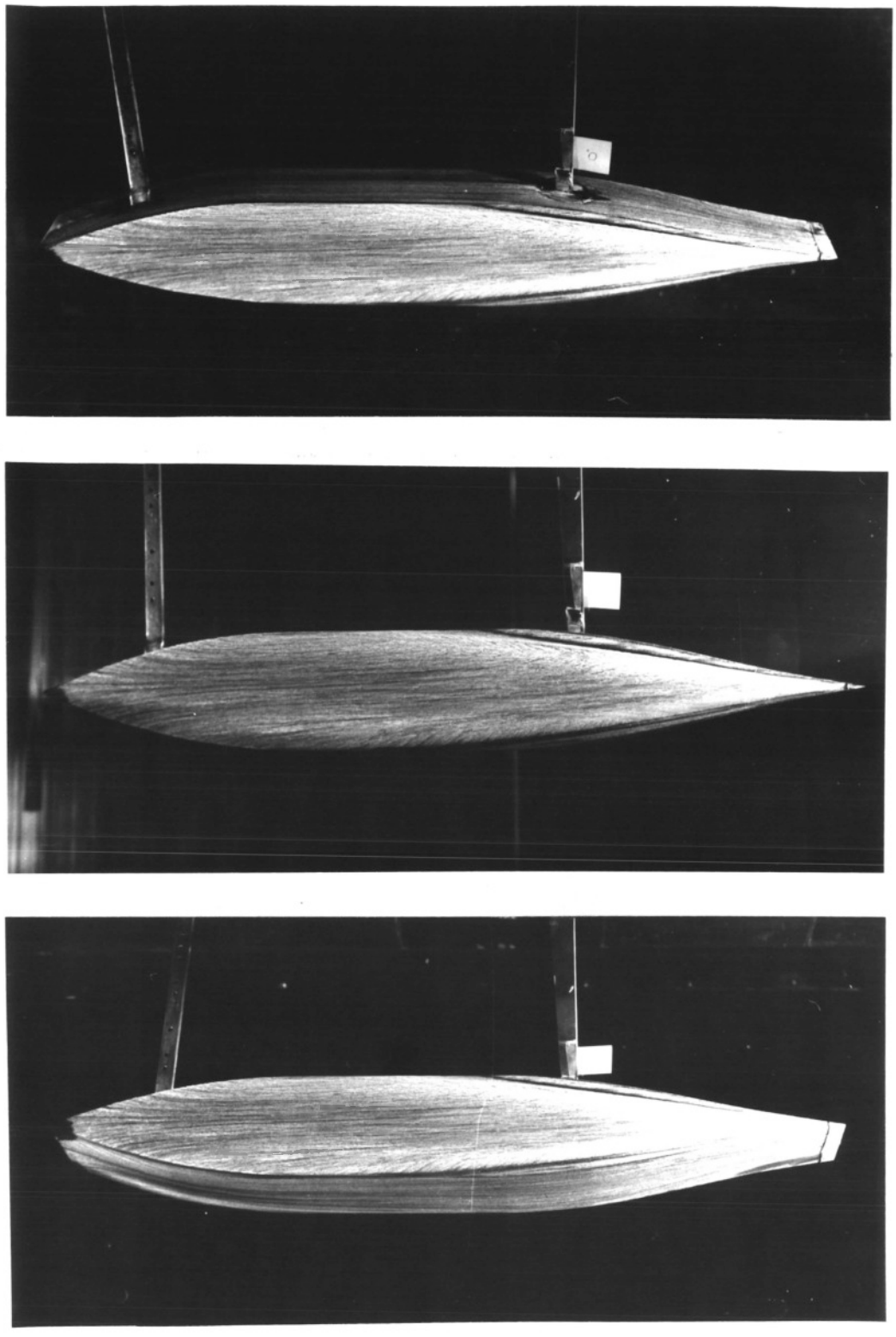

Figure 3.22

Oil flow pattern: hull-like block at 0° incidence

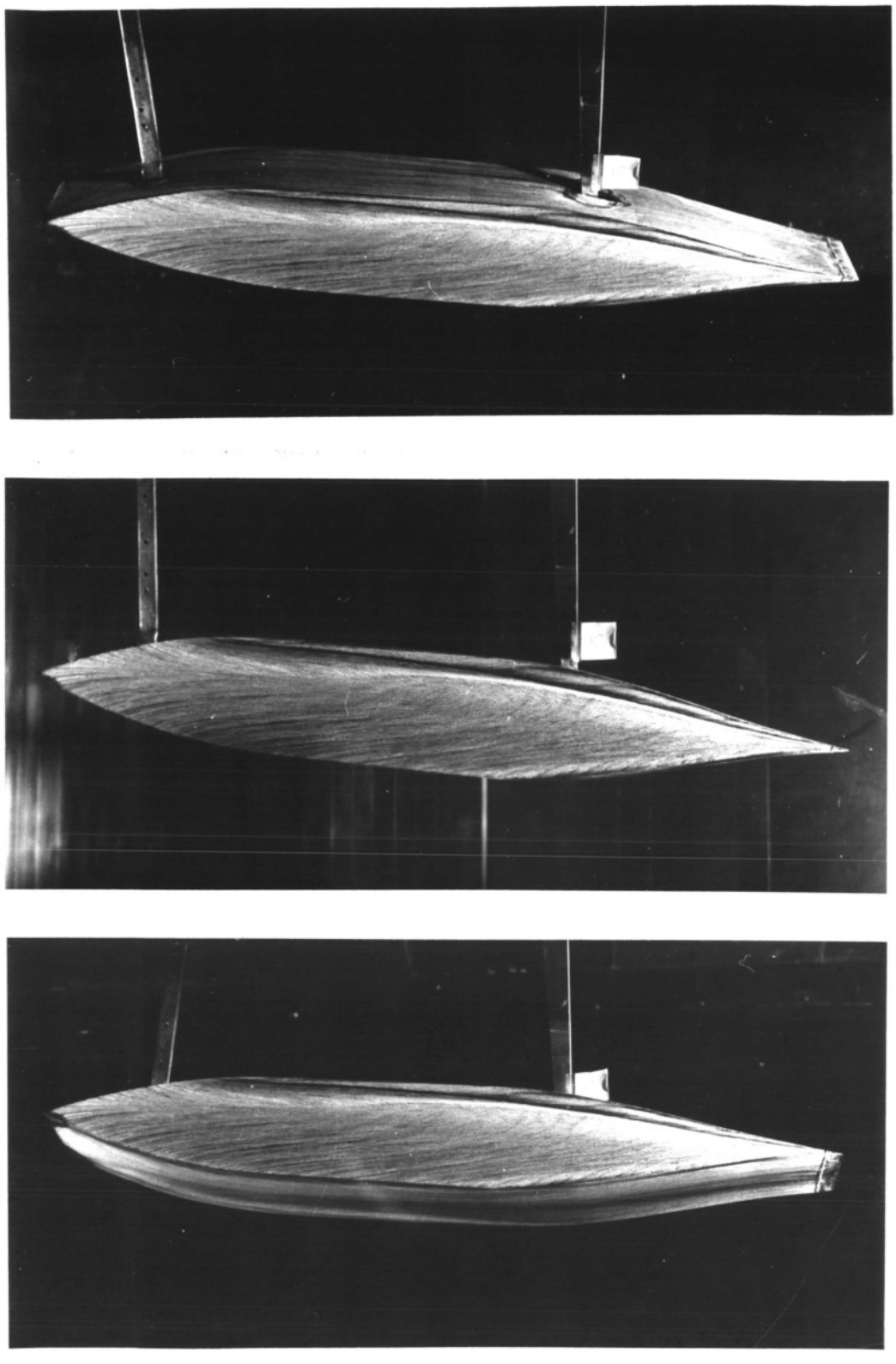

Figure 3.23

Oil flow pattern: hull-like block at 5° incidence

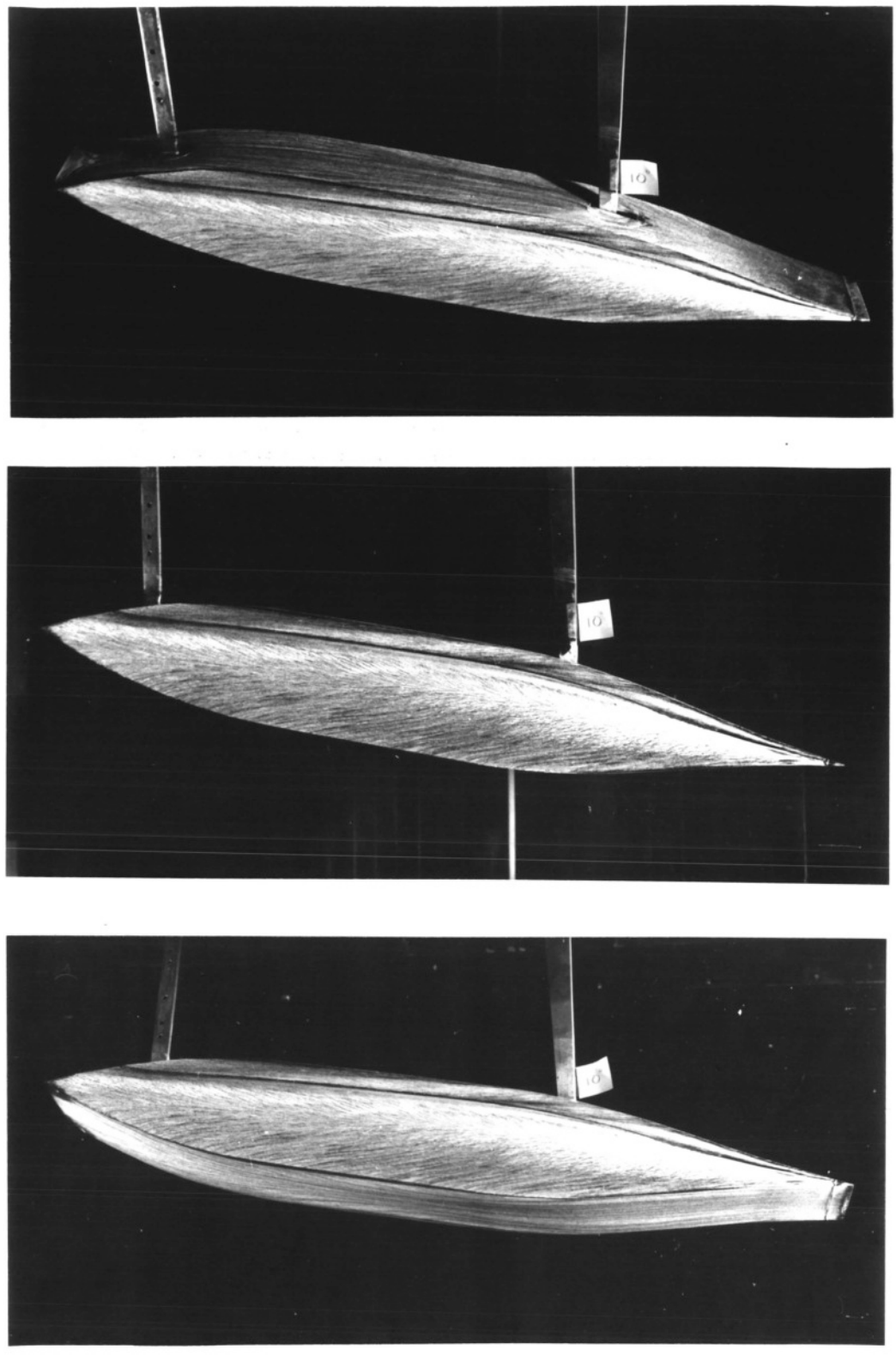

Figure 3.24

Oil flow pattern: hull-like block at 10° incidence

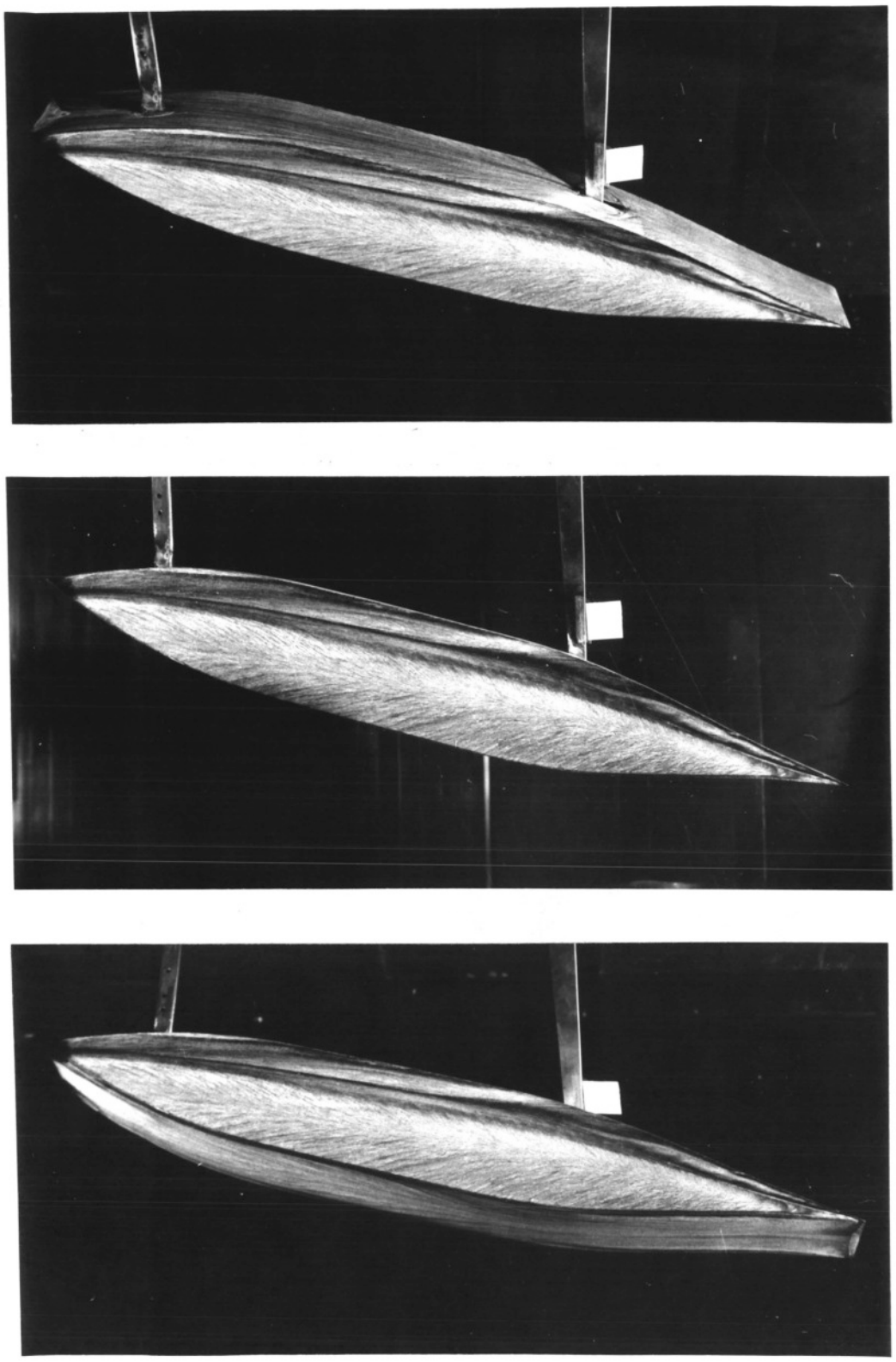

Figure 3.25

Oil flow pattern: hull-like block at 15° incidence

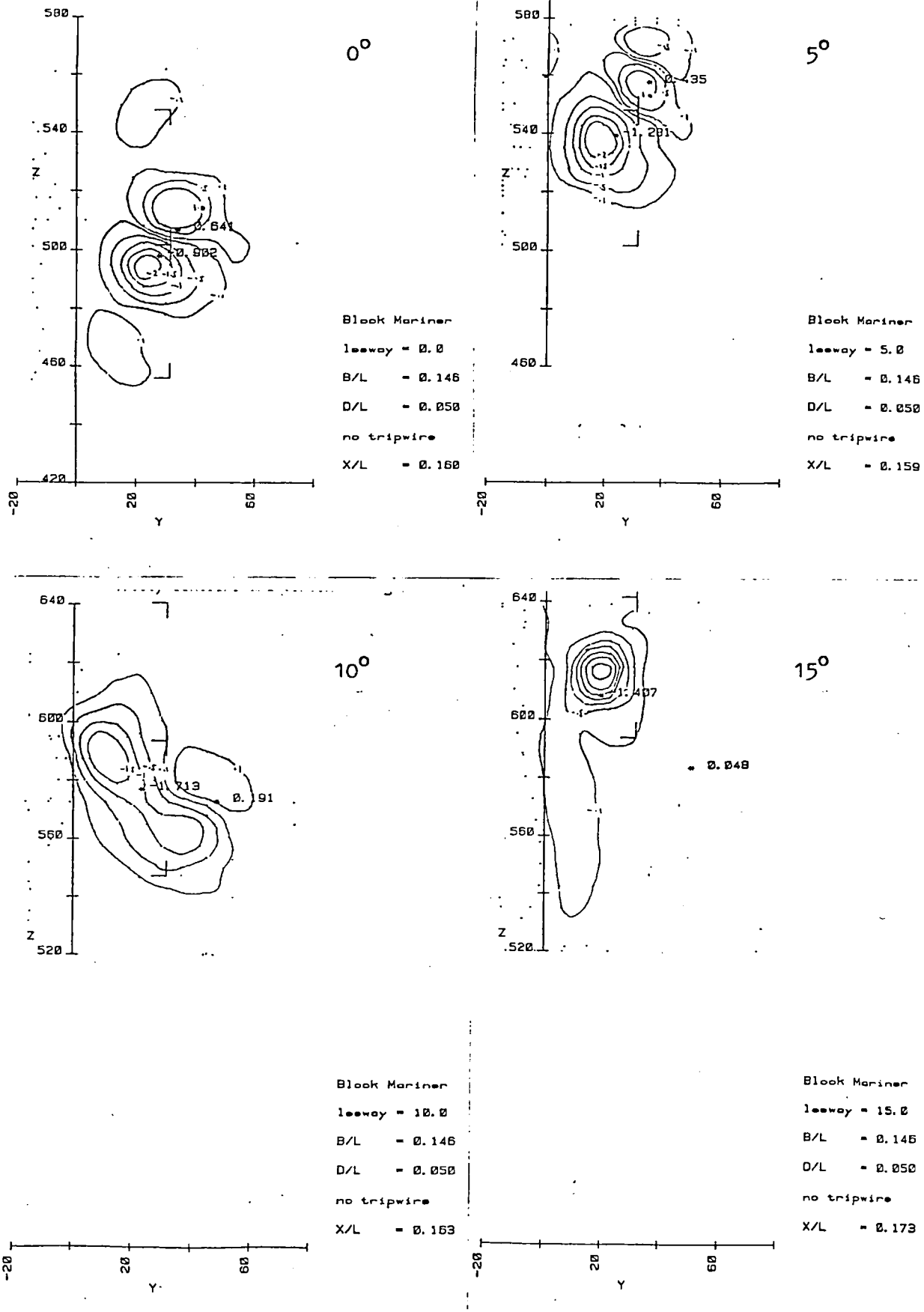

Figure 3.26

Vorticity plots: flow behind the block Mariner.

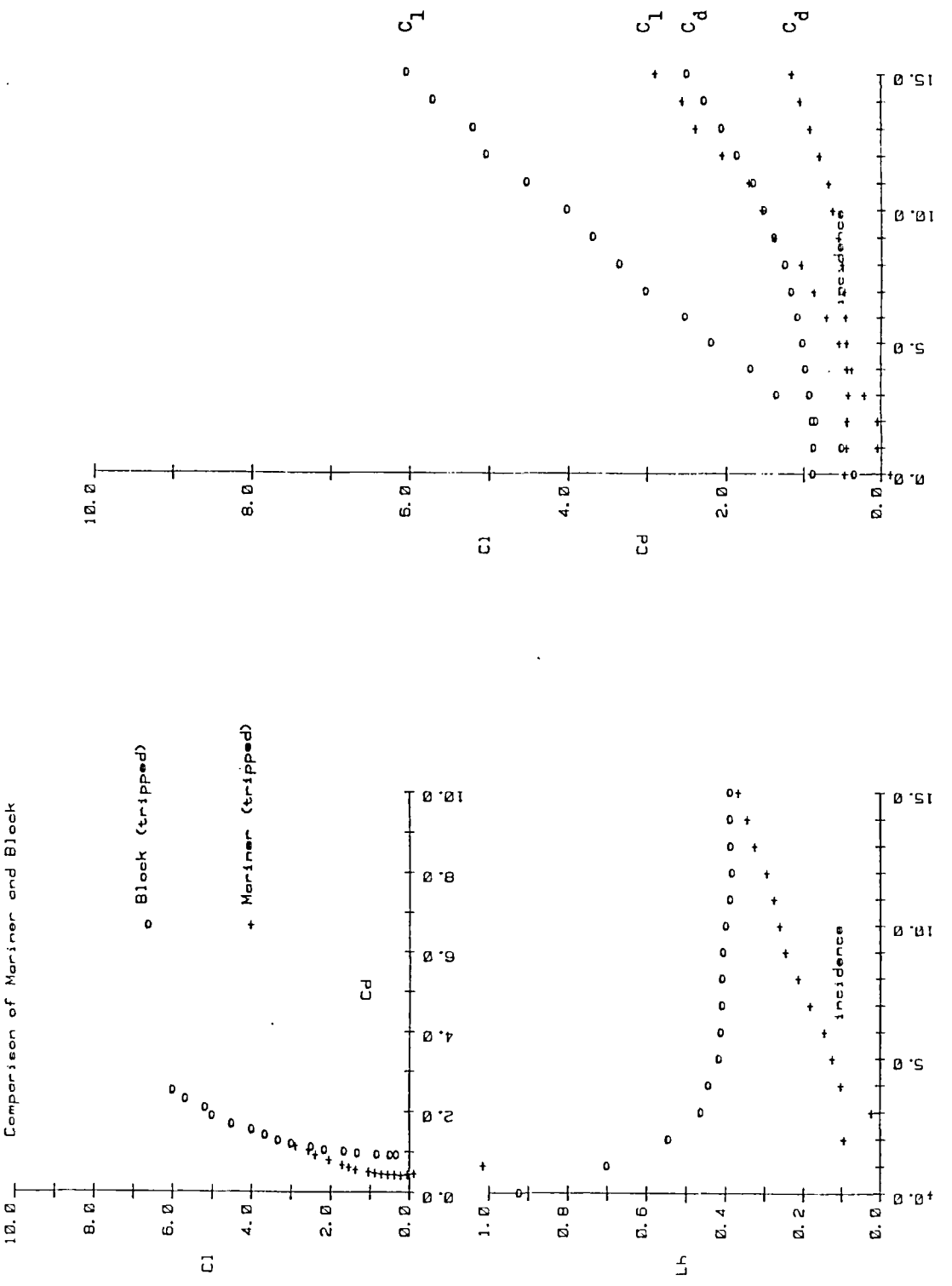

Figure 3.27

Comparison of Mariner and block Mariner forces

3.4(c) Results: influence of beam

Flow visualisation. Increasing beam is associated with increasingly strong vortices. At 0° incidence the entrance vortices have been swept outwards and upwards to about the depth of the run vortices. At all beams the run vortices approximately maintain their positions relative to the keel. The distance of the entrance vortices from the keel increases with increasing beam. At 10° incidence the relative positions of vortices at the stern vary considerably with beam. For the wide beam hull the leading bilge vortex passes on the leading side of the stern, while for the narrow beam hull the leading vortex crosses the trailing bilge about half way along the run. The flow induced by the leading vortex in this position decreases the cross flow round the trailing run bilge. This would be expected to reduce the strength of the trailing run vortex. This appears to be true from the vorticity plot.

Note that a vorticity plot could not be produced for the wide beam hull at 10°. This was because the very strong vortices induced cross flow velocities that are outside the limits of the probe.

Force Measurements. For this set of hull-like blocks, increased beam considerably increases the drag and marginally increases lift. It reduces the maximum lift to drag ratio. Changes in beam have little effect on the position of the apparent centre of effort.

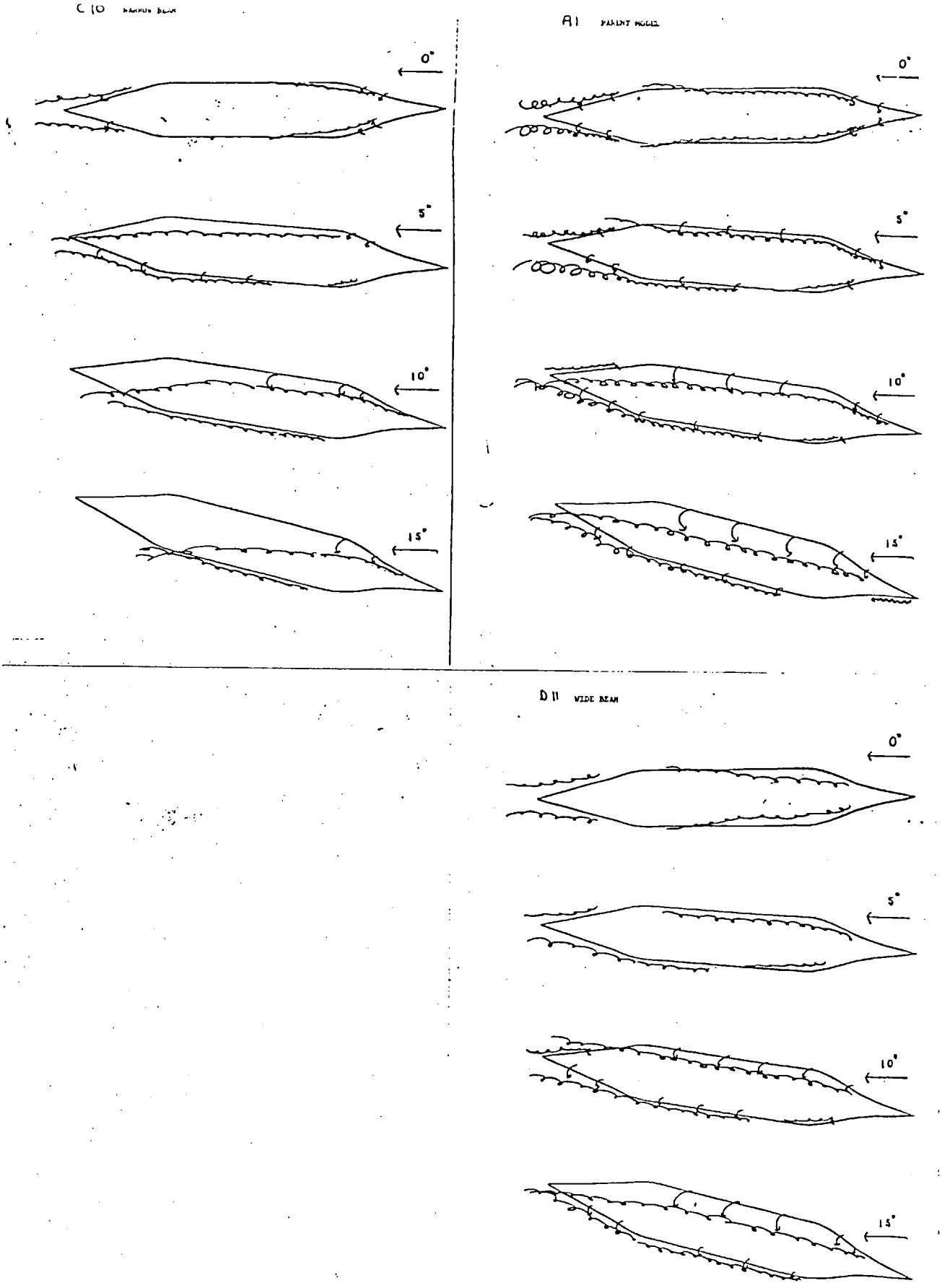

Figure 3.28

Influence of beam on vortex positions.

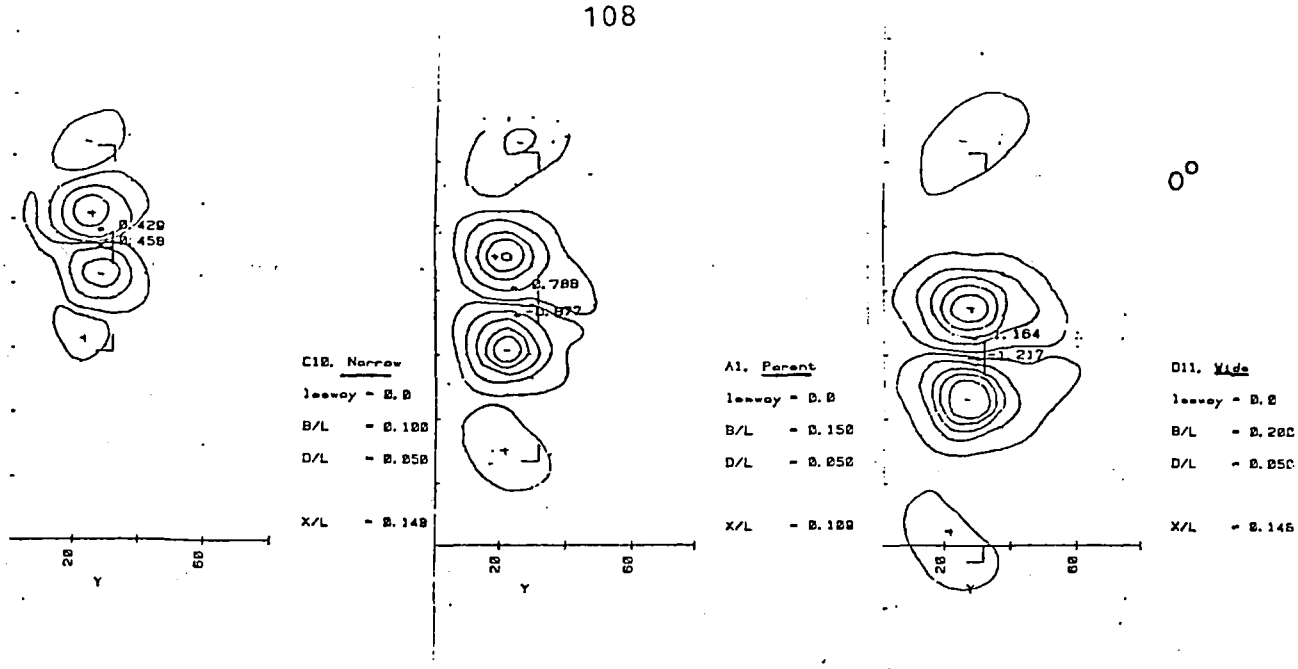

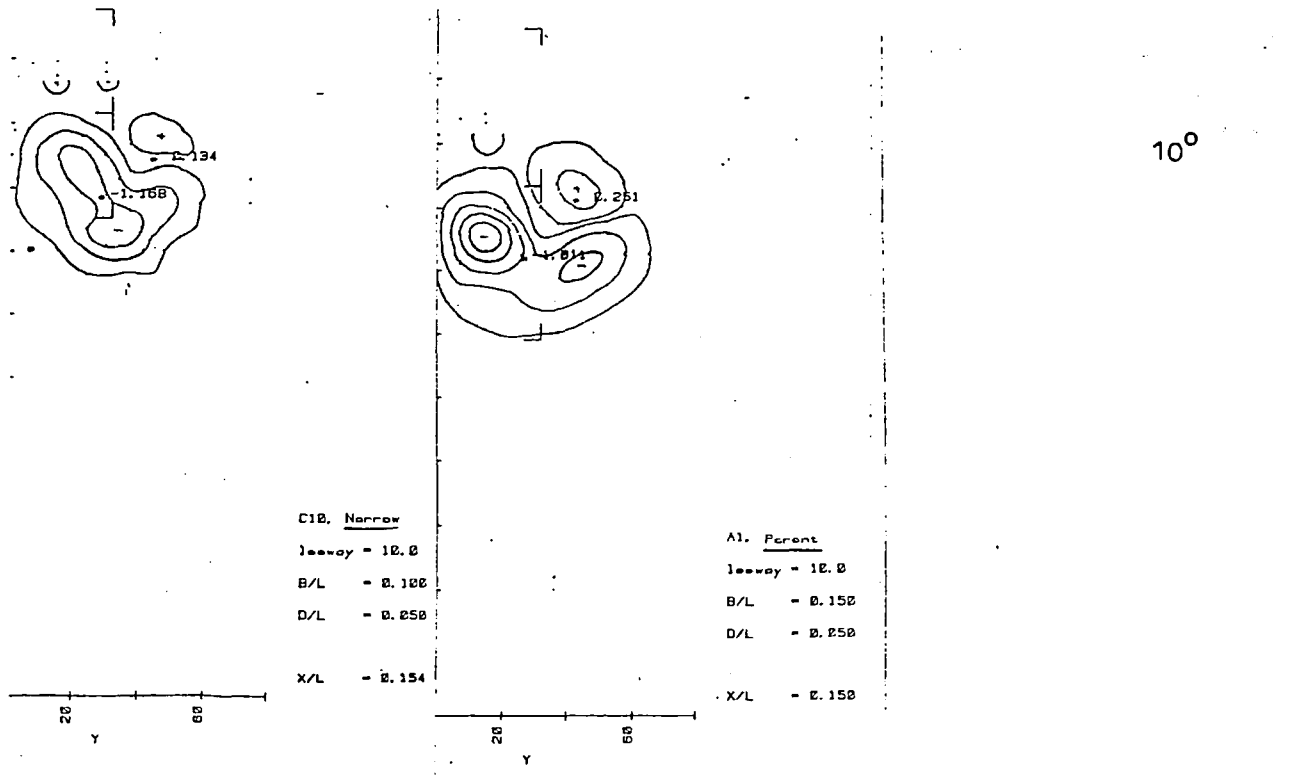

Figure 3.29
Vorticity plots: influence of beam

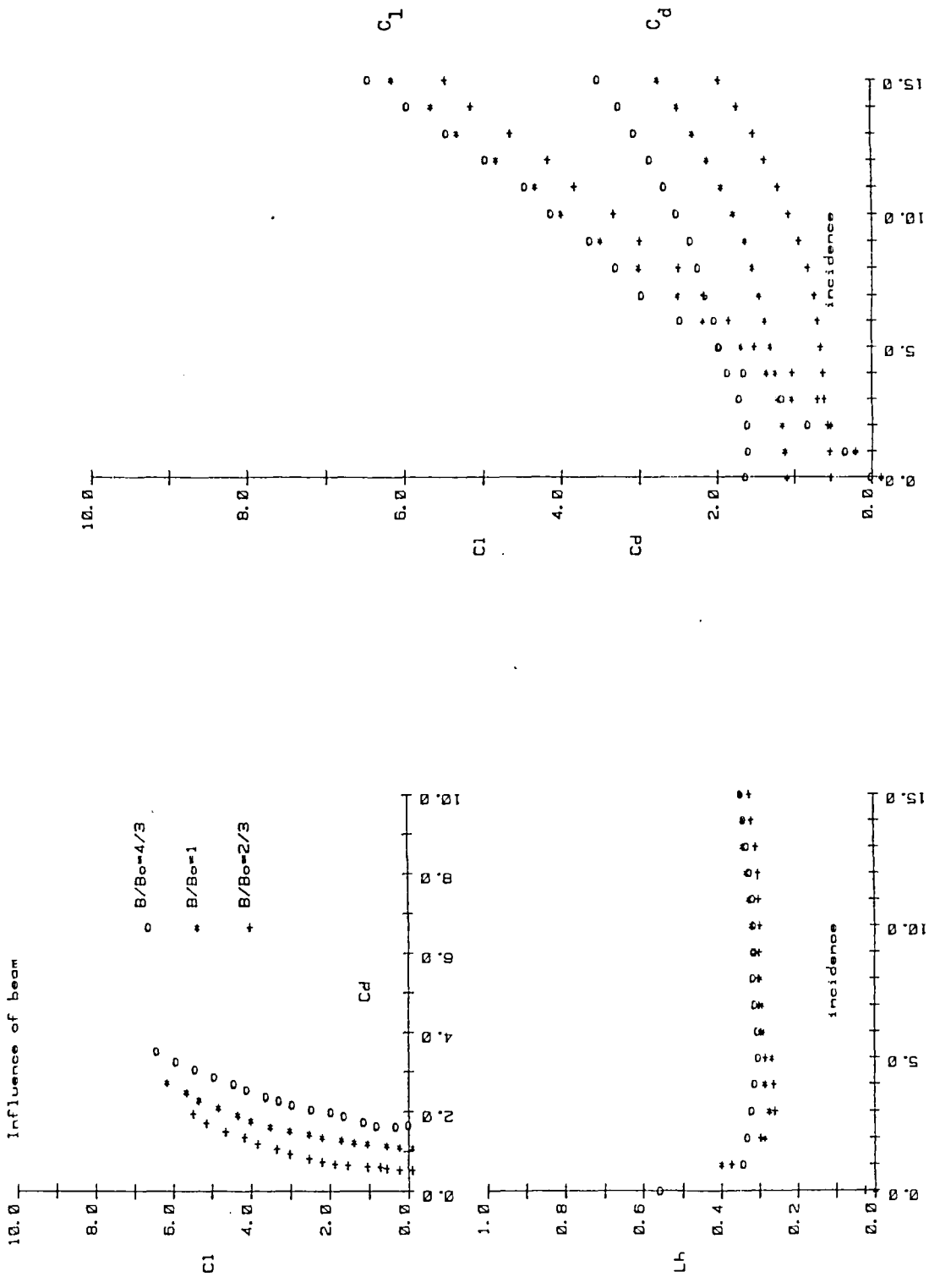

Figure 3.30

Influence of beam on forces

3.4(d) Results: influence of draft

Flow visualisation observations. Increasing draft is associated with increasingly strong vortices. At 0° leeway the run vortices approximately maintain their positions relative to the ship's keel. The weaker entrance vortices are swept outwards and upwards by the run vortices. At the wake survey plane they are at about the same depth as the run vortices for the shallow draft hull. At the same distance aft they have been swept above the run vortices for the deep draft hull. At 10° incidence the wake flow is dominated by the trailing edge vortex shed from the middle body and run. At all drafts the two leading edge vortices have been swept round this vortex which maintains its depth at about 1/2 draft.

Force Measurements. For this set of hull-like blocks, the drag coefficient increases approximately linearly with aspect ratio whereas the lift coefficient increases at a greater rate. This results in deep draft vessels producing higher maximum lift/drag ratios than shallow draft vessels. The position of the centre of effort moves forward slightly with increasing draft.

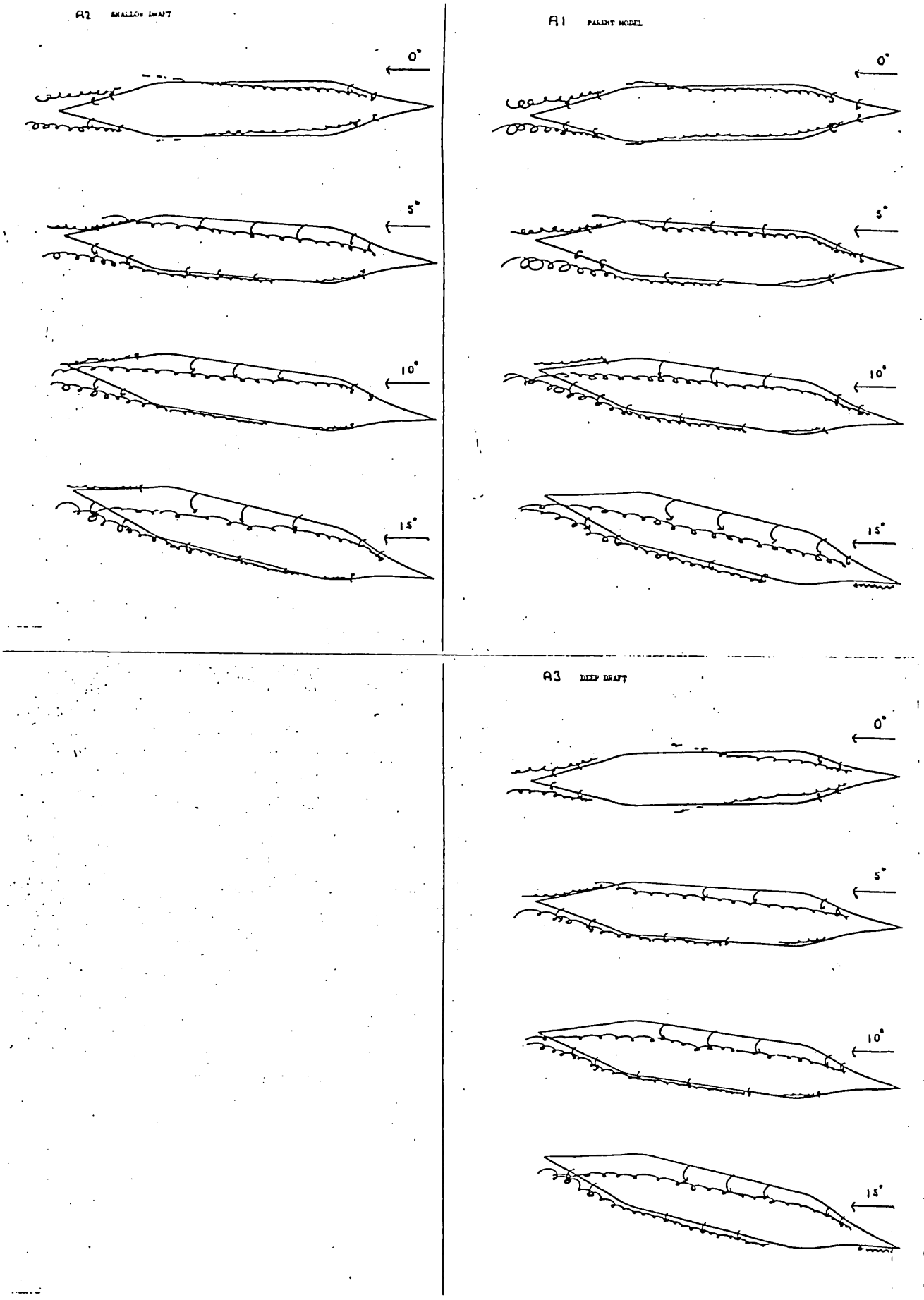

Figure 3.31

Influence of draft on vortex positions.

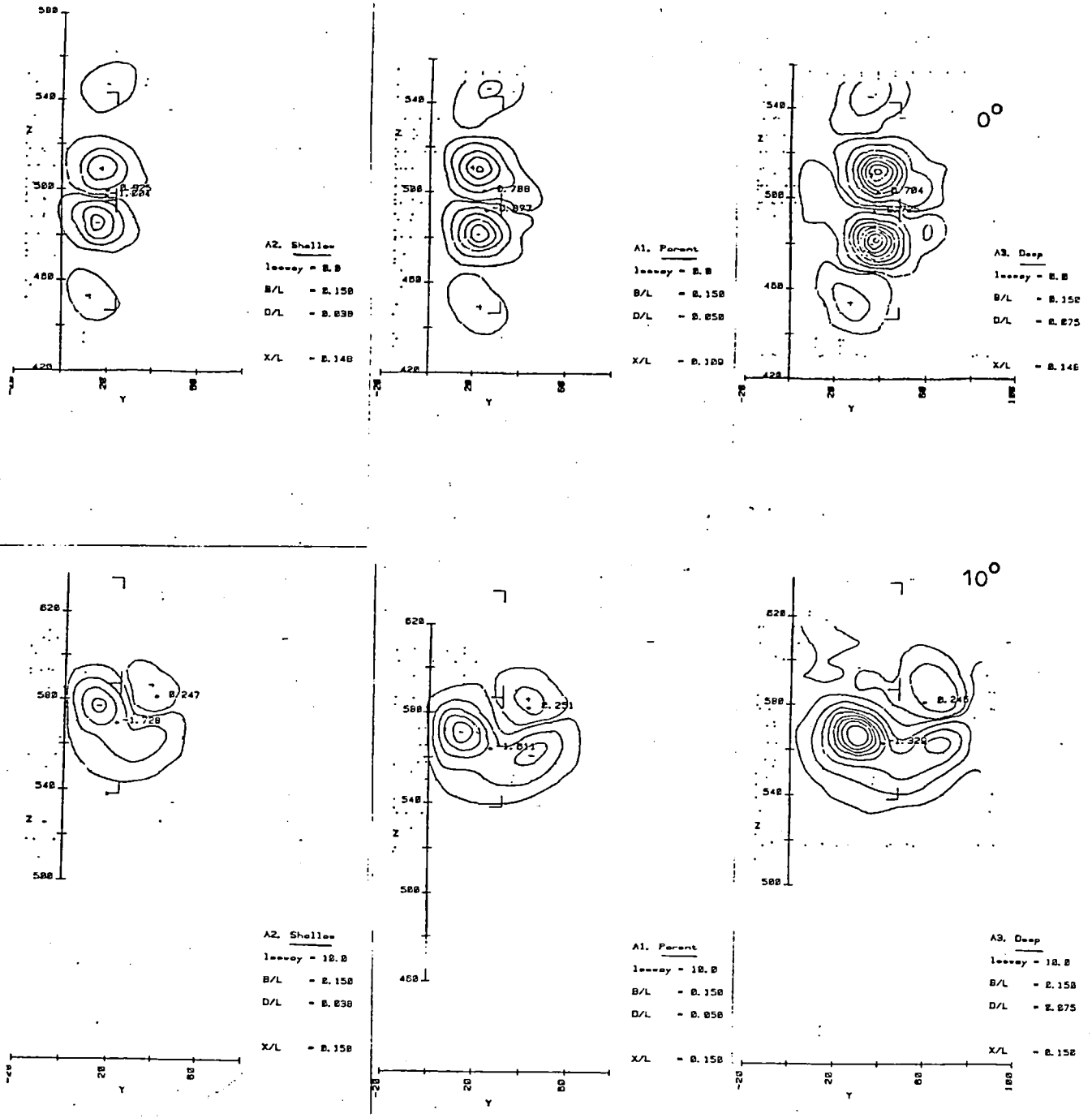

Figure 3.32

Vorticity plots: influence of draft.

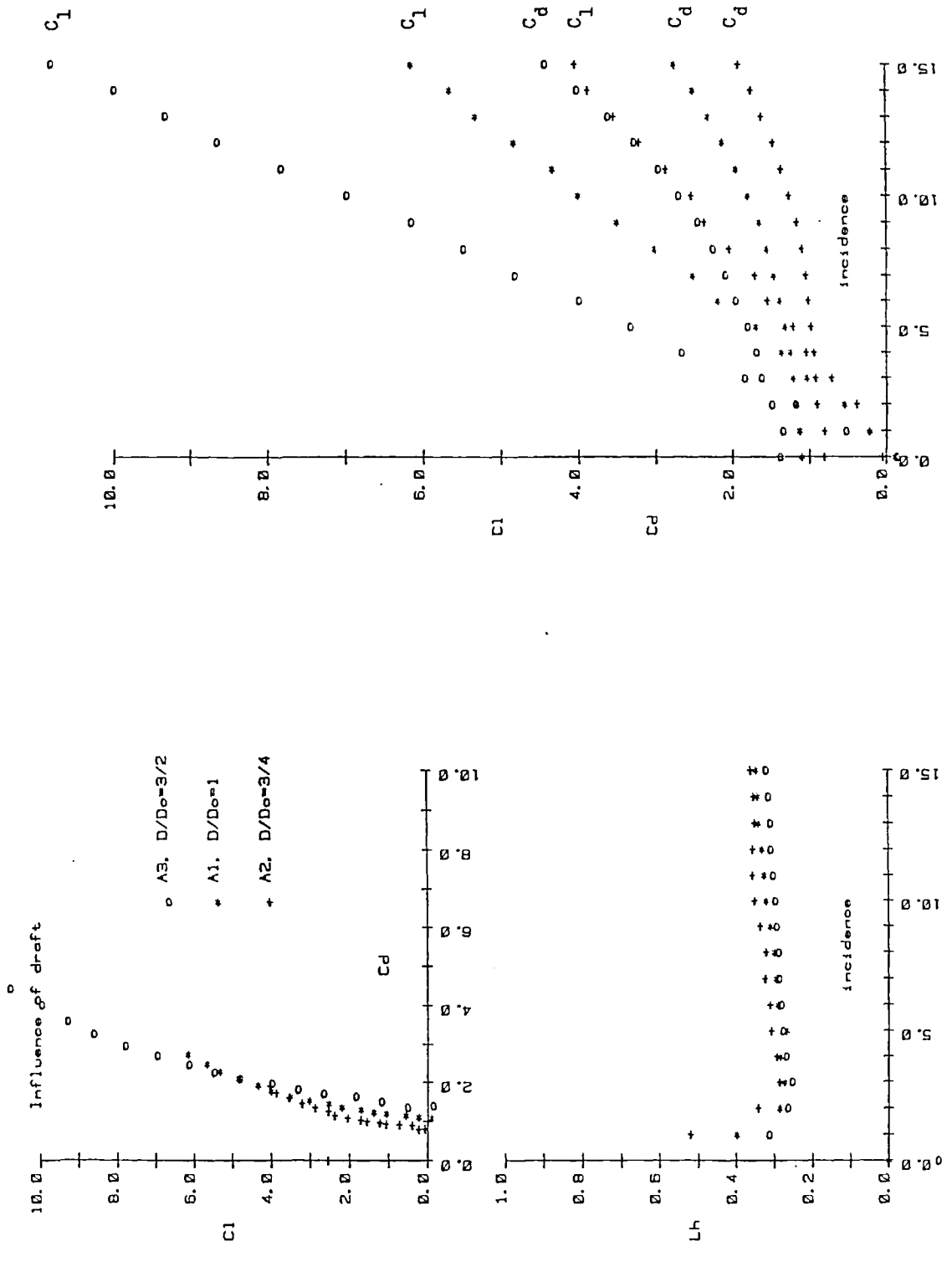

Figure 3.33

Influence of draft on forces

3.4(e) Results: influence of cross sectional area

Force measurements. This test compares two hulls of equal length with identical cross sectional shape. One ship has cross sectional dimensions (draft and beam) increased by 50% compared with the other. This increase in thickness more than doubles drag and almost doubles lift. The maximum lift/drag ratio is slightly reduced. The position of the apparent centre of effort remains fairly constant.

It is interesting to compare the hydrodynamic repercussions of increasing, in three different ways, the cross sectional area, and hence the capacity, of a ship. Simply increasing the beam (see figure 3.30) causes a large decrease in the lift/drag ratio and a large increase in the zero-leeway drag. Increasing the cross sectional area, while maintaining the ratio of beam to draft (see figure 3.34), causes a much smaller decrease in the lift to drag ratio and a slightly smaller increase in the zero-leeway drag. Simply increasing the draft (see figure 3.33) causes a slight improvement in the lift/drag ratio and a still smaller increase in zero-leeway drag.

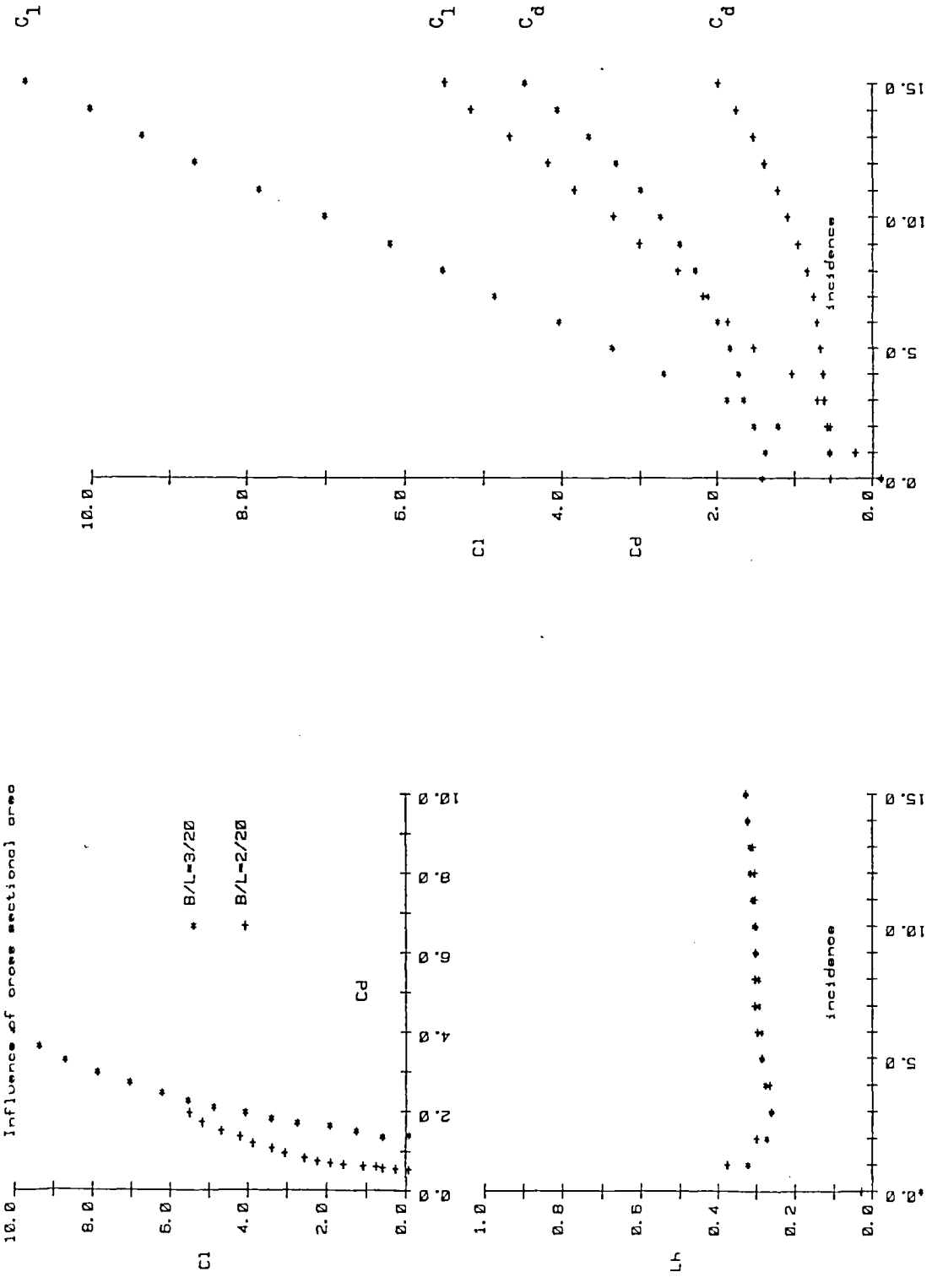

Figure 3.34

Influence of cross sectional area on forces

3.4(f) Results: rounded bilges

Flow visualisation observations. Separation lines are generally fixed in position by the sharp rectangular bilges of most of the block models. This is not true for this model. The flow geometry may well be slightly dependent on Reynolds number, particularly as a greater proportion of the model flow is laminar than would be so for a larger hull. Note that no trip wire was used, but that appendix A3.2 indicates that flow tripping has minimal effects.

The flow past the rounded bilge model produces much weaker vortices than the flow past the block model. The vortices are, however, generally in similar positions. The main difference is that, for the block model, the leading entrance bilge vortex continues to be fed along the middle body and remains close to the bilge, while for the rounded bilge model this leading entrance bilge vortex is convected downstream in approximately the free stream direction.

Force Measurements. The model with square bilges experiences lift and drag forces of about 50% greater than those experienced by the rounded bilge model. The maximum lift/drag ratios are similar for the two models. At small angles of leeway, square bilges are associated with a centre of effort slightly nearer the bow; at larger angles of leeway the centre of effort is similarly positioned for the two models.

As discussed earlier, a greater pressure difference can be maintained across a sharp bilged hull and stronger vortex suctions are likely on the ship's side near the

trailing sharp bilge. These two effects contribute to the greater lift of the sharp bilged hull. The greater drag is mainly increased vortex drag.

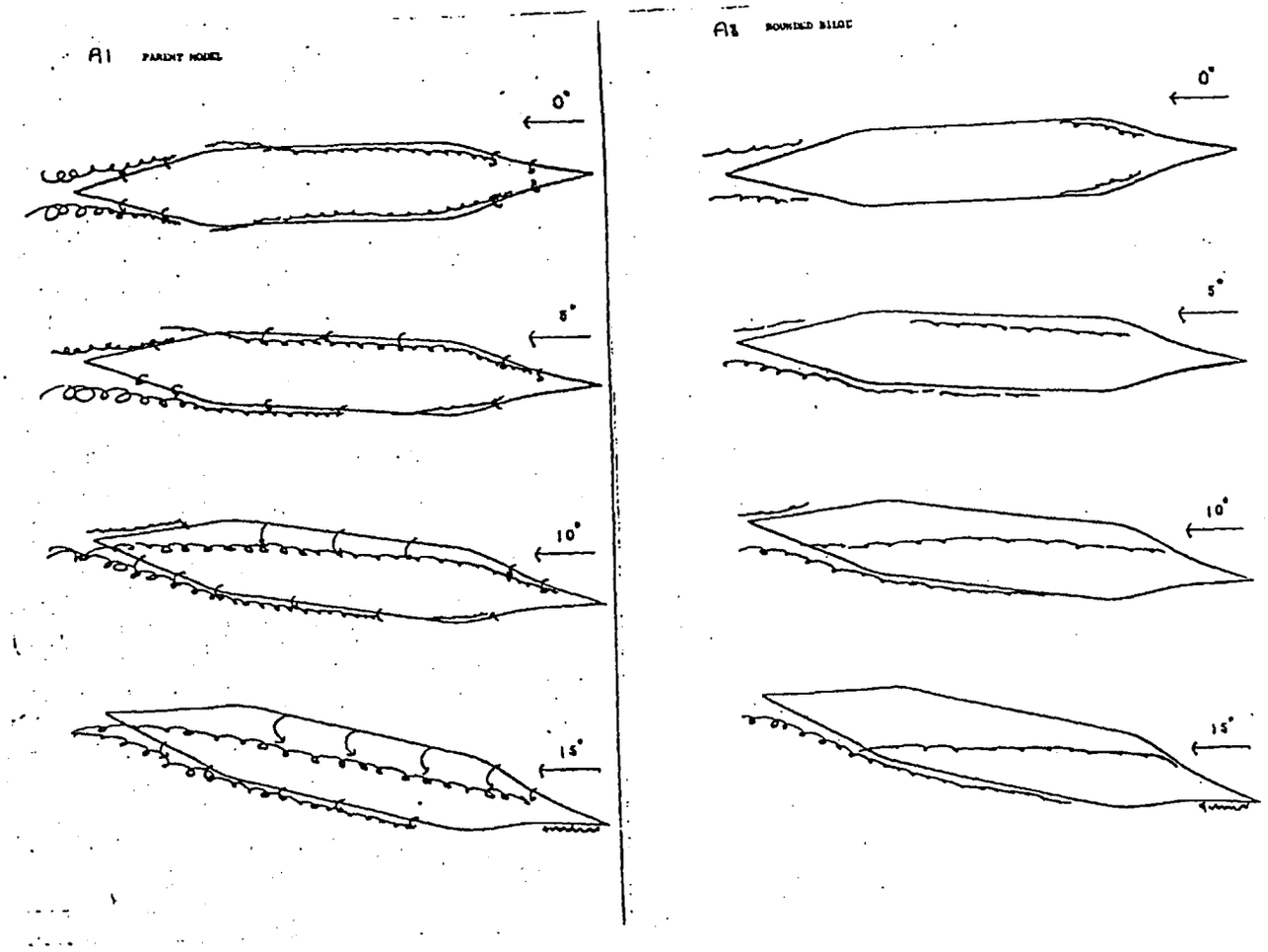

Figure 3.35

Effect of rounded bilges on vortex positions.

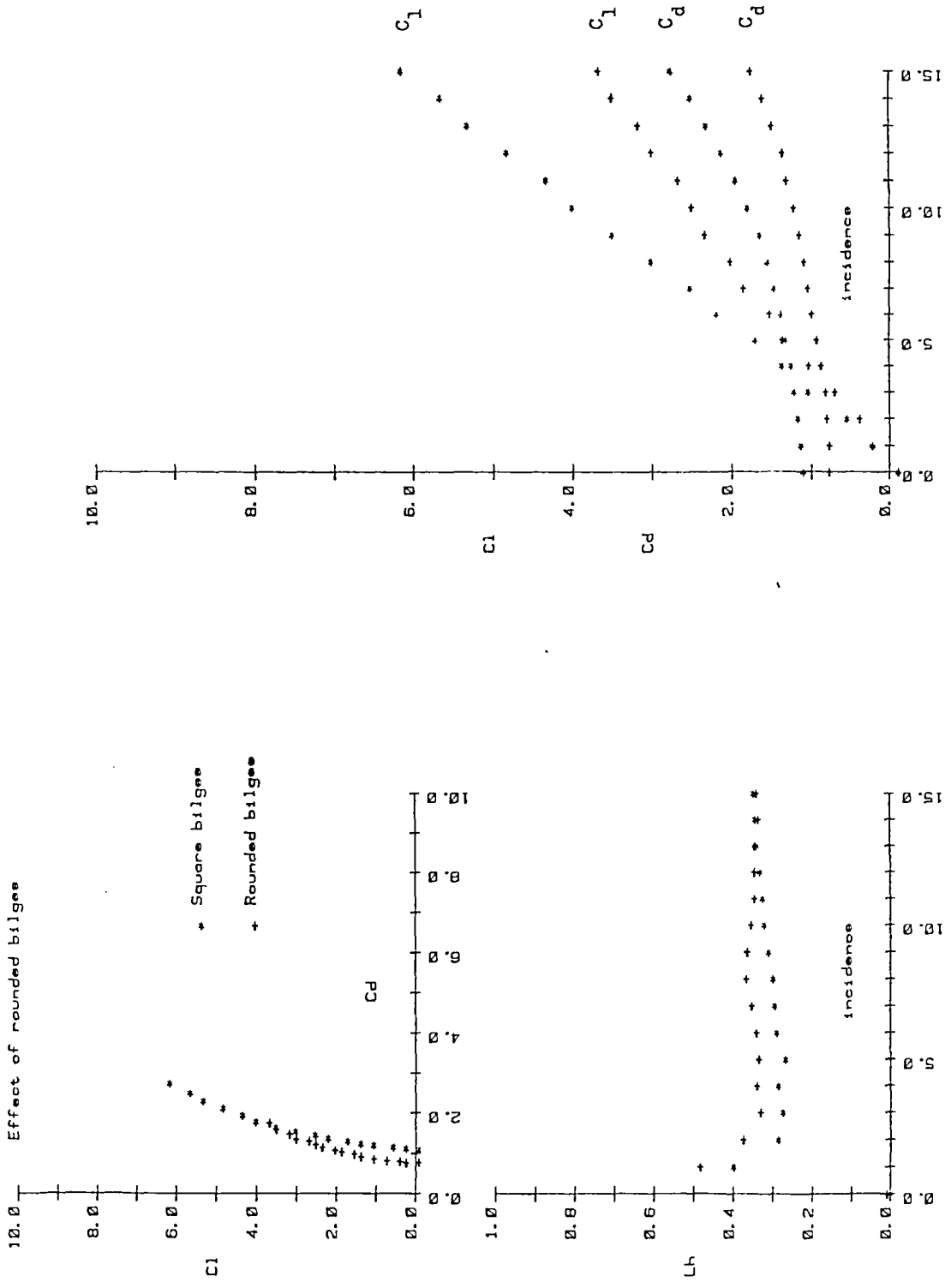

Figure 3.36

Effect of rounded bilges on forces

3.4(g) Results: rounded bow

Flow visualisation observations. The flow at the foremost part of the ship is likely to be particularly dependent on Reynolds number. Model B9 was given a rounded bow planform for comparison with the parent model's sharp bow. The flow round the sides of the model bow is laminar, and scale effects are likely.

For the parent model the flow near the bow is attached for leeway of up to 10°. At 15° leeway very turbulent flow is detected on the trailing side of the bow. That is probably associated with a small separation bubble close to the bow initiated at the sharp leading edge. For the rounded bow model very turbulent flow is detected on the trailing side of the bow at 10° leeway. This is probably associated with a separation bubble initiating from smooth surface separation. At 15° leeway an area of recirculating flow can be detected in this position. An additional feature of the flow, which may not be so dependent on Reynolds number, is a region of separated flow on the underside of the hull near the bows. This region is indicated by hatched lines.

Force Measurements. The model with a rounded planform bow was found to have a greater drag than the parent model. Flow visualisation shows that there is a region of separated flow on the ship's bottom near the bow. Separated flow and its associated drag are to be expected near a bow with a rounded planform but sharp corners at the bottom. The bow of this model is crudely shaped and unlikely to have good hydrodynamic characteristics. As noted earlier, there is laminar flow near

the bow; and the flow in this region is therefore very dependent on Reynolds number. It is unwise to draw conclusions concerning full scale flows from this experiment; indeed, no experiments at this scale comparing bow characteristics can reliably model full scale effects.

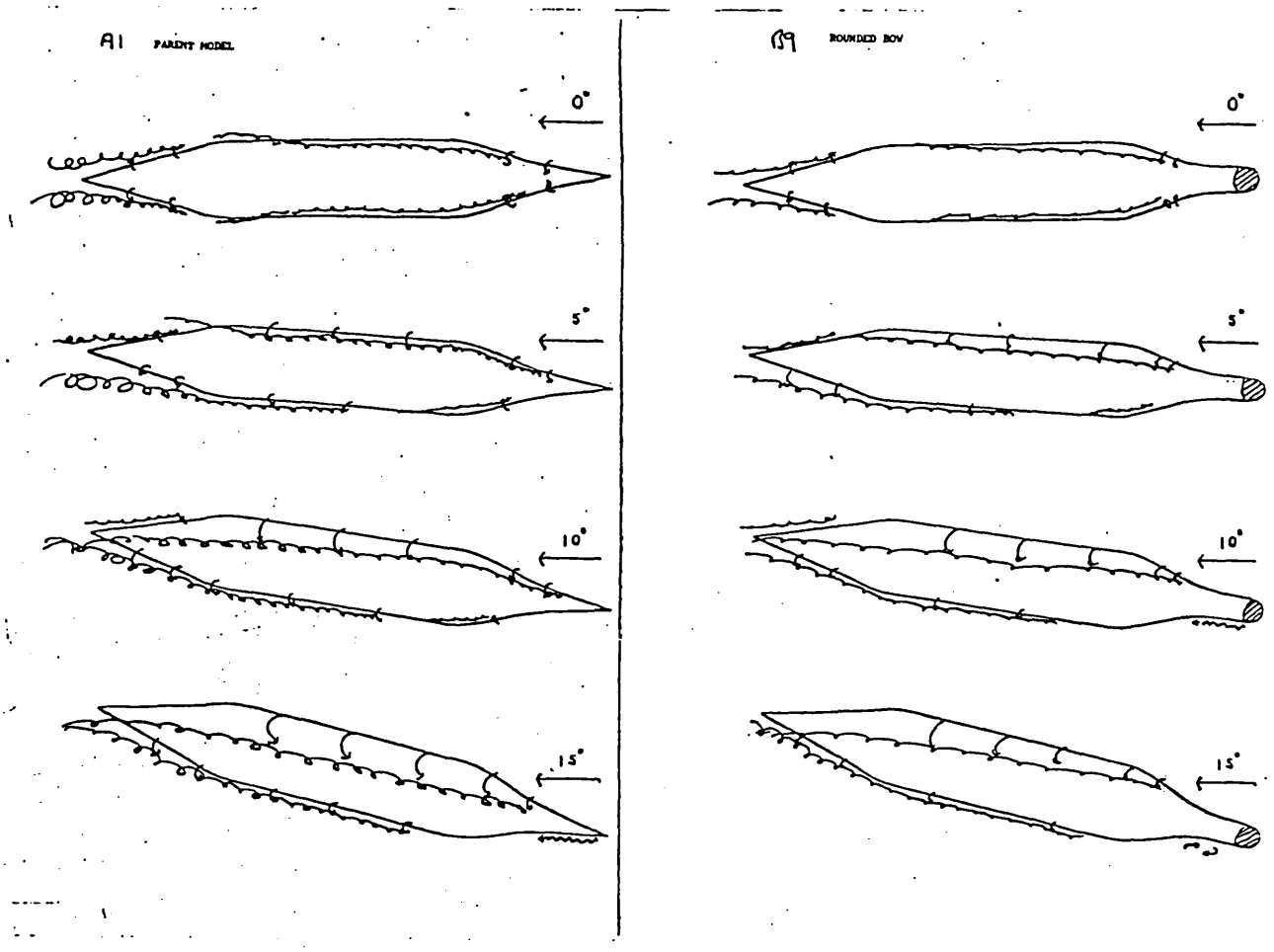

Figure 3.37

Effect of a rounded bow on vortex positions.

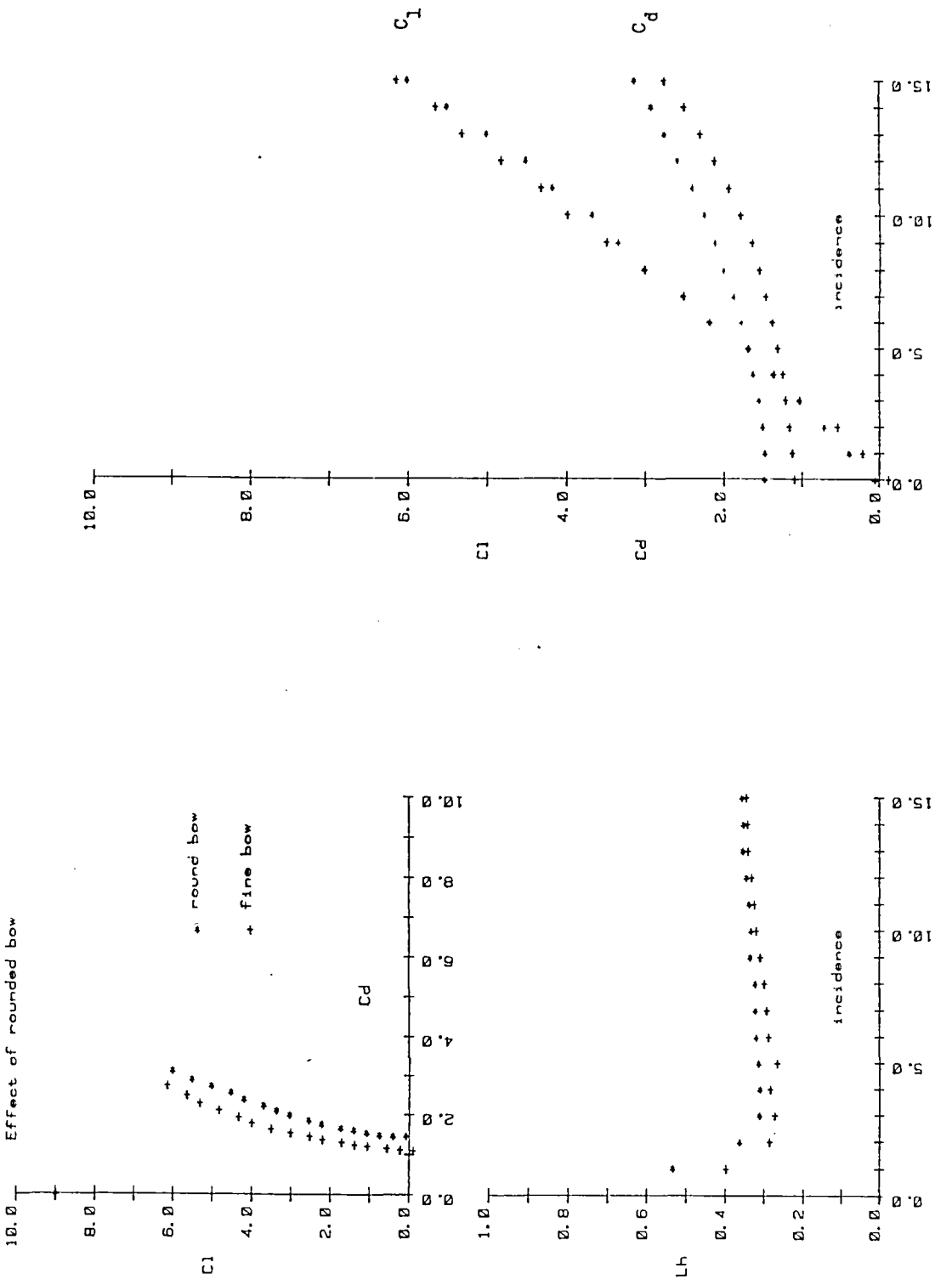

Figure 3.38

Effect of rounded bow on forces

3.4(h) Results: influence of trim

Flow visualisation observations. When a hull is trimmed by the bows (that is, so that the bows are deeper than the stern), flow is induced from the ship's side to the ship's bottom as the draft decreases towards the stern. The opposite is true when the hull is trimmed by the stern. Trim has a significant influence on the vortices shed because of this induced flow. At 0° leeway the entrance vortices are fed and remain strong along the whole length of the middle body for a hull trimmed by the bow, whereas they are very quickly convected back round the bilge and become undetectable for a hull trimmed by the stern. The run vortices are strongest for vessels trimmed by the stern. Towards the stern, at 10° leeway, whichever way the hull is trimmed, the vortex shed at the entrance and middle body leading bilge combines with the vortex shed at the trailing bilge. The vorticity plots show that the leading edge vortex remains the stronger of the two when trimmed by the bow, but is weaker when trimmed by the stern.

Note that this set of vorticity plots were made from data obtained at grid points separated by 15mm. It was subsequently decided (see appendix A3.4) that a 15mm grid was too coarse as too much detail was lost at this spacing. These plots are nevertheless useful for indicating the main features of the wake flow.

Force Measurements. Trimming a hull by the bow marginally reduces the drag at low leeway and increases it at large leeway; it has little effect on the lift. Trimming the hull 1/20 by the bow moves the apparent centre of effort

forward by about 1/4 ship length. Trimming a hull by the stern marginally increases the drag and considerably increases the lift. Trimming the hull 1/20 by the stern moves the apparent centre of effort aft by about 1/4 ship length.

These results suggest that a sailing vessel might benefit from being trimmed by the stern. This would move the hydrodynamic centre of effort aft, reducing the rudder moment required to maintain a straight course; it would also increase the lift/drag ratio of the hull which would improve sailing performance. It is interesting to note that traditional sailing vessels do appear to have been sailed trimmed by the stern. Kemp (1897) writes, "A much greater draft aft than forward has been found of great use in keeping the centre of lateral resistance in (at) a required distance aft"; however, his explanation continues "as the lower parts of what may be termed a raking keel are continually being moved into solid or undisturbed water." Laas (1907) gives extensive technical details and plans of a great many 19th century sailing ships. Unfortunately he makes no comment on sailing trim and only gives sailing trim for one ship; this is for a successful fast clipper which is probably trimmed in a conventional fashion. This information is for the 49m ship "France et Chile": her sailing trim is reported as 1/69 by the stern.

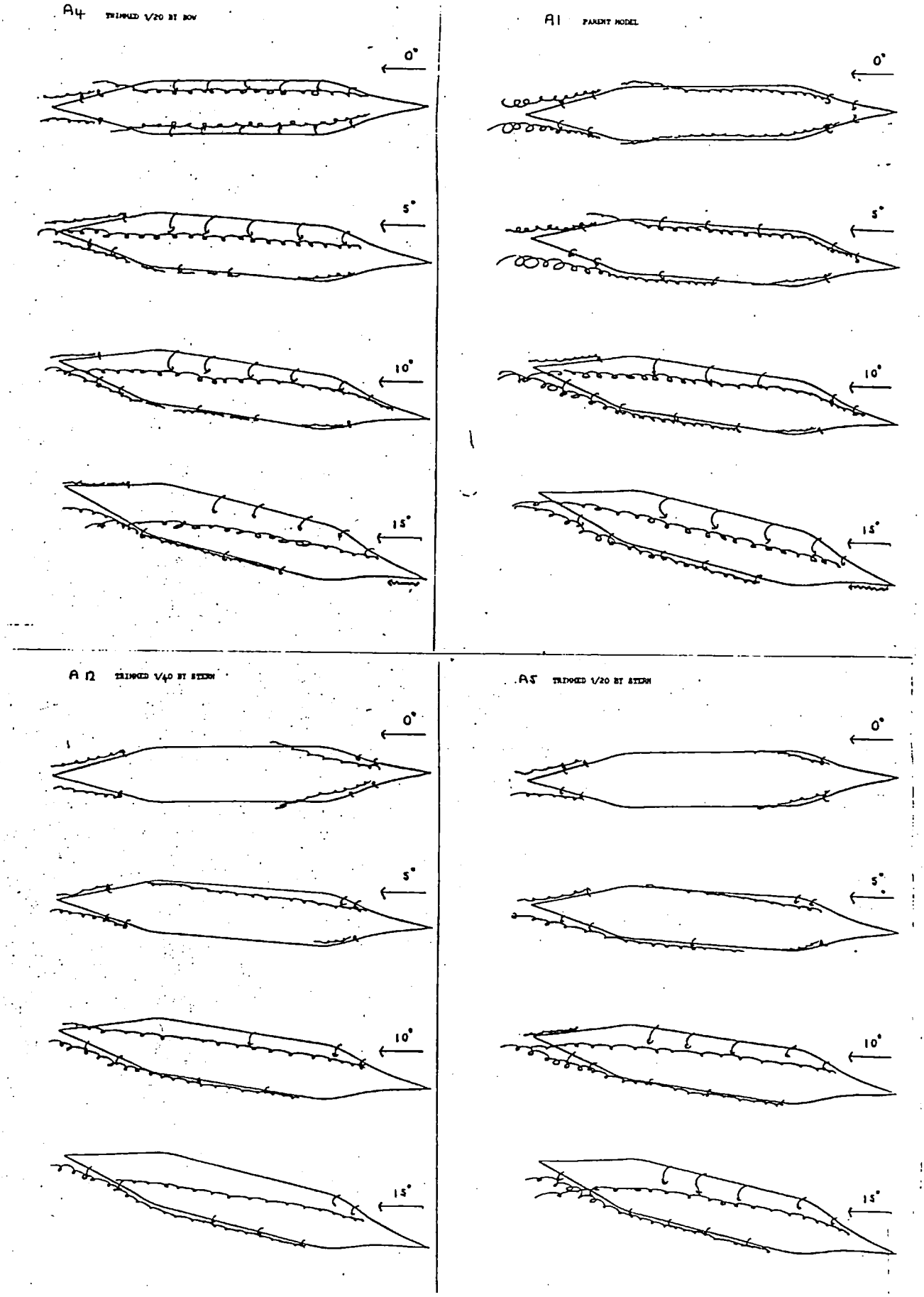

Figure 3.39

Influence of trim on vortex positions

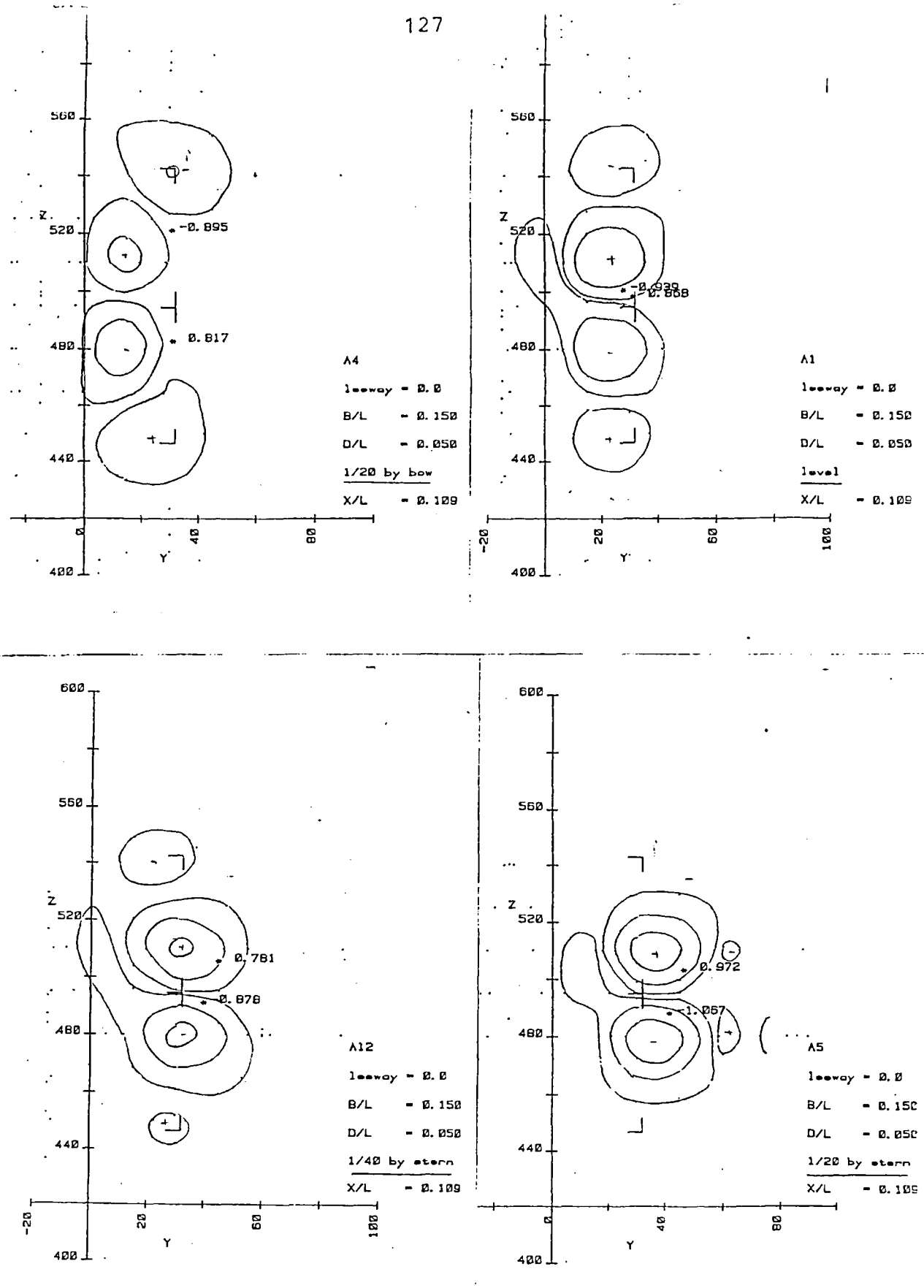

Figure 3.40

Influence of trim, no leeway.

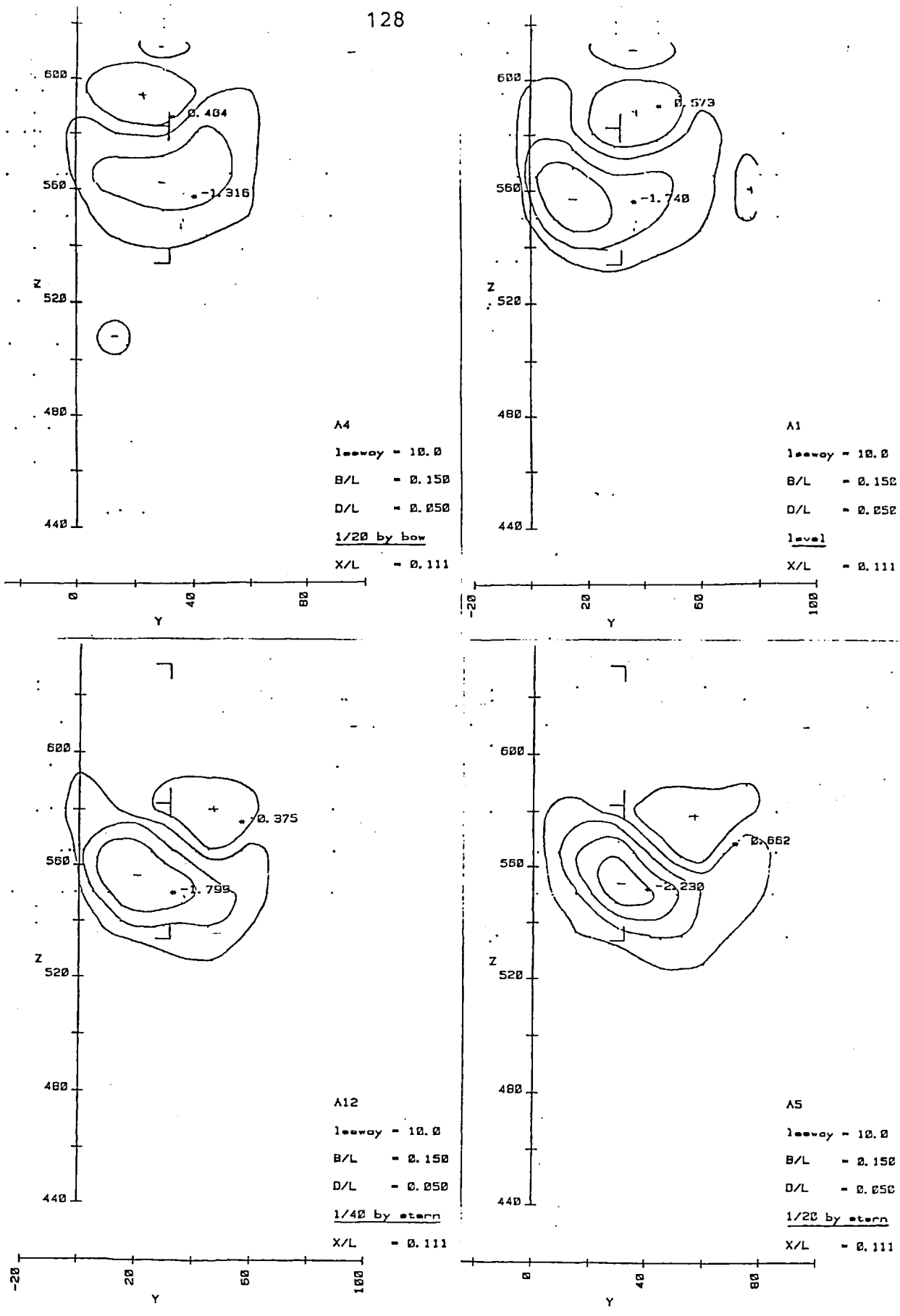

Figure 3.41

Influence of trim, at leeway (10^{o})

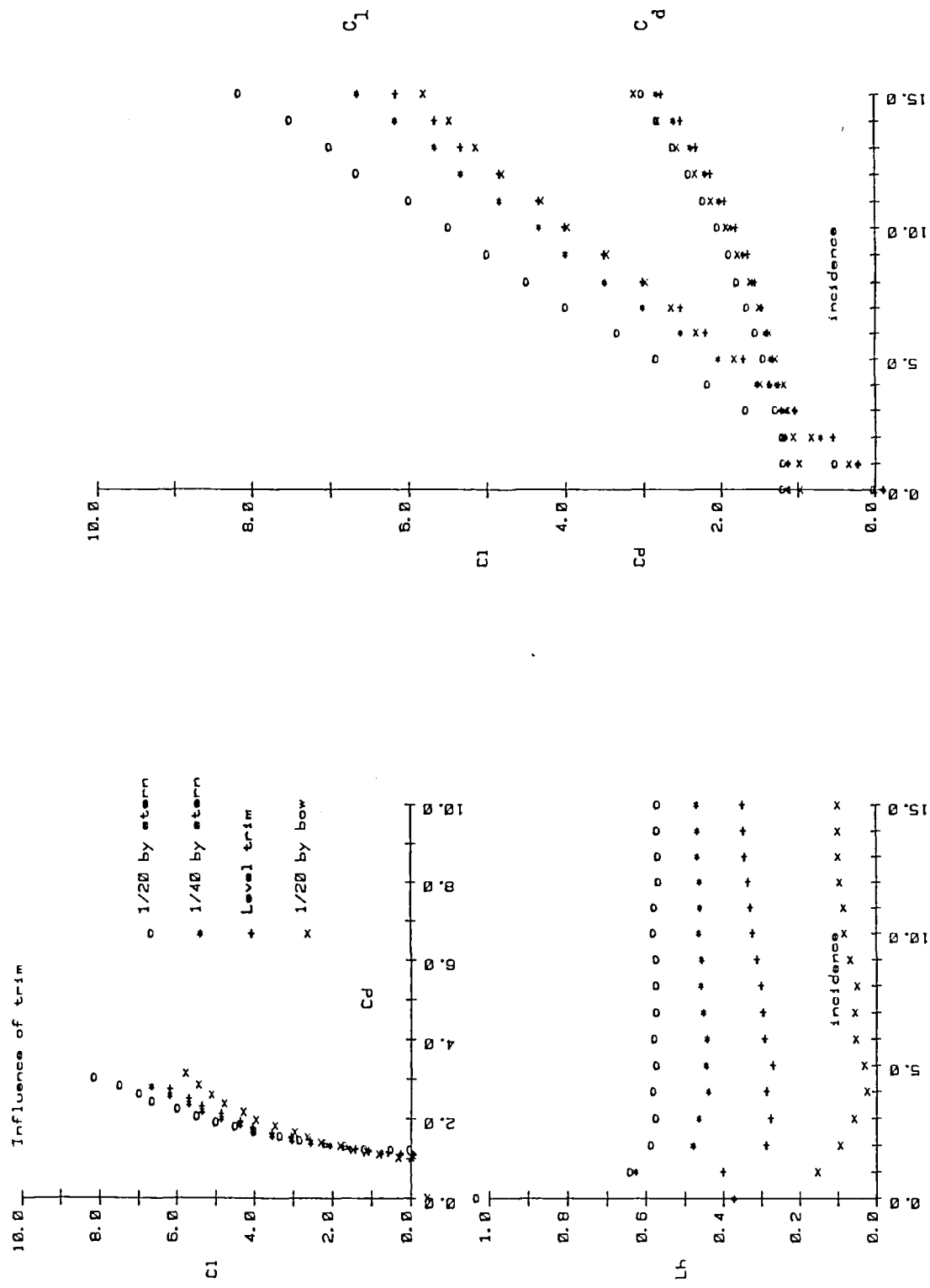

Figure 3.42

Influence of trim on forces

3.4(i) Results: influence of heel

Flow visualisation observations. When a sailing vessel is heeled by windforces the hull is rotated so that the leading bilge is pushed deeper into the water. As the depth of the trailing bilge decreases, the underwater cross section approaches a triangular shape with the leading bilge as apex. It is the flow round this leading bilge which produces the main vortex features. The wool tuft flow visualisation shows that at large angles of heel and leeway the main feature of the wake is a strong vortex shed from the entrance and middle body leading bilge. This vortex becomes increasingly deep at the stern as heel is increased.

Force Measurements. The heeled hulls develop side-force and yawing moment at zero leeway. This is not surprising as the underwater part of a heeled hull is asymmetric. At small leeway angles, heel is associated with slightly reduced drag and reduced lift. At zero leeway, this lift force is in the opposite direction to that required to balance the heeling force. At large leeway angles, heel is associated with slightly increased drag and considerably increased lift, giving an improved lift/drag ratio. The hydrodynamic centre of effort moves forward with increasing heel. The trailing vortex becomes very weak with increasing heel and presumably causes a slight reduction to the vortex suction lift. However, the leading vortex becomes very strong with increasing heel and large vortex suction forces are expected on the hull bottom near the leading bilge; for the heeled hull there will be a (horizontal) lift component to this suction force:

it seems likely that this more than compensates for the reduction in vortex suction on the trailing side.

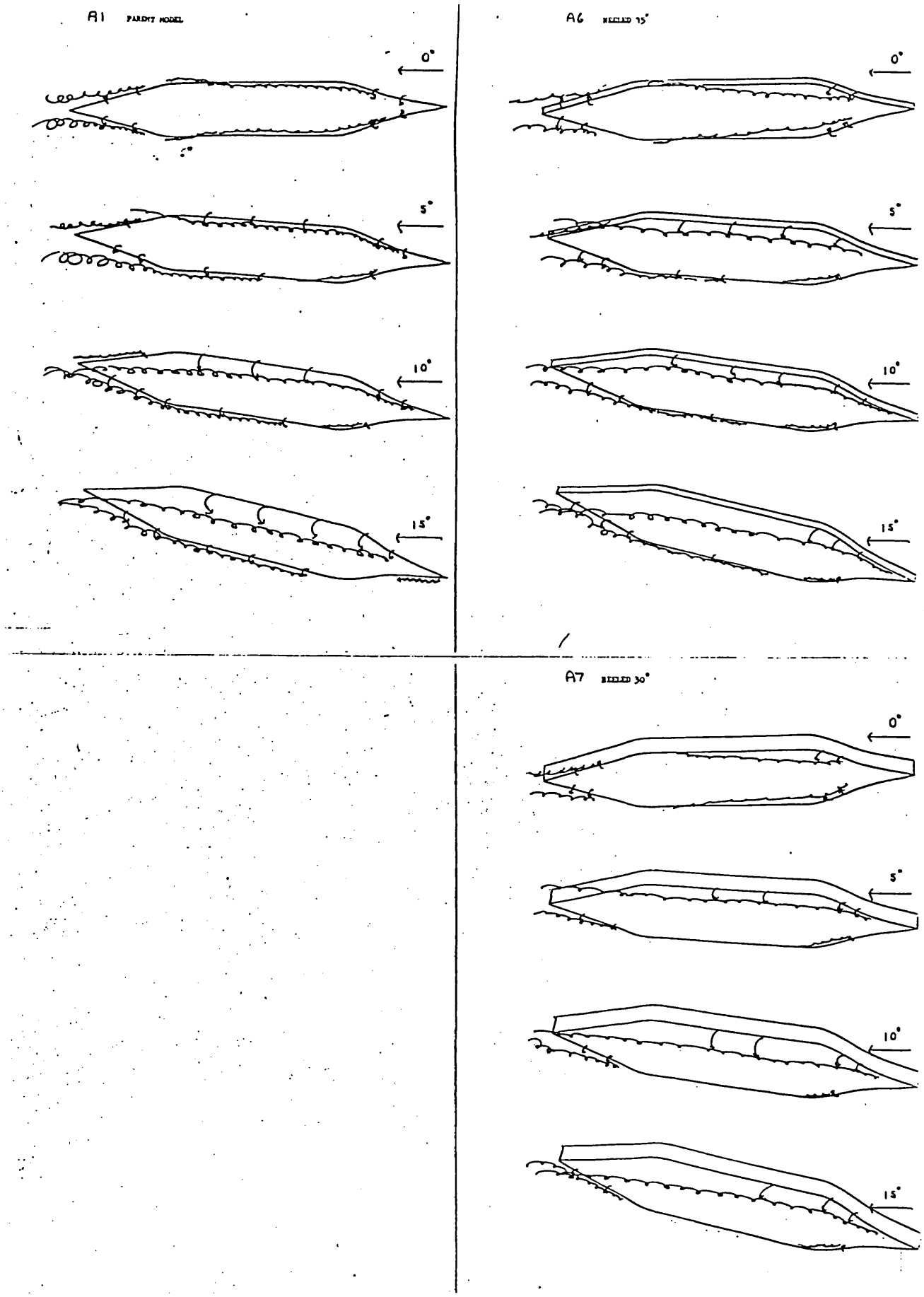

Figure 3.43

Influence of heel on vortex positions.

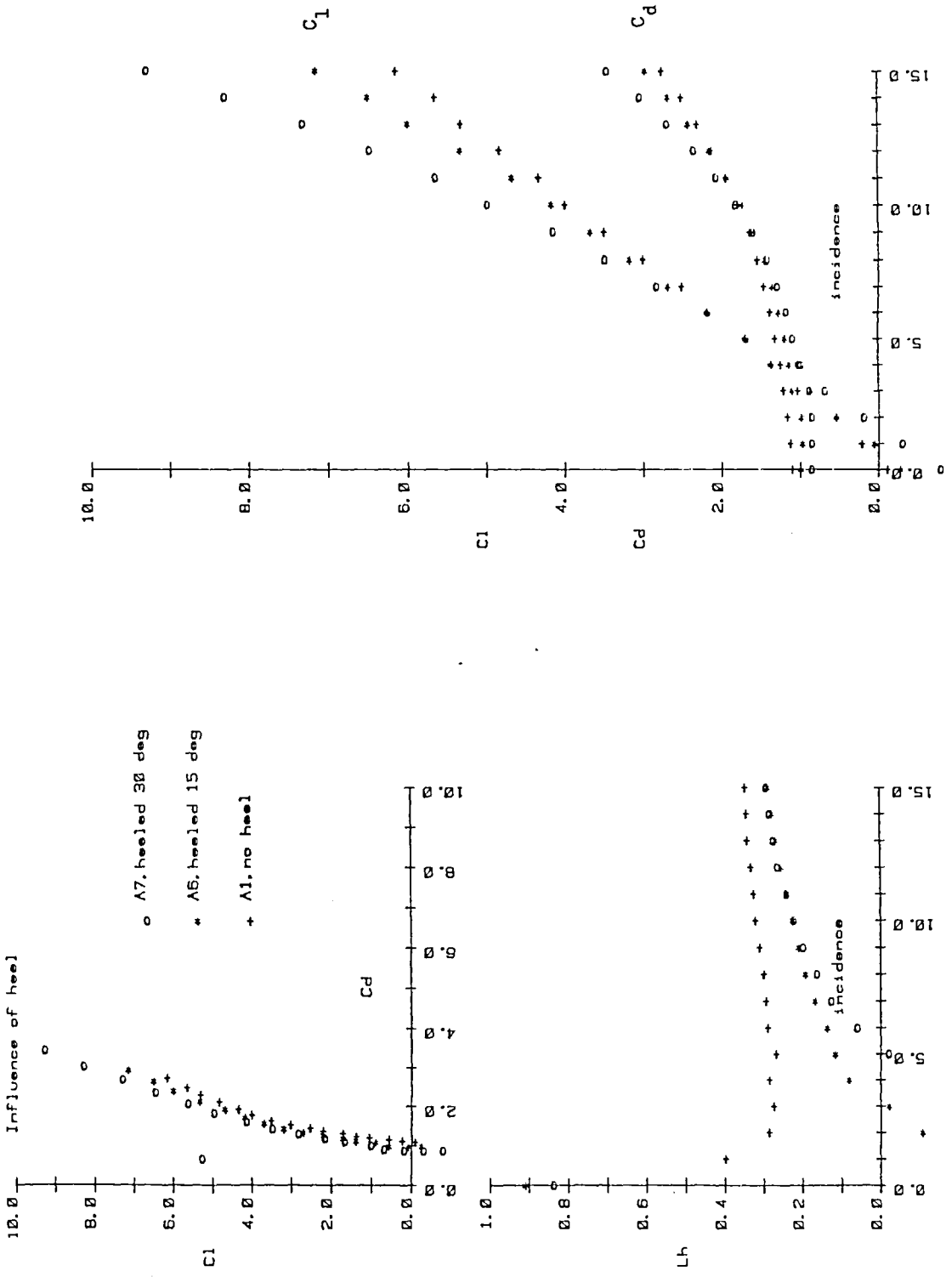

Figure 3.44

Influence of heel on forces

3.5 Conclusions

The underwater Mariner hull has a slender shape with small longitudinal curvature; nevertheless, oblique flow across the comparatively high transverse curvature at the bilges leads to some separation, even at zero leeway. This separation from the bilges produces longitudinal vortices which are convected along the hull and into the wake. At low angles of leeway the flow separates in passing from the sides to the bottom at the entrance, and in passing from the bottom to the sides at the run. At leeway asymmetric vortices associated with the cross flow become important; the flow separates on passing from the leading side to the bottom and on passing from the bottom to the trailing side. This asymmetric flow marginally modifies the symmetric flow at low incidence, but becomes dominant for much of the hull's length at large angles of leeway. The shed vortices maintain their identity at least for the length of the hull; there is, however, some merging of vorticity at the edges of proximate vortices.

The hull is a low aspect ratio lifting body which develops a maximum lift/drag ratio of nearly 3. Vortex suction on the trailing side of the hull contributes to the lift; this contribution is probably small, but no experiment has been conducted to confirm this.

The flow about a Mariner waterplane block has the same general characteristics although the vortices are stronger and greater forces are developed. The major difference is that for this block hull the position of separation is fixed at the sharp bilges.

The similarities between the flows justify the

use of simplified block models to investigate the general effects on the flow of variations in hull form. Conclusions drawn from the results of these experiments relate to the flow past the block hulls; it is likely, however, that general trends are repeated in flows past realistic hulls. Important conclusions of these systematic experiments are:

(1) Increased beam produces marginally increased lift at a considerably worsened maximum lift drag ratio;

(2) Increased draft (increased aspect ratio) increases lift and improves the maximum lift/drag ratio;

(3) Rounding the bilge of the model reduces the forces developed, but scarcely changes the maximum lift/drag ratio (this conclusion cannot be applied to full-scale hulls because of possible Reynolds number effects).

(4) Rounding the bows of the model increases the drag but scarcely affects the lift (this conclusion, again, cannot be applied to full-scale hulls due to Reynolds number effects).

(5) Trimming a hull by the head or the stern increases the strength of the entrance or run vortices; small changes in trim cause large changes in the position of the centre of pressure; increasing the trim by the stern increases the lift and improves the maximum lift/drag ratio.

(6) Heeling the hull increases the strength of the leading bilge vortex; the lift increases and the maximum lift/drag ratio is improved.

All the experimental techniques employed were found to be useful (in the sense that each contributed some information about the overall flow which was not supplied by any of the others). No serious unexpected experimental difficulties were encountered.

4 : A MATHEMATICAL MODEL OF THE FLOW PAST A BLOCK HULL AT LEEWAY

4.1 Introduction

An attempt is made to model the essential features of the flow past a block hull at leeway. An experimental investigation of this flow is described in Chapter 3. The predominant velocity field is a uniform flow nearly parallel to the ship's centre-line, which is perturbed as the hull has thickness and may be at an angle of leeway. An important feature of the flow is the longitudinal vortices trailing from the sharp bilges. There are rarely less than 4 such vortices detectable near a block hull.

When there is oblique flow across a sharp bilge the flow does not remain attached, but leaves the body approximately tangentially to one or other of the hull faces. A thin shear layer is formed between the flows from the two faces. The velocity is different on the two sides of the shear layer, but the pressure is continuous, and hence this thin shear layer has the characteristics of a vortex sheet. Such shear layers are unstable and tend to roll up to form the longitudinal vortices referred to. Diffusion of the bilge vortices is slow, and they appear to maintain their identity at least for flow distances of the order of the hull length. The effects of viscosity are small except near the body surface and near the centre of rolled up vortices, and this makes the flow amenable to inviscid flow modelling. In some circumstances the proximity of one of these bilge vortices to the hull produces a sufficiently adverse pressure gradient within the boundary layer on the surface beneath the vortex to cause secondary separation.

This occurs away from the bilge and a secondary vortex is formed by the rolling up of a shed shear layer.

The inviscid model used to investigate this flow is adapted from the line vortex models produced at O.N.E.R.A. and N.A.C.A. in the 1950s. Each rolled up vortex sheet is modelled as a single concentrated line vortex together with a force-carrying mathematical discontinuity in velocity potential connecting the line vortex to the bilge. The condition of continuous pressure is relaxed and replaced by the condition that the combined vortex-plus-cut sustains no net force. The slender body assumption is made which allows step-by-step streamwise solution of two-dimensional differential equations governing the evolution of the vortices. No attempt is made to model secondary vortices. However, additional vortices are allowed to form once previously attached vortices have ceased to gain in strength. This model is a very simplified model of a complicated flow; the flow could conceivably be modelled by more realistic vortex sheet models, but considerable computing resources would be required. Even this simplified model made sufficiently large demands to justify thrift in the use of resources: this is reflected as large time steps and comparatively loose convergence criteria in iterative schemes.

The model is used to predict the shedding and evolution of bilge vortices and to determine the associated surface pressure distributions and forces. The effects of varying incidence and beam are investigated. Comparisons are made with experimental results.

4.2 Review: slender-body line-vortex calculations

Jones (1946) noted that the slender body assumption made by Munk (1924) is applicable to low aspect ratio delta wings: that is, the streamwise derivative term $(1-M^2)\frac{\partial^2\varphi}{\partial z^2}$ can be neglected in the linearised potential equation

$$(1-M^2)\frac{\partial^2\varphi}{\partial z^2} + \frac{\partial^2\varphi}{\partial x^2} + \frac{\partial^2\varphi}{\partial y^2} = 0$$

which then reduces to the two-dimensional Laplace equation in the cross flow plane. He attempted to determine the lift of a delta wing by considering an inviscid flow with no separation at sharp leading edges.

Roy (1952) reported the results of a series of delta-wing flow-visualisation experiments conducted with the guidance of Legendre; the results showed the existence of twin vortices on the upper surface of delta-wings at incidence. He deduced that these arose from the rolling up of "cornet" vortex sheets shed from the leading edges because of the difference in velocity between fluid flowing from the upper and lower surfaces. He also noted evidence of weak secondary vortices at large angles of incidence.

Adams and Sears (1953) reported that Brown and Adams had considered flow separation from delta-wing leading-edges, and had modelled the rolled vortex sheets as a pair of line vortices near the wing's upper surface. The following month, Legendre (1952) published results of calculations made according to such a conical slender-body line-vortex model. In this model the line vortices were assumed to sustain no force (that is, they were convected

with the fluid); the potential field was continuous but multi-valued, and the law of conservation of circulation about a free vortex was violated. Adams (1953) noted that this was because the vortex feed-lines to the core had been ignored. He proposed a mathematical barrier (or "cut") to represent the vortex sheet; this could sustain a potential jump and render the potential field single valued. An unphysical consequence was that there was then a pressure difference across the barrier. It should be noted that this cut need not be straight, but could be the same shape as the true vortex sheet; however, since the correct boundary condition for a vortex sheet is not realised, this is of little consequence. Legendre (1953) incorporated this concept in a subsequent paper later that year. Edwards (1954) noted that there is no net force on the true vortex sheet system, and proposed that the assumption of no force on the vortex (made by Legendre and Adams) should be replaced by one of no net force on the combined barrier-plus-vortex system. Two months later, apparently unaware of Edward's proposal, Brown and Michael (1954) published the results of various calculations made with this assumption of zero total force on the vortex-plus-cut. Legendre (1966) defended the earlier French work and criticised the hypothesis adopted by Brown and Michael, commenting, "They were obliged to abandon the fundamental condition of equilibrium of forces for the vortex axis itself and their results are farther away from the experimental data.".

Brown and Michael (1954 and 1955) used this (zero force on vortex-plus-cut) method to determine the lift and pressure distribution on a delta wing at incidence. Even at subsonic speeds the actual flow is nearly conical away from the

trailing edge. By developing slender-body flow equations which were exactly conical, they were able to simplify the mathematics and obtain algebraic solutions. The method has subsequently been used for various flows including a number that are non-conical.

Smith (1957) applied the method to slender wings with curved leading edges; Squire (1966) considered wings with cross-sectional (conical) camber; and Portnoy and Russel (1971) considered wings with a small conical thickness distribution. Hanin and Mishne (1973) considered the rather different problem of a rolling wing; this flow is steady (in body axes), but non-conical. Barsby (1973) applied the method to delta wings at low angles of incidence; he noted the convergence of results predicted by line vortex and vortex sheet models at low incidence. Smith (1974) investigated the effects on the Brown and Michael model results of separation moving inboard of the leading edge. This occurs at very low angles of incidence. He found the effects to be small. Subsequently Clark, Smith and Thompson (1975) produced asymptotic algebraic solutions for various wings at low angles of incidence; the wings considered included several with thick cross-sections.

Time dependent flows have also been analysed: Randall (1966) and Lowson (1963) used the Brown and Michael model to investigate the aerodynamics of an oscillating slender wing; Dore (1964) used it to investigate the effects of step changes in flow conditions, such as meeting a sudden gust.

4.3(a) Model: mathematical statement of problem

A potential model is used which assumes that the only effect of viscosity on the hull flow is that thin vortex sheets can be shed at the bilges. Such sheets will tend to roll up, and are each modelled here as a concentrated line vortex together with a feeding sheet. A physical requirement of the problem is that the fluid pressure in the flow field is continuous. Brown and Michael (1954) show that for this type of model it is necessary to relax this continuous pressure condition, replacing it by the requirement that the integral of pressure about the assumed vortex system vanishes. In simpler terms, the assumed vortex system, consisting of a feeding sheet together with a longitudinal line-vortex, must have zero net force acting upon it, since only the body and not the fluid can sustain force.

Equation of Motion: a velocity potential function, φ, is sought, which represents a slightly perturbed main stream velocity; this must satisfy Laplace's equation (for incompressible flow):

$$\frac{\partial^2\varphi}{\partial x^2} + \frac{\partial^2\varphi}{\partial y^2} + \frac{\partial^2\varphi}{\partial z^2} = 0$$

Boundary conditions: this potential function must satisfy the following boundary conditions:-

(1) The body is solid, hence all normal velocities on the body surface are zero.

(2) The sea surface is level and flat, hence all normal velocities at the fluid surface are zero.

(3) The disturbance vanishes at infinity within the half space bounded by the free surface.

(4) The flow separates tangentially at the bilges. In this model this condition is replaced by the condition that infinite velocities do not occur at the bilges.

(5) The integral of pressure about each of the assumed vortex systems vanishes.

4.3(b) Model: slender body assumption

The flow is about a body which is slender and lying closely parallel to the z axis; this justifies making the slender body assumption that $\frac{\partial^2\varphi}{\partial z^2}$ is small compared with the other terms in the three-dimensional Laplace equation (this is the assumption made by Munk (1924)).

Equations of motion. With the slender body assumption, the equation of motion reduces to the two-dimensional Laplace equation in the cross-flow plane:

$$\frac{\partial^2\varphi}{\partial x^2} + \frac{\partial^2\varphi}{\partial y^2} = 0$$

together with the requirement that circulation is convected into each plane from its neighbouring upstream plane.

Boundary conditions: in the cross-flow plane represented in figure 4.1, these become:-

(1) On the body surface normal components of velocity are equal to normal components of the rate of change of body surface position. In the Z plane, on a hull with constant draft D and beam varying at rate $2\frac{dC}{dt}$ this velocity condition is:

$$\begin{aligned} V_z &= \frac{dC}{dt} + i f(Z) && R(Z) = C \\ &= -\frac{dC}{dt} + i f(-Z) && R(Z) = -C \\ &= f(Z) + i0 && \text{elsewhere} \end{aligned}$$

where f(Z) is an undetermined real function.

(2) At the sea surface, all normal velocity components are zero:

$$V_z = f(Z) + i0$$

where f(Z) is an undetermined real function.

(3) The disturbance vanishes at infinity:

$$\frac{dW}{dZ} \longrightarrow V_\infty \qquad \text{as} \qquad Z \longrightarrow \infty \qquad (\mathrm{Im}(Z) \geq 0)$$

(4) Velocities are not infinite at the bilges:

$$\frac{dW}{dZ} \not\longrightarrow \infty \qquad \text{as} \qquad Z \longrightarrow Z_e$$

where Z_e is the bilge.

(5) There is zero net force acting on each combined feeding sheet and longitudinal vortex. Figure 4.2 represents a thin cross-flow slice of the flow. The feeding sheet is assumed to be composed of filaments stretching from the bilge to the longitudinal vortex. An elemental slice of thickness Δq is considered. The force on the feeding filament is

$$F_f = -i\rho U \frac{dG}{dq} \Delta q (Z_o - Z_e)$$

The force on the line vortex is produced by a relative flow normal to the vortex of velocity V*. This force is

$$F_v = i\rho V^* G \Delta q$$

Setting the sum of these to zero gives:

$$U \frac{dG}{dq} (Z_o - Z_e) - V^* G = 0$$

Alternatively, writing $q = Ut$

$$(Z_o - Z_e) \frac{dG}{dt} - V^* G = 0$$

Now,

$$V^* = \left(\bar{V}_o - \frac{dZ_o}{dt} \right)$$

where $\overline{V}_o$ is the appropriate solution to the Laplace equation in the cross-flow plane given by

$$\overline{V}_o = u + iv = \lim_{z \to z_o} \left(\frac{dW}{dz} - \frac{iG}{2\pi(z - z_o)} \right)$$

By substitution, the zero force condition is

$$(z_o - z_e)\frac{dG}{dt} - G \lim_{z \to z_o} \overline{\left(\frac{dW}{dz} - \frac{iG}{2\pi(z - z_o)} \right)} + G\frac{dz_o}{dt} = 0$$

or

$$\frac{dz_o}{dt} = \lim_{z \to z_o} \overline{\left(\frac{dW}{dz} - \frac{iG}{2\pi(z - z_o)} \right)} - \frac{dG}{dt}\frac{(z_o - z_e)}{G}$$

4.3(c) Model: conformal transformation

It is not possible to simply write down a solution to this problem; however, it is possible to determine a solution by solving a simpler problem which can be mapped onto the given problem by a conformal transformation. A Schwarz Christoffel transformation (described below) provides a suitable mapping between a simple half plane and the physical cross-flow plane. The boundary conditions in the physical cross-flow plane are transformed to give corresponding, but simpler, boundary conditions in the mathematical half plane. A potential function is determined which is a solution to Laplace's equation and satisfies the transformed boundary conditions in this half plane. It is noted that this potential function, on transformation, is also a solution to Laplace's equation in the cross-flow plane (this is because any analytic complex function satisfies Laplace's equation in the S plane; and if there is a conformal transformation between the S plane and the Z plane, then $W(S(Z))$ is also analytic; and hence W(Z) satisfies Laplace's equation in the Z plane). The transformed potential function satisfies the boundary conditions in the cross-flow plane as the corresponding boundary conditions are satisfied in the simple half plane.

Figure 4.1 represents the physical cross flow plane (Z plane) and the simple half plane (S plane). The Schwarz Christoffel transformation between these two infinite half planes is

$$\frac{dS}{dZ} = K \sqrt{\frac{S^2 - b^2}{S^2 - a^2}}$$

On integration, this gives

$$KZ = \int_0^S \sqrt{\frac{S^2 - a^2}{S^2 - b^2}}\, dS + L$$

The constants K and L are determined by requiring that (1) transformed positions are identical at infinity, and (2) the point Z=iD is transformed onto the point S=0. Hence, the transformation function between the planes is

$$Z = \int_0^S \sqrt{\frac{S^2 - a^2}{S^2 - b^2}}\, dS + iD$$

This equation can be evaluated numerically. An iterative procedure can be used to determine the parameters a and b corresponding to desired values of the beam (2C) and draft (D).

The corresponding transformed boundary conditions in the simple half plane are:-

(1) Body surface condition. On the real, x, axis:

$$V_S = V_Z \frac{dZ}{dS} = \left(\frac{dC}{dt} + if(x)\right)\frac{dZ}{dS} \qquad a < x < b$$

$$= \left(-\frac{dC}{dt} + if(-x)\right)\frac{dZ}{dS} \qquad -a > x > -b$$

$$= g(x) + i0 \qquad \text{elsewhere}$$

where $f(x)$ and $g(x)$ are undetermined real functions.

(2) Flat sea condition. On the real, x, axis:

$$V_S = V_Z \frac{dZ}{dS} = g(x) + i0 \qquad |x| > |b|$$

where is an undetermined real function.

(3) Condition at infinity. Noting that

$$\frac{dZ}{dS} \longrightarrow 1 \qquad \text{and} \qquad S \longrightarrow \infty \qquad \text{as} \qquad Z \longrightarrow \infty$$

then,

$$\frac{dW}{d\zeta} = \frac{dW}{dz}\frac{dz}{d\zeta} \longrightarrow 0 \qquad \text{as} \qquad \zeta \longrightarrow \infty$$

(4) Condition at the bilges. Noting that

$$\frac{dW}{dz} = \frac{dW}{d\zeta}\frac{d\zeta}{dz}$$

and

$$\frac{d\zeta}{dz} \longrightarrow \infty \qquad \text{as} \qquad \zeta \longrightarrow \zeta_e$$

where ζ_e is the transformed bilge, then this condition becomes

$$\frac{dW}{d\zeta} \longrightarrow 0 \qquad \text{as} \qquad \zeta \longrightarrow \zeta_e$$

(5) Zero force condition. The hull shape varies along the streamwise axis. It is therefore necessary for the transformation function to be a function of streamwise position as well as of position in the S plane: that is

$$z = z(\zeta, t)$$

which implies

$$\delta z = \frac{\partial z}{\partial \zeta}\delta\zeta + \frac{\partial z}{\partial t}\delta t$$

Less generally,

$$\frac{dz}{dt} = \frac{\partial z}{\partial \zeta}\frac{d\zeta}{dt} + \frac{\partial z}{\partial t}$$

which can be rearranged as

$$\frac{d\zeta}{dt} = \left(\frac{dz}{dt} - \frac{\partial z}{\partial t}\right)\frac{\partial \zeta}{\partial z}$$

from which it follows that the zero force condition for each vortex system becomes:

$$\frac{d\zeta_o}{dt} = \frac{\partial \zeta}{\partial z}\left(\lim_{z \to z_o}\left(\frac{dW}{dz} - \frac{i\Gamma}{2\pi(z-z_o)}\right) - \frac{d\Gamma}{dt}\frac{(z_o - z_e)}{\Gamma} - \left.\frac{\partial z}{\partial t}\right|_{\zeta_o}\right)$$

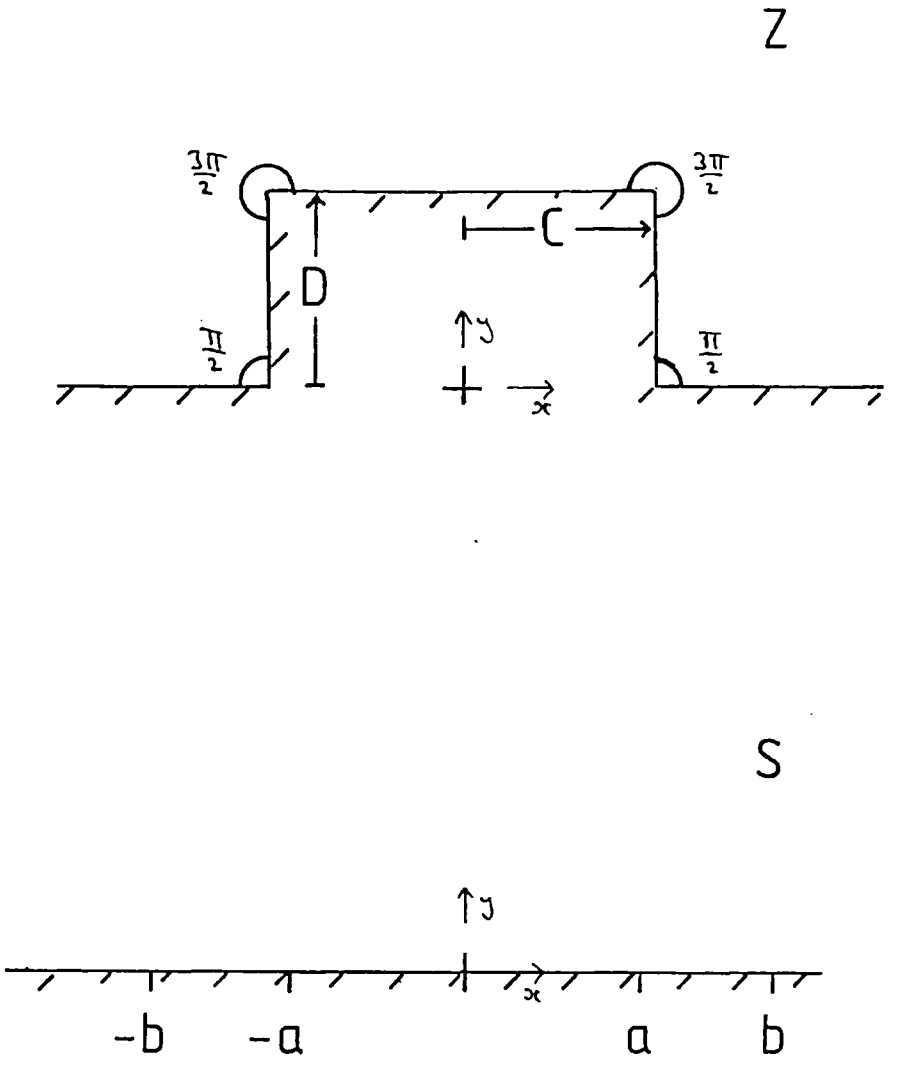

Figure 4.1

Hull cross-flow planes: physical plane (top)and

simplified half plane (bottom)

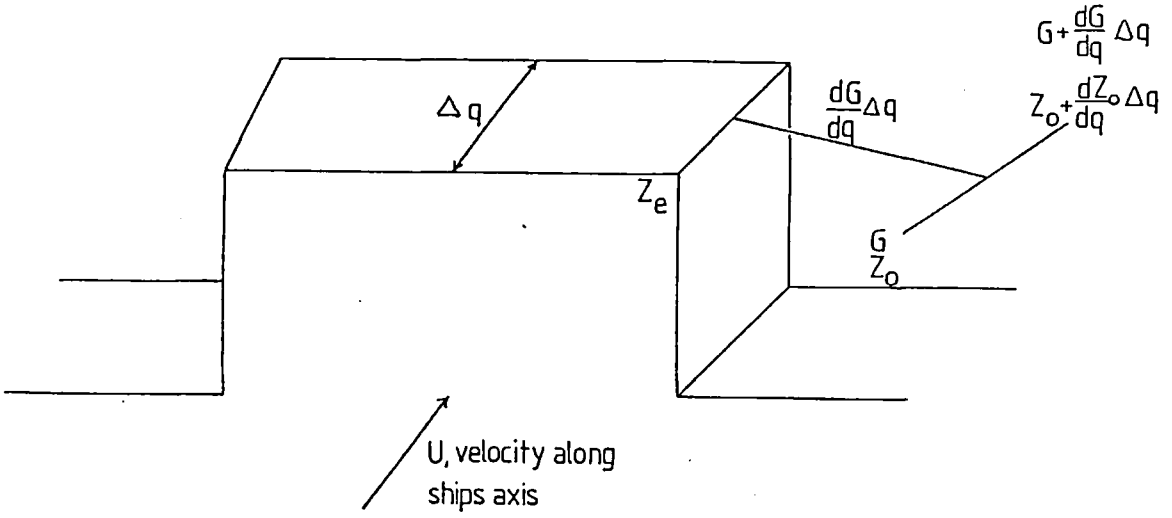

Figure 4.2

Incremental slice of hull flow showing a section of the longitudinal vortex G at Z_o and a concentrated vortex feedline $\frac{dG}{dq}\Delta q$ from the bilge to the longitudinal vortex.

4.3(d) Model: potential solution

The conformal transformation described in the last section maps the flow boundaries (both sea surface and hull surface) onto the y = 0 boundary of an infinite half plane. This is exploited by seeking a potential solution in a full plane which is symmetric about the y = 0 axis and satisfies the conditions of the transformed plane boundary on this axis. It is attempted to solve the problem with a potential function of the form:

$$W(\zeta) = V\zeta + \sum_{j=1,m} \frac{iC_j}{2\pi} \ln\left(\frac{\zeta - \zeta_{oj}}{\zeta - \bar{\zeta}_{oj}}\right) + \int_{-\infty}^{\infty} \frac{m(x)}{2\pi} \ln(\zeta - x)\, dx$$

where the first term on the right is the potential describing uniform cross flow velocity parallel to the x axis. The second term is the potential describing the flow associated with point vortices C_j at ζ_{oj} together with symmetrically placed images at $\bar{\zeta}_{oj}$. These point vortices are convected downstream through successive cross-flow planes and represent the concentrated line vortices. The third term is the potential associated with a source distribution on the x axis; this provides the non-zero normal velocities on the flow boundary and represents instantaneous rates of change of the hull cross section moving downstream with the flow. The potential function $W(\zeta)$ satisfies Laplace's equation as it is analytic in ζ. The complete solution is determined by the following boundary conditions:-

(1 & 2) Flow surface (y=0) conditions. These conditions concern the imaginary part of the velocity on the x axis. Due to the symmetric disposition about the x axis of each

vortex and its image, only the line source term of the potential function can contribute to this component of the velocity field. It is noted that a line source distribution m(x) on the x axis is associated with a boundary velocity

$$V = h(x) - \frac{i\, m(x)}{2}$$

where h(x) is an undetermined real function. Comparison of the imaginary part of this velocity and the specified boundary velocity shows the required source distribution to be

$$\begin{aligned} m(x) &= \frac{-2}{i}\frac{dC}{dt}\frac{dZ}{dS} && a < x < b \\ &= \frac{2}{i}\frac{dC}{dt}\frac{dZ}{dS} && -a > x > -b \\ &= 0 && \text{elsewhere} \end{aligned}$$

Hence, the source-distribution term of the potential function is

$$W_p = \frac{1}{2\pi}\int_{-b}^{-a} \frac{2}{i}\frac{dC}{dt}\frac{dZ}{dS}(x^*)\, \ln(S - x^*)\, dx^* + \frac{1}{2\pi}\int_{a}^{b} \frac{-2}{i}\frac{dC}{dt}\frac{dZ}{dS}(x)\, \ln(S - x)\, dx$$

which simplifies to

$$W_p = \frac{i}{\pi}\int_{a}^{b} \frac{dC}{dt}\sqrt{\frac{x^2 - a^2}{x^2 - b^2}}\, \ln(S^2 - x^2)\, dx$$

(3) Condition at infinity. This condition is satisfied, provided the singularities are finite and are concentrated in a finite region of the S plane.

(4) Condition at the bilges. After differentiating the potential function, this boundary condition is that

$$V + \sum_{j=1,m} \frac{iC_j}{2\pi}\left(\frac{1}{\zeta_{ek}-\zeta_{oj}} - \frac{1}{\zeta_{ek}-\bar{\zeta}_{oj}}\right) + \frac{2\zeta_{ek}\, i}{\pi}\frac{dC}{dt}\int_a^b \sqrt{\frac{x^2-a^2}{x^2-b^2}}\,\frac{dx}{(\zeta_{ek}^2-x^2)} = 0$$

at the two bilges ζ_{e1} and ζ_{e2}. Writing, for convenience

$$x_{jk} = \frac{i}{\pi}\left(\frac{1}{\zeta_{ek}-\zeta_{oj}} - \frac{1}{\zeta_{ek}-\bar{\zeta}_{oj}}\right)$$

and

$$y_k = -V - \sum_{j=1,m} \frac{iC_j}{2\pi}\left(\frac{1}{\zeta_{ek}-\zeta_{oj}} - \frac{1}{\zeta_{ek}-\bar{\zeta}_{oj}}\right) - \frac{2\zeta_{ek}\, i}{\pi}\frac{dC}{dt}\int_a^b \sqrt{\frac{x^2-a^2}{x^2-b^2}}\,\frac{dx}{(\zeta_{ek}^2-x^2)}$$

then rearranging, the conditions at the two bilges imply

$$C_1 = \frac{x_{22}\,y_1 - x_{21}\,y_2}{x_{22}\,x_{11} - x_{21}\,x_{12}}$$

and

$$C_2 = \frac{x_{12}\,y_1 - x_{11}\,y_2}{x_{12}\,x_{21} - x_{11}\,x_{22}}$$

5) <u>Zero force condition</u>. Writing, for convenience,

$$V_{ok} = \lim_{z \to z_{ok}} \left(\frac{dW}{dz} - \frac{iC_k}{2\pi(z-z_{ok})}\right)$$

noting that

$$\frac{dW}{dz} = \frac{dW}{d\zeta}\frac{d\zeta}{dz} = \frac{dW}{d\zeta}\sqrt{\frac{\zeta^2-b^2}{\zeta^2-a^2}}$$

and

$$\frac{dW}{d\zeta} = V + \sum_{j=1,m} \frac{iC_j}{2\pi}\left(\frac{1}{\zeta-\zeta_{oj}} - \frac{1}{\zeta-\bar{\zeta}_{oj}}\right) + \int_a^b \frac{2i\zeta}{\pi}\frac{dC}{dt}\sqrt{\frac{x^2-a^2}{x^2-b^2}}\,\frac{dx}{(\zeta^2-x^2)}$$

and using the result given in appendix A4.2(a)

$$V_{ok} = \text{conj}\left(\frac{\partial S}{\partial Z}\left(V + \frac{2S_{ek}\,i}{\pi}\frac{dC}{dt}\int_a^b \sqrt{\frac{x^2-a^2}{x^2-b^2}}\,\frac{dx}{S^2-x^2}\right.\right.$$

$$\left.\left. + \sum_{\substack{j=1,m \\ j\neq k}} \frac{i\Gamma_j}{2\pi}\left(\frac{1}{S_{ok}-S_j} - \frac{1}{S_{ok}-\bar{S}_j}\right) + \frac{i\Gamma_k}{2\pi}\left(\frac{S_{ok}}{2}\left(\frac{1}{S_{ok}^2-b^2} - \frac{1}{S_{ok}^2-a^2}\right) - \frac{1}{S_{ok}-\bar{S}_k}\right)\right)\right)$$

The zero force condition on each vortex, Γ_k , can then be written

$$\frac{dS_{ok}}{dt} = \frac{\partial S}{\partial Z}\left(V_{ok} - \frac{d\Gamma_k}{dt}\frac{(Z_{ok}-Z_{ek})}{\Gamma_k} - \left.\frac{\partial Z}{\partial t}\right|_{S_{ok}}\right)$$

4.3(e) Model: solution procedure

The vortex evolutions are determined by a streamwise marching calculation. Differentials of the vortex positions and strengths are determined from each cross flow plane solution. Integration, assuming linear plane-by-plane increments, determines position and strength of each vortex at any plane downstream from the bows.

An iterative procedure is used to determine a solution in each cross flow plane which may contain several shed vortices in addition to the two being fed by sheets from the bilges. It was found that the procedure of simply looping through the zero-force-condition equations and the bilge-condition equations is convergent; this loop is repeated until the differences between successive values of differential quantities are considered acceptably small; this procedure produces values of $\frac{d\zeta_o}{dt}$ (for all vortices) and $\frac{dG}{dt}$ (for the two growing vortices) corresponding to previously calculated values of ζ_o and G.

This procedure can not deal with the inception of new vortices and a starting solution is required to give the values of vortex positions (ζ_{ok}) and strengths (C_k) and initial estimates of $\frac{d\zeta_{ok}}{dt}$ and $\frac{dG_k}{dt}$ in the first plane; in subsequent planes the vortex characteristics and initial estimates of differential quantities are provided by the calculations conducted in the previous plane. The iterative procedure is then conducted to determine the differentials of vortex strengths and positions. The magnitudes of these quantities are determined by a linear downstream marching incrementation:

$$\Gamma_{new} = \Gamma_{old} + \frac{d\Gamma}{dt}\Delta t$$

and

$$S_{new} = S_{old} + \frac{dS}{dt}\Delta t$$

These differential quantities are also used as initial estimates for the iterative procedure in the subsequent plane.

Bow conditions. At the foremost part, a block hull is thin, and a single vortex may be formed if the hull is at leeway. Shortly aft, thickness becomes important, and vortices are formed near both bilges. Details of this bow flow are obscure and difficult to model. However, it seems likely that slightly modified bow conditions will have little effect on the overall hull flow characteristics. For the calculations described in this chapter, an unphysical bow flow is assumed: the bow is allowed to start abruptly with finite thickness, but the slender body assumption is still applied, although this must be locally violated.

The slender body marching calculation requires a starting solution. The starting solutions used are adapted from analysis by Graham (1977); these are local right-angle-wedge solutions which can be embedded into the flow according to the similarity theory of Maskell (1960). These starting solutions are used at the bows and also for the initial growth of new vortices formed after existing vortices have been shed (in this discussion vortices are said to be "shed" when they cease to be fed by a vortex sheet from the bilge). The starting solutions are discussed in appendix A4.1.

Vortex shedding. Graham (1977) discusses several

criteria for vortex shedding. The first suggested criterion is that shedding should occur when a vortex ceases to grow. This is the criterion used here. It avoids vorticity being "sucked" back along the feed sheet from a vortex; such behaviour is mathematically feasible but physically unrealistic. At each plane, the sign of each vortex and the sign of its rate of growth are compared; if they are not the same, the vortex is shed and a new vortex is allowed to form. Other possible criteria suggested by Graham, which are not used here, are the occurrence of minimum values of vortex growth rate and sudden changes in the flow direction near the bilge.

Merging of vortex pairs. A number of unphysical modelled flow traits are discussed in section 4.4(c). One particular problem concerns strong artificial vortex pairs. The expedient described below is adopted in the example calculations to prevent these strong vortex pairs from looping back near to the hull where they could have major unrealistic effects. This expedient is that vortices are arbitrarily merged if their mutual separation is less than 1/10 of their distance from the hull (this rule is not applied to vortex-plus-image pairs). The two vortices are replaced by a single vortex having their combined total strength, and located at their centroid if they are of the same sign, or (arbitrarily) at the position of the stronger existing vortex if they are not.

4.3(f) Model: calculation of lift

The calculated flow field can be used to determine the surface pressure distribution on the body and this can be integrated to give the total (horizontal) lift force. The lift force developed forward of any cross-flow plane can alternatively be determined by calculating the total flux of horizontal cross-flow momentum at this plane. The first (pressure) method is used, however, as a map of the pressure distribution in each cross flow plane gives more information on how this lift is generated than is available from the second (momentum) method.

At any point in the three dimensional flow field the total velocity vector ($\underline{V}_T$) can be considered as the sum of two vector parts, the velocity vector at infinity (the "free stream velocity", $\underline{V}_S$) and the difference between the total velocity vector and this free stream velocity vector (the "perturbation velocity", $\underline{V}_P$). Each of these parts can be resolved into two components, a component parallel to the ship's axis (subscript z) and a component in the cross flow plane (subscript c). These velocity components are indicated in the first sketch of figure 4.3.

Bernoulli's theorem is applied along a streamline from infinity to a point near the body:

$$\frac{2}{\rho} p_\infty + \underline{V}_S \cdot \underline{V}_S = \frac{2}{\rho} p + \underline{V}_T \cdot \underline{V}_T$$

which implies

$$C_p = \frac{2(p - p_\infty)}{\rho \, \underline{V}_S \cdot \underline{V}_S}$$

$$= \frac{1}{\underline{V}_S \cdot \underline{V}_S} \left\{ -2 \underline{V}_{SZ} \cdot \underline{V}_P - (\underline{V}_{SC} + \underline{V}_P) \cdot (\underline{V}_{SC} + \underline{V}_P) + \underline{V}_{SC} \cdot \underline{V}_{SC} \right\}$$

noting that

$$\frac{dW}{dz} = \underline{v}_{sc} + \underline{v}_{pc}$$

and making the slender body assumptions that

$$\underline{v}_{pz} \ll \frac{dW}{dz} \ll \underline{v}_{sz}$$

the pressure coefficient equation reduces to

$$C_p = \frac{-2v_{pz}\cos\lambda}{V_s} - \frac{1}{V_s^2}\frac{dW}{dz}\overline{\frac{dW}{dz}} + \sin^2\lambda$$

Smith (1980) comments that the form of this equation indicates a departure from two-dimensionality of the slender body model: the first term on the right represents a linear thin wing approximation for C_p, while the subsequent terms represent the contribution from the cross flow.

The changing strength of the vortices, while they continue to be fed by sheets from the bilges, is associated with a vortex sheet on the surface of the hull. This situation is schematically indicated in the second sketch of figure 4.3. A vortex sheet strength k_i can be determined by assuming that the surface vorticity $\partial\Gamma_i/\partial z$ lies across the stream:

$$k_i = \frac{\partial\Gamma_i}{\partial z} = \frac{\partial\Gamma_i}{v_{sz}\,\partial t}$$

To evaluate the "thin wing" contribution to the lift, a further assumption is made. This thin wing approximation is that the two surface vortex sheets are modelled as a single vortex sheet at the hull's plane of symmetry and

that the required longitudinal velocity components are evaluated at either side of this sheet. This model is indicated as the third sketch of figure 4.3. The difference in axial perturbation velocity components is

$$v_{p2}^{+} - v_{p2}^{-} = k_1 + k_2 = \frac{1}{V_{s2}} \frac{d}{dt}(\Gamma_1 + \Gamma_2)$$

where Γ_1 and Γ_2 are the strengths of the growing leading and trailing vortices. The non-dimensional lift-force/unit-area, P_{co}, is:

$$p_{co} = -(c_p^{+} - c_p^{-})$$

so, on substitution,

$$p_{co} = \frac{1}{V_s^2}\left(2\frac{d\Gamma_{total}}{dt} + \left(\frac{dw}{ds}\overline{\frac{dw}{ds}}\Big|_{s} - \frac{dw}{ds}\overline{\frac{dw}{ds}}\Big|_{-s} \right) \frac{dz}{dz}\overline{\frac{dz}{dz}} \right)$$

The first term is the linear thin wing lift contribution; this is associated with reduced longitudinal velocity on one side of the hull and increased longitudinal velocity on the other. The subsequent terms represent the cross flow pressure contributions on the trailing and leading sides respectively. The total lift coefficient is obtained by integrating P_{co} over the hull's length and draft. The value of C_1 obtained is non-dimensionalised by a reference area of (draft)^2 whereas a reference area of (length)$^2 \rho_H / \rho_A$ is used in Chapters 3 and 7. Using the latter reference area, the thin wing lift component is approximately $4.25\Gamma_{total}$.

Schematic reflex hull indicating velocity vectors

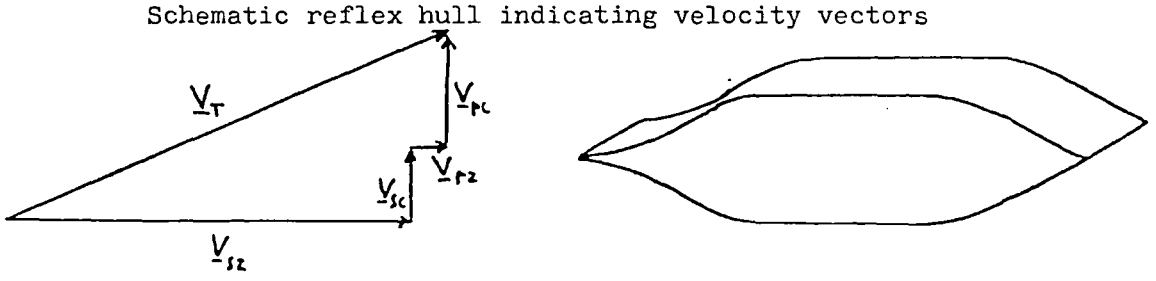

Schematic reflex hull indicating vortex sheet

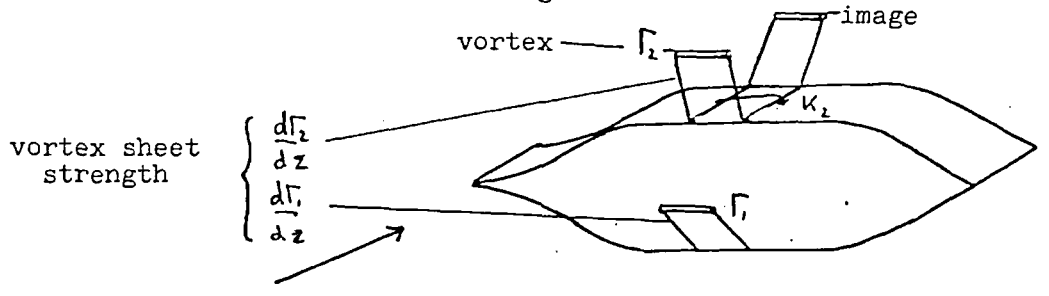

Schematic representation of thin wing approximation to reflex hull

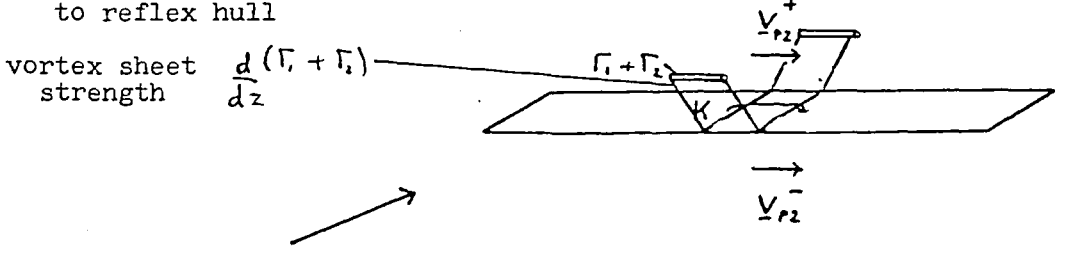

FIGURE 4.3

THIN WING HULL REPRESENTATION

4.4(a) Results: example calculations

Example calculations have been conducted for block hulls similar to the block hulls tested in Chapter 3. The shape is the same, except near the bow, where it has been modified slightly, as described in section 4.3(e).

Figures 4.4 to 4.7 show calculated flow past parent-form block hulls at a range of leeway angles (the flow is from right to left). The composition of these diagrams is described in this paragraph and annotated on figure 4.5. The bottom figure represents the vortex paths past the hull. This figure is produced by drawing a succession of cross flow planes - each showing the hull section outline and the vortex positions - so that the lines indicating the hull bottom map out the hull plan at the appropriate angle of leeway. The vortices are indicated as small circles with diameter proportional to the vortex strengths; the two attached vortices are indicated by lines from the bilges representing the mathematical feedlines. The middle figure shows some of these cross flow planes to help clarify the flow features; the vortex directions-of-rotation are indicated by the curved arrows. The top figure indicates how the (horizontal) lift is distributed along the hull. This figure consists of a series of hull cross sections laid out as before. The direction and relative magnitude of the "thin wing" lift component is indicated by the single line issuing from the hull-section's line of symmetry. The direction and relative magnitude of the "cross-flow" lift component is indicated by the set of lines with their zero at a distance of one draft off the hull's sides.

Figures 4.8 to 4.10 show how the calculated vortex

evolutions vary with leeway for hulls of three different beams. Figure 4.11 (which is also figure 3.28) shows the approximate vortex paths determined in the wind tunnel tests of block hulls; these are at various leeway angles and for various beams. Figure 4.12 reproduces the corresponding calculated results for easy comparison.

Figure 4.13 shows how the "thin wing" component lift coefficients and total lift coefficients vary with leeway angle. Table 4.1 lists the results of calculations made for hulls with various beams.

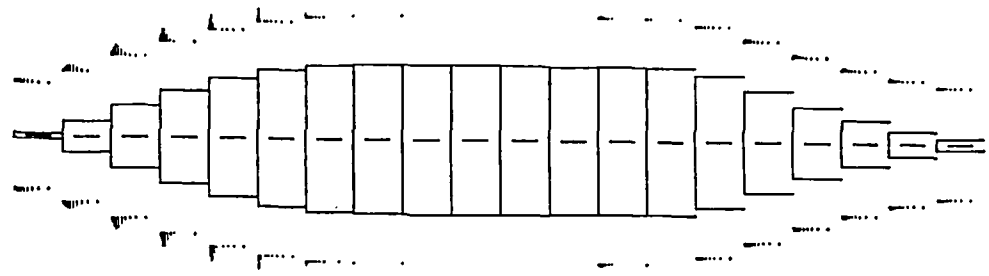

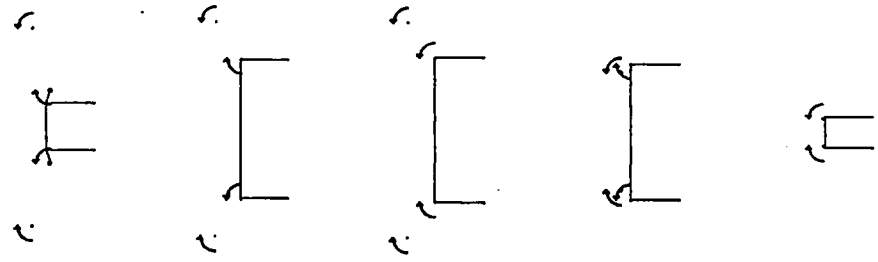

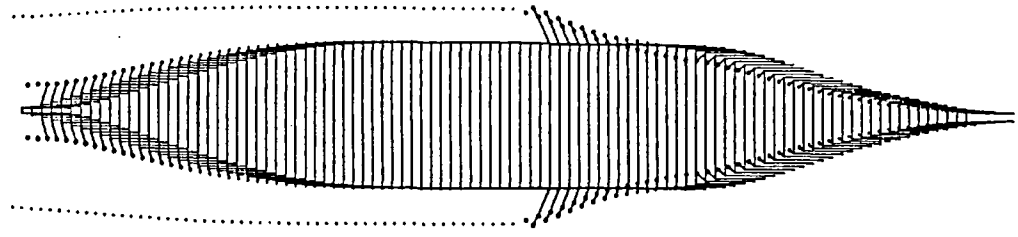

Figure 4.4

VORTEX POSITIONS AND PRESSURE DISTRIBUTION: 0° LEEWAY.

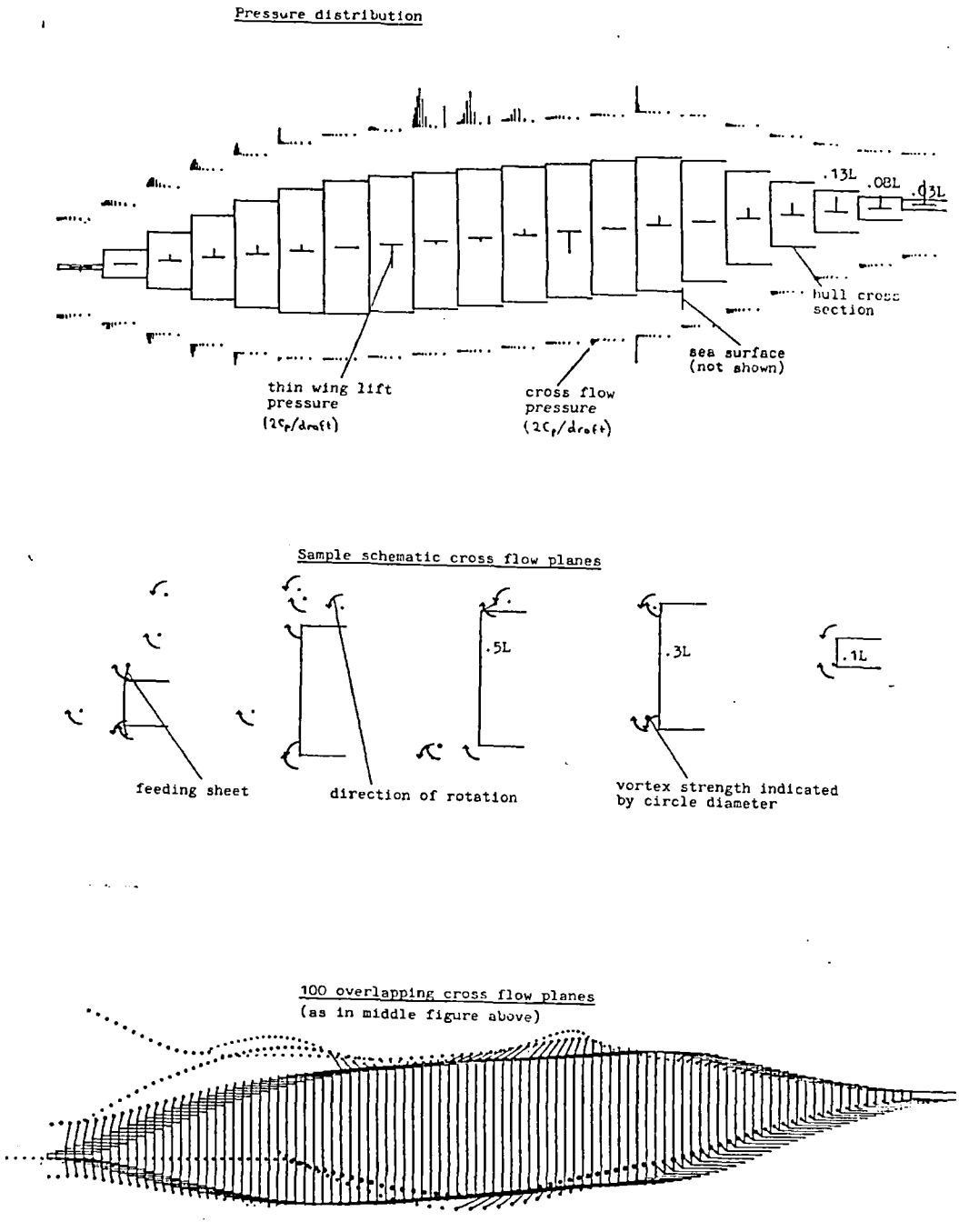

Figure 4.5

Vortex positions and pressure distribution: 5^{o} leeway

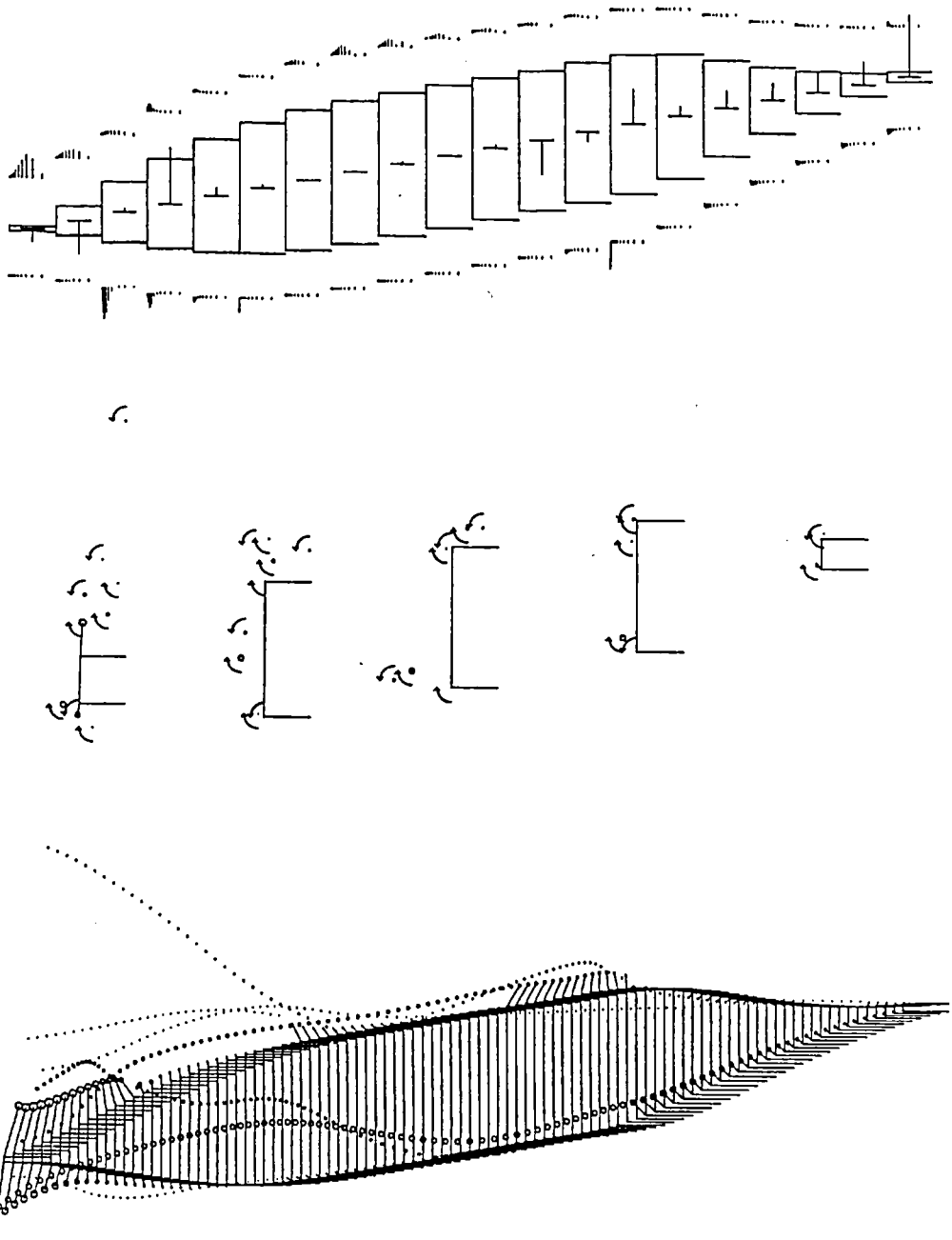

Figure 4.6

VORTEX POSITIONS AND PRESSURE DISTRIBUTION: 10° LEEWAY.

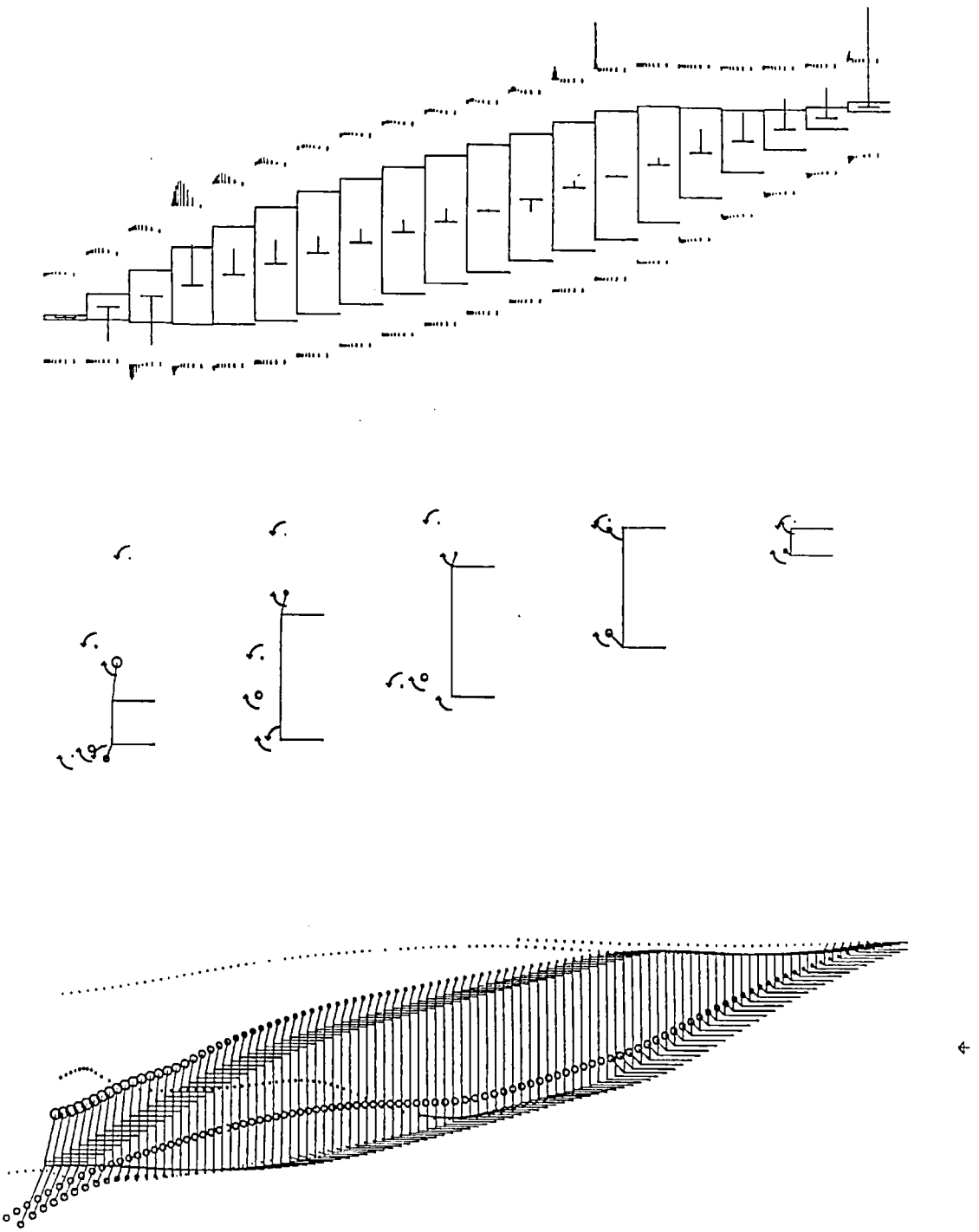

Figure 4.7

VORTEX POSITIONS AND PRESSURE DISTRIBUTION: 15° LEEWAY

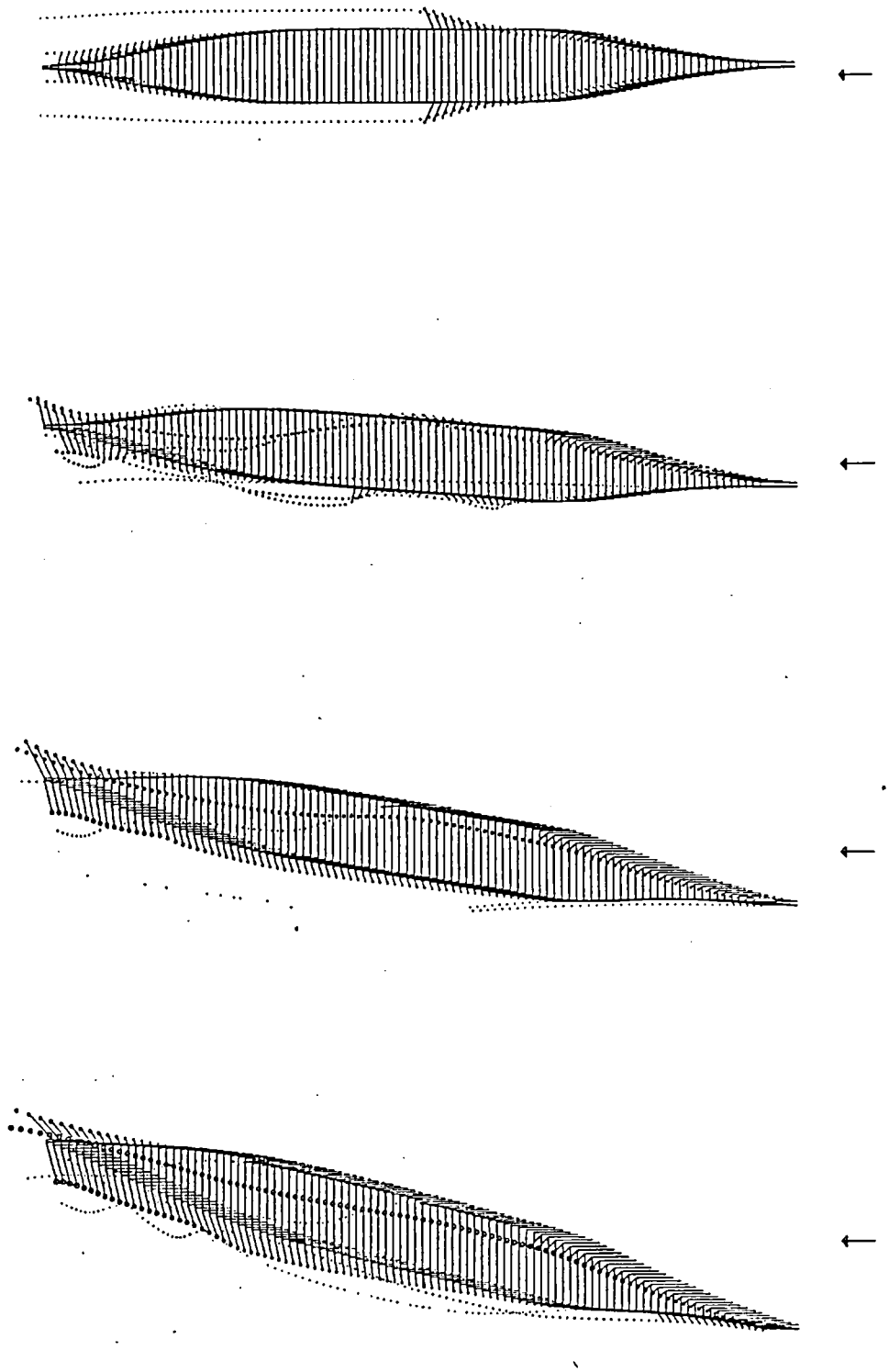

Figure 4.8

Calculated vortex positions: narrow beam

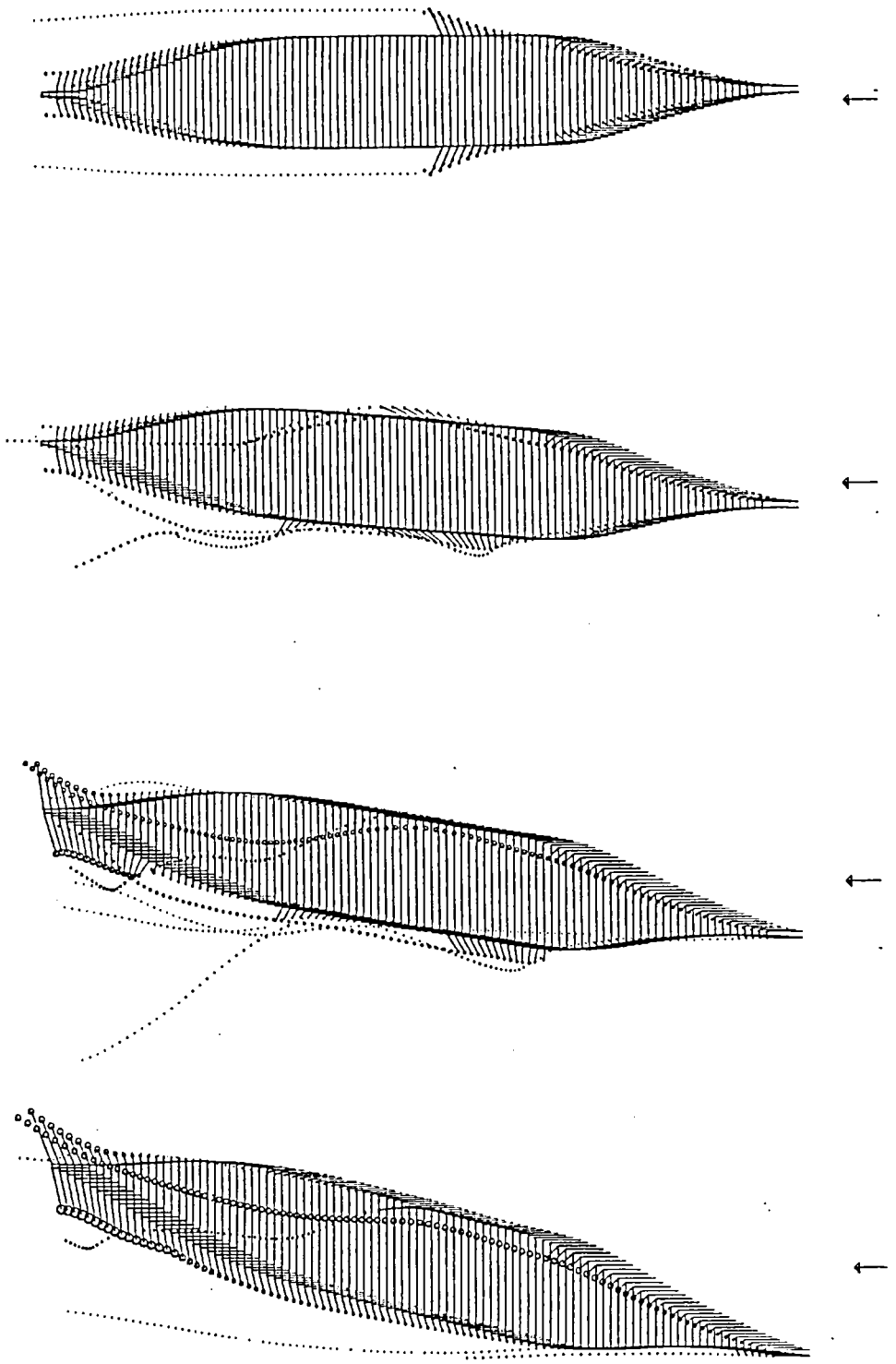

Figure 4.9

Calculated vortex positions: parent model

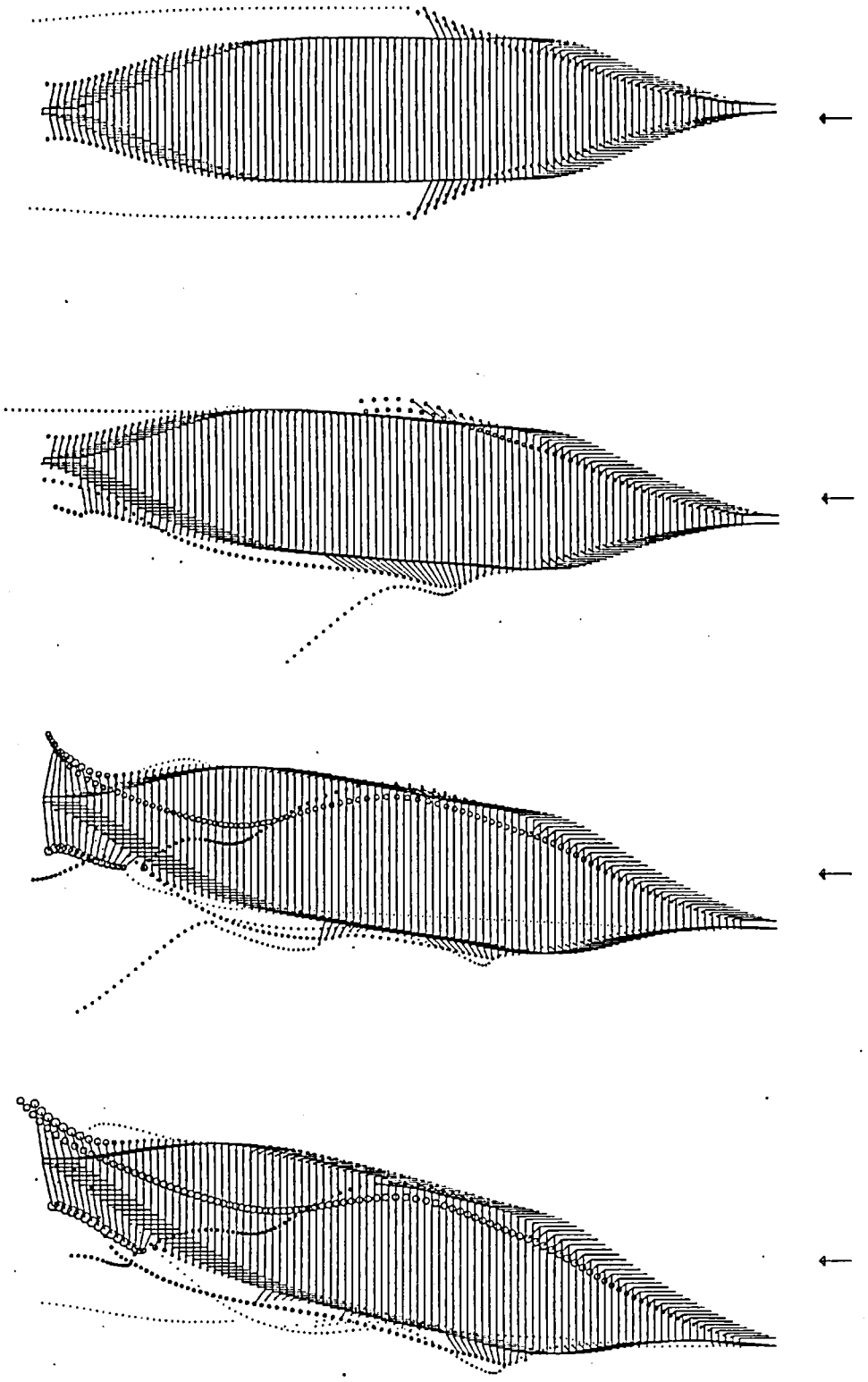

Figure 4.10

Calculated vortex positions: wide beam

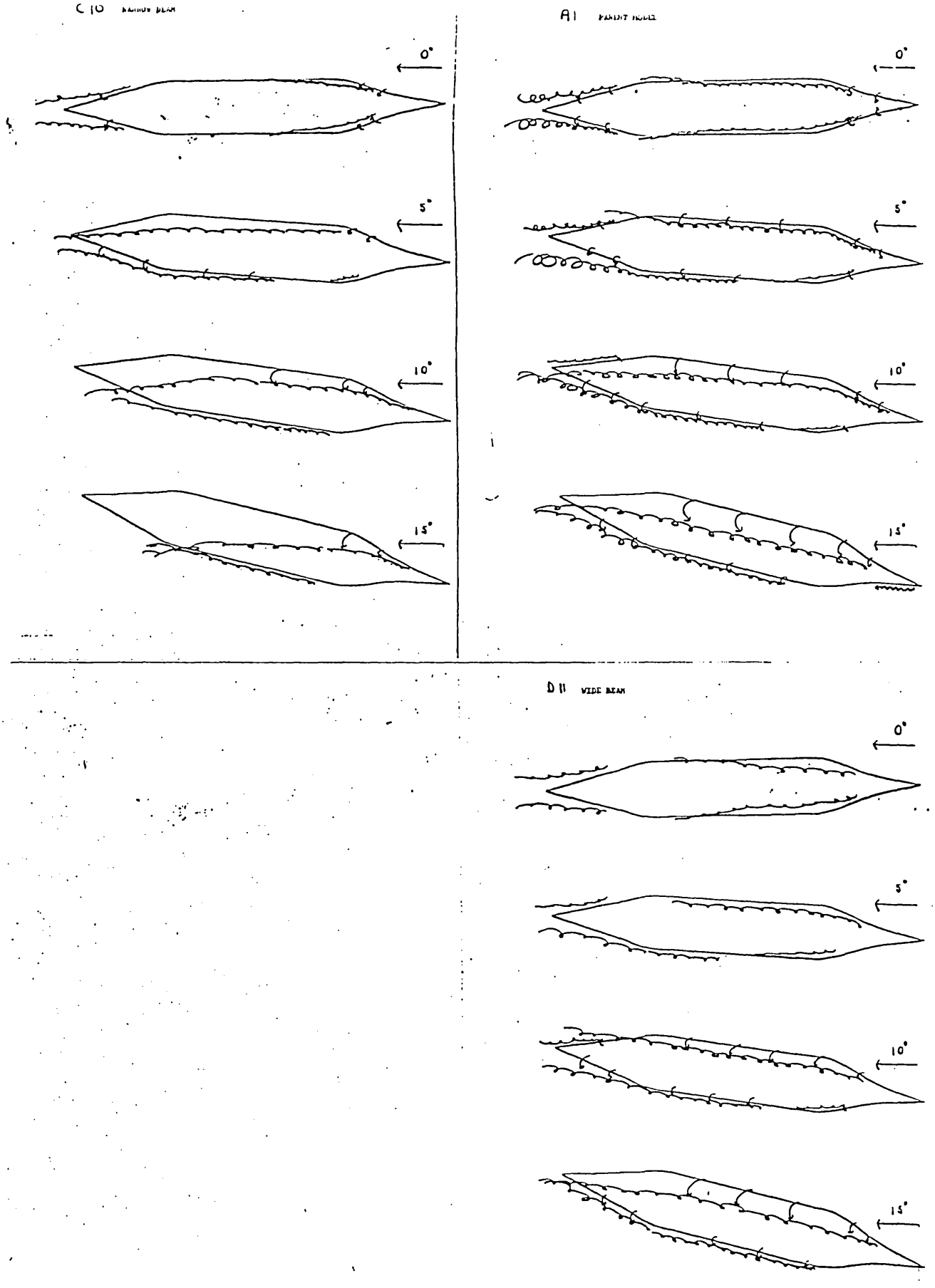

Figure 4.11

Influence of beam on vortex positions - experimental

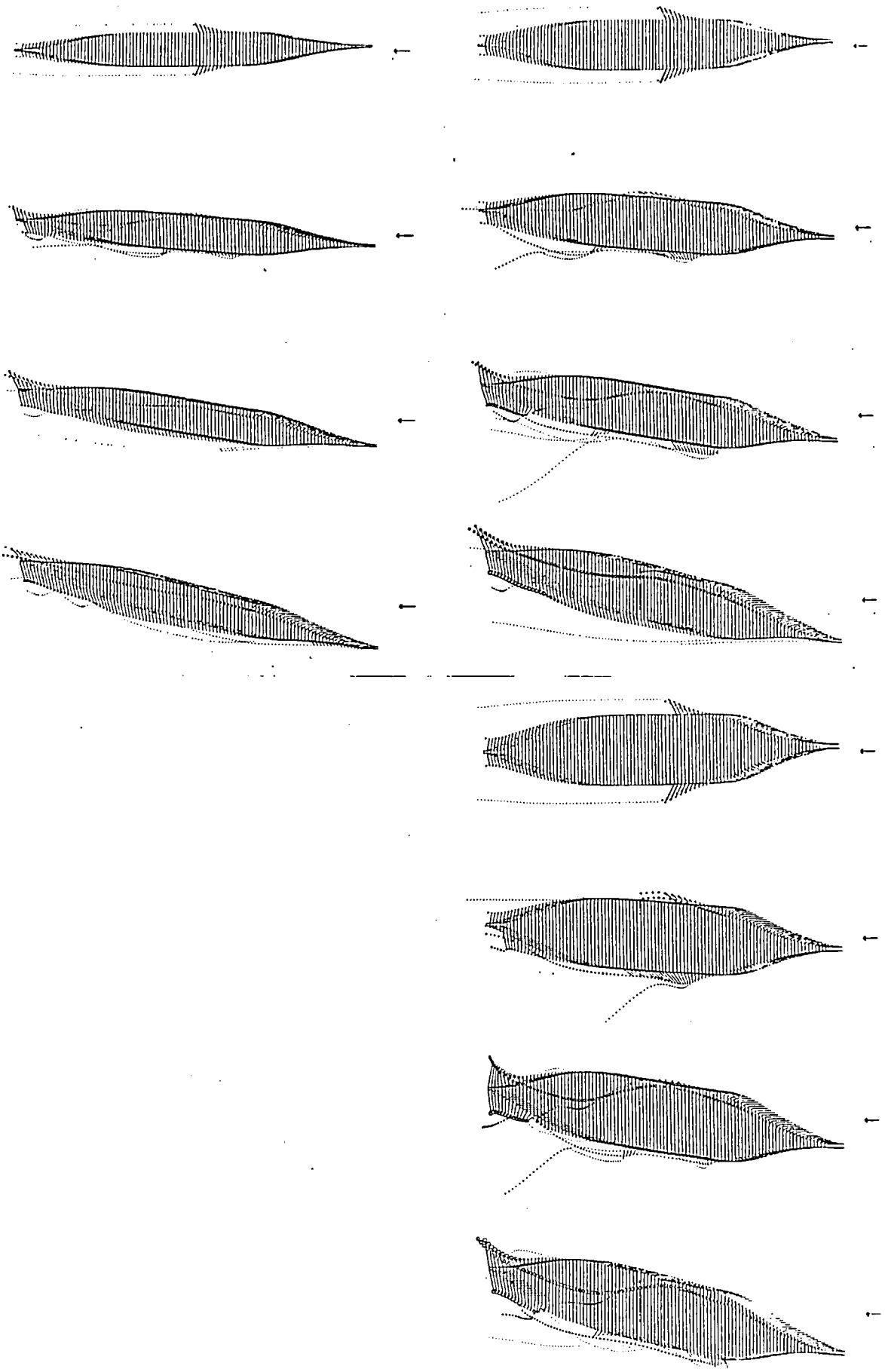

Figure 4.12

Influence of beam on vortex positions - calculated.

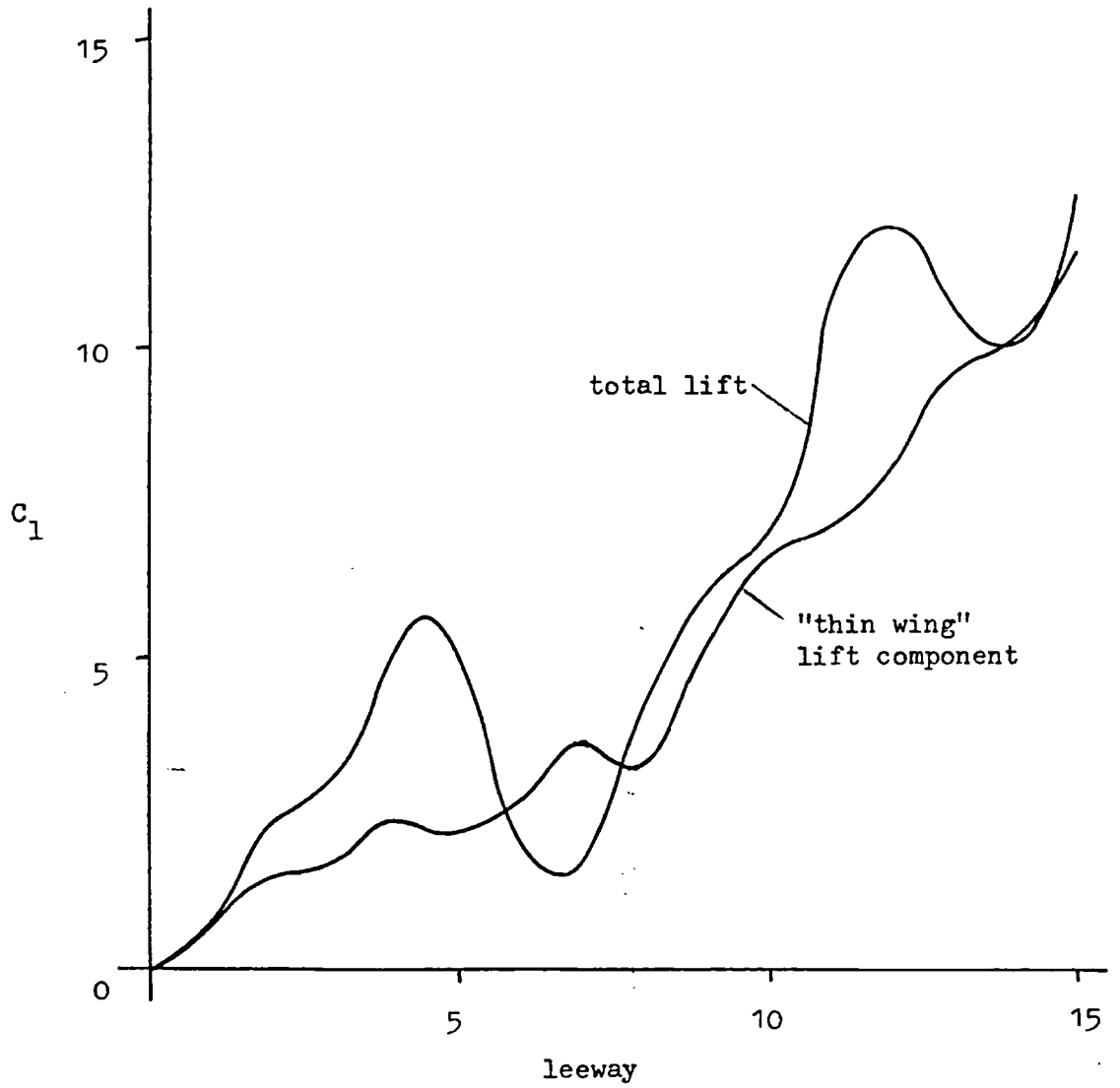

Figure 4.13
Calculated lift/leeway curves for parent-form hull-like block.

TABLE 4.1: CALCULATED LIFT COEFFICIENTS

(LISTED AS CROSS-FLOW-COMPONENT + THIN-WING-COMPONENT)

BEAM/DRAFT	2	3	4
LEEWAY(D)			
0	0+0	0+.02	-.01+-.02
1		-.03+.79	
2		.82+1.58	
3		1.38+1.79	
4		2.72+2.47	
5	.95+2.21	2.84+2.30	.84+3.66
6		-.72+2.76	
7		-1.98+3.69	
8		1.11+3.39	
9		.98+5.23	
10	.39+5.84	.30+6.71	5.62+6.22
11			
12			
13			
14			
15	.56+10.08	.96+11.56	246.11+10.88

Table 4.2 COMPARISON OF CALCULATION AND EXPERIMENT

Incidence (deg)	0	5	10
CALCULATED			
positive vortex strength	.684	1.650	4.114
negative vortex strength	-.680	-1.109	-2.537
net vortex strength	.004	.541	1.577
thin wing lift coefficient	.017	2.300	6.702
total lift coefficient	.016	5.144	7.006
EXPERIMENTAL			
positive vortex strength	.877		1.611
negative vortex strength	-.788		-.251
net vortex strength	.089		1.360
thin wing lift coefficient	.378		5.780
total lift coefficient	-.122		3.488

/

4.4(b) Results: comparison with experiment

Vortex paths. Experimental and calculated vortex paths are compared in figures 4.11 and 4.12. The calculation introduces some spurious flow characteristics which are discussed at some length in section 4.4(c). Nevertheless, comparison of the figures shows that the modelled flows do correctly reproduce the important qualitative features of the real flows. The paths of dominant vortices are generally similar to the approximate paths indicated by the wool-tuft wind-tunnel tests, although significant differences sometimes occur at the stern. For example, the leading bilge vortex is often swept off the wrong side of the stern.

Vortex magnitudes. The calculations are conducted for flows about a hull-like block (model A1) which has been tested as part of the experiment described in Chapter 3. Comparison of calculated and experimentally determined vortex strengths is of considerable interest. Wake surveys were conducted at 0° and 10° for this model. Analysis of the wake survey data provides a rough estimate of the total strengths of positive and negative vortices. This estimate is not accurate for three reasons discussed in appendix A3.1: a very primitive "block-integration" technique is used, spurious vorticity due to mathematical curve fitting is included, and some real vorticity may be excluded if it lies outside the survey plane. The experimental and calculated vortex strengths are tabulated together for comparison in table 4.2.

At 0° incidence, the calculation predicts positive and negative vortex strengths of about 0.7. The difference of less than 1% is produced by cumulative iteration-limit

and integration errors. The experimental positive and negative vortex strengths are about 0.8. Their magnitudes differ by about 10% because of asymmetries caused by the model support and errors in the vorticity integration procedure. As expected, the net total vortex strengths are close to 0 in both cases.

At 10° incidence, the calculated and experimental net vortex strengths are similar, being about 1.6 and 1.4. This is despite considerable differences in the calculated and experimental magnitudes of total positive and total negative vortex strengths. The greater strengths of total positive and negative vortices predicted by the calculation result mainly from the unrealistic vortex shedding discussed in section 4.4(c). It is thought that the unrealistic shedding should produce roughly equal quantities of positive and negative spurious vorticity. This is not contradicted by this comparison.

Lift forces. The calculated lift/leeway curve (figure 4.13) shows very considerable fluctuations associated with the spurious modelled-vortex behaviour discussed in the next section. Separation of the lift into attributable components shows that most of the fluctuation occurs in the cross-flow (vortex suction) component. The cross-flow component is generally smaller than the "thin wing" component and even becomes negative at some angles of leeway.

The calculated lift coefficients can be compared with the experimental values obtained in the tests referred to in the discussion of vortex strengths. The relevant data is given in table 4.2. The calculated and experimental thin wing lift components are determined from the calculated

and experimental net total vortex strengths. The calculated total lift is determined by integration of the calculated hull surface pressures and the experimental total lift is measured directly. At 0° incidence all calculated and experimentally determined lift coefficient values are acceptably close to 0. At 10° incidence the calculated total lift is about twice the experimental value, although the thin wing contributions are of similar magnitude. In view of the expected errors in both the experimental and calculated thin wing contributions, this latter similarity may be fortuitous. Comparison of figures 3.30 and 4.13 shows that the calculated lift forces are generally larger than the experimental values. The discrepancies can only be partly attributed to the concentrated line vortex representation used and the spurious vortex evolution traits previously discussed. Smith (1980) notes that agreement with overall lift cannot be expected because the Kutta condition at the trailing edge is violated as a consequence of the slender body assumption and hence the lift force is not correctly predicted at the after part of the ship.

4.4(c) Results: spurious model flow characteristics

The calculated flows show the general features of real flows described in the previous chapter; however, they also display some unphysical traits which can be attributed particularly to two of the model simplifications. These are, that real vortices which are diffuse regions of vorticity can be represented as single concentrated line vortices, and that the vortex evolutions can be determined by integration of linear increments. The first of these causes spurious vortex behaviour, particularly when a modelled line vortex has approached another vortex or flow boundary so closely that the separation is less than some typical radius of a real diffuse vortex. The second causes spurious vortex behaviour when the second or higher order derivatives of vortex characteristics are large. For example, when a highly curved vortex path is modelled as a series of linear tangential steps, considerable inaccuracy can result. A number of particular associated problems are now considered.

(1) Excessive vortex suction: the model sometimes convects line vortices unrealistically close to the hull's side; and this can lead to excessive vortex suction forces. For example, in the wide beam, 15° leeway calculation a comparatively weak vortex is convected very close to the trailing side near the stern; this produces a vortex suction component of the lift which is more than twenty times the "thin wing" lift component.

(2) Excessive image induced velocity: in some cases the model convects a line vortex unrealistically close to the flow boundary; its own induced velocity field

(that is, the velocity field of its image in the potential model) then convects it rapidly parallel to the surface. Figure 4.7 provides an example; a vortex near to the sea surface moves away at a very broad angle on the trailing side.

(3) Unrealistic vortex shedding. Firstly, when a model concentrated line vortex is convected past a bilge, the changes in the induced velocity at the bilge are more severe than when a real diffuse vortex is convected past; this can cause artificial reversals of flow direction and hence lead to unrealistic vortex shedding. Figure 4.5 provides an example of probably unrealistic multiple vortex shedding on the trailing side of the middle body. Secondly, when a real diffuse vortex is convected past a bilge it is likely to merge with the vorticity being produced (as a vortex sheet) at the bilge; diffusion then results in cancellation of opposite vorticity. The concentrated line vortex model can indicate quite different behaviour; frequently, when a modelled line vortex is convected back round a bilge a line vortex of similar magnitude but opposite sign is produced very close to the vortex, and the resultant vortex pair is convected away by its own induced velocity. Examples of strong vortex pairs occur on the leading side near the stern in figures 4.6 and 4.7.

(4) Unrealistic proximity of vortices: if the centres of two real diffuse vortices approach closer than some typical radius of vorticity (that is the radius of a circle which includes most of the vorticity of a vortex), then some merging of vorticity occurs. However, two similarly close modelled line vortices maintain their individual characters and can misbehave in two ways.

Firstly, if they are of similar magnitude and opposite sign the self induced velocity of the vortex pair can be quite large, whereas the induced velocity of a similar real pair would be less as their proximity would have led to some merging and cancellation of vorticity. Examples of strong vortex pairs have already been given in case (3). Secondly, the real flow path of a vortex close to another, when they are not of similar magnitude and opposite sign, is likely to have high curvature, hence the model's finite time steps can lead to serious inaccuracies. An interesting example is the one given in case (1); the vortex which caused the extreme vortex suction reached its unphysical position after being convected in unrealistic tangential steps round a strong trailing-run-vortex.

(5) Stern "water-shed" effect; as noted before, the leading bilge vortex is often swept off the wrong side of the stern. This occurs because the fluid near the hull-bottom at the run is effectively at a "water-shed": there is some dividing surface so that fluid on one side of it flows off the leading bilge, while fluid on the other flows off the trailing bilge. In most cases the predicted (and actual observed) leading bilge vortex path passes near to this "water-shed". The subsequent vortex evolution is very critical to small errors in the previous predicted path as a small error in position can cause this vortex to flow off the wrong side of the hull. Figures 4.11 and 4.12 show that this does indeed usually happen at angles of incidence greater than 5°, and in consequence the predicted and actual vortex positions will be very dissimilar down-stream of the stern in these cases.

4.5 Conclusions

Model. A slender-body line-vortex potential model is described which models the flow past hull-like blocks at leeway. The downstream evolution of the flows is determined by a marching calculation procedure. At each cross flow plane an iterative procedure is used to solve a transformed problem with simpler boundary conditions, and the solution is conformally mapped to provide a potential solution to the cross flow problem. When bilge vortices cease growing they are shed and new vortices are allowed to form near the bilge. The lift force is determined by integration of pressure forces.

Realistic flow characteristics. Despite various artificial and spurious effects, the modelled flows do correctly reproduce the important qualitative features of the real flows. The paths of dominant vortices are generally similar to the approximate paths indicated by the wool-tuft wind-tunnel tests although significant differences sometimes occur at the stern, for example, the leading bilge vortex is often swept off the wrong side of the stern.

Artificial flow characteristics. The calculated flows display various unphysical traits which can be attributed to the line vortex representation of real diffuse vortices and to the finite time step marching procedure used to model the real vortex evolutions. Some particular effects discussed are: excessive vortex suction, excessive image induced velocity, unrealistic vortex shedding, unrealistic proximity of vortices and the stern "water-shed" effect.

Force characteristics. The calculated lift-leeway curve shows very significant fluctuations about the mean

curve; these fluctuations result from spurious modelled-vortex behaviour. Separation of the lift into attributable components shows that most of the fluctuation occurs in the cross-flow (vortex suction) component. The cross flow component is generally smaller than the "thin wing" component and even becomes negative at some angles of leeway. The calculated lift forces are generally larger than the experimentally determined lift forces. Although this model correctly reproduces the major features of the real flow field, it can not, for various reasons discussed, accurately predict the lift forces experienced by real hulls.

Future developments. The model has been shown to be successful in modelling some important features of the very complex flow near a ship's hull at leeway. It is interesting to speculate on the further evolution of this type of slender-body vortex calculation.

Firstly, in its present primitive form, using appropriate Schwarz Christoffel transformations, it can be used to model important features of the flow past a variety of basically polygonal bodies such as cars, trains, parts of offshore oil structures and buildings. A number of simple improvements could be made to the model for this type of application: a more sophisticated marching procedure could be used; theoretical or empirical considerations might suggest vortex merging criteria which could be incorporated; and Smith (1980) type vortex-sheets could be used to represent the vortices.

Secondly, coupled with a boundary-layer calculation procedure, this type of model could be used to investigate flows near rounded slender bodies. This type of calculation could again be conducted using a line-vortex model but a

vortex-sheet model would probably be more appropriate. As separation would be predicted by the boundary-layer calculation it should additionally be possible to model secondary vortices. This type of calculation could be expected to reasonably model well organised flows near slender bodies such as most of the flow near a realistic ship's hull. However, it could not be expected to model complex disorganised flows such as the wake near the stern of a ship.

Thirdly, and perhaps most importantly, it is hoped that this type of slender body calculation could be used as one part of a more complicated procedure for modelling complete viscous flows in which longitudinal vortices occur. The full equations of motion for viscous flow (the Navier-Stokes and continuity equations) are well known. They are highly coupled and complicated, and can not be solved exactly; indeed, the problem is so difficult that no useful numerical solution can be produced for complete flows about arbitrary bodies with present-day computing resources. Although there seems little hope of finding numerical solutions to the full set of equations it seems likely that progress will be made by patching together appropriate approximate subsolutions. In some circumstances slender-body line-vortex or vortex-sheet calculations may be used as part of such a procedure. For example, it may be possible to produce a useful model of the viscous flow past a realistic ship's hull at leeway by embedding, in a potential flow solution, a boundary-layer solution near the body surface, a slender-body solution for the vortices, and perhaps an approximate

Navier-Stokes solution for the separated flow region near the stern.

5. AN EXPERIMENTAL INVESTIGATION OF THE FLOW THROUGH SIMPLIFIED MULTI-MAST SAILING RIGS

5.1 Introduction

A successful sailing vessel is required to have both good hydrodynamic and good aerodynamic characteristics. The hydrodynamic characteristics are discussed in Chapters 3 and 4: the aerodynamic characteristics are discussed in this chapter and Chapter 6. Traditional large sailing vessels had multi-mast arrays of sails, and it seems likely for various practical reasons that a modern vessel with a large sail area will have the sail divided into a number of elements. These experiments investigate some features of the flow through simplified multi-mast arrays and compare various configurations.

It is not a simple matter to state what constitute good aerodynamic characteristics, nor are characteristics that are good for one type of sailing vessel necessarily good for another (for example, a high-speed motor-sailing vessel might require a very different rig from a low speed trade-wind vessel). There are some aerodynamic similarities between sailing rigs and aeroplane wings, but the requirements of the latter are far simpler than those of the former: an aeroplane wing is required to develop a sufficiently large lift force together with a reasonably low drag force; a sailing rig is required to develop a large drag when sailing with the wind, a large lift when sailing at right angles to the wind, and a fairly large lift, together with a fairly low drag, when sailing close to the wind.

These complex requirements can make comparison of different rig geometries difficult. A simple indication of relative merits can be obtained by simply comparing the components of sail force along the ship's centreline (the "driving force") at various headings relative to the wind; a better indication can be obtained by adjusting the driving force component by an empirical correction to allow for the detrimental effects of "heeling-" (or "side-") force (such a procedure is described by Wagner (1966)); the best way of comparing rigs is to conduct complete performance calculations (as described in Chapter 7) and then to calculate the returns and costs of the ship according to suitable meteorological and economic assumptions. Simple consideration of the driving force component is usually adequate for qualitative comparison of rig configurations and is used throughout this chapter.

Future sailing rigs could take a variety of shapes and sizes. An array of eight simplified rectangular sails of plausible dimensions are arbitrarily chosen for this investigation; this array has the general features of traditional and proposed multi-mast rigs. The characteristics of various simplified aerofoil-sail sections are compared individually and combined as sailing rigs; various reefing and trimming strategies are compared; the effects of end-plates, mast-number and heel on sail forces are also investigated.

The experiment is conducted using a model of the above-water part of the hull which can be fitted with the various model sail rigs to be tested. This model is mounted in a wind tunnel close to the tunnel wall which simulates the sea surface. The mounting is linked to a

weigh-beam balance which measures the aerodynamic lift and drag. The flow is investigated using a wool-tuft probe.

5.2(a) Review : sail wind tunnel tests

Yacht sails. The first reported wind tunnel tests of a yacht's sail were conducted by Everett (1915) at the Massachusetts Institute of Technology. He tested a single model gaff mainsail to determine the position of the centre of pressure and the magnitude of the total sail-force at a range of incidence angles. The sail was made of a single unseamed piece of silk and must have taken up a camber distribution unlike that of a full-sized seamed sail. Various subsequent experiments at M.I.T. are reported by Warner and Ober (1925). They made systematic comparative tests with rectangular-silhouette rigid model sails to investigate the influence of sectional shape and the effect of mast interference. They also tested a triangular model sail near to a sheet of plywood which modelled the sea surface; rather surprisingly they report that closing the gap between the modelled sea and sail reduced the driving component of the sail-force.

Curry (1930) reports various wind tunnel and water tank tests of model sails; he conducted flow visualisation experiments, mapped pressure distributions and measured sail-forces. Parameters investigated include sail silhouette, aspect ratio, degree of camber, distribution of camber and sail-twist; he also investigated the effect of sealing the gap between the mast and the sail's leading edge, and the effect of fitting a lower edge end-plate (a "Plank boom").

Tanner (1962) comments that little success had been achieved (by 1962) in determining sail-force coefficients. He discusses the difficulties of modelling,

in a wind tunnel, a flexible sail on a heeled yacht near to the sea surface. He reports systematic tests using rigid sheet-metal model sloop rigs in the working section of Southampton University's largest (7 ft by 5½ ft) wind tunnel; these investigate effects of sail-silhouette and position of maximum sail-camber. Crago (1963) considers modelling difficulties to "almost render wind tunnel tests useless" and suggests that only qualitative information can be obtained from such tests. He discusses a number of problems; these are associated with hull aerodynamic interference, modelling sail elasticity and porosity, modelling the wind gradient and full-scale turbulence, and Reynolds number effects. Tanner (1963) agrees in general with Crago, but thinks he is being too critical. Tanner goes on to describe tests conducted with 8ft high models in the largest part of the return duct of the Southampton 7ft by 5½ft wind tunnel. These apparently include tests of a flexible 2/5 scale model of a dinghy mainsail. He remarks, "at last we shall be able to produce some valuable sail-force coefficients, if only for relatively small models." Milgram (1972) refers to the Southampton experiments and comments, "First of all, most of the wind-tunnel results have been given without any correction for wind-tunnel blockage, which can have a significant effect. Second, there has been no connection between the various experiments, each one having been made on a different arbitrary sail shape, which was not even known in some experiments."

The lightly loaded shape of a sail depends primarily on the cut of the sailcloth (that is on the

shapes of the panels from which it is constructed); in normal sailing conditions this shape is deformed by both dynamic loads due to the wind and static (control) tensions applied by the crew; the nature of the deformation also depends on the elastic properties of the sail, battens and spars. Marchaj (1979) reports a number of tests with a 2/5 scale model "Finn" sail made in the Southampton University wind tunnel; most of these investigate the interaction between sail shape and sail forces. The Finn Sail is also used to investigate the effect of changing the gap between the sail's lower edge (the "foot") and the modelled sea surface. Unlike Warner and Ober (1925), Marchaj finds that reducing this gap increases the lift/drag ratio, which would increase the driving force on some headings; this increase indicates reduced vortex drag associated with the reduced flow under the sail foot. He reports various other experiments on a variety of rigs tested with or without the above-water-hull; subjects investigated include faired sail leading edges and thick sails, sail interaction and genoa overlap, and unstable downwind rolling.

Ship sails. Flettner (1926) conducted tests with a model barquentine in the Göttingen wind tunnel; smoke flow visualisation and force tests were carried out with the full rig, and with individual sails. Wagner (1967c) refers to earlier tests of a barquentine by Croseck, and of the "Preussen" mainmast by himself. He reports tests of a "Pamir" type barque in the Hamburg 1m x 1.75m open section tunnel; one surprising result is that the model has improved force characteristics with the staysails removed: this probably reflects the difficulty of

correctly modelling flexible sails at this scale, as it seems unlikely that sailors would have used sails that slowed their progress!

Despite the recent interest in advanced technology sailing vessels, there is very little experimental data available from wind tunnel tests of suitable rigs. Flettner (1926) reports experiments with a triplane aerofoil rig conducted at Göttingen. Wagner (1966 and 1967b) carried out a series of experiments as part of the "Dynaship" project. Prölss had proposed roller-furled square sails on cantilever masts for this ship; a series of tests were conducted to optimise the geometry of these sails. Subsequent tests were made to determine suitable ways of combining these sails as a rig and to produce data for performance calculations. NKK (1979) report a series of wind tunnel tests conducted to optimise the design of practical sails suitable for wind-assistance of powered vessels. The problems associated with individual or isolated sails for wind-assistance are much less complex than those associated with rigs intended to provide a large part of the propulsive power. With admirable directness, NKK exploited this simplicity and quickly moved from fairly simple wind tunnel tests to prototype, then full-scale sea-going tests.

5.2(b) Review: Aerofoil characteristics

An aerofoil is a sharp tailed slender device whose purpose is to deflect flow. It experiences an aerodynamic force equal and opposite to the rate of change of the fluid's momentum. This force is conventionally resolved into two components; the lift (perpendicular to both the relative inflow and the aerofoil span direction), and the drag (parallel to the relative inflow). An aerofoil is normally considered efficient if it develops a reasonably large lift force and a comparatively small drag force.

Most of the flow near an aerofoil is inviscid, and the viscid regions of the flow are concentrated as thin "boundary-layers" on the body surface and thin "shear-layers" trailing downstream from separation lines on the body. Although these regions of viscid flow are small, they are essential to the generation of aerodynamic lift. It can be shown that a hypothetical finite body in purely inviscid flow would experience no aerodynamic forces. In particular, purely inviscid calculations of the flow past finite-aspect-ratio aerofoils indicate that no fluid would be deflected (and no lift would be developed). This purely inviscid flow is considerably altered by the effects of viscosity at the trailing edge. The hypothetical flow discussed generally does not separate from the aerofoil at the trailing edge; indeed, it predicts extremely unphysical behaviour of the flow at this edge. Observations show that real flows do separate at the trailing edge of real finite aspect ratio aerofoils for a useful range of incidence angles. The normality of this condition is postulated as "the extended Kutta-Joukowski hypothesis", which is that

"the rear dividing streamline leaves the aerofoil at the trailing edge. Its tangent at the trailing edge, in general, passes through the interior of the aerofoil" (Thwaites, 1960). This hypothesis is only strictly applicable to unseparated flow. It can easily be demonstrated experimentally, but it is much more difficult to justify it theoretically. A useful and interesting consequence of this modification to the purely inviscid flow is that the real flow does deflect fluid, and hence a real aerofoil does develop lift.

The effects of viscosity in localised regions of the flow can cause large modifications to the external inviscid flow in another important way. This is when viscous forces and pressure forces act together to cause flow separation. This is a complicated phenomenon and only the basic nature of the mechanism for separation is indicated in this paragraph. Firstly, it is noted that the lift force is experienced as differences in pressure across the aerofoil and the pressure varies on the body surface. The surface pressure gradient is described as "favourable" when the pressure force tends to accelerate the boundary-layer flow, and "adverse" when it acts in the opposite direction. Secondly, it is noted that in the boundary-layer on the body surface, viscous friction decelerates the flow. In certain circumstances the combined effects of adverse pressure gradient and viscous friction are sufficient to reverse the surface flow direction. Where this first occurs the boundary-layer leaves the body surface and separation is said to occur. This phenomenon depends critically on the boundary-layer

characteristics which in turn depend on the ratio of typical inertial forces to typical viscous forces. This ratio is characterised by the "Reynolds number" $\rho V c/\mu$. Reynolds number dependency is discussed in some detail in section 5.2(e) and appendix A5.1.

Another interesting feature of the flow about finite-aspect-ratio aerofoils is the vortices which trail from their ends. As noted before, there is a pressure difference across the aerofoil. This difference drives flow round the ends of the aerofoils from their high to low pressure sides. Two particular effects are: firstly, the pressure difference is reduced near the ends and so the lift decreases towards these ends; secondly, the circulatory flow about the ends is convected downstream as trailing vortices and these represent stores of kinetic energy and hence contribute to the aerofoil drag.

Published experimental investigations of the aerofoil sections tested as possible sail sections are now described.

Thin cambered plates: one of the earliest aerodynamic experiments reported by the Göttingen model testing institute was an investigation of "wind pressure on curved plates of different camber" (Anon., 1910). Eight circular-arc plates with cambers varying between 0% and 12.5%, and with a constant aspect ratio of 4, were compared; in this range of cambers, the largest camber (12.5%) is found to give the greatest maximum lift, while the camber of 4% gives the highest maximum lift/drag ratio.

Eiffel (1913) reports similar tests conducted in the open section wind tunnel at Paris. These were made

with 4 curved plates of aspect ratio 4 in the camber range 0 - 14.3%. Of these four, the 7.4% camber gives the highest maximum lift/drag ratio, and the maximum camber gives the highest maximum lift. Eiffel's results have been used in a number of papers on sail aerodynamics; this appears to have resulted from their being quoted by Curry (1933).

Wallis (1946) tested 7 circular-arc plates with camber varying between 0% and 12%; these were tested between end-plates to simulate two-dimensional flow conditions and within this range of cambers, the largest camber (12%) gives the greatest maximum lift, while the camber of 8% gives the highest maximum lift/drag ratio.

Milgram (1971) tested three circular arc plates with cambers of 12%, 15% and 18%; these were tested with their ends very close to the tunnel walls to simulate two-dimensional flow conditions; in this camber-range, the largest (18%) gives the greatest maximum lift, while the smallest (12%) gives the highest maximum lift/drag ratio. Milgram comments that the lift characteristics of moderately thick, slightly cambered aerofoils are close to the theoretical (attached flow) predictions, while those of thin cambered plates are not: this is due to the extensive separation which occurs on the cambered plates. At low angles of incidence the flow separates from the bottom surface at the leading edge; with increasing angle of incidence the position of flow separation, from the upper surface, moves progressively forward from the trailing edge.

Thick circular-arc aerofoils: no tests have been

reported (to the author's knowledge) of aerofoils with the section of the thick circular-arc aerofoil tested in this experiment. However, tests of aerofoils of similar sections have been reported: the thick circular-arc aerofoil tested in this experiment has 3% camber on the lower surface and 15% camber on the upper surface; the reported results are for zero camber on the lower surface and 12% or 16% camber on the upper surface (that is to say, for aerofoil sections which are segments of circles, so that the camber of the upper surface is equal to the thickness). Briggs and Dryden (1930) conducted experiments with these thick circular-arc aerofoils. 8 of these aerofoils were tested with thicknesses varying between 6% and 20%. The minimum Mach number of these tests was 0.5. At this speed the thick circular-arc sections were found to be "extremely inefficient": they produce lower maximum lift and lower maximum lift/drag ratios than conventional aerofoils of the same thickness with which they were compared.

NACA aerofoils: the two aerofoil sections tested as possible sail sections are from the NACA 4-digit-series. These aerofoils have thickness distributions derived from the Göttingen and Clark Y aerofoil thickness distributions. Abbott, Von Doenhoff and Stivers (1945) describe these aerofoils and discuss the flow about such aerofoils. Both aerofoils tested have a thickness of 18%. The characteristics of the NACA 0018 (symmetric) aerofoil are described by Jacobs and Sherman (1937) and Goett and Bullivant (1939), those of the NACA 6518 (cambered) aerofoil are described by Jacobs, Ward and Pinkerton (1933).

Effects of camber and thickness. As an example,

the characteristics of four thick and thin, cambered and uncambered NACA aerofoils are compared. The aerofoil sections and characteristics are shown in figures 5.1 and 5.2 which are taken from Jacobs, Ward and Pinkerton (1933).

Firstly, the effects of thickness are considered for both cambered and uncambered aerofoils: the thin aerofoils produce the higher maximum lift/drag ratios which occur at low angles of incidence, while at moderate angles of incidence the thick aerofoils produce the better lift/drag ratios; the thick aerofoils develop greater maximum lift, and stall at greater angles of incidence. The better lift/drag ratios of the thin aerofoils reflect their low profile drag; the delayed stall characteristics of the thick aerofoils result from the more gentle streamline curvature and reduced adverse pressure gradients on the upper surfaces of their thick rounded fore-parts (see Batchelor, 1967).

Secondly, the effects of camber are considered for both thin and thick aerofoils; the uncambered aerofoils produce a slightly higher maximum lift/drag ratio which occurs at a small angle of incidence; the cambered aerofoils develop a greater maximum lift and have a greater incidence range between zero-lift and stall. The delayed stall characteristics of the cambered foils again reflect the more gentle streamline curvature and reduced adverse pressure gradients on the forward parts of the upper surfaces, which now result from the leading parts of the cambered aerofoils being tilted into the flow so that they are at lower angles of attack than would otherwise be the case (see Batchelor, 1967).

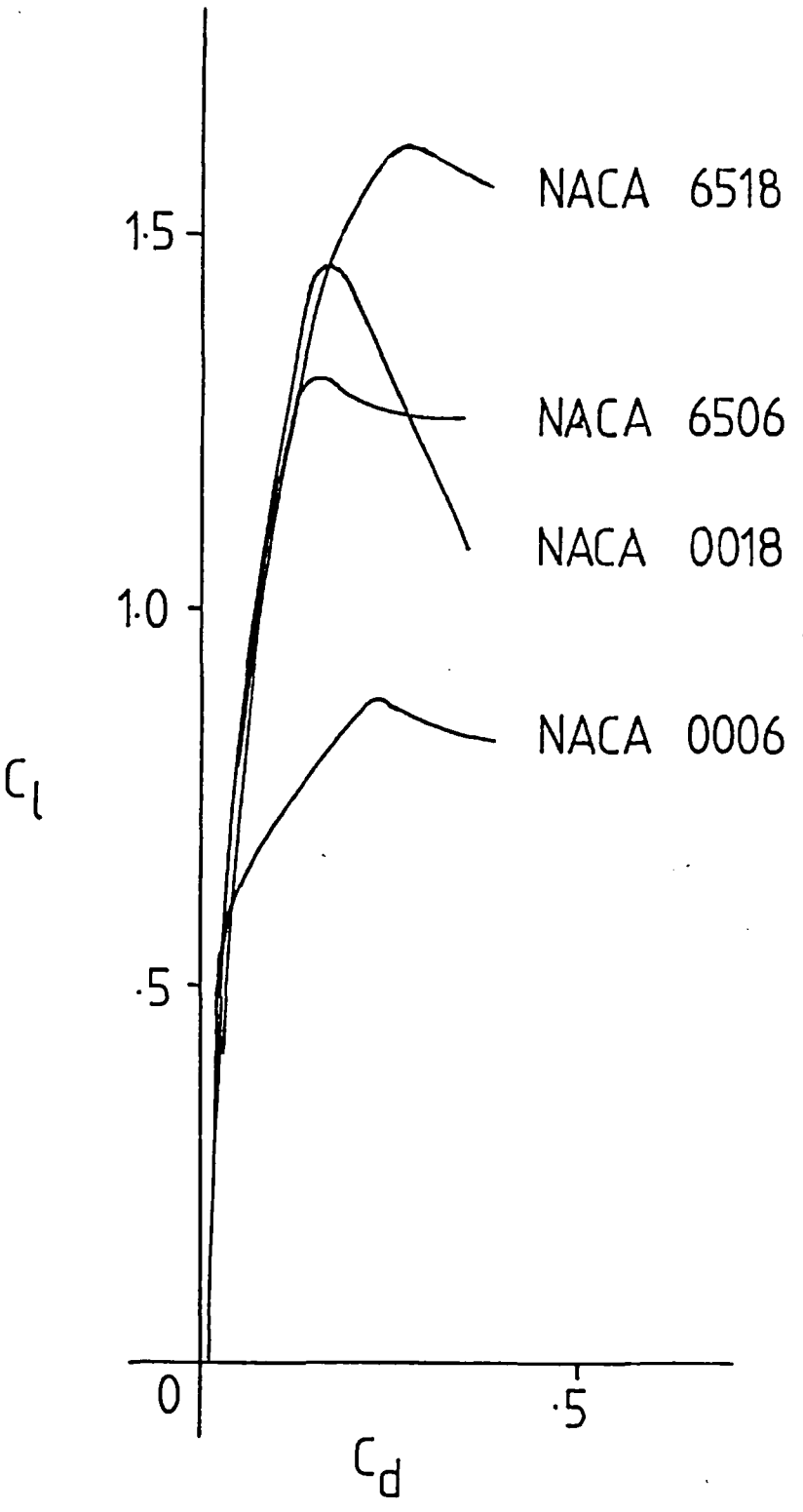

Figure 5.1

A comparison of the lift-drag characteristics of four NACA aerofoils.

after Jacobs, Ward and Pinkerton (1933)

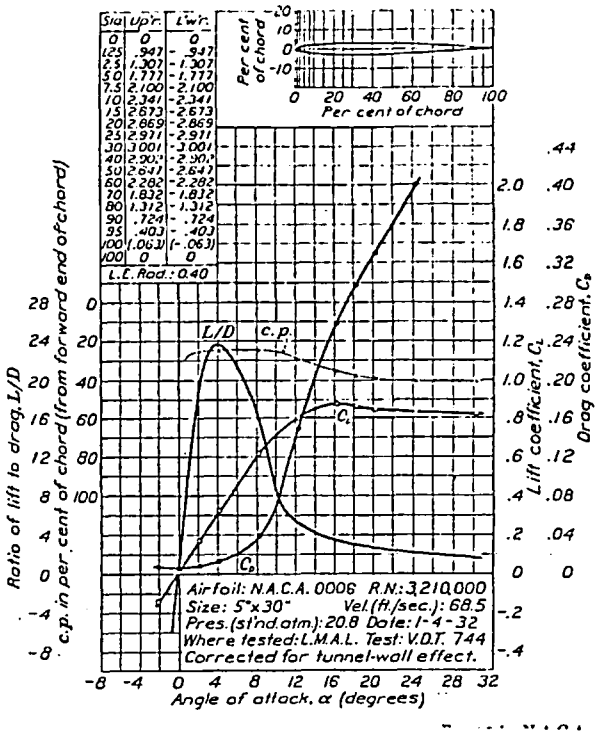

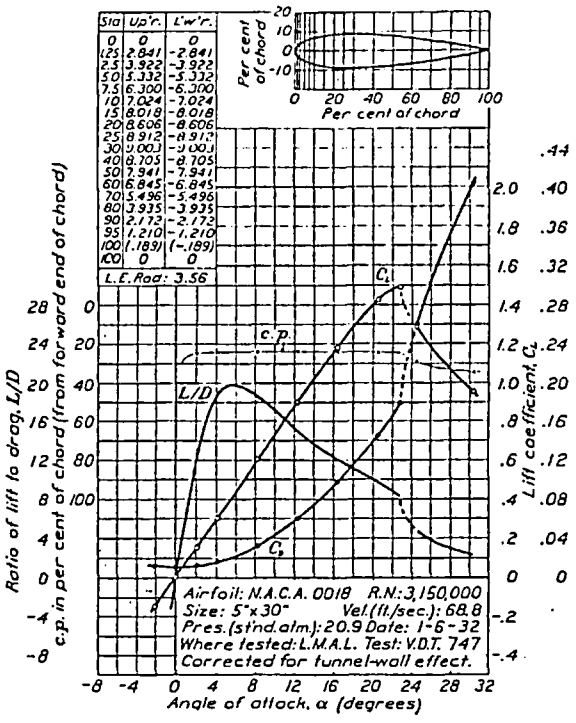

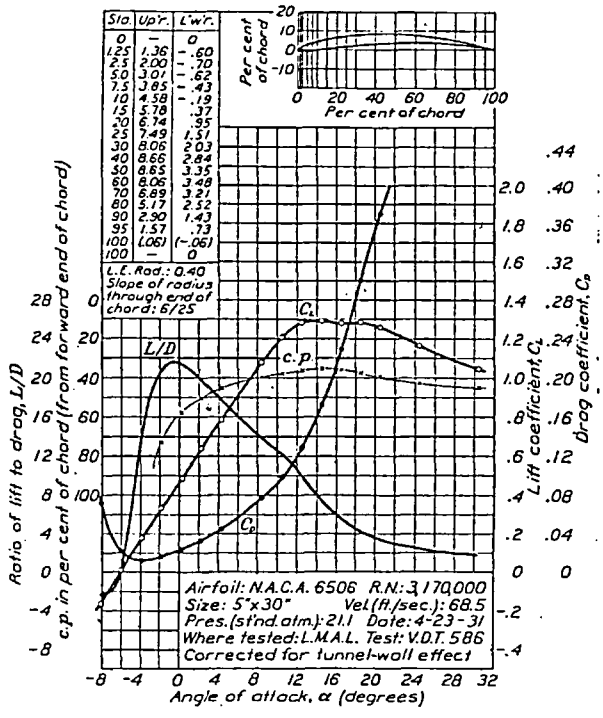

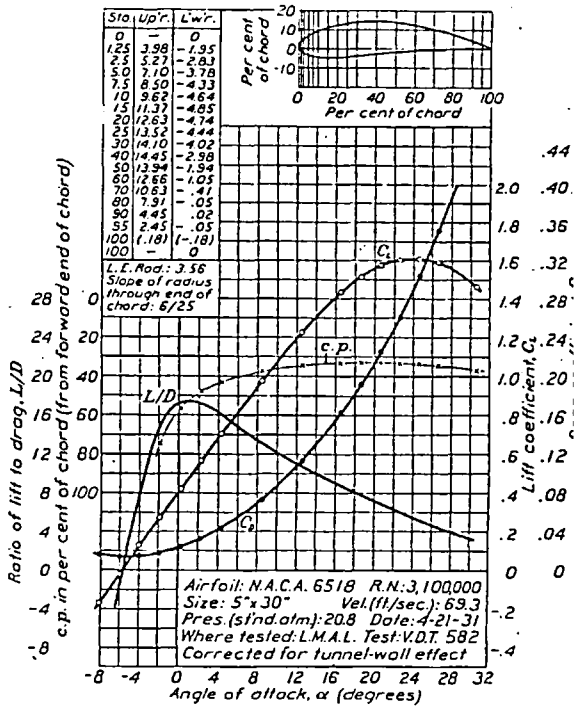

Figure 5.2

Comparison of the aerodynamic characteristics of four NACA aerofoils

After Jacobs, Ward and Pinkerton (1933).

5.2(c) Review : multi-element sail interaction

Yacht-sail interaction. Warner and Ober (1925) measured pressure distributions and made smoke flow visualisation observations with sails of a yacht while she was underway. They conclude that the jib serves to guide the air onto the lower part of the mainsail, thus reducing the harmful effects of mainsail twist; the sail is normally twisted so that the angle of incidence near the foot is much larger than that near the head; and without a jib, the flow is likely to be stalled near the foot while it is at a very low incidence near the head. In a delightful book, Curry (1930) discusses the flow past sails largely by analogy with his conception of bird-flight. He argues (wrongly) that the suction forces on the leeside of a stalled mainsail are reduced by forces due to a return jet of air striking this side of the sail; and that the jib improves the suction forces as the "return flow of the eddies is blocked from reaching the mainsail by the current of air off the jib flowing directly across its path". He also argues (correctly) that the presence of the mainsail changes the local angle of incidence at the jib, so that a greater component of the resultant force acts in the direction of motion through the water.

Morwood (1953) and Millward (1961) note that the jib acts like a Handley Page leading edge slot; the presence of the auxiliary aerofoil (jib) improves the airflow over the back of the aerofoil (mainsail) at high angles of attack so that the flow does not stall so readily. Figure 2.3 shows a multi-element aerofoil sail designed to produce high lift forces. Tests on this sail

are described by Otto-Scherer (1974). He states that flow through the slots increases the surface velocity over the after part of the aerofoil sail where there is an adverse pressure gradient; this makes boundary-layer separation less likely, delays stall, and so increases the maximum lift attainable. Marchaj (1979) criticises this explanation which he attributes to Prandtl; he considers that a better explanation is not that the slot flow makes the boundary layer better able to overcome the adverse pressure gradient, but that the slot flow changes the pressure gradient so that it is not so adverse.

Gentry (1971 and 1981) investigated the flow past two-dimensional aerofoils with an "analog field plotter"; this models the potential velocity field as a potential voltage field across a poorly conducting sheet with highly conducting, aerofoil shaped regions. He concludes that the flow at the jib is influenced by the (horizontal) "upwash" forward of the mainsail, and the flow at the mainsail is influenced by the (horizontal) "downwash" aft of the jib. A particular effect on the jib is that the velocity at the trailing edge is increased, so that the Kutta condition is satisfied at a higher velocity, and so the velocity over the entire lee surface is increased; this results in the high observed performance of jibs. A particular effect on the mainsail is that adverse pressure gradients near the leeside leading edge are made more favourable due to the accelerating flow in the slot; and so mainsail stall is less likely. Wiersma (1979) solved the exact equations describing the potential flow past a pair of overlapping two-dimensional sails with parabolic camber. He confirms all Gentry's conclusions.

Marchaj (1979) considers a controversy amongst yachtsmen as to whether the jib accelerates or decelerates the flow over the mainsail's leeside. Confusion appears to be caused because the flow at the trailing end of the slot is accelerated compared with the velocity at the leading end of the slot, but the trailing end flow has been decelerated compared with the velocity which would occur at this point if the jib was absent.

"Dynaship" sail interaction. Wagner (1966) experimented with several linearly graduated arrays while investigating suitable sails for the proposed "Dynaship". He notes that the favourable sail interaction avoids partial stall and produces greater rig forces. Subsequently (Wagner, 1967b) he attempts to determine optimum linear graduation for this ship; he finds that on a close reach ($\lambda_H \approx 60°$) a fore-to-aft sail trim range of about 30° is needed and that this decreases with inflow angle so that no graduation is required on a broad reach ($\lambda_H \approx 120°$). He makes no further comments on the aerodynamics of this sail interaction.

Multi-component aerofoils. Handley Page (1921) attempted to achieve higher maximum lift forces from aerofoils by putting a slot near to the leading edge; this allows some air to flow fairly smoothly from the lower to upper sides and results in increased maximum lift and decreased maximum lift/drag ratio. The explanation given is that stall is delayed as the flow of "fresh air" through the slot helps to preserve the "live air stream" flowing over the back of the aerofoil. Experiments with larger numbers of slots show that large lift coefficients can be developed: for example, a R.A.F. 19 section aerofoil with

6 slots develops more than twice the maximum lift of such an aerofoil with no slots; on the other hand, the drag is also considerably increased so that the best lift/drag ratio is reduced by about half.

Le Page (1923) tested a rather different arrangement: he investigated the effect of fitting a small auxiliary aerofoil below and downstream of the main aerofoil. It was thought that the flow induced by the auxiliary aerofoil would increase the velocity at the trailing edge of the main aerofoil; this would reduce the pressure at the trailing edge and hence it would reduce the adverse pressure gradient between the minimum pressure point and the trailing edge; this might be expected to delay stall and hence increase the maximum achievable lift of the main aerofoil. It is found that this arrangement does increase the maximum lift coefficient and also decreases the best lift/drag ratio; however, it is said not to be clear that this is, in fact, because stall has been delayed.

A number of investigations were subsequently conducted to determine suitable arrangements of slots and auxiliary aerofoils; two further examples are referred to in this paragraph. Weick and Shortal (1932) tested a low camber Clark Y aerofoil with up to 4 slots; they find that a single leading edge slot greatly improves the maximum lift, but that additional slots only produce a marginal further increase. They make no attempt to explain the aerodynamic mechanism responsible for this improvement. Weick and Bamber (1932) tested a Clark Y aerofoil with a small auxiliary aerofoil near the leading edge. They attempted to determine the best position for this

auxiliary aerofoil; the exact position of the auxiliary aerofoil is found not to be critical, and considerable increases in maximum lift can be achieved. Again the aerodynamics of this interaction are not discussed.

Prandtl and Tietjens (1934) discuss stall on conventional wings: separation occurs if the kinetic energy of the particles in the boundary layer has been so reduced by the action of viscosity that they are unable to reach the trailing edge against the adverse pressure gradients which exist on the latter part of the upper surface. Slotted wings delay stall and achieve greater maximum lift as "the air coming out of the slot blows into the boundary layer on the top of the wing and imparts fresh momentum to the particles in it, which have been slowed down by the action of viscosity. Owing to this help, the particles are able to reach the sharp rear edge without breaking away."

Thwaites (1960) gives a different explanation of the slot effect - "The leading edge slat amounts to an auxiliary aerofoil at a high lift coefficient; the strong downwash from its trailing edge forces the boundary layer on the main part of the wing to adhere to the surface instead of separating as it otherwise would, or to reattach quickly if separation does occur. Alternatively, we may explain the action of the slat by saying that the circulation about it decreases the fluid velocity which would otherwise occur near the leading edge of the main wing; the rise in pressure undergone later by the boundary layer is therefore diminished and separation possibly prevented." He notes that the flow may well separate

from the upper surface of the slat, but its wake is discharged into the mainstream where it cannot seriously affect the lift on the main wing.

Smith (1972) notes five primary effects of slots between aerofoil elements: firstly, the circulation on a forward element runs counter to the circulation on the downstream element and reduces negative pressure peaks on the downstream element; secondly, the downstream element places the trailing edge of the adjacent upstream element in a region of high velocity that is inclined to the mean camber line at the rear of this forward element, and this flow inclination induces appreciably greater circulation on the forward element; thirdly, because the trailing edge of the forward element is in a region of higher velocity, the boundary layer flow "dumps" at higher velocity, and this higher discharge velocity relieves the pressure rise impressed on the boundary layer, so alleviating separation problems; fourthly, the boundary layer from forward elements is dumped at velocities appreciably higher than free stream, and the final deceleration of the wake is done efficiently out of contact with a wall; and finally, each new element starts out with a fresh boundary layer at its leading edge, and thin boundary layers can withstand stronger adverse pressure gradients than can thick ones.

Cascades. There are a number of important fundamental differences between the flow through an array of sails and the flow through an infinite cascade. Characteristics peculiar to cascade flows include:

- there is only a finite flux associated with each aerofoil;

- the distant free stream velocities are different in magnitude and direction upstream and downstream of a cascade;
- secondary flows can be of great importance in rotating cascade flows;
- and the aerofoils are all parallel and flow conditions are identical at each.

Thwaites (1960) notes that the direct effects of viscosity (such as the influence of the boundary layer on the external flow, and the mutual interaction between closely spaced blades) may be greater for cascades than for isolated aerofoils.

Nevertheless, the flow through an array of aerofoil-sails (away from the ends of the array) has some similarity to the flow through a cascade. The main similarity is that the flow over each aerofoil upper surface is strongly influenced by the induced flow of its "upper" neighbour. Thwaites (1960) notes that the pressure distribution over the rear half of aerofoils in cascade changes more slowly with incidence than it does for isolated aerofoils; in consequence there is an appreciable range of incidence over which unseparated flow can be expected. Even in conditions where separation does occur the mutual interaction of the aerofoils is important. The induced flow from neighbouring aerofoils constrains the flow so that the regions of separated flow near the "upper" surface remain thin and close to this surface. In consequence the cascade continues to usefully deflect flow, even in conditions of stall; and for this reason cascades do not experience a dramatic loss of lift at stall.

5.2(d) Review: trimming strategies

Wagner (1967b) found that graduated sail trim often gives better performance than parallel sail trim. He investigated a large number of Dynaship sail arrays with the sails linearly graduated so that the forward sails were at a smaller angle of incidence to the distant free stream than the after sails. The experiment described in section 5.4(d) compares three strategies for trimming arrays of sails. These strategies are described below. This experiment was conducted with both the symmetric NACA aerofoil rig and the 12% camber thin circular arc rig.

(1) Parallel trim strategy: the obvious and simplest way of setting an array of sails is to have them all parallel. If there was no interaction between sails this would be a very good way of setting the sails. There is, however, considerable interaction. The array of aerofoils act together as a multipart aerofoil and impart curvature to the streamlines. For example, when close reaching (when the inflow angle is less than 90°), this streamline curvature increases the local angle of incidence at the bows and decreases it at the stern. This could result in the leading aerofoils being stalled while the trailing aerofoils are at very low angles of incidence to the local flow. This does not distribute loads equally between the masts and might reduce the attainable useful aerodynamic forces. One possible advantage in having heavier aerodynamic loading forward is that the hydrodynamic sideforce generated by a hull sailing at leeway is also forward, so the required helming moment might be reduced. Otherwise, equal loading would be optimum.

(2) Calculated graduated trim strategy: another possibility is to graduate the sail trim angles so that equal aerodynamic loading occurs on each aerofoil. If the array could be graduated to give identical local flow conditions at all aerofoils there would be several advantages. Firstly, they could all be set at the same most advantageous local angle of incidence; secondly, they would all have to withstand equal structural loads. It is not actually possible to obtain identical local flow conditions as end effects, hull interference and local radius of streamline curvature all vary with position in the array. However, an approximation to this state of affairs is desirable. Some method of predicting suitable arrays is required as an iterative experimental procedure would be prohibitive. Predicting such arrays is problematic. A full three dimensional viscous flow calculation would be impossible with present knowledge. Two simplifications can be made to make the problem tractable. The answers, while not precise, should still give a meaningful approximation to the desired conditions. The first is to use a potential flow model for conditions that correspond to flow being attached everywhere. The second is to use a two dimensional model. The heights of the aerofoils are large compared with typical widths of gaps between them, so away from the ends the flow will not be very different from two dimensional flow. Using the approximation of two dimensional, attached, potential flow, an iterative procedure can be used to calculate arrays of aerofoil angles which give equal local angles of incidence on all aerofoils. For the eight aerofoils used in these test, arrays have been calculated for a

number of inflow angles and for a number of modelled local angles of incidence. Arrays have also been calculated by this method for a few angles of incidence so large that the flow would no longer be attached. In these cases there is no reason to expect the aerofoils to be even approximately evenly loaded. The method used to predict these arrays is described in Chapter 6.

(3) Linearly graduated trim strategy: a third and arbitrary way of setting sails is to have them linearly graduated. That is to have the trim angle reduced in equal steps of n degrees working from bow to stern. This should give some of the advantages of the calculated graduation described above. For practical use this is a slightly simpler scheme. As the most favourable magnitude of n for particular circumstances is unknown, a range of values was tested.

5.2(e) Review: Reynolds number effects

Jacobs and Sherman (1937) and Scholz (1965) discuss the influence of Reynolds number on the flow past an aerofoil. The flow alters gradually with Reynolds number except in a limited range (typically lying somewhere between Re = 10^5 and Re = 10^6) where the flow alters more rapidly. The former gradual changes are associated with gradual changes in the boundary-layer thickness which produce gradual variations in the aerofoil's pressure and force characteristics. The latter major changes to the flow are associated with the fundamental transition from laminar to turbulent flow in the boundary layer. A consequence of this transition can be that separation is avoided or delayed, which leads to important alterations to the outer inviscid flow and significantly affects the aerofoil's force and pressure characteristics. The range of Reynolds number where these comparatively rapid changes occur is known as the "critical" range.

The critical behaviour of separation reflects differences in the ability of laminar and turbulent boundary-layers to withstand adverse pressure gradients without separation occurring: the turbulent boundary-layer displays a greater resistance to separation than the laminar boundary-layer. The pressure on the upper surface of an aerofoil generally falls, then rises in a downstream direction; there is an adverse pressure gradient downstream of the minimum pressure point which becomes more severe as the angle of incidence is increased. When the boundary-layer is laminar at the minimum pressure point, separation may be expected to occur very quickly downstream of the minimum pressure point if there is a sufficiently large

adverse pressure gradient. If, however, in this case, the boundary layer changes from laminar to turbulent before the minimum pressure point, then the position of the separation point will move in a downstream direction due to the turbulent boundary layer's ability to withstand greater adverse pressure gradients.

Below the critical range, the position of (laminar) separation virtually does not change with Reynolds number. Above the critical range, the position of (turbulent) separation changes gradually with Reynolds number.

Simulating above-critical flow. Ideally tests should be conducted at the full-scale Reynolds number: for practical reasons, this is often not possible and frequently tests conducted at subcritical Reynolds number are expected to give information on an above-critical full-scale flow. The differences between model and full-scale flows can be much reduced by artifically tripping the flow to prevent laminar separation. The flow can be tripped to achieve transition in several ways: for example, Abbott, Von Doenhoff and Stivers (1945) report the use of strips of carborundum, Wallis (1946) reports the use of a trip-cord. A disadvantage is that the carborundum roughness or trip-wire causes a slight increase in drag.

Thick aerofoils: Jacobs and Sherman (1937) conducted experiments with various NACA section aerofoils in the Reynolds number range of 4×10^4 - 3.1×10^6. The critical test Reynolds number was found, typically, to be of the order of 3×10^5. (This value was considered to be low because of the turbulence of the wind tunnel air stream). The minimum profile drag of the aerofoils generally

displays similar characteristics to those of a flat plate: below critical conditions the profile drag drops off with Reynolds number, in the critical range the profile drag usually increases, above the critical range the drag again drops off gradually with Reynolds number; the lift/incidence slope hardly changes with Reynolds number. The value of the maximum attainable lift coefficient, which is entirely dependent on boundary layer behaviour, is considerably influenced by the Reynolds number (for example, C_{Lmax} for the NACA0018 aerofoil varies between about 1.1 at Re = $3x10^5$ to about 1.4 at Re = $3x10^6$). Goett and Bullivant (1939) conducted tests of NACA aerofoils in the NACA full-scale tunnel and achieved a test Reynolds number of $7x10^6$. They found that at these higher Reynolds numbers the minimum profile drag continued to decrease gradually and the maximum lift coefficient continued to increase slightly, with Reynolds number.

Thin aerofoils: Milgram (1971) tested thin highly cambered plates in the Reynolds number range $6x10^5$ to $12x10^5$. He found that in this range, maximum lift increases slightly with Reynolds number (although the highest Reynolds number produces slightly lower lift at low angles of incidence); the lift/incidence slope and minimum drag show little dependence on Reynolds number. Marchaj (1979) quotes results of force test for a thin (417a) and thick (N60) aerofoil section in the Reynolds number range, $2.1x10^4$ to $1.7x10^5$. In this low range, typical changes in force coefficients for the thin cambered plate aerofoil (417a) are an order of magnitude smaller than those for the thick (N60) aerofoil:

this comparative insensitivity to Reynolds number is almost certainly due to a small separation bubble which starts at the leading edge (except when the leading edge is almost aligned with the local inflow). This bubble initiates with laminar separation and trips the flow so that it is subsequently turbulent. In this way above-critical conditions are produced even at these lower Reynolds numbers.

Cascades: Scholz (1965) reproduces results of various investigations into the effects of Reynolds number on the flow through cascades. The effects of Reynolds number on flow and therefore on force and pressure characteristics, show similar trends to those of individual aerofoils. Diffuser-type cascades have been tested in the Reynolds number range 3×10^4 to 5×10^5 by Stuart (1955): compressor-type cascades have been tested in the same range by Rhoden (1956).

Yacht sails: Marchaj (1979) gives an interesting general discussion of Reynolds number effects on yacht sails. Critical behaviour is particularly important to yachts as the operating range for yacht sails includes the critical range: the operating range is from about 5×10^6 down to almost zero. There are two reasons why low Reynolds number conditions are experienced on yacht sails; firstly they are often triangular so the chord length, upon which a local Reynolds number will be based, tapers to zero at one or both ends; secondly, yachting being recreational, the sails are sometimes used when the wind is light. The normal minimum operating Reynolds number for a rectangular sail on a powered commercial

sailing vessel would probably be above the critical range, (for example, a 10m chord sail in a 10 kt relative wind gives a Reynolds number of about 3×10^6).

5.3(a) Method: outline

The experiment is conducted using a model of the above water part of the ship which can be fitted with the various model sail rigs to be tested. The model is mounted in a wind tunnel close to the tunnel wall which simulates the sea surface. The mounting is linked to a balance which is used to measure the aerodynamic lift and drag. The model's angle of incidence and the trim of the sails are adjusted by hand for each run. The tunnel is run at about 20 m/s while the force measurements are made. The velocity is then reduced to about 10 m/s so that the flow can be investigated with a wool tuft on a stiff wire.

Sections 5.4(a) to 5.4(g) report investigations on the following: single sail characteristics, combined rig characteristics, effect of end-plates, influence of mast-number, reefing strategy, trimming strategy and influence of heel.

Appendix A5.1 reports a Reynolds number test, A5.2 reports a repeatability test and A5.3 is a table of all results obtained.

5.3(b) Method: The model ship

Figure 5.3 shows the wooden-hulled model ship used for this experiment. Figure 5.4 is a plan drawing of the model defining various dimensions and angles. The hull has a length of 640mm, beam of 80mm and height of 40mm. 7 alternative types of aerofoil sail were tested. These have various combinations of camber and thickness. Figure 5.5 shows these various sections. When normally rigged, the ship has 8 aerofoil sails which rotate about their quarter points (for NACA aerofoil sections) or their mid points (for circular-arc aerofoil sections). They are 240mm high and have a chord of 80mm. Sand roughness extends for 10mm along the upper surface from the leading edge of each aerofoil. Sail trim angles of aerofoils and the inflow angle of the ship were set by hand.

To model the sea surface, the model ship was tested near a tunnel wall; to enable simple coupling to the balance this was a vertical side wall. The clearance between ship and wall was less than 1mm. The ship's vertical axis was usually normal to the wall (representing an upright ship): some tests, however, were made with the ship heeled.

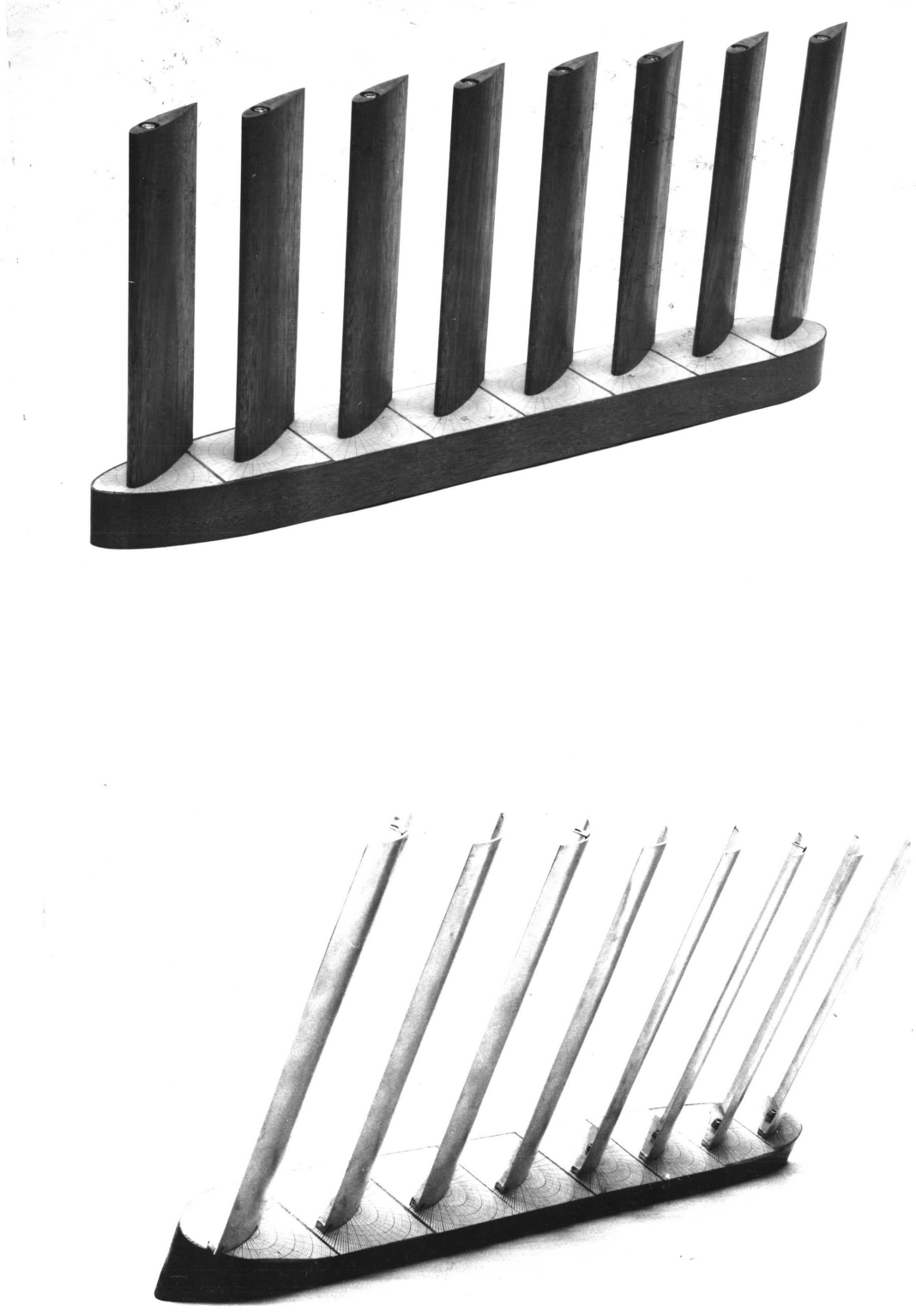

Figure 5.3

Model ship: upright with symmetric aerofoil-sails (top) and heeled with 12% camber thin sails (bottom)

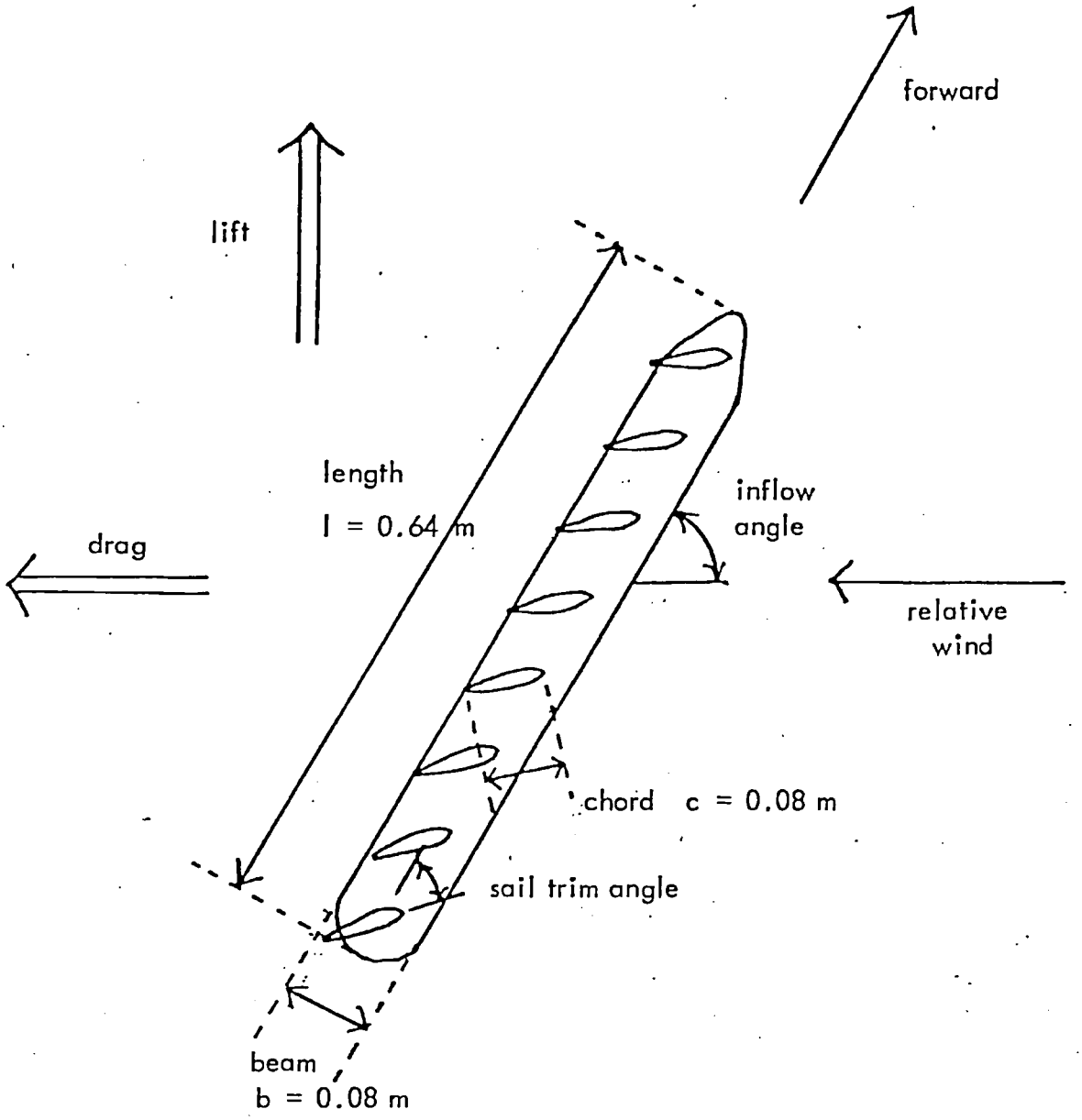

Figure 5.4

Plan view of model ship

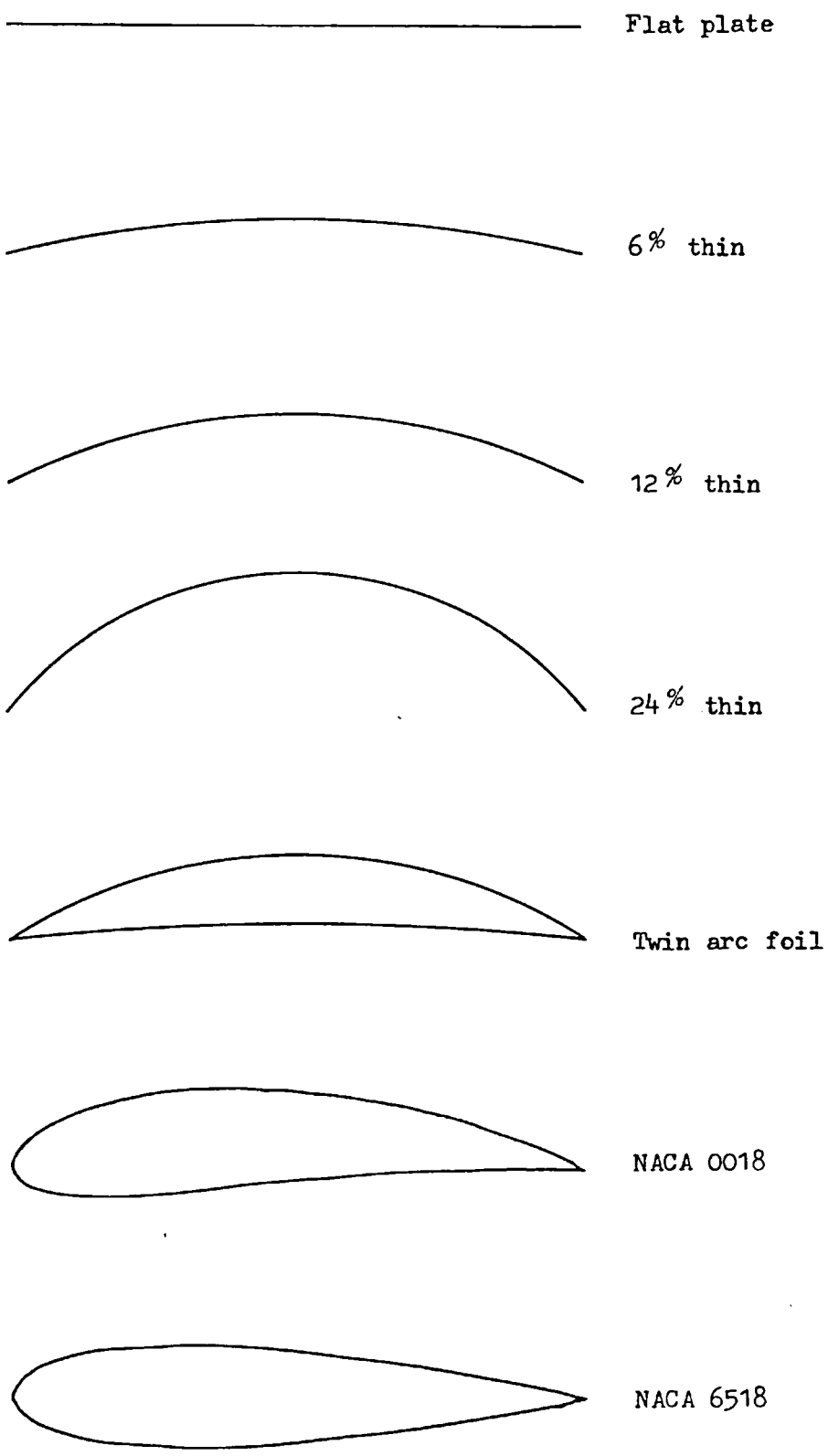

Figure 5.5

Sections of tested aerofoil sails.

5.3(c) Method: the wind tunnel

Tunnel. The tests were conducted in the Donald Campbell Low Speed Wind Tunnel in the Imperial College, Aeronautics Department. This is a closed return circuit tunnel. The working section is 4.5ft wide, 4ft high and 10ft long. Breather slots at the downstream end of the working section help to maintain static pressure close to atmospheric pressure within the test section. The flow ahead of the contraction is smoothed by passing through a small cell honeycomb and a screen which reduce the turbulence level to 0.2% in the working section. Calibration and details are given by Bearman, Harvey and Gardner (1976).

Speed measurement. To infer with minimum error the wind speed, the difference in static pressure upstream and downstream of the contraction is measured using a Betz manometer with a resolution of 0.1mm H_2O. The relationship between pressure difference and speed, for the empty tunnel, is known from previous calibrations. This method of determining wind speed is described by Pope and Harper (1966). Most sail experiments were run at a speed of about 20 m/s, giving a Reynolds number ($\rho V c/\mu$) of about 10^5.

Force measurement. The tunnel is equipped with a three component balance mounted above the working section which can measure lift, drag and pitching moment. The balance is of moving weight weighbeam type. The mechanism is shown in figure 5.6. The resolution of the balance is 0.01 lbf lift, 0.001 lbf drag and 0.001 ftlbf pitching moment. The weighbeam controls are interfaced to a computer. A computer routine developed by Davis is used to

balance the weighbeam automatically. During the experiment, force coefficients were calculated and plotted immediately so that interesting features or possible errors could be identified during the test. The forces are non-dimensionalised by $(\frac{1}{2}\rho_a V^2) \times S_A$ The reference area, S_A, is the normal total sail area.

Flow visualisation. After each force measurement the tunnel wind speed was reduced to about 10 m/s and the flow was investigated with a wool tuft on a stiff wire. In every case, brief notes were made on the extent of separation. A few fairly detailed surveys of separated regions were made; a series of these made at a range of Reynolds number are produced in appendix A5.2.

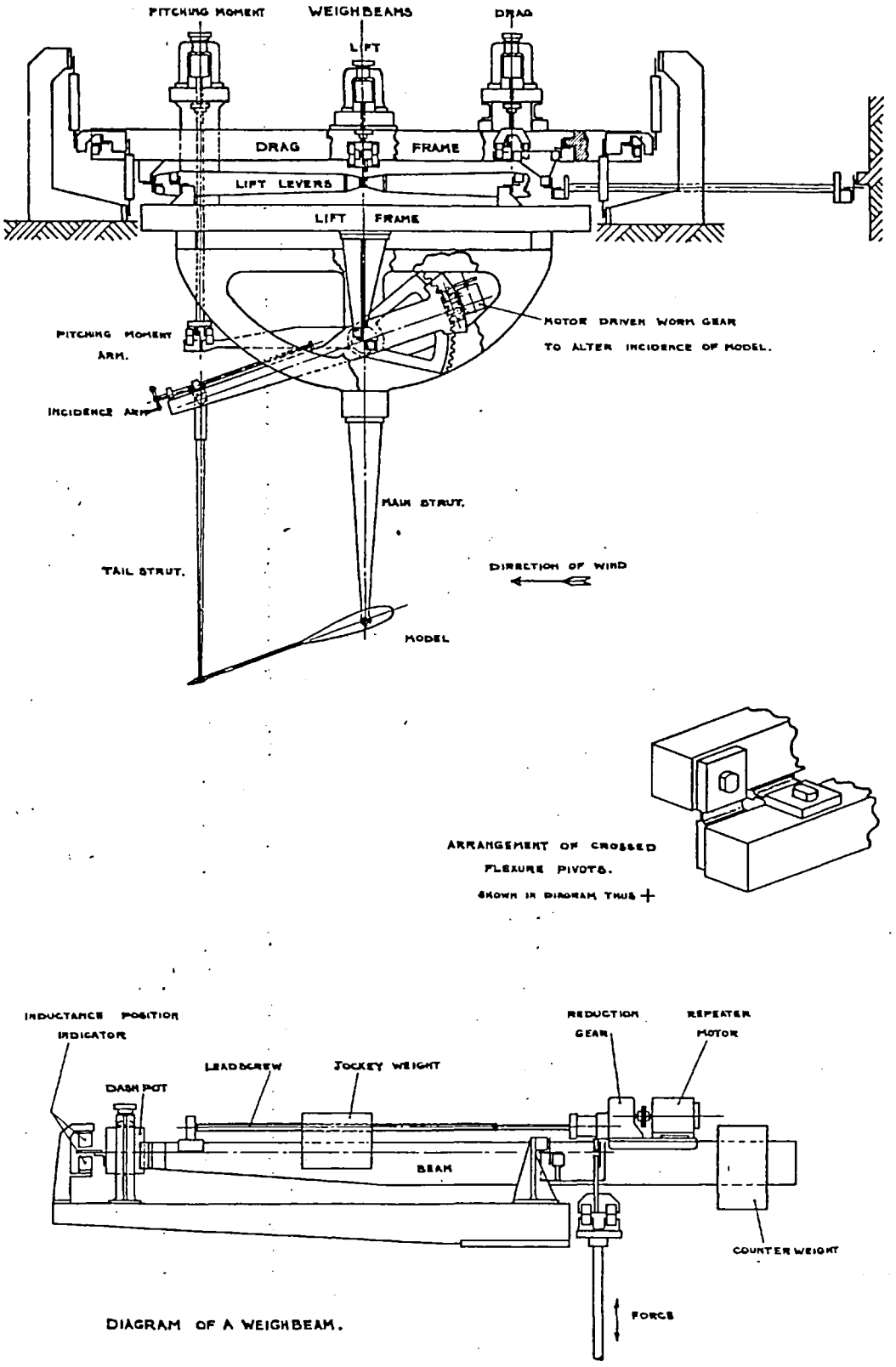

Figure 5.6

Balance mechanism

5.4(a) Results: single aerofoil-sails

Single aerofoils of aspect ratio 3 were tested at the forward station of a head-to-wind hull. Graph 5.7 shows the sail force coefficient non dimensionalised by the single sail area.

After subtracting the drag of the naked hull, the two thick NACA aerofoils show greater maximum lift to drag ratios than thin aerofoils of equal camber. In every other respect the thick aerofoils perform less well than the thin aerofoils: they show a lower maximum lift, more catastrophic loss of lift at stall, and lower total forces in all stalled conditions.

The thick circular arc foil with 9% camber performs less well in all respects than either the 6% or 12% camber thin circular arc aerofoils.

Thin circular arc foils with camber of 0%, 6%, 12% and 24% are compared. Maximum lift to drag ratio is highest at 6% and then drops off with camber. Maximum lift increases with camber, as does total force in stalled conditions.

As discussed in section 5.2(e), Reynolds number scale effects tend to be more serious for thick aerofoils than for thin aerofoils. Comparison of the force curves in figure 5.7 with published results (for the same effective aspect ratio) referred to in section 5.2(b) show that the maximum lift coefficients obtained for the sharp edged aerofoils are close to their expected values, while those for the rounded nose aerofoils are not: the maximum lift coefficients obtained here at a Reynolds number of about 10^5 are 0.7 (for the NACA 0018) and 1.15 (for the

NACA 6518); corresponding values at a Reynolds number of about $3x10^6$ reported by Jacobs, Ward and Pinkerton (1933) are 1.5 and 1.6. Some difference can be expected due to hull interference, but this would undoubtedly be smaller than the observed differences. It is apparent that the strip of sand roughness has not successfully produced turbulent flow over the NACA aerofoils, so the model flow is not similar to the above-critical flow.

There are at least three possible ways that the sand roughness could fail to simulate above-critical flow on the thick NACA aerofoils; firstly, the sand roughness could fail to trip turbulent flow; secondly, the flow could separate before reaching the sand roughness (the sand roughness only starts at the leading edge while the stagnation point is below the leading edge); or thirdly, the forward edge of the roughness strip, which is a very low step on the surface, could induce separation where it would not otherwise occur. It is not clear which of these is the correct explanation, although tests made at a range of Reynolds numbers, and described in appendix A5.1, indicate that the first is unlikely.

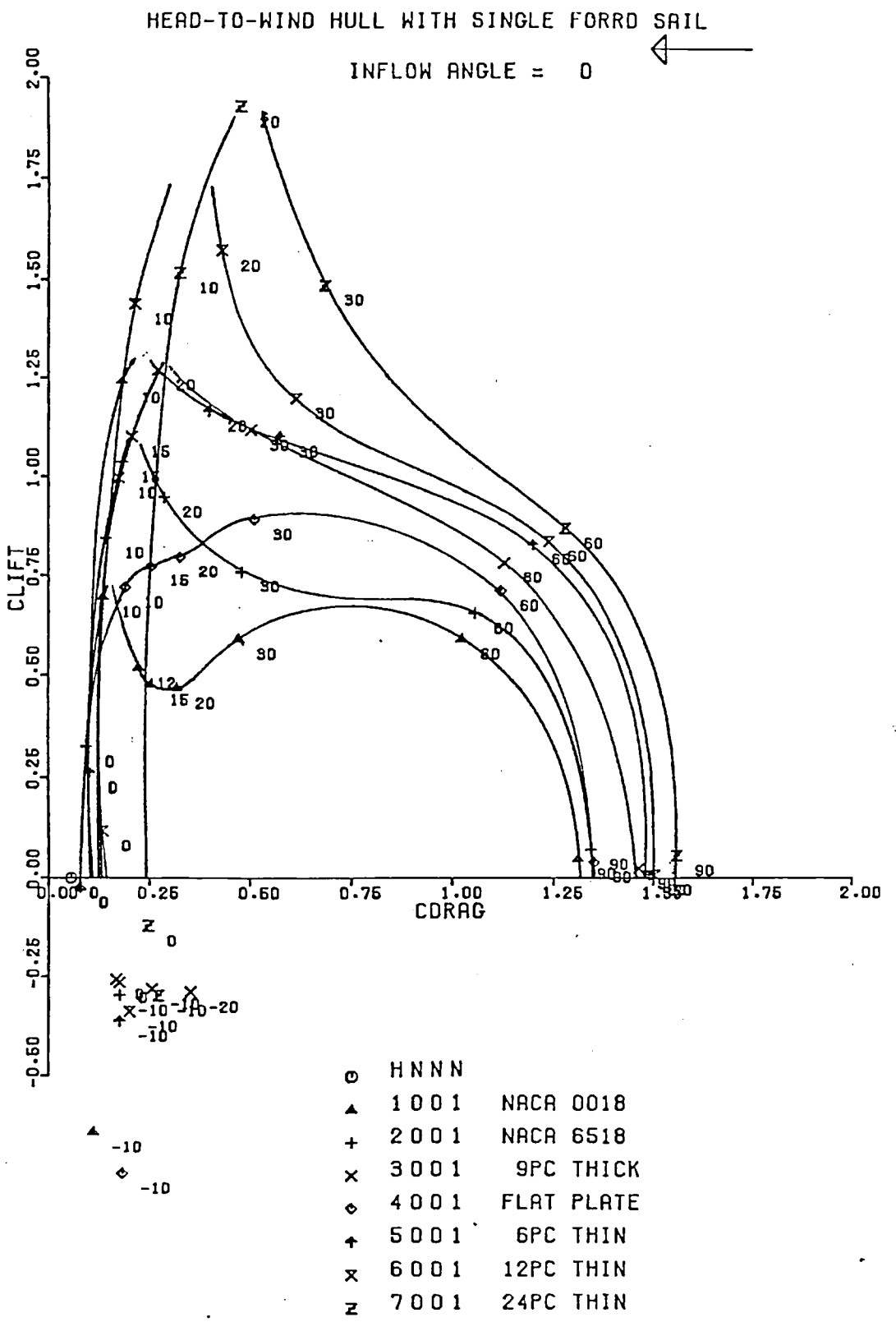

Figure 5.7

Characteristics of individual aerofoils.

5.4(b) Results: comparison of rigs

Standard rigs of 8 parallel trimmed sails were compared with the sails set in a range of sensible configurations and with the ship at a range of inflow angles. In the subsequent discussion the rigs are normally compared in terms of their useful (or "driving") component of force. This is the best component of force acting along the ship's centre line. Comparison of this useful force gives a good qualitative indication of the relative merits of the rigs.

At 10° incidence no rig gives a positive useful force. The NACA 6518 produces less retarding force than a 6% camber thin foil. At all other angles of incidence the two NACA section aerofoil rigs perform less well than thin circular arc foils of the same camber. As noted in section 5.4(a), Reynolds number scale effects make this result inapplicable to full-size rigs.

The 9% camber thick circular arc aerofoil performs less well at all headings than the 6% or 12% camber thin circular arc aerofoils.

Rigs with 0%, 6%, 12% and 24% camber thin circular arc foils were tested. Comparison of the rigs showed that the optimum camber increases with inflow angles from an optimum of 6% camber at low inflow angles to an optimum of 24% camber for inflow angles of 90° and above.

It is interesting to compare the force coefficients of a single sail with those of a rig consisting of an array of such sails. The rig has considerably more drag and a considerably lower maximum lift to drag ratio. The rig does not display the same catastrophic loss of lift at

stall. The maximum lift coefficients of the best single sails are similar to those of rigs of these sails. The maximum lift coefficients of the poorer sails are actually increased when they are part of a rig. (This is presumably because favourable interaction between sails is delaying stall). That is to say, sails which perform poorly alone perform comparatively better when they are part of a rig. The relative order of performance of rigs could, however, have been inferred from the relative order of performance of single sails.

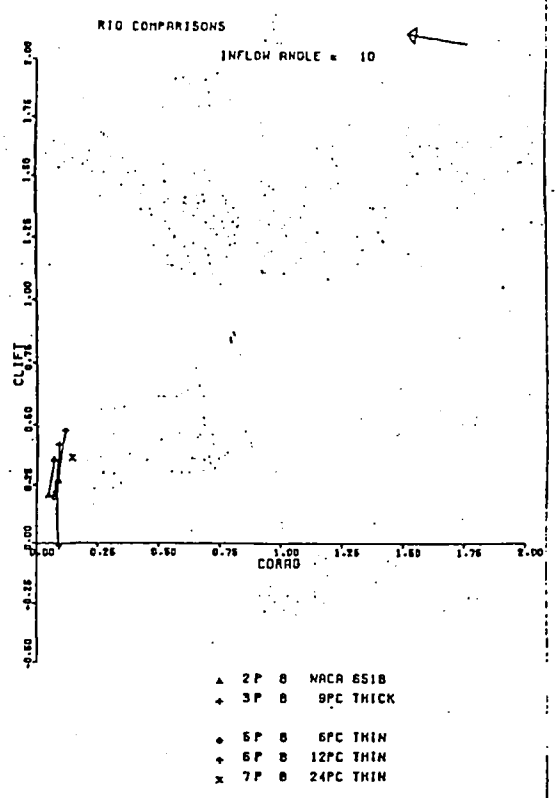

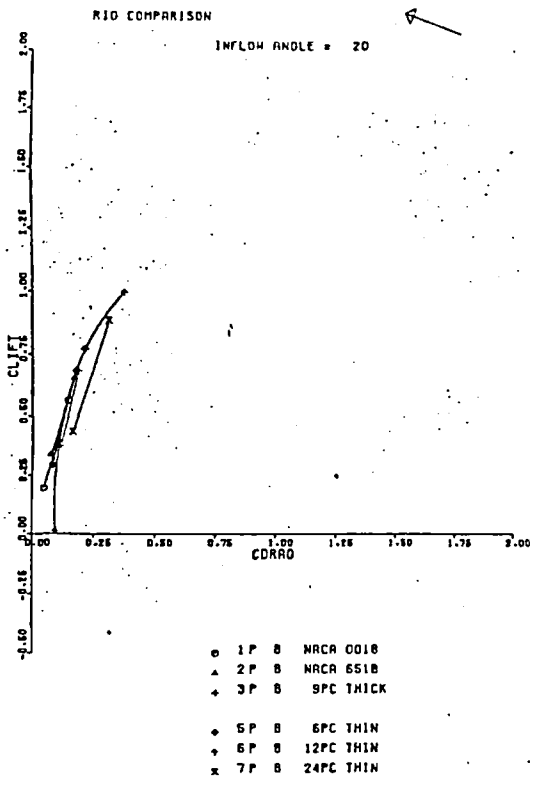

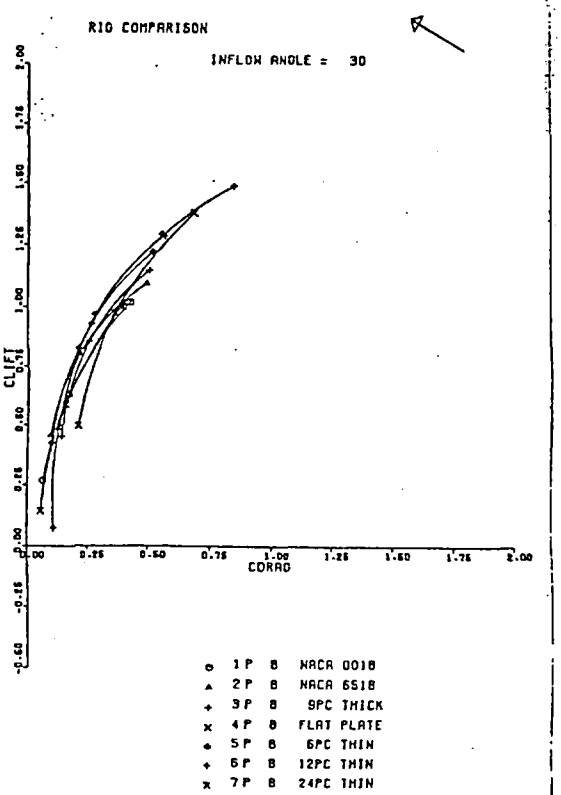

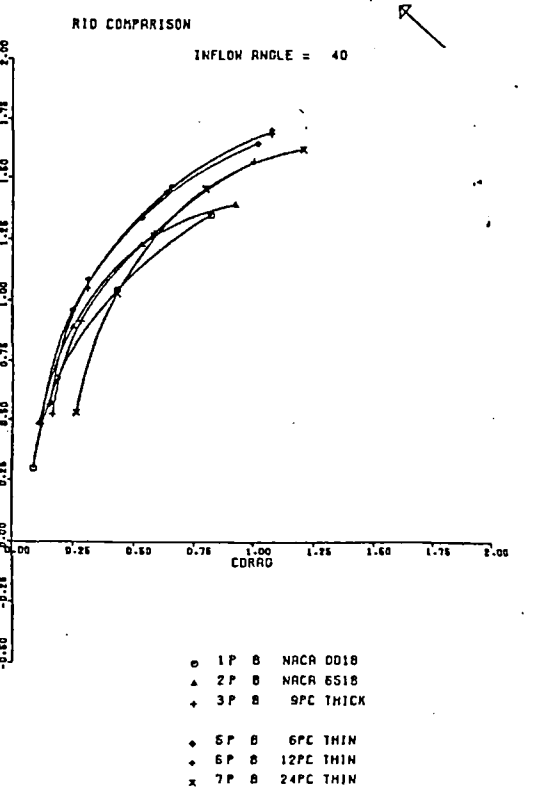

Figure 5.8

Comparison of the various rigs tested.

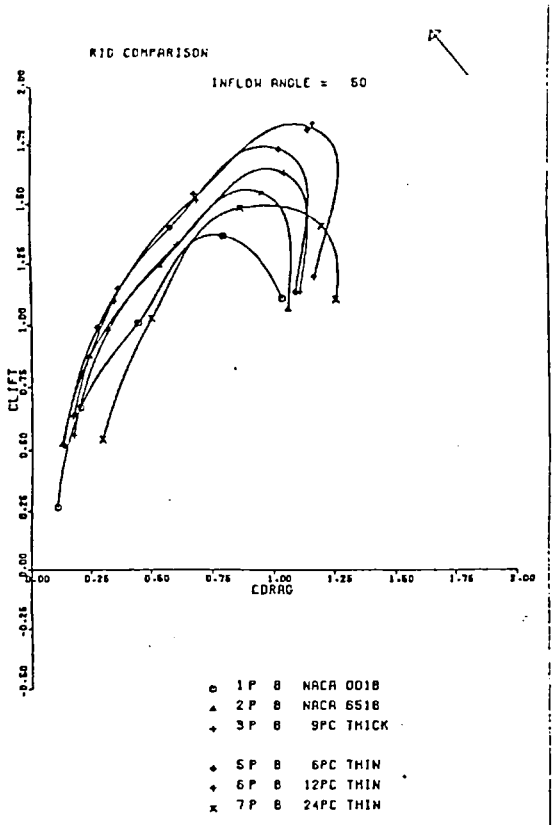

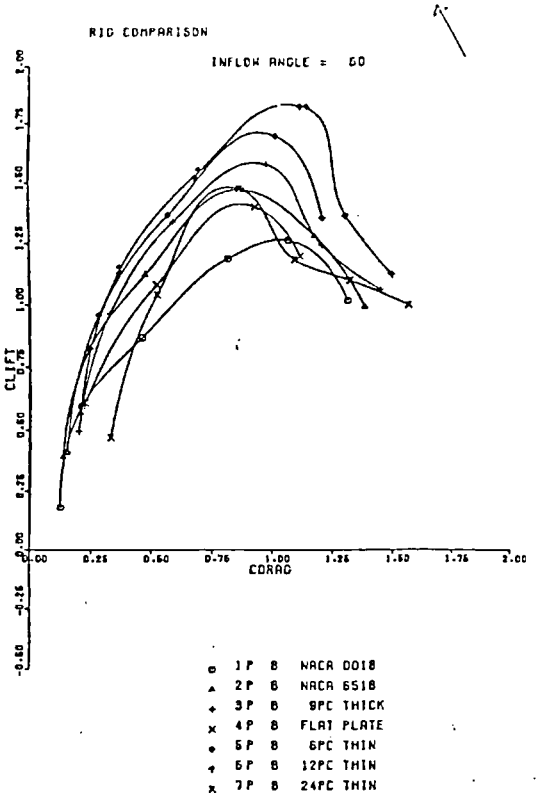

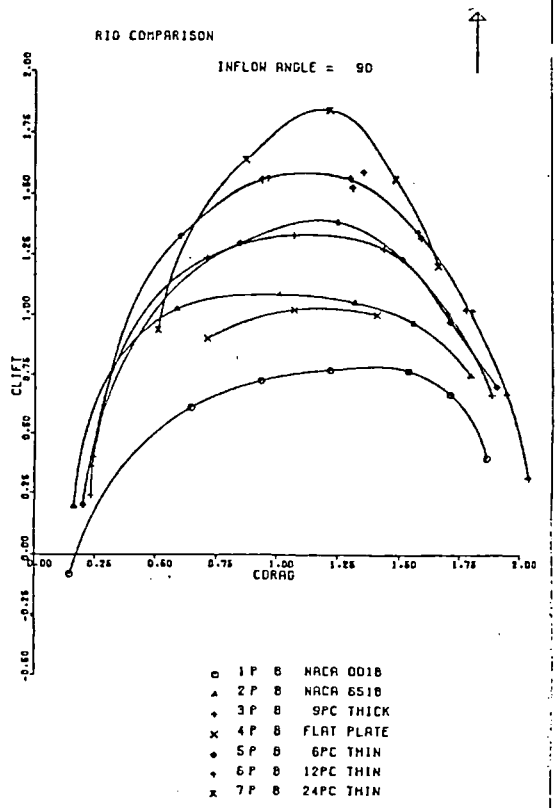

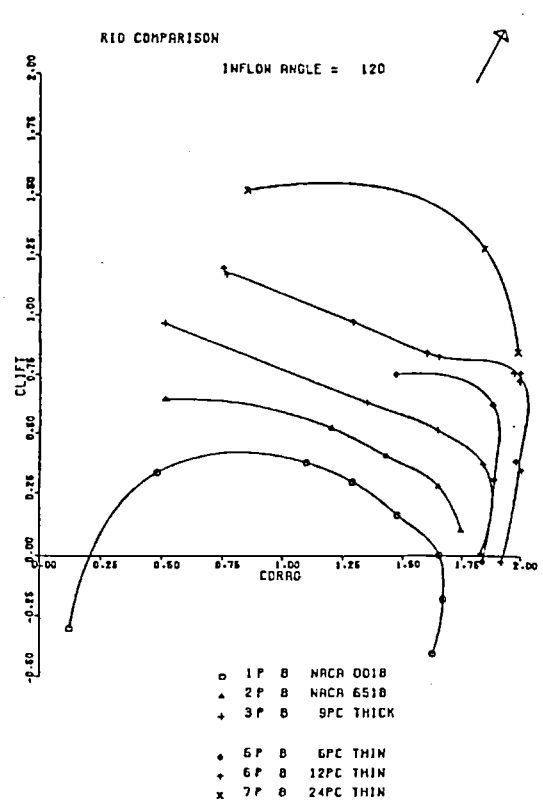

Figure 5.9

Comparison of the various rigs tested.

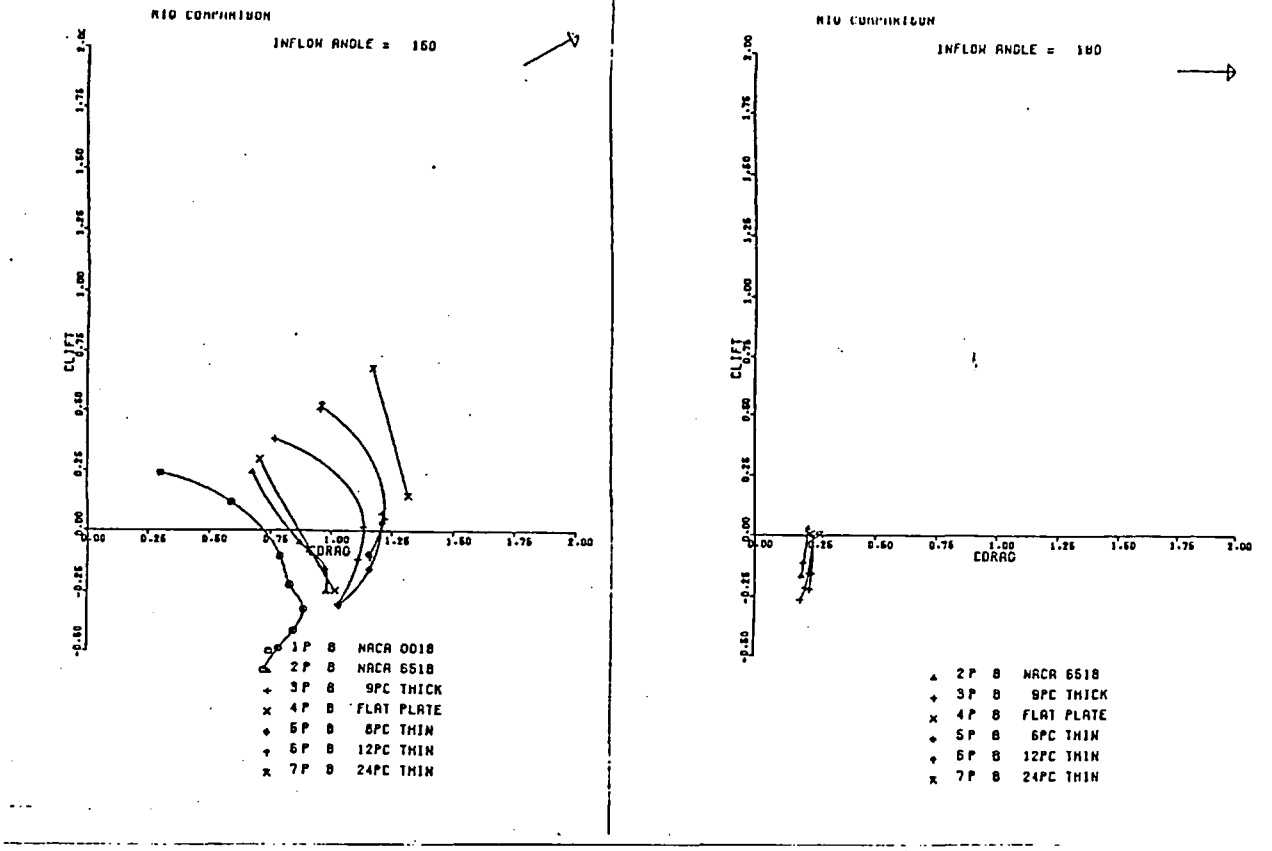

Figure 5.10

Comparison of the various rigs tested.

5.4(c) Results: effects of end-plates

Two mast-head end-plates were tested. The smaller had the same planform as the ship, the larger was twice as wide as the ship. Graph 5.11 compares a normal rig with a rig fitted with the end-plates at all angles of incidence. The sails are NACA 0018 section and are graduated from 28° to 0°. At low angles of incidence (20°-30°) the flow is fully attached and the plate increases lift slightly. At larger angles of incidence (35°-40°) the flow is partially separated and the plate results in a loss of lift. At angles of incidence greater than 60° the flow is very bluff and the plate increases both lift and drag. At all angles the larger plate produced marginally more effect than the small plate. Only the large plate was tested in the second part of this test.

The plate was tested at 30° and 90° incidence with the two NACA aerofoil section rigs and the 12% cambered thin plate rig. Figures 5.12 and 5.13 show the results. At 30° incidence the plate does not increase the useful component of force for any rig. At 90° incidence the plate reduces the useful component of force for the thin sail rig but marginally increases it for the two aerofoil rigs.

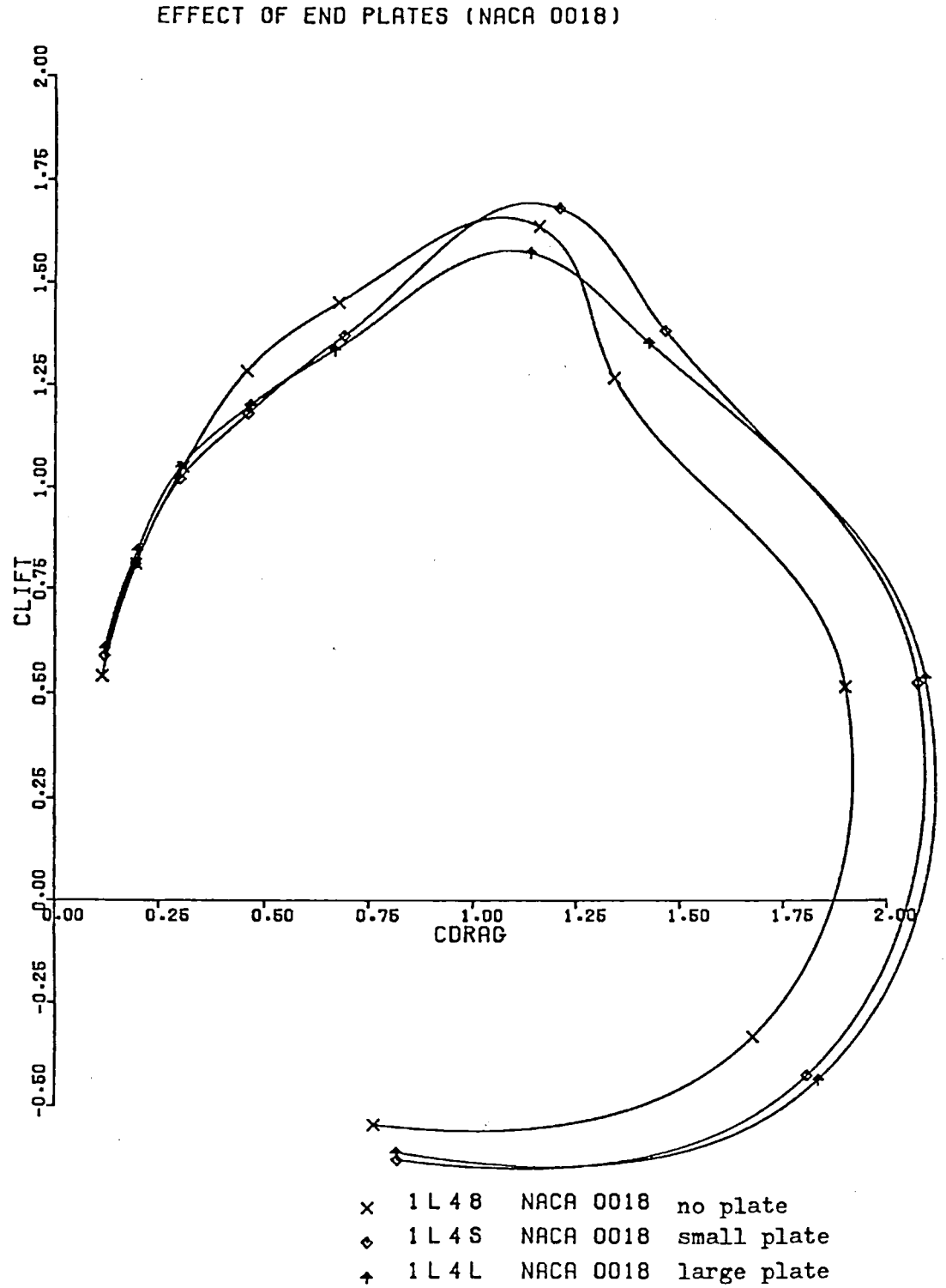

Figure 5.11

Effect of end plates: symmetric aerofoil section sails.

These force coefficients are for constant trim at varying inflow angles.

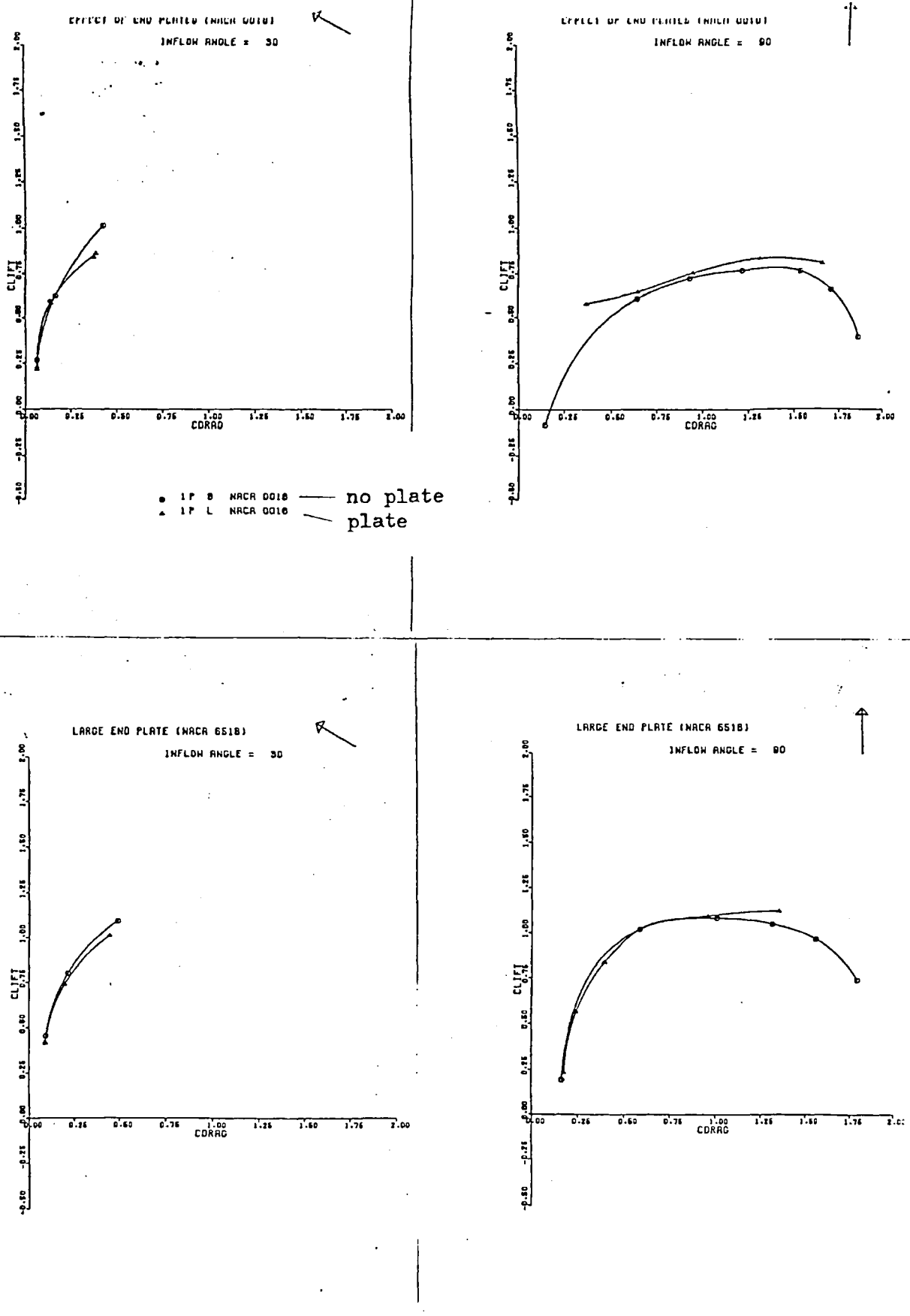

Figure 5.12

Effect of end plate for symmetric(top) and asymmetric (bottom) aerofoil section sail rigs.

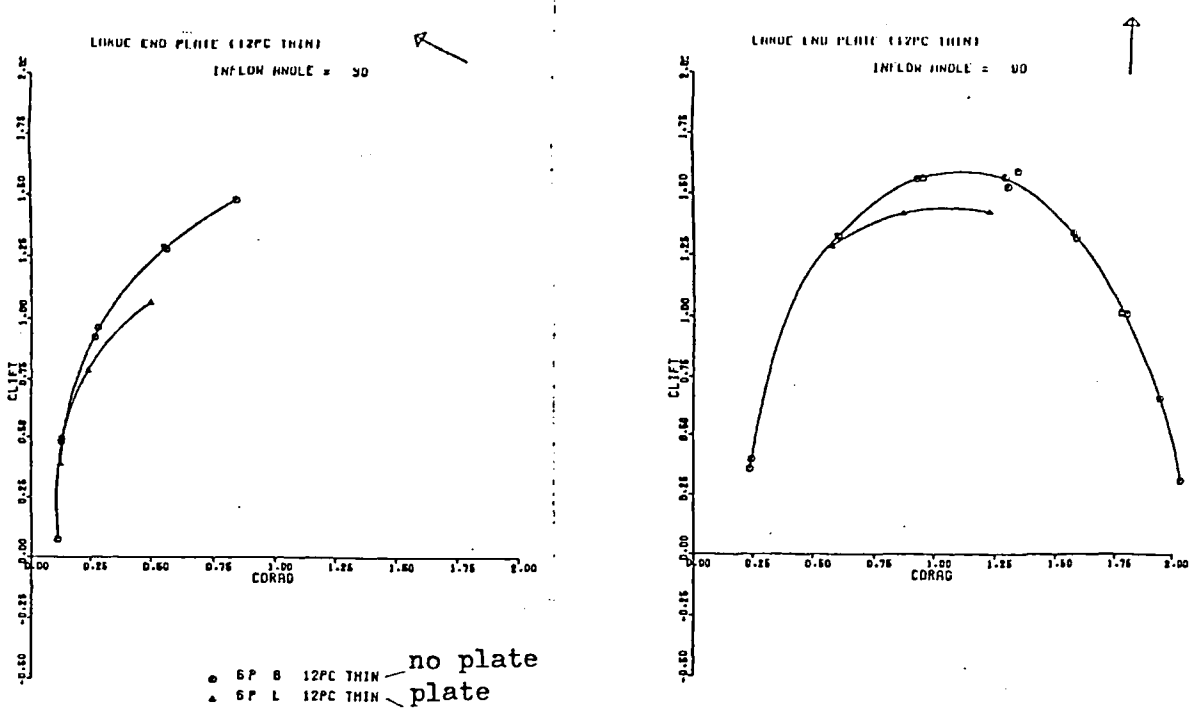

Figure 5.13

Effect of end plate for thin cambered plate sail rig.

5.4(d) Results: influence of mast-number

The ship was tested with 8, 6 or 4 sails. When 6 sails were fitted they were equally spaced between the normal 1st and 8th positions; when 4 sails were fitted these were equally spaced between the 1st and 7th positions. The main test was made with 12% cambered thin sails; some parts of the test were repeated with flat thin sails or symmetric NACA section aerofoil sails.

Figure 5.14 shows the results of the tests made with the thin cambered plate sails. At low angles of incidence 6 sails provide as much useful component of force as 8 sails. This is a result of the lower drag of the 6 sails. 4 sails have a better lift to drag ratio than 6, but do not provide a better useful force as the lift developed is too small. With increased inflow angle the larger number of sails become increasingly beneficial. At 90° inflow angle a larger number of sails produce a disproportionately large increase in useful force. This is probably due to the closer proximity of neighbouring aerofoils delaying stall by reducing adverse pressure gradients on the aerofoil leeward surfaces so that separation does not occur as it would on an isolated aerofoil. This allows the aerofoils to generate greater maximum lift forces than would otherwise be the case. At larger angles of incidence the larger number of sails still increases the useful component of force, but not in the same disproportionate way.

The flat plate rig appears to show similar characteristics (see figure 5.15 - bottom). The two tests with the NACA aerofoil rigs suggest that the useful force component remains more nearly proportional to number of sails for

this rig (see figure 5.15 - top); again, Reynolds number scale effects, discussed in section 5.4(a), make this particular result inapplicable to full-size ships.

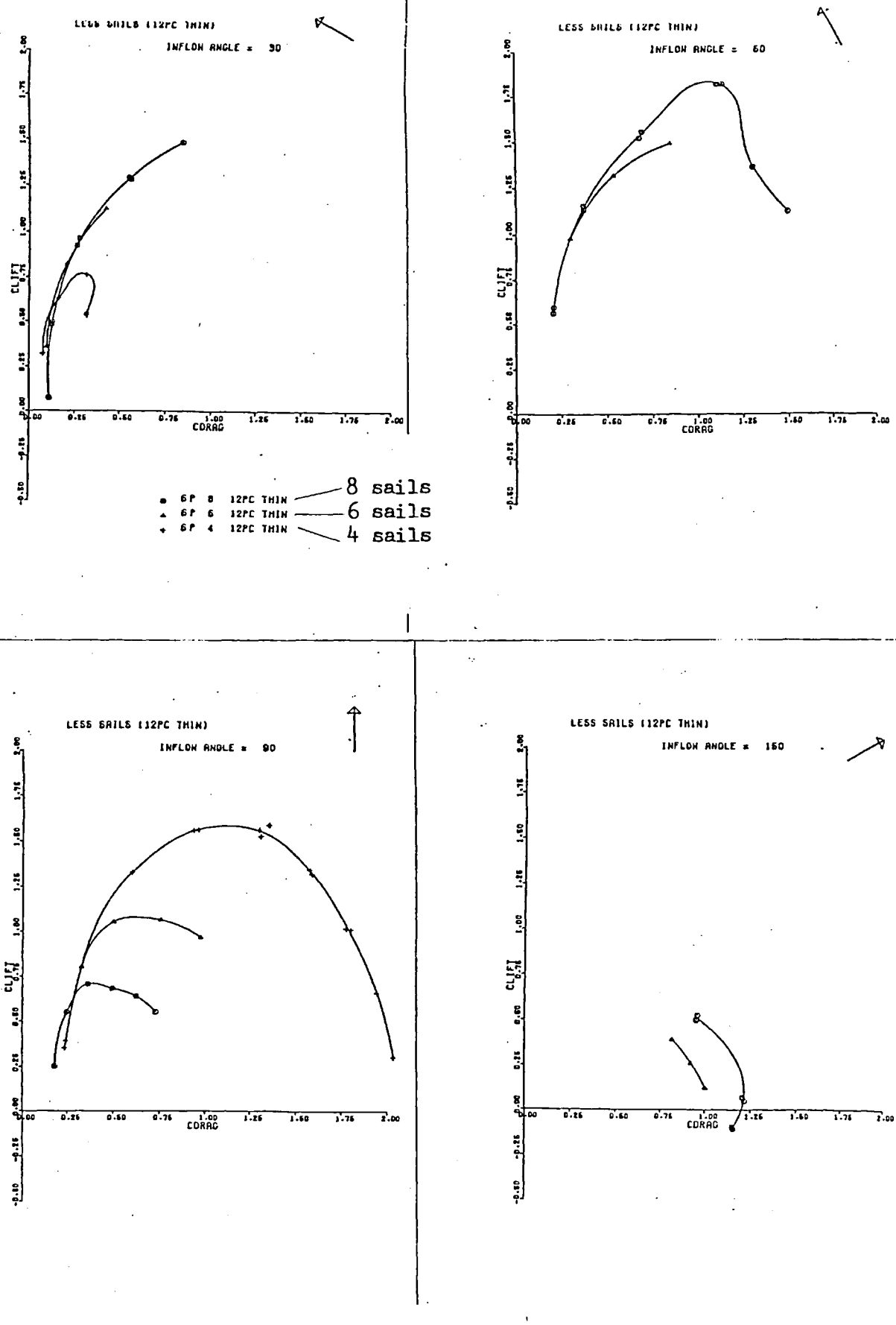

Figure 5.14

The effect of reducing mast-number: thin cambered plate sails.

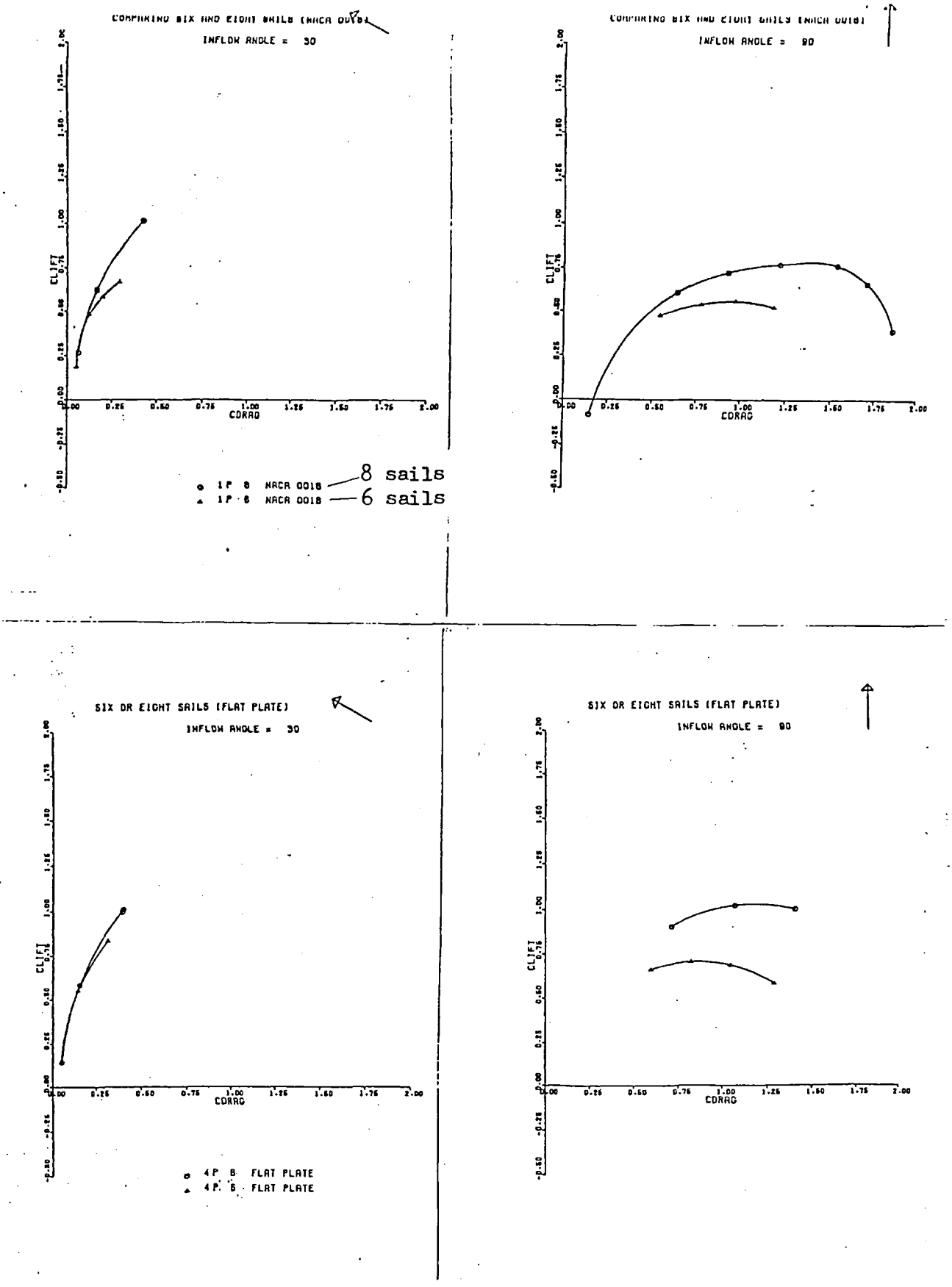

Figure 5.15

The effect of reducing the mast-number for symmetric aerofoil section sails (top), and flat plate sails (bottom).

5.4(e) Results: reefing strategies

This test investigates the relative merits of three possible reefing strategies. The sail area is halved either by reducing the height of all sails, by removing the four after sails, or by removing alternate sails. These strategies referred to in the figures as (H), (4) and (A) respectively, are compared at 30° and 90° inflow angle for the 12% camber thin sail rig.

The reduced height strategy (H) results in considerably more drag than either of the other strategies. This is to be expected as a low aspect ratio lifting surface produces more induced drag for the same lift. The reduced-from-aft strategy (4) produces better maximum lift than the alternate removal strategy (A). This is probably because when the four sails are in closer proximity they act together more like a single multislot aerofoil, separation at each being discouraged by the flow induced by the forward neighbouring sail.

Reduction of sail is likely to be required as the result of severe weather. It is not clear, without making further assumptions, which strategy would be best in these circumstances. At 30° inflow angle the reduced-from-aft strategy (4) gives the best useful force component but the reduced height strategy gives lower sideforce component and a lower heeling moment. At 90° inflow angle the reduced height strategy (H) gives marginally the best useful force component. It also gives a considerably higher sideforce component but heeling moment is smaller than either of the other strategies because of the lowering of the centre of pressure.

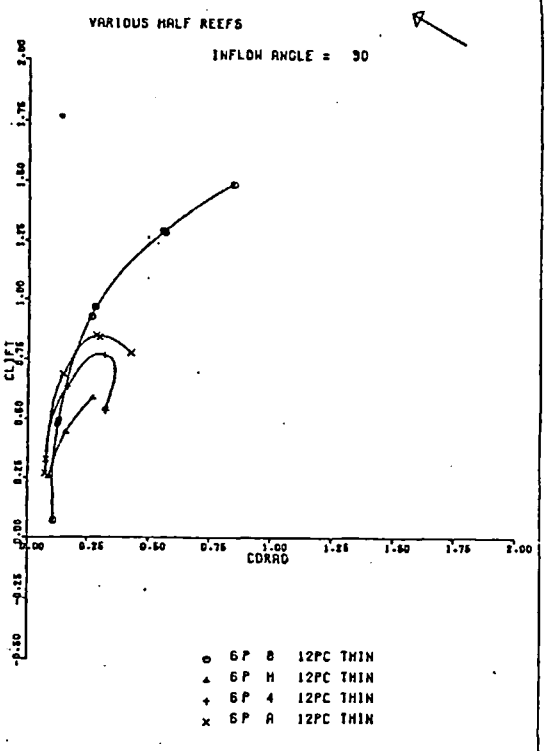

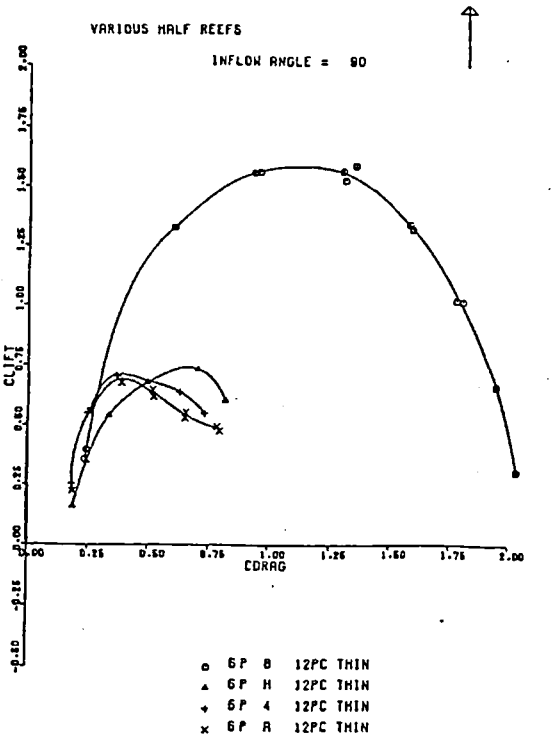

Figure 5.16

Comparison of reefing strategies.

5.4(f) Results: trimming strategies

NACA 0018 section. At low ship inflow angles the parallel arrays give a lower maximum lift than the better graduated arrays. At angles of inflow greater than 90° the parallel arrays produce the best lift. The parallel arrays produce comparatively low maximum lift to drag ratios. This may be because the sails are never all near to conditions of individual maximum lift to drag ratio as they are at a range of local angles of incidence. The calculated graduated arrays produce higher lift to drag ratios than the arrays linearly graduated by 2° or 4° per aerofoil. However, the linearly graduated arrays usually produce a greater maximum lift than the calculated graduated arrays.

Differences in maximum lift seem to be associated with differences in the way stall occurs. Two extreme stall modes can be distinguished. These are diagrammatically represented in figure 5.17, the upper illustration showing a catastrophic forward sail stall, and the lower a widespread individual sail stall. The first mode is often observed near conditions of maximum lift for parallel arrays where the aerofoils are successively less heavily aerodynamically loaded. The flow separates from the leading edge of the forward aerofoil, producing a wide bluff body type wake. The flow is attached over the subsequent aerofoils. Although stalled, the forward aerofoil and its wide wake deflect the flow over subsequent aerofoils, perhaps reducing adverse pressure gradients and delaying separation. The second mode is often observed near conditions of maximum lift for some of the graduated arrays where all the aerofoils are at similar

local angles of incidence. Partial stall can be observed on a number of aerofoils. Typically separation bubbles or pre-trailing-edge separation occur along much of the length of these aerofoils. A further difference is observable between linearly graduated arrays and calculated graduated arrays. As the arrays approach conditions of maximum lift the stall often starts with the forward sails for the linearly graduated arrays, but often with the after sails for the calculated graduated arrays. This suggests that the two dimensional potential flow calculation produces arrays which are too severely graduated at the after part of a three-dimensional ship like array.

As discussed before, the "driving force" component along the ship's centreline is a good criterion for practical comparison. For inflow angles of less than 90° the various graduated arrays generally give a higher maximum driving force than the parallel arrays. For greater inflow angles the parallel arrays give the highest maximum driving force.

These conclusions may not be valid for a full size thick symmetric-aerofoil rig because of the Reynolds number scale effects discussed in section 5.4(a).

12% camber thin sails. With these sails, the calculated graduated arrays always produce lower lift to drag ratios and lower maximum lift than the linearly graduated or parallel arrays. The linearly graduated arrays generally give the best maximum lift.

The parallel arrays often stall with the catastrophic sail stall described before. There is often attached flow over most of the aerofoils, although the

after sails are at small local angles of incidence and probably do not contribute much to the total lift. The arrays linearly graduated by 2° per aerofoil tend to stall on the forward sail or sails while the flow is largely attached on subsequent sails. In this case the after sails are not at the small local angles of incidence of the previous case. In consequence these after sails are probably producing more lift. In the case of the calculated graduated arrays there is often widespread individual stall at conditions near to maximum lift. Often regions of leading edge separation could be detected on all 8 aerofoils.

The performance of graduated arrays calculated by the two-dimensional potential model is worse for the thin circular aerofoil rig than it was for the NACA 0018 aerofoil rig. This is probably associated with the sensitivity of these aerofoils with sharp leading edge to the local flow direction; there is very often leading edge separation on these aerofoils while the calculation was for fully attached flow.

For practical comparison, the linearly graduated arrays give the best driving force components with this rig except at large inflow angles.

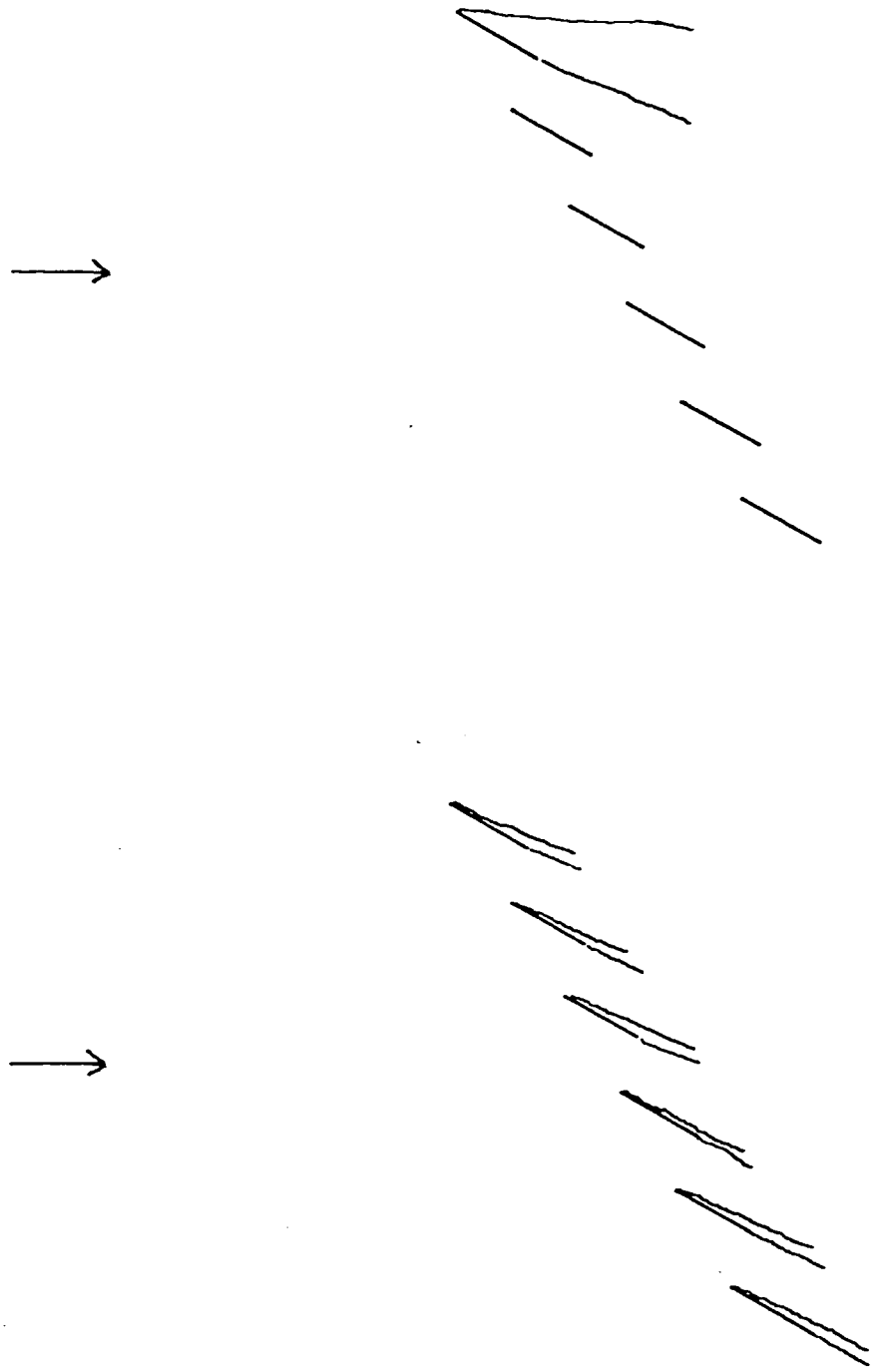

Figure 5.17

Schematic representation of extreme stall modes:
catastrophic forward-sail stall(top) and
widespread individual stall (bottom)

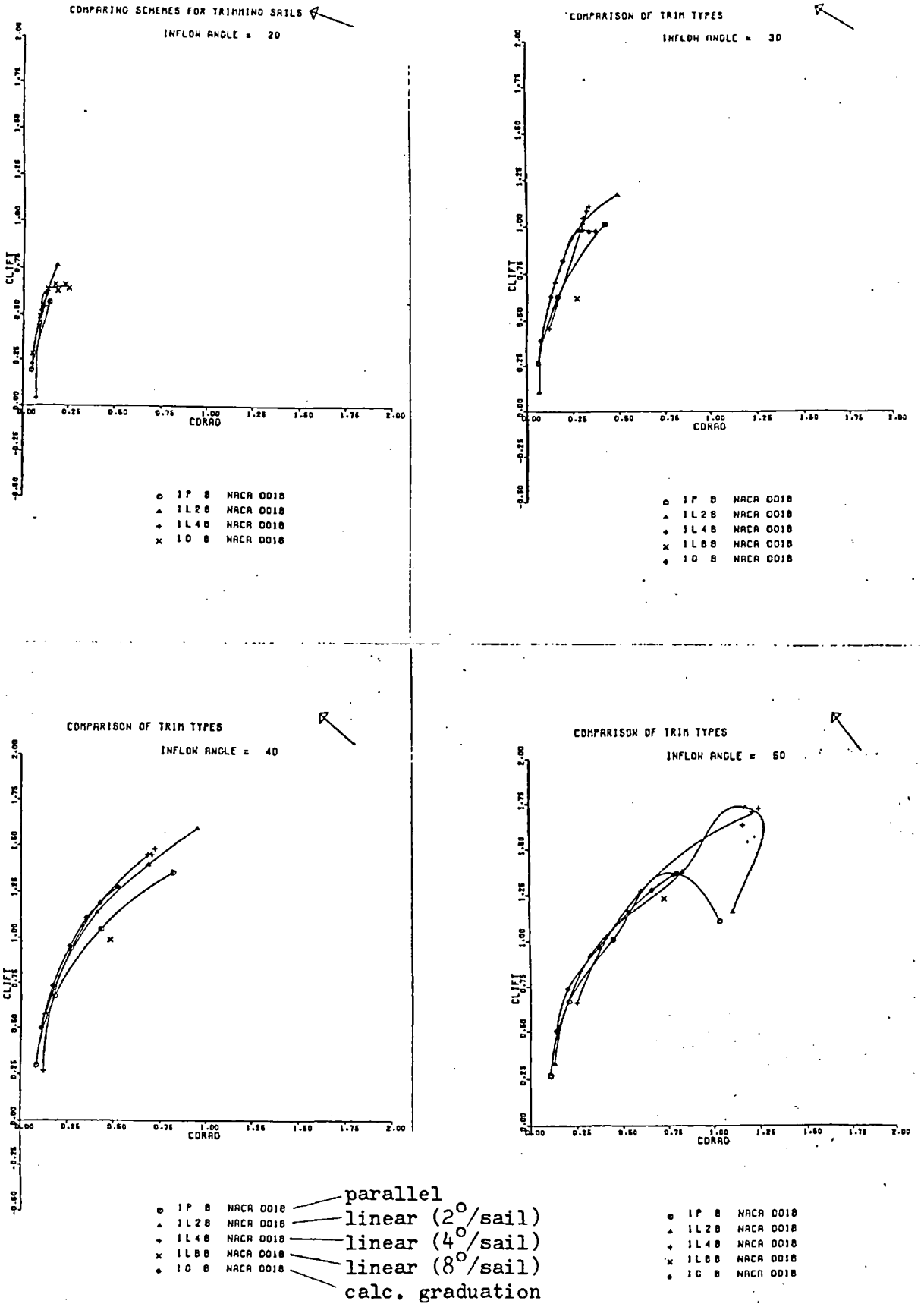

Figure 5.18

Comparison of sail-trim strategies: symmetric aerofoil section sails

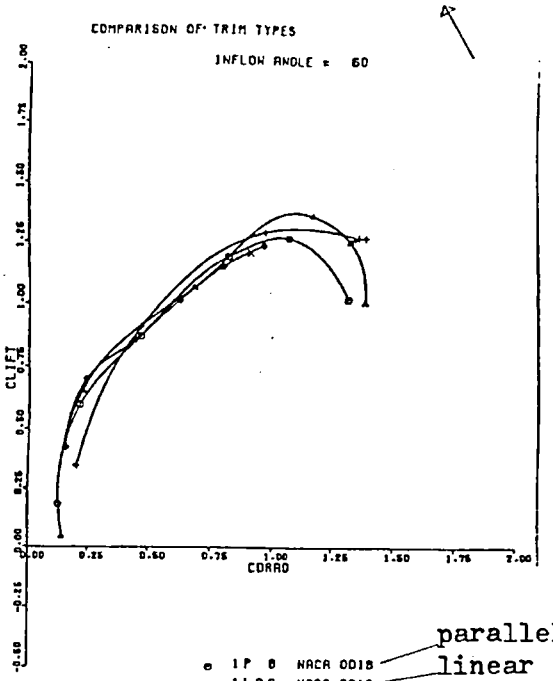

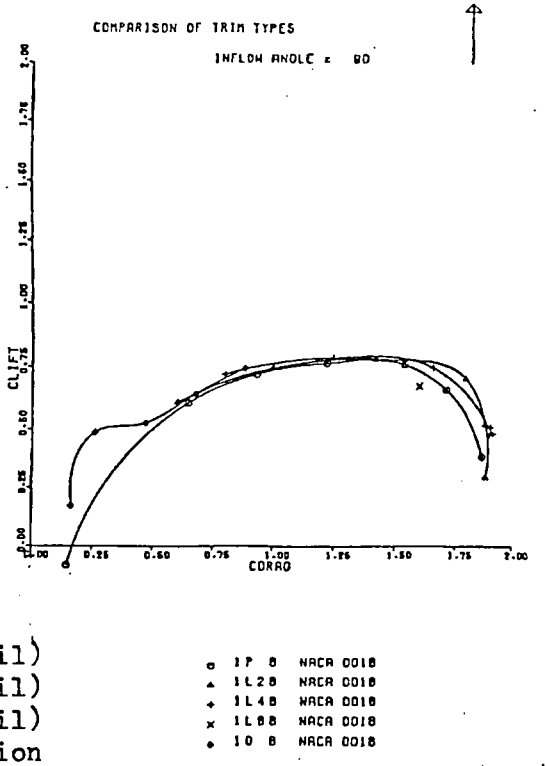

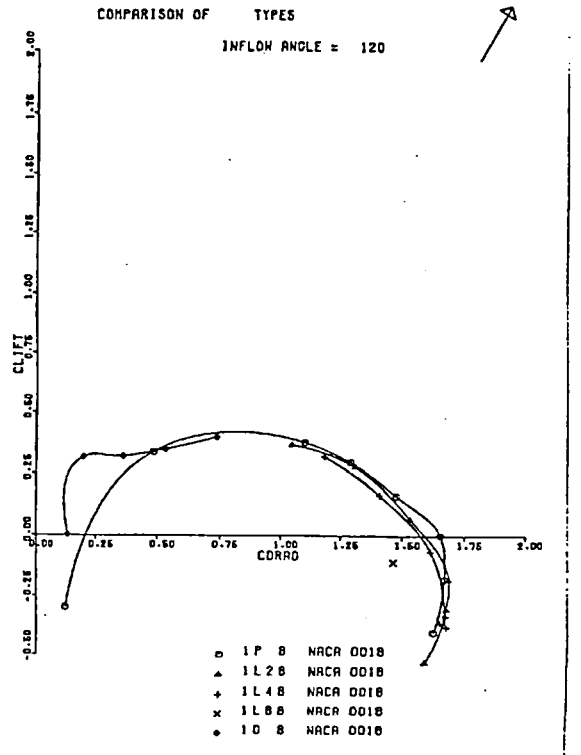

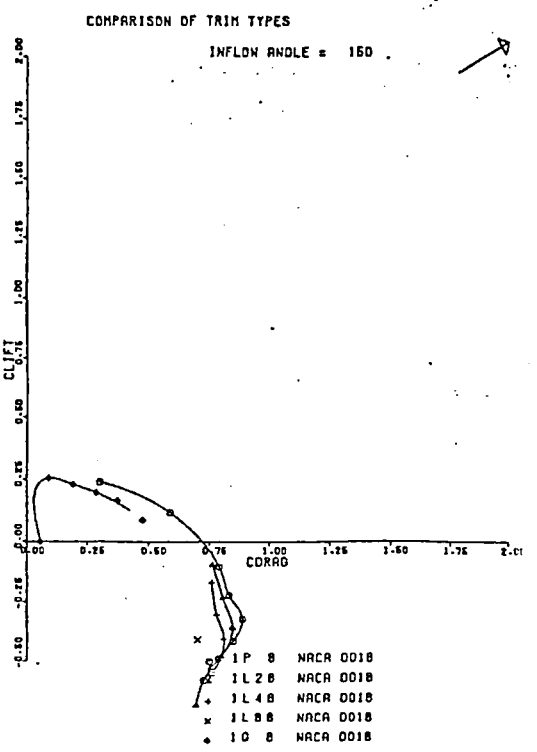

Figure 5.19

Comparison of sail-trim strategies: symmetric aerofoil section sails.

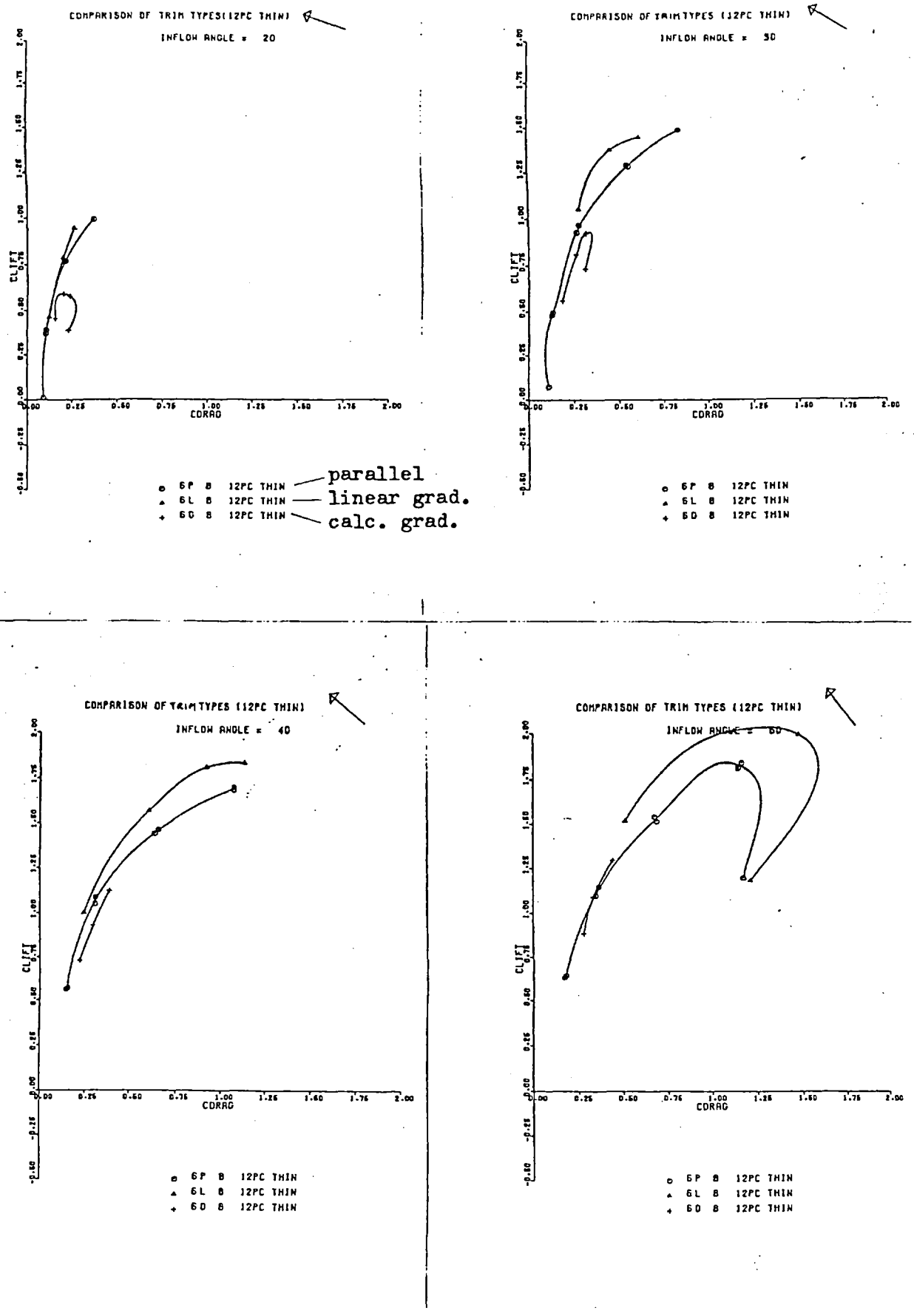

Figure 5.20

Comparison of trimming strategies: thin cambered plate sails.

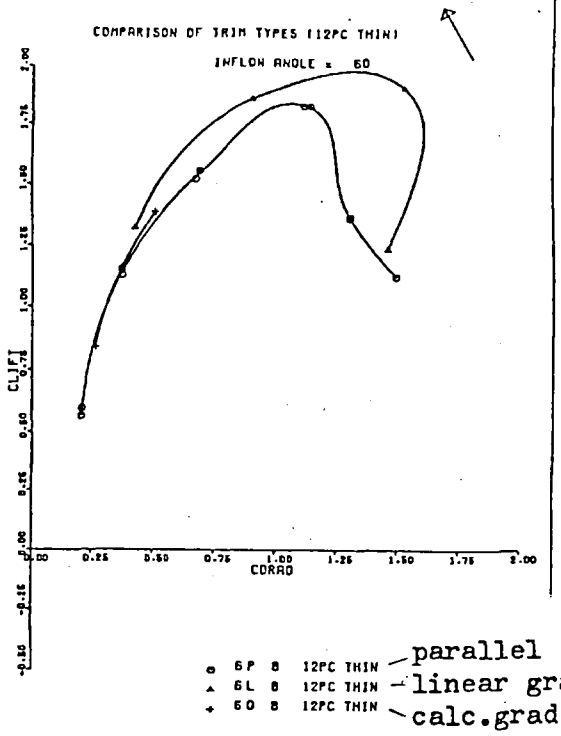

parallel
linear grad.
calc.grad.

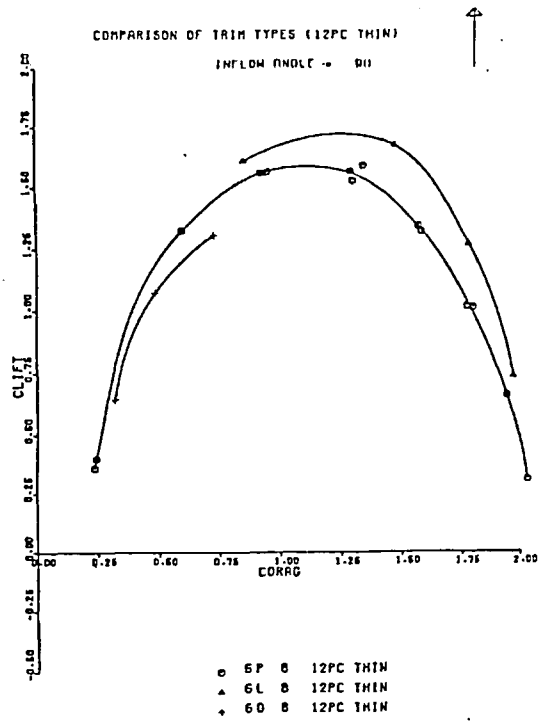

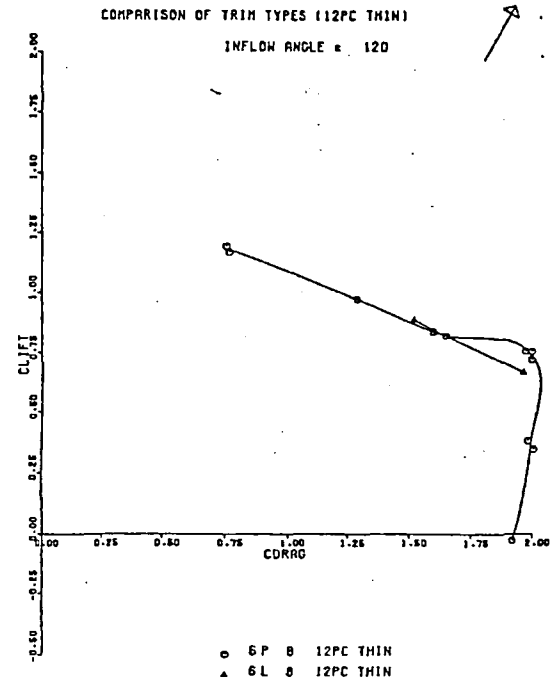

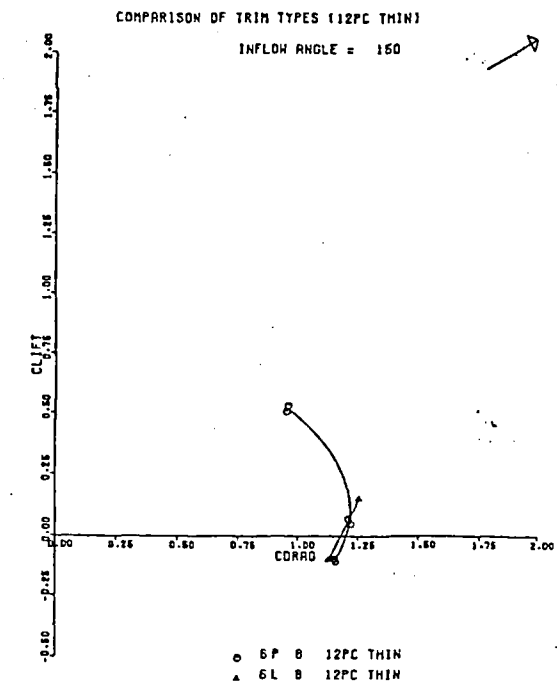

Figure 5.21

Comparison of sail-trim strategies: thin cambered plate sails.

5.4(g) Results: influence of heel

Heel changes the flow over an array of sails in a complicated and unpredictable way: it changes all three components of the free stream velocity relative to the ships' axes; it also tips the hull so that a greater part of the sail array is likely to be within a separated flow region. This latter separated flow region exists above the deck, and initiates with sharp-edge separation from the windward side of the hull at the shear strake (the outside top corner of the hull).

Figures 5.23 to 5.25 show the effects of heel at a range of inflow angles. In conditions where sails are mainly at low angles of incidence, heel slightly decreases drag and considerably decreases lift; heeling an upright vessel by 15° causes very much less effect than heeling a vessel from 15° to 30°. When the sails are near to conditions of maximum lift, heel again decreases lift more severely than drag; the effects of heeling an upright vessel 15° are slightly less than those of heeling a vessel from 15° to 30°. Incomplete tests were made to investigate the effects of heel for vessels at inflow angles corresponding to sailing "off the wind" or "downwind" (i.e. at inflow angles greater than 90°): however, it does appear that heel again reduces both lift and drag; the effect of heeling an upright vessel 15° is of a similar magnitude to that of heeling a vessel from 15° to 30°.

Figure 5.22 shows the effect of heel on the component of force along the ship's centreline (the "useful" or "driving" force component). This is only for the

range of inflow angles of 30° to 90° as insufficient tests were made outside this range. At low inflow angles the effect of heel is severe; it becomes less pronounced at inflow angles of about 45° and marginally more pronounced at inflow angles of about 70°; it again becomes less pronounced for larger inflow angles. The effect of heel on useful force can be expected to diminish as the inflow angle approaches 180°: this is because, at this angle, the useful force is entirely produced as drag which is hardly affected by heel.

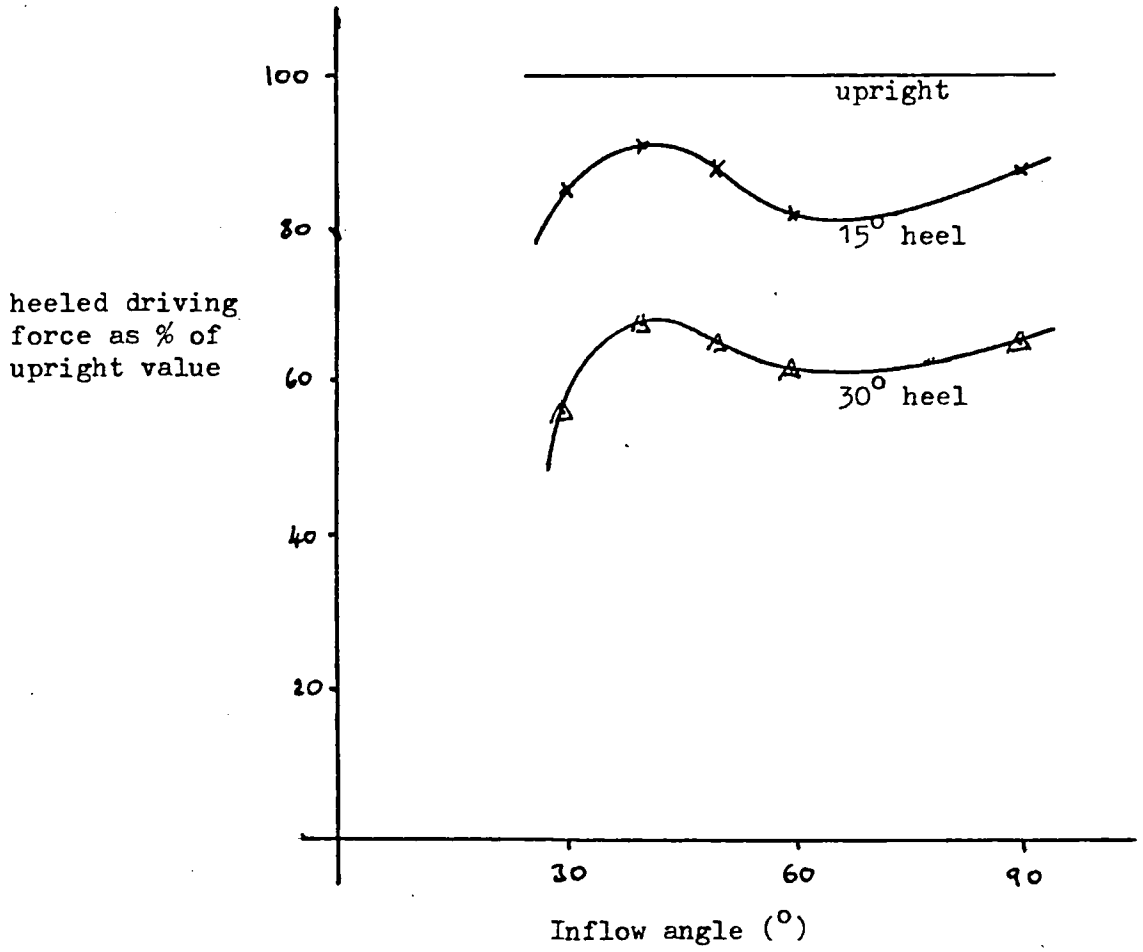

Figure 5.22

Effect of heel on driving component of sail-force;

12% camber thin plate sails

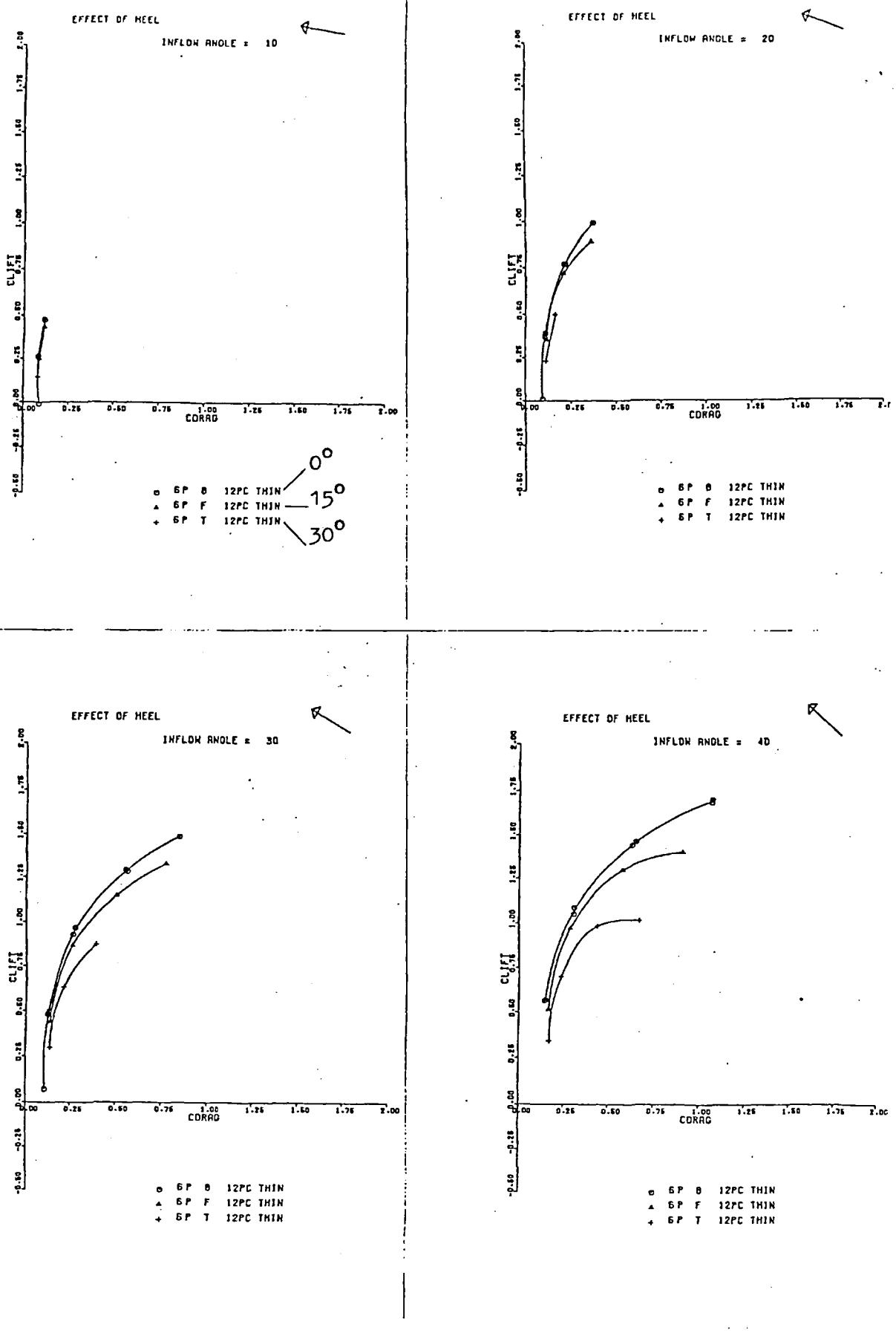

Figure 5.23

Influence of heel: thin cambered plate sails.

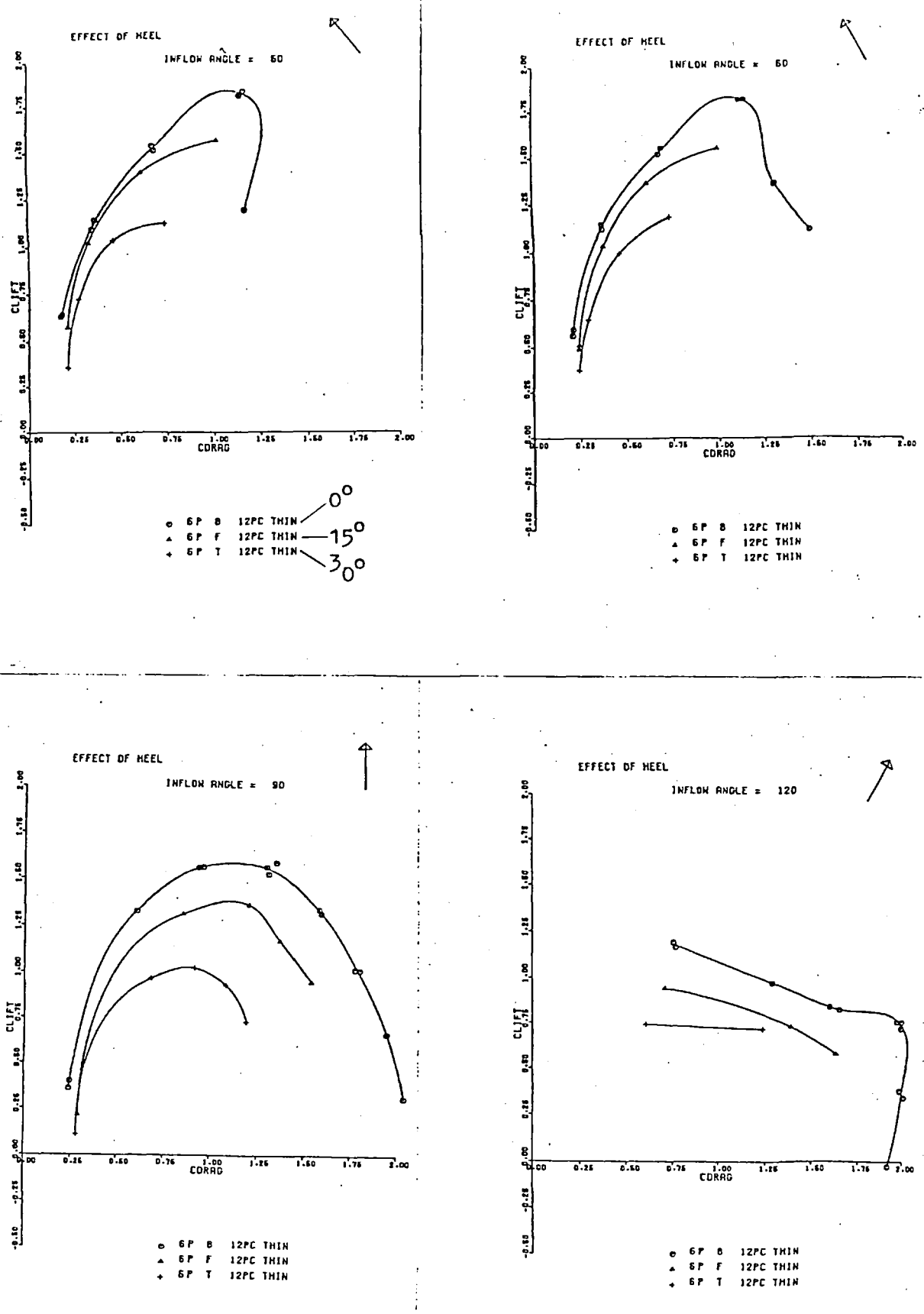

Figure 5.24

Influence of heel: thin cambered plate sails.

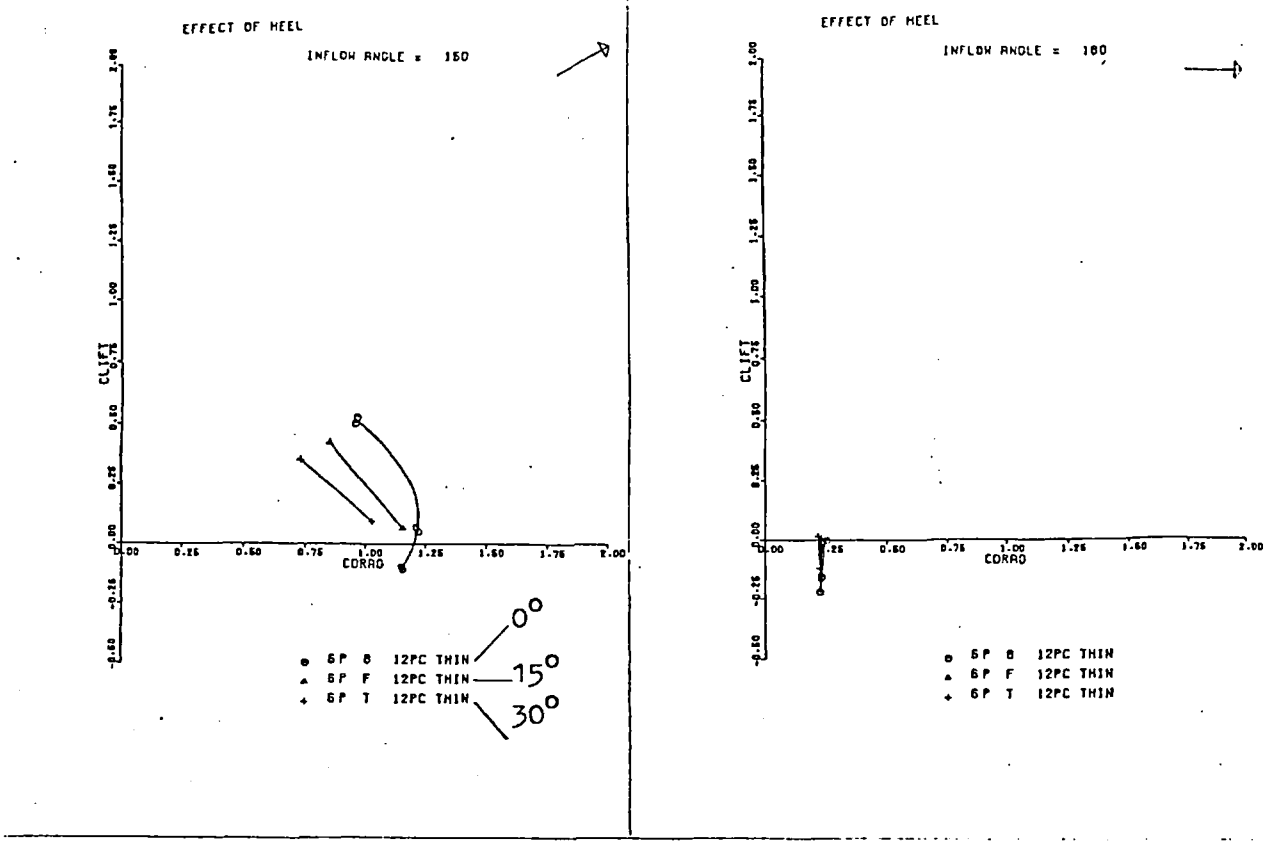

Figure 5.25

Influence of heel: thin cambered plate sails

5.5 Observations and conclusions

A multi-mast sailing rig acts as a low aspect ratio multi-element aerofoil. Away from the ends of aerofoil-sails the gaps between sails are fairly small compared with the sail's heights and the flow is substantially two dimensional. Near the hull, the effects of hull interference and sea boundary layer are significant; and near the mast-heads there is significant flow around the sail ends and trailing vortices are shed into the wake. There are important interaction effects between the array's constituent aerofoils: the primary effect is that the local apparent direction of flow varies from sail to sail because of the flow induced by the whole array; the secondary effect is that the flow induced by upstream neighbouring aerofoils tends to reduce adverse pressure gradients on the aerofoil lee-surfaces, and in some circumstances this prevents separation where it would otherwise occur. Even if separation does occur, the flow is still deflected (i.e. a force is generated due to a momentum flux) because the separation region is forced to remain close to the lee-side of each sail. An interesting result of the interaction is that catastrophic forward-sail stall (with the flow largely attached on the other sails) is a very common stall mode, particularly for parallel arrays of sails.

Important specific conclusions follow -

(1) For thin sails, the low cambers give best maximum lift/drag ratios, but the larger cambers give better maximum lift and maximum drag forces. The thin sharp edged aerofoils have better force characteristics than

the thick sharp edged foils. The relative merits of thick NACA section aerofoils cannot be deduced from these experiments because of Reynolds number effects; however, published data suggests that these NACA aerofoils, particularly the cambered aerofoils, are likely to have favourable characteristics.

(2) It is interesting to note that the relative merits of combined rigs could have been deduced from the relative merits of individual aerofoils. For the thin sails, 6% camber is best when sailing close to the wind, but increasing camber is required for courses further off the wind; a fixed camber of 12% would give good overall performance, but better performance would be obtained from a sail which could be trimmed fairly flat when sailing close to the wind but trimmed with more camber when sailing off the wind (this is, of course, a characteristic of most normal flexible sailing rigs). The thin circular arc rigs perform better than the thick circular arc rigs; the thick NACA aerofoil rigs cannot be compared because of Reynolds number effects.

(3) The effects of fitting a mast-head end-plate are fairly small and are not always advantageous; there appears to be no justification for fitting such a device with its attendant severe practical problems!

(4) When sailing across the wind, a reduction in mast number produces an approximately proportional reduction in driving force; however, when sailing close to the wind, 6 masts or 8 masts produce similar driving forces.

(5) Three reefing strategies are compared. The two better strategies are reefing-from-aft and reefing-from-aloft; both have their particular advantages.

(6) Graduated trim arrays perform better than parallel trim arrays when sailing up wind or across the wind but parallel trim arrays perform better when sailing downwind. In upwind sailing conditions (at the test Reynolds number) the calculated graduated arrays perform better than the linearly graduated arrays for the NACA aerofoil rig, but not for the thin circular arc sails.

(7) Heel can cause a significant reduction in sail forces at normal angles of heel; the effect on the side (heeling) force is often greater than the effect on the driving force, and this has beneficial repercussions for ship safety.

The main experimental problem encountered was that of simulating above-critical flow over the rounded nose aerofoils. It was initially thought that the poor performance of the arrays of thick NACA aerofoils was a characteristic of thick aerofoil arrays; it was not until the aerofoils were tested individually that it was realised that this poor performance indicated a Reynolds number effect associated with the failure of the sand roughness to prevent laminar separation. A lesser difficulty was that of accurately setting the sail trim angles; an accuracy of about 1° was achieved. One other point worth noting is that the lower part of the model hull was in the wind tunnel wall boundary layer; a full-size sailing ship also operates in a boundary layer, but the velocity profile is certainly quite different.

6. A POTENTIAL FLOW PREDICTION OF GRADUATED TRIM ARRAYS

6.1 Introduction

Various strategies for trimming multi-mast arrays of aerofoil-sails are discussed in section 5.2(d). In a very low solidity array of aerofoils, the flow past each aerofoil would be scarcely affected by the flow past its neighbours ("solidity" is the ratio of typical aerofoil-sail chord to mast spacing); in this case, the aerofoils could be trimmed parallel to one another so that each is near to its most advantageous angle of incidence. As solidity is increased, the local flow conditions at each aerofoil become increasingly influenced by the induced flow of neighbouring aerofoils. To achieve the most advantageous local flow conditions for each aerofoil a graduated array of trim angles is required. Wagner (1966) conducted a series of tests with a model "Dynaship" rig; these included tests made with all sails set parallel and with the sail trim angles linearly graduated from bow to stern. He found that the latter often have more advantageous aerodynamic characteristics than the parallel arrays. The best graduated arrays are not linearly graduated, but must be determined by considering the local flow conditions throughout the array. One criterion for an optimum graduation is that the aerodynamic loading should be equal on each mast (this implies that the local individual angles of incidence are all approximately equal). This equal-loading criterion is adopted here.

In attempting to investigate arrays with all aerofoil-sails bearing equal given aerodynamic loading, a model ship

could be put in a wind tunnel, loads on individual aerofoils measured and the individual sail trim angles varied in some systematic and iterative manner until each aerofoil bore the required load. This would involve a large number of test runs for each investigated inflow angle and for each investigated aerodynamic load. An alternative approach, which is adopted here, is to predict possibly advantageous arrays using an approximate analytic method, and then to test these in a wind tunnel to determine whether they are, in fact, advantageous.

The analytic representation used is a two-dimensional, attached flow, potential model. A three-dimensional potential analysis for attached flow could have been used, but would have been much more complicated and time consuming; a potential flow analysis for separated flow about an aerofoil-sail rig appeared quite impossible as part of an investigation of this scale. The two-dimensional model used should reasonably well predict the flow geometry in three-dimensions away from the aerofoil ends. Thus arrays calculated to exactly meet the equal-load criterion for two-dimensional aerofoils are expected to approximately meet the criterion for real (three-dimensional) aerofoil-sails.

In this two-dimensional attached flow analysis, each aerofoil is modelled by an array of line vortices and sources. The vortices are calculated to model the flow past acurved plate at incidence; the sources are calculated to model the flow about a slender aerofoil aligned with the flow. Batchelor (1967) shows that these singularities can be superposed to model the flow past an aerofoil at

incidence. The calculations are conducted for arrays of eight aerofoils with a solidity of one. The aerofoils can be given any desired camber and thickness distribution. The aerofoils are hinged at their quarter-points and an iterative procedure is used to find, for a given free stream inflow angle, arrays with all aerofoils at the same specified local angle of incidence, and hence approximately equally loaded.

This model assumes that the distribution of vorticity calculated for a single aerofoil in a uniform free stream gives a good representation of the flow round an aerofoil in a stream with some curvature due to the presence of the other aerofoils. Small curvature should only slightly change the distribution of vorticity. A more sophisticated representation could be used which would eliminate this problem; however, any errors thus introduced are likely to be small compared with those introduced by using a two-dimensional analysis to model this three-dimensional flow. This model also assumes attached flow, so it is only a good model provided that the local inflow angles are not so large that the aerofoils are stalled.

6.2(a) Review: potential flow past sails

Thwaites (1961) and Nielsen (1963) independently consider the two-dimensional inviscid flow past a flexible membrane (a sail) at incidence; they determine the aerodynamic equation connecting the shape of the sail and its pressure distribution, and show how this can be numerically solved. Tuck and Haselgrove (1972) modify Thwaites' analysis to account for a more realistic sheeting arrangement (i.e. for a non-rigid attachment of the trailing edge). Irvine (1979) reports an approximate analytic theory to predict the threshold of shape-instability for a simple flexible sail. Dugan (1970) investigates the sail shape and pressure distributions found on a fully stalled sail; the method used is a two-dimensional free streamline separated flow model. Newman (1981) reviews various solutions for incompressible flow past membranes of simple geometry.

Milgram (1968 and 1972) describes a three-dimensional lifting line and vortex lattice lifting surface method of determining the sail shapes required to give a specified pressure distribution; this method can be used for single sails or multi-element rigs. Gentry (1971) uses an electrical analogue method to investigate the two-dimensional potential flow past interacting sails.

6.2(b) Review: multicomponent aerofoil flows

A number of potential models of the flow past two-dimensional multi-component thick aerofoils have been reported. These all use a distribution of finite singularity elements over surface streamlines; the distribution is determined by solving an appropriate matrix equation. Hess and Smith (1966) use linear source elements, as do Foster, Irwin and Williams (1971) and De Vries (1972). Wilkinson (1968), Ormsbee and Chen (1972) and Kennedy and Marsden (1976 and 1978) use linear vortex elements. Beatty and Narramore (1976) attempt to improve accuracy by using parabolic vortex elements. Bhately and Bradley (1972) investigate the flow through multi-component aerofoils near stall; they place vortex elements on the displacement surface of the boundary layer, and use an internal source distribution to model the wake flows.

6.3(a) Model: two-dimensional aerofoil potential flow

Potential flow past bodies satisfies Laplace's equation and the boundary condition that there is no flow perpendicular to the body surfaces at the surfaces. This condition, alone, does not specify a unique potential flow field; the circulation round each body must also be specified. For slender aerofoil-like bodies the circulation is specified by the "Kutta condition": this requires that the rear stagnation points are at the trailing edges so that on the two sides of each aerofoil the stream flows smoothly off the rear edge. Various distributions of singularities (sources, vortices, dipoles, etc.) within and on the body surface provide appropriate solutions. The distributions are not unique, so a convenient singularity distribution can be sought. In this case, a distribution of singularities along the aerofoil chord enables reasonably tractable calculations.

6.3(b) Model: cambered plate at incidence

This simulation is discussed by Batchelor (1967). Figure 6.1 represents a cambered plate at a small angle, α, to a free stream of velocity U. The camber is small and the camber line can be written as

$$y = y_c(x) \qquad 0 \leq x \leq c$$

There is no flow through the plate and there is a discontinuity in the tangential velocity at the plate; so the plate has the characteristics of a vortex sheet and can be modelled as such. To the first order in the perturbation velocity (u,v) due to the presence of the plate, the condition of no flow across the plate can be written as

$$\frac{v - \alpha U}{U} = \frac{dy}{dx} \qquad \text{on } y = y_c, \quad 0 \leq x \leq c$$

The Kutta condition is that the fluid flows smoothly from the trailing edge, so to the first order in the perturbation velocity

$$\frac{v - \alpha U}{U} = \frac{dy}{dx} \qquad \text{at } x = c$$

For the purpose of evaluation of the perturbation velocity, the sheet is assumed to lie on the x axis rather than on the line $y = y_c(x)$. An element δx of the x axis acts as a line vortex of strength $\Gamma(x)\,\delta x$; so the perturbation velocity v is approximately

$$v = \frac{1}{2\pi} \int_0^c \frac{\Gamma(x')}{x - x'}\, dx'$$

By substitution the vortex strength distribution satisfies

the integral equation

$$\frac{1}{2\pi U}\int_0^c \frac{\Gamma(x')}{x-x'}\,dx' = \alpha + \frac{dy}{dx} \qquad 0 \leq x \leq c$$

and the Kutta condition which is equivalent to

$$\Gamma(x) = 0 \qquad \text{at} \quad x = c$$

There are not analytic solutions to this type of equation and a numerical solution procedure must be adopted. For this calculation the vortex sheet is modelled as a set of line vortices. The sheet is considered as n equal sections, each with a line vortex, of strength K_j, at its quarter point and a collocation point, C_j, at its three-quarter point. The condition of no flow through the plate remains

$$\frac{v - \alpha U}{U} = \frac{dy}{dx} \qquad \text{at } C_i, \quad 1 \leq i \leq n-1$$

The Kutta condition is approximated by the requirement that this is also true at the n^{th} collocation point;

$$\frac{v - \alpha U}{U} = \frac{dy}{dx} \qquad \text{at } C_n$$

The perturbation velocity at the i^{th} collocation point is

$$v = \frac{1}{2\pi}\,\frac{K_j}{\frac{c}{n}\left(i - j + \frac{1}{2}\right)}$$

so that the boundary integral equation is replaced by

$$\sum_{j=1}^{n} \frac{n K_j}{U c \pi (2i - 2j + 1)} = \alpha + \frac{dy}{dx}$$

This equation can be solved for $\{K_j\}$ by matrix inversion.

6.3(c) Model: aligned slender symmetric aerofoil

For a thin aerofoil, the effect of non-zero thickness on the flow can be simulated separately from the vortex simulation of the effect of camber and incidence. This simulation is discussed by Batchelor (1967). Figure 6.1 represents a slender symmetric aerofoil aligned with a flow of velocity V. The aerofoil surface is described by the curve

$$y = \frac{1}{2} y_t(x) \qquad 0 \leq x \leq c$$

The body surface is a stream-surface of the flow, and the external flow is at a small angle to the free stream everywhere except near the aerofoil nose. A distribution of singularities is required along the aerofoil x axis such that a stream-surface of the irrotational flow associated with these singularities in combination with the uniform stream approximately reproduces the aerofoil surface. A distribution of line sources conveniently meets this requirement. Batchelor shows that, for a slender aerofoil, the streamline component of velocity can be taken as U to a first approximation. It follows that the flux, f, between the stream surfaces representing the aerofoil surface is

$$f = U y_t(x) \qquad 0 \leq x \leq c$$

Hence the gradient of flux between the stream-surfaces is

$$\frac{df}{dx} = U \frac{dy_t}{dx} \qquad 0 \leq x \leq c$$

The boundaries of this internal flow are stream-surfaces, so the conservation of mass requires that changes in flux

must be supplied by flow sources. If these are distributed along the x axis the strength of the source distribution, m, is given by

$$\frac{dm}{dx} = \frac{dF}{dx} = U\frac{dy_t}{dx}$$

In this numerical calculation the source sheet is modelled as n discrete line sources. For convenience, the aerofoil is considered as n sections of equal length with the line sources located at the positions of the line vortices previously discussed. The change in flux is considered between the start and finish of each section. Conservation of mass now relates the i^{th} line source strength, S_i, to the increase in thickness along the i^{th} aerofoil section, Δt_i ;

$$S_i = U\Delta t_i$$

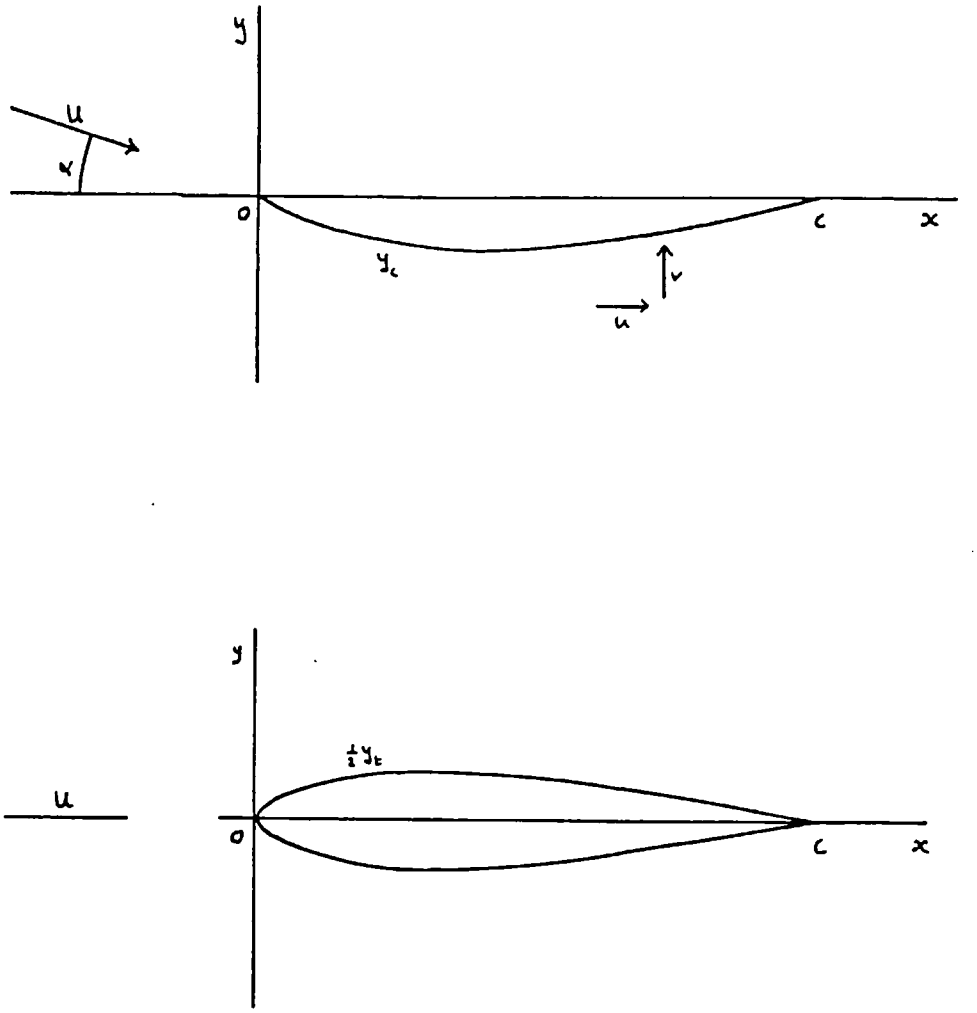

Figure 6.1

Defining sketches: aerofoil camber line (top) and

aerofoil thickness distribution (bottom)

6.3(d) Model: iterative procedure

An array of aerofoil-sails is required with each at approximately the same specified local angle of incidence. Figure 6.2 represents the model of the aerofoil arrays used in the computer program. The ship centre-line can rotate about the position of the foremost mast; the calculations are performed with the centre-line at a range of inflow angles (ε) to the free stream (U). As discussed before, each aerofoil is represented by a distribution of line sources ($\{S_{ij}\}$ $j=1,n$) and line vortices ($\{k_{ij}\}$ $j=1,n$) along a straight aerofoil chord line pivoted about its quarter point, and at an angle α_i to the free stream. When the aerofoil is at the modelled local angle of incidence, the Kutta condition is satisfied by requiring that there is no cross flow velocity component at the trailing edge collocation point (C_{in}).

An iterative procedure is required to determine the geometry of the array of modelled aerofoils which satisfies the Kutta condition at the eight collocation points. This state is achieved by estimating the array of inflow angles, $\{\alpha_i\}$; determining the flow directions at the Kutta points, $\{C_{in}\}$, associated with the free stream and the line singularities; and re-estimating the inflow angles by aligning the aerofoils with this calculated flow direction. This procedure is repeated until the cross flow velocities at the trailing edge collocation points are all below a specified minimum value. The initial estimate made is that all the aerofoils are parallel to the free stream. This iterative procedure is found to converge for the range of local incidence angles for which

the assumptions of attached flow past slender aerofoils are justified.

Note. The flow induced at a position (x,y) relative to a source, S, is;

$$\underline{v} = \frac{S}{2\pi(x^2 + y^2)} \quad (x, y)$$

and the corresponding velocity induced by a vortex k is;

$$\underline{v} = \frac{k}{2\pi(x^2 + y^2)} \quad (-y, x)$$

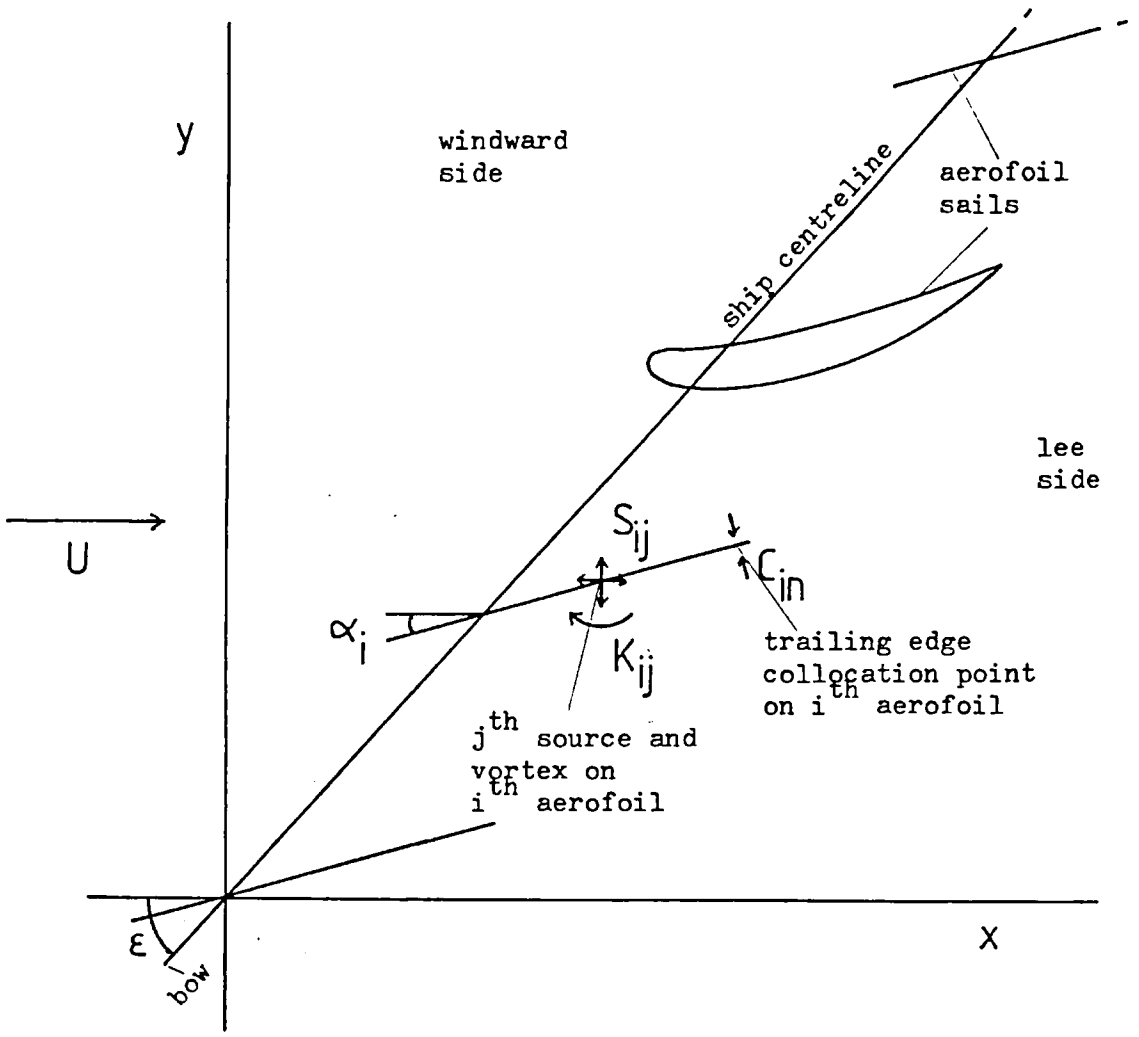

Figure 6.2

Defining sketch indicating axes and subscripts for the computer model of the multi-component aerofoil rig

6.4 Calculated arrays

The procedure described was conducted at various ship inflow angles (ε) and at a range of local angles of incidence (α). Some calculations were also performed for local angles of incidence so large that the flow could no longer be expected to be attached and the slender aerofoil assumptions could not be justified. A number of calculated graduated arrays of aerofoil-sails were tested in the wind tunnel; the results are described in the previous chapter.

Figures 6.3 to 6.5 show typical graphical output from the computer procedure. These arrays are for a NACA 0018 aerofoil section at a modelled local incidence angle of 11°. The dashed lines are streamlines; the numbers near the aerofoils are the angles, in degrees, between the free stream flow direction and the aerofoil x axis. Table 6.1 is computer output produced in another example application. These arrays of angles are for a thin plate aerofoil with a camber of 6% at a range of modelled local angles of incidence.

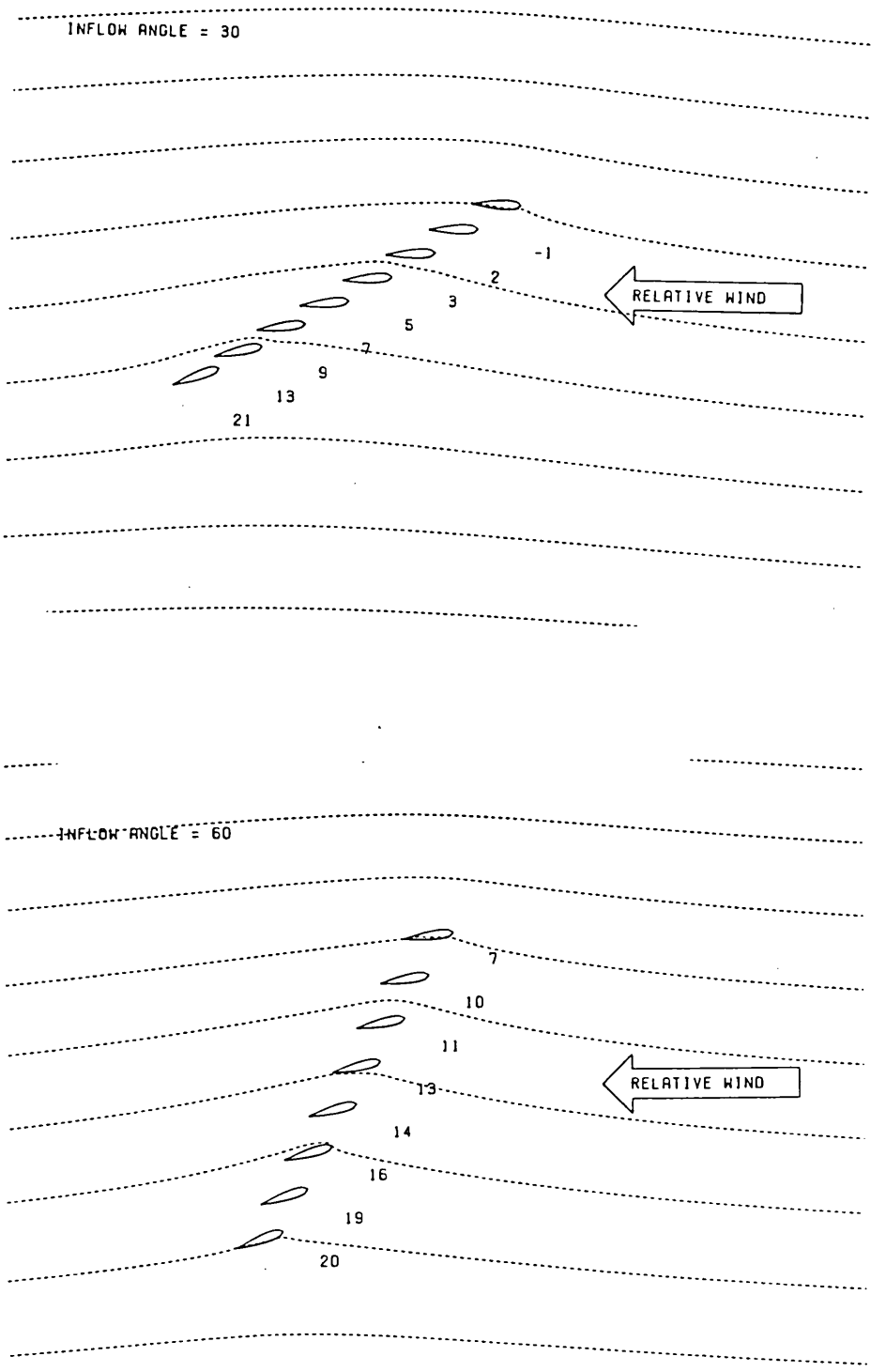

Figure 6.3

Streamlines through a graduated trim array of two-dimensional NACA 0018 aerofoils.

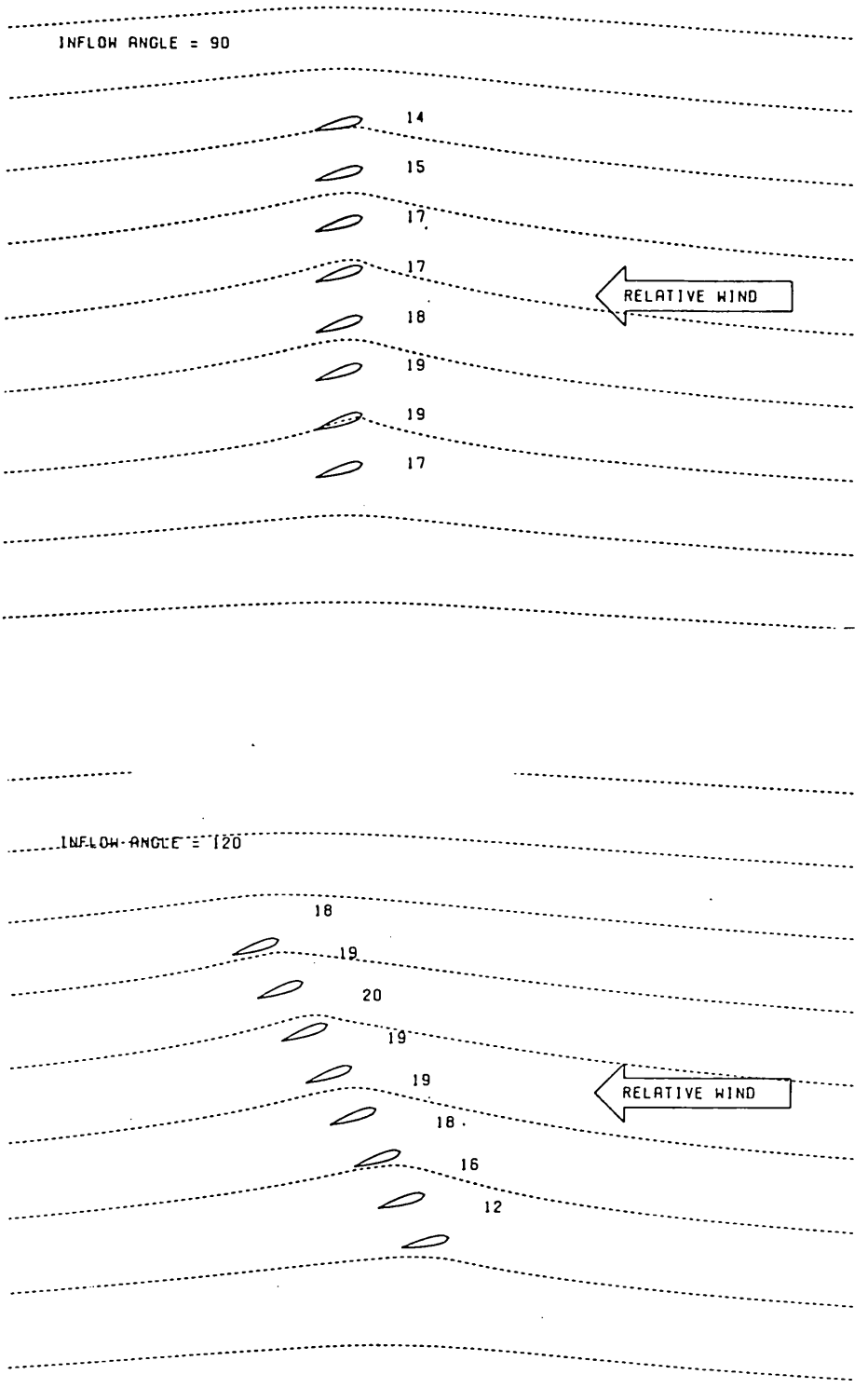

Figure 6.4

Streamlines through a graduated trim array of two-dimensional NACA 0018 aerofoils.

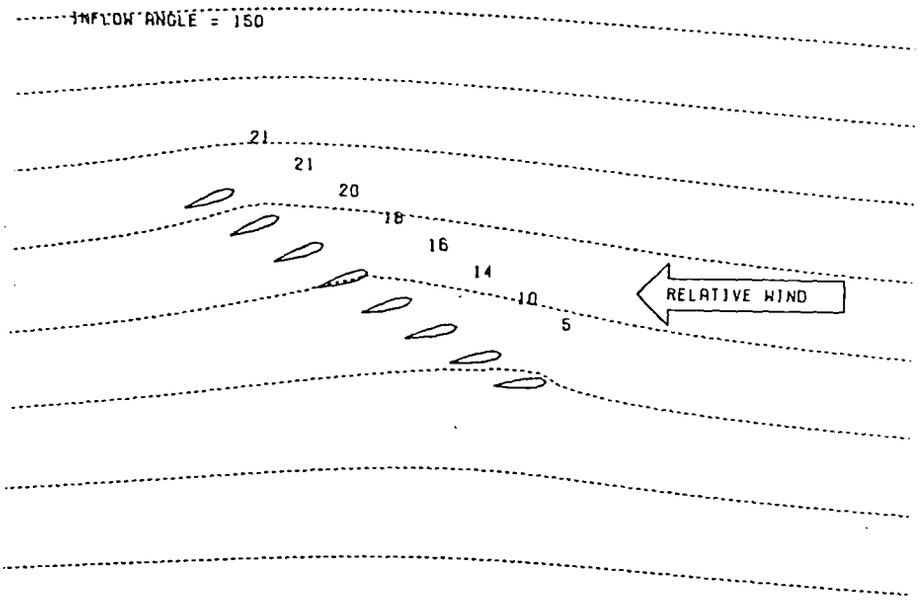

Figure 6.5

Streamlines through a graduated trim array of two-dimensional NACA 0018 aerofoils

Table 6.1

Example graduated trim arrays

THICKNESS = 0 PERCENT
CAMBER = 6. PERCENT
LOCAL INFLOW ANGLE = 0

	SAIL ANGLES REL TO SHIP							
INFLOW ANGLE = 20	29.5	27.1	25.5	24.0	22.6	20.9	18.6	12.9
INFLOW ANGLE = 25	33.7	31.3	29.7	28.2	26.8	25.2	22.8	17.9
INFLOW ANGLE = 30	37.9	35.6	33.9	32.5	31.1	29.5	27.2	22.9
INFLOW ANGLE = 35	42.2	39.8	38.2	36.8	35.5	33.9	31.7	27.9
INFLOW ANGLE = 40	46.4	44.1	42.5	41.2	39.9	38.4	36.3	33.1
INFLOW ANGLE = 50	55.0	52.8	51.3	50.0	48.8	47.5	45.7	43.3
INFLOW ANGLE = 60	63.7	61.5	60.2	59.0	58.0	56.8	55.4	53.7
INFLOW ANGLE = 90	90.1	88.4	87.6	87.0	86.6	86.1	85.8	86.0
INFLOW ANGLE = 120	117.2	116.4	116.5	116.8	117.2	117.7	118.4	120.2
INFLOW ANGLE = 150	144.7	146.0	147.7	149.2	150.7	152.3	154.3	157.6

THICKNESS = 0 PERCENT
CAMBER = 6. PERCENT
LOCAL INFLOW ANGLE = 5.0

	SAIL ANGLES REL TO SHIP							
INFLOW ANGLE = 20	30.5	27.1	24.6	22.5	20.3	17.9	14.5	2.7
INFLOW ANGLE = 25	34.3	30.8	28.3	26.1	23.9	21.3	17.7	7.6
INFLOW ANGLE = 30	38.0	34.5	32.0	29.8	27.6	25.0	21.2	12.5
INFLOW ANGLE = 35	41.8	38.3	35.8	33.6	31.4	28.8	25.0	17.4
INFLOW ANGLE = 40	45.7	42.1	39.7	37.5	35.3	32.7	29.0	22.4
INFLOW ANGLE = 50	53.5	49.9	47.5	45.4	43.3	40.8	37.5	32.6
INFLOW ANGLE = 60	61.3	57.9	55.5	53.6	51.6	49.3	46.4	42.9
INFLOW ANGLE = 90	85.6	82.5	80.7	79.4	78.2	77.1	75.9	75.8
INFLOW ANGLE = 120	110.7	108.4	107.8	107.7	107.9	108.4	109.4	112.4
INFLOW ANGLE = 150	136.6	136.2	138.3	140.5	142.9	145.7	149.6	156.5

THICKNESS = 0 PERCENT
CAMBER = 6. PERCENT
LOCAL INFLOW ANGLE = 10.0

SAIL ANGLES REL TO SHIP

INFLOW ANGLE								
20	31.3	27.0	24.0	21.3	18.7	15.8	13.2	-7.9
25	34.7	30.3	27.2	24.4	21.7	18.6	15.0	-3.2
30	38.1	33.6	30.5	27.7	24.9	21.6	17.2	1.5
35	41.5	37.1	33.9	31.0	28.1	24.8	20.0	6.2
40	45.0	40.5	37.3	34.5	31.5	28.1	23.0	11.0
50	52.1	47.6	44.4	41.5	38.6	35.1	30.1	20.8
60	59.3	54.8	51.6	48.9	46.0	42.7	38.0	31.1
90	81.6	77.2	74.5	72.3	70.2	68.0	65.3	63.8
120	104.8	100.9	99.4	98.6	98.1	97.9	98.5	102.2
150	129.0	126.6	128.0	130.1	132.9	136.7	142.6	155.0

THICKNESS = 0 PERCENT
CAMBER = 6. PERCENT
LOCAL INFLOW ANGLE = 15.0

SAIL ANGLES REL TO SHIP

INFLOW ANGLE								
20	32.0	27.0	23.5	20.5	17.6	14.4	14.2	-19.1
25	35.0	29.9	26.4	23.2	20.2	16.8	14.8	-14.8
30	38.1	33.0	29.3	26.1	22.8	19.2	15.9	-10.5
35	41.3	36.1	32.3	29.0	25.7	21.9	17.3	-6.1
40	44.5	39.2	35.4	32.1	28.6	24.6	19.3	-1.6
50	51.0	45.6	41.8	38.3	34.8	30.6	24.3	7.6
60	57.6	52.2	48.3	44.9	41.3	37.0	30.5	17.2
90	78.1	72.6	69.1	66.0	62.9	59.2	54.2	49.0
120	99.6	94.2	91.6	89.7	88.1	86.5	85.4	88.6
150	121.5	117.0	116.9	118.1	120.2	124.0	131.2	156.1

6.5 Observations and conclusions

The potential flow representation described can be used to predict graduated arrays of sail trim angles. The model assumes two dimensional attached flow past slender aerofoil-sails at small angles of incidence. It is most suitable, therefore, for modelling the flow through rigs when "close hauled" (that is, when the ship inflow angle to the relative wind is less than about 60°); in this condition the sails are trimmed fairly close to the ship centre-line and are required to produce a fairly high lift/drag ratio; in consequence, the gaps between aerofoils are small compared with their height, which results in a comparatively two-dimensional flow away from their ends, and the sails are trimmed to be below the stall angle so that the thin aerofoil assumptions are justified.

A number of graduated arrays were tested in the wind tunnel. These tests are considered in the previous chapter. The arrays calculated for the NACA 0018 aerofoil section have good close hauled aerodynamic characteristics while those calculated for the thin cambered plate sails do not; this difference is associated with the separation which is almost always present, sometimes on both surfaces, on thin cambered plate aerofoils. At large inflow angles the calculated graduated arrays always perform poorly; this is because at such inflow angles the best force characteristics are associated with stalled flow, so the model assumptions become quite unjustified.

The predicted graduation is usually not severe near the centre of the array where the influence of up-

stream and downstream aerofoils tend to change the flow in opposing ways. It becomes more severe towards the ends, and particularly so at the trailing aerofoil in close hauled arrays. This trailing aerofoil-sail (which is the "mizzen" in a conventional rig) must be at a considerably smaller trim angle than the others to experience the same local flow incidence; it is sometimes required to be at a negative sail trim angle.

It is worth noting that the mizzen of a real sailing craft is often sheeted much nearer the fore-and-aft line than other sails. It is also interesting to consider the effect of sheeting the mizzen still harder, so that it is sheeted to windward (that is of giving the trailing aerofoil a negative trim angle); it is possible in some circumstances that this could increase the driving component of the total rig aerodynamic force even though the mizzen itself would now be producing a retarding force. An increase in the rig aerodynamic lift is expected if this change in the mizzen trim angle increases the total induced circulation; the additional force would be experienced by the sails forward of the mizzen; the local angles of incidence at these would be increased by the mizzen and, in consequence, these sails could provide a better driving force component.

7. THE MATHEMATICAL MODELLING OF SAILING SHIPS' PERFORMANCE

7.1 Introduction

The complex and fascinating mathematics of sailing have attracted the attention of many people for whom sailing is often a much loved recreation. A number of these people have attempted to mathematically model the performance of sailing vessels. These attempts have been biased towards a range of related objectives: for example, Herreshoff (1964) and Myers (1975) wished to highlight ways of improving racing sailing yachts; Baker and Douglas (1971) and Bradfield and Madhaven (1977) wished to analyse the potential of high speed craft; Myers (1975) and Kerwin (1976) wished to develop a model as a standard for handicapping yachts; while Hafner (1980) investigated the optimisation of existing yachts' performance. A lot of performance models, particularly recent ones, have been motivated by interest in modern large commercial sailing ships: examples are Wagner (1967a), Woodward, Beck, Scher and Cary (1975), Schenzle (1976), NKK (1979) and Rainey (1980).

The basic mathematics of propelling a vessel at the interface between two fluids (air and sea) with motion relative to one another are simple: however, there are a number of complicating phenomena at the sea surface; the motions of sea and air are randomly unsteady and the sea surface itself is often far from flat. As noted by Hafner (1980), this results in "an utterly unsteady state of proceedings in all the six degrees of freedom in space".

There is no possibility of accurately modelling all the features affecting sailing performance; however, by making suitable assumptions and approximations, reasonable simplified models can be produced. Where calculated performance has been compared with actual performance agreement has generally been considered acceptable, and seems good enough to justify drawing conclusions about actual sailing performance from mathematical performance models.

The model described in this chapter was derived to make qualitative comparisons between various sailing ship configurations tested in the wind tunnel.

7.2(a) Review: equations of motion

In steady sailing equilibrium the performance parameters of a vessel at a simplified air/sea interface satisfy three vector equations; one kinematic relationship and two equilibrium conditions. The kinematic equation is the "wind triangle" relationship between true and relative wind speeds. The other two equations concern the equilibrium of forces and moments acting on the hull and sails. Symbols used in this chapter are listed with their meanings in appendix A7.1.

Kinematics: except for small vessels on large waves, the vertical velocities of sailing craft are usually very small: they are not considered in most performance models. This reduces the kinematic vector equation to the two dimensional wind triangle relationships. Figure 7.7 shows the relationship of the relative wind speed (V_A), relative water speed (V_H) and true wind speed (V_T) to the course angle (γ) and the angle between ship's track and relative wind ($\lambda_A + \lambda_H$). Application of the cosine formula gives:

$$V_T^2 = V_A^2 + V_H^2 - 2 V_A V_H \cos(\lambda_A + \lambda_H)$$

and

$$V_A^2 = V_H^2 + V_T^2 - 2 V_H V_T \cos(\pi - \gamma)$$

Equilibrium of forces: in steady sailing conditions, the total gravitational forces ($\underline{F}_G$), hydrodynamic forces ($\underline{F}_H$), and aerodynamic forces ($\underline{F}_A$) acting on the ship, are in equilibrium. That is:

$$\underline{F}_C + \underline{F}_H + \underline{F}_A = 0$$

Vertical components of forces: the equilibrium of vertical force components is not considered in most performance models. This implies that vertical components of fluid dynamic forces can be neglected in comparison with the weight and bouyancy forces. This assumption can not be made for non-displacement craft employing fluid dynamic lift. In this case the vertical force component equation must be considered. Writing G for buoyancy and weight forces, H for hydrodynamic forces, A for aerodynamic forces and using the subscript Z to indicate vertical components, this equation is:

$$G_z + H_z + A_z = 0$$

Horizontal components of forces: the equilibrium of horizontal force components is usually considered by resolving forces along two perpendicular horizontal axes. The axes chosen vary between models. Using the subscripts X and Y to indicate components in two perpendicular directions, the equations are:

$$A_x + H_x = 0$$

and

$$A_Y + H_Y = 0$$

An equivalent method, which is sometimes more convenient, is to require that the force vectors have the same magnitude:

$$|\underline{F}_A| = |\underline{F}_H|$$

and act in opposite directions:

$$\underline{F}_A \cdot \underline{F}_H = - |\underline{F}_A||\underline{F}_H|$$

Equilibrium of moments: in steady sailing conditions the total gravitational moments ($\underline{M}_G$), hydrodynamic moments ($\underline{M}_H$) and aerodynamic moments ($\underline{M}_A$) acting on the ship are in equilibrium. That is:

$$\underline{M}_G + \underline{M}_H + \underline{M}_A = 0$$

The moments acting on the ship are resolved into three components; yawing moments about a vertical axis, heeling moments about a longitudinal axis of the ship, and pitching moments about a horizontal axis perpendicular to the longitudinal axis of the ship. Most models do not consider all three of the component equations. In some cases attempts are made to show that this simplification does not lead to large errors in predicted performance. The component equations are:

$$M_{H\,yaw} + M_{A\,yaw} = 0$$

$$M_{G\,heel} + M_{H\,heel} + M_{A\,heel} = 0$$

$$M_{G\,pitch} + M_{H\,pitch} + M_{A\,pitch} = 0$$

The component equations of these vector equations are non-linear, extremely complicated and highly coupled. There seems no possibility at present of exactly solving the complete set of the equations of motion: this is prevented both by inadequate theory and inadequate data.

Nevertheless, by making reasonable simplifications approximate solutions to the equations of motion can be found. All the models discussed subsequently attempt to solve exactly the kinematic equations. They differ in the approximations and simplifications made to the equilibrium conditions, and in their attempts to model some real features of the air/sea interface.

7.2(b) Review: history of performance models

Thieme (1955) produced a thorough treatise on the mechanics of sailing. This includes a very complete review of the existing sailing literature. It appears to have been the starting point for much of the subsequent German analysis of sailing. It is implied that the governing equations for a sailing vessel are: the kinematic equations, 2 horizontal force equations and the heeling moment equation. Thieme proceeds by making various assumptions and simplifications to analyse the qualitative effects of changes in various factors. Despite many simplifications the analysis becomes very complicated and unwieldy.

Davidson (1956) wrote a chapter on sailing mechanics in a book edited by Batchelor. Much of the chapter considers the performance achieved by various existing sailing craft. Davidson does not explicitly identify the governing equations for sailing performance. He deduces the importance of maximising both aerodynamic and hydrodynamic lift to drag ratios to improve upwind performance. He also analyses the advantages of decreasing hull area and increasing stability.

Barnaby (1960) includes a section on sailing ships in his comprehensive book of naval architecture. He identifies the governing equations as; the kinematic equations and 2 horizontal force equations. He subsequently makes deductions by considering the component of aerodynamic force along the ship's track. He considers the effects of heel and leeway on hull resistance and discusses the balance of yawing moments. He also discusses

the effects of wind gradient and of air deflected over the hull on the relative wind direction at various heights.

Herreshoff (1964) wrote a long and useful paper on the fluid dynamics of the sailing yacht. His main interest was the optimisation of racing sailing yacht design. He identifies the full set of governing equations. His performance model solves the following equations; the kinematic equations, 2 horizontal force equations, and the heeling moment equation. A computer program solves the equations using two nested iterative loops. The hydrodynamic data are basically obtained from model tests. The aerodynamic data are basically obtained from full size tests. Various assumptions are made in adapting the data which is represented by complicated analytic functions. An attempt is made to allow for rough water effects.

Wagner (1967a) produced a performance model based on the work of Thieme. He suggests that the model can be used to predict the performance of existing and proposed ships, to investigate design modifications or changes in the set of sails, and as a basis for handicapping racing yachts. The model solves the following equations; the kinematic equations, 2 horizontal force equations, and the yawing moment equation. The heeling moment equation is subsequently solved, but the only feedback is by sail reduction in the event of excessive heel. Experimental results are quoted which indicate that moderate heel causes minimal changes to hydrodynamic forces. The effect of heel on aerodynamic forces is not

considered. The equations are solved using a computer programme consisting essentially of two nested iterative loops. The aerodynamic data is obtained from wind tunnel tests. The hydrodynamic data is taken from oblique towing tests and standard series test data. The model considers rough water effects. An effective root mean squared wind velocity is used to allow for the effect of the vertical wind gradient. The wind is taken to be proportional to the 6th root of height above sea surface. Wagner compares the results of his calculations for a four masted barque with log book data from five old trading barques. The quality of the historic data is poor. Nevertheless, Wagner considers the agreement to be satisfactory.

Baker and Douglas (1971) attempted to optimise the design of a hydrofoil/aerofoil craft capable of record breaking speeds for short runs. Their performance model solves the kinematic equations, and all 3 force equations. It is necessary to consider the vertical equilibrium of forces as their craft is supported by hydrodynamic lift. The model is not required to consider equilibrium of heeling moments as the craft is designed so that equilibrium always occurs at zero heel. Baker and Douglas do not solve the equations but investigate the effects of changing various factors by making suitable approximations and assumptions to make the equations tractable. The data are obtained from towing tests, from systematic aerodynamic data and from aerodynamic theory.

Myers (1975) developed a performance model in order to understand and improve yacht performance and to improve the handicapping system for racing yachts.

The model solves the kinematic equations, 2 horizontal force equations and the heeling moment equation. The equations are solved using a computer program consisting of two nested iterative loops. A fairly simple functional representation of aerodynamic force coefficients is chosen after considering sail force data from a number of sources. The hydrodynamic data is produced using naval architects' rule of thumb and aerodynamic theory. Changes in aerodynamic and hydrodynamic forces due to heeling are considered. An estimate is made of rough water effects. A guess is made about the effects of "rough air". It is noted that the wind speed varies as the sixth root of height above sea surface. Myers concludes that "the present theory fits all the data within the measurement errors".

Woodward, Beck, Scher and Cary (1975) investigated the feasibility of sailing ships for the American merchant navy. The model used appears to be based on Wagner's model but is more primitive. Unlike Wagner's, the equilibrium of yawing moments is not considered. The model solves the kinematic equations, and the 2 horizontal force equations. Like Wagner's model, this one also solves a very simplified equation to determine heeling angle. Again, the only feedback is by reduction of sail in excessive winds. The computer programme used consists of two nested iterative loops. Much of the data used is taken from Wagner's paper. Different standard series data is used for the straight line hull resistance. There are other slight differences in the data used.

Kerwin (1976) produced a program which, it was claimed, would predict the speed of any yacht at any point of sailing in any wind velocity. This claim is clearly somewhat optimistic in view of the considerable difficulties encountered, for example, when trying to predict the flow past even fairly simple bodies in uniform velocity fields. The program was developed both to investigate possible yacht improvements and as a basis for a fair handicapping system for racing yachts. Kerwin calls it the V.P.P. (Velocity Prediction Program). It solves 2 horizontal force equations and the heeling moment equation. Although this is a fairly sophisticated performance model, no attempt is made to consider the equilibrium of yawing moments. The implicit assumption is that the rudder is midships in sailing equilibrium. Schenzle (1976) and Barnaby (1960) discuss the advantages of having the rudder at a greater angle of incidence than the hull to the water. Spens (1964) notes that performance models tend to overestimate leeway; this may be due to the above assumption. The effect of heel on hull and sail forces is considered. It is assumed that sail force coefficients are reduced linearly with heel angle. No justification is made for this assumption. Heeling angle is also used as a criterion for reefing in excessive winds. The computer program used consists of two nested iterative loops. Hull forces are taken from towing tests and are adapted using the I.T.T.C. friction allowance. The sail force coefficients are obtained from full scale yacht tests of the yacht "Baybea" and are adapted for the geometry of other possible rigs.

Schenzle (1976) wished to compare the performance of proposed large sailing vessels. He makes some improvements to Wagner's model. The equations solved are; the kinematic equations, 2 horizontal force equations and the yawing moment equation. He also determines the angle of heel, but feedback is only by reefing in the event of excessive heel. The set of equations is solved using an advanced precompiler for computer aided design. Hydrodynamic data are based on towing tank results. The frictional component is calculated using the I.T.T.C. empirical formula. Allowance is made for roughness and fouling and for the added resistance in a seaway. Sail force coefficients are taken from Wagner's wind tunnel tests. Allowance is made for a wind gradient approximating to a 10th root of height formula. It is shown that the effects of relative wind twist with height are small. This model is probably the most soundly based and thorough produced.

Bradfield and Madhaven (1977) were interested in comparing the performance of two particular single sail high performance catamarans. Together with Riise, they developed a model suitable for this particularly simple application. Their program solves the kinematic equations and the 2 horizontal force equations. The heeling moment equation is only required to calculate a maximum permissible heeling force: the craft is normally sailed with minimum heel. It is assumed that the craft always requires no helm and that variable angle keel boards allow the hulls to be sailed with no leeway. Unlike a multi-element rig, the single sail rig allows the sail force coefficients to be represented by single

polar curves. The sail force coefficients are obtained from the results of water and wind tunnel tests. The hull force coefficients are adapted from standard systematic series data. The wind profile is assumed to be constant over the sails and then to reduce linearly to zero across the above water hull. Comparison of predicted and observed sailing performance suggests acceptable agreement. This is a fairly primitive model, but it is adequate for its intended purpose.

Hafner (1980) produced a novel method of achieving optimum sailing performance. This method was intended to be used by sailors to get the best from their crafts. In developing his method, Hafner reduced the mathematics of sailing to an exceptionally elegant form. He derives expression for performance in terms of two quantities; β (the angle between relative wind and track), and V_H/V_A (the ratio of relative water speed to relative wind speed). He shows how these quantities can be derived directly from suitably non-dimensionalised polar force curves for hull and sails. In effect his procedure solves the kinematic equations and the 2 horizontal force equations. Hafner shows how this method can be simply modified to consider; Froude number dependency, variety of sail sets, heeling, etc. In this way the model can be adapted to simultaneously satisfy various other governing equations.

Marchaj (1979) produced an encyclopaedic book on the theory of sailing. This is a good source of references. Marchaj discusses the full set of governing equations. His analysis of performance tends to be piecemeal but very thorough. He comments that "moderate optimism with respect to the possibility of speed prediction based on

specific model tests is justified by past records".

NKK (1979) investigated a proposed sail equipped motor ship for the Japanese merchant navy. Their performance model is of particular interest as it is the first to consider the use of sails and engine together. It estimates the performance of a vessel motor sailing with the engine working at constant power. The program apparently solves; the kinematic equations, the 2 horizontal force equations, and the yawing moment equation. The model is very simple and fairly primitive. This model has been used to predict the performance of a prototype scale model sailing ship and a full scale 1,600 ton sailing tanker. It is concluded that "... the measured ship speeds ... coincide fairly well with the estimated ship speeds".

Rainey (1980) developed a program to calculate ship performance curves for ships using power and sail together. Unlike the NKK performance model this model is used to calculate auxiliary power requirements for a vessel maintaining constant speed. The model apparently solves the kinematic equations and 2 horizontal force equations. This model is more primitive than Schenzle's as there are more implicit simplifying assumptions. It does, however, have the following advantages; it is written in a general way to predict performance for a variety of types of wind craft including wind turbine ships and rotor ships from suitable data curves; it is particularly useful for comparative economic evaluation as it calculates the reduction in power requirements.

Letcher (1982) produced a very simplified performance

model for the analysis of large powered sailing vessels. Like the NKK (1979) model, it estimates the performance of a vessel motorsailing with the engine working at constant power. It solves the kinematic equations and the 2 horizontal force equations. However, it is assumed that force coefficients are independent of velocity; this is a very unrealistic assumption except at low velocities where heel effects, rough water effects and Froude drag effects are small. For real sailing ships an increase in an already strong wind will usually only produce a marginal improvement or even a deterioration in ship speed: the model, however, produces no scale effects in strong winds, and predicts a fairly uniform increase in ship speed with wind speed. The model has severe limitations which are acknowledged by Letcher. He claims, however, that his assumptions are appropriate to the analysis of large sailing ships over the greater part of their operating range, especially in the conditions where auxiliary power will be useful. The performance curves of Wagner (1967) and Schenzle (1976) show that scale effects are important when close hauled in even a force 5 breeze; hence Letcher's claims are not fully justified.

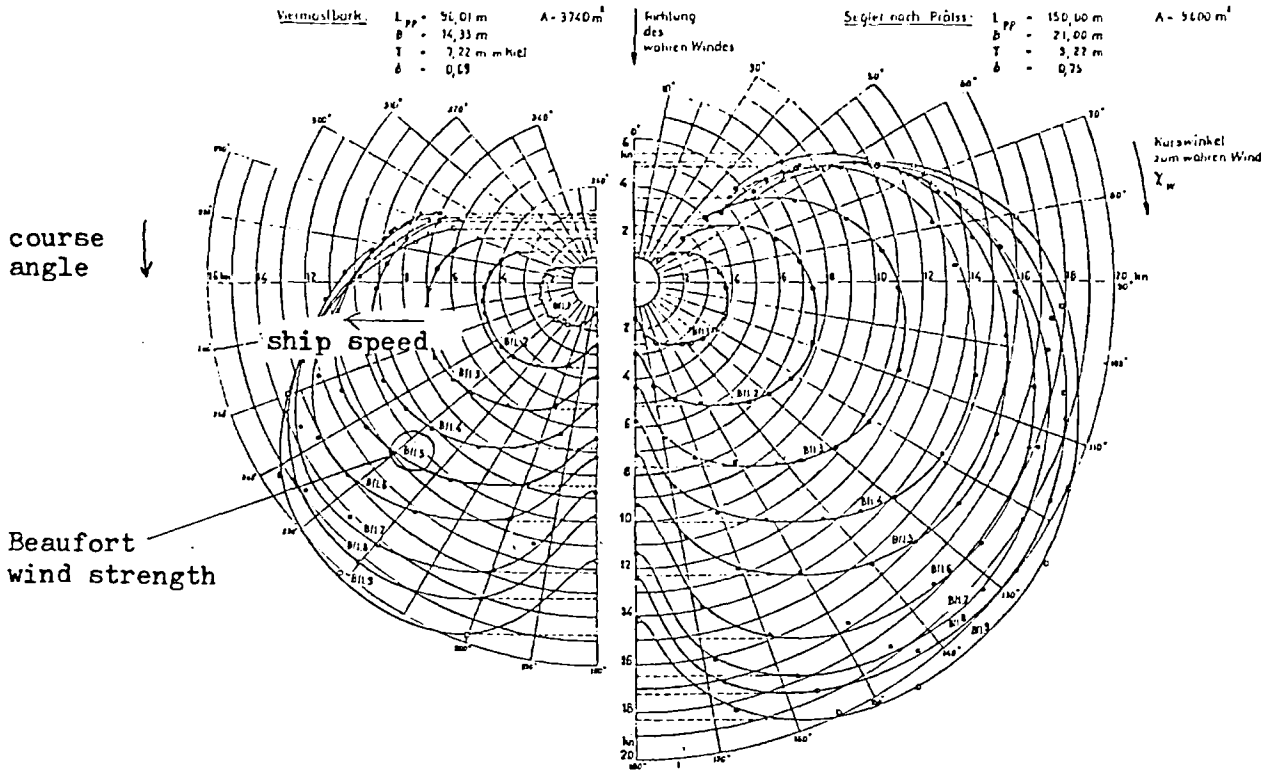

Geschwindigkeitsdiagramme für Viermastbark (links, linke Hälfte des Diagramms) und Segler nach Prölss (rechts, rechte Hälfte des Diagramms). Fahrtgeschwindigkeiten V_H als Funktion des Kurswinkels zum wahren Wind χ_W für verschiedene Windstärken in Beaufort.

Figure 7.1

Performance curves for a traditional barque (left) and the proposed "Dynaship" (right):

Wagner (1967)

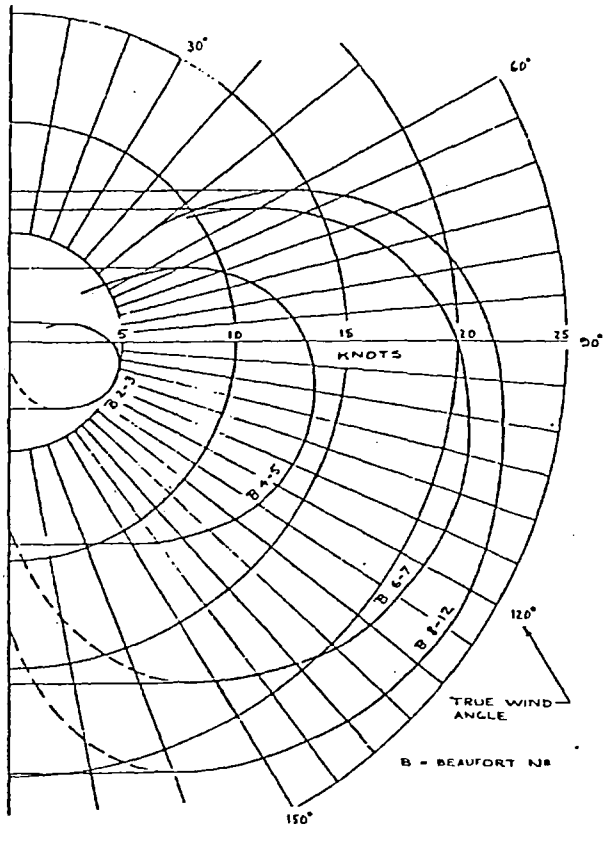

Speed Polar for 15,000 ton Sailing Ship,
Full Load, $\overline{GM}$ = 6.3 ft

Figure 7.2

Performance curves for a possible sailing ship:

Woodward, Beck, Scher and Cary(1976)

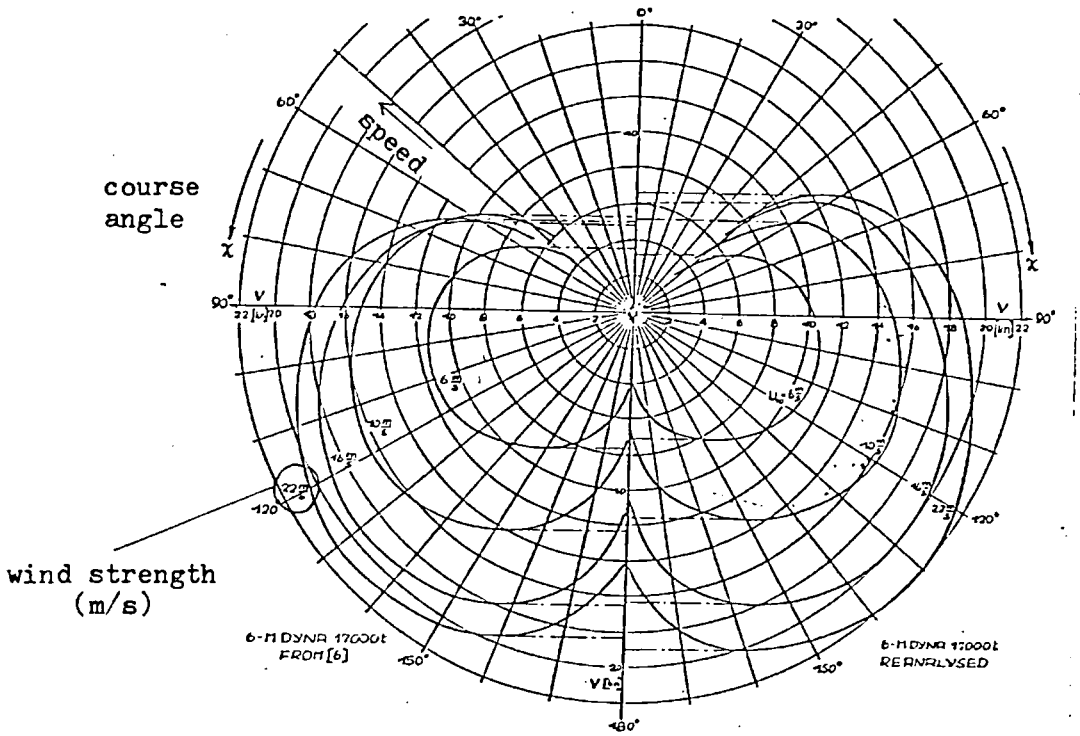

Figure 7.3

Performance curves for the "Dynaship", comparing those produced by Wagner (left) with those of Schenzle (right):

Schenzle (1976)

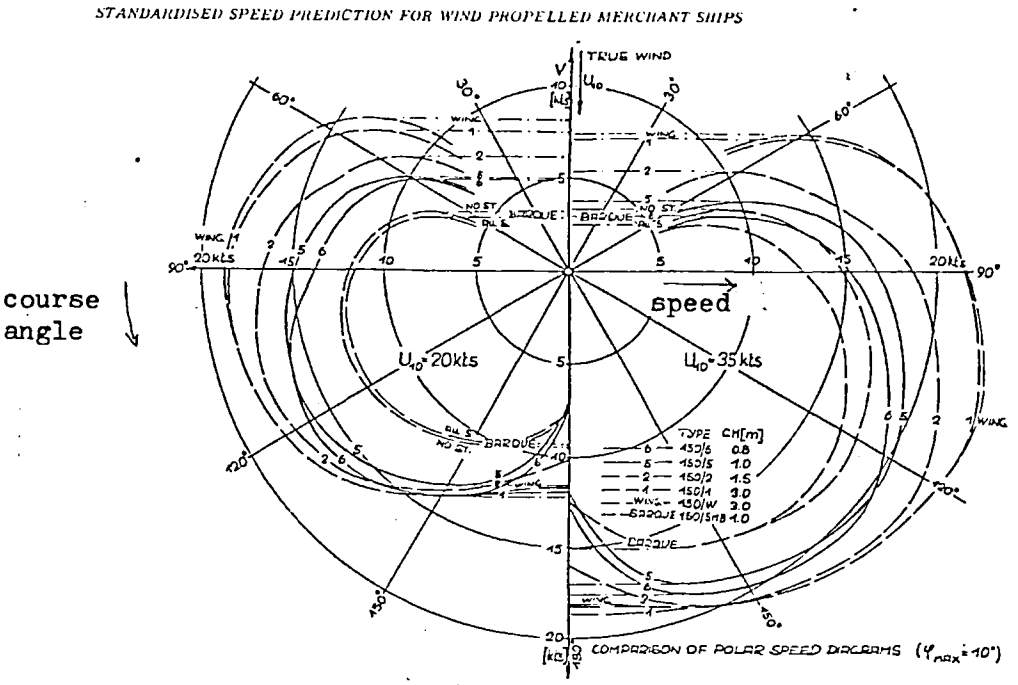

Comparison of Polar Speed Diagrams, $\phi_{max} = 10°$

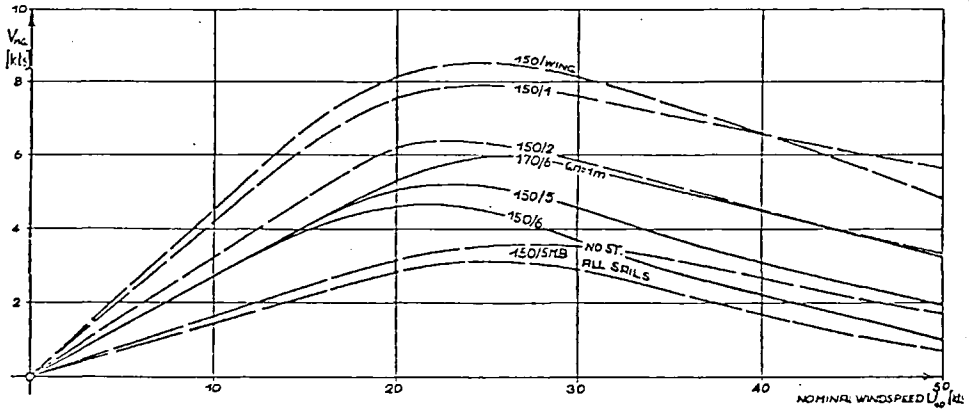

Speed Made Good to Windward for Different Rigs, $\phi_{max} = 10°$

Figure 7.4

Performance curves comparing similar possible vessels with various sail-numbers and sail-types: Schenzle(1980)

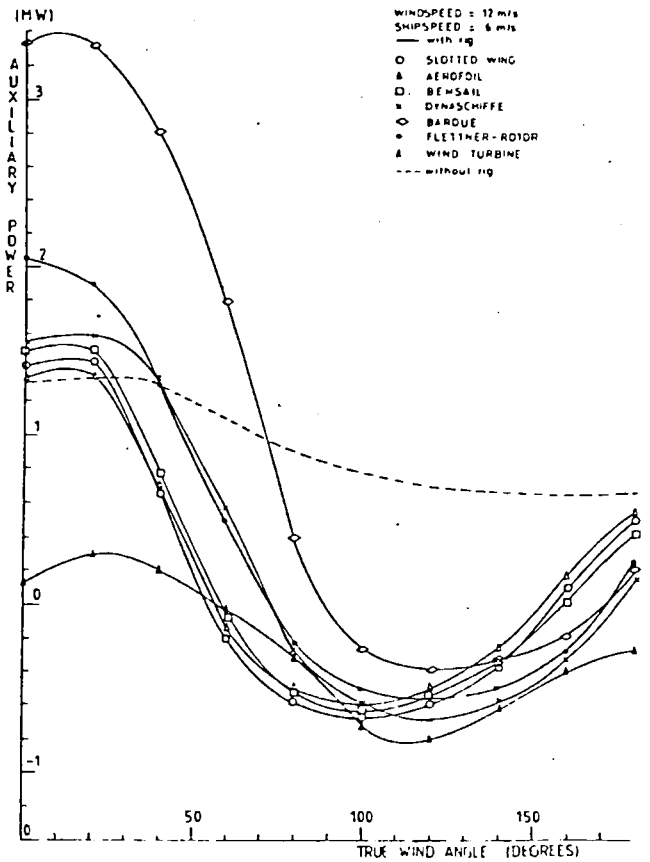

Fig. 2. Fuel Power Requirement vs True Wind Angle

Figure 7.5

Performance curves produced by Rainey's program for various possible wind-powered vessels:

Nance (1980)

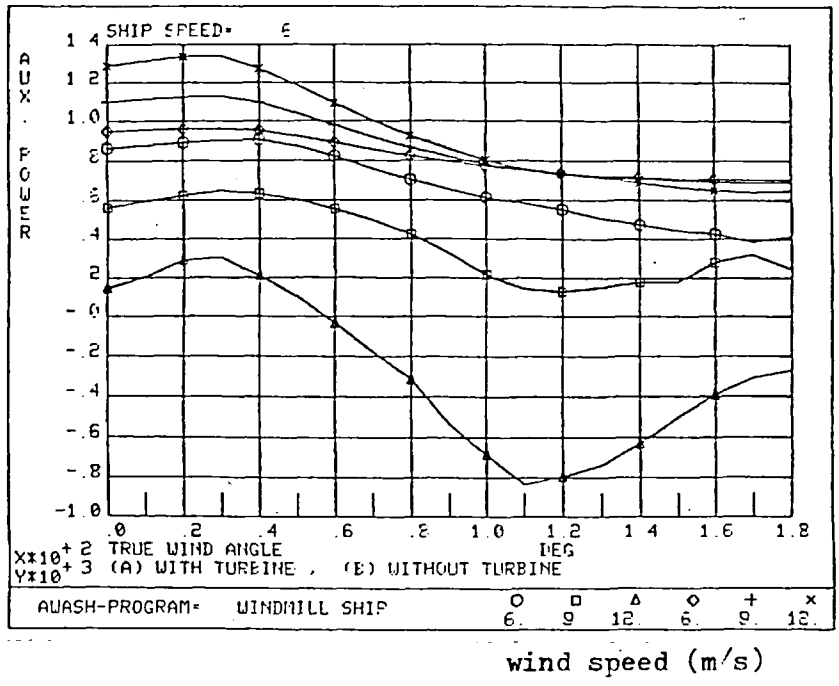

Figure 7.6

Performance curves for a proposed windmill ship:

Rainey (1980)

7.3(a) Model: outline

The new performance model described below has been derived by the author for comparative analysis of possible sailing ship configurations. It uses a single iterative loop to solve the following equations; two kinematic equations, 2 horizontal force equations, the yawing moment equation and the heeling moment equation. It is assumed that pitching moments and vertical components of forces cause small enough change in draft and trim to be neglected in estimating performance. Attempts are made to model the vertical wind profile and rough water effects. The program is written so that the performance can be calculated for various sailing or motor-sailing modes; these are pure sailing, constant power motor-sailing and constant speed motor-sailing.

The governing equations are derived in section 7.3(b). They are summarised below:

The kinematic equations;

$$V_T^2 = V_A^2 + V_H^2 - 2 V_A V_H \cos(\lambda_A + \lambda_H) \qquad 1$$

$$V_A^2 = V_T^2 + V_H^2 - 2 V_T V_H \cos(\pi - \gamma) \qquad 2$$

Equilibrium of horizontal forces;

$$C_{TA} / C_{TH} = (V_H / V_A)^2 \qquad 3$$

$$\lambda_A + \lambda_H = \varepsilon_A + \varepsilon_H \qquad 4$$

Equilibrium of moments;

$$\varphi = f_n (C_{TH} , \lambda_H , \varepsilon_H , V_H) \quad 5$$

$$L_A = L_H \quad 6$$

Hydrodynamic data equations;

$$C_{TH} = f_n(\lambda_H , V_H , L_H , \rho , V_T , \gamma) \quad 7$$

$$\varepsilon_H = f_n(\lambda_H , V_H , L_H , \rho , V_T , \gamma) \quad 8$$

Aerodynamic heel equations;

$$C_{TA} = f_n (C_{TAO} , \lambda_{AO} , \varepsilon_{AO} , \varphi) \quad 9$$

$$\varepsilon_A = f_n (\lambda_{AO} , \varepsilon_{AO} , \varphi) \quad 10$$

$$\lambda_A = f_n (\lambda_{AO} , \varphi) \quad 11$$

Aerodynamic data equations;

$$C_{TAO} = f_n (\lambda_{AO}) \quad 12$$

$$\varepsilon_{AO} = f_n (\lambda_{AO}) \quad 13$$

$$L_A = f_n (\lambda_{AO}) \quad 14$$

There are fourteen equations relating seventeen variables,

$$V_T , V_H , V_A , \varphi , \gamma , \lambda_H , \lambda_A , \lambda_{AO} , \varepsilon_H , \varepsilon_A , \varepsilon_{AO} , C_{TH} , C_{TA} , C_{TAO} , L_H , L_A , \rho$$

The set of equations is closed by specifying the values of three of these variables. Two of these are normally the true wind speed, V_T, and the no-heel aerodynamic inflow angle, λ_{AO} (λ_{AO} is specified as a value for which wind

tunnel test data is available). The third specified variable can be V_H or P: if the relative water speed, V_H, is specified, the model calculates constant speed motor-sailing performance; if the engine power, P, is specified, the model calculates constant power motor-sailing performance (or pure sailing performance if $P = 0$).

Note: the symbols used in this chapter are listed and defined in appendix A7.3.

7.3(b) Model: derivation of model equations

Kinematic relationships: figure 7.7 indicates the relationship between the true wind velocity (V_T), the relative fluid speeds (V_A and V_H) and the inflow angles (λ_A and λ_H). Application of the cosine formula gives;

$$V_T^2 = V_A^2 + V_H^2 - 2 V_A V_H \cos(\lambda_A + \lambda_H) \quad 1$$

$$V_A^2 = V_T^2 + V_H^2 - 2 V_T V_H \cos(\pi - \gamma) \quad 2$$

Equilibrium of horizontal force components: figure 7.8 indicates the relationship between velocities, inflow angles, forces ($\underline{F}_A$ and $\underline{F}_H$) and drag angles (ε_A and ε_H). Firstly, aerodynamic and hydrodynamic forces must be of equal magnitude: that is;

$$|\underline{F}_A| = |\underline{F}_H|$$

Using non-dimensionalised force coefficients as described in appendix A7.1, this becomes;

$$\tfrac{1}{2}\rho_A (L^2) V_A^2 C_{TA} = \tfrac{1}{2}\rho_H \left(\frac{\rho_A}{\rho_H} L^2\right) V_H^2 C_{TH}$$

$$\Rightarrow \quad \frac{C_{TA}}{C_{TH}} = \left(\frac{V_H}{V_A}\right)^2 \quad 3$$

Secondly, the aerodynamic and hydrodynamic forces act in opposite directions, so the angle between $\underline{F}_A$ and $\underline{F}_H$ is π, which requires;

$$\pi = \varepsilon_A + \frac{\pi}{2} - \lambda_A - \lambda_H + \frac{\pi}{2} + \varepsilon_H$$

$$\Rightarrow \quad \lambda_A + \lambda_H = \varepsilon_A + \varepsilon_H \quad 4$$

Equilibrium of heeling moments: figure 7.9 consists of three sketches indicating the heeling and righting forces acting on a sailing ship. In steady sailing conditions, the aerodynamic and hydrodynamic heeling couple are in equilibrium with the buoyancy and weight righting couple. The heeling couple is considered first. The heeling force is the component of the total force acting perpendicular to the ship's centre line. Simple trigonometry gives this component as;

$$\text{heeling force} = C_{TH} \cos(\lambda_H - \varepsilon_H) \tfrac{1}{2} \rho_H \left(\frac{\rho_A}{\rho_H} L^2\right) V_H^2$$

writing h_A as the height of the aerodynamic centre of pressure, h_H as the depth of the hydrodynamic centre of pressure, and φ as the angle of heel;

$$\text{heeling moment arm} = (h_A + h_H) \cos\varphi$$

$$\Rightarrow \quad \text{heeling couple} = (h_A + h_H) \cos\varphi \, C_{TH} \cos(\lambda_H - \varepsilon_H) \tfrac{1}{2} \rho_A L^2 V_H^2$$

The righting couple is now considered; this is exerted by the vessel's total weight (acting downwards through the centre of gravity, G) and the total buoyancy force (acting vertically upwards through the centre of buoyancy, B). KG, the distance of the centre of gravity from the keel, is determined for a given ship by the distribution of ship's structure, bunkers, cargo, etc. KM, the distance of the metacentre from the keel, is determined by the underwater shape of the hull. (The metacentre is the point of intersection of a vertical through the centre of buoyancy with the ship's plane of symmetry.) Taylor and Trim (1948) and

Hind (1982) describe the stability (buoyancy) calculations needed to estimate KM. It can be shown that for a conventionally shaped ship (and provided the vessel is not so far heeled that she is "gunwales under");

$$KM \approx \frac{D}{2} + \frac{B^2}{18\,D\,C_B}\left(1 + \frac{\tan^2\varphi}{2}\right)$$

that is, KM is a function of φ ;

$$KM = KM(\varphi)$$

(The condition on maximum heel is;

$$\varphi < \operatorname{atan}\left(\frac{2(D_{deck} - D)}{B}\right) \qquad)$$

Equating the heeling and righting couples requires;

$$(h_A + h_H)\cos\varphi\, C_{TH}\cos(\lambda_H - \varepsilon_H)\tfrac{1}{2}\rho_A L^2 V_H^2 = (KM(\varphi) - KG)\sin\varphi\,\nabla\rho_H g$$

This is an implicit equation in φ : hence;

$$\varphi = f_n(C_{TH}, \lambda_H, \varepsilon_H, V_H) \qquad 5$$

Equilibrium of yawing moments: figure 7.10 indicates the yawing forces acting on the above-water ship (A_Y), on the underwater hull (H_{YH}) and on the rudder (H_{YR}). As discussed by Davidson (1956), Barnaby (1960) and Wagner (1967a), the centre of effort for hull side force generally lies forward of the centre of effort for sail side force. The resultant couple is usually balanced by putting the rudder over so that it produces part of the hydrodynamic side force. The condition that there is no resultant yawing couple is that the total aerodynamic and hydro-

dynamic forces act at the same distance from the bows: that is;

$$L_A = L_H \qquad 6$$

The hydrodynamic data used here is in a form which includes hull and rudder side forces and moments as functions of lee-way, λ_H, and rudder angle, λ_R. The total hydrodynamic moment about the bows (M_H) is equal to the sum of the hull moment (M_{HH}) and the rudder moment (M_{HR}): that is;

$$M_H = M_{HH} + M_{HR}$$

Substituting the functional expressions for side forces and moments on hull and rudder gives;

$$L_H\left(H_{YH}(\lambda_H) + H_{YR}(\lambda_R)\right) = M_{HH}(\lambda_H) + M_{HR}(\lambda_R)$$

This is an implicit functional relationship of the form;

$$\lambda_R = f_n(L_H, \lambda_H)$$

There is an upper limit to the turning moment that a rudder can exert. The results of the example applications of the performance model indicate that, in this case, the required rudder moment is below this limit in normal sailing conditions.

Hydrodynamic force data: figure 7.11 indicates the hydrodynamic inflow and drag angles (λ_H and ε_H) and the components of total horizontal hydrodynamic force (C_{HX} and C_{HY}). In this analysis hydrodynamic force coefficients are most conveniently considered resolved parallel and perpendicular to the ship's centre-line. Two relationships

are obtained from the figure;

$$C_{TH} = \sqrt{C_{HX}^2 + C_{HY}^2}$$

$$\varepsilon_H = \text{atan}\left(\frac{C_{HX}}{C_{HY}}\right) + \lambda_H$$

The resolved force components C_{HX} and C_{HY} are modelled as consisting of the following constituent components;

$$C_{HX} = C_X + C_{XR} + C_{XW} + C_{X\varphi} + C_{X\lambda} - C_{XT}$$

$$C_{HY} = C_{Y\lambda}$$

The device of considering the hydrodynamic force as the sum of attributable components is justified in section 3.2(d). The various constituent components are now considered in turn. $C_X = C_X(V_H)$ represents the "straight line" resistance of the hull. For a given hull, C_X is a complicated and imperfectly known function of Reynolds number and Froude number. C_X is most easily estimated from standard series data. These data have been obtained from model tests and adapted by empirical and theoretical corrections to predict full size ship resistance.

C_{XR} represents the hull roughness and fouling increment to resistance. It is estimated from empirical data.

$C_{XW} = C_{XW}(V_T, \gamma)$ represents the rough water increment to resistance for a ship in a seaway. It can be estimated from theoretical considerations or empirical data.

$C_{X\varphi} = C_{X\varphi}(\varphi)$ represents the resistance

increment due to heeling. The form of this function for a conventional ship hull is unknown. Wagner (1967a) experimented with a ship's hull on an even keel and heeled by 10°. He concluded that "the influence of the heel on the resistance in the case investigated is so small that it can be neglected." This assumption is made here $(C_{x\varphi} = 0)$.

$C_{x\lambda} = C_{x\lambda}(\lambda_H, L_H)$ and $C_{y\lambda} = C_{y\lambda}(\lambda_H, L_H)$ represent the components of force associated with leeway. Limited suitable oblique towing tests have been conducted at several establishments; results from these tests can be adapted to give these coefficients. Alternatively, the wind tunnel tests of hulls at leeway described elsewhere in this thesis provide suitable data.

$C_{xT} = C_{xT}(P, V_H)$ represents the thrust of the propeller. Note that for this performance model, P, the power coefficient, is defined as follows:- the power coefficient is the ratio of the product of propeller's actual thrust and ship's actual speed to the product of the propeller's thrust and ship's speed when motoring at service speed in flat conditions with no relative wind.

$$P = \frac{C_{xT}\,\frac{1}{2}\,\rho_H\left(\frac{\rho_A}{\rho_H}L^2\right)V_H^2\,V_H}{\left(C_x(V_S) + C_{xR}\right)\frac{1}{2}\rho_H\left(\frac{\rho_A}{\rho_H}L^2\right)V_S^2\,V_S}$$

$$\Rightarrow \quad C_{xT} = P\left(\frac{V_S}{V_H}\right)^3\left(C_x(V_S) + C_{xR}\right)$$

Substituting the various force constituents into the expressions for C_{TH} and ε_H gives;

$$C_{TH} = f_n(V_H, V_T, \gamma, \lambda_H, L_H, \rho) \quad 7$$

$$\varepsilon_H = f_n(V_H, V_T, \gamma, \lambda_H, L_H, \rho) \quad 8$$

The effect of heel on aerodynamic forces: few attempts have been made to determine the effects of heel on sail forces. Herreshoff (1964) analyses the geometric effects of heel. Milgram (1972) performs a lifting surface analysis of heeled yacht sail aerodynamics; he states that the aerodynamic effects of heel are negligible for heel angles of less than 30° and that the heeled case can be considered by simple resolution of velocities, forces and moments. Myers (1975) simply assumes that sail forces vary with cosine of heel angle, while Kerwin (1976) assumes that the relationship is linear. Curtis (1979) discusses the importance of aerodynamic effects of heel such as the changing flow interference on sails from the hull. The wind tunnel tests described in section 5.4(g) indicate that the aerodynamic effects of heel are not negligible and vary in a complicated way with sail and ship geometry. Only the geometric effects of heel are considered in this performance model as there seems no simple way of modelling the aerodynamic effects.

The aerodynamic data used for this performance model are obtained from wind tunnel tests. The (upright) aerodynamic force vectors are determined at a variety of inflow angles; hence the aerodynamic data consists of corresponding sets of $\{ \lambda_{Ao}, C_{TAo}(\lambda_{Ao}), \varepsilon_{Ao}(\lambda_{Ao}) \}$ The data relates to force and velocity vectors in a plane

parallel to the plane of the deck. The geometric effects of heel can be calculated by determining the relationship between the wind vector in the horizontal plane and its component in the (heeled) deck plane and the relationship between the force vector in the (heeled) deck plane and its component in the horizontal plane. This assumes that the spanwise flow component (up the mast) induces no additional forces. Figures 7.12 and 7.13 show the components of forces and vectors in the horizontal and deck planes. The following geometric relationships are obtained by consideration of the diagrams;

$$\tan(\lambda_A - \varepsilon_A) = \frac{\sin(\lambda_{AO} - \varepsilon_{AO})}{\cos(\lambda_{AO} - \varepsilon_{AO})\cos\varphi}$$

$$T_A = T_N \sqrt{\sin^2(\lambda_{AO} - \varepsilon_{AO}) + \cos^2(\lambda_{AO} - \varepsilon_{AO})\cos^2\varphi}$$

$$\tan\lambda_A = \frac{\sin\lambda_{AO}}{\cos\lambda_{AO}\cos\varphi}$$

$$V_A = V_N \sqrt{\frac{\sin^2\lambda_{AO}}{\cos^2\varphi} + \cos^2\lambda_{AO}}$$

The relationship between force and coefficient are;

$$T_N = \tfrac{1}{2}\rho_A L^2 V_N^2 C_{TAO}$$

$$T_A = \tfrac{1}{2}\rho_A L^2 V_A^2 C_{TA}$$

hence;

$$\frac{T_A}{T_N} = \frac{V_A^2 C_{TA}}{V_N^2 C_{TAO}}$$

So, by substitution,

$$C_{TA} = \frac{\sqrt{\sin^2(\lambda_{Ao} - \varepsilon_{Ao}) + \cos^2(\lambda_{Ao} - \varepsilon_{Ao})\cos^2\varphi}}{\left(\frac{\sin^2\lambda_{Ao}}{\cos^2\varphi} + \cos^2\lambda_{Ao}\right)} \qquad 9$$

$$\varepsilon_A = \operatorname{atan}\left(\frac{\tan\lambda_{Ao}}{\cos\varphi}\right) - \operatorname{atan}\left(\frac{\tan(\lambda_{Ao} - \varepsilon_{Ao})}{\cos\varphi}\right) \qquad 10$$

$$\lambda_A = \operatorname{atan}\left(\frac{\tan\lambda_{Ao}}{\cos\varphi}\right) \qquad 11$$

Aerodynamic force data: this data is obtained from the wind tunnel tests described elsewhere in this thesis. The various sail geometries were tested at a number of inflow angles; the data is therefore available as sets of aerodynamic quantities corresponding to each test inflow angle: that is;

$$C_{TAo} = f_n(\lambda_{Ao}) \qquad 12$$

$$\varepsilon_{Ao} = f_n(\lambda_{Ao}) \qquad 13$$

$$L_A = f_n(\lambda_{Ao}) \qquad 14$$

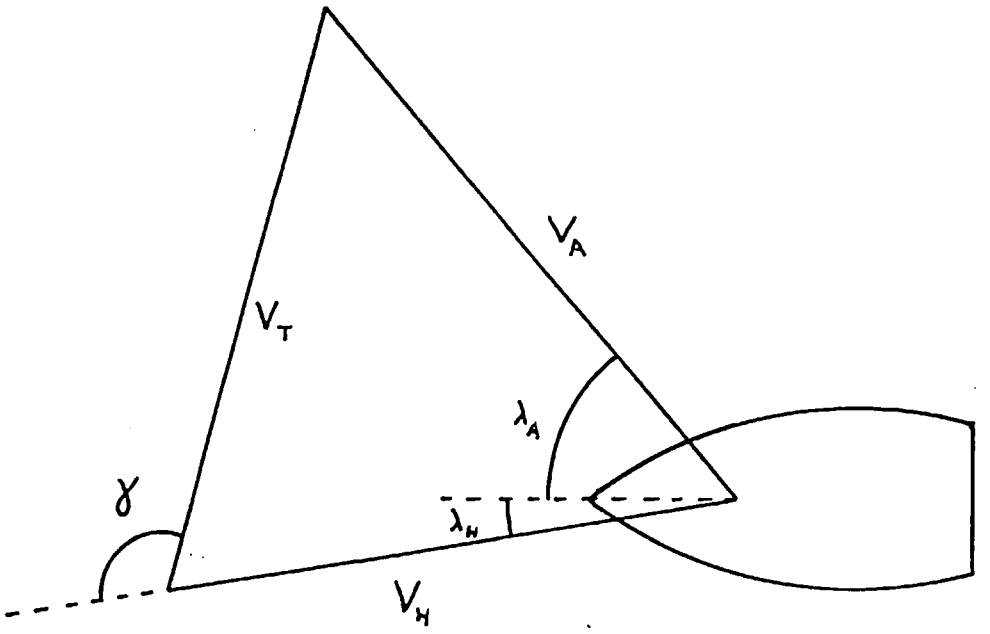

Figure 7.7

Sketch indicating trigonometry of velocity components

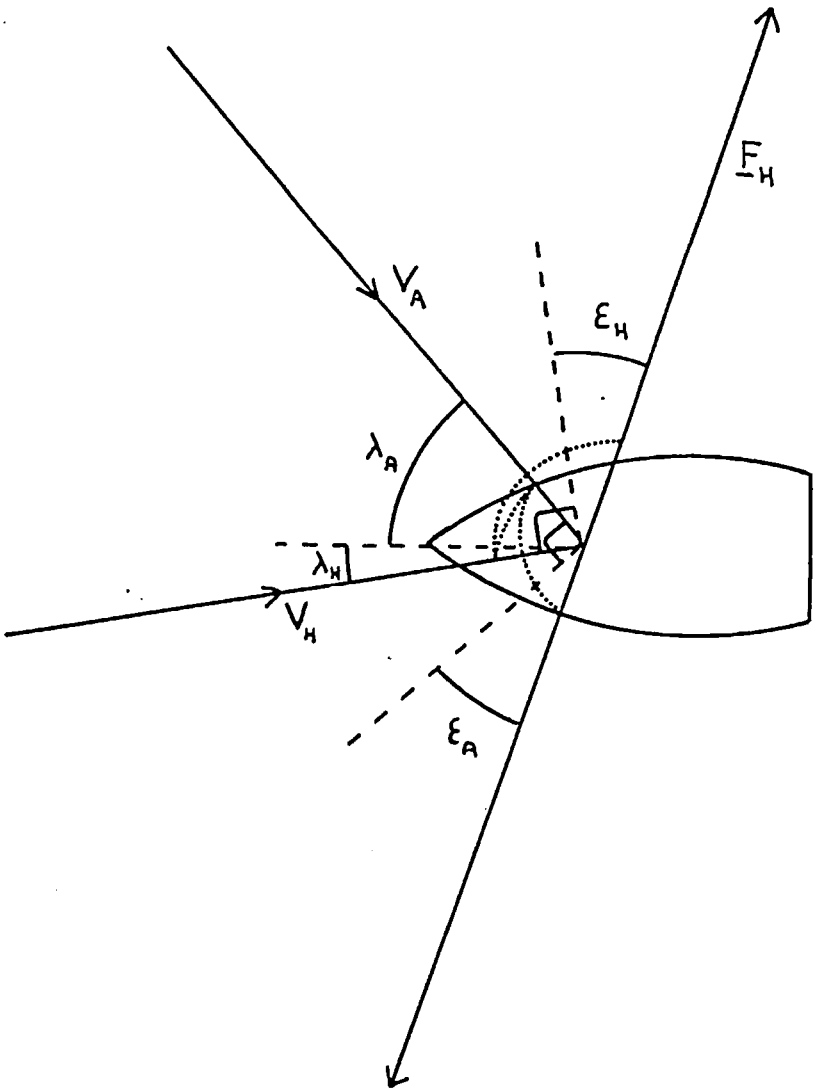

Figure 7.8

Geometry of horizontal velocity and force components

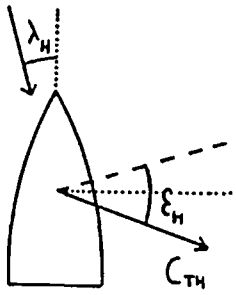

plan view of
hydrodynamic forces

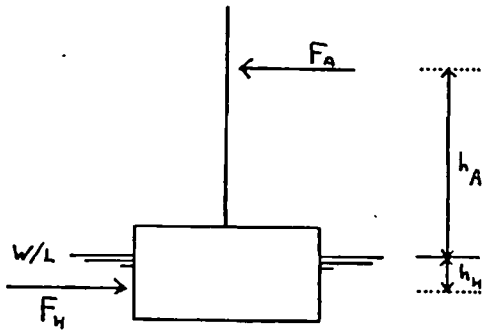

end view of
heeling forces

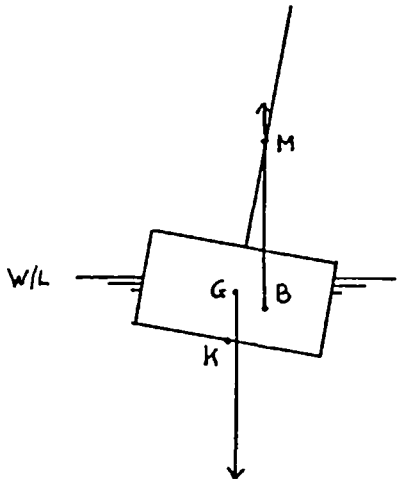

end view of
righting forces

Figure 7.9

Sketches indicating heeling and righting forces

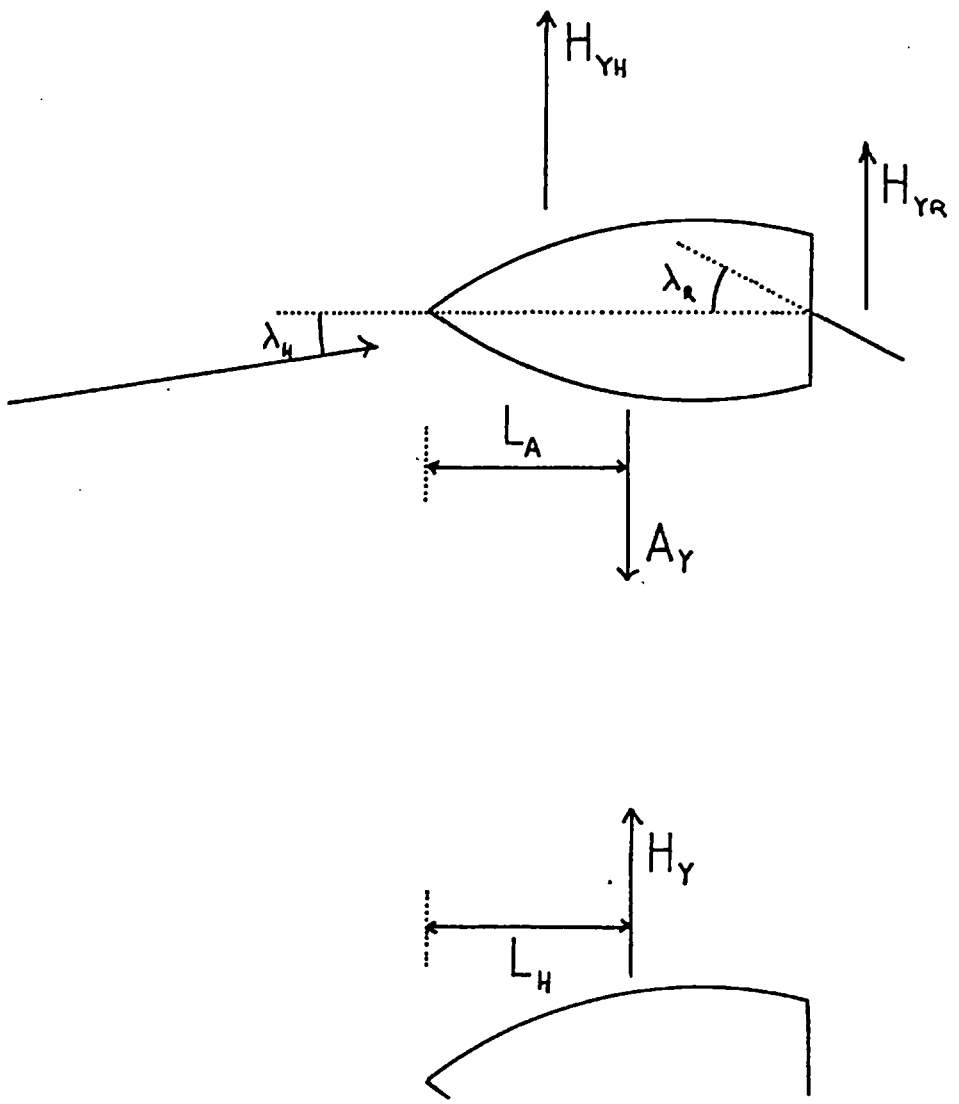

Figure 7.10

Sketches indicating yawing forces

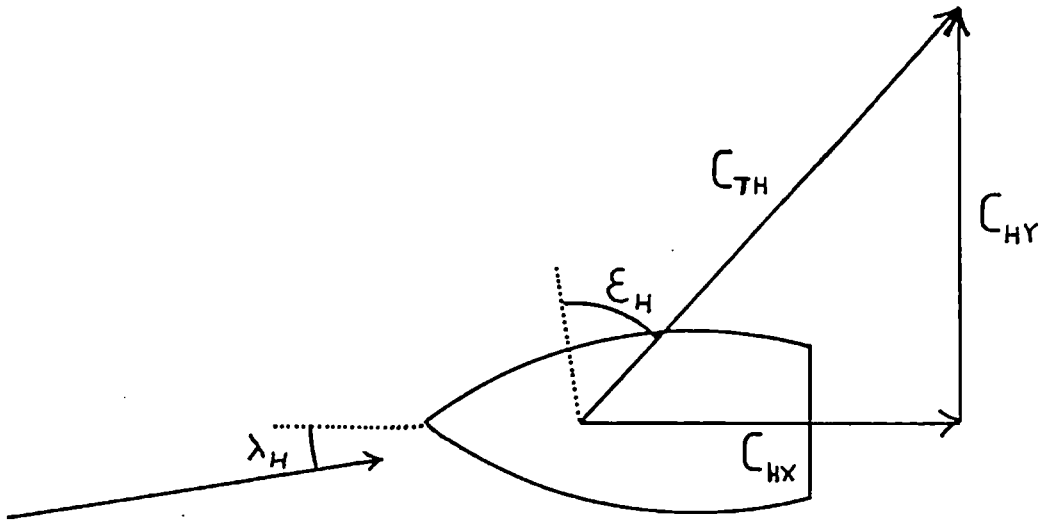

Figure 7.11

Trigonometry of resolved hydrodynamic force components

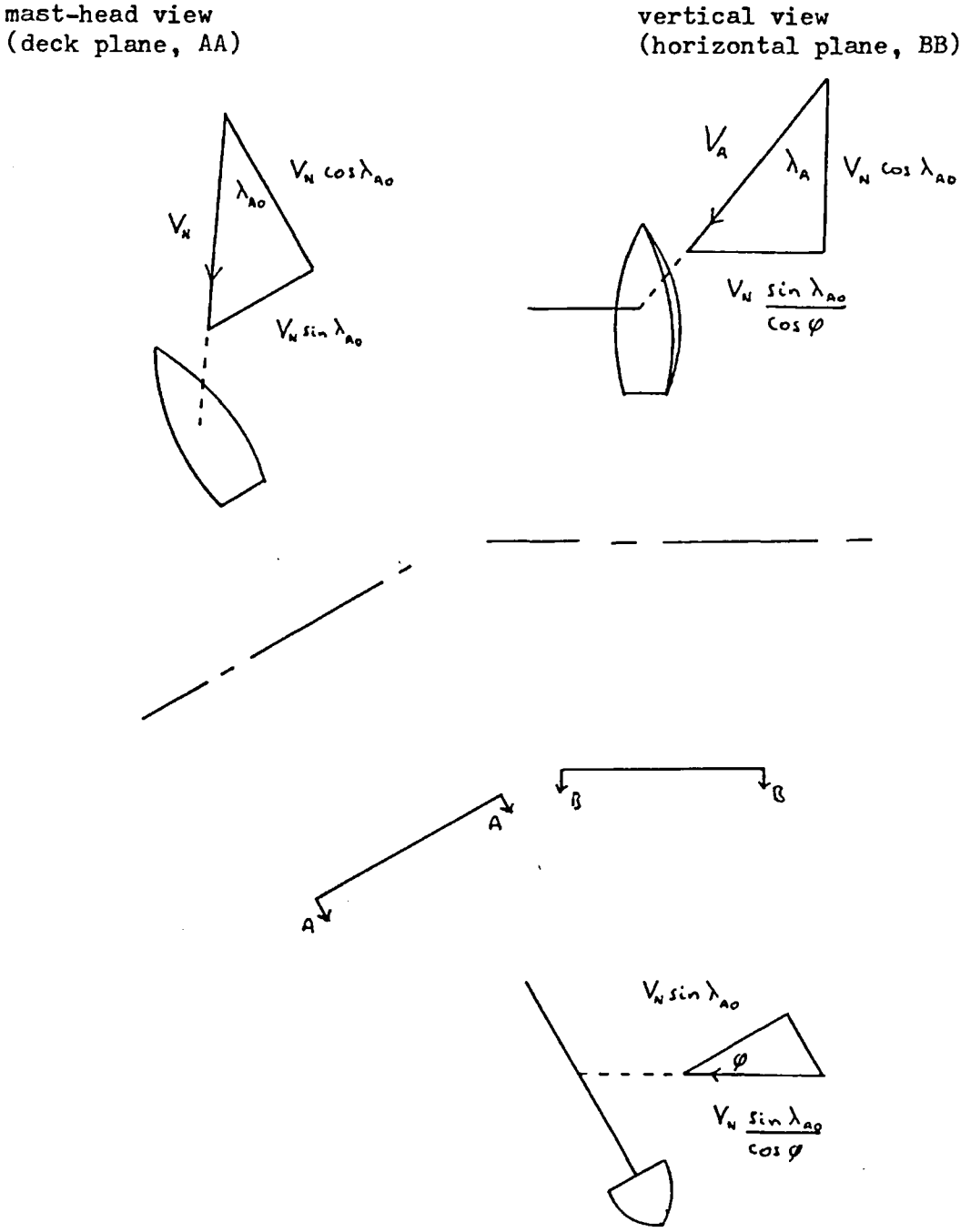

Figure 7.12

Geometric effects of heel on relative velocity

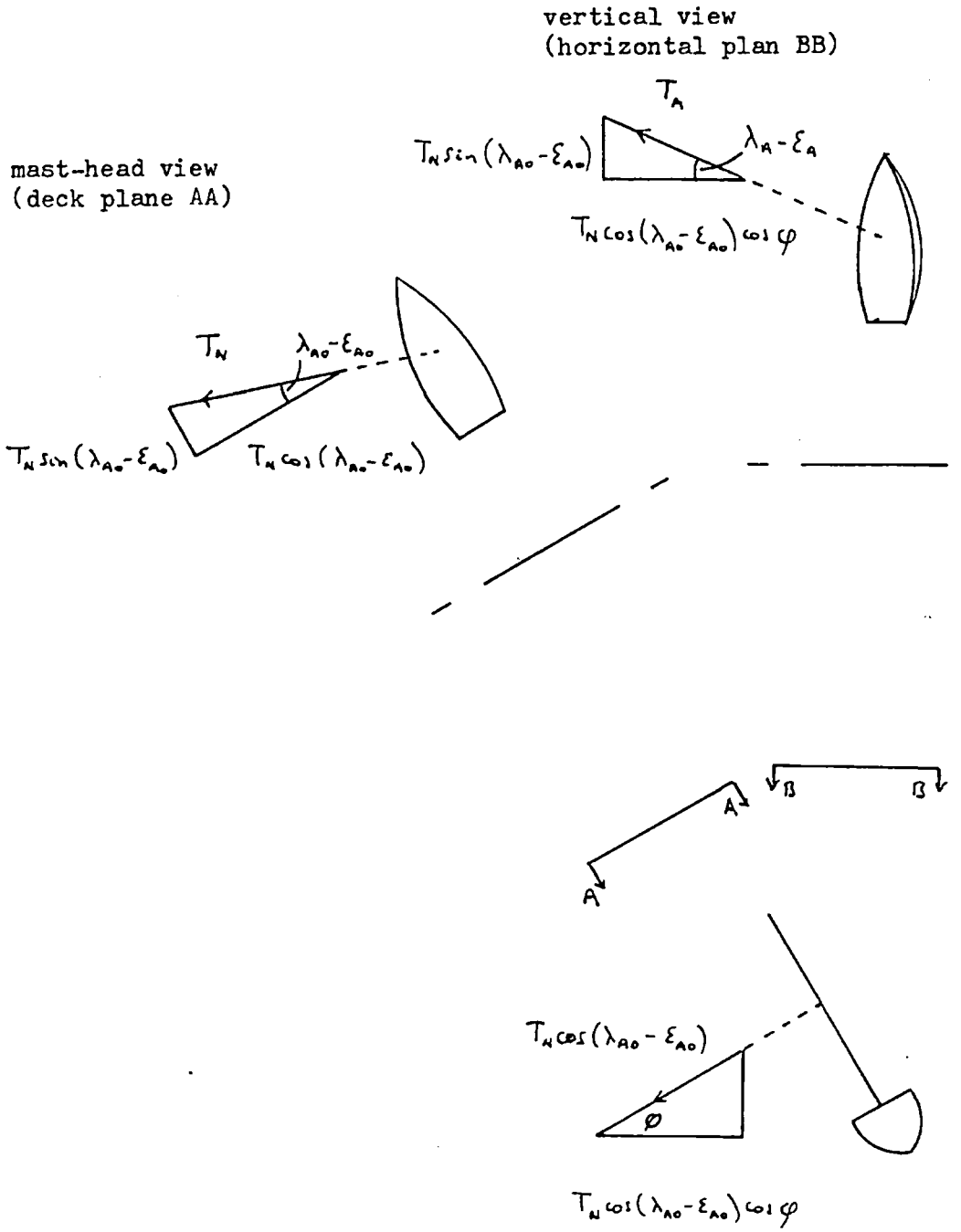

Figure 7.13

Geometric effects of heel on force components

7.3(c) Model: the wind

The Beaufort scale: a relationship between Beaufort wind strength and wind velocity is required. Mariners estimate the strength of the wind from the appearance of the sea surface. A more precise relationship is required for performance calculations. A suitable relationship is the "1946 International Scale" quoted by Wagner (1967a). This gives the velocity at a height of 10m above the sea surface as;

$$V_{10} = 0.8366 \text{ (Beaufort number)}^{3/2}$$

The wind profile: ships sail in the atmospheric boundary layer; the wind velocity varies with height. Milgram (1968) assumes that the wind profile between the sail's head and foot (top and bottom) varies linearly with height;

$$V / V_{10} = 1 + KZ$$

Hoerner (1965) suggests that the undisturbed wind profile is, approximately, of the form;

$$V / V_{10} = \sqrt[6]{Z/Z_0}$$

This profile is used by Wagner (1967a) and Baker and Douglas (1971). Schenzle (1976) quotes data from Wieghardt which suggests that a better approximation in moderate and strong winds is;

$$V/V_{10} = \sqrt[10]{Z/Z_0}$$

This is the profile given for strong (V_{10} > 10 m/s) ocean winds by Cermak (1976); it is also the profile

adopted for this model for most example calculations performed.

7.4 Example applications

Three example applications of the model are now discussed; the calculations are performed for various types of rig, and according to various engine-use-strategies. Firstly, various rigs are compared according to their constant-speed power requirements; secondly, the pure-sailing performance of a vessel rigged with eight thin circular-arc sails is estimated at various wind speeds; and thirdly, a realistic engine-use strategy is considered for a thick circular-arc sailing rig.

The calculations are performed for a possible 160 m auxiliary sailing vessel; this would be rigged with 8 60m x 20m rectangular sails. Table 7.1 gives the specifications of the vessel. The data used in this example application are discussed fully in appendix A7.3: the aerodynamic data are provided by the wind tunnel tests described in Chapter 5; the hydrodynamic data used aretaken from a variety of published sources.

Constant-speed example. A realistic engine-use strategy for an auxiliary cargo vessel is determined in a complicated way by the relative economic importance of fuel used and time spent at sea. Many of the factors affecting an economic strategy are discussed by Alderton (1981). For comparative analysis consideration of a simple, if unrealistic, strategy avoids the need for, possibly controversial, economic assumptions. One suitable strategy is the constant-speed motor-sailing strategy. This gives an immediate indication of the power available from the sailing rig in the assumed conditions. It is the strategy used by Rainey (1980) for

comparative analysis of rig configurations. The performance is calculated in terms of the power required to maintain a constant service speed. The power requirements are non-dimensionalised by the "service speed power" which is the power required by a similar, conventional, powered vessel making the same speed on a calm sea. A value of P greater than 1 indicates that the service speed power is insufficient to maintain the desired speed; a realistic strategy in such a case might be to motor-sail at service-speed power (P=1) making a slower speed. A value of P less than 0 indicates a surplus of power available; theoretically, some of this power is available for storage. Wynne (1981) discusses the advantages of storing energy in strong winds for use in light winds; lacking suitable cheap technology to do this, a realistic strategy might be to allow the vessel to sail faster than the desired speed with the engine off (P=0).

Figure 7.14 shows an example set of performance curves for a 15 kt vessel in a force 5 wind. The vessel is rigged with thin 12% camber circular-arc sails. Each curve represents a range of performance achievable with the sails trimmed in a particular way. For example, the curve labelled p20 represents the locus of performance achievable with all sails trimmed 20° from fore-and-aft. The dotted line represents the envelope of performance achievable by such a rig with all sails parallel. The individual curves do not diverge rapidly from this envelope: and this indicates that if a vessel has its sails trimmed for optimum performance at a given course

angle, the performance will remain near optimum as the course fluctuates about this given angle.

Figure 7.15 is a graph consisting of a number of performance envelopes for a variety of rigs. In every case the sails are trimmed parallel. The rigs are identified by sail camber (c%) and thickness (t%); N denotes a NACA four-figure-series thickness distribution and C denotes a distribution described by two circular arcs. Curve 9 is the power required by a conventional powered vessel to maintain service speed in this wind. It should be noted that curves have been included for the two NACA aerofoil rigs; these were calculated using model data which cannot be scaled, with any confidence, to full size because of severe Reynolds number effects discussed in Chapter 5. Hence, although the curves for the NACA aerofoil rigs are included on the graph, these two curves cannot be expected to be similar to the actual performance of such an aerofoil ship. Comparison of the performance curves of the remaining 5 rigs shows that the 12% camber circular-arc thin sail rig has the lowest overall power requirements, but all the other rigs, except the flat plate rig, perform nearly as well.

Note. For this first example, the wind velocity is assumed not to change with height (E=1). For the subsequent two examples it is assumed to vary as the tenth root of height (E=1.129 with the assumptions made in appendix A7.2).

Pure-sail example. Another simplified strategy that is useful for comparative analysis of rig configurations is the pure-sailing strategy. This is not a realistic strategy for an auxiliary vessel as economic

considerations would require the use of the engine in certain conditions to prevent the sailing speed from falling below some minimum value. In this example the performance curves are not produced for comparative analysis of configurations, but are used to show how achievable sailing speed varies with the (Beaufort) wind strength. The calculations are performed for a vessel fitted with thin 12% camber circular-arc sails.

Figure 7.16 shows the results of the calculations. It can be seen that the ship can sail within about 50° of the wind, although best speed to windward is made at about 60° off the wind; the best progress downwind is made by sailing about 150° off the wind. The effects of Froude wave drag become apparent in wind strengths above about force 5: large additional increases in wind strength produce modest additional increases in ship speed. The rough water effects become important in gale conditions (wind strengths of force 8 and above): these are manifest as a reduction in the vessel's best speed to windward in a force 8 and a reduction in maximum speed except when running with the wind in a force 9. No attempt is made to estimate performance in stronger winds because of the difficulties in modelling rough water effects in storm conditions.

Realistic engine strategy. Figure 7.17 shows example performance curves for a vessel fitted with 9% camber, 12% thick circular-arc section sails. These curves represent a possible realistic engine-use strategy. The vessel attempts to maintain a nominal service speed by using engine and sails together; in very favourable

conditions the vessel sails faster than this speed with the engine off; in unfavourable conditions the vessel motor-sails at a slower speed with the engine at normal service power. This example is for a vessel with a nominal service speed of 15 kts in a force 5 wind. This example curve shows that the ship sails faster than 15 kts under sail alone at course angles between 72° and 145°; it motor-sails at 15 kts at course angles between 30° and 72° and at course angles greater than 145°; and when motor-sailing closer than 30° to the wind its speed falls below 15 kts.

Table 7.1

Vessel specifications for example application of performance model

L, length between perpendiculars	: 160 m
B, beam	: 23.2 m
D_{deck}, deck height above keel	: 15 m
D, mean draft	: 7.5 m
Trim	: 1/130 by stern
LCB, location of centre of buoyancy	: 2% aft of amidships
C_B, box coefficient	: 0.625
∇, displacement volume	: 17400 m
Δ, displacement tonnage	: 17850 tonnes
Number of masts	: 8
Rig height	: 60 m
Rig length	: 160 m
Sail chord	: 20 m

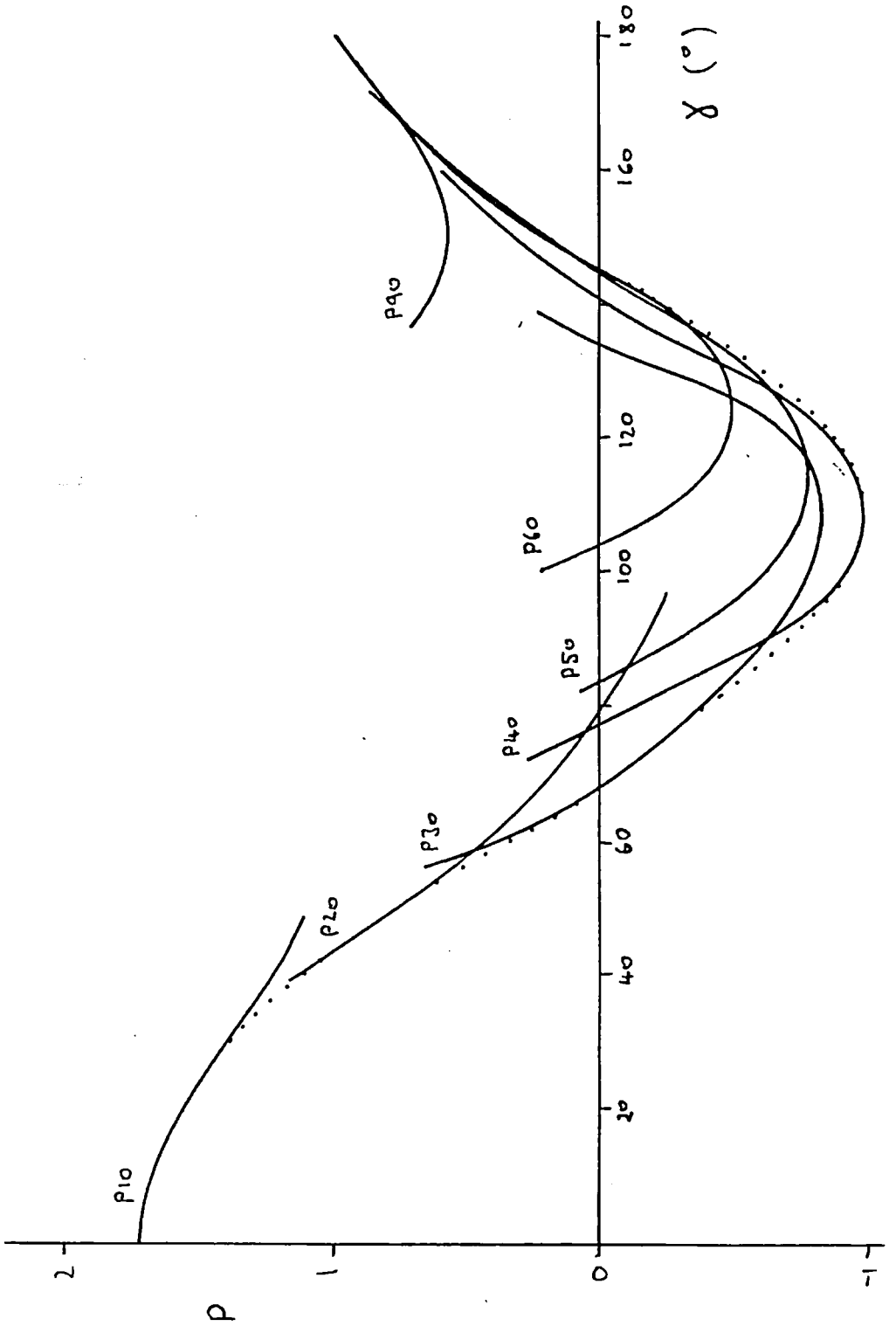

Figure 7.14

Auxiliary power requirements; 15 kt ship in force 5 wind;

12% camber thin plate sails; parallel trim

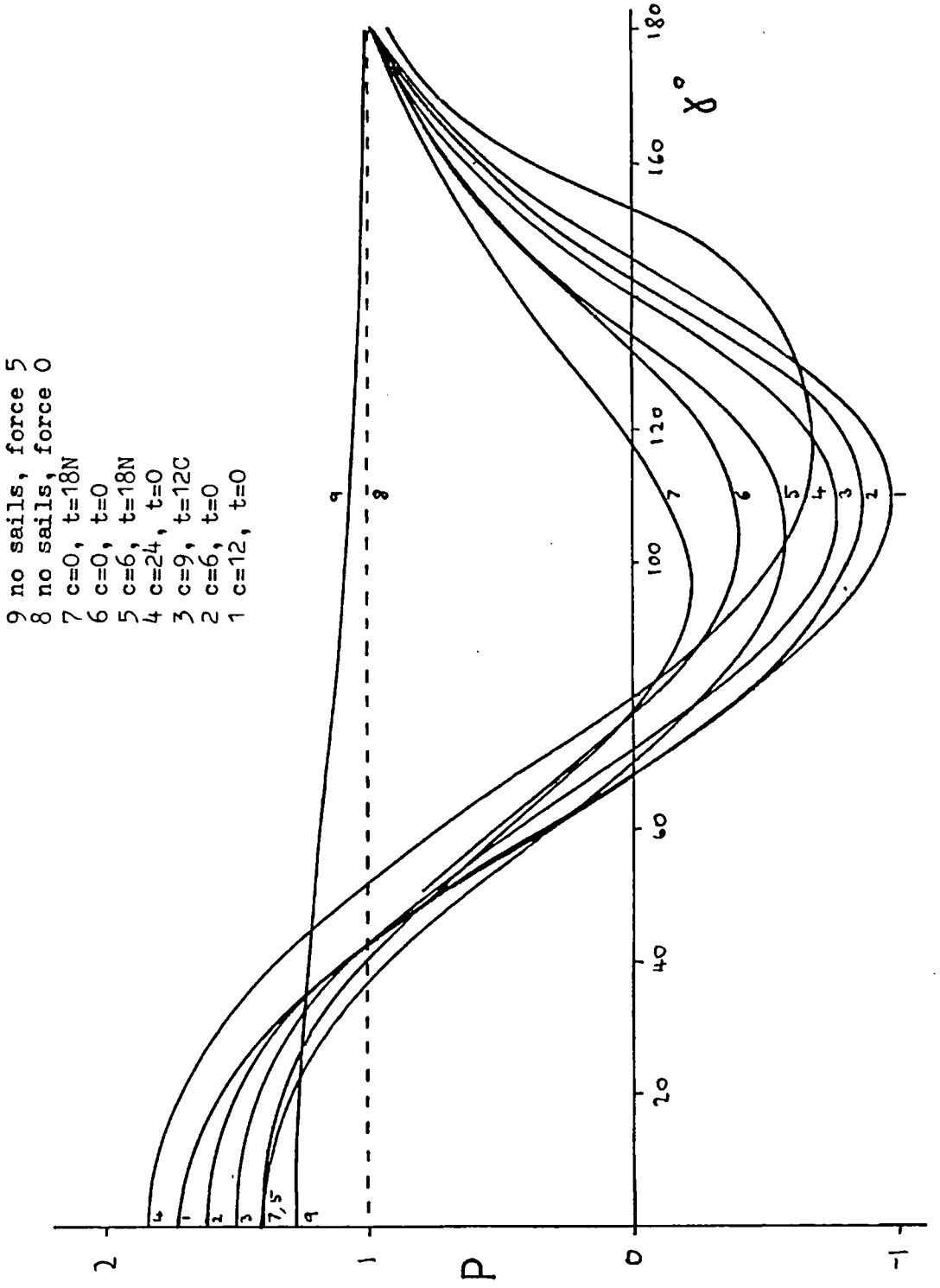

Figure 7.15

Auxiliary power requirements; 15kt ship in a force 5 wind; comparing various rigs; parallel trim

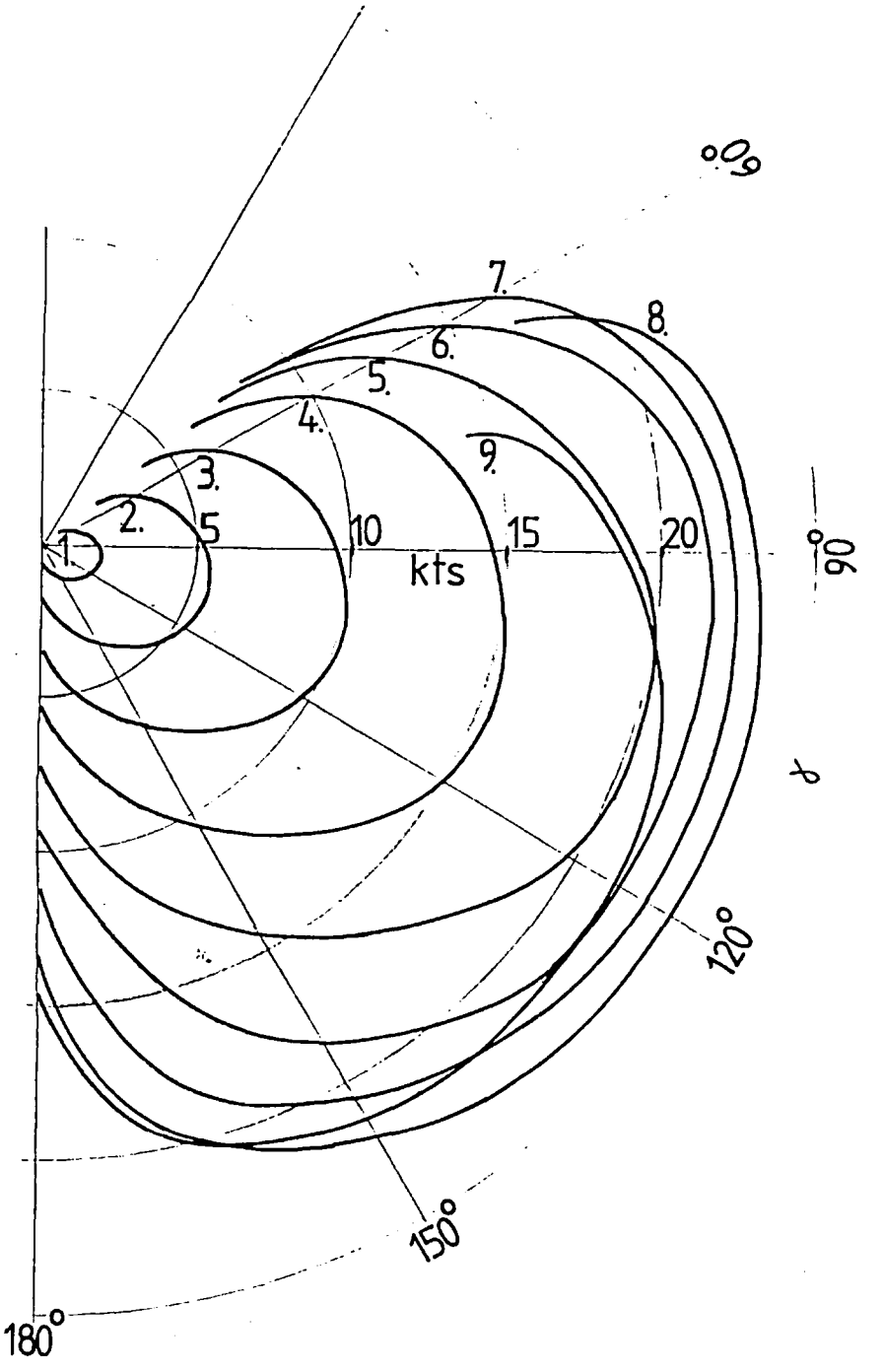

Figure 7.16

Polar performance graph: achievable speed V_h at course angle γ ; pure sail strategy; 12% camber thin sails; Beaufort force1. to 9.

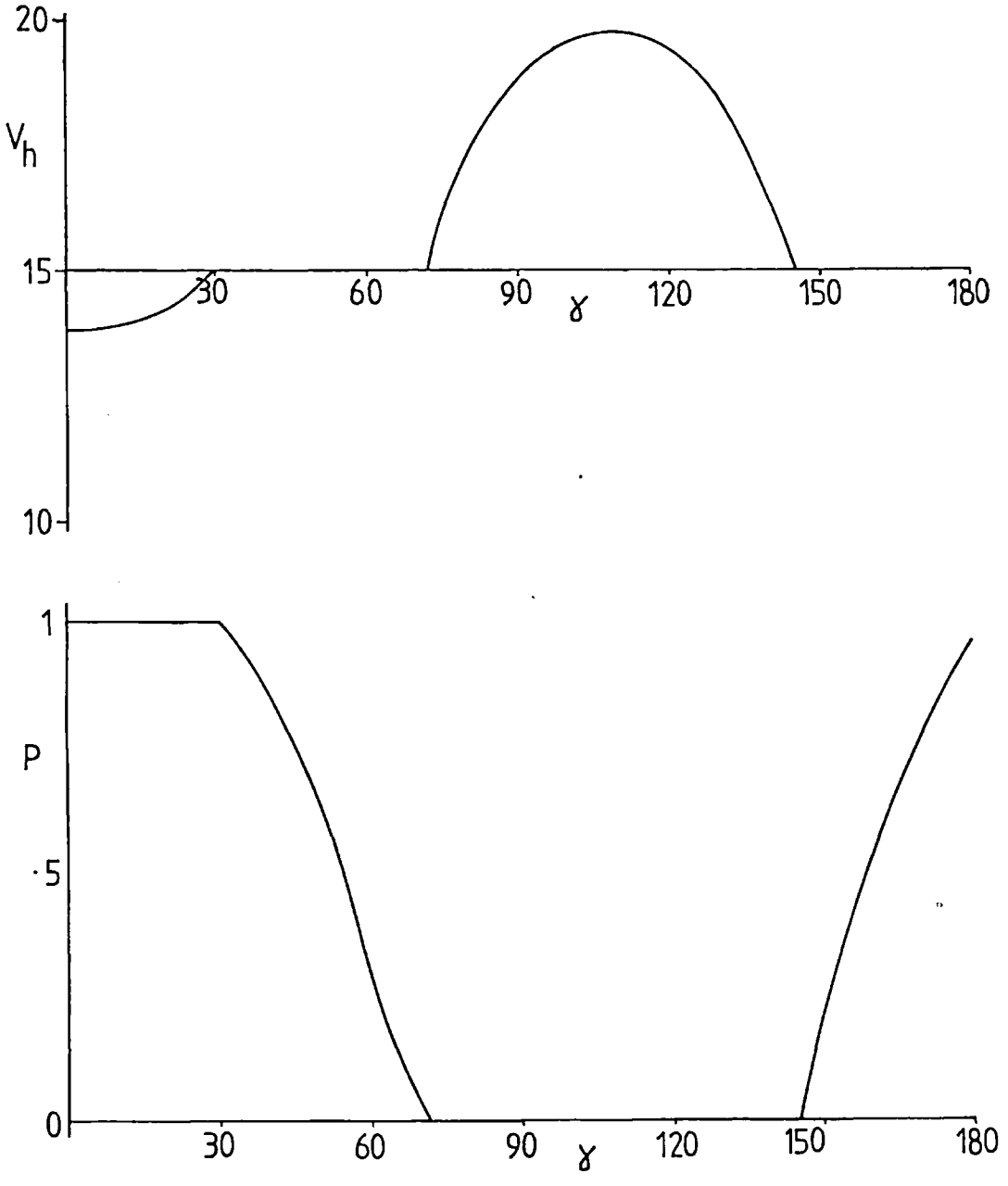

Figure 7.17

Performance curves: realistic engine strategy;
speed through the water and power coefficient plotted against
course angle γ ; twin arc thick sails; force 5 wind;
15kt service speed.

7.5 Observations and conclusions

The performance of a sailing vessel can be estimated by considering the kinematic relationships, the equilibrium of moments and forces, and various complicating phenomena at the sea surface. The history of mathematical performance models shows that these have been successively improved as simplifying assumptions have been removed and additional features of real sailing conditions have been considered. A number of models, particularly recent ones, have been written to estimate performance of large commercial sailing ships. Where real performance data have been compared with calculated performance the agreement has been found acceptable.

A new model is derived which can estimate performance according to various engine-use strategies. The basic equations are written in a non-dimensional form inspired by Hafner (1980); and this enables them to be solved using a single iterative loop and therefore allows economic use of computer time. The model can be simply adapted to consider additional features of real sailing conditions. It considers the kinematic relationships, the equilibrium of horizontal forces, and the equilibrium of yawing and heeling moments. It also includes consideration of the following features; hull wave making resistance, hull roughness and fouling resistance, rough water effects, variable propeller thrust, effect of heel on sail forces, and the wind profile.

A possible 8 masted, 160 m vessel is considered in several example applications. It is found that, provided the sails are trimmed in a near-optimum way, performance is not very sensitive to variations in sail

trim and inflow angle. Comparison of various circular-arc section sail rigs shows that the 12% thin sails are the best tested, but that the other circular-arc rigs are nearly as good. Pure sail performance curves are calculated for the 12% camber thin rig and a realistic engine strategy is considered for a thick circular-arc rig.

8: CONCLUSION

General. The indications are that wind-assisted or wind-powered ships once again have a role to play in the world's ocean-going merchant trade. These modern ships are unlikely to depend entirely on sail; they will be fitted with engines whose size will depend on the vessel's design philosophy for sail and engine use. This can vary between "wind-assistance" - where the engines are used for main propulsion and sails are used to reduce fuel consumption - to "wind-propulsion" - where sails are used for main propulsion and a comparatively small engine is used to maintain a minimum speed in poor sailing conditions. The first new wind ships to be constructed or converted are all at the wind-assistance end of the sail-use spectrum. Many proposed and actual wind ship projects are for vessels fitted with aerofoil-sails or more conventional thin fabric sails; other proposed systems include the rotor, the kite and the wind-turbine.

Hydrodynamics. The flow about a Mariner type hull has been investigated. The hull is a very low aspect ratio lifting body which can develop (horizontal) lift to balance sail side-force; it does this at the expense of considerable induced drag. The body is slender and fairly streamlined, but flow separation occurs at the bilges and shed vortex sheets roll up to form longitudinal vortices. These vortices, responsible for much of the drag penalty, trail downstream near to the hull; they generally maintain their identities, at least for the length of the ship; there is, however, some merging of vorticity between proximate vortices.

A series of experiments were made with hull-like blocks. The flow about these shows the same general features as that about realistic hulls. Specific conclusions for the block hulls indicate that the hydrodynamic repercussions on sailing ship performance of various changes are as follows:

- An increase in beam is marginally detrimental.
- An increase in draft is beneficial.
- Allowing the vessel to heel is beneficial.
- Trimming the vessel by the stern is beneficial.

A slender-body line-vortex method is used to model the flow past a block hull at leeway. Despite the complicated nature of the problem, the model is found to reproduce the main features of the flow; the calculation does, however, introduce some unphysical flow traits. It is clear that more realistic vortex representations and hull shapes could be considered using a similar slender body method. The mathematical modifications would not be great, although very considerably increased computer resources would be required.

Aerodynamics. The flow through multi-mast sailing rigs has been investigated. A multi-mast sailing rig acts as a low aspect ratio multi-element aerofoil. There are significant interaction effects between aerofoil-sails: the primary effect is that the local direction of flow varies throughout the array; the secondary, but also significant, effect is that the interaction between aerofoils can delay stall on individual aerofoils by reducing adverse pressure gradients.

Various rigs and rig configurations have been

experimentally compared. Particular conclusions for the rigs tested are as follows:

- For thin sails a camber of 12% has good all-round aerodynamic characteristics. However, sails which could be trimmed flatter at low angles of inflow and set fuller at large angles of inflow would give better performance.
- The thick sharp edged sails perform less well than similarly cambered thin sharp edged sails.
- There appears to be no justification for fitting mast-head end-plates.
- Reefing-from-aft and reefing-from-aloft can both be justifiable strategies for shortening sail according to circumstances.
- Good graduated trim arrays perform better than good parallel trim arrays when sailing close to the wind.
- Heel can cause considerable reductions in sail forces and this has beneficial repercussions for ship safety.

Experiments were also conducted with thick aerofoil section sails. A failure to correctly simulate above-critical flow prevents meaningful conclusions being drawn about the full scale behaviour of such aerofoil-sails.

A two-dimensional attached-flow thin-wing potential calculation was used to determine possibly advantageous graduated trim arrays. Predicted graduation of sail trim is often found to be particularly severe at the aft end of the arrays; the practical repercussions of this observation are discussed. The predicted graduated arrays were tested in a wind tunnel. The calculated arrays perform well in conditions where the real flow is largely attached; they

perform poorly in conditions where it is not.

Performance model. In steady sailing conditions, the total forces and moments on hull and sails are in equilibrium. These conditions form the bases of various previous performance models which are reviewed. A new performance model has been derived. It is based on these equilibrium conditions and includes consideration of the following complicating features: hull wave making resistance, hull roughness and fouling resistance, rough water effects, variable propeller thrust, effects of heel on sail forces, and the wind profile.

Various example performance calculations have been conducted and discussed.

REFERENCES

I.H. Abbott, A.E. Von Doenhoff and L.S. Stivers (1945), "Summary of airfoil data", N.A.C.A. report 824

F.D. Adams (1959), "Aeronautical dictionary", United States Government Printing Office

M.C. Adams (1953), "Leading-edge separation from delta wings at supersonic speeds", Journal of Aeronautic Sciences, 20, 430

M.C. Adams and W.R. Sears (1953), "Slender body theory - review and extension", Journal of Aeronautic Sciences, 20, 85-98

G. Aertssen (1969), "Service performance and trials at sea", Twelfth International Towing Tank Conference, proceedings, 210-214

G. Aertssen, G.E. Gadd and P.E. Colin (1980), "A method of ship resistance prediction: wave resistance and viscous resistance", Royal Institution of Naval Architects, transactions, 122, 407-426

P.M. Alderton (1981), "The optimum speed of ships", Journal of Navigation, 34, 341-355

J.F. Allan, D.J. Doust and B.E. Ware (1957), "Yacht testing", Royal Institution of Naval Architects, transactions, 99, 136-154

H.J. Allen and E.W. Perkins (1951), "A study of effects of viscosity on flow over slender inclined bodies of revolution", N.A.C.A. report 1048

Anon. (1910), "Wind pressure on curved plates of different camber", Engineering, 91, 804-805

Anon. (1975a), "Dynaship - resurgence of sail?", Marine Week, 2, no. 20, 33-35

Anon. (1975b), "Return of the cargo sailing vessel", Dock & Harbour Authority, 56, 48-49

Anon. (1976), "Give sail a chance", Marine Week, 3, no. 45, 13-15

Anon. (1978a), "Hands to the braces again", News, Portsmouth, 7 July, 14

Anon. (1978b), "Wind propulsion concept", Ship & Boat International, 31, no. 6, 22-26

Anon. (1979a), "Back to sail", Shipping World & Shipbuilder, 172, 738

Anon. (1979b), "Fuel economy in ship propulsion", Marine Engineers Review, March, 30-31

Anon. (1979c), "NKK sail research", Ship & Boat International, 32, no. 12, 52

Anon. (1980a), "A 5,000 tdw five-masted auxiliary barque proposed", Shipbuilding and Marine Engineering International, March, 110

Anon. (1980b), "Japanese sail on regardless", Marine Engineers Review, March, 37

Anon. (1980c), "Japan launches first wind assisted ship", Marine Engineers Review, Oct., 19

Anon. (1980d), "Japan to launch sail fleet", Observer, 6 July, 14

Anon. (1980e), "Windpower - a history of the future", Marine Engineers Review, Dec, 16-18

Anon. (1981), "States windship study", Marine Engineers Review, May, 30

Anon. (1982a), "Now a 12,000 dwt German sailing ship", Shipbuilding and Marine Engineering International, Nov., 515

Anon. (1982b), "Sail equipped cargo carrier ordered", Marine Engineers Review, Nov., 34

Anon. (1982c), "Sailpower progress continues in Japan", Marine Engineers Review, July, 28

Anon. (1982d), "Wind propulsion dynamometer", M.A.R.I.N. report no. 11, 98

Anon. (1983a), "American wind power: new demonstration sails through first tests", Marine Engineers Review, Jan., 15

Anon. (1983b), "BP flies an alternative kite", New Scientist, 98, 371

J.L. Armand, P. Marol and G. Saint-Blancat (1982), "Aero-dynamics of sail assisted propulsion of commercial ships: a preliminary study", Twelfth A.I.A.A. symposium on the aero/hydronautics of sailing, proceedings, 230-237

P. Arnold (1982), "Sail-bitten", Ship & Boat International, 112, no. 3, 5

S.A. Azad (1978), "Commercial Sailing Ships NewsBulletin", no. 3, Liverpool Polytechnic Department of Maritime Studies

S.A. Azad (1980), "Commercial Sailing Ships NewsBulletin", no. 5, Liverpool Polytechnic Department of Maritime Studies

M. Baily (1980), "Oil prices put sails back on horizon", Times, 9 Aug., 1

R.M.L. Baker and J.S. Douglas (1971), "Preliminary mathematical analysis of a rigid airfoil/hydrofoil water conveyance", Journal of Hydronautics, 5, no. 4, 140-147

H.M. Barkla (1951), "High speed sailing", Royal Institution of Naval Architects, transactions, 93, 248

K.C. Barnaby (1960), 'Basic Naval Architecture', Hutchinson

J.E. Barsby (1973), "Separated flow past a slender delta wing at incidence", Aeronautics Quarterly, 24, 120-128

G.K. Batchelor (1967), 'An introduction to fluid dynamics', Cambridge University Press

P.W. Bearman, J.K. Harvey and C.M. Gardner (1976), "Preliminary calibration of the 4.5' x 4.0' (1.37m x 1.21m) low speed wind tunnel", Imperial College Aero. report 76-01

T.D. Beatty and J.C. Narramore (1976), "Inverse methods for the design of multielement high-lift systems", Journal of Aircraft, 13, 393-398

I.C. Bhately and R.G. Bradley (1972), "A simplified mathematical analysis of multi-element airfoils near stall", A.G.A.R.D. C.P. 102, paper 12

A. Bowbee (1980), "Sail cargo ships - progress", Ship & Boat International, 33, no. 11, 60

W.M.S. Bradbury (1980a), "An investigation of graduated trim for an aerofoil rig", at Royal Institution of Naval Architects (1980), paper 12

W.M.S. Bradbury (1980b), "Wind tunnel tests of a model aerofoil ship", Imperial College Aero. report 80-04

W.S. Bradfield and S. Madhaven (1977), "Wing sail versus soft rig: an analysis of the successful Little Americas Cup challenge of 1976", 3rd S.N.A.M.E. Chesapeake sailing yacht symposium, 97-110

L.J. Briggs and H.L. Dryden (1930), "Aerodynamic characteristics of circular-arc airfoils at high speed", N.A.C.A. report 365

C.E. Brown and W.H. Michael (1954), "Effect of leading-edge separation on the lift of a delta wing", Journal of Aeronautic Sciences, 21, 690-694 and 706

C.E. Brown and W.H. Michael (1955), "On slender delta wings with leading-edge separation", N.A.C.A. technical note 3430

R.K. Burcher (1972), "Developments in ship manoeuvrability", Royal Institution of Naval Architects, transactions, 114, 1-32

J.E. Cermak (1976), "Aerodynamics of buildings", Annual Reivew of Fluid Mechanics, 8, 75-106

R.W. Clark, J.H.B. Smith and C.W. Thompson (1975), "Some series-expansion solutions for slender wings with leading-edge separation", R.A.E. technical report 75004

J. Cornell (1979), "Modern auxiliary schooner and ferry for Fiji", Ship & Boat International, 32, no. 1, 15

J. Cornell (1980), "Notes on Fiji shipping", Ship & Boat International, 33, no. 4, 26

A.D. Couper (1977), "The economics of sail", at Royal Institute of Navigation (1977), 164-171

A.D. Couper, J. King and P.B. Marlow (1979), "An evaluation of commercial sail", at Department of Industry (1979), paper 1

A.D. Couper and J. King (1980), "Commercial sail - present operations and future prospects", at Royal Institution of Naval Architects (1980), paper 3

W.A. Crago (1963), "The prediction of yacht performance from tank tests", Royal Institution of Naval Architects, transactions, 105, 155-176

M. Cross (1983), "Setting sail on wind-power with - the Pru", New Scientist, 98, 141

E.P. Crowdy (1980), "The economics of sail" at Royal Institution of Naval Architects (1980), paper 5

A.E. Cullinson (1980), "Tanker powered by sails", Daily Telegraph, 2 Aug., 5

M. Curry (1930), 'Yacht racing: the aerodynamics of sails and racing tactics', Bell and Sons

H.C. Curtis (1979), "The influence of heel angle on windward performance of sailing craft", Ninth A.I.A.A. symposium on the aero/hydronautics of sailing, proceedings, paper 24

K.S.M. Davidson (1936), "Some experimental studies of the sailing yacht", Society of Naval Architects and Marine Engineers, transactions, 44, 288-334

K.S.M. Davidson (1956), "The mechanics of sailing ships and yachts", published in 'Surveys in mechanics', edited by G.K. Batchelor and H. Bondi, Cambridge

J.P. Davis (1982), "Wind tunnel investigation of road vehicle wakes", Ph.D. Thesis, Department of Aeronautics, Imperial College

Department of Commerce (1979), "Marad awards contract for sailing ship study", News report MA NR 79-8

Department of Industry (1979), "DoI to study commercial sail", Press notice, 19 Sep.

Department of Industry, S.M.T.R.B. (1979), 'Symposium on the viability of commercial sailing ships', proceedings

P. De Saix (1964), Discussion of Herreshoff (1964)

O. De Vries (1972), "Comments on the methods developed at NLR for conducting two-dimensional research on high-lift devices", A.G.A.R.D. C.P. 102, Paper 8

B.D. Dore (1964), "The unsteady motion of slender wings with leading-edge vortices", A.R.C. C.P. 810

J.P. Dugan (1970), "A free streamline model of the two-dimensional sail", Journal of Fluid Mechanics, 42, 433-446

Dynaship Corporation (1975), "Dynaship - Modern wind powered cargo ships to 45,000 dwt", brochure

H. Eda and C. Lincoln Crane (1965), "Steering characteristics of ships in calm water and waves", Society of Naval Architects and Marine Engineers, transactions, 73, 135-177

H. Eda and D. Savitsky (1969), "Experimental and analytic studies of ship controllability in canals", Eleventh International Towing Tank Conference, proceedings, 649-654

R.H. Edwards (1954), "Leading-edge separation from delta wings", Journal of Aeronautical Sciences, 21, 134-135

G. Eiffel (1913), 'The resistance of the air and aviation', Constable

H.A. Everett (1915), "Aerodynamical experiments upon a yacht's mainsail", Society of Naval Architects and Marine Engineers, transactions, 23, 1-16

J.E. Fiddler, R.C. Schwind and J.N. Nielsen (1977), "Investigation of slender-body vortices", A.I.A.A. Journal, 15, 1736-1741

A. Flettner (1926), 'The story of the rotor', Crosby, Lockwood and Son

D.N. Foster, M.P.A.H. Irwin and B.R. Williams (1970), "The two-dimensional flow around a slotted flap", A.R.C. R&M 3681

H.B. Freeman (1933), "Pressure-distribution measurements on the hull and fins of a 1/40-scale model of the U.S. Airship 'Akron', N.A.C.A. report 443

A.E. Gentry (1971), "The aerodynamics of sail interaction", Third A.I.A.A. symposium on the aero-hydrodynamics of sailing, proceedings, 80-97

A.E. Gentry (1981), "A review of modern sail theory", Eleventh A.I.A.A. Symposium on the Aero/hydronautics of sailing, proceedings, 1-18

M. Gertler (1966), "The I.T.T.C. standard captive-model-test program", Eleventh International Towing Tank Conference, proceedings, 508-516

M. Gertler (1969), "Final analysis of first phase of I.T.T.C. standard captive-model-test-programme", Twelfth International Towing Tank Conference, proceedings, 609-626

A.D. Gill (1980), "The Analysis and Synthesis of Ship Manoeuvring", Royal Institution of Naval Architects, transactions, 122, 209-225

H.J. Goett and W.K. Bullivant (1939), "Tests of N.A.C.A. 0009, 0012 and 0018 airfoils in the full-scale tunnel", N.A.C.A. report 647

J.M.R. Graham (1977), "Vortex shedding from sharp edges", Imperial College Aero. report 77-06

P. Green (1980), "Will the windjammers return?", Port of London, 55, 78-79

B. Greenhill (1972), "The sailing ship in a fuel crisis", Ecologist, 2, no. 9, 8-10

F.R. Grosche (1971), "Wind tunnel investigation of the vortex system near an inclined body of revolution with and without wings", A.G.A.R.D. Conference proceedings, 71, paper 2

R. Hafner (1980), "A novel method to achieve optimum sailing performance", The Royal Institution of Naval Architecture, transactions, 122, 151-170

F. Handley Page (1921), "The Handley Page Wing", Aeronautical Journal, 25, 263-289

M. Hanin and O. Mischne (1973), "Flow about a rolling slender wing with leading-edge separation", Israel Journal of Technology, II, 131-136

H.G. Hasler (1977), "A rig for coastal trades", at Royal Institute of Navigation (1977), paper 7

C.C. Herbert (1976), "Commercial sail", Marine Week, August 20, 4

C.C. Herbert (1980), "The design challenge of the wind powered ship", at Royal Institution of Naval Architects (1980), paper 15

H.C. Herreshoff (1964), "Hydrodynamics and aerodynamics of the sailing yacht", Society of Naval Architects and Marine Engineers, transactions, 72, 445-492

H.C. Herreshoff and J.N. Newman (1966), "The Study of Sailing Yachts", Scientific American, 215, No. 2, 61-68

J.L. Hess and A.M.O. Smith (1967), "Calculation of potential flow about arbitrary bodies", 'Progress in Aeronautical Sciences', 8, Pergamon, 1-138

J.A. Hind (1982), 'Stability and trim of fishing vessels and other small ships', Fishing News Books Ltd.

S.F. Hoerner (1965), 'Fluid-dynamic drag', Otterbein Press, Dayton Ohio

R. Hogben (1978), "The return of the square rig?", Ships Monthly, 13, no. 4, 35

R. Hogben (1979a), "Trading under sail", Ships Monthly, 14, no. 2, 11

R. Hogben (1979b), "More commercial sail", Ships Monthly, 14, no. 12, 12

R. Hogben (1980a), "Cargo under sail", Ships Monthly, 15, no. 4, 12-13

R. Hogben (1980b), "What price the wind?", Ships Monthly, 15, no. 10, 30

R. Hogben (1982a), "Towage under sail", Ships Monthly, 17, no. 2, 29

R. Hogben (1982b), "Theory and practice", Ships Monthly, 17, no. 4, 13

R. Hogben (1982c), "Under sail - commercial talk and action", Ships Monthly, 18, no. 2, 10-11

W.J. Hood (1979), "The future of commercial sailing ships", 'Man and Navigation', symposium proceedings, International Congress of the Institutes of Navigation, 300-310

W.J. Hood (1980), "Using wind reliable routes for bulk cargo transport", at Royal Institution of Naval Architects (1980), paper 2

J.P. Howell (1979), "A consideration of some aerodynamic problems related to advanced ground transport", Magnetic Levitation Project report, University of Warwick Department of Engineering

J.P. Howell, R.G. Rhodes and K.W. Everitt (1980), "The influence of ground simulation on the aerodynamics of high speed trains", Magnetic Levitation Project, University of Warwick Department of Engineering

J.C.R. Hunt, C.J. Abell, J.A. Peterka and H. Woo (1978), "Kinematic studies of the flows around free or surface mounted obstacles; applying topology to flow visualisation", Journal of Fluid Mechanics, 86, 179-200

K. Illies (1977), "Energie für Schiffsantriebe - eine Zukunftsbetrachtung", Jahrbuch der Schiffbautechnischen Gesellschaft, 71, 68-79

D.B. Irani (1980), "Country craft and sailing vessels of India", The Naval Architect, 189-191

H.M. Irvine (1979), "A note on luffing in sails", Royal Society, proceedings, A365, 345-347

E.N. Jacobs and A. Sherman (1937), "Airfoil section characteristics as affected by variations of the Reynolds number", N.A.C.A. report 586

E.N. Jacobs, K.E. Ward and R.M. Pinkerton (1933), "The characteristics of 78 related airfoil sections from tests in the variable-density wind tunnel", N.A.C.A. report 460

M.A. Jacquemin (1980), "A multi-purpose tuna fishing boat with combined propulsion", at Royal Institution of Naval Architects (1980), paper 17

R.T. Jones (1946), "Properties of low-aspect-ratio pointed wings at speeds below and above the speed of sound", N.A.C.A. report 835

P.N. Joubert and P.N. Hoffman (1979), "An experimental study of the viscous resistance of a 0.564 C_B form", Journal of Ship Research 23, 140-156

P.N. Joubert and N. Matheson (1970), "Wind tunnel tests of two Lucy Ashton reflex geosims", Journal of Ship Research, 14, 241-276

P.N. Joubert and N. Matheson (1973), "Experimental Determination of the Components of Resistance of a small 0.80 C_B Tanker Model", Journal of Ship Research, 17, 162-180

D. Kemp (1897), 'Yacht architecture: a treatise on the laws which govern the resistance of bodies moving in water; propulsion by steam and sail; yacht designing; and yacht building', Cox, London

J.L. Kennedy and D.J. Marsden (1976), "Potential flow velocity distributions on multi-component airfoil sections", Canadian Aeronautics and Space Journal, 22, 243-256

J.L. Kennedy and D.J. Marsden (1978), "A potential flow design method for multi-component airfoil sections", Journal of Aircraft, 15, 47-52

J.E. Kerwin (1976), "A velocity prediction program for ocean racing yachts", Proceedings of the New England sailing yacht symposium, paper 7

J.F.R. King (1975), "A technical description and performance analysis of the Dynaship", at Royal Institution of Naval Architects (1975), paper 1

J.F.R. King (1976), "A forecast for sailing ships", Futures, 517-524

K. Kirkman and D. Pedrich (1974), "Scale effects in yacht hydronautic testing", Society of Naval Architects and Marine Engineers, transactions, 82, 78-101

W. Laas (1907), "Entwickelung und Zukunft der grossen Segelschiffe", Jahrbuch der Schiffbautechnischen Gesellschaft, 8, 275-379

W. Laas (1912), quoted by Flettner (1926), 52-53

H. Lackenby and M.N. Parker (1966), "The B.S.R.A. Methodical Series - An overall presentation: variation of resistance with breadth-draft ratio and length-displacement ratio", Royal Institution of Naval Architects, transactions, 108, 363-388

H.G. Lawrence (1975), "A modern fore and aft rigged sailing cargo ship", at Royal Institution of Naval Architects (1975), paper 2

R. Legendre (1952), "Ecoulement au voisinage de la point avant d'une aile a forte fleche aux incidences moyennes", La Recherche Aeronautique, no. 30, 3-6

R. Legendre (1953), "Ecoulement au voisinage de la point avant d'une aile a forte fleche aux incidences moyennes", La Recherche Aeronautique, no. 35

R. Legendre (1966), "Vortex sheet rolling-up along leading-edges of delta wings", Progress in Aeronautical Sciences, 7, Pergamon, 7-33

J.B. Lemon (1975), "Dynaship", Marine Week, 2, no. 26, 20

W.L. Le Page (1923), "Further experiments on tandem aero-foils", A.R.C. R&M 886

J.S. Letcher (1975), "Sailing hull hydrodynamics, with reanalysis of the 'Antiope' data", Society of Naval Architects and Marine Engineers, transactions, 83, 22-40

W. Letko (1953), "A low speed experimental study of the directional characteristics of a sharp-nosed fuselage through a large angle-of-attack range at zero angle of sideslip", N.A.C.A. technical note 2911

M.J. Lighthill (1963), "Attachment and Separation in Three-Dimensional Flow", in 'Laminar Boundary Layers', Ed. L. Rosenhead, Oxford University Press, 72-82

Liverpool Polytechnic, Department of Maritime Studies (1976), 'Symposium on technical and economic feasibility of commercial sailing ships', proceedings

M.V. Lowson (1963), "The separated flows on slender wings in unsteady motion", A.R.C. R&M 3448

R.L. Maltby and R.F.A. Keating (1962), "The surface oil flow technique for use in low speed wind tunnels", AGARDOgraph no. 70, 29-38

C.A. Marchaj (1979), 'Aero-Hydrodynamics of Sailing', Adlard Coles Ltd.

E.C. Maskell (1955), "Flow Separation in Three Dimensions", Royal Aircraft Establishment, Aeronautics report 2565

E.C. Maskell (1960), "Similarity laws governing the initial growth of leading edge vortex sheets in conical flow past sharp-edged slender bodies", Tenth International Congress of Applied Mechanics, Stresa, proceedings

A.S. Miles (1973), "Reviving the commercial sailing ship", privately circulated paper

J.H. Milgram (1968), "The analytic design of yacht sails", Society of Naval Architects and Marine Engineers, transactions, 76, 118-160

J.H. Milgram (1971), "Section data for thin, highly cambered airfoils in incompressible flow", N.A.S.A. CR-1767

J.H. Milgram (1972), "Sailing vessels and sails", Annual Review of Fluid Mechanics, 4, 397-430

A. Millward (1961), "The aerodynamics of sails", Journal of the Royal Aeronautical Society, 66, 760-764

D.I. Moor, M.N. Parker and R.N.M. Pattullo (1961), "The B.S.R.A. Methodical Series - An overall presentation", Royal Institution of Naval Architects, transactions, 103, 329-415

H.F. Morin Scott (1980), A full scale experiment in commercial auxiliary sail, at Royal Institution of Naval Architects (1980), paper 14

J. Morwood (1953), 'Sailing aerodynamics', privately published

C. Mudie (1977a), "Reducing the running costs at sea", at Royal Institute of Navigation (1977), paper 2

C. Mudie (1977b), "Some reflections on the optimal use of wind power", at Royal Institute of Navigation (1977), paper 8

C. Mudie (1980), "Some aspects of commercial sail", Journal of Navigation, 33, 56-63

M.M. Munk (1924), "The aerodynamic forces on airship hulls", N.A.C.A. report 184

H.A. Myers (1975), "Theory of sailing applied to ocean racing yachts", Marine Technology, 12, 223-241

C.T. Nance (1976a), "Can sailers make a come-back?", Sea Breezes, 296-301

C.T. Nance (1976b), "Outlook for the Dynaship", Sea Breezes, 478-483

C.T. Nance (1976c), "A triad of schooners", Sea Breezes, 635-637

C.T. Nance (1978a), "Proving race plan", Sea Breezes, 326-329

C.T. Nance (1978b), "Ideas from Australia", Sea Breezes, 611-615

C.T. Nance (1979), "The role of the engineer in the windship revolution", at Department of Industry (1979), paper 2

C.T. Nance (1980), "Wind power for ships - a general survey", at Royal Institution of Naval Architects (1980), paper 1

B.G. Newman (1981), "The aerodynamics of flexible membranes", Eighth Canadian Congress of Applied Mechanics, proceedings, Moncton, 63-78

J.N. Nielsen (1963), "Theory of flexible aerodynamic surfaces", Journal of Applied Mechanics, 30, 435-442

NKK (1979), "Sail equipped motor ship - Interim summary", Nippon Kokan technical bulletin

R. North (1979), "Will tall ships return?", Observer Magazine, 10 June, 67-69

S. Okada and T. Tsuda (1966), "On some results of form factor measurements obtained in wind tunnel tests", Eleventh International Towing Tank Conference, proceedings, 66-68

A.I. Ormsbee and A.W. Chen (1972), "Multiple element airfoils optimised for maximum lift coefficient", A.I.A.A. Journal, 10, 1620-1624

J. Otto-Scherer (1974), "Aerodynamics of high performance wing sails", Marine Technology, 11, 270-276

D.J. Peake, F.K. Owen and H. Higuchi (1978), "Symmetrical and Asymmetrical Separations about a Yawed Cone", A.G.A.R.D. conference proceedings, 247, paper 16

D.J. Peake, W.J. Rainbird and E.G. Atraghji (1972), "Three-dimensional flow separations on aircraft and missiles", A.I.A.A. Journal, 10, 567-580

D. Pike (1980), "Magnus-effect rudder", Ship & Boat International, 33, no. 10, 39

D. Pike (1982), "A sail assisted cargo vessel", Ship & Boat International, 35, no. 10, 24

A. Pope and J.J. Harper (1966), 'Low Speed Wing Tunnel Testing', John Wiley and Son, New York

H. Portnoy and S.C. Russel (1971), "The effect of conical thickness distributions on the separated flow past slender delta wings", A.R.C. C.P. 1189

L. Prandtl and O.G. Tietjens (1934), 'Applied hydro- and aero- mechanics', McGraw-Hill

P.D. Priebe (1981), "The evolution of commercial sailing ship technology", Eleventh A.I.A.A. symposium on the aero/hydronautics of sailing, proceedings, 19-42

W. Prolss (1967), "Zur Frage der Wirtschaftlichkeit von windangetriebenen Handelschiffen", Jahrbuch der Schiffbautechnischen Gesellschaft, 61, 36-54

R.C.T. Rainey (1979), "The AWASH (Atkins Wind Assisted Ship) computer program", information leaflet, Atkins R. and D.

R.C.T. Rainey (1980), "The wind turbine ship", at Royal Institution of Naval Architects (1980), paper 8

D.G. Randall (1966), "Oscillating slender wings with leading-edge separation", Aeronautics Quarterly, 17, 311-333

H.G. Rhoden (1956), "Effects of Reynolds number on the flow of air through a cascade of compressor blades", A.R.C. R&M 2919

Royal Institution of Naval Architects (1975), 'The future of commercial sail', symposium proceedings

Royal Institution of Naval Architects (1980), 'Symposium on wind propulsion of commercial ships', proceedings

Royal Institute of Navigation (1977), 'The practicability of commercial sail', symposium proceedings, Journal of Navigation, 30, 163-206

T. Rocca (1980), "Now what are the Japanese up to? Launching sail ships", Sunday Times Magazine, 28 Sep., 34-42

M. Roy (1952), "Caractères de l'écoulement autour d'une aile en flèche accentuée", Comptes rendus Académie des Sciences, Paris, 234, 2501-2504

Scantling (1978a), "Tonga sail schemes", Ship & Boat International, 31, no. 6, 3

Scantling (1978b), "Vegetables or wind?", Ship & Boat International 31, no. 6, 3

Scantling (1979), "Sailing tugs?", Ship & Boat International, 32, no. 7, 3

Scantling (1982a), "Selling sail", Ship & Boat International, 35, no. 9, 3-4

Scantling (1982b), "Lucander on sail", Ship & Boat International, 35, no. 12, 3

G.W. Schaefer and K. Allsop (1980), "Kite sails for wind-assisted ship propulsion", at Royal Institution of Naval Architects (1980), paper 9

P. Schenzle (1976), "Comparative sailing speed in wind propulsion", at Liverpool Polytechnic (1976), 67-102

N. Scholz (1965), "Aerodynamics of cascades", AGARDOgraph no. 220

S.D. Sharma and G.E. Bellows (1976), "Experiments on the wavemaking of a drifting ship", International seminar on wave resistance, Japan, 369-372

A.M.O. Smith (1972), "Aerodynamics of high-lift aerofoil systems", A.G.A.R.D. Conference proceedings, 102, paper 10

J.H.B. Smith (1957), "A theory of the separated flow from the curved leading edge of a slender wing", A.R.C. R&M 3116

J.H.B. Smith (1974), "The isolated-vortex model of leading-edge separation revised for small incidence", R.A.E. technical report 73160

J.H.B. Smith (1980), "Vortical flows and their computation", R.A.E. technical memo. AERO 1866

L.W. Smitt and M.S. Chislett (1974), "Large amplitude P.M.M. tests and manoeuvring predictions for a Mariner class vessel", Tenth Naval Hydrodynamics Symposium, proceedings, Cambridge USA, 131-151

W.H. Smyth (1897), "The sailor's word-book: an alphabetical digest of nautical terms", Blackie and Son

N.E. Sorensen-Viale (1981), "A 35,000 ton motor and sailing bulk carrier", Eleventh A.I.A.A. symposium on the aero/hydronautics of sailing, proceedings, 43-71

P.G. Spens (1964), discussion of Herreshoff (1964)

L.C. Squire (1962), "The motion of a thin oil sheet under the boundary layer on a body", AGARDograph no. 70, 7-28

L.C. Squire (1966), "Camber effects on the non-linear lift of slender wings with sharp leading edges", A.R.C. C.P. 924

T.M. Stoeckert (1968), "Sailboat wings through water", Product Engineering, 39, no. 15, 8

D.J.K. Stuart (1955), "Analysis of Reynolds number effect in fluid flow through two-dimensional cascades", A.R.C. R&M 2920

T. Tagori (1966), "Investigations on vortices generated at the bilge", Eleventh International Towing Tank Conference, proceedings, 54-57

T. Tanner (1962), "A survey of yacht research at Southampton University", Journal of the Royal Aeronautical Society, 66, 642-648

T. Tanner (1963), discussion of Crago (1963)

L.G. Taylor and F.H. Trim (1948), "The principle of ship stability", Brown, Son and Ferguson

H. Thieme (1955), "Mechanik des Segelantriebes", Jahrbuch der Schiffbautechnischen Gesellschaft, 49, 305-351

G.R. Thomson and B.S. Bowden (1977), "The B.S.R.A. Methodical Series - An overall presentation: variation in parallel middle body", Royal Institution of Naval Architects, transactions, 119, 203-212

B. Thwaites (1960), 'Incompressible aerodynamics', Oxford

B. Thwaites (1961), "The aerodynamic theory of sails: I. two-dimensional sails", Royal Society, proceedings, A261, 402-422

W. Tidy (1983), "Grimbledon Down", New Scientist, 97, 93

B.E. Tinling and C.Q. Allen (1962), "An investigation of the normal-force and vortex-wake characteristics of an ogive-cylinder body at subsonic speeds", N.A.S.A. technical note D-1297

F.H. Todd (1957), "Skin friction and turbulence stimulation; formal discussion", Eighth International Towing Tank Conference, proceedings, 88-99

V.N. Treshchevsky and A.I. Korotkin (1976), "Some characteristics of flow around ships at different drift angles in shallow water", The Eleventh Symposium on Naval Hydrodynamics, proceedings, Office of Naval Research and University College London, 693-713

E.O. Tuck and M. Hazelgrove (1972), "An extension of two-dimensional sail theory", Journal of Ship Research, 16, 148-152

T. Von Kármán (1936), discussion of Davidson (1936)

B. Wagner (1966), "Windkanalversuche mit gewölbten Plattensegeln bei Mehrmastanordnung", Institut für Schiffbau der Universität Hamburg, report 171

B. Wagner (1967a), "Fahrtgeschwindigkeitsberechnung für Segelschiffe", Jahrbuch der Schiffbautechnischen Gesellschaft, 61, 14-35

B. Wagner (1967b), "Windkanalversuche für einen sechsmastigen Segler nach Prölss", Schiff und Hafen, 19, 165-172

B. Wagner (1967c), "Windkanalversuche mit dem Takelagemodell einer Viermastbark", Schiff und Hafen, 19, 13-20

B. Wagner (1976), "Sailing ship research at the Hamburg University", at Liverpool Polytechnic (1976), 21-57

E.P. Warner and S. Ober (1925), "The aerodynamics of yacht sails", Society of Naval Architects and Marine Engineers, transactions, 33, 207-232

R.A. Wallis (1946), "Wind tunnel tests on a series of circular arc plate aerofoils", (Australian) Council for Scientific and Industrial Research, Aerodynamics, Note 74

P.R. Warner and W.J. Hood (1975), "A commercial sailing ship for the South West Pacific Ocean", at R.I.N.A. (1975), paper 3

T. Watanabe, Y. Endo, K. Nakanishi and K. Takeda (1982), "Sail-equipped motor ship 'Shin Aitoku Maru' and studies on larger ship", Twelfth A.I.A.A. symposium on the aero-hydronautics of sailing, proceedings, 238-249

F.E. Weick and M.J. Bamber (1932), "Wind tunnel tests of a Clark Y wing with a narrow auxiliary airfoil in different positions", N.A.C.A. report 428

F.E. Weick and J.A. Shortal (1932), "The effect of multiple fixed slots and a trailing-edge flap on the lift and drag of a Clark Y aerofoil", N.A.C.A. report 427

J. Wellicome (1975), "A broad appraisal of the economic and technical requisites for a wind driven merchant vessel", at Royal Institution of Naval Architects (1975), paper 5

K. Wieghardt (1972), "Zum Windprofil über See", Schiffstechnik, 19, 22

A.K. Wiersma (1979), "Note on the interaction of two overlapping rigid sails, Part I: two-dimensional sails", International Shipbuilding Progress, 26, no. 293, 9-20

D.H. Wilkinson (1968), "A numerical solution of the analysis and design problems for the flow past one or more aerofoils or cascades", A.R.C. R&M 3545

R.M. Willoughby (1979), "The Windrose ship - why square rig?", at Department of Industry (1979), paper 6

R.M. Willoughby and E.C.B. Corlett (1980), "Design problems of a commercial sailing ship", at Royal Institution of Naval Architects (1980), paper 16

Windrose Ships Limited (1978), brochure

D.A. Wise and J.W. English (1975), "Tank and wind tunnel tests for a drill-ship with dynamic position control", Offshore Technology Conference, proceedings, paper O.T.C. 2345

J.B. Woodward, R.F. Beck, R. Scher and C.M. Cary (1975), "Feasibility of sailing ships for the American merchant marine", University of Michigan Department of Naval Architecture and Marine Engineering report 168

J.B. Wynne (1975), "Sails for the auxiliary propulsion of a V.L.C.C. trading on the Northern Europe - Persian Gulf route", at Royal Institution of Naval Architects (1975), 47-56

J.B. Wynne (1979), "Possibilities for higher speeds under sail", North East Coast Institution of Engineers and Shipbuilders, transactions, 96, no. 1, 45-60

J.B. Wynne (1981), discussion of H.H. Pearcey (1981), "Hydrodynamics and aerodynamics - cross fertilisation in research and design", presented at a joint meeting of Royal Aeronautical Society and Royal Institution of Naval Architects.

A3 : APPENDIX TO CHAPTER 3

A3.1(a) Interpretation - of flow visualisation data

The interpretation of oil-flow patterns is discussed in section 3.3(d). Two examples are now considered.

Mariner at 10°. Figure A3.2 and figure 3.16 show the surface flow pattern on the Mariner hull at 10° incidence. Figure A3.1 indicates the lines of attachment and separation where they can be clearly deduced from the surface pattern. Near the bows a leading bilge separation line and a reattachment line can be easily detected. At about 1/5 length from the bow the flow pattern changes considerably; interpretation of the surface flow pattern is difficult here, although other flow visualisation techniques indicate a region of diffuse weak vortices across the body. There is a clear separation line along the trailing middle body and run bilge.

Block Mariner at 10°. Figure A3.5 is a photograph showing the surface flow pattern on the block Mariner at 10° incidence. Lines of attachment and separation are indicated in figure A3.4. Figures 3.22 to 3.25 show the surface patterns at a range of angles of incidence. There is a consistent difference in the complexity of leading and trailing bilge separation patterns. Figure A3.6 is a schematic interpretation of the flow near the leading and trailing bilges. Near the leading bilge the surface flow pattern always indicates secondary separation and sometimes, perhaps, tertiary separation. The details of the more complicated separation patterns can not be discerned with

certainty from these oil flow patterns. Near the trailing bilge the surface flow pattern always indicates a single separation line and a single attachment line.

A3.1(b) Interpretation - of wake survey data

The technique for conducting the wake surveys is discussed in section 3.3(b). The position of the survey plane relative to the hull is indicated in figure 3.12.

Cross-flow velocity vectors. The information most directly available from the wake survey is the cross flow velocity field. Figures A3.3 and A3.7 include maps of the cross flow velocity vectors which are simply determined from the inclination of the aligned probe. These cross flow vectors give a general idea of the wake flow. More detail becomes apparent when vorticity contours are plotted.

Vorticity contours. Figures A3.3 and A3.7 also include maps of vorticity contours. The vorticity is calculated by differentiation of quartic-fits to the velocity profile through sets of five co-linear survey points. For most of the plane the quartic-fit is determined using information from both sides of any given point, and hence differentials of the quartic representation of the velocity profile provide a good approximation to the true velocity derivatives. At the edge of the survey plane all information for the quartic fit is obtained from one side of an edge point and hence differentials of the quartic can take quite different values to the true velocity derivatives. In consequence, good estimates of vorticity can be obtained away from survey-plane edges, but spurious regions of vorticity are sometimes indicated at these edges.

The vortex contours give a clear graphical indication of the wake characteristics. Figure A3.3 shows the results

of the wake survey conducted behind a Mariner type hull at 10° leeway. The dominant trailing run bilge can be identified as the region of approximately circular vorticity contours, corresponding in position to the centre of rotation apparent in the cross-flow vector map. The leading entrance vortex can be identified as the region of vorticity extending along the z axis from the dominant vortex. The weak leading bilge vortex has been swept round the dominant vortex and can be identified as the positive vorticity contour adjacent to the dominant vortex.

Figure A3.7 consists of a vorticity plot and a cross flow velocity component map for the block Mariner at 10°. These are basically similar to the corresponding figures for the Mariner hull; the main difference is that the leading entrance bilge vortex has not been swept so close to the waterplane (the z axis) by the dominant trailing run bilge; the vortices and cross flow velocity components are also stronger.

Vortex strengths. Smith (1980) gives two equivalent expressions for the vortex strengths:

$$\Gamma = \oint_C \underline{V} \cdot \underline{d\sigma}$$

where $\underline{V}$ is the velocity and $\underline{d\sigma}$ is an element of arc along a closed curve C enclosing the vortex, and

$$\Gamma = \int \underline{\omega} \cdot \underline{dS}$$

where $\underline{\omega}$ is the vorticity and the integration is over any surface spanning C and $\underline{dS}$ is an elemental areal vector on this surface.

It was initially decided to use the latter areal integration to determine estimates of vortex strengths from the wake survey data. A simple block integration is used to estimate total strengths and centroids of positive and negative vortices. Although positive and negative vorticity are integrated separately, no attempt is made to differentiate between vortices of the same sign because of the difficulties of determining a boundary between adjacent merged vortices. The estimated centroids and strengths are indicated on the vorticity plots; so that, for example, the total negative vortex strength (or "circulation") is indicated "*-0.980" in figure A3.3.

The total vortex strengths and centroid positions are only approximately determined for three reasons; firstly, spurious vorticity produced by mathematical curve fitting at the edge of the plane is included, secondly, real regions of weak vorticity may lie outside the survey plane, and thirdly, a simple and approximate numerical integration scheme is used. The first problem could have been avoided by using the more direct contour integration expression for the vortex strength. Accuracy could also have been improved if a more refined integration procedure had been used.

Figure A3.1 Mariner separation and attachment lines (10°)

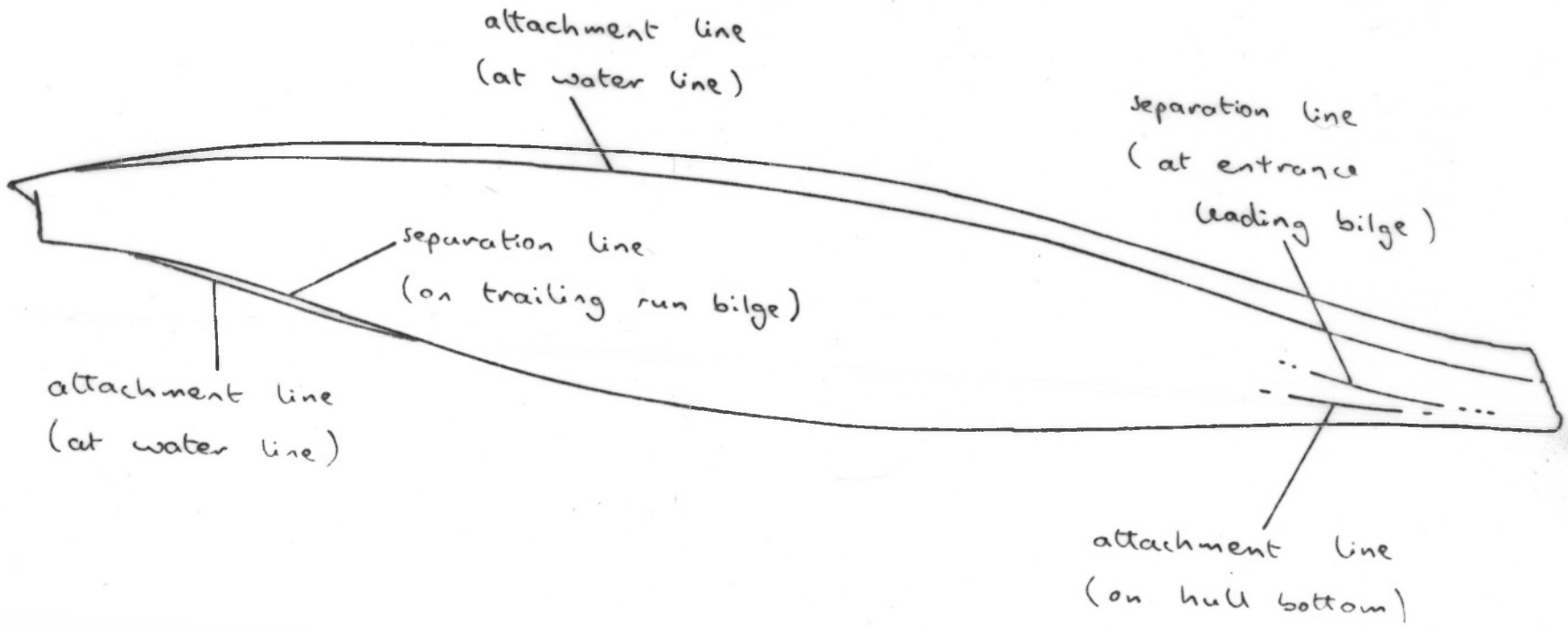

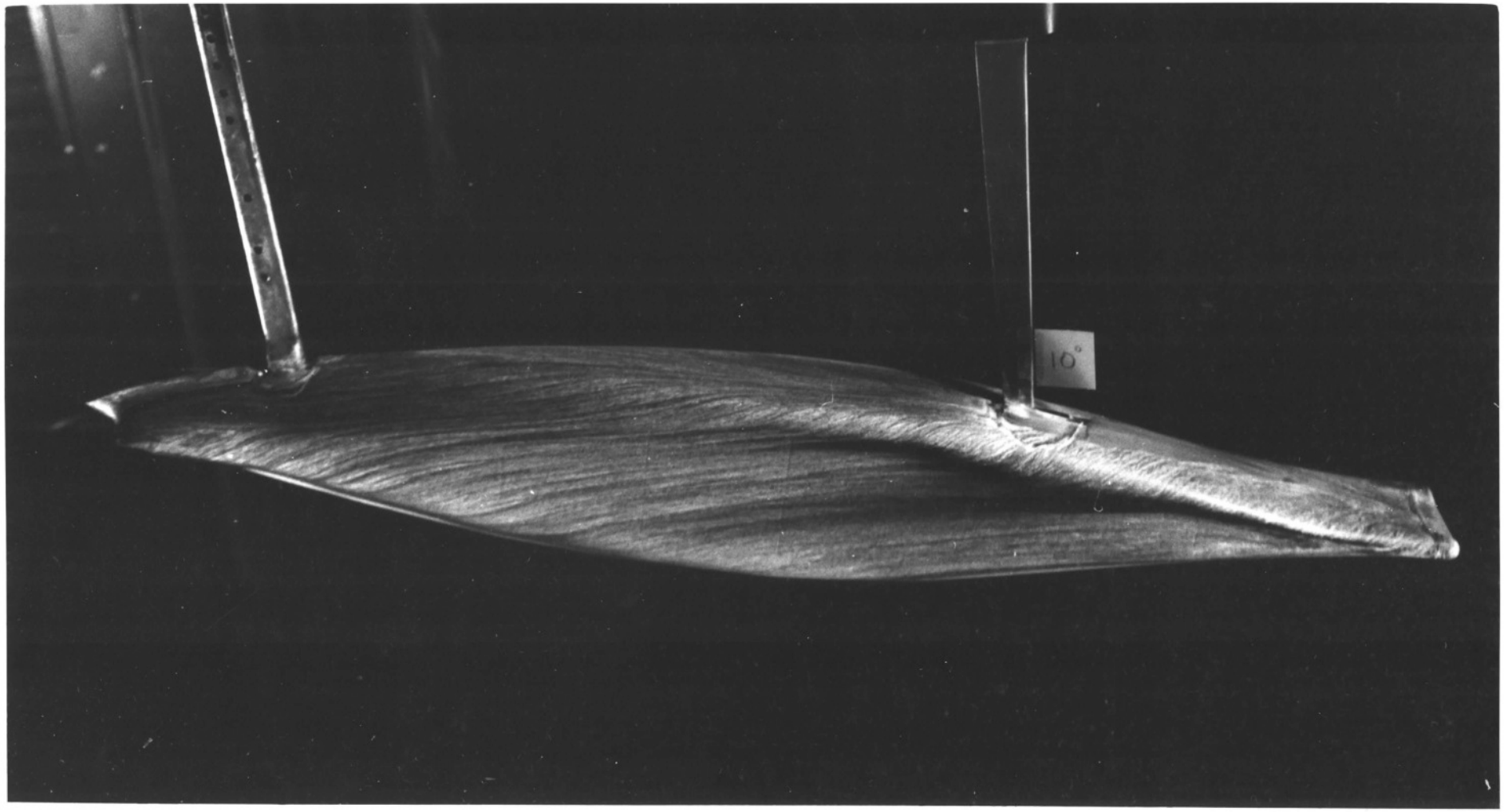

Oil flow pattern: Mariner type hull at 10° incidence.

Figure A3.2

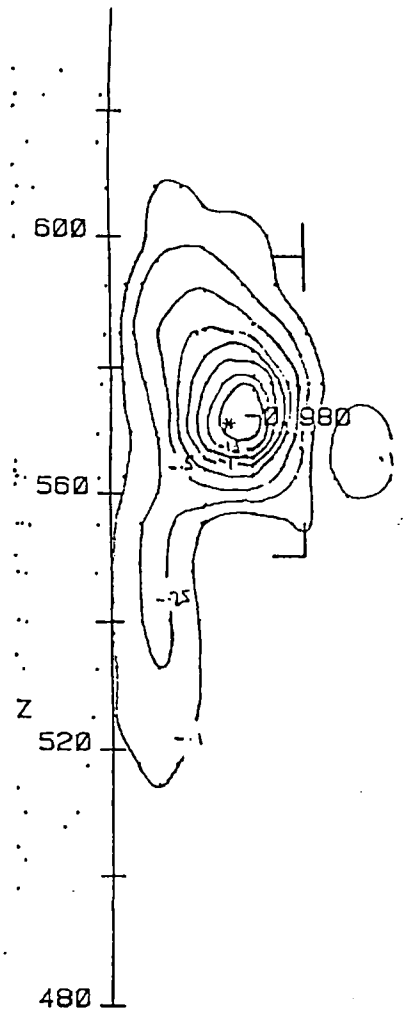

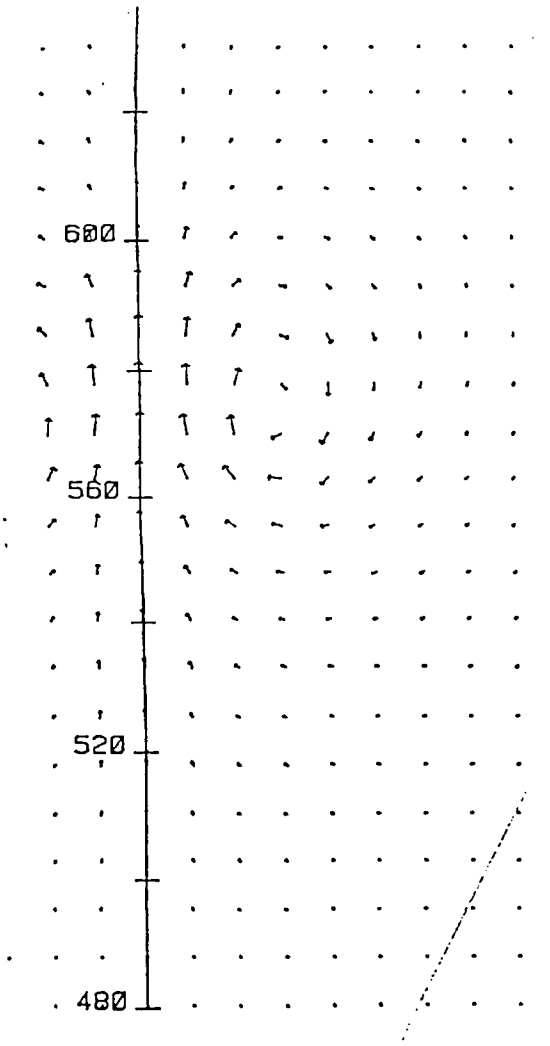

Figure A3.3

Flow behind Mariner

Mariner

leeway = 10.0

B/L = 0.146

D/L = 0.049

flow tripped

X/L = 0.164

Figure A3.4 Block Mariner separation and attachment lines (10°)

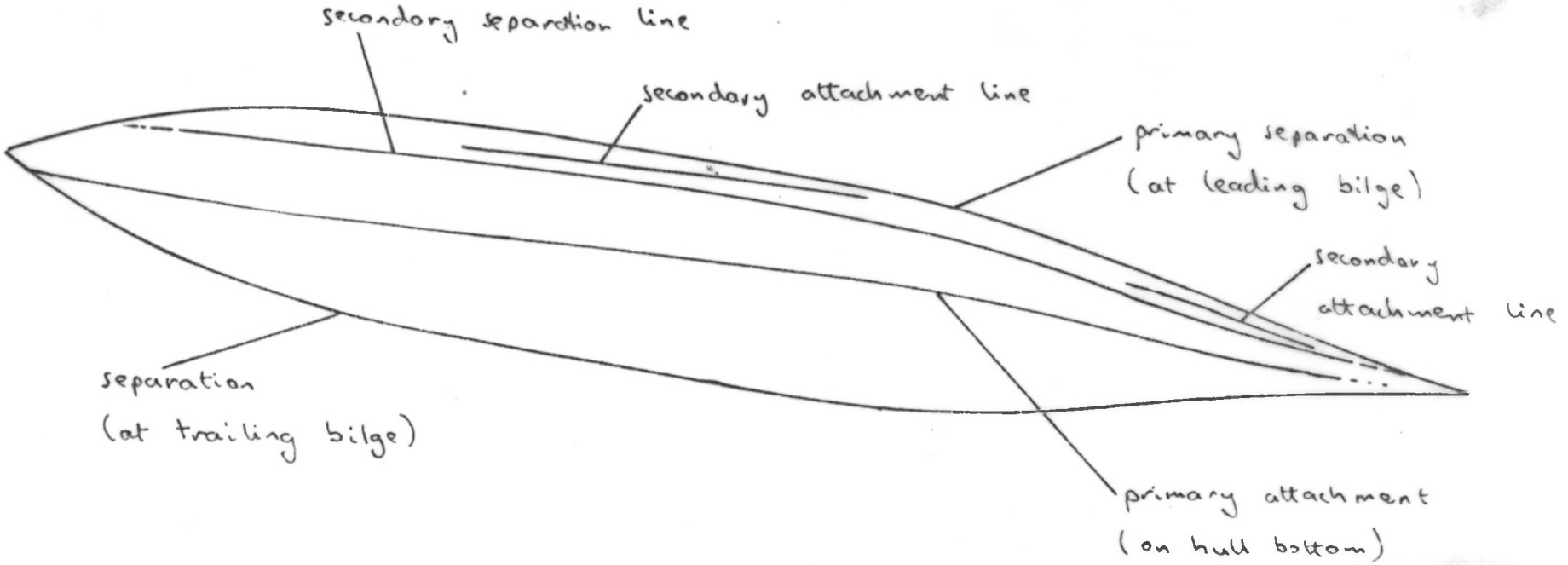

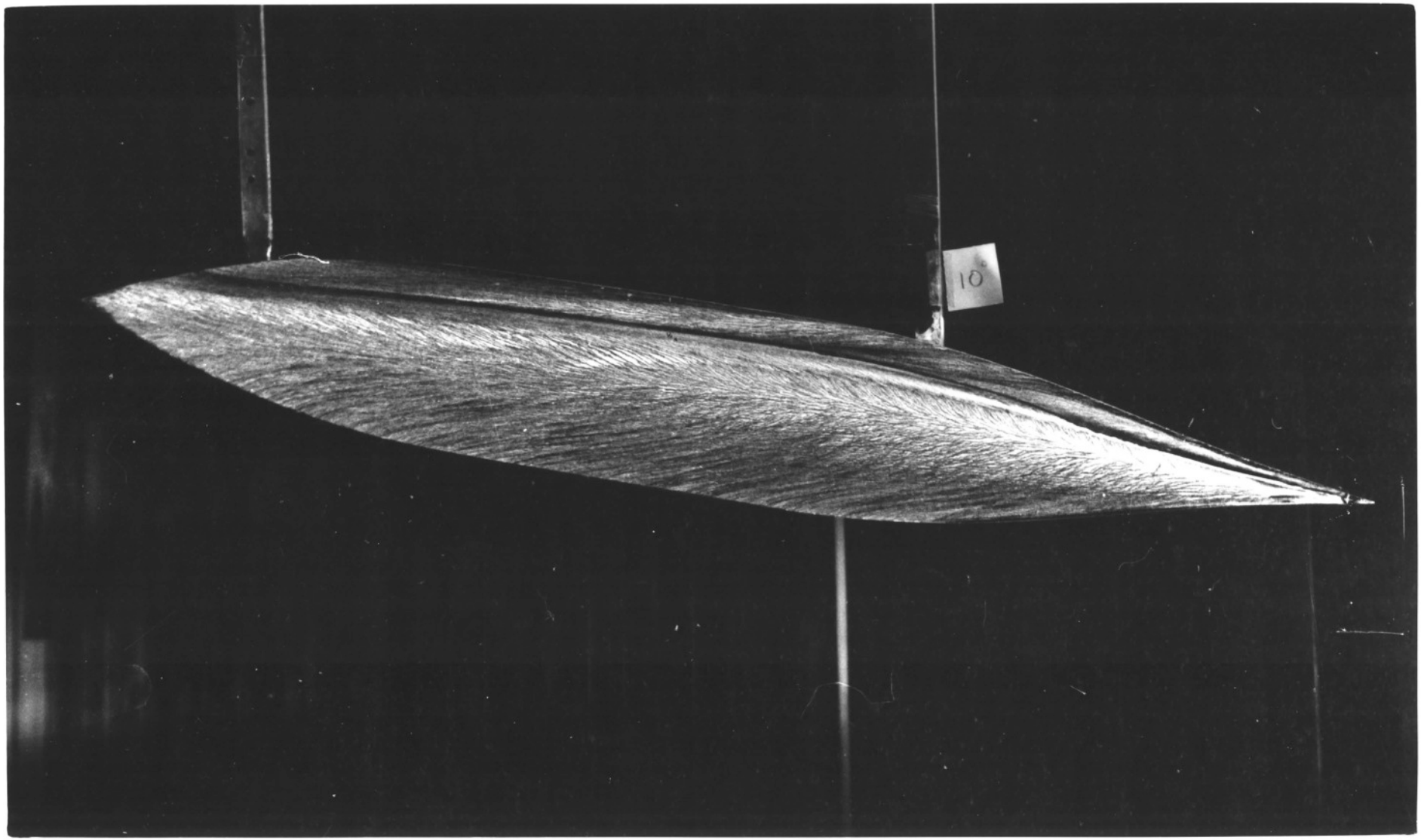

Oil flow pattern: hull-like block at 10° incidence.

Figure A3.5

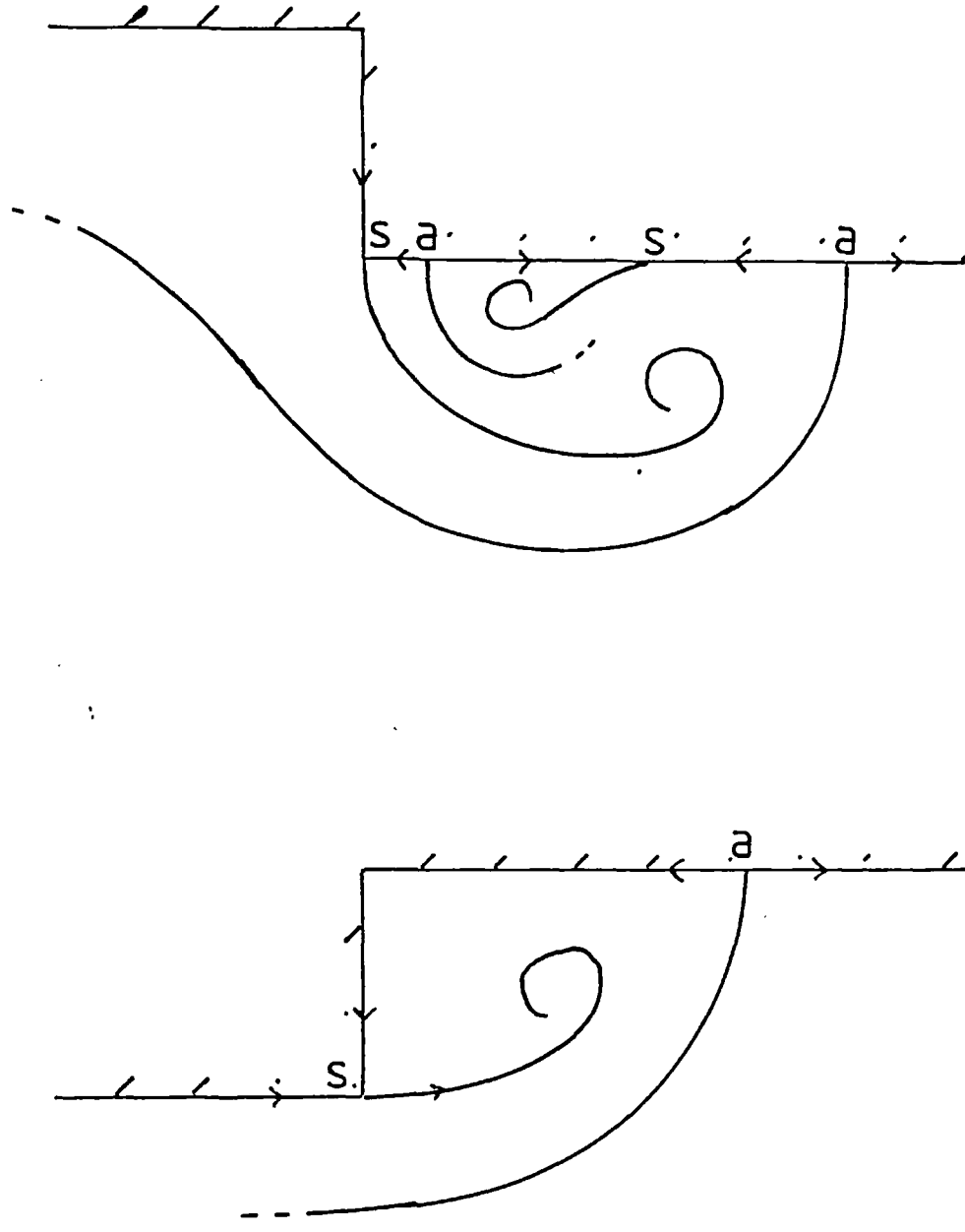

Figure A3.6

Schematic cross section through flow indicating separation and attachment lines and stream surfaces:
typical leading bilge pattern (top) and
typical trailing bilge pattern (bottom)

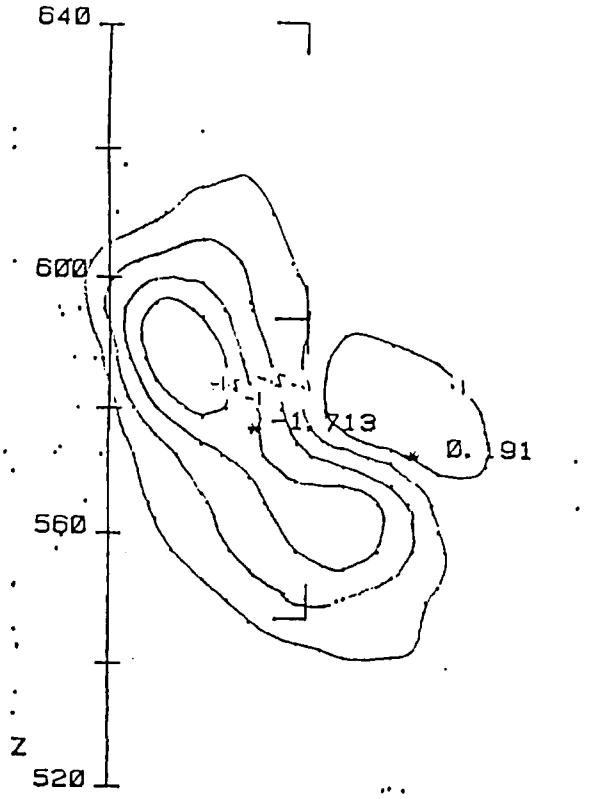

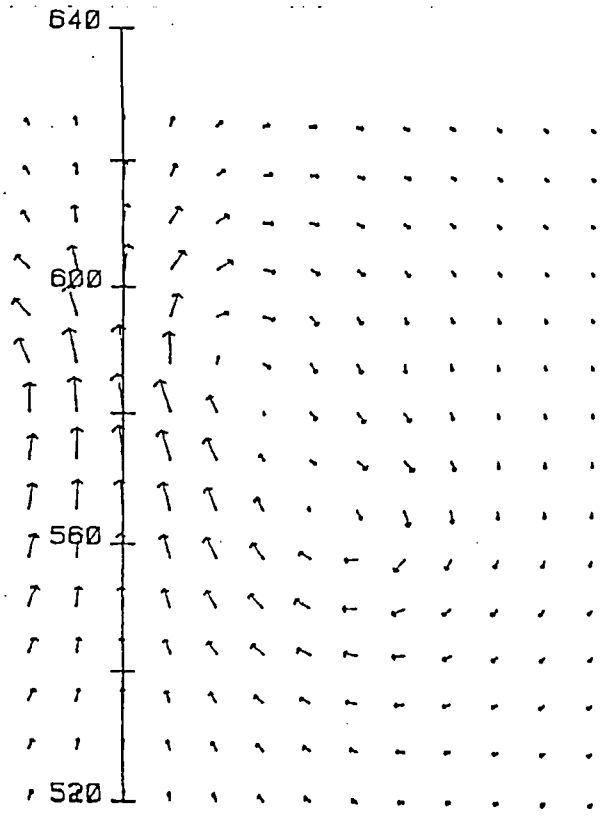

Block Mariner

leeway = 10.Ø

B/L = Ø.146

D/L = Ø.Ø5Ø

no tripwire

X/L = Ø.163

Figure A3.7

Flow behind Block Mariner

Vorticity contours and vortex strengths

A3.2 Comparative tests with and without a tripwire

The justification for artificially tripping the flow is discussed in sections 3.2(d) and 3.3(a). Tripping was expected to be important when separation is from surfaces with gentle streamwise curvature but unimportant when the separation is from a salient edge; this is because transition does not affect separation from salient edges, and these tend to trip subsequent flow. The tests described below indicate that the effects are minimal, even for the Mariner-type hull.

Mariner-type hull. The wool tuft and oil flow tests detect no changes in vortex or separation-line positions caused by the trip wire. It seems that major flow features are hardly affected by any region of laminar flow near the bow. Figure A3.8 shows the results of the wake surveys. Positions of vorticity contours are similar with and without a tripwire.

Figure A3.9 consists of the corresponding force curves. At low angles of incidence the effect of a tripwire is to increase the drag, while at larger angles its effect is negligible. This may imply that part of the untripped flow is laminar at low angles of incidence. The lift force and the position of the hydrodynamic centre of effort are almost unchanged by the tripwire.

Block Mariner hull. Figure A3.10 shows the oil flow patterns obtained with and without a tripwire near the bow. The most obvious difference is observed on the hull's side: when the flow is tripped, the surface flow is approximately along the ship; when it is not tripped, the surface flow appears to converge near the forward end of the middle body. There is an abrupt boundary between a region

largely cleared of French chalk and a downstream chalky region. This boundary appears to be associated with transition rather than separation or attachment; the wool tuft showed that the flow near the surface in this region was approximately parallel to the free stream, the stethoscope showed that the flow was laminar upstream of this boundary and turbulent downstream of it. The positions of all separation and attachment lines were unaffected by the tripwire. This model has sharp bilges so the position of separation lines are fixed at the bilges. Major features of the flow may be expected to be fairly well independent of Reynolds number or of tripping. The wool tuft, which can only be used to indicate the approximate positions of flow features, gives no indication of changes in vortex positions. Figure A3.11 shows the results of the wake survey. Positions of vorticity contours are similar with and without a tripwire.

Figure A3.12 compares the block Mariner forces with and without a tripwire. At low angles of incidence the effect of a tripwire is to increase the drag; at large angles its effect is negligible. This implies, as is confirmed by flow visualisation, that part of the untripped flow is laminar at low angles of incidence. The lift force and the position of the hydrodynamic centre of effort are almost unchanged by the tripwire.

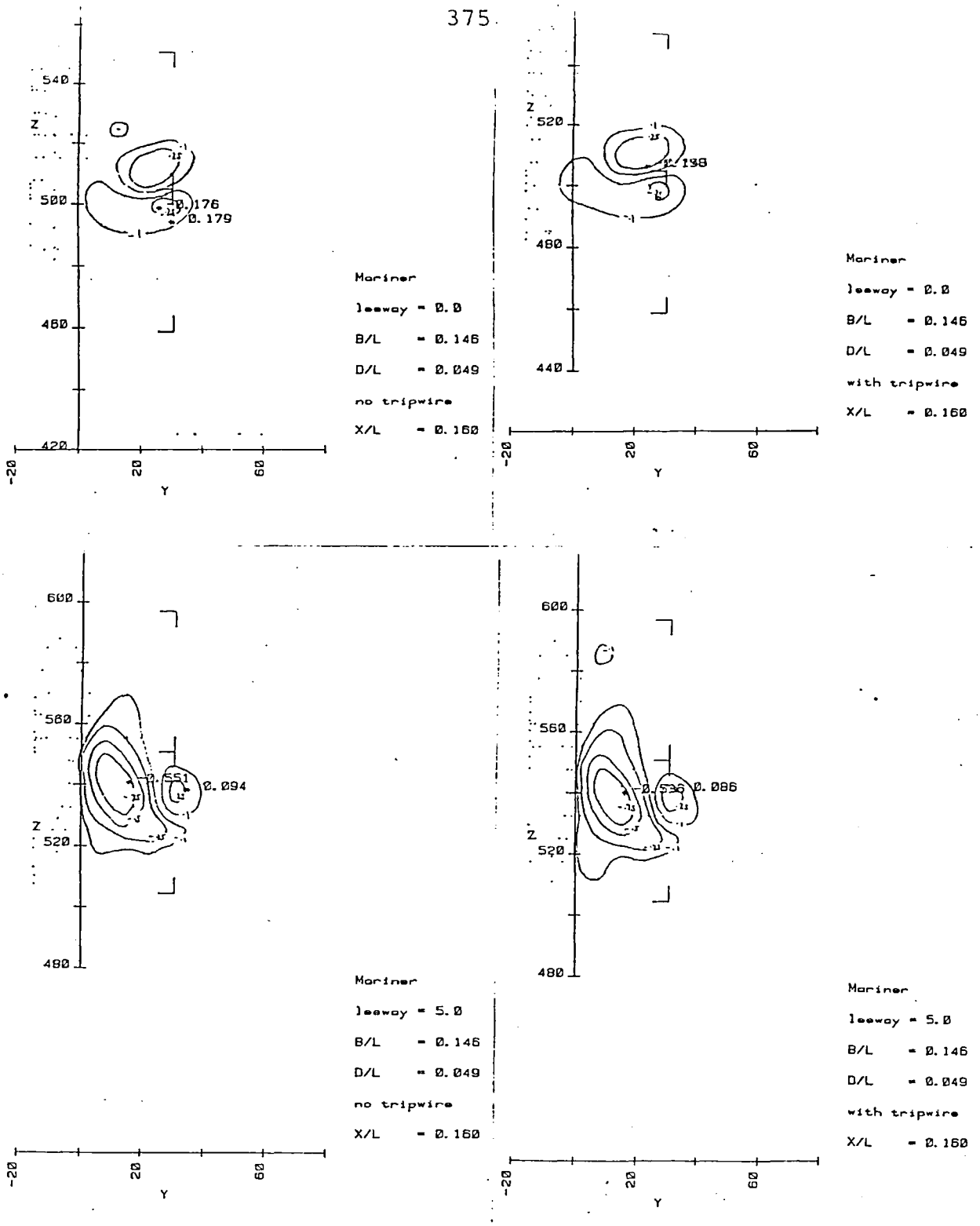

Figure A3.8

Vorticity plots: effect of trip-wire, Mariner type hull.

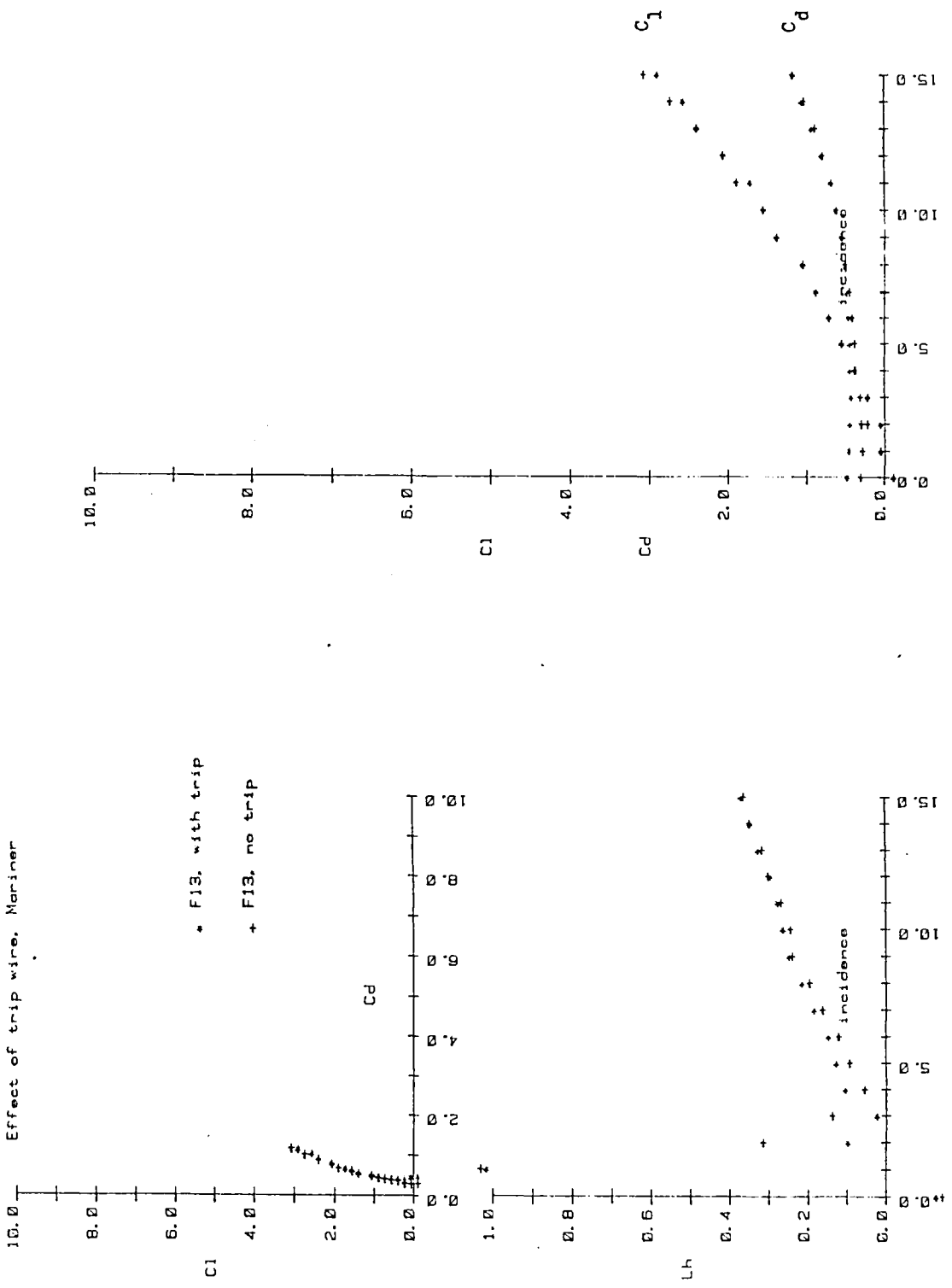

Figure A3.9

Effect of tripwire on forces: Mariner hull

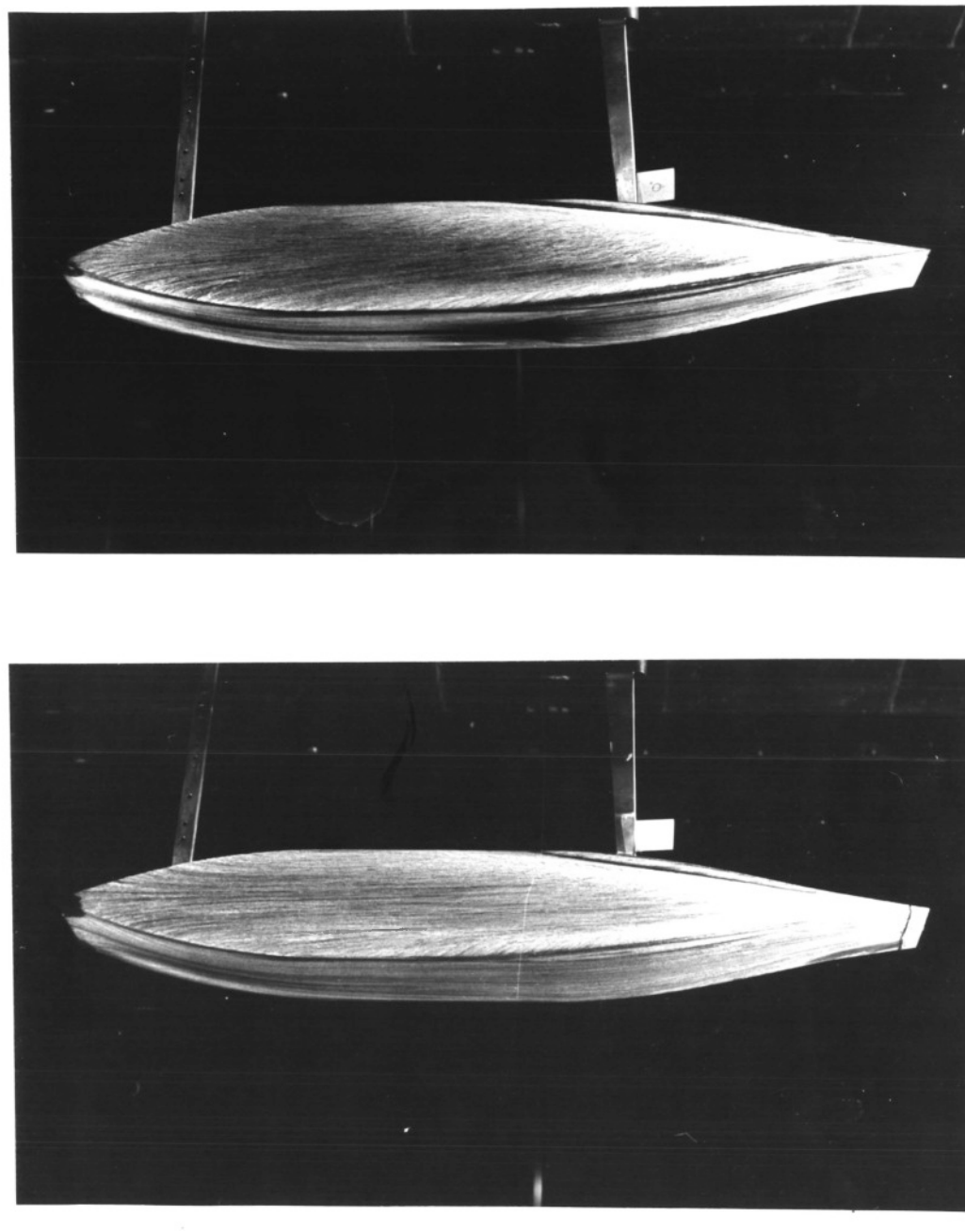

Figure A3.10

Effect of trip-wire: top - without, bottom - with.

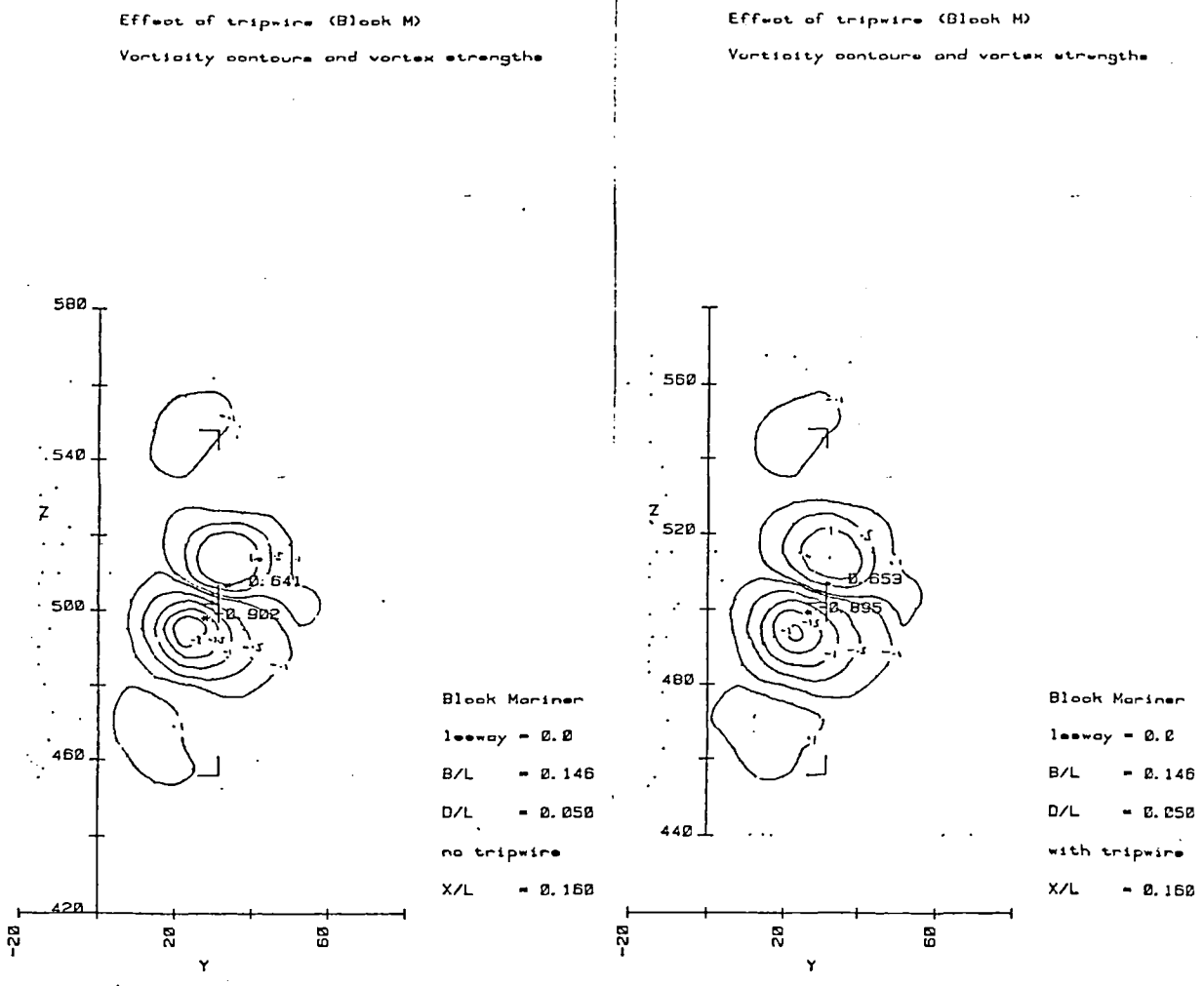

Figure A3.11

Vorticity plots: effect of tripwire, block Mariner.

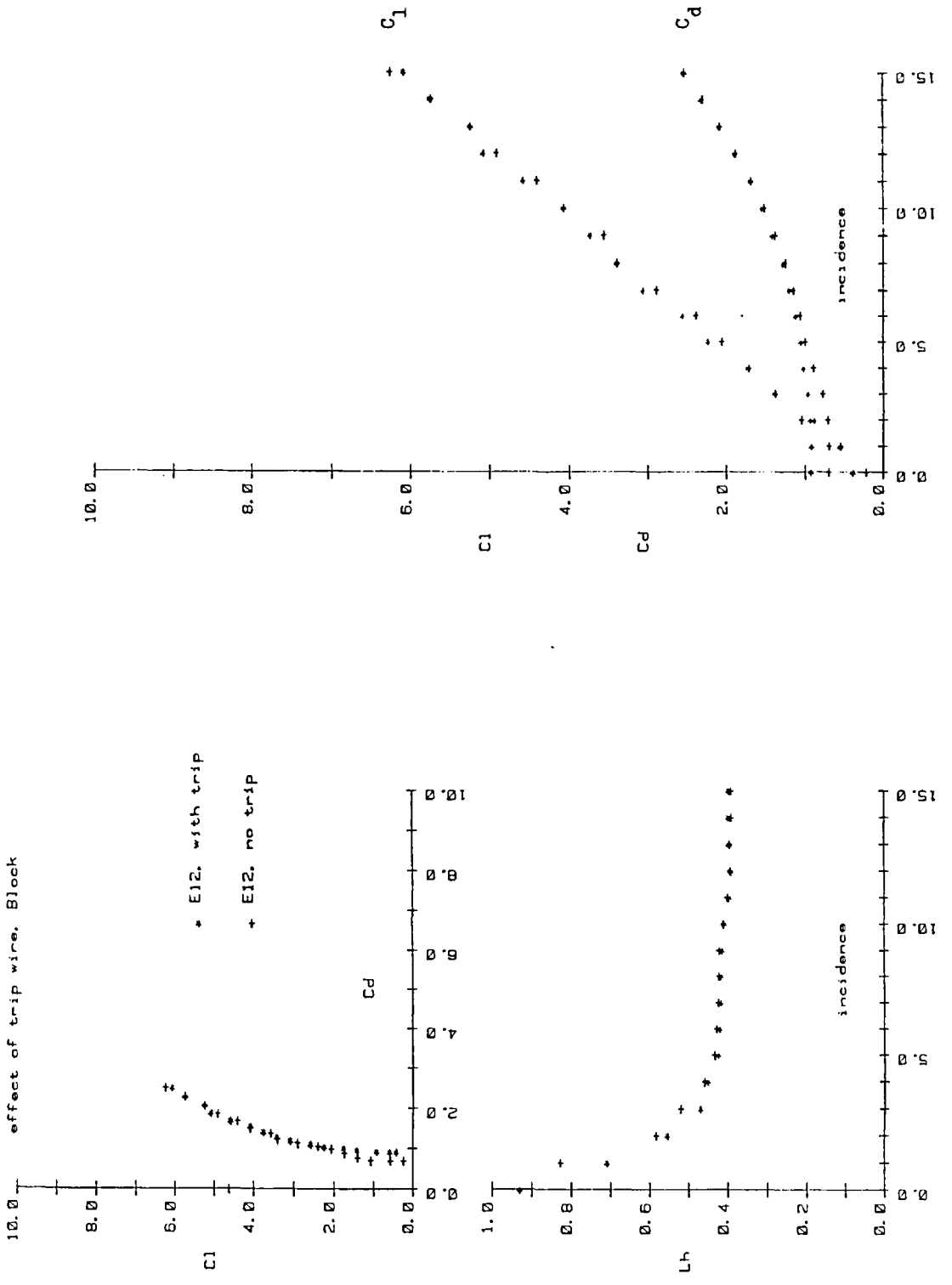

Figure A3.12

Effect of tripwire on forces: Block Mariner

A3.3 Flow waterplane symmetry tests

In these experiments using reflex hull models the plane of symmetry is used to model the sea surface. As noted before, this is only a valid modelling technique if the flow does remain symmetric about the reflex model's plane of symmetry.

Figure A3.13 shows the time averaged flow past a Mariner type hull at leeway. It can be seen that the flow is substantially symmetric. The slight asymmetries probably result from; imperfect alignment of the model and support, variations in the free stream tunnel flow direction and asymmetries of the model itself. A symmetric time averaged flow does not preclude the possibility of a periodically or randomly varying flow. However, wool tuft tests of this model, and all other models, showed that the flow features are approximately symmetric and fixed in position. Figure A3.14 shows wake surveys for a block model tested with and without a splitter plate. This splitter plate was about 30mm wide and was fitted, on the trailing side of the model, at the plane of symmetry. It can be seen that the wake cross flows are very similar with and without the splitter plate. If the flow was asymmetric and oscillating, it would be changed by the presence of a splitter plate. This therefore confirms that the flow remains approximately symmetric about the modelled waterplane.

Figure A3.15 compares force curves obtained with and without a splitter plate. Absence or presence of the plate seems to make little qualitative difference. Its presence causes a slight increase in the drag; this is

presumably the viscous drag on the plate, and perhaps additional drag due to small corner vortices forming at the junction of the plate and hull. Lift seems to have been slightly reduced; this could be the results of the negative circulation associated with the plate's drag (the splitter plate was only fitted to the trailing side, so its drag is likely to have slowed the flow over the trailing side). This, again, confirms the flow visualisation indications that the flow is approximately symmetric and fixed with respect to time.

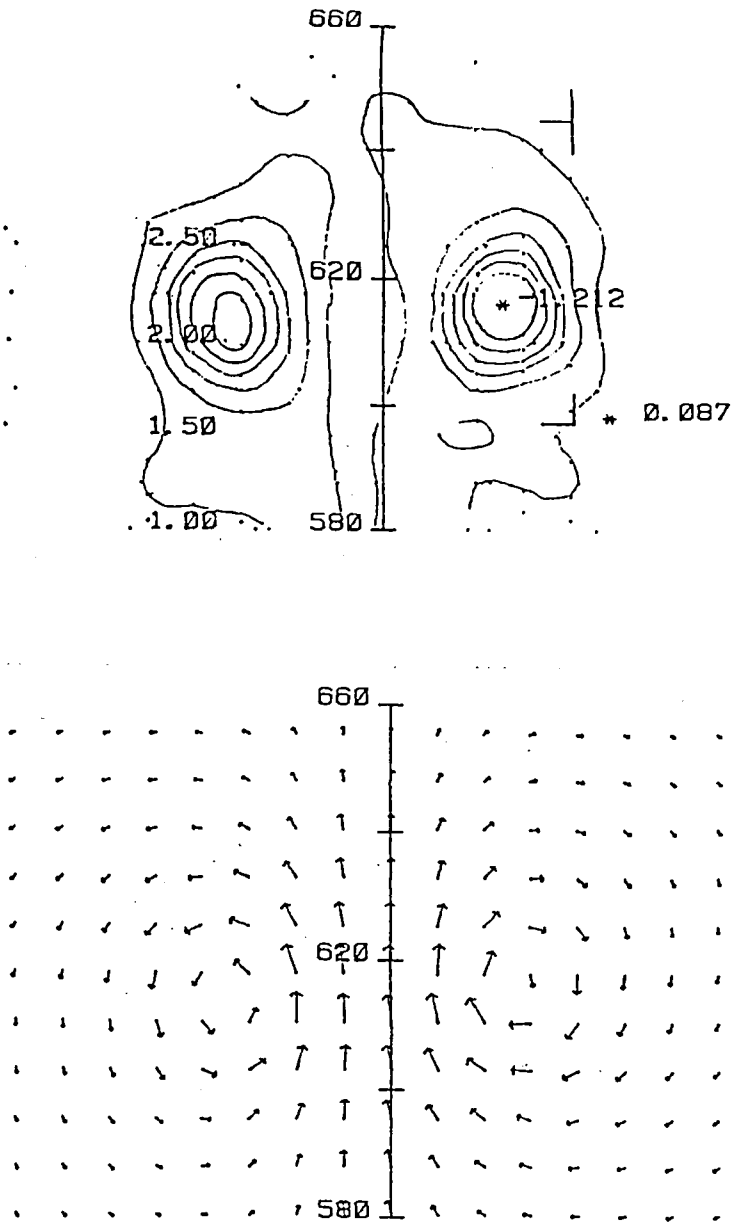

Figure A3.13

Symmetry test (Mariner hull)

Mariner

leeway = 15.0

B/L = 0.146

D/L = 0.049

flow tripped

X/L = 0.174

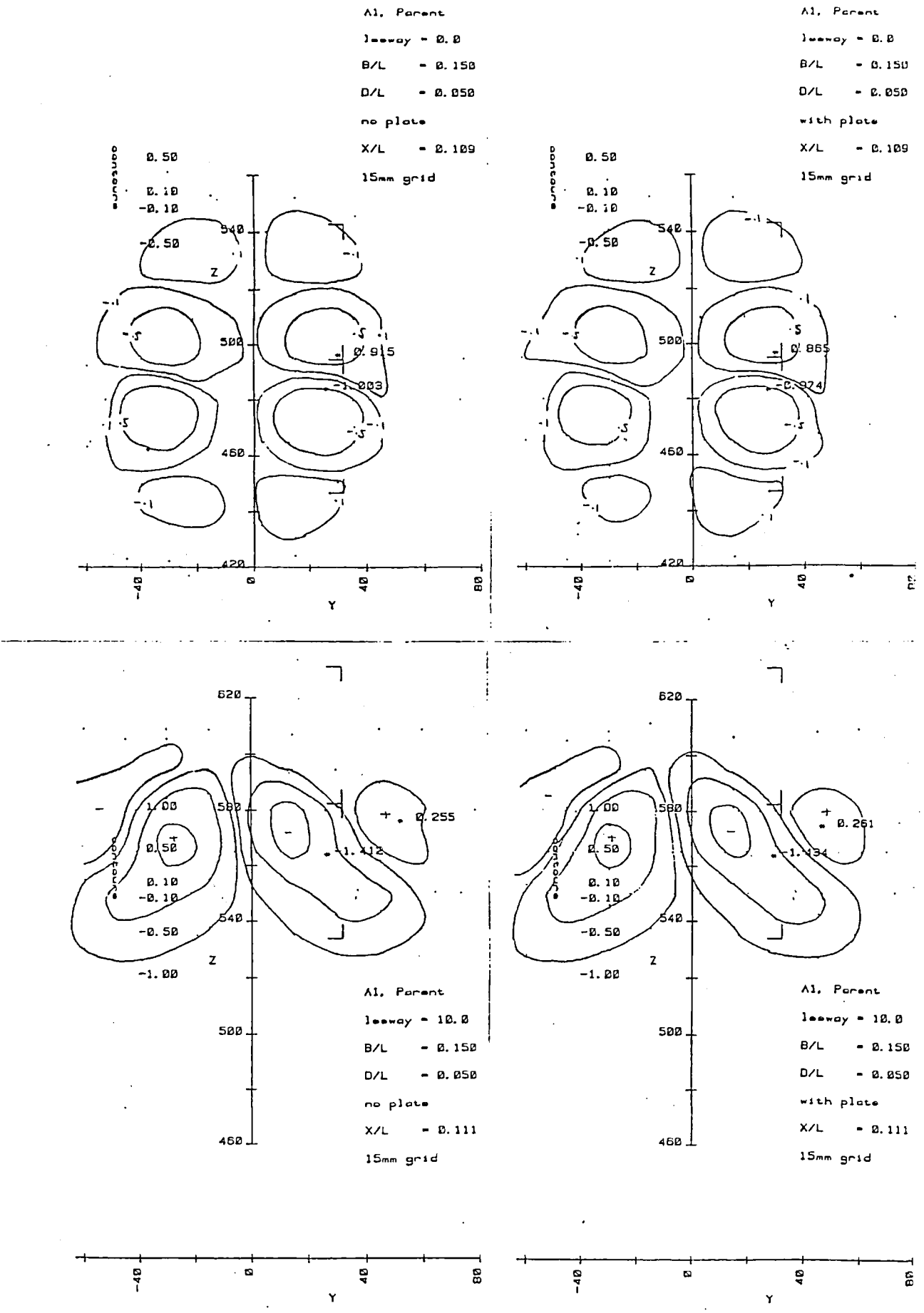

Figure A3.14

Vorticity plots: splitter plate test.

Without plate (left) and with plate (right).

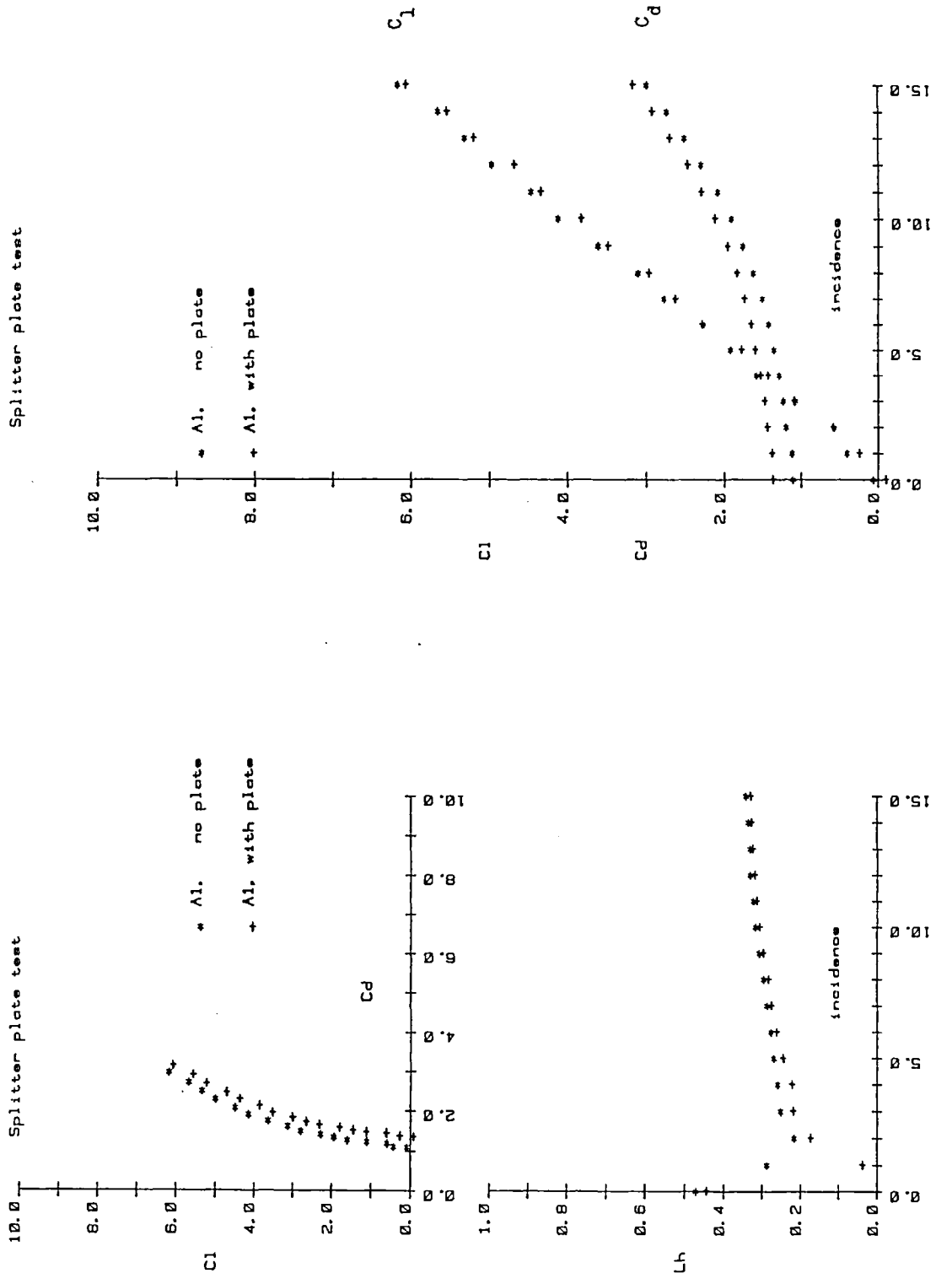

Figure A3.15

Forces: splitter plate test

A3.4 Traverse and probe array spacing test

Three wake surveys were made, behind a block model at leeway, to indicate the effect of array spacing on the vorticity contours obtained. These were made with grid spacings of 15mm, 7.5mm and 2.5mm. A large grid spacing will produce a plot which does not accurately show all details; features which lie wholly between grid points may be distorted or lost by the curve fitting used to determine vorticity. Reducing the grid spacing will improve the detail shown. However, spurious details will be indicated on the vorticity plots if the grid spacing is so small, that typical changes in flow direction, between neighbouring points, are of similar magnitude to the angular resolution of the probe. Surveys made with a very small array spacing also take a long time to conduct. Figure A3.16 shows these wake surveys. The 7.5mm grid produces a plot showing considerably more detail than the 15mm grid. The 2.5mm grid produces a plot which shows only slightly more detail than the 7.5mm grid. The 2.5mm grid is not so small that spurious resolution details are produced. Despite the slight superiority of surveys conducted with a 2.5mm grid, it was decided to generally use a 7.5mm grid. This required only 1/9 of the time to map the same area, and this allowed a much greater number of surveys to be undertaken.

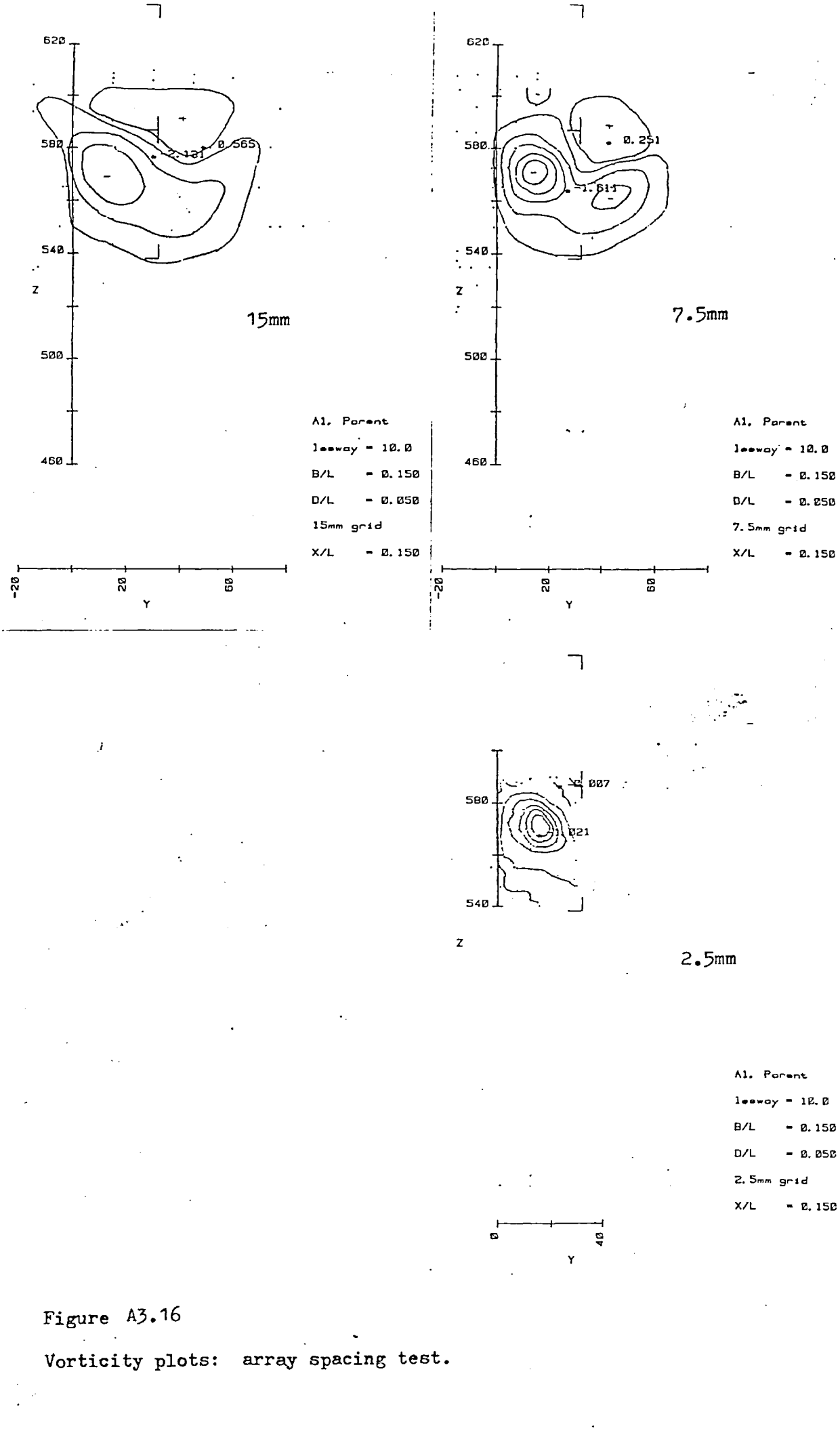

Figure A3.16

Vorticity plots: array spacing test.

A3.5 Tabulated results of the hull force tests

Table A3.1

A1, Parent model

Run	Vel	Incidence	Cl	Cd	Cm	Lh
1	21.88	0.00	-0.122	1.090	-0.016	-0.002
2	21.89	1.00	0.205	1.117	-0.045	0.396
3	21.88	2.00	0.534	1.154	-0.082	0.284
4	21.88	3.00	1.026	1.203	-0.119	0.271
5	21.88	4.00	1.353	1.235	-0.126	0.283
6	21.88	5.00	1.681	1.302	-0.172	0.266
7	21.88	6.00	2.174	1.368	-0.165	0.287
8	21.88	7.00	2.502	1.450	-0.175	0.291
9	21.87	8.00	2.995	1.534	-0.187	0.296
10	21.87	9.00	3.488	1.633	-0.178	0.307
11	21.86	10.00	3.982	1.782	-0.164	0.318
12	21.86	11.00	4.310	1.930	-0.161	0.323
13	21.86	12.00	4.804	2.112	-0.154	0.329
14	21.86	13.00	5.299	2.294	-0.127	0.339
15	21.86	14.00	5.629	2.492	-0.136	0.340
16	21.85	15.00	6.126	2.742	-0.141	0.343

Data recorded on file 3

A2, Shallow draft

Run	Vel	Incidence	Cl	Cd	Cm	Lh
1	21.79	0.00	0.043	0.801	0.007	1.453
2	21.80	1.00	0.208	0.798	-0.004	0.519
3	21.79	2.00	0.374	0.900	-0.043	0.341
4	21.79	3.00	0.705	0.916	-0.078	0.285
5	21.78	4.00	1.036	0.935	-0.087	0.292
6	21.78	5.00	1.201	0.968	-0.079	0.306
7	21.78	6.00	1.532	1.002	-0.088	0.308
8	21.78	7.00	1.698	1.035	-0.074	0.321
9	21.78	8.00	2.030	1.086	-0.087	0.319
10	21.78	9.00	2.360	1.151	-0.065	0.334
11	21.77	10.00	2.527	1.252	-0.040	0.348
12	21.77	11.00	2.859	1.352	-0.030	0.354
13	21.77	12.00	3.191	1.452	-0.035	0.354
14	21.76	13.00	3.523	1.602	-0.057	0.349
15	21.76	14.00	3.855	1.735	-0.059	0.351
16	21.76	15.00	4.022	1.903	-0.048	0.358

Data recorded on file 4

A3, Deep draft

Run	Vel	Incidence	Cl	Cd	Cm	Lh
1	21.78	0.00	-0.122	1.398	-0.016	-0.129
2	21.80	1.00	0.539	1.361	-0.077	0.317
3	21.80	2.00	1.199	1.508	-0.149	0.268
4	21.80	3.00	1.860	1.640	-0.217	0.256
5	21.80	4.00	2.685	1.705	-0.241	0.272
6	21.82	5.00	3.341	1.816	-0.260	0.280
7	21.80	6.00	4.006	1.970	-0.289	0.284
8	21.80	7.00	4.831	2.101	-0.313	0.290
9	21.80	8.00	5.492	2.267	-0.347	0.291
10	21.79	9.00	6.157	2.468	-0.358	0.296
11	21.79	10.00	6.984	2.717	-0.386	0.299
12	21.78	11.00	7.821	2.972	-0.392	0.305
13	21.79	12.00	8.641	3.281	-0.389	0.311
14	21.77	13.00	9.313	3.618	-0.418	0.313
15	21.77	14.00	9.979	4.018	-0.423	0.317
16	21.77	15.00	10.803	4.430	-0.418	0.322

Data recorded on file 5

A4, 1/20 by bow

Run	Vel	Incidence	Cl	Cd	Cm	Lh
1	21.82	0.00	0.043	1.007	-0.016	1.165
2	21.83	1.00	0.372	1.022	-0.113	0.159
3	21.84	2.00	0.865	1.101	-0.247	0.100
4	21.84	3.00	1.194	1.166	-0.363	0.063
5	21.83	4.00	1.524	1.217	-0.495	0.031
6	21.83	5.00	1.853	1.316	-0.581	0.037
7	21.82	6.00	2.350	1.401	-0.676	0.058
8	21.83	7.00	2.679	1.532	-0.756	0.061
9	21.82	8.00	3.009	1.649	-0.856	0.055
10	21.81	9.00	3.507	1.817	-0.929	0.074
11	21.82	10.00	3.999	1.963	-0.998	0.089
12	21.82	11.00	4.329	2.161	-1.064	0.090
13	21.81	12.00	4.828	2.363	-1.131	0.101
14	21.81	13.00	5.158	2.594	-1.180	0.105
15	21.80	14.00	5.491	2.844	-1.246	0.105
16	21.80	15.00	5.824	3.144	-1.306	0.105

Data recorded on file 6

A5, 1/20 by stern

Run	Vel	Incidence	Cl	Cd	Cm	Lh
1	21.78	0.00	0.043	1.217	-0.032	1.036
2	21.79	1.00	0.539	1.215	0.100	0.643
3	21.79	2.00	1.200	1.281	0.236	0.589
4	21.80	3.00	1.695	1.311	0.331	0.576
5	21.80	4.00	2.190	1.376	0.453	0.583
6	21.79	5.00	2.852	1.460	0.582	0.575
7	21.79	6.00	3.350	1.562	0.700	0.580
8	21.79	7.00	4.011	1.677	0.824	0.576
9	21.79	8.00	4.508	1.810	0.921	0.576
10	21.78	9.00	5.007	1.911	1.017	0.577
11	21.79	10.00	5.498	2.056	1.133	0.583
12	21.78	11.00	6.000	2.243	1.202	0.580
13	21.78	12.00	6.664	2.426	1.253	0.569
14	21.77	13.00	7.000	2.628	1.295	0.570
15	21.76	14.00	7.504	2.831	1.375	0.572
16	21.76	15.00	8.162	3.027	1.467	0.571

Data recorded on file 7

A6, heeled 15 deg

Run	Vel	Incidence	Cl	Cd	Cm	Lh
1	21.85	0.00	-0.286	0.982	-0.212	0.907
2	21.86	1.00	0.042	0.963	-0.235	-7.143
3	21.87	2.00	0.535	0.978	-0.266	-0.110
4	21.87	3.00	0.863	1.092	-0.336	-0.023
5	21.86	4.00	1.356	1.127	-0.375	0.079
6	21.86	5.00	1.684	1.175	-0.399	0.114
7	21.86	6.00	2.177	1.258	-0.463	0.134
8	21.86	7.00	2.670	1.340	-0.482	0.166
9	21.87	8.00	3.161	1.437	-0.494	0.189
10	21.85	9.00	3.659	1.574	-0.509	0.207
11	21.85	10.00	4.153	1.723	-0.517	0.222
12	21.85	11.00	4.647	1.921	-0.513	0.237
13	21.84	12.00	5.306	2.135	-0.511	0.252
14	21.83	13.00	5.971	2.403	-0.505	0.265
15	21.83	14.00	6.468	2.653	-0.494	0.275
16	21.83	15.00	7.124	2.947	-0.487	0.285

Data recorded on file 8

A7, heeled 30 deg

Run	Vel	Incidence	Cl	Cd	Cm	Lh
1	21.82	0.00	-0.781	0.874	-0.440	0.841
2	21.83	1.00	-0.287	0.872	-0.462	1.730
3	21.83	2.00	0.207	0.871	-0.484	-2.184
4	21.84	3.00	0.701	0.903	-0.536	-0.429
5	21.83	4.00	1.030	1.003	-0.576	-0.223
6	21.83	5.00	1.690	1.104	-0.604	-0.017
7	21.82	6.00	2.186	1.188	-0.607	0.063
8	21.82	7.00	2.846	1.304	-0.602	0.130
9	21.82	8.00	3.504	1.435	-0.614	0.167
10	21.82	9.00	4.163	1.616	-0.591	0.201
11	21.81	10.00	4.993	1.835	-0.598	0.225
12	21.81	11.00	5.654	2.083	-0.580	0.243
13	21.81	12.00	6.480	2.364	-0.532	0.265
14	21.79	13.00	7.314	2.700	-0.528	0.277
15	21.80	14.00	8.301	3.044	-0.528	0.287
16	21.79	15.00	9.301	3.462	-0.536	0.294

Data recorded on file 9

A8, Rounded bilges

Run	Vel	Incidence	Cl	Cd	Cm	Lh
1	21.93	0.00	-0.122	0.765	-0.000	0.006
2	21.94	1.00	0.204	0.762	-0.010	0.481
3	21.94	2.00	0.367	0.795	-0.027	0.372
4	21.94	3.00	0.693	0.810	-0.044	0.328
5	21.94	4.00	1.020	0.860	-0.039	0.337
6	21.93	5.00	1.346	0.910	-0.047	0.333
7	21.92	6.00	1.511	0.978	-0.045	0.338
8	21.92	7.00	1.838	1.028	-0.027	0.350
9	21.92	8.00	2.002	1.077	-0.003	0.364
10	21.92	9.00	2.329	1.143	-0.007	0.361
11	21.91	10.00	2.493	1.210	-0.031	0.352
12	21.90	11.00	2.660	1.295	-0.056	0.343
13	21.90	12.00	2.987	1.344	-0.058	0.344
14	21.90	13.00	3.152	1.477	-0.072	0.342
15	21.90	14.00	3.478	1.590	-0.106	0.334
16	21.89	15.00	3.646	1.741	-0.109	0.337

Data recorded on file 10

B9, Rounded bow

Run	Vel	Incidence	Cl	Cd	Cm	Lh
1	21.84	0.00	0.042	1.461	-0.000	2.094
2	21.86	1.00	0.371	1.456	-0.006	0.530
3	21.86	2.00	0.699	1.487	-0.057	0.360
4	21.87	3.00	1.027	1.536	-0.101	0.308
5	21.85	4.00	1.357	1.606	-0.113	0.308
6	21.85	5.00	1.686	1.655	-0.118	0.312
7	21.85	6.00	2.179	1.754	-0.124	0.317
8	21.84	7.00	2.510	1.855	-0.132	0.319
9	21.84	8.00	3.004	1.988	-0.150	0.318
10	21.84	9.00	3.333	2.104	-0.125	0.331
11	21.84	10.00	3.662	2.235	-0.141	0.330
12	21.84	11.00	4.158	2.385	-0.139	0.334
13	21.83	12.00	4.488	2.567	-0.125	0.342
14	21.83	13.00	4.982	2.732	-0.101	0.350
15	21.83	14.00	5.480	2.900	-0.122	0.348
16	21.82	15.00	5.978	3.117	-0.118	0.352

Data recorded on file 11

C10, Narrow beam

Run	Vel	Incidence	Cl	Cd	Cm	Lh
1	21.92	0.00	-0.122	0.520	0.023	0.024
2	21.93	1.00	0.204	0.536	-0.006	0.371
3	21.93	2.00	0.531	0.568	-0.033	0.295
4	21.92	3.00	0.695	0.603	-0.064	0.257
5	21.92	4.00	1.021	0.619	-0.084	0.260
6	21.92	5.00	1.512	0.653	-0.086	0.283
7	21.91	6.00	1.840	0.688	-0.083	0.294
8	21.91	7.00	2.167	0.737	-0.085	0.300
9	21.90	8.00	2.496	0.821	-0.098	0.300
10	21.89	9.00	2.990	0.938	-0.121	0.298
11	21.89	10.00	3.319	1.070	-0.141	0.297
12	21.89	11.00	3.810	1.201	-0.155	0.298
13	21.88	12.00	4.142	1.369	-0.164	0.300
14	21.90	13.00	4.625	1.509	-0.159	0.306
15	21.88	14.00	5.122	1.726	-0.126	0.318
16	21.88	15.00	5.452	1.958	-0.117	0.322

Data recorded on file 12

D11, Broad beam

Run	Vel	Incidence	Cl	Cd	Cm	Lh
1	21.89	0.00	0.042	1.658	-0.117	0.562
2	21.89	1.00	0.369	1.625	-0.119	0.346
3	21.90	2.00	0.860	1.640	-0.122	0.336
4	21.90	3.00	1.187	1.738	-0.142	0.324
5	21.88	4.00	1.681	1.890	-0.172	0.316
6	21.88	5.00	2.009	1.990	-0.203	0.307
7	21.87	6.00	2.502	2.058	-0.221	0.309
8	21.88	7.00	2.994	2.172	-0.225	0.316
9	21.87	8.00	3.325	2.274	-0.231	0.320
10	21.86	9.00	3.654	2.373	-0.255	0.318
11	21.87	10.00	4.145	2.553	-0.282	0.319
12	21.86	11.00	4.476	2.703	-0.303	0.319
13	21.85	12.00	4.973	2.871	-0.296	0.328
14	21.85	13.00	5.466	3.069	-0.291	0.335
15	21.85	14.00	5.963	3.269	-0.273	0.344
16	21.84	15.00	6.460	3.536	-0.275	0.350

Data recorded on file 13

A12, 1/40 by stern

Run	Vel	Incidence	Cl	Cd	Cm	Lh
1	21.89	0.00	-0.122	1.117	-0.063	0.369
2	21.90	1.00	0.205	1.115	-0.003	0.621
3	21.90	2.00	0.696	1.149	0.036	0.475
4	21.90	3.00	1.024	1.198	0.061	0.459
5	21.90	4.00	1.515	1.264	0.081	0.434
6	21.89	5.00	2.008	1.332	0.132	0.440
7	21.89	6.00	2.499	1.398	0.169	0.437
8	21.88	7.00	2.992	1.465	0.238	0.447
9	21.89	8.00	3.480	1.575	0.297	0.453
10	21.88	9.00	3.978	1.696	0.333	0.451
11	21.87	10.00	4.307	1.845	0.375	0.457
12	21.86	11.00	4.806	1.998	0.399	0.454
13	21.85	12.00	5.301	2.181	0.436	0.456
14	21.85	13.00	5.633	2.364	0.477	0.462
15	21.84	14.00	6.130	2.580	0.500	0.461
16	21.86	15.00	6.614	2.804	0.532	0.462

Data recorded on file 14

E12, with trip wire

Run	Vel	Incidence	Cl	Cd	Cm	Lh
1	21.86	0.00	0.379	0.916	0.190	0.928
2	21.88	1.00	0.545	0.911	0.162	0.706
3	21.88	2.00	0.879	0.929	0.150	0.551
4	21.89	3.00	1.378	0.958	0.143	0.467
5	21.89	4.00	1.712	1.009	0.152	0.448
6	21.89	5.00	2.212	1.042	0.150	0.422
7	21.89	6.00	2.545	1.108	0.163	0.418
8	21.89	7.00	3.045	1.191	0.189	0.415
9	21.89	8.00	3.379	1.276	0.205	0.414
10	21.89	9.00	3.713	1.409	0.211	0.412
11	21.89	10.00	4.044	1.541	0.198	0.405
12	21.88	11.00	4.548	1.678	0.174	0.394
13	21.87	12.00	5.053	1.881	0.163	0.389
14	21.88	13.00	5.218	2.080	0.173	0.393
15	21.87	14.00	5.721	2.298	0.187	0.394
16	21.87	15.00	6.054	2.515	0.182	0.394

Data recorded on file 64

E12, no trip wire

Run	Vel	Incidence	Cl	Cd	Cm	Lh
1	21.87	0.00	0.212	0.695	0.254	1.660
2	21.89	1.00	0.545	0.692	0.237	0.825
3	21.89	2.00	1.045	0.710	0.229	0.581
4	21.89	3.00	1.378	0.775	0.221	0.519
5	21.89	4.00	1.711	0.891	0.174	0.458
6	21.89	5.00	2.044	0.991	0.158	0.433
7	21.89	6.00	2.378	1.057	0.172	0.427
8	21.89	7.00	2.879	1.143	0.201	0.423
9	21.88	8.00	3.382	1.245	0.227	0.421
10	21.89	9.00	3.547	1.377	0.226	0.420
11	21.87	10.00	4.051	1.514	0.214	0.409
12	21.88	11.00	4.384	1.679	0.181	0.398
13	21.87	12.00	4.889	1.867	0.168	0.392
14	21.86	13.00	5.226	2.069	0.174	0.393
15	21.86	14.00	5.726	2.285	0.165	0.390
16	21.86	15.00	6.231	2.522	0.166	0.389

Data recorded on file 63

F13, with trip wire

Run	Vel	Incidence	Cl	Cd	Cm	Lh
1	21.87	0.00	-0.122	0.464	0.039	-0.131
2	21.89	1.00	0.045	0.443	0.009	1.014
3	22.00	2.00	0.043	0.434	-0.022	0.094
4	22.00	3.00	0.208	0.416	-0.072	0.021
5	22.00	4.00	0.373	0.433	-0.094	0.101
6	22.00	5.00	0.538	0.434	-0.118	0.125
7	21.99	6.00	0.704	0.452	-0.138	0.145
8	21.98	7.00	0.870	0.471	-0.138	0.182
9	21.97	8.00	1.036	0.505	-0.133	0.213
10	21.97	9.00	1.367	0.555	-0.132	0.245
11	21.96	10.00	1.534	0.624	-0.127	0.260
12	21.95	11.00	1.701	0.676	-0.118	0.274
13	21.94	12.00	2.035	0.795	-0.105	0.293
14	21.91	13.00	2.375	0.921	-0.058	0.324
15	21.89	14.00	2.545	1.042	-0.023	0.343
16	21.89	15.00	2.880	1.143	0.031	0.367

Data recorded on file 61

F13, no trip wire

Run	Vel	Incidence	Cl	Cd	Cm	Lh
1	21.88	0.00	-0.122	0.295	0.047	-0.146
2	21.89	1.00	0.045	0.276	0.018	1.029
3	21.89	2.00	0.211	0.292	-0.014	0.312
4	21.90	3.00	0.211	0.306	-0.049	0.136
5	21.88	4.00	0.378	0.359	-0.111	0.053
6	21.88	5.00	0.546	0.378	-0.136	0.091
7	21.88	6.00	0.712	0.410	-0.156	0.119
8	21.88	7.00	0.879	0.444	-0.156	0.161
9	21.88	8.00	1.046	0.495	-0.151	0.195
10	21.88	9.00	1.380	0.545	-0.142	0.237
11	21.87	10.00	1.547	0.612	-0.152	0.242
12	21.87	11.00	1.881	0.679	-0.141	0.266
13	21.87	12.00	2.049	0.780	-0.095	0.299
14	21.86	13.00	2.385	0.883	-0.076	0.315
15	21.86	14.00	2.719	1.016	-0.013	0.347
16	21.86	15.00	3.053	1.166	0.023	0.362

Data recorded on file 62

Alr with splitter plate

Run	Vel	Incidence	Cl	Cd	Cm	Lh
1	21.61	0.00	-0.122	1.346	-0.083	0.440
2	21.62	1.00	0.220	1.359	-0.128	0.083
3	21.63	2.00	0.561	1.424	-0.156	0.169
4	21.64	3.00	1.072	1.485	-0.191	0.215
5	21.63	4.00	1.414	1.509	-0.226	0.218
6	21.64	5.00	1.754	1.575	-0.229	0.241
7	21.63	6.00	2.268	1.630	-0.241	0.258
8	21.64	7.00	2.608	1.712	-0.239	0.272
9	21.64	8.00	2.950	1.816	-0.246	0.278
10	21.63	9.00	3.466	1.939	-0.241	0.292
11	21.62	10.00	3.807	2.110	-0.229	0.302
12	21.62	11.00	4.321	2.282	-0.230	0.309
13	21.62	12.00	4.663	2.453	-0.226	0.315
14	21.62	13.00	5.176	2.676	-0.228	0.321
15	21.62	14.00	5.519	2.899	-0.234	0.324
16	21.61	15.00	6.036	3.142	-0.254	0.325

Data recorded on file 52

Alr no splitter plate

Run	Vel	Incidence	Cl	Cd	Cm	Lh
1	21.72	0.00	0.047	1.091	-0.050	0.468
2	21.74	1.00	0.385	1.103	-0.073	0.294
3	21.74	2.00	0.554	1.186	-0.121	0.213
4	21.75	3.00	1.061	1.220	-0.145	0.249
5	21.75	4.00	1.567	1.270	-0.177	0.256
6	21.75	5.00	1.905	1.338	-0.186	0.267
7	21.75	6.00	2.244	1.405	-0.197	0.274
8	21.74	7.00	2.751	1.490	-0.209	0.283
9	21.74	8.00	3.091	1.611	-0.207	0.292
10	21.74	9.00	3.597	1.745	-0.199	0.303
11	21.73	10.00	4.107	1.899	-0.186	0.314
12	21.72	11.00	4.449	2.073	-0.185	0.319
13	21.73	12.00	4.958	2.289	-0.171	0.328
14	21.72	13.00	5.296	2.496	-0.185	0.328
15	21.72	14.00	5.635	2.716	-0.188	0.332
16	21.72	15.00	6.143	2.971	-0.179	0.328

Data recorded on file 51

A4 : APPENDIX TO CHAPTER 4

A4.1 Starting solution for hull flow calculation

As discussed in section 4.3(e), starting solutions are required for the marching calculation of vortex evolutions. These are required at the first cross-flow plane and subsequently at the first appearance of new vortices when existing vortices are shed. When the distance of a vortex from a bilge is small compared with hull cross flow dimensions, the local bilge flow will be similar to the local flow at the corner of an infinite right-angled wedge in an appropriate velocity field.

The notation of Chapter 4 is used. In the transformed S plane, W_{XK} is defined as the total potential function excluding any part associated with vortex k :

$$W_{xk} = W_p + VS + \sum_{j=1,m}^{j\neq k} \frac{iG_j}{2\pi}\left(\ln(S-S_{oj}) - \ln(S-\bar{S}_{oj})\right)$$

and by differentiating, the velocity at the transformed bilge is

$$V_{ek} = \left.\frac{dW_p}{dS}\right|_{S_{ek}} + V + \sum_{j=1,m}^{j\neq k} \frac{iG_j}{2\pi}\left(\frac{1}{S_{ek}-S_{oj}} - \frac{1}{S_{ek}-\bar{S}_{oj}}\right)$$

Graham (1977) gives single-point-vortex similarity solutions for the starting flows about infinite wedges. These solutions are obtained by transforming the wedge flow into the flow past an infinite half plane. These solutions can be used by assuming that the local flow at the transformed bilge is similar to uniform flow past a straight flow boundary:

$$W_{xu} \approx V_{eu} \int$$

Single point vortex starting flow. The time dependent flow past an infinite edge of $\frac{\pi}{2}$ is considered. This edge flow and the corresponding transformed flow are represented in the top sketch of figure A4.1. In the absence of shed vorticity, uniform flow past the transformed plane is represented by the complex potential

$$W_o(\zeta) = i\hat{V}\zeta$$

where $\hat{V}$ is a real constant. The corresponding potential in the physical plane is

$$W_o(Z) = i\hat{V}Z^{\frac{2}{\pi}}$$

In the initial stages of the starting flow, the flow separates from the upper surface of the physical edge. A highly simplified flow consisting of a single growing point vortex $\Gamma_o(t)$ at $Z_o''(t)$ is considered. As discussed in Chapter 4, since the point vortex represents a growing spiral vortex sheet attached to the edge, the point Z_o'' must be joined to the edge Z_e'' by a cut representing this sheet. The potential in this transformed plane is

$$W(\zeta) = i\hat{V}\zeta + \frac{i\Gamma_o}{2\pi}\ln(\zeta-\zeta_o) - \frac{i\Gamma_o}{2\pi}\ln(\zeta-\bar{\zeta}_o)$$

The Kutta condition. Infinite velocities must be eliminated at the edge. That is, in the transformed plane

$$-i\hat{V} + \frac{i\Gamma_o}{2\pi\zeta_o} + \frac{i\Gamma_o}{2\pi\bar{\zeta}_o} = 0$$

$$\Rightarrow \quad \Gamma_0 \left(Z_0^{\frac{1}{\lambda}} + \bar{Z}_0^{\frac{1}{\lambda}} \right) = 2\pi \hat{V} Z_0''^{\frac{1}{\lambda}} \bar{Z}_0''^{\frac{1}{\lambda}}$$

where

$$\lambda = \frac{3}{2}$$

The zero force condition. The bottom sketch of figure A4.1 indicates a vortex Γ_0 at Z_0'' with a cut to Z_e'' such that across the cut $\varphi_2 - \varphi_1 = \Gamma_0$. Bernoulli's theorem is applied at a point Z on the cut:

$$p_1 - p_2 = \rho \frac{\partial}{\partial t}(\varphi_2 - \varphi_1) + \frac{1}{2}\left(u_2^2 - u_1^2\right)$$

All vorticity is concentrated on Z_0'', so

$$u_2 = u_1 \qquad \text{and} \qquad \varphi_2 - \varphi_1 = \Gamma_0$$

$$\Rightarrow \quad p_1 - p_2 = \rho \frac{\partial \Gamma_0}{\partial t}$$

So, the force on the cut

$$= \int_{Z_e''}^{Z_0''} (p_1 - p_1)\, dZ = \rho \frac{\partial}{\partial t}(\Gamma_0 Z_0'') - \rho \Gamma_0 \frac{\partial Z_0''}{\partial t} - \rho Z_e'' \frac{\partial \Gamma_0}{\partial t}$$

and, the force on the vortex

$$= \rho \Gamma_0 \left(\frac{\partial Z_0''}{\partial t} - \bar{V}_0 \right)$$

where $\bar{V}_0$ is the velocity of the fluid at Z_0'', and

$$V_0 = u - iv = \lim_{Z'' \to Z_0''} \left(\frac{\partial W}{\partial Z''} - \frac{i\Gamma_0}{2\pi (Z'' - Z_0'')} \right)$$

Hence, the requirement of zero total force is

$$\frac{\partial}{\partial t}(\Gamma_0 \bar{Z}_0^*) - Z_e^* \frac{\partial \Gamma_0}{\partial t} = \Gamma_0 \lim_{Z'' \to Z_0''} \left(\frac{\partial W}{\partial Z^*} - \frac{i\Gamma_0}{2\pi(Z^* - Z_0^*)} \right)$$

Noting that

$$\frac{\partial W}{\partial \zeta} = i\hat{V} + \frac{i\Gamma_0}{2\pi}\left(\frac{1}{\zeta - \zeta_0} - \frac{1}{\zeta + \zeta_0}\right)$$

and

$$\frac{\partial \zeta}{\partial Z''} = \frac{1}{\lambda} Z''^{\left(\frac{1}{\lambda}-1\right)}$$

then

$$\frac{\partial W}{\partial Z''} = \frac{i\hat{V}}{\lambda} Z''^{\left(\frac{1}{\lambda}-1\right)} + \frac{i\Gamma_0}{2\pi}\frac{Z''^{\left(\frac{1}{\lambda}-1\right)}}{\lambda}\left(\frac{1}{Z^{*\frac{1}{\lambda}} - Z_0''^{\frac{1}{\lambda}}} - \frac{1}{Z''^{\frac{1}{\lambda}} + Z_0''^{\frac{1}{\lambda}}}\right)$$

Also, noting that Z_e'' is the origin, and taking complex conjugates of all terms, the zero force condition becomes

$$\frac{\partial}{\partial t}(\Gamma_0 \bar{Z}_0'') = \Gamma_0 \lim_{Z'' \to Z_0''} \left(\frac{i\hat{V} Z''^{\left(\frac{1}{\lambda}-1\right)}}{\lambda} + \frac{i\Gamma_0}{2\pi}\frac{Z''^{\left(\frac{1}{\lambda}-1\right)}}{\lambda}\left(\frac{1}{Z''^{\frac{1}{\lambda}} - Z_0''^{\frac{1}{\lambda}}} - \frac{1}{Z''^{\frac{1}{\lambda}} + Z_0''^{\frac{1}{\lambda}}}\right) - \frac{i\Gamma_0}{2\pi}\frac{1}{(Z'' - Z_0'')}\right)$$

And, using lemma A4.2(c) for terms with singular values at Z_0''; the zero force condition is

$$\frac{\partial}{\partial t}(\Gamma_0 \bar{Z}_0'') = \Gamma_0 \left\{ \frac{i\hat{V} Z_0''^{\left(\frac{1}{\lambda}-1\right)}}{\lambda} - \frac{i\Gamma_0}{4\pi\lambda Z_0''}\left(\lambda - 1 + \frac{2 Z_0''^{\frac{1}{\lambda}}}{Z_0''^{\frac{1}{\lambda}} + \bar{Z}_0''^{\frac{1}{\lambda}}}\right)\right\}$$

Blenderman similarity solution. The kutta condition and zero force condition are

$$\begin{cases} \Gamma_0\left(Z_0''^{\frac{1}{\lambda}} + \bar{Z}_0''^{\frac{1}{\lambda}}\right) = 2\pi\hat{V} Z_0''^{\frac{1}{\lambda}} \bar{Z}_0''^{\frac{1}{\lambda}} \\ \frac{\partial}{\partial t}(\Gamma_0 \bar{Z}_0'') = \Gamma_0\left(\frac{i\hat{V} Z_0''^{\left(\frac{1}{\lambda}-1\right)}}{\lambda} - \frac{i\Gamma_0}{4\pi\lambda Z_0''}\left(\lambda - 1 + \frac{2 Z_0''^{\frac{1}{\lambda}}}{Z_0''^{\frac{1}{\lambda}} + \bar{Z}_0''^{\frac{1}{\lambda}}}\right)\right) \end{cases}$$

These equations have similarity solutions of the Blenderman form when $\hat{V} = \overset{*}{V} t^{\alpha}$ (that is for starting flows round an edge). Writing

$$L_v = (\hat{V} t)^{\frac{\lambda}{2\lambda-1}}$$

$$\theta = -\lambda \cos^{-1}\left(\tfrac{1}{2}\sqrt{\lambda}\right)$$

$$K = \frac{\sqrt{4-\lambda}\,(\lambda-1)(2\lambda-1)}{2\lambda^2(3\alpha\lambda+\lambda+1)}$$

then the similarity solutions can be shown to be

$$Z_o'' = K^{\frac{\lambda}{2\lambda-1}} L_v e^{i\theta}$$

$$\Gamma_o = \frac{2\pi}{\sqrt{\lambda}} K^{\frac{1}{2\lambda-1}} L_v^2 t^{-1}$$

Notes. These solutions assume $\hat{V}$ to be positive. If $\hat{V}$ is negative the flow would separate from the opposite surface. Appropriate solutions would then be found by making Γ_o and θ negative.

The parameter $\hat{V}$ is determined in terms of V_{ek} by considering successive transformations between complex planes. It is shown to be

$$\hat{V} = \left(\frac{9}{4}\left(\frac{b^2-a^2}{2f_e}\right)\right)^{\frac{1}{3}} V_{ek}$$

The parameter α is determined by considering the recent history of the flow. For the first time step α is given the value 0; this represents a flow which suddenly starts with the appropriate velocity. Subsequently it is assumed that initially, after a vortex has been shed,

$$V_r \approx \overset{*}{V} t^{\alpha}$$

where V_r is the velocity that would occur at the transformed

bilge in the absence of the new vortex, V^* is some constant, and t is the time since the velocity was zero. Then α can be determined at time t as

$$\alpha = \frac{t \frac{dV_r}{dt}}{V_r}$$

Transformation between planes

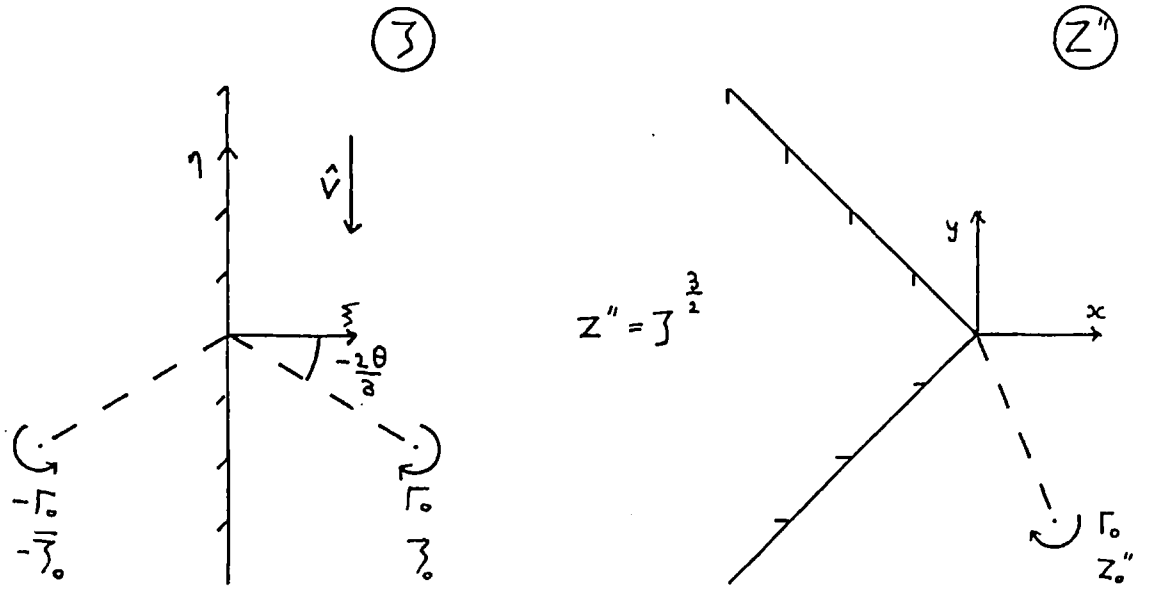

Vortex and cut

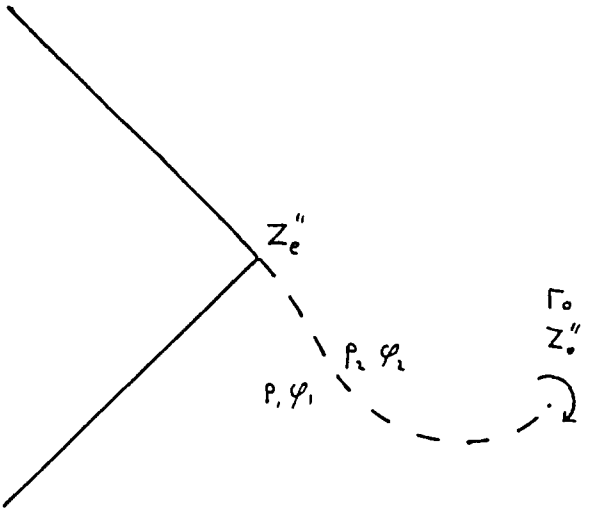

Figure A4.1

Defining sketches: hull calculation starting solutions

A4.2(a) Lemma

$$\lim_{z\to z_0}\left\{\frac{1}{s-s_0}\sqrt{\frac{s^2-b^2}{s^2-a^2}}-\frac{1}{z-z_0}\right\}$$

substitute $z=\int_0^s\sqrt{\frac{s^2-a^2}{s^2-b^2}}\,ds+c_0$

$$=\lim_{z\to z_0}\left\{\frac{1}{s-s_0}\sqrt{\frac{s^2-b^2}{s^2-a^2}}-\frac{1}{\left(\int_0^s\sqrt{\frac{s^2-a^2}{s^2-b^2}}\,ds+c_0\right)-\left(\int_0^{s_0}\sqrt{\frac{s^2-a^2}{s^2-b^2}}\,ds+c_0\right)}\right\}$$

$$=\lim_{z\to z_0}\left\{\frac{1}{s-s_0}\sqrt{\frac{s^2-b^2}{s^2-a^2}}-\frac{1}{\int_{s_0}^s\sqrt{\frac{s^2-a^2}{s^2-b^2}}\,ds}\right\}$$

write $s\sim s_0(1-\alpha)\quad\Rightarrow\quad ds=-s_0\,d\alpha$

and using lemma A4.2(b)

$$=\lim_{\alpha\to0}\left\{\frac{-1}{s_0\alpha}\sqrt{\frac{s_0^2-b^2}{s_0^2-a^2}}\left(1+\alpha s_0^2\left(\frac{1}{s_0^2-a^2}-\frac{1}{s_0^2-b^2}\right)+O(\alpha^2)\right)\right.$$
$$\left.-\left(\int_0^{\alpha}\sqrt{\frac{s_0^2-a^2}{s_0^2-b^2}}\left(1+\alpha s_0^2\left(\frac{1}{s_0^2-b^2}-\frac{1}{s_0^2-a^2}\right)+O(\alpha^2)\right)-s_0\,d\alpha\right)^{-1}\right\}$$

$$=\frac{-1}{s_0}\sqrt{\frac{s_0^2-b^2}{s_0^2-a^2}}\lim_{\alpha\to0}\left\{\frac{1}{\alpha}\left(1+s_0^2\left(\frac{1}{s_0^2-a^2}-\frac{1}{s_0^2-b^2}\right)\alpha+O(\alpha^2)\right)-\left(\alpha+\frac{\alpha^2}{2}s_0^2\left(\frac{1}{s_0^2-b^2}-\frac{1}{s_0^2-a^2}\right)+O(\alpha^3)\right)^{-1}\right\}$$

$$=\frac{-1}{s_0}\sqrt{\frac{s_0^2-b^2}{s_0^2-a^2}}\lim_{\alpha\to0}\left\{\frac{1}{\alpha}\left(1+s_0^2\left(\frac{1}{s_0^2-a^2}-\frac{1}{s_0^2-b^2}\right)\alpha-1-\frac{s_0^2}{2}\left(\frac{1}{s_0^2-a^2}-\frac{1}{s_0^2-b^2}\right)\alpha+O(\alpha^2)\right)\right\}$$

$$=\frac{s_0}{2}\sqrt{\frac{s_0^2-b^2}{s_0^2-a^2}}\left(\frac{1}{s_0^2-b^2}-\frac{1}{s_0^2-a^2}\right)$$

A4.2(b) Lemma

$$\sqrt{\frac{s^2-a^2}{s^2-b^2}}$$

For $s \to s_0$, $s_0 \neq \pm a$, $s_0 \neq \pm b$

write $s \sim s_0(1-\alpha) \Rightarrow \left(\frac{s}{s_0}\right)^n = 1 - n\alpha + O(\alpha^2)$

$$= \sqrt{\frac{(s/s_0)^2 - (a/s_0)^2}{(s/s_0)^2 - (b/s_0)^2}}$$

$$= \sqrt{\frac{1 - 2\alpha + O(\alpha^2) - (a/s_0)^2}{1 - 2\alpha + O(\alpha^2) - (b/s_0)^2}}$$

$$= \sqrt{\frac{1-(a/s_0)^2}{1-(b/s_0)^2}} \sqrt{\frac{1 - (2\alpha - O(\alpha^2))/(1-(a/s_0)^2)}{1 - (2\alpha - O(\alpha^2))/(1-(b/s_0)^2)}}$$

$$= \sqrt{\frac{s_0^2-a^2}{s_0^2-b^2}} \sqrt{\left(1 - \frac{2\alpha}{1-(a/s_0)^2} + O(\alpha^2)\right)\left(1 + \frac{2\alpha}{1-(b/s_0)^2} + O(\alpha^2)\right)}$$

$$= \sqrt{\frac{s_0^2-a^2}{s_0^2-b^2}} \sqrt{1 + 2\alpha\left(\frac{1}{1-(b/s_0)^2} - \frac{1}{1-(a/s_0)^2}\right) + O(\alpha^2)}$$

$$= \sqrt{\frac{s_0^2-a^2}{s_0^2-b^2}} \left(1 + \alpha s_0^2\left(\frac{1}{s_0^2-b^2} - \frac{1}{s_0^2-a^2}\right) + O(\alpha^2)\right)$$

A4.2(c) Lemma

$$\lim_{z \to z_0} \left\{ \frac{z^{\frac{1}{\lambda}-1}}{\lambda} \left(\frac{1}{z^{\frac{1}{\lambda}} - z_0^{\frac{1}{\lambda}}} \right) - \left(\frac{1}{z - z_0} \right) \right\}$$

write $z \sim z_0(1-\alpha) \quad \Rightarrow \left(\frac{z}{z_0}\right)^n = 1 - n\alpha + \frac{n(n-1)}{2}\alpha^2 + O(\alpha^3)$

$$= \lim_{\alpha \to 0} \left\{ \frac{z_0^{\frac{1}{\lambda}-1}}{\lambda} \frac{\left(1 - \left(\frac{1}{\lambda}-1\right)\alpha + \frac{1}{2}\left(\frac{1}{\lambda}-1\right)\left(\frac{1}{\lambda}-2\right)\alpha^2 + O(\alpha^3)\right)}{z_0^{\frac{1}{\lambda}}\left(1 - \frac{1}{\lambda}\alpha + \frac{1}{2}\frac{1}{\lambda}\left(\frac{1}{\lambda}-1\right)\alpha^2 + O(\alpha^3) - 1\right)} - \frac{1}{z_0(1-\alpha-1)} \right\}$$

$$= \lim_{\alpha \to 0} \frac{1}{z_0} \left\{ \frac{\left(1 - \left(\frac{1}{\lambda}-1\right)\alpha + O(\alpha^2)\right)}{-\lambda\alpha\frac{1}{\lambda}\left(1 - \frac{1}{2}\left(\frac{1}{\lambda}-1\right)\alpha + O(\alpha^2)\right)} - \frac{1}{\alpha} \right\}$$

$$= \lim_{\alpha \to 0} \frac{1}{z_0} \left\{ \frac{\left(1 - \left(\frac{1}{\lambda}-1\right)\alpha + O(\alpha^2)\right)\left(1 + \frac{1}{2}\left(\frac{1}{\lambda}-1\right)\alpha + O(\alpha^2)\right)}{-\alpha} + \frac{1}{\alpha} \right\}$$

$$= \lim_{\alpha \to 0} \frac{1}{z_0} \left\{ \frac{1}{\alpha} \left(\frac{1}{2}\left(\frac{1}{\lambda}-1\right)\alpha + O(\alpha^2) \right) \right\}$$

$$= \frac{1}{2z_0}\left(\frac{1}{\lambda} - 1\right)$$

$$= \frac{1-\lambda}{2\lambda z_0}$$

A5 : APPENDIX TO CHAPTER 5

A5.1 Sail experiment Reynolds number test

The Reynolds Number Test was made with the NACA 0018 rig at an inflow angle of 35° and a linearly graduated array. The following sail trim angles, working from bow to stern, describe the sail-set: 28°, 24°, 20°, 16°, 12°, 8°, 4°, 0°. This sail-set was chosen as one for which both attached and separated flow could be observed past different aerofoils. Nine runs were made (numbers 206-214) at Reynolds numbers varying from 0.25×10^5 to 2.5×10^5. Regions of recirculating flow, identified by the wool probe test, are mapped in figure A5.1. The hatched areas represent these regions of recirculating flow on aerofoil upper surfaces. The force coefficients are plotted against Reynolds number in figure A5.2. Note that the Reynolds number scale is logarithmic.

Figure A5.1 shows that the regions of separated flow show some change with Reynolds number in this range. In particular the flow over the fourth aerofoil is largely separated at the lower speed but fully attached at the higher speed. The drag varies by 10% in this range, while the lift varies by only 2%.

These results show that the flow, and therefore the forces, are not independent of Reynolds number. This indicates a failure in simulating above-critical flow. This problem is discussed in section 5.4(a) where three possible reasons for this failure are postulated. It is interesting to note that the separated flow region on the fourth aerofoil, which is Reynolds number dependent, initiates at the leading edge. This indicates that the low

Reynolds number (laminar) separation occurs at, or before, the forward edge of the strip of sand roughness.

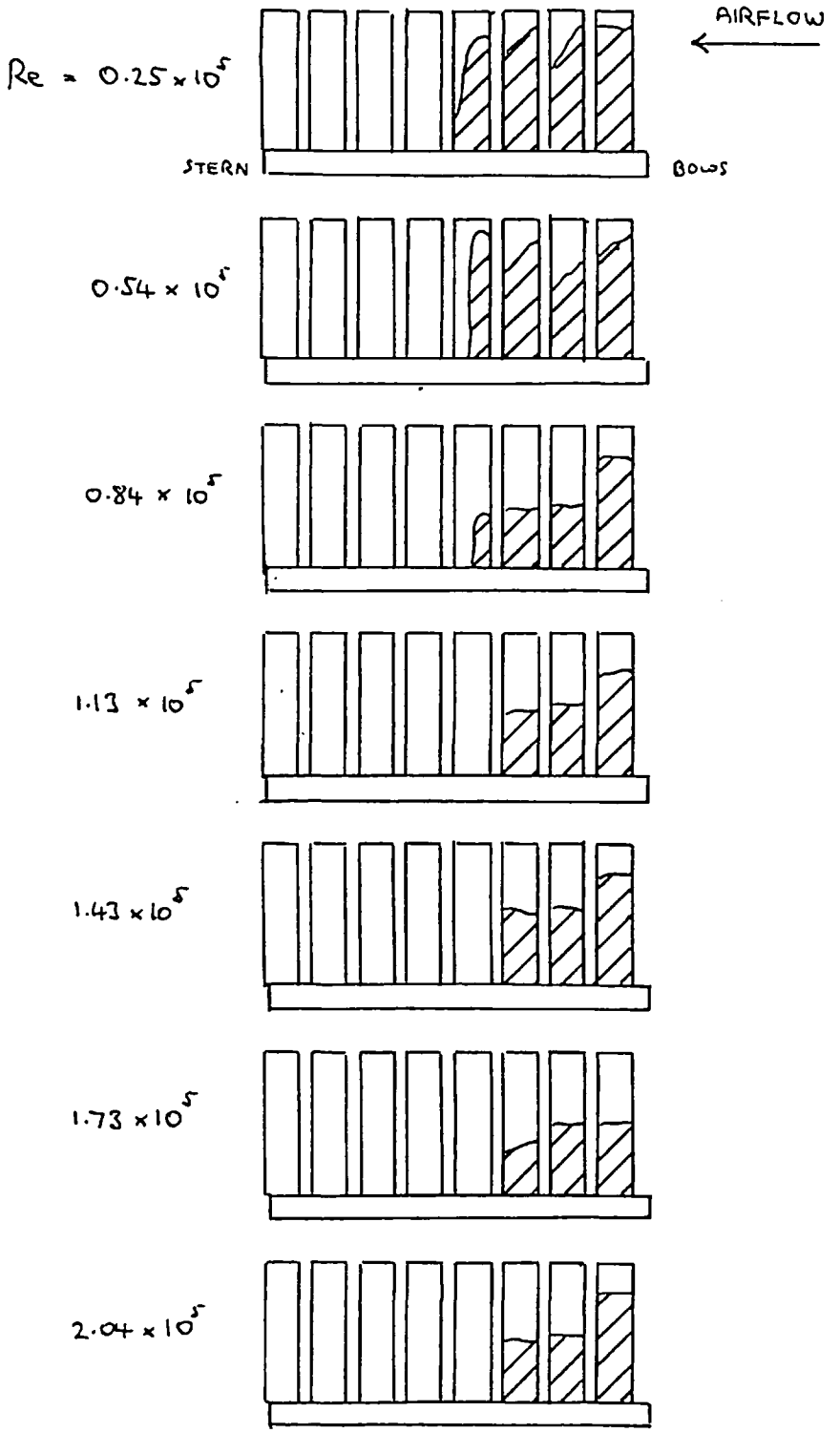

Figure A5.1

Reynolds number test:

NACA 0018 aerofoil-sails; recirculating regions (viewed from leeward)

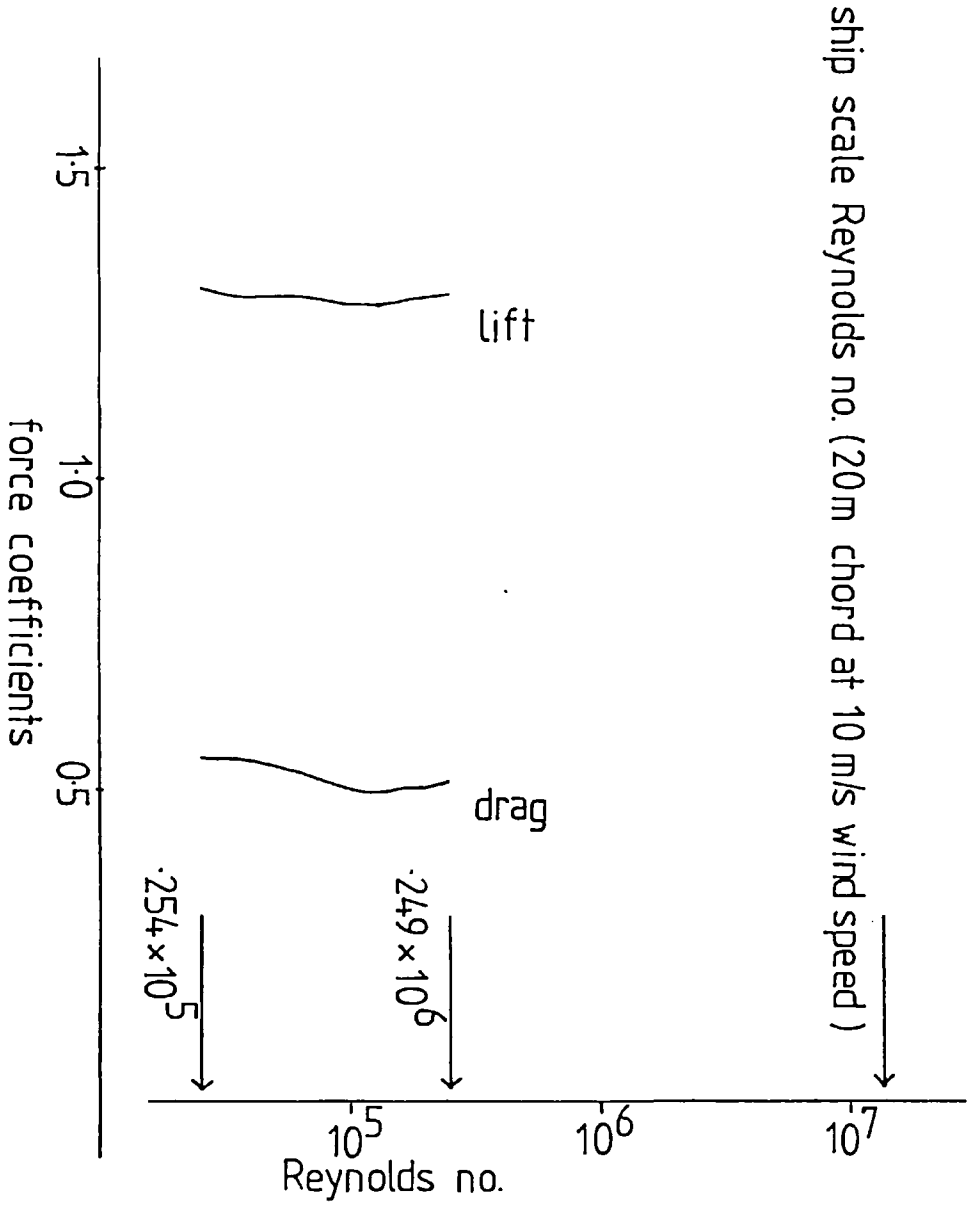

Inflow angle 35°

Graduated linear trim 28° ..... 0°

Figure A5.2

A5.2 Repeatability test

10 test runs with the NACA 0018 rig at a range of incidence angles were repeated after several days. This was to provide an indication of the repeatibility of the test results. At 20 m/s the resolution of the balance is equivalent to .0012 on the lift coefficient and .0001 on the drag coefficient, the resolution of the Betz is equivalent to .4% of a force coefficient. In stalled flow conditions the flow is often fluctuating and this causes errors in finding the mean balance points and in reading a fluctuating tunnel speed. However, the largest errors are probably associated with difficulties in accurately setting the sail angles and the hull incidence angles. It is estimated that hull incidence could be set to ± 1/4° and sail incidence could be set to ± 1°. Figure A5.3 shows the two sets of results. The mean difference in corresponding force magnitudes is 3.1%. The worst variation occurs near conditions of maximum lift when the flow is on the point of stalling.

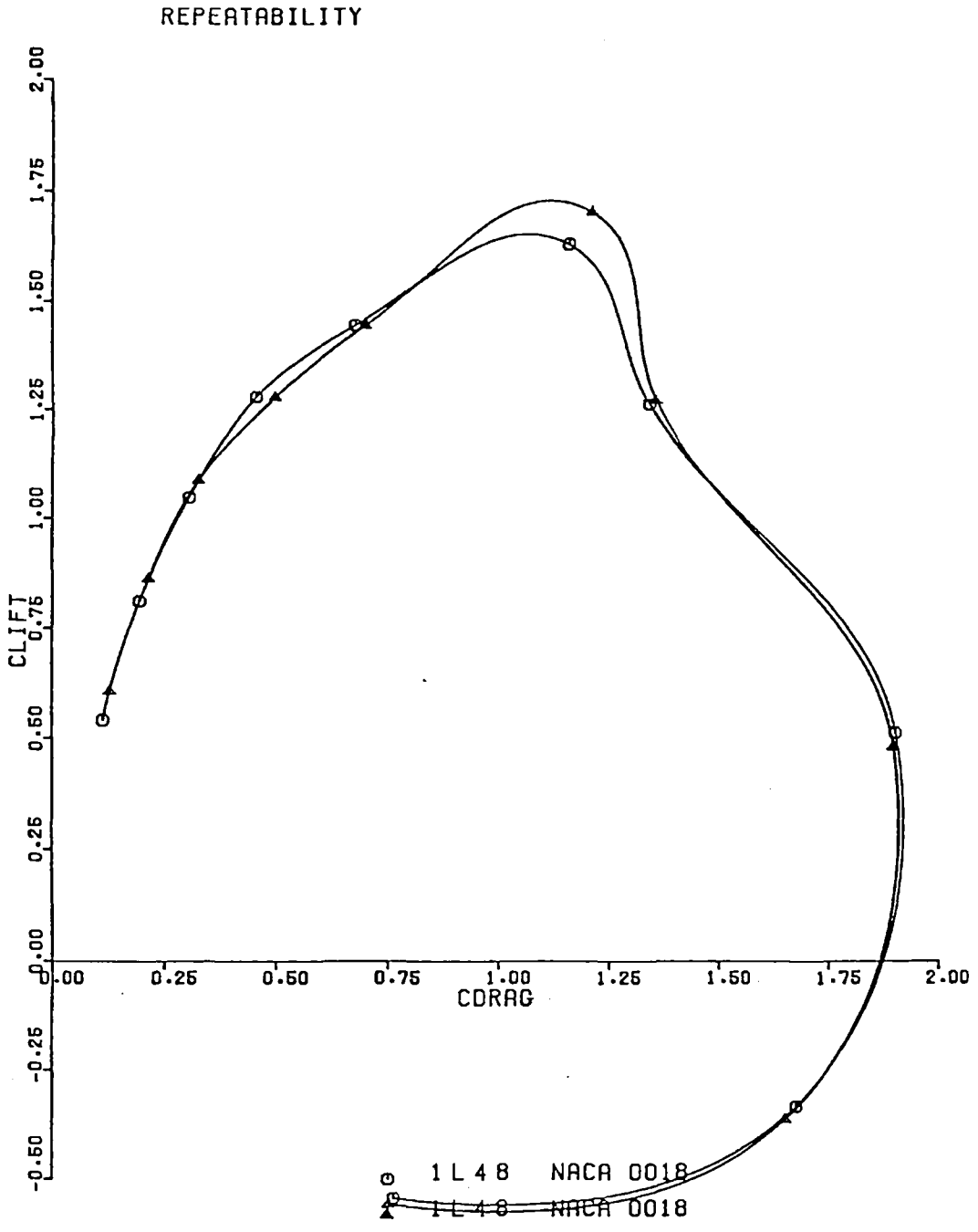
REPEATABILITY
CLIFT
CDRAG
2.00
1.75
1.50
1.25
1.00
0.75
0.50
0.25
0.00
-0.25
-0.50
0.00
0.25
0.50
0.75
1.00
1.25
1.50
1.75
2.00
1 L 4 8 NACA 0018
1 L 4 8 NACA 0018

Figure A5.3

A5.3 Tabulated results of sail tests

Table A5.1 contains the result of the wind tunnel tests of the various sailing ship rigs. For each run it lists a key word, the inflow angle, the sailset angles, the force coefficients, the test Reynolds number and the comments. The keyword contains information about the rig tested. A key word of this type was used as it facilitates computer sorting. The force coefficients are non dimensionalised by the dynamic pressure and a reference area which is the product of the ship's length and the normal sail height. The Reynolds number is based on aerofoil chord. The comments are aerodynamic notes made during the tests. The comments sometimes also include information contained in the key word.

Key word: the first character generally indicates the type of sail according to the following code.

1 - NACA 0018 section

2 - NACA 6518 section

3 - 9% camber, 12% thick circular arc foil

4 - flat thin foil

5 - 6% camber, thin circular arc foil

6 - 12% camber, thin circular arc foil

7 - 24% camber, thin circular arc foil

H - hull tested without sails

X - small stump tested without sails

Y - 15° heel small stump tested without sails

Z - 30° heel small stump tested without sails

The second and third characters generally give information about how the sails are trimmed.

Pn - parallel trim, all sails set at 10n°

Ln - linear graduation of -n° per foil

Gn - graduated trim calculated by the 2-dimensional model for a local angle of incidence of 5n°

OO - a single sail

NN - no sails

The fourth character gives other information.

8 - standard rig of 8 sails

S - small end plate fitted

L - large end plate fitted

6 - 6 sails only

4 - 4 sails at forward 4 stations

A - 4 sails at alternate stations

H - 8 sails of half normal height

1 - sail at bow station of head-to-wind hull

N - no sails

F - hull heeled 15°

T - hull heeled 30°

X - sail mounted on small stump

Y - sail heeled 15° on small stump

Z - sail heeled 30° on small stump.

Comments: the first group contains information on recirculating flow. Recirculating flow was recorded if it was detected over at least half the foil length.

N - on no foils

numbers - on numbered foils

(numbers)R - on rear face of numbered foils

A - on all foils.

The second group indicated the degree of oscillation of sail forces. These categories are inevitably somewhat subjective.

N - no oscillation

S - slight oscillation

Y - considerable oscillation but allowing a good estimate of the mean value to be obtained

B - considerable oscillation not allowing a good estimate of mean values to be obtained.

Table A5.1

Results of the sail tests

RUN NO	KEY	INFLOW ANGLE	SAIL SET								LIFT COEFF	DRAG COEFF	REYNOLDS NUMBER	COMMENTS		
1	1P08	0	0	0	0	0	0	0	0	0	-.029	.024	.1040E+06	N	N	0018NOPLATE
2	1P18	20.	10	10	10	10	10	10	10	10	.566	.147	.1039E+06	12	N	P10 NACA
3	1P18	25.	10	10	10	10	10	10	10	10	.781	.264	.1030E+06	12	N	0018
4	1P18	30.	10	10	10	10	10	10	10	10	1.015	.427	.1017E+06	1	N	
5	1P18	35.	10	10	10	10	10	10	10	10	1.251	.637	.1002E+06	1	N	
6	1P18	40.	10	10	10	10	10	10	10	10	1.350	.819	.9840E+05	1	N	
7	1P18	50.	10	10	10	10	10	10	10	10	1.109	1.036	.9680E+05	1	Y	
8	1P18	60.	10	10	10	10	10	10	10	10	1.022	1.314	.9480E+05	1	Y	
9	1P18	90.	10	10	10	10	10	10	10	10	.391	1.865	.9085E+05	1	Y	
10	1P18	120.	10	10	10	10	10	10	10	10	-.402	1.625	.9263E+05	1	Y	
11	1P18	150.	10	10	10	10	10	10	10	10	-.579	.729	.9838E+05	18	S	
12	1P28	20.	20	20	20	20	20	20	20	20	.196	.047	.1042E+06	N	N	P20
13	1P28	25.	20	20	20	20	20	20	20	20	.429	.090	.1039E+06	1	N	
14	1P28	30.	20	20	20	20	20	20	20	20	.627	.168	.1035E+06	1	N	
15	1P28	35.	20	20	20	20	20	20	20	20	.849	.286	.1026E+06	1	N	
16	1P28	40.	20	20	20	20	20	20	20	20	1.043	.433	.1014E+06	1	N	
17	1P28	50.	20	20	20	20	20	20	20	20	1.369	.799	.9852E+05	1	N	
18	1P28	60.	20	20	20	20	20	20	20	20	1.266	1.069	.9636E+05	1	Y	
19	1P28	90.	20	20	20	20	20	20	20	20	.662	1.711	.9187E+05	A	Y	
20	1P28	120.	20	20	20	20	20	20	20	20	-.180	1.670	.9223E+05	A	Y	
21	1P28	150.	20	20	20	20	20	20	20	20	-.488	.790	.9776E+05	A	N	
22	1P38	30.	30	30	30	30	30	30	30	30	.268	.065	.1039E+06	N	N	P30
23	1P38	35.	30	30	30	30	30	30	30	30	.488	.109	.1037E+06	1	N	
24	1P38	40.	30	30	30	30	30	30	30	30	.675	.183	.1034E+06	12	N	
25	1P38	50.	30	30	30	30	30	30	30	30	1.011	.448	.1012E+06	12345	Y	
26	1P38	60.	30	30	30	30	30	30	30	30	1.190	.817	.9831E+05	A	Y	
27	1P38	90.	30	30	30	30	30	30	30	30	.764	1.538	.9326E+05	A	Y	
28	1P38	120.	30	30	30	30	30	30	30	30	.002	1.655	.9248E+05	A	Y	
29	1P38	150.	30	30	30	30	30	30	30	30	-.414	.850	.9745E+05	A	Y	
30	1P48	40.	40	40	40	40	40	40	40	40	.298	.087	.1039E+06	N	N	P40
31	1P48	50.	40	40	40	40	40	40	40	40	.671	.205	.1032E+06	123	N	
32	1P48	60.	40	40	40	40	40	40	40	40	.871	.464	.1012E+06	A	N	
33	1P48	90.	40	40	40	40	40	40	40	40	.769	1.219	.9534E+05	A	Y	
34	1P48	120.	40	40	40	40	40	40	40	40	.162	1.479	.9353E+05	A	Y	
35	1P48	150.	40	40	40	40	40	40	40	40	-.320	.891	.9714E+05	A	Y	
36	1P58	50.	50	50	50	50	50	50	50	50	.269	.109	.1036E+06	N	N	P50
37	1P58	60.	50	50	50	50	50	50	50	50	.597	.213	.1032E+06	12	N	
38	1P58	90.	50	50	50	50	50	50	50	50	.724	.934	.9718E+05	A	Y	
39	1P58	120.	50	50	50	50	50	50	50	50	.296	1.293	.9480E+05	A	Y	
40	1P58	150.	50	50	50	50	50	50	50	50	-.220	.833	.9764E+05	A	S	
41	1P68	60.	60	60	60	60	60	60	60	60	.181	.128	.1034E+06	N	N	P60
42	1P68	90.	60	60	60	60	60	60	60	60	.609	.646	.9951E+05	A	S	
43	1P68	120.	60	60	60	60	60	60	60	60	.376	1.102	.9619E+05	A	Y	
44	1P68	150.	60	60	60	60	60	60	60	60	-.104	.792	.9793E+05	A	Y	
45	1P98	90.	90	90	90	90	90	90	90	90	-.081	.147	.1033E+06	N	N	P90
46	1P98	120.	90	90	90	90	90	90	90	90	.336	.485	.1008E+06	A	S	
47	1P98	150.	90	90	90	90	90	90	90	90	.119	.590	.9979E+05	A	Y	
48	1PT8	120.	120	120	120	120	120	120	120	120	-.300	.124	.1034E+06	N	N	P120
49	1PT8	150.	120	120	120	120	120	120	120	120	.241	.303	.1023E+06	A	N	
50	1L28	20.	14	12	10	8	6	4	2	0	.764	.188	.1034E+06	1	N	L2, 0

RUN NO	KEY	INFLOW ANGLE				SAIL SET					LIFT COEFF	DRAG COEFF	REYNOLDS NUMBER	COMMENTS
51	1L28	25.	14	12	10	8	6	4	2	0	.988	.318	.1028E+06	12 N
52	1L28	30.	14	12	10	8	6	4	2	0	1.174	.493	.1010E+06	12 N
53	1L28	35.	14	12	10	8	6	4	2	0	1.409	.723	.9928E+05	18 N
54	1L28	40.	14	12	10	8	6	4	2	0	1.589	.953	.9740E+05	18 N
55	1L28	50.	14	12	10	8	6	4	2	0	1.158	1.108	.9607E+05	18 Y
56	1L28	60.	14	12	10	8	6	4	2	0	1.008	1.382	.9416E+05	1 Y
57	1L28	90.	14	12	10	8	6	4	2	0	.300	1.881	.9067E+05	12 B
58	1L28	120.	14	12	10	8	6	4	2	0	-.530	1.591	.9266E+05	12 Y
59	1L28	150.	14	12	10	8	6	4	2	0	-.682	.700	.9850E+05	78 Y
60	1L28	20.	21	19	17	15	13	11	9	7	.522	.103	.1038E+06	N N L2, 7
61	1L28	25.	21	19	17	15	13	11	9	7	.793	.188	.1032E+06	N N
62	1L28	30.	21	19	17	15	13	11	9	7	1.023	.305	.1025E+06	12 N
63	1L28	35.	21	19	17	15	13	11	9	7	1.215	.481	.1012E+06	123 N
64	1L28	40.	21	19	17	15	13	11	9	7	1.391	.684	.9953E+05	1234 N
65	1L28	50.	21	19	17	15	13	11	9	7	1.731	1.178	.9573E+05	1234 N
66	1L28	60.	21	19	17	15	13	11	9	7	1.252	1.326	.9463E+05	1234 Y
67	1L28	90.	21	19	17	15	13	11	9	7	.526	1.879	.9031E+05	1234 Y
68	1L28	120.	21	19	17	15	13	11	9	7	-.303	1.678	.9197E+05	1234 Y
69	1L28	150.	21	19	17	15	13	11	9	7	-.526	.757	.9781E+05	12348 Y
70	1L28	20.	28	26	24	22	20	18	16	14	.232	.054	.1037E+06	N N L2,14
71	1L28	25.	28	26	24	22	20	18	16	14	.471	.092	.1037E+06	N N
72	1L28	30.	28	26	24	22	20	18	16	14	.708	.155	.1032E+06	N N
73	1L28	35.	28	26	24	22	20	18	16	14	.940	.261	.1026E+06	12 N
74	1L28	40.	28	26	24	22	20	18	16	14	1.132	.413	.1015E+06	1234 N
75	1L28	50.	28	26	24	22	20	18	16	14	1.376	.833	.9788E+05	12345 N
76	1L28	60.	28	26	24	22	20	18	16	14	1.359	1.172	.9519E+05	12345 S
77	1L28	90.	28	26	24	22	20	18	16	14	.708	1.793	.9100E+05	1234567 Y
78	1L28	120.	28	26	24	22	20	18	16	14	-.180	1.689	.9174E+05	A Y
79	1L28	150.	28	26	24	22	20	18	16	14	-.478	.802	.9733E+05	234567 Y
80	1L28	30.	42	40	38	36	34	32	30	28	.107	.070	.1032E+06	N N L2,28
81	1L28	35.	42	40	38	36	34	32	30	28	.351	.092	.1034E+06	N N
82	1L28	40.	42	40	38	36	34	32	30	28	.578	.133	.1030E+06	N N
83	1L28	50.	42	40	38	36	34	32	30	28	.925	.323	.1016E+06	A Y
84	1L28	60.	42	40	38	36	34	32	30	28	1.065	.678	.9916E+05	A S
85	1L28	90.	42	40	38	36	34	32	30	28	.784	1.420	.9341E+05	A B
86	1L28	120.	42	40	38	36	34	32	30	28	.069	1.534	.9243E+05	A B
87	1L28	150.	42	40	38	36	34	32	30	28	-.357	.848	.9675E+05	A B
88	1L28	50.	56	54	52	50	48	46	44	42	.332	.131	.1029E+06	N N L2,42
89	1L28	60.	56	54	52	50	48	46	44	42	.654	.223	.1022E+06	345678 S
90	1L28	90.	56	54	52	50	48	46	44	42	.749	1.002	.9585E+05	A S
91	1L28	120.	56	54	52	50	48	46	44	42	.276	1.312	.9406E+05	A Y
92	1L28	150.	56	54	52	50	48	46	44	42	-.232	.807	.9694E+05	A Y
93	1L28	60.	70	68	66	64	62	60	58	56	.043	.144	.1025E+06	N N L2,56
94	1L28	90.	70	68	66	64	62	60	58	56	.612	.601	.9916E+05	A S
95	1L28	120.	70	68	66	64	62	60	58	56	.366	1.049	.9568E+05	A Y
96	1L28	150.	70	68	66	64	62	60	58	56	-.095	.764	.9738E+05	A S
97	1L48	20.	28	24	20	16	12	8	4	0	.541	.117	.1031E+06	N N L4, 0
98	1L48	25.	28	24	20	16	12	8	4	0	.811	.197	.1025E+06	N N
99	1L48	30.	28	24	20	16	12	8	4	0	1.049	.307	.1020E+06	N N
100	1L48	35.	28	24	20	16	12	8	4	0	1.280	.457	.1009E+06	1234 S

1

RUN NO	KEY	INFLOW ANGLE				SAIL SET					LIFT COEFF	DRAG COEFF	REYNOLDS NUMBER	COMMENTS
101	1L48	40.	28	24	20	16	12	8	4	0	1.446	.680	.9890E+05	1234 S
102	1L48	50.	28	24	20	16	12	8	4	0	1.633	1.162	.9507E+05	12345 Y
103	1L48	60.	28	24	20	16	12	8	4	0	1.263	1.344	.9401E+05	12345 B
104	1L48	90.	28	24	20	16	12	8	4	0	.514	1.903	.8976E+05	12345 B
105	1L48	120.	28	24	20	16	12	8	4	0	-.333	1.676	.9144E+05	1234 B
106	1L48	150.	28	24	20	16	12	8	4	0	-.544	.763	.9721E+05	12348 Y
107	1L48	20.	42	38	34	30	26	22	18	14	.043	.077	.1034E+06	12R N L4,14
108	1L48	25.	42	38	34	30	26	22	18	14	.240	.086	.1033E+06	1R N
109	1L48	30.	42	38	34	30	26	22	18	14	.460	.122	.1034E+06	N N
110	1L48	35.	42	38	34	30	26	22	18	14	.705	.182	.1030E+06	34567 N
111	1L48	40.	42	38	34	30	26	22	18	14	.927	.267	.1024E+06	234567 N
112	1L48	50.	42	38	34	30	26	22	18	14	1.272	.605	.9993E+05	A S
113	1L48	60.	42	38	34	30	26	22	18	14	1.288	.967	.9692E+05	A S
114	1L48	90.	42	38	34	30	26	22	18	14	.752	1.655	.9174E+05	A B
115	1L48	120.	42	38	34	30	26	22	18	14	-.065	1.615	.9230E+05	A B
116	1L48	150.	42	38	34	30	26	22	18	14	-.406	.812	.9716E+05	A Y
117	1L48	40.	56	52	48	44	40	36	32	28	.267	.126	.1031E+06	1R,7 N L4,28
118	1L48	50.	56	52	48	44	40	36	32	28	.664	.248	.1023E+06	45678 S
119	1L48	60.	56	52	48	44	40	36	32	28	.907	.464	.1009E+06	2345678 S
120	1L48	90.	56	52	48	44	40	36	32	28	.791	1.244	.9431E+05	A Y
121	1L48	120.	56	52	48	44	40	36	32	28	.165	1.410	.9363E+05	A Y
122	1L48	150.	56	52	48	44	40	36	32	28	-.304	.782	.9757E+05	A Y
123	1L48	60.	70	66	62	58	54	50	46	42	.351	.204	.1030E+06	5678 S L4,42
124	1L48	90.	70	66	62	58	54	50	46	42	.723	.800	.9847E+05	A S
125	1L48	120.	70	66	62	58	54	50	46	42	.318	1.184	.9541E+05	A S
126	1L48	150.	70	66	62	58	54	50	46	42	-.170	.760	.9828E+05	A S
127	1L88	30.	56	48	40	32	24	16	8	0	.621	.274	.1026E+06	1R,456 N L8,0
128	1L88	35.	56	48	40	32	24	16	8	0	.796	.371	.1019E+06	1R,456 S
129	1L88	40.	56	48	40	32	24	16	8	0	.985	.482	.1013E+06	34567 S
130	1L88	50.	56	48	40	32	24	16	8	0	1.232	.732	.9909E+05	234567 Y
131	1L88	60.	56	48	40	32	24	16	8	0	1.207	.908	.9750E+05	A B
132	1L88	90.	56	48	40	32	24	16	8	0	.677	1.599	.9230E+05	A Y
133	1L88	120.	56	48	40	32	24	16	8	0	-.109	1.466	.9343E+05	A B
134	1L88	150.	56	48	40	32	24	16	8	0	-.409	.701	.9852E+05	A Y
135	1G18	20.	24	23	22	21	20	19	18	11	.285	.055	.1040E+06	N N G 5
136	1G18	25.	28	27	26	25	24	23	21	16	.328	.066	.1041E+06	N N
137	1G18	30.	32	31	30	29	28	27	25	21	.395	.079	.1041E+06	N N
138	1G18	35.	36	35	34	33	32	31	29	26	.452	.096	.1039E+06	N N
139	1G18	40.	40	39	38	37	36	35	33	31	.497	.112	.1038E+06	N N
140	1G18	50.	48	47	46	46	45	44	43	42	.505	.139	.1036E+06	N N
141	1G18	60.	57	56	55	54	54	53	52	52	.429	.158	.1034E+06	N N
142	1G18	90.	83	83	82	82	82	82	82	84	.170	.167	.1031E+06	N N
143	1G18	120.	111	111	111	111	112	112	113	115	.004	.134	.1032E+06	N N
144	1G18	150.	140	140	140	141	142	143	145	147	0	.057	.1037E+06	N N
145	1G28	20.	24	22	20	19	18	16	14	1	.489	.095	.1041E+06	N N G10
146	1G28	25.	28	26	24	22	21	19	17	6	.538	.107	.1038E+06	N N
147	1G28	30.	31	29	27	26	24	22	19	11	.630	.132	.1037E+06	N N
148	1G28	35.	35	32	31	29	28	26	23	16	.664	.144	.1036E+06	N N
149	1G28	40.	38	36	34	33	31	29	26	21	.731	.172	.1034E+06	8 N
150	1G28	50.	46	44	42	40	39	37	35	32	.740	.201	.1032E+06	568 N

RUN NO	KEY	INFLOW ANGLE	SAIL SET								LIFT COEFF	DRAG COEFF	REYNOLDS NUMBER	COMMENTS		
151	1G28	60.	53	51	50	48	47	45	43	43	.703	.241	.1029E+06	A	N	
152	1G28	90.	78	76	75	74	74	73	73	75	.489	.262	.1031E+06	123457	S	
153	1G28	120.	104	102	102	103	103	104	106	110	.316	.200	.1030E+06	12	N	
154	1G28	150.	131	131	132	134	136	138	141	146	.256	.094	.1036E+06	1	N	
155	1G38	20.	25	22	20	18	16	14	13	-10	.632	.138	.1037E+06	N	N	G15
156	1G38	25.	27	24	22	20	18	16	14	-5	.746	.170	.1035E+06	8	N	
157	1G38	30.	31	27	25	23	21	19	16	0	.823	.197	.1032E+06	8	N	
158	1G38	35.	34	31	28	26	24	22	18	5	.902	.229	.1035E+06	8	N	
159	1G38	40.	37	34	32	29	27	25	21	11	.950	.265	.1032E+06	148	N	
160	1G38	50.	44	41	38	36	34	31	27	21	.970	.370	.1026E+06	A	Y	
161	1G38	60.	51	48	45	43	41	39	35	32	.857	.443	.1021E+06	A	S	
162	1G38	90.	73	70	68	67	66	64	63	66	.528	.472	.1015E+06	A	Y	
163	1G38	120.	97	95	94	94	94	95	97	103	.319	.364	.1023E+06	A	S	
164	1G38	150.	123	121	123	125	128	131	136	144	.231	.193	.1034E+06	17	S	
165	1G48	20.	25	21	19	17	15	12	14	-21	.660	.178	.1040E+06	8	N	G20
166	1G48	25.	27	24	21	19	17	14	14	-16	.885	.242	.1037E+06	8	N	
167	1G48	30.	30	26	24	21	19	16	15	-11	.983	.278	.1032E+06	8	N	
168	1G48	35.	33	29	26	24	21	19	16	-6	1.025	.308	.1031E+06	2358	N	
169	1G48	40.	36	32	29	27	24	21	17	-1	1.105	.358	.1028E+06	1234568	N	
170	1G48	50.	42	38	35	33	30	27	22	9	1.160	.535	.1014E+06	A	S	
171	1G48	60.	49	45	42	39	36	33	28	20	1.016	.622	.1004E+06	A	S	
172	1G48	120.	91	87	86	85	85	85	86	94	.347	.535	.1009E+06	A	S	
173	1G48	150.	115	112	113	115	118	122	129	142	.200	.289	.1026E+06	1234567	S	
174	1G58	20.	25	21	18	16	14	11	16	-32	.625	.192	.1039E+06	8	N	G25
175	1G58	25.	27	23	20	18	15	13	16	-28	.814	.247	.1038E+06	8	N	
176	1G58	30.	30	26	23	20	17	14	16	-23	.984	.302	.1032E+06	8	N	
177	1G58	35.	33	28	25	22	19	16	16	-18	1.120	.371	.1026E+06	8	N	
178	1G58	40.	35	31	28	25	22	18	17	-14	1.185	.429	.1024E+06	1234568	S	
179	1G58	50.	41	36	33	30	27	23	19	-4	1.280	.667	.1003E+06	A	S	
180	1G58	60.	47	42	39	36	32	28	23	6	1.152	.796	.9928E+05	A	S	
181	1G58	90.	66	61	58	55	52	48	43	40	.747	.883	.9828E+05	A	S	
182	1G58	120.	86	81	78	76	75	74	73	82	.397	.738	.9963E+05	A	S	
183	1G58	150.	107	103	103	104	106	110	119	140	.168	.377	.1022E+06	A	S	
184	1G68	20.	25	21	18	15	13	10	16	-45	.658	.233	.1036E+06	8	N	G30
185	1G68	25.	27	23	19	17	14	11	17	-42	.827	.283	.1033E+06	8	N	
186	1G68	30.	30	25	22	19	16	13	18	-38	.978	.340	.1028E+06	8	N	
187	1G68	35.	32	27	24	21	18	15	18	-34	1.150	.423	.1023E+06	2348	N	
188	1G68	40.	35	30	26	23	20	16	18	-30	1.273	.523	.1015E+06	123458	S	
189	1G68	50.	40	35	31	28	24	20	19	-22	1.361	.785	.9930E+05	A	N	
190	1G68	60.	45	40	36	33	29	25	20	-14	1.236	.963	.9781E+05	A	S	
191	1G68	150.	100	94	92	91	92	94	103	142	.089	.478	.1011E+06	A	N	
192	1G78	20.	25	20	17	15	12	9	13	-61	.639	.254	.1032E+06	8	N	G35
193	1G78	25.	27	22	19	16	14	10	15	-60	.824	.316	.1027E+06	8	S	
194	1G78	30.	29	24	21	18	15	12	17	-58	.976	.375	.1024E+06	8	N	
195	1G78	90.	69	65	63	60	58	56	53	54	.646	.677	.9956E+05	A	S	
196	1L48	20.	28	24	20	16	12	8	4	0	.606	.133	.1042E+06		ERROR	
197	1L48	25.	28	24	20	16	12	8	4	0	.863	.217	.1035E+06		TEST	
198	1L48	30.	28	24	20	16	12	8	4	0	1.089	.328	.1029E+06			
199	1L48	35.	28	24	20	16	12	8	4	0	1.279	.500	.1016E+06			
200	1L48	40.	28	24	20	16	12	8	4	0	1.445	.703	.9996E+05			

1

RUN NO	KEY	INFLOW ANGLE	SAIL SET								LIFT COEFF	DRAG COEFF	REYNOLDS NUMBER	COMMENTS
201	1L48	50.	28	24	20	16	12	8	4	0	1.705	1.215	.9588E+05	
202	1L48	60.	28	24	20	16	12	8	4	0	1.271	1.360	.9490E+05	
203	1L48	90.	28	24	20	16	12	8	4	0	.482	1.898	.9075E+05	
204	1L48	120.	28	24	20	16	12	8	4	0	-.363	1.651	.9271E+05	
205	1L48	150.	28	24	20	16	12	8	4	0	-.558	.753	.9845E+05	
206	1L48	35.	28	24	20	16	12	8	4	0	1.305	.552	.2539E+05	RE NO
207	1L48	35.	28	24	20	16	12	8	4	0	1.292	.535	.5438E+05	TEST
208	1L48	35.	28	24	20	16	12	8	4	0	1.286	.511	.8370E+05	
209	1L48	35.	28	24	20	16	12	8	4	0	1.279	.497	.1134E+06	
210	1L48	35.	28	24	20	16	12	8	4	0	1.282	.499	.1427E+06	
211	1L48	35.	28	24	20	16	12	8	4	0	1.287	.503	.1730E+06	
212	1L48	35.	28	24	20	16	12	8	4	0	1.292	.505	.2037E+06	
213	1L48	35.	28	24	20	16	12	8	4	0	1.298	.509	.2353E+06	
214	1L48	35.	28	24	20	16	12	8	4	0	1.299	.514	.2492E+06	
215	1L48	20.	28	24	20	16	12	8	4	0	.623	.136	.1034E+06	N N L4,0 0018
216	1L48	25.	28	24	20	16	12	8	4	0	.880	.222	.1028E+06	N N
217	1L48	30.	28	24	20	16	12	8	4	0	1.112	.340	.1020E+06	1 N
218	1L48	35.	28	24	20	16	12	8	4	0	1.299	.510	.1010E+06	1234 S
219	1L48	40.	28	24	20	16	12	8	4	0	1.477	.720	.9921E+05	1234 S
220	1L48	50.	28	24	20	16	12	8	4	0	1.723	1.248	.9502E+05	1234 Y
221	1L48	60.	28	24	20	16	12	8	4	0	1.270	1.388	.9378E+05	1234 Y
222	1L48	90.	28	24	20	16	12	8	4	0	.487	1.914	.8982E+05	1234 B
223	1L48	120.	28	24	20	16	12	8	4	0	-.380	1.677	.9162E+05	12348 B
224	1L48	150.	28	24	20	16	12	8	4	0	-.558	.761	.9781E+05	12348 B
225	1L4S	20.	28	24	20	16	12	8	4	0	.589	.123	.1034E+06	N N L4,0 SMALL
226	1L4S	25.	28	24	20	16	12	8	4	0	.812	.196	.1030E+06	N N END
227	1L4S	30.	28	24	20	16	12	8	4	0	1.020	.300	.1023E+06	N N PLATE
228	1L4S	35.	28	24	20	16	12	8	4	0	1.178	.460	.1012E+06	1234 N
229	1L4S	40.	28	24	20	16	12	8	4	0	1.365	.693	.9928E+05	1234 S
230	1L4S	50.	28	24	20	16	12	8	4	0	1.677	1.213	.9546E+05	1234 S
231	1L4S	60.	28	24	20	16	12	8	4	0	1.376	1.468	.9366E+05	1234 Y
232	1L4S	90.	28	24	20	16	12	8	4	0	.522	2.078	.8979E+05	1234 B
233	1L4S	120.	28	24	20	16	12	8	4	0	-.427	1.807	.9149E+05	1234 B
234	1L4S	150.	28	24	20	16	12	8	4	0	-.630	.820	.9771E+05	1238 Y
235	1L4L	20.	28	24	20	16	12	8	4	0	.608	.123	.1048E+06	N N L4,0 LARGE
236	1L4L	25.	28	24	20	16	12	8	4	0	.845	.200	.1043E+06	N N END
237	1L4L	30.	28	24	20	16	12	8	4	0	1.050	.302	.1037E+06	1 N PLATE
238	1L4L	35.	28	24	20	16	12	8	4	0	1.198	.466	.1023E+06	1234 N
239	1L4L	40.	28	24	20	16	12	8	4	0	1.330	.670	.1010E+06	1234 S
240	1L4L	50.	28	24	20	16	12	8	4	0	1.570	1.140	.9699E+05	1234 S
241	1L4L	60.	28	24	20	16	12	8	4	0	1.347	1.428	.9495E+05	1234 B
242	1L4L	90.	28	24	20	16	12	8	4	0	.534	2.096	.9067E+05	1234 B
243	1L4L	120.	28	24	20	16	12	8	4	0	-.437	1.834	.9218E+05	1234 Y
244	1L4L	150.	28	24	20	16	12	8	4	0	-.611	.817	.9899E+05	1234 Y
245	1P1L	30.	10	10	10	10	10	10	10	10	.843	.375	.1013E+06	12 N 0018+PLATE
246	1P2L	30.	20	20	20	20	20	20	20	20	.584	.146	.1032E+06	12 N
247	1P3L	30.	30	30	30	30	30	30	30	30	.218	.065	.1037E+06	N N
248	1P5L	90.	50	50	50	50	50	50	50	50	.754	.952	.9714E+05	A Y
249	1P6L	90.	60	60	60	60	60	60	60	60	.650	.648	.9935E+05	A S
250	1P7L	90.	70	70	70	70	70	70	70	70	.580	.376	.1015E+06	A S

RUN NO	KEY	INFLOW ANGLE	SAIL SET								LIFT COEFF	DRAG COEFF	REYNOLDS NUMBER	COMMENTS
251	1P4L	90.	40	40	40	40	40	40	40	40	.835	1.317	.9443E+05	A Y 0018+PLATE
252	1P3L	90.	30	30	30	30	30	30	30	30	.808	1.660	.9220E+05	A S
253	1P1L	30.	10	10	10	10	10	10	10	10	.864	.389	.1013E+06	0018+PLATE
254	1P2L	30.	20	20	20	20	20	20	20	20	.597	.140	.1037E+06	
255	1P3L	30.	30	30	30	30	30	30	30	30	.231	.066	.1041E+06	
256	1P16	30.	10	10	10	10	10	10	-0	-0	.673	.292	.1022E+06	A S NACA0018
257	1PF6	30.	15	15	15	15	15	15	-0	-0	.585	.200	.1031E+06	12345 S
258	1P26	30.	20	20	20	20	20	20	-0	-0	.484	.128	.1034E+06	123 N
259	1P36	30.	30	30	30	30	30	30	-0	-0	.187	.053	.1038E+06	N N
260	1P56	90.	50	50	50	50	50	50	-0	-0	.538	.782	.9809E+05	A Y
261	1P66	90.	60	60	60	60	60	60	-0	-0	.478	.549	.1003E+06	A Y
262	1P46	90.	40	40	40	40	40	40	-0	-0	.558	.978	.9677E+05	A Y
263	1P36	90.	30	30	30	30	30	30	-0	-0	.521	1.187	.9532E+05	A Y
264	2P08	0	0	0	0	0	0	0	0	0	.014	.025	.1045E+06	N N P0 NACA
265	2P08	10.	0	0	0	0	0	0	0	0	.360	.071	.1041E+06	N N 6518
266	2P18	10.	10	10	10	10	10	10	10	10	.201	.048	.1044E+06	N N P10
267	2P18	20.	10	10	10	10	10	10	10	10	.657	.171	.1036E+06	1 N
268	2P18	30.	10	10	10	10	10	10	10	10	1.091	.493	.1013E+06	1 S
269	2P18	40.	10	10	10	10	10	10	10	10	1.391	.922	.9776E+05	1 Y
270	2P18	50.	10	10	10	10	10	10	10	10	1.063	1.061	.9694E+05	1 B
271	2P18	60.	10	10	10	10	10	10	10	10	.996	1.383	.9450E+05	1 B
272	2P28	20.	20	20	20	20	20	20	20	20	.343	.076	.1039E+06	12 N P20
273	2P28	30.	20	20	20	20	20	20	20	20	.801	.215	.1033E+06	A N
274	2P28	40.	20	20	20	20	20	20	20	20	1.229	.532	.1010E+06	1345678 N
275	2P28	50.	20	20	20	20	20	20	20	20	1.547	.958	.9762E+05	1 S
276	2P28	60.	20	20	20	20	20	20	20	20	1.282	1.179	.9573E+05	1 B
277	2P28	90.	20	20	20	20	20	20	20	20	.742	1.797	.9154E+05	12 B
278	2P38	30.	30	30	30	30	30	30	30	30	.457	.095	.1038E+06	A N P30
279	2P38	40.	30	30	30	30	30	30	30	30	.891	.250	.1030E+06	1345678 N
280	2P38	50.	30	30	30	30	30	30	30	30	1.243	.536	.1011E+06	145678 N
281	2P38	60.	30	30	30	30	30	30	30	30	1.474	.888	.9788E+05	1 S
282	2P38	90.	30	30	30	30	30	30	30	30	.965	1.561	.9331E+05	123 B
283	2P38	120.	30	30	30	30	30	30	30	30	.103	1.747	.9208E+05	A B
284	2P48	40.	40	40	40	40	40	40	40	40	.486	.107	.1035E+06	45678 N P40
285	2P48	50.	40	40	40	40	40	40	40	40	.873	.243	.1029E+06	1345678 N
286	2P48	60.	40	40	40	40	40	40	40	40	1.126	.478	.1011E+06	14678 N
287	2P48	90.	40	40	40	40	40	40	40	40	1.049	1.318	.9478E+05	A B
288	2P48	120.	40	40	40	40	40	40	40	40	.276	1.651	.9251E+05	A Y
289	2P48	150.	40	40	40	40	40	40	40	40	-.246	.984	.9646E+05	A Y
290	2P58	50.	50	50	50	50	50	50	50	50	.524	.127	.1033E+06	345678 N P50
291	2P58	60.	50	50	50	50	50	50	50	50	.829	.247	.1027E+06	45678 N
292	2P58	90.	50	50	50	50	50	50	50	50	1.082	1.012	.9687E+05	A Y
293	2P58	120.	50	50	50	50	50	50	50	50	.401	1.430	.9386E+05	A Y
294	2P58	150.	50	50	50	50	50	50	50	50	-.153	.979	.9646E+05	A B
295	2P58	180.	50	50	50	50	50	50	50	50	-.164	.194	.1024E+06	A B
296	2P68	60.	60	60	60	60	60	60	60	60	.395	.139	.1032E+06	45678 N P60
297	2P68	90.	60	60	60	60	60	60	60	60	1.022	.587	.1004E+06	1258 Y
298	2P68	120.	60	60	60	60	60	60	60	60	.520	1.207	.9539E+05	A Y
299	2P68	150.	60	60	60	60	60	60	60	60	-.050	.873	.9730E+05	A Y
300	2P68	180.	60	60	60	60	60	60	60	60	-.108	.203	.1024E+06	A Y

RUN NO	KEY	INFLOW ANGLE				SAIL SET					LIFT COEFF	DRAG COEFF	REYNOLDS NUMBER	COMMENTS
301	2P98	90.	90	90	90	90	90	90	90	90	.194	.165	.1030E+06	N N P90
302	2P98	120.	90	90	90	90	90	90	90	90	.644	.518	.1005E+06	A S
303	2P98	150.	90	90	90	90	90	90	90	90	.244	.678	.9883E+05	A S
304	2P98	180.	90	90	90	90	90	90	90	90	.029	.222	.1021E+06	A B
305	2P9L	90.	90	90	90	90	90	90	90	90	.234	.179	.1026E+06	A N 6518+PLATE
306	2P8L	90.	80	80	80	80	80	80	80	80	.566	.244	.1024E+06	2345678 N
307	2P7L	90.	70	70	70	70	70	70	70	70	.839	.399	.1013E+06	15678 S
308	2P6L	90.	60	60	60	60	60	60	60	60	1.023	.590	.9930E+05	1 S
309	2P5L	90.	50	50	50	50	50	50	50	50	1.094	.960	.9716E+05	A S
310	2P4L	90.	40	40	40	40	40	40	40	40	1.120	1.353	.9450E+05	A Y
311	2P3L	30.	30	30	30	30	30	30	30	30	.418	.092	.1033E+06	123 N
312	2P3L	30.	30	30	30	30	30	30	30	30	.423	.092	.1037E+06	123 N
313	2P2L	30.	20	20	20	20	20	20	20	20	.740	.198	.1031E+06	123 S
314	2P1L	30.	10	10	10	10	10	10	10	10	1.010	.449	.1011E+06	1 S
315	3P08	0	0	0	0	0	0	0	0	0	.052	.038	.1051E+06	1234567 N P0 TWO
316	3P08	10.	0	0	0	0	0	0	0	0	.421	.091	.1048E+06	1234567 N ARC
317	3P18	10.	10	10	10	10	10	10	10	10	.218	.076	.1051E+06	N N P10 FOIL
318	3P18	20.	10	10	10	10	10	10	10	10	.686	.189	.1047E+06	1 N
319	3P18	30.	10	10	10	10	10	10	10	10	1.144	.503	.1021E+06	12 S
320	3P18	40.	10	10	10	10	10	10	10	10	1.569	1.004	.9816E+05	1 Y
321	3P18	50.	10	10	10	10	10	10	10	10	1.134	1.112	.9721E+05	1 Y
322	3P18	60.	10	10	10	10	10	10	10	10	1.065	1.449	.9455E+05	1 Y
323	3P28	20.	20	20	20	20	20	20	20	20	.381	.117	.1047E+06	1 N P20
324	3P28	30.	20	20	20	20	20	20	20	20	.855	.256	.1039E+06	1 N
325	3P28	40.	20	20	20	20	20	20	20	20	1.276	.582	.1016E+06	A N
326	3P28	50.	20	20	20	20	20	20	20	20	1.631	1.048	.9766E+05	A Y
327	3P28	60.	20	20	20	20	20	20	20	20	1.247	1.208	.9651E+05	178 B
328	3P28	90.	20	20	20	20	20	20	20	20	.659	1.884	.9215E+05	1 B
329	3P38	30.	30	30	30	30	30	30	30	30	.451	.140	.1045E+06	1278 N P30
330	3P38	40.	30	30	30	30	30	30	30	30	.916	.283	.1038E+06	A S
331	3P38	50.	30	30	30	30	30	30	30	30	1.330	.612	.1011E+06	1345678 S
332	3P38	60.	30	30	30	30	30	30	30	30	1.580	.980	.9809E+05	1345678 S
333	3P38	90.	30	30	30	30	30	30	30	30	1.005	1.703	.9321E+05	1 S
334	3P38	120.	30	30	30	30	30	30	30	30	.011	1.828	.9245E+05	A Y
335	3P48	40.	40	40	40	40	40	40	40	40	.523	.160	.1044E+06	A N P40
336	3P48	50.	40	40	40	40	40	40	40	40	.978	.322	.1033E+06	A S
337	3P48	60.	40	40	40	40	40	40	40	40	1.341	.592	.1015E+06	145678 S
338	3P48	90.	40	40	40	40	40	40	40	40	1.274	1.435	.9514E+05	A Y
339	3P48	120.	40	40	40	40	40	40	40	40	.368	1.842	.9263E+05	A Y
340	3P48	150.	40	40	40	40	40	40	40	40	-.300	1.032	.9714E+05	A B
341	3P48	180.	40	40	40	40	40	40	40	40	-.261	.190	.1039E+06	A Y
342	3P58	50.	50	50	50	50	50	50	50	50	.561	.177	.1042E+06	A N P50
343	3P58	60.	50	50	50	50	50	50	50	50	.968	.331	.1032E+06	A N
344	3P58	90.	50	50	50	50	50	50	50	50	1.331	1.070	.9781E+05	1278 S
345	3P58	120.	50	50	50	50	50	50	50	50	.507	1.648	.9378E+05	A S
346	3P58	150.	50	50	50	50	50	50	50	50	-.117	1.112	.9697E+05	A B
347	3P58	180.	50	50	50	50	50	50	50	50	-.212	.210	.1035E+06	A S
348	3P68	60.	60	60	60	60	60	60	60	60	.497	.201	.1041E+06	A N
349	3P68	90.	60	60	60	60	60	60	60	60	1.236	.711	.1008E+06	18 S
350	3P68	120.	60	60	60	60	60	60	60	60	.629	1.349	.9551E+05	A Y

RUN NO	KEY	INFLOW ANGLE	SAIL SET								LIFT COEFF	DRAG COEFF	REYNOLDS NUMBER	COMMENTS
351	3P68	150.	60	60	60	60	60	60	60	60	.015	1.134	.9687E+05	A B
352	3P68	180.	60	60	60	60	60	60	60	60	-.154	.222	.1034E+06	A S
353	3P98	90.	90	90	90	90	90	90	90	90	.238	.234	.1036E+06	A S
354	3P98	120.	90	90	90	90	90	90	90	90	.967	.515	.1021E+06	15678 S
355	3P98	150.	90	90	90	90	90	90	90	90	.380	.768	.9939E+05	A S
356	3P98	180.	90	90	90	90	90	90	90	90	.006	.244	.1034E+06	A B
357	4P18	30.	10	10	10	10	10	10	10	10	.998	.396	.1014E+06	123 N P10 FLAT
358	4P18	30.	10	10	10	10	10	10	10	10	1.011	.401	.7171E+05	123 N THIN
359	4P28	30.	20	20	20	20	20	20	20	20	.584	.156	.7304E+05	12 N P20 FOIL
360	4P28	60.	20	20	20	20	20	20	20	20	1.201	1.120	.6804E+05	2345678 Y
361	4P38	30.	30	30	30	30	30	30	30	30	.144	.056	.7329E+05	N N P30
362	4P38	60.	30	30	30	30	30	30	30	30	1.404	.935	.6875E+05	2345678
363	4P48	60.	40	40	40	40	40	40	40	40	1.086	.524	.7119E+05	A N P40
364	4P48	90.	40	40	40	40	40	40	40	40	.998	1.408	.6661E+05	A Y
365	4P58	60.	50	50	50	50	50	50	50	50	.610	.227	.7272E+05	12345 N P50
366	4P58	90.	50	50	50	50	50	50	50	50	1.019	1.072	.6804E+05	2345678 N
367	4P58	150.	50	50	50	50	50	50	50	50	-.242	1.019	.6790E+05	A Y
368	4P68	90.	60	60	60	60	60	60	60	60	.902	.713	.6997E+05	2345678 S P60
369	4P68	150.	60	60	60	60	60	60	60	60	-.076	.914	.6848E+05	A S
370	4P98	150.	90	90	90	90	90	90	90	90	.297	.707	.6983E+05	A N P90
371	4P98	180.	90	90	90	90	90	90	90	90	.005	.223	.7210E+05	A Y
372	4P16	30.	10	10	10	10	10	10	-0	-0	.833	.315	.7255E+05	A N FLAT PLATE
373	4P26	30.	20	20	20	20	20	20	-0	-0	.551	.146	.7367E+05	123 N
374	4P36	30.	30	30	30	30	30	30	-0	-0	.145	.051	.7367E+05	N N
375	4P36	90.	30	30	30	30	30	30	-0	-0	.583	1.290	.6738E+05	A Y
376	4P46	90.	40	40	40	40	40	40	-0	-0	.686	1.049	.6858E+05	A Y
377	4P56	90.	50	50	50	50	50	50	-0	-0	.704	.824	.6997E+05	A Y
378	4P66	90.	60	60	60	60	60	60	-0	-0	.662	.597	.7129E+05	A S
379	5P18	0	10	10	10	10	10	10	10	10	-.096	.063	.1039E+06	N N 6PCNOPLATE
380	5P18	10.	10	10	10	10	10	10	10	10	.196	.071	.1039E+06	N N
381	5P18	20.	10	10	10	10	10	10	10	10	.686	.178	.1034E+06	1 N
382	5P28	20.	20	20	20	20	20	20	20	20	.297	.080	.1037E+06	N N
383	5P28	30.	20	20	20	20	20	20	20	20	.825	.210	.1032E+06	1 N
384	5P28	40.	20	20	20	20	20	20	20	20	1.341	.534	.1007E+06	1 N
385	5P28	50.	20	20	20	20	20	20	20	20	1.732	1.024	.9685E+05	1 S
386	5P28	60.	20	20	20	20	20	20	20	20	1.358	1.212	.9529E+05	1 Y
387	5P28	90.	20	20	20	20	20	20	20	20	.695	1.904	.9062E+05	A B
388	5P38	30.	30	30	30	30	30	30	30	30	.423	.099	.1036E+06	N N
389	5P38	40.	30	30	30	30	30	30	30	30	.961	.250	.1028E+06	1 N
390	5P38	50.	30	30	30	30	30	30	30	30	1.401	.582	.1004E+06	1 S
391	5P38	60.	30	30	30	30	30	30	30	30	1.698	1.018	.9699E+05	1 S
392	5P38	90.	30	30	30	30	30	30	30	30	.970	1.712	.9185E+05	A B
393	5P38	120.	30	30	30	30	30	30	30	30	-.023	1.836	.9146E+05	A B
394	5P48	40.	40	40	40	40	40	40	40	40	.479	.115	.1035E+06	1 N
395	5P48	50.	40	40	40	40	40	40	40	40	.991	.277	.1027E+06	1 N
396	5P48	60.	40	40	40	40	40	40	40	40	1.371	.573	.1004E+06	1 N
397	5P48	90.	40	40	40	40	40	40	40	40	1.232	1.514	.9351E+05	A Y
398	5P48	120.	40	40	40	40	40	40	40	40	.305	1.890	.9123E+05	A B
399	5P48	150.	40	40	40	40	40	40	40	40	-.303	1.035	.9588E+05	A B
400	5P58	50.	50	50	50	50	50	50	50	50	.520	.135	.1034E+06	N N

1

RUN NO	KEY	INFLOW ANGLE	SAIL SET								LIFT COEFF	DRAG COEFF	REYNOLDS NUMBER	COMMENTS			
401	5P58	60.	50	50	50	50	50	50	50	50	.961	.284	.1026E+06	1	N		
402	5P58	90.	50	50	50	50	50	50	50	50	1.387	1.249	.9546E+05	A	S		
403	5P58	120.	50	50	50	50	50	50	50	50	.619	1.885	.9129E+05	A	Y		
404	5P58	150.	50	50	50	50	50	50	50	50	-.155	1.159	.9539E+05	A	B		
405	5P68	60.	60	60	60	60	60	60	60	60	.413	.156	.1031E+06	N	N		
406	5P68	90.	60	60	60	60	60	60	60	60	1.297	.847	.9845E+05	A	Y		
407	5P68	120.	60	60	60	60	60	60	60	60	.747	1.472	.9378E+05	A	Y		
408	5P68	150.	60	60	60	60	60	60	60	60	.033	1.211	.9549E+05	A	B		
409	5P18	30.	10	10	10	10	10	10	10	10	1.221	.516	.1010E+06	1	S		
410	5P18	40.	10	10	10	10	10	10	10	10	1.644	1.019	.9706E+05	1	S		
411	5P18	50.	10	10	10	10	10	10	10	10	1.133	1.093	.9644E+05	1	B		
412	5P98	90.	90	90	90	90	90	90	90	90	.200	.203	.1029E+06	N	N		
413	5P98	180.	90	90	90	90	90	90	90	90	.008	.248	.1025E+06	A	B		
414	6P18	0	10	10	10	10	10	10	10	10	-.012	.079	.1038E+06	(A)R	N	P10	12PC
415	6P18	10.	10	10	10	10	10	10	10	10	.265	.090	.1041E+06	1	N		THIN
416	6P18	20.	10	10	10	10	10	10	10	10	.772	.218	.1037E+06	1	N		PLATE
417	6P18	30.	10	10	10	10	10	10	10	10	1.284	.562	.1009E+06	1	N		
418	6P18	40.	10	10	10	10	10	10	10	10	1.686	1.074	.9661E+05	1	Y		
419	6P28	20.	20	20	20	20	20	20	20	20	.375	.108	.1038E+06	1	N	P20	
420	6P28	30.	20	20	20	20	20	20	20	20	.927	.266	.1031E+06	1	N		
421	6P28	40.	20	20	20	20	20	20	20	20	1.442	.635	.1005E+06	1	S		
422	6P28	50.	20	20	20	20	20	20	20	20	1.815	1.147	.9641E+05	1	S		
423	6P28	60.	20	20	20	20	20	20	20	20	1.368	1.312	.9509E+05	1	B		
424	6P38	30.	30	30	30	30	30	30	30	30	.495	.130	.1036E+06	1	N	P30	
425	6P38	40.	30	30	30	30	30	30	30	30	1.049	.310	.1026E+06	1	N		
426	6P38	50.	30	30	30	30	30	30	30	30	1.515	.689	.9970E+05	1	S		
427	6P38	60.	30	30	30	30	30	30	30	30	1.824	1.145	.9641E+05	1	Y		
428	6P38	90.	30	30	30	30	30	30	30	30	1.012	1.803	.9187E+05	A	B		
429	6P48	40.	40	40	40	40	40	40	40	40	.569	.154	.1034E+06	N	N	P40	
430	6P48	50.	40	40	40	40	40	40	40	40	1.096	.348	.1023E+06	N	N		
431	6P48	60.	40	40	40	40	40	40	40	40	1.524	.683	.9984E+05	178	S		
432	6P48	90.	40	40	40	40	40	40	40	40	1.342	1.578	.9323E+05	A	Y		
433	6P48	120.	40	40	40	40	40	40	40	40	.377	1.985	.9093E+05	A	Y		
434	6P58	50.	50	50	50	50	50	50	50	50	.645	.179	.1032E+06	N	N	P50	
435	6P58	60.	50	50	50	50	50	50	50	50	1.132	.372	.1022E+06	2345678	N		
436	6P58	90.	50	50	50	50	50	50	50	50	1.589	1.353	.9465E+05	A	S		
437	6P58	90.	50	50	50	50	50	50	50	50	1.565	1.300	.9514E+05				
438	6P58	120.	50	50	50	50	50	50	50	50	.718	2.000	.9067E+05	A	B		
439	6P58	120.	50	50	50	50	50	50	50	50	.754	1.976	.9093E+05				
440	6P58	120.	50	50	50	50	50	50	50	50	.752	2.002	.9067E+05				
441	6P58	150.	50	50	50	50	50	50	50	50	-.095	1.155	.9563E+05	A	B		
442	6P68	60.	60	60	60	60	60	60	60	60	.565	.209	.1032E+06	N	N	P60	
443	6P68	90.	60	60	60	60	60	60	60	60	1.559	.936	.9824E+05	A	Y		
444	6P68	120.	60	60	60	60	60	60	60	60	.834	1.602	.9318E+05	A	Y		
445	6P68	120.	60	60	60	60	60	60	60	60	.839	1.603	.9301E+05				
446	6P68	150.	60	60	60	60	60	60	60	60	.071	1.212	.9558E+05	A	B		
447	6P68	180.	60	60	60	60	60	60	60	60	-.154	.236	.1023E+06	A	B		
448	6P78	90.	70	70	70	70	70	70	70	70	1.328	.603	.9951E+05	1	S		
449	6P78	120.	70	70	70	70	70	70	70	70	.971	1.294	.9519E+05	A	Y		
450	6P98	90.	90	90	90	90	90	90	90	90	.357	.238	.1028E+06	N	N	P90	

RUN NO	KEY	INFLOW ANGLE				SAIL SET					LIFT COEFF	DRAG COEFF	REYNOLDS NUMBER	COMMENTS
451	6P98	120.	90	90	90	90	90	90	90	90	1.192	.757	.9925E+05	A S
452	6P98	150.	90	90	90	90	90	90	90	90	.530	.963	.9709E+05	A S
453	6P98	180.	90	90	90	90	90	90	90	90	-.001	.256	.1022E+06	A B
454	6P1A	30.	10	-0	10	-0	10	-0	10	-0	.850	.284	.1018E+06	13 N P10 12PC
455	6P2A	30.	20	-0	20	-0	20	-0	20	-0	.686	.146	.1027E+06	3 N THIN
456	6P3A	30.	30	-0	30	-0	30	-0	30	-0	.270	.073	.1028E+06	N N FOIL AT
457	6P4A	90.	40	-0	40	-0	40	-0	40	-0	.496	.786	.9754E+05	A Y 1,3,5,7
458	6P5A	90.	50	-0	50	-0	50	-0	50	-0	.556	.655	.9862E+05	A Y ONLY
459	6P6A	90.	60	-0	60	-0	60	-0	60	-0	.649	.519	.9998E+05	A Y
460	6P7A	90.	70	-0	70	-0	70	-0	70	-0	.706	.381	.1010E+06	1 S
461	6P8A	90.	80	-0	80	-0	80	-0	80	-0	.555	.258	.1019E+06	N S
462	6P1L	30.	10	10	10	10	10	10	10	10	1.067	.495	.9963E+05	1 N 12PC
463	6P2L	30.	20	20	20	20	20	20	20	20	.788	.236	.1016E+06	1 N THIN
464	6P3L	30.	30	30	30	30	30	30	30	30	.388	.122	.1025E+06	N N FOIL,
465	6P6L	90.	60	60	60	60	60	60	60	60	1.421	.875	.9742E+05	1 Y LARGE
466	6P5L	90.	50	50	50	50	50	50	50	50	1.426	1.234	.9455E+05	12345 Y END
467	6P7L	90.	70	70	70	70	70	70	70	70	1.285	.577	.9961E+05	1 S PLATE
468	6G08	20.	41	36	33	30	27	24	19	5	.460	.161	.1041E+06	(1234567)R N G0 12PC
469	6G18	20.	42	37	33	29	26	22	17	-5	.596	.205	.1039E+06	(123456)R N G5
470	6G28	20.	43	37	33	29	25	21	17	-17	.582	.241	.1036E+06	345678 S G10
471	6G38	20.	44	37	32	28	24	20	19	-29	.392	.235	.1035E+06	345678,(123456)R S G15
472	6G08	30.	49	44	41	38	35	31	27	14	.560	.183	.1040E+06	2345678,(123456)R N G0
473	6G18	30.	49	43	40	36	33	28	22	3	.810	.264	.1032E+06	234568,(1234)R N G5
474	6G28	30.	50	43	39	35	31	26	21	-10	.922	.317	.1032E+06	568,(1234)R N G10
475	6G38	30.	50	43	38	34	29	24	21	-25	.734	.314	.1030E+06	5678,(1234)R N G15
476	6G08	40.	56	51	48	45	42	39	34	24	.729	.223	.1036E+06	(1234)R N G0
477	6G18	40.	56	50	46	43	39	35	29	12	.930	.301	.1031E+06	(123)R N G5
478	6G28	40.	56	50	45	41	37	32	25	-3	1.121	.392	.1024E+06	8,(123)R N G10
479	6G08	50.	64	59	56	53	50	47	42	33	.886	.279	.1030E+06	2345678,(1234)R N G0
480	6G18	50.	63	57	53	50	46	42	35	20	1.090	.334	.1028E+06	2345678,(1234)R N G5
481	6G28	50.	63	56	51	47	43	38	30	4	1.298	.446	.1022E+06	1238,(12)R N G10
482	6G08	60.	71	67	64	61	58	55	51	43	.841	.266	.1032E+06	1234567,(123)R N G0
483	6G18	60.	70	64	60	57	53	49	43	30	1.166	.373	.1026E+06	12348,(12)R N G5
484	6G28	60.	69	62	58	53	49	44	35	12	1.389	.513	.1015E+06	1238,(1)R
485	6G08	90.	95	90	88	86	84	82	79	76	.645	.321	.1024E+06	1235678,(1)R S G0
486	6G18	90.	92	86	82	79	76	73	68	60	1.073	.487	.1014E+06	13568,(1)R S G5
487	6G28	90.	89	82	78	73	69	64	55	33	1.307	.732	.9972E+05	235678,(1)R S G10
488	6L28	0	14	12	10	8	6	4	2	0	.049	.066	.1039E+06	1234,(1234567)R N L2,
489	6L28	0	14	12	10	8	6	4	2	0	.048	.066	.1040E+06	1234,(1234567)R N
490	6L28	10.	14	12	10	8	6	4	2	0	.401	.111	.1039E+06	123,(12345)R N
491	6L28	20.	14	12	10	8	6	4	2	0	.949	.267	.1029E+06	1,(2345)R N
492	6L28	30.	14	12	10	8	6	4	2	0	1.445	.621	.1004E+06	1 S
493	6L28	40.	14	12	10	8	6	4	2	0	1.838	1.136	.9617E+05	1 Y
494	6L28	50.	14	12	10	8	6	4	2	0	1.181	1.211	.9544E+05	1 B
495	6L28	20.	21	19	17	15	13	11	9	7	.791	.205	.1031E+06	1,(23456)R N L2,7
496	6L28	30.	21	19	17	15	13	11	9	7	1.374	.461	.1016E+06	1234 N
497	6L28	40.	21	19	17	15	13	11	9	7	1.812	.921	.9814E+05	1 N
498	6L28	50.	21	19	17	15	13	11	9	7	1.994	1.479	.9383E+05	134 Y
499	6L28	60.	21	19	17	15	13	11	9	7	1.239	1.464	.9366E+05	1 B
500	6L28	20.	28	26	24	22	20	18	16	14	.468	.127	.1035E+06	1,(123456)R N L2,14

RUN NO	KEY	INFLOW ANGLE	SAIL SET								LIFT COEFF	DRAG COEFF	REYNOLDS NUMBER	COMMENTS
501	6L28	30.	28	26	24	22	20	18	16	14	1.054	.280	.1028E+06	12 N
502	6L28	40.	28	26	24	22	20	18	16	14	1.571	.607	.1005E+06	134567 S
503	6L28	50.	28	26	24	22	20	18	16	14	2.016	1.124	.9658E+05	1567 S
504	6L28	60.	28	26	24	22	20	18	16	14	1.904	1.532	.9321E+05	1 B
505	6L28	90.	28	26	24	22	20	18	16	14	.738	1.976	.9005E+05	1 B
506	6L28	40.	42	40	38	36	34	32	30	28	1.000	.247	.1025E+06	12378,(2)R N L2,28
507	6L28	50.	42	40	38	36	34	32	30	28	1.518	.514	.1011E+06	2345678 N
508	6L28	60.	42	40	38	36	34	32	30	28	1.853	.906	.9807E+05	18 S
509	6L28	90.	42	40	38	36	34	32	30	28	1.270	1.788	.9126E+05	A B
510	6L28	60.	56	54	52	50	48	46	44	42	1.325	.428	.1018E+06	123678 N L2,42
511	6L28	90.	56	54	52	50	48	46	44	42	1.670	1.484	.9371E+05	A B
512	6L28	120.	56	54	52	50	48	46	44	42	.665	1.967	.9041E+05	A S
513	6L28	150.	56	54	52	50	48	46	44	42	-.098	1.130	.9546E+05	A Y
514	6L28	90.	70	68	66	64	62	60	58	56	1.608	.861	.9859E+05	145678 S L2,56
515	6L28	120.	70	68	66	64	62	60	58	56	.885	1.524	.9341E+05	A S
516	6L28	150.	70	68	66	64	62	60	58	56	.152	1.258	.9490E+05	A Y
517	6L28	180.	70	68	66	64	62	60	58	56	-.165	.270	.1018E+06	A B
518	6P16	30.	10	10	10	10	10	10	-0	-0	1.123	.427	.1014E+06	12 N 12PC 60NLY
519	6P26	30.	20	20	20	20	20	20	-0	-0	.827	.208	.1033E+06	12345 N
520	6P36	30.	30	30	30	30	30	30	-0	-0	.357	.099	.1039E+06	A N
521	6P36	60.	30	30	30	30	30	30	-0	-0	1.494	.851	.9812E+05	1 S
522	6P46	60.	40	40	40	40	40	40	-0	-0	1.317	.539	.1009E+06	16 N
523	6P56	60.	50	50	50	50	50	50	-0	-0	.980	.301	.1026E+06	456 N
524	6P56	90.	50	50	50	50	50	50	-0	-0	.969	.977	.9699E+05	A Y
525	6P66	90.	60	60	60	60	60	60	-0	-0	1.064	.760	.9909E+05	A S
526	6P76	90.	70	70	70	70	70	70	-0	-0	1.052	.501	.1011E+06	1 S
527	6P86	90.	80	80	80	80	80	80	-0	-0	.803	.329	.1025E+06	56 N
528	6P86	150.	80	80	80	80	80	80	-0	-0	.265	.926	.9726E+05	A Y
529	6P76	150.	70	70	70	70	70	70	-0	-0	.125	1.005	.9639E+05	A Y
530	6P96	150.	90	90	90	90	90	90	-0	-0	.398	.818	.9785E+05	A Y
531	6P08	0	0	0	0	0	0	0	0	0	.077	.054	.1028E+06	1234567,(A)R N P0 12PC
532	6P08	10.	0	0	0	0	0	0	0	0	.477	.116	.1028E+06	1234567,(24567)R N
533	6P08	20.	0	0	0	0	0	0	0	0	.996	.375	.1013E+06	A,(246)R S P0
534	6P08	30.	0	0	0	0	0	0	0	0	1.486	.844	.9730E+05	A,(123456)R Y P0
535	6P18	0	10	10	10	10	10	10	10	10	-.022	.072	.1025E+06	345678,(A)R S
536	6P18	10.	10	10	10	10	10	10	10	10	.260	.085	.1029E+06	1,(23467)R N
537	6P18	20.	10	10	10	10	10	10	10	10	.771	.213	.1024E+06	1,(34567)R N
538	6P18	30.	10	10	10	10	10	10	10	10	1.292	.553	.9977E+05	1,(4567)R S P10
539	6P18	40.	10	10	10	10	10	10	10	10	1.702	1.076	.9566E+05	1 Y P10
540	6P18	50.	10	10	10	10	10	10	10	10	1.196	1.173	.9436E+05	1 B
541	6P18	60.	10	10	10	10	10	10	10	10	1.126	1.497	.9235E+05	1 B
542	6P18	90.	10	10	10	10	10	10	10	10	.308	2.038	.8885E+05	1,(12345)R B
543	6P28	20.	20	20	20	20	20	20	20	20	.395	.111	.1025E+06	(2345678)R N
544	6P28	30.	20	20	20	20	20	20	20	20	.966	.280	.1018E+06	1,(467)R S
545	6P28	40.	20	20	20	20	20	20	20	20	1.463	.655	.9918E+05	1 Y
546	6P28	50.	20	20	20	20	20	20	20	20	1.842	1.168	.9500E+05	1 Y
547	6P28	60.	20	20	20	20	20	20	20	20	1.364	1.306	.9368E+05	1 B
548	6P28	90.	20	20	20	20	20	20	20	20	.661	1.947	.8966E+05	1,(12345)R B
549	6P28	10.	20	20	20	20	20	20	20	20	-.012	.092	.1027E+06	(A)R S
550	6P38	20.	30	30	30	30	30	30	30	30	.011	.095	.1024E+06	(A)R, N

RUN NO	KEY	INFLOW ANGLE	SAIL SET								LIFT COEFF	DRAG COEFF	REYNOLDS NUMBER	COMMENTS
551	6P38	30.	30	30	30	30	30	30	30	30	.481	.125	.1024E+06	(A)R N
552	6P38	40.	30	30	30	30	30	30	30	30	1.084	.313	.1015E+06	234567,(4678)R S
553	6P38	50.	30	30	30	30	30	30	30	30	1.541	.678	.9873E+05	1 Y
554	6P38	60.	30	30	30	30	30	30	30	30	1.823	1.118	.9524E+05	1 Y
555	6P38	90.	30	30	30	30	30	30	30	30	1.017	1.778	.9088E+05	1,(1)R Y
556	6P38	120.	30	30	30	30	30	30	30	30	-.026	1.918	.9002E+05	A,(A)R B
557	6P48	30.	40	40	40	40	40	40	40	40	.073	.110	.1026E+06	2345678,(A(R NN
558	6P48	40.	40	40	40	40	40	40	40	40	.564	.148	.1024E+06	8,(14568)R N
559	6P48	50.	40	40	40	40	40	40	40	40	1.146	.365	.1011E+06	N S
560	6P48	60.	40	40	40	40	40	40	40	40	1.557	.699	.9862E+05	1 Y
561	6P48	90.	40	40	40	40	40	40	40	40	1.319	1.591	.9205E+05	A B
562	6P48	120.	40	40	40	40	40	40	40	40	.342	2.008	.8956E+05	A,(1234)R B
563	6P58	50.	50	50	50	50	50	50	50	50	.635	.172	.1021E+06	(5678)R N
564	6P58	60.	50	50	50	50	50	50	50	50	1.155	.372	.1011E+06	N S
565	6P58	90.	50	50	50	50	50	50	50	50	1.527	1.310	.9408E+05	A Y
566	REDO	120.	50	50	50	50	50	50	50	50	.001	.002	.3058E+077	A B
567	6P58	150.	50	50	50	50	50	50	50	50	-.106	1.159	.9463E+05	A,(A)R B
568	6P58	180.	50	50	50	50	50	50	50	50	-.220	.228	.1011E+06	A,(A) Y
569	6P68	60.	60	60	60	60	60	60	60	60	.597	.211	.1021E+06	(45678)R N
570	6P68	90.	60	60	60	60	60	60	60	60	1.563	.961	.9690E+05	1 Y
571	6P68	120.	60	60	60	60	60	60	60	60	.820	1.653	.9169E+05	A B
572	6P68	150.	60	60	60	60	60	60	60	60	.050	1.222	.9411E+05	A,(8)R B
573	6P68	180.	60	60	60	60	60	60	60	60	-.159	.233	.1012E+06	A,(A)R B
574	6P98	90.	90	90	90	90	90	90	90	90	.397	.245	.1018E+06	(A)R S
575	6P98	120.	90	90	90	90	90	90	90	90	1.166	.770	.9847E+05	A Y
576	6P98	150.	90	90	90	90	90	90	90	90	.505	.956	.9622E+05	A S
577	6P98	180.	90	90	90	90	90	90	90	90	-.005	.240	.1017E+06	A,(A)R B
578	6P0F	0	0	0	0	0	0	0	0	0	.059	.054	.1025E+06	1,(135678)R N 15H*
579	6P0F	10.	0	0	0	0	0	0	0	0	.438	.115	.1029E+06	3457 N
580	6P0F	20.	0	0	0	0	0	0	0	0	.894	.361	.1015E+06	A,(34567)R S
581	6P0F	30.	0	0	0	0	0	0	0	0	1.326	.772	.9809E+05	A,(367)R B
582	6P0F	31.	0	0	0	0	0	0	0	0	1.307	.815	.9766E+05	A,(3467)R B
583	6P1F	0	10	10	10	10	10	10	10	10	-.031	.074	.1029E+06	1,(A)R S
584	6P1F	10.	10	10	10	10	10	10	10	10	.249	.092	.1032E+06	(234567)R N
585	6P1F	20.	10	10	10	10	10	10	10	10	.721	.210	.1027E+06	(234567)R N
586	6P1F	30.	10	10	10	10	10	10	10	10	1.147	.506	.1005E+06	12,(45678)R S
587	6P1F	40.	10	10	10	10	10	10	10	10	1.401	.915	.9723E+05	1,(457)R B
588	6P2F	20.	20	20	20	20	20	20	20	20	.357	.118	.1029E+06	(2345678)R N
589	6P2F	30.	20	20	20	20	20	20	20	20	.866	.262	.1023E+06	(45678)R N
590	6P2F	40.	20	20	20	20	20	20	20	20	1.298	.582	.1000E+06	1,(78)R S
591	6P2F	50.	20	20	20	20	20	20	20	20	1.569	1.024	.9644E+05	1 Y
592	6P3F	30.	30	30	30	30	30	30	30	30	.439	.138	.1026E+06	(2345678)R N
593	6P3F	31.	30	30	30	30	30	30	30	30	.478	.147	.1026E+06	(2345678)R N
594	6P3F	40.	30	30	30	30	30	30	30	30	.969	.293	.1020E+06	(78)R N
595	6P3F	50.	30	30	30	30	30	30	30	30	1.394	.618	.9968E+05	1(8)R S
596	6P3F	60.	30	30	30	30	30	30	30	30	1.557	1.003	.9651E+05	1 Y
597	6P3F	61.	30	30	30	30	30	30	30	30	1.553	1.031	.9617E+05	1 Y
598	6P3F	90.	30	30	30	30	30	30	30	30	.949	1.541	.9228E+05	A,(1)R B
599	6P4F	40.	40	40	40	40	40	40	40	40	.513	.171	.1024E+06	(2345678)R S
600	6P4F	50.	40	40	40	40	40	40	40	40	1.022	.324	.1017E+06	(78)R N

1

RUN NO	KEY	INFLOW ANGLE	SAIL SET								LIFT COEFF	DRAG COEFF	REYNOLDS NUMBER	COMMENTS
601	6P4F	60.	40	40	40	40	40	40	40	40	1.370	.616	.9961E+05	1 Y
602	6P4F	90.	40	40	40	40	40	40	40	40	1.171	1.372	.9363E+05	A Y
603	6P5F	50.	50	50	50	50	50	50	50	50	.576	.209	.1022E+06	(2345678)R N
604	6P5F	60.	50	50	50	50	50	50	50	50	1.041	.374	.1013E+06	N N
605	6P5F	90.	50	50	50	50	50	50	50	50	1.365	1.204	.9485E+05	A Y
606	6P5F	120.	50	50	50	50	50	50	50	50	.579	1.635	.9182E+05	A,(78)R B
607	6P6F	60.	60	60	60	60	60	60	60	60	.515	.243	.1021E+06	(345678) S
608	6P6F	61.	60	60	60	60	60	60	60	60	.507	.260	.1020E+06	8,(4578)R B
609	6P6F	90.	60	60	60	60	60	60	60	60	1.313	.851	.9783E+05	A Y
610	6P6F	119.	60	60	60	60	60	60	60	60	.746	1.370	.9371E+05	A Y P60
611	6P6F	120.	60	60	60	60	60	60	60	60	.727	1.389	.9341E+05	A Y
612	6P6F	149.	60	60	60	60	60	60	60	60	.079	1.194	.9463E+05	A,(78)R B
613	6P6F	150.	60	60	60	60	60	60	60	60	.066	1.159	.9487E+05	A,(78)R B
614	6P6F	180.	60	60	60	60	60	60	60	60	-.140	.232	.1016E+06	A,(A)R Y
615	6P6F	60.	60	60	60	60	60	60	60	60	.492	.240	.1020E+06	8,(345678)R Y
616	6P6F	61.	60	60	60	60	60	60	60	60	.547	.248	.1022E+06	8,(345678)R Y
617	6P9F	90.	90	90	90	90	90	90	90	90	.213	.291	.1017E+06	(8)R Y
618	6P9F	119.	90	90	90	90	90	90	90	90	.963	.699	.9831E+05	A Y
619	6P9F	120.	90	90	90	90	90	90	90	90	.942	.710	.9892E+05	A Y
620	6P9F	149.	90	90	90	90	90	90	90	90	.446	.858	.9733E+05	A Y
621	6P9F	150.	90	90	90	90	90	90	90	90	.428	.848	.9735E+05	A Y
622	6P9F	180.	90	90	90	90	90	90	90	90	.009	.234	.1021E+06	A B
623	6P0T	0	0	0	0	0	0	0	0	0	.036	.054	.1037E+06	1,(136)R N 30H
624	6P1T	0	10	10	10	10	10	10	10	10	-.049	.079	.1036E+06	(A)R S
625	6P1T	10.	10	10	10	10	10	10	10	10	.143	.084	.1035E+06	(4689R N
626	6P1T	20.	10	10	10	10	10	10	10	10	.499	.164	.1030E+06	(2345678)R N
627	6P1T	30.	10	10	10	10	10	10	10	10	.871	.394	.1017E+06	1,(345678)R S
628	6P1T	40.	10	10	10	10	10	10	10	10	1.015	.675	.9939E+05	1,(4678)R B
629	6P2T	20.	20	20	20	20	20	20	20	20	.229	.113	.1033E+06	(A)R N
630	6P2T	30.	20	20	20	20	20	20	20	20	.633	.212	.1029E+06	(34678)R N
631	6P2T	40.	20	20	20	20	20	20	20	20	.983	.445	.1013E+06	1,(678)R S
632	6P2T	50.	20	20	20	20	20	20	20	20	1.127	.742	.9895E+05	1,(8)R B
633	6P3T	30.	30	30	30	30	30	30	30	30	.298	.138	.1030E+06	(A)R N
634	6P3T	34.	30	30	30	30	30	30	30	30	.468	.168	.1028E+06	(2345678)R N
635	6P3T	40.	30	30	30	30	30	30	30	30	.697	.240	.1029E+06	(345678)R N
636	6P3T	50.	30	30	30	30	30	30	30	30	1.037	.459	.1011E+06	1,(78)R S
637	6P3T	60.	30	30	30	30	30	30	30	30	1.190	.738	.9892E+05	1 Y
638	6P3T	63.	30	30	30	30	30	30	30	30	1.099	.787	.9850E+05	1 B
639	6P3T	90.	30	30	30	30	30	30	30	30	.726	1.192	.9468E+05	A,(12)R B
640	6P4T	40.	40	40	40	40	40	40	40	40	.341	.175	.1027E+06	(A)R S
641	6P4T	50.	40	40	40	40	40	40	40	40	.725	.273	.1025E+06	(678)R N
642	6P4T	60.	40	40	40	40	40	40	40	40	1.001	.460	.1012E+06	1 S
643	6P4T	90.	40	40	40	40	40	40	40	40	.931	1.082	.9624E+05	A B
644	6P5T	50.	50	50	50	50	50	50	50	50	.359	.213	.1024E+06	A S
645	6P5T	60.	50	50	50	50	50	50	50	50	.650	.292	.1022E+06	(78)R S
646	6P5T	90.	50	50	50	50	50	50	50	50	1.023	.916	.9750E+05	A Y
647	6P6T	60.	60	60	60	60	60	60	60	60	.376	.243	.1022E+06	(A)R S
648	6P6T	63.	60	60	60	60	60	60	60	60	.447	.252	.1023E+06	(2345678)R S
649	6P6T	90.	60	60	60	60	60	60	60	60	.965	.682	.9925E+05	123456 B
650	6P6T	117.	60	60	60	60	60	60	60	60	.723	1.176	.9509E+05	A B

RUN NO	KEY	INFLOW ANGLE	SAIL SET								LIFT COEFF	DRAG COEFF	REYNOLDS NUMBER	COMMENTS
651	6P6T	120.	60	60	60	60	60	60	60	60	.715	1.239	.9443E+05	A B
652	6P6T	146.	60	60	60	60	60	60	60	60	.167	1.129	.9532E+05	A,(8)R B
653	6P6T	150.	60	60	60	60	60	60	60	60	.093	1.029	.9600E+05	A,(8)R B
654	6P6T	180.	60	60	60	60	60	60	60	60	-.118	.228	.1021E+06	A Y
655	6P9T	90.	90	90	90	90	90	90	90	90	.108	.282	.1017E+06	(45678)R Y
656	6P9T	117.	90	90	90	90	90	90	90	90	.717	.553	.1001E+06	A Y
657	6P9T	120.	90	90	90	90	90	90	90	90	.742	.606	.9951E+05	A Y
658	6P9T	146.	90	90	90	90	90	90	90	90	.434	.759	.9785E+05	A Y
659	6P9T	150.	90	90	90	90	90	90	90	90	.357	.729	.9795E+05	A Y
660	6P9T	180.	90	90	90	90	90	90	90	90	.015	.220	.1018E+06	A Y
661	6P04	30.	0	0	0	0	-0	-0	-0	-0	.537	.323	.1012E+06	A,(234)R Y REEFED
662	6P04	30.	0	0	0	0	-0	-0	-0	-0	.547	.326	.1014E+06	A,(234)R Y
663	6P04	30.	0	0	0	0	-0	-0	-0	-0	.535	.326	.1015E+06	A,(234)R Y
664	6P14	30.	10	10	10	10	-0	-0	-0	-0	.767	.321	.1019E+06	1 S
665	6P24	30.	20	20	20	20	-0	-0	-0	-0	.634	.163	.1027E+06	(3)R S
666	6P34	30.	30	30	30	30	-0	-0	-0	-0	.320	.079	.1038E+06	(234)R S
667	6P44	90.	40	40	40	40	-0	-0	-0	-0	.552	.733	.9850E+05	A Y
668	6P54	90.	50	50	50	50	-0	-0	-0	-0	.641	.628	.9930E+05	A Y
669	6P64	90.	60	60	60	60	-0	-0	-0	-0	.684	.497	.1005E+06	A Y
670	6P74	90.	70	70	70	70	-0	-0	-0	-0	.709	.366	.1016E+06	1 S
671	6P84	90.	80	80	80	80	-0	-0	-0	-0	.552	.250	.1024E+06	N N
672	6P94	90.	90	90	90	90	-0	-0	-0	-0	.254	.185	.1029E+06	(A)R S
673	6P4A	90.	40	-0	40	-0	40	-0	40	-0	.477	.797	.9774E+05	A Y
674	6P5A	90.	50	-0	50	-0	50	-0	50	-0	.533	.652	.9914E+05	A Y
675	6P6A	90.	60	-0	60	-0	60	-0	60	-0	.620	.523	.1002E+06	A S
676	6P7A	90.	70	-0	70	-0	70	-0	70	-0	.677	.390	.1013E+06	123 Y
677	6P8A	90.	80	-0	80	-0	80	-0	80	-0	.562	.263	.1023E+06	N S
678	6P9A	90.	90	-0	90	-0	90	-0	90	-0	.223	.188	.1026E+06	(A)R S
679	6P0A	30.	0	-0	0	-0	0	-0	0	-0	.777	.427	.1008E+06	A Y
680	6P1A	30.	10	-0	10	-0	10	-0	10	-0	.842	.298	.1021E+06	12 N
681	6P2A	30.	20	-0	20	-0	20	-0	20	-0	.686	.148	.1030E+06	N N
682	6P3A	30.	30	-0	30	-0	30	-0	30	-0	.328	.078	.1032E+06	(A)R S
683	6P1H	30.	10	10	10	10	10	10	10	10	.588	.271	.1031E+06	1,(345678)R S
684	6P2H	30.	20	20	20	20	20	20	20	20	.444	.160	.1040E+06	(45678)R S
685	6P3H	30.	30	30	30	30	30	30	30	30	.255	.090	.1043E+06	(2345678)R S
686	6P3H	60.	30	30	30	30	30	30	30	30	.902	.594	.1005E+06	1 Y
687	6P4H	60.	40	40	40	40	40	40	40	40	.731	.384	.1022E+06	1 S
688	6P5H	60.	50	50	50	50	50	50	50	50	.529	.236	.1033E+06	1 S
689	6P2H	60.	20	20	20	20	20	20	20	20	.905	.818	.9871E+05	1 Y
690	6P4H	90.	40	40	40	40	40	40	40	40	.605	.820	.9847E+05	A Y
691	6P5H	90.	50	50	50	50	50	50	50	50	.734	.705	.9944E+05	A Y
692	6P6H	90.	60	60	60	60	60	60	60	60	.676	.495	.1014E+06	A Y
693	6P7H	90.	70	70	70	70	70	70	70	70	.542	.338	.1026E+06	1 S
694	6P8H	90.	80	80	80	80	80	80	80	80	.348	.247	.1030E+06	N S
695	6P9H	90.	90	90	90	90	90	90	90	90	.159	.190	.1034E+06	(5678)R S
696	7P18	0	10	10	10	10	10	10	10	10	.073	.094	.1044E+06	A S 24PCNOPLATE
697	7P18	10.	10	10	10	10	10	10	10	10	.368	.144	.1043E+06	A S
698	7P18	20.	10	10	10	10	10	10	10	10	.885	.313	.1032E+06	A S
699	7P18	30.	10	10	10	10	10	10	10	10	1.377	.684	.1008E+06	A S
700	7P18	40.	10	10	10	10	10	10	10	10	1.619	1.207	.9610E+05	A Y

RUN NO	KEY	INFLOW ANGLE	SAIL SET								LIFT COEFF	DRAG COEFF	REYNOLDS NUMBER	COMMENTS	
701	7P18	50.	10	10	10	10	10	10	10	10	1.104	1.259	.9571E+05	A	Y
702	7P18	60.	10	10	10	10	10	10	10	10	1.003	1.568	.9366E+05	A	Y
703	7P28	20.	20	20	20	20	20	20	20	20	.438	.165	.1041E+06	A	S
704	7P28	30.	20	20	20	20	20	20	20	20	.970	.366	.1027E+06	A	S
705	7P28	40.	20	20	20	20	20	20	20	20	1.456	.797	.9939E+05	A	S
706	7P28	50.	20	20	20	20	20	20	20	20	1.408	1.206	.9585E+05	A	B
707	7P28	60.	20	20	20	20	20	20	20	20	1.103	1.325	.9517E+05	A	B
708	7P38	30.	30	30	30	30	30	30	30	30	.496	.209	.1035E+06	A	Y
709	7P38	40.	30	30	30	30	30	30	30	30	1.029	.432	.1021E+06	A	S
710	7P38	50.	30	30	30	30	30	30	30	30	1.484	.868	.9838E+05	A	S
711	7P38	60.	30	30	30	30	30	30	30	30	1.187	1.095	.9692E+05	A	Y
712	7P48	40.	40	40	40	40	40	40	40	40	.530	.261	.1030E+06	A	S
713	7P48	50.	40	40	40	40	40	40	40	40	1.028	.504	.1014E+06	A	S
714	7P48	60.	40	40	40	40	40	40	40	40	1.479	.868	.9854E+05	A	S
715	7P48	90.	40	40	40	40	40	40	40	40	1.199	1.662	.9296E+05	A	B
716	7P58	50.	50	50	50	50	50	50	50	50	.543	.297	.1026E+06	A	S
717	7P58	60.	50	50	50	50	50	50	50	50	1.045	.526	.1011E+06	A	S
718	7P58	90.	50	50	50	50	50	50	50	50	1.560	1.485	.9423E+05	A	S
719	7P58	120.	50	50	50	50	50	50	50	50	.842	1.992	.9141E+05	A	Y
720	7P68	60.	60	60	60	60	60	60	60	60	.472	.333	.1025E+06	A	S
721	7P68	90.	60	60	60	60	60	60	60	60	1.843	1.216	.9661E+05	A	S
722	7P68	120.	60	60	60	60	60	60	60	60	1.275	1.848	.9210E+05	A	B
723	7P68	150.	60	60	60	60	60	60	60	60	.149	1.319	.9519E+05	A	B
724	7P78	90.	70	70	70	70	70	70	70	70	1.640	.869	.9911E+05	A	S
725	7P88	90.	80	80	80	80	80	80	80	80	.937	.510	.1016E+06	A	S
726	7P98	120.	90	90	90	90	90	90	90	90	1.519	.855	.9923E+05	A	S
727	7P98	150.	90	90	90	90	90	90	90	90	.685	1.170	.9583E+05	A	S
728	7P98	180.	90	90	90	90	90	90	90	90	.003	.271	.1024E+06	A	B
729	HNNN	0	-0	-0	-0	-0	-0	-0	-0	-0	0	.007	.1047E+06		ONE FLAT PLATE
730	4001	0	-10	-0	-0	-0	-0	-0	-0	-0	-.093	.023	.1046E+06		
731	4001	0	0	-0	-0	-0	-0	-0	-0	-0	-.003	.010	.1047E+06		
732	4001	0	10	-0	-0	-0	-0	-0	-0	-0	.090	.024	.1045E+06		
733	4001	0	20	-0	-0	-0	-0	-0	-0	-0	.100	.041	.1044E+06		
734	4001	0	15	-0	-0	-0	-0	-0	-0	-0	.097	.032	.1045E+06		
735	4001	0	30	-0	-0	-0	-0	-0	-0	-0	.112	.064	.1042E+06		
736	4001	0	60	-0	-0	-0	-0	-0	-0	-0	.089	.140	.1034E+06		
737	4001	0	90	-0	-0	-0	-0	-0	-0	-0	.005	.169	.1032E+06		
738	5001	0	-10	-0	-0	-0	-0	-0	-0	-0	-.045	.022	.1046E+06		ONE 6 PC
739	5001	0	0	-0	-0	-0	-0	-0	-0	-0	.033	.013	.1047E+06		
740	5001	0	10	-0	-0	-0	-0	-0	-0	-0	.155	.023	.1047E+06		
741	5001	0	20	-0	-0	-0	-0	-0	-0	-0	.146	.050	.1044E+06		
742	5001	0	30	-0	-0	-0	-0	-0	-0	-0	.138	.072	.1042E+06		
743	5001	0	60	-0	-0	-0	-0	-0	-0	-0	.104	.150	.1034E+06		
744	5001	0	90	-0	-0	-0	-0	-0	-0	-0	.001	.186	.1031E+06		
745	6001	0	-10	-0	-0	-0	-0	-0	-0	-0	-.042	.025	.1045E+06		ONE 12 PC
746	6001	0	0	-0	-0	-0	-0	-0	-0	-0	.015	.017	.1046E+06		
747	6001	0	10	-0	-0	-0	-0	-0	-0	-0	.180	.027	.1046E+06		
748	6001	0	20	-0	-0	-0	-0	-0	-0	-0	.197	.054	.1044E+06		
749	6001	0	30	-0	-0	-0	-0	-0	-0	-0	.150	.077	.1042E+06		
750	6001	0	60	-0	-0	-0	-0	-0	-0	-0	.105	.155	.1034E+06		

RUN NO	KEY	INFLOW ANGLE				SAIL SET					LIFT COEFF	DRAG COEFF	REYNOLDS NUMBER	COMMENTS
751	6001	0	90	-0	-0	-0	-0	-0	-0	-0	.001	.188	.1032E+06	
752	7001	0	-10	-0	-0	-0	-0	-0	-0	-0	-.037	.034	.1042E+06	ONE 24 PC
753	7001	0	0	-0	-0	-0	-0	-0	-0	-0	-.015	.031	.1042E+06	
754	7001	0	10	-0	-0	-0	-0	-0	-0	-0	.190	.041	.1043E+06	
755	7001	0	20	-0	-0	-0	-0	-0	-0	-0	.241	.060	.1041E+06	
756	7001	0	30	-0	-0	-0	-0	-0	-0	-0	.186	.086	.1038E+06	
757	7001	0	60	-0	-0	-0	-0	-0	-0	-0	.109	.160	.1032E+06	
758	7001	0	90	-0	-0	-0	-0	-0	-0	-0	.007	.195	.1028E+06	
759	1001	0	-10	-0	-0	-0	-0	-0	-0	-0	-.080	.014	.1044E+06	ONE NACA0018
760	1001	0	0	-0	-0	-0	-0	-0	-0	-0	-.003	.010	.1045E+06	
761	1001	0	10	-0	-0	-0	-0	-0	-0	-0	.087	.017	.1044E+06	
762	1001	0	20	-0	-0	-0	-0	-0	-0	-0	.059	.040	.1041E+06	
763	1001	0	15	-0	-0	-0	-0	-0	-0	-0	.060	.032	.1042E+06	
764	1001	0	12	-0	-0	-0	-0	-0	-0	-0	.065	.028	.1043E+06	
765	1001	0	30	-0	-0	-0	-0	-0	-0	-0	.074	.059	.1041E+06	
766	1001	0	60	-0	-0	-0	-0	-0	-0	-0	.074	.128	.1034E+06	
767	1001	0	90	-0	-0	-0	-0	-0	-0	-0	.006	.164	.1030E+06	
768	2001	0	-10	-0	-0	-0	-0	-0	-0	-0	-.037	.022	.1040E+06	ONE NACA6518
769	2001	0	0	-0	-0	-0	-0	-0	-0	-0	.041	.012	.1041E+06	
770	2001	0	10	-0	-0	-0	-0	-0	-0	-0	.106	.018	.1040E+06	
771	2001	0	15	-0	-0	-0	-0	-0	-0	-0	.130	.023	.1040E+06	
772	2001	0	20	-0	-0	-0	-0	-0	-0	-0	.119	.036	.1038E+06	
773	2001	0	30	-0	-0	-0	-0	-0	-0	-0	.095	.060	.1036E+06	
774	2001	0	60	-0	-0	-0	-0	-0	-0	-0	.082	.132	.1029E+06	
775	2001	0	90	-0	-0	-0	-0	-0	-0	-0	.009	.168	.1026E+06	
776	3001	0	-10	-0	-0	-0	-0	-0	-0	-0	-.035	.032	.1036E+06	ONE TWO ARC
777	3001	0	0	-0	-0	-0	-0	-0	-0	-0	-.032	.021	.1040E+06	
778	3001	0	10	-0	-0	-0	-0	-0	-0	-0	.125	.022	.1040E+06	
779	3001	0	15	-0	-0	-0	-0	-0	-0	-0	.138	.026	.1040E+06	
780	3001	0	20	-0	-0	-0	-0	-0	-0	-0	.159	.034	.1040E+06	
781	3001	0	30	-0	-0	-0	-0	-0	-0	-0	.140	.063	.1037E+06	
782	3001	0	60	-0	-0	-0	-0	-0	-0	-0	.098	.141	.1030E+06	
783	3001	0	90	-0	-0	-0	-0	-0	-0	-0	.003	.183	.1026E+06	
784	3001	0	0	-0	-0	-0	-0	-0	-0	-0	-.033	.022	.1039E+06	
785	3001	0	-20	-0	-0	-0	-0	-0	-0	-0	-.036	.044	.1039E+06	
786	HNNN	20.		-0	-0	-0	-0	-0	-0	-0	.027	.016	.1045E+06	HULL
787	HNNN	25.		-0	-0	-0	-0	-0	-0	-0	.037	.022	.1045E+06	ONLY
788	HNNN	30.		-0	-0	-0	-0	-0	-0	-0	.044	.029	.1044E+06	
789	HNNN	35.		-0	-0	-0	-0	-0	-0	-0	.053	.039	.1043E+06	
790	HNNN	40.		-0	-0	-0	-0	-0	-0	-0	.061	.050	.1043E+06	
791	HNNN	50.		-0	-0	-0	-0	-0	-0	-0	.068	.073	.1044E+06	
792	HNNN	60.		-0	-0	-0	-0	-0	-0	-0	.065	.095	.1041E+06	
793	HNNN	90.		-0	-0	-0	-0	-0	-0	-0	-.005	.129	.1038E+06	
794	HNNN	120.		-0	-0	-0	-0	-0	-0	-0	-.073	.100	.1039E+06	
795	HNNN	150.		-0	-0	-0	-0	-0	-0	-0	-.047	.030	.1045E+06	
796	600X	-0	0	-0	-0	-0	-0	-0	-0	-0	.042	.012	.1053E+06	()R N HO
797	600X	-0	0	-0	-0	-0	-0	-0	-0	-0	.044	.012	.1053E+06	()R N
798	600X	-0	10	-0	-0	-0	-0	-0	-0	-0	.152	.028	.1053E+06	N N
799	600X	-0	20	-0	-0	-0	-0	-0	-0	-0	.155	.055	.1052E+06	1 Y
800	600X	-0	30	-0	-0	-0	-0	-0	-0	-0	.129	.073	.1048E+06	1 Y

RUN NO	KEY	INFLOW ANGLE				SAIL SET					LIFT COEFF	DRAG COEFF	REYNOLDS NUMBER	COMMENTS
801	600X	-0	60	-0	-0	-0	-0	-0	-0	-0	.085	.140	.1043E+06	1 Y
802	600X	-0	90	-0	-0	-0	-0	-0	-0	-0	-.003	.176	.1040E+06	1,(1)R Y
803	600X	-0	5	-0	-0	-0	-0	-0	-0	-0	.117	.020	.1052E+06	N N
804	600X	-0	15	-0	-0	-0	-0	-0	-0	-0	.180	.038	.1051E+06	N N
805	600Y	0	0	-0	-0	-0	-0	-0	-0	-0	.014	.013	.1052E+06	()R S H15
806	600Y	0	0	-0	-0	-0	-0	-0	-0	-0	.026	.012	.1050E+06	()R S
807	600Y	0	15	-0	-0	-0	-0	-0	-0	-0	.164	.038	.1049E+06	N N
808	600Y	0	31	-0	-0	-0	-0	-0	-0	-0	.118	.077	.1047E+06	1 S
809	600Y	0	61	-0	-0	-0	-0	-0	-0	-0	.074	.141	.1041E+06	1 Y
810	600Y	0	30	-0	-0	-0	-0	-0	-0	-0	.120	.076	.1046E+06	1 S
811	600Y	0	60	-0	-0	-0	-0	-0	-0	-0	.078	.141	.1041E+06	1 Y
812	600Y	31.	0	-0	-0	-0	-0	-0	-0	-0	.118	.073	.1047E+06	1 S
813	600Y	31.	-30	-0	-0	-0	-0	-0	-0	-0	.070	.135	.1040E+06	1 Y
814	600Y	31.	-60	-0	-0	-0	-0	-0	-0	-0	-.014	.161	.1038E+06	1,()R Y
815	600Y	31.	30	-0	-0	-0	-0	-0	-0	-0	.020	.012	.1049E+06	()R S
816	600Y	61.	0	-0	-0	-0	-0	-0	-0	-0	.071	.128	.1040E+06	1 S
817	600Y	61.	30	-0	-0	-0	-0	-0	-0	-0	.121	.069	.1046E+06	1 S
818	600Y	61.	60	-0	-0	-0	-0	-0	-0	-0	.029	.014	.1049E+06	()R S
819	600Y	90.	30	-0	-0	-0	-0	-0	-0	-0	.080	.125	.1040E+06	1 Y
820	600Y	90.	60	-0	-0	-0	-0	-0	-0	-0	.126	.068	.1045E+06	1 S
821	600Y	119.	30	-0	-0	-0	-0	-0	-0	-0	.010	.155	.1036E+06	1,()R Y
822	600Y	119.	60	-0	-0	-0	-0	-0	-0	-0	.086	.126	.1039E+06	1 Y
823	600Y	119.	90	-0	-0	-0	-0	-0	-0	-0	.126	.068	.1045E+06	1 Y
824	600Y	149.	60	-0	-0	-0	-0	-0	-0	-0	.013	.160	.1036E+06	1,()R Y
825	600Y	149.	90	-0	-0	-0	-0	-0	-0	-0	.095	.120	.1042E+06	1 Y
826	600Z	34.	0	-0	-0	-0	-0	-0	-0	-0	.105	.073	.1045E+06	1 S H30
827	600Z	34.	30	-0	-0	-0	-0	-0	-0	-0	.024	.016	.1048E+06	()R N
828	600Z	63.	30	-0	-0	-0	-0	-0	-0	-0	.107	.066	.1045E+06	1 Y
829	600Z	90.	30	-0	-0	-0	-0	-0	-0	-0	.075	.109	.1041E+06	1 Y
830	600Z	90.	60	-0	-0	-0	-0	-0	-0	-0	.122	.063	.1045E+06	1 Y
831	600Z	117.	60	-0	-0	-0	-0	-0	-0	-0	.092	.111	.1041E+06	1 Y
832	600Z	117.	90	-0	-0	-0	-0	-0	-0	-0	.124	.063	.1045E+06	1 S
833	XNNN	-0	-0	-0	-0	-0	-0	-0	-0	-0	0	.002	.1052E+06	NOSAILS H0
834	YNNN	0	-0	-0	-0	-0	-0	-0	-0	-0	0	.002	.1050E+06	H15
835	YNNN	15.	-0	-0	-0	-0	-0	-0	-0	-0	0	.002	.1050E+06	
836	YNNN	31.	-0	-0	-0	-0	-0	-0	-0	-0	-.003	.003	.1049E+06	
837	YNNN	61.	-0	-0	-0	-0	-0	-0	-0	-0	-.003	.004	.1050E+06	
838	YNNN	90.	-0	-0	-0	-0	-0	-0	-0	-0	-.003	.004	.1049E+06	
839	YNNN	119.	-0	-0	-0	-0	-0	-0	-0	-0	0	.003	.1048E+06	
840	YNNN	149.	-0	-0	-0	-0	-0	-0	-0	-0	-.005	.002	.1048E+06	
841	ZNNN	0	-0	-0	-0	-0	-0	-0	-0	-0	0	.002	.1049E+06	H30
842	ZNNN	90.	-0	-0	-0	-0	-0	-0	-0	-0	-.001	.007	.1048E+06	
843	ZNNN	34.	-0	-0	-0	-0	-0	-0	-0	-0	-.005	.005	.1049E+06	
844	ZNNN	63.	-0	-0	-0	-0	-0	-0	-0	-0	-.003	.007	.1049E+06	
845	ZNNN	117.	-0	-0	-0	-0	-0	-0	-0	-0	-.001	.005	.1049E+06	

A7 : APPENDIX TO CHAPTER 7

A7.1 Iterative procedures for performance calculations

Figure A7.1 is a flow chart indicating the iterative procedure used to calculate constant-speed motor-sailing performance corresponding to any particular wind-tunnel test configuration. The ship speed and true wind speed are specified; the leeway is estimated; and then a single iterative loop is used to improve this estimate until all equations are satisfied to within specified limits. It is found that errors in heel and course angle only cause small errors to calculated performance; and this allows estimates of heel and course angle to be simultaneously iteratively improved.

Figure A7.2 is the corresponding flow chart for constant-power motor-sailing. In this case the procedure iteratively improves estimates of the ship speed until a satisfactory solution is found.

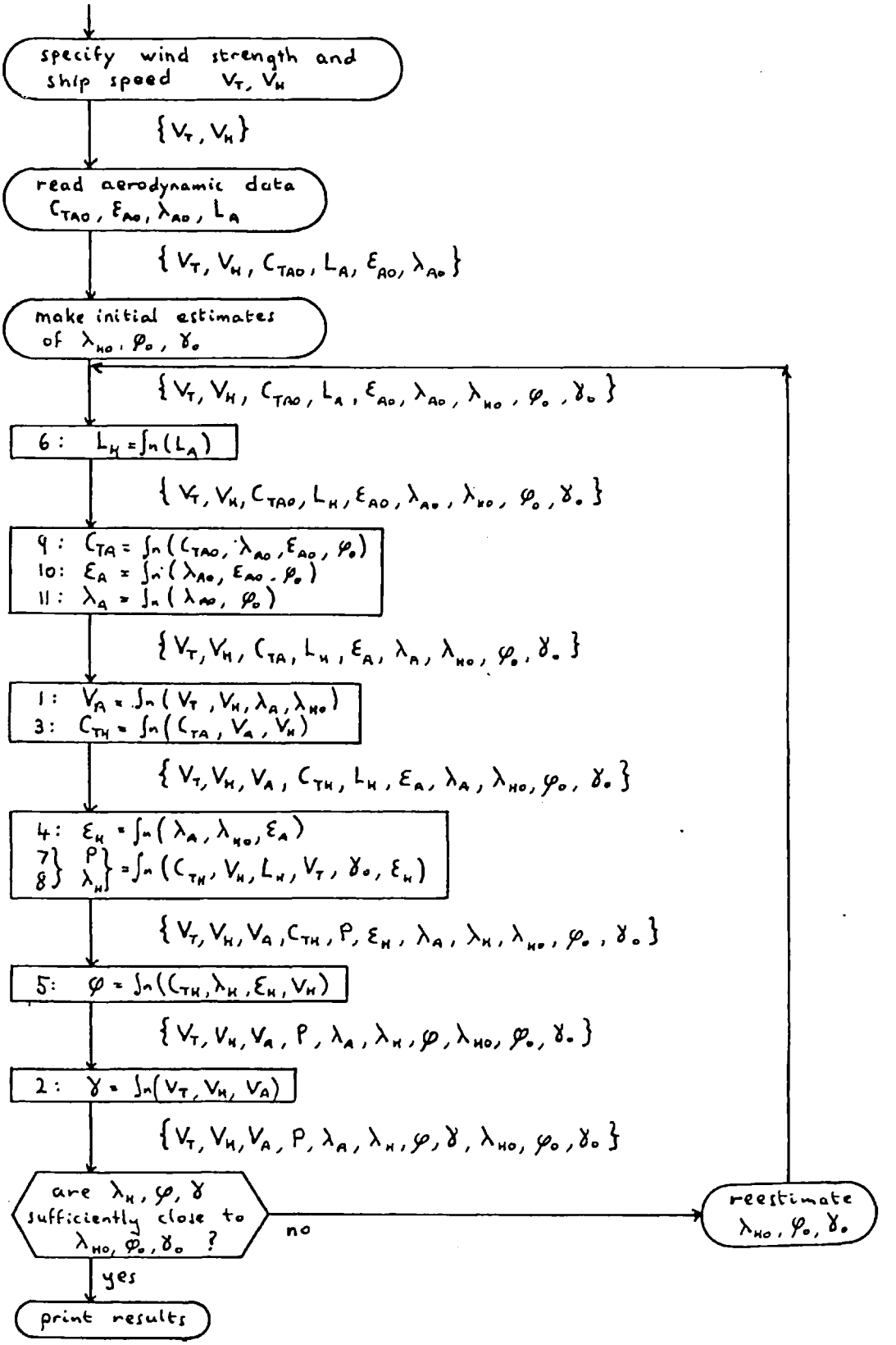

Figure A7.1

Iterative procedure for determining constant speed motor-sailing performance

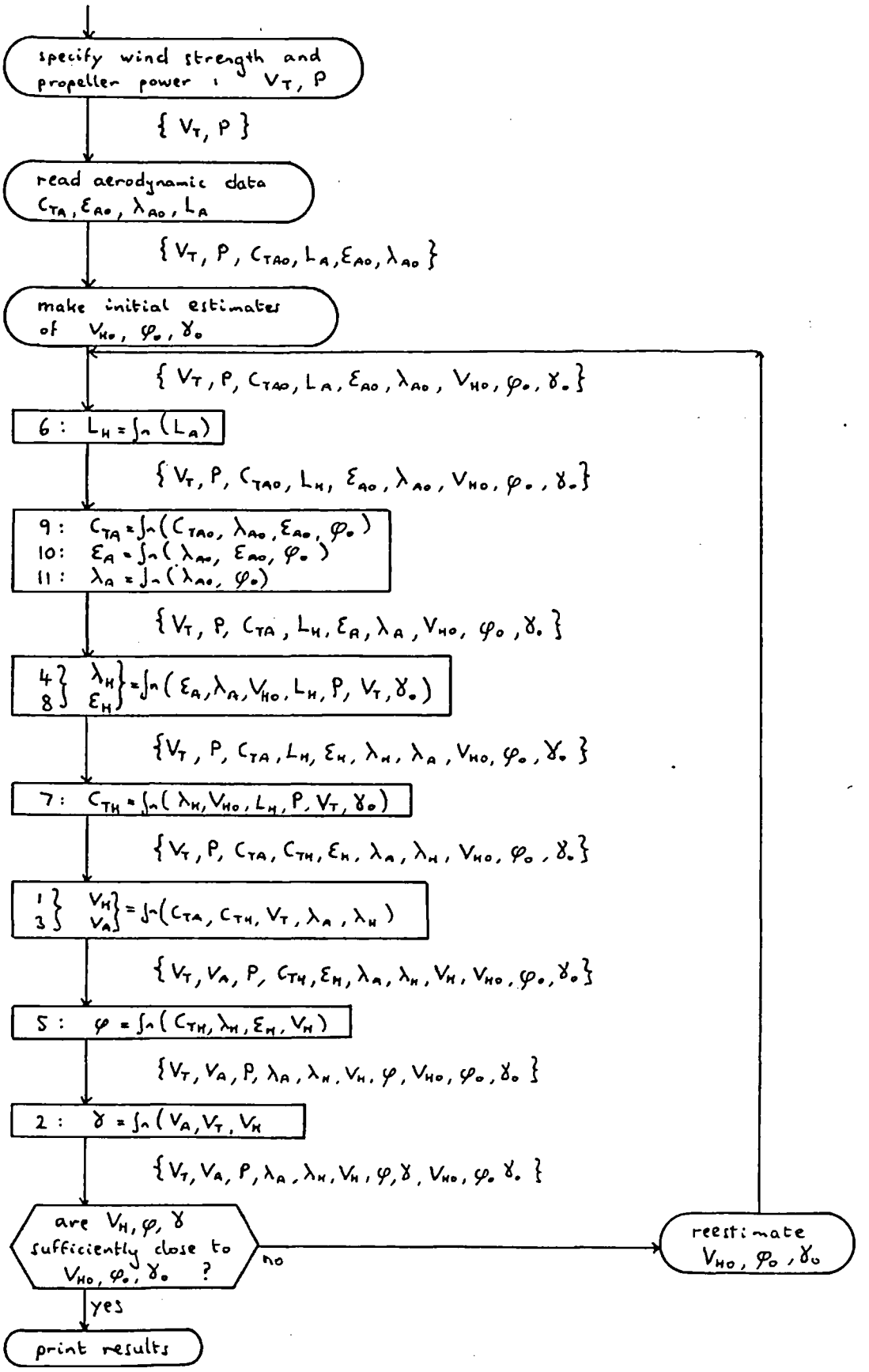

Figure A7.2

Iterative procedure for determining constant power motor-sailing performance

A7.2 Data for example performance calculation

Aerodynamic data: the aerodynamic data was obtained from tests described elsewhere in this thesis. These tests were part of an investigation comparing a number of possible rigs for modern commercial sailing ships. Each rig was tested at a variety of inflow angles and with the sails set in a variety of ways. The results obtained from each test run were processed to give a set of data in the form $\{ \lambda_{Ao} , C_{TAo}(\lambda_{Ao}) , \varepsilon_{Ao}(\lambda_{Ao}) \}$. Yawing moments were not measured. In this example application of the performance model it is assumed that the centre of effort for the sails is approximately amidships (i.e. $L_A = L/2$). This is probably a reasonable assumption for a multimast array, particularly at near-optimal settings when each sail is likely to be producing similar forces.

"Straight Line" resistance: C_x is estimated using BSRA methodical series data. This series data allows resistance to be estimated at a range of speeds for normal merchant ship forms of given size and proportions. The series data is described by Moor, Parker and Pattullo (1961), Lackenby and Parker (1966), and Thomson and Bowden (1977). Thomson and Bowden explain the use of this series data. Resistance coefficients are presented graphically for a 400ft long basis ship. Other graphs give correction factors to adapt these coefficients for a ship of the desired proportions. A further graphical procedure is used to scale the coefficients for a ship of the desired dimensions. Todd (1957) discusses the Froude assumption used in this scaling. The skin friction formula used is the 1957 ITTC formulation.

The numerical steps to calculate this resistance are now described. Table A7.1 lists the values calculated at each stage of the calculation. These calculations are performed for a basis (120 m) ship speed range of 10kts to 19kts; this corresponds to a full-scale (160m) ship speed range of 5.2m/s to 11.2m/s.

(1) The Froude number is calculated;

$$F_N = V/\sqrt{gL} = 0.01489\ V_{kts}$$

(2) The corresponding speed for the (160m) ship is calculated;

$$V = \sqrt{gL}\ F_N = 39.61\ F_N$$

(3) The basis resistance coefficient © is taken from figure 48 of Moor, Parker and Pattullo (1961) (note; $C_B = 0.625$).

(4) The beam/draft ratio correction is taken from figure 6 of Lackenby and Parker (1966) (note; B/D = 3.093).

(5) The length/cube-root-displacement ratio correction is taken from figures 7 and 8 of Lackenby and Parker (1966) (note; $L/\nabla^{\frac{1}{3}} = 6.175$).

(6) The Location-of-Centre-of-Buoyancy correction is taken from figures 51 to 58 of Moor, Parker and Pattullo (1961) (note; standard LCB = 1% aft, desired LCB = 2% aft).

(7) The various corrections are applied to the basis resistance coefficient for the required ship proportions.

(8) The Froude friction correction is taken from figure 97 of Moor, Parker and Pattullo (1961); this correction allows for Reynolds-number-dependent differences in the resistance of the basis and 160m ships. (note; an

approximate expression for the wetted surface coefficient (S) is provided by Lackenby and Parker (1966));

$$S/\nabla^{\frac{2}{3}} = (S) = 3.4 + 0.5L/\nabla^{\frac{1}{3}} = 6.487$$

(9) A friction correction modification is taken from figure 98 of Moor, Parker and Pattullo (1966). This modification is made to adapt the method so that the resistance scaling is made according to the 1957 ITTC formula for the variation of skin friction resistance with Reynolds number.

(10) These two corrections are applied to give the resistance coefficient $(C)_{ITTC}$ for the 160m ship. This is defined so that;

$$\text{resistance} = \frac{\pi \rho_H \nabla^{\frac{2}{3}} V_H^2 (C)_{ITTC}}{250}$$

(11) For the performance model, the resistance coefficient has to be non-dimensionalised differently: the resistance coefficient C_x is calculated from $(C)_{ITTC}$;

$$\text{resistance} = \frac{1}{2}\rho_H \left(\frac{\rho_A}{\rho_H} L^2\right) V_H^2 C_x$$

$$\Rightarrow \quad C_x = 0.5613 (C)_{ITTC}$$

Figure 7.3 is a graph of the resistance coefficient C_x against velocity. The values calculated from BSRA data cover a normal working velocity range for conventional ships. This range is extrapolated by assuming that C_x is constant at low speeds and approximately a cubic function

of velocity at high speeds.

Roughness and fouling resistance increment; Aertssen (1969) proposes an empirical formula for the coefficient of roughness and fouling resistance, C_{XR};

$$100 \frac{C_{XR}}{C_{FO}} = \frac{ad}{b+d} + \frac{d_o}{c}$$

where a, b and c are coefficients, d and d_o are the number of days since launch and since last dry docking, and C_{FO} is the Reynolds number dependent part of C_X. He quotes data for three cargo liners as coefficients for this equation. The mean values (a=29, b=145, c=90) are used in this example; the ship is taken to be 100 days out of dry dock (d=100) and 5 years from launching (d_o = 1825). This gives;

$$C_{XR} = 0.321\, C_{FO}$$

The 1957 ITTC formulation for frictional resistance is;

$$R_F = \frac{0.075}{(\log R_e - 2)^2} \frac{1}{2} \rho_H S V_H^2$$

so, by substitution;

$$C_{XR} = \frac{3.49}{(\log_{10}(1.6 V_H) + 6)^2}$$

Rough water resistance increment; Aertssen (1969) proposes an empirical formula for the speed loss in rough water, ΔV_H;

$$100 \frac{\Delta V_H}{V_H} = \frac{m}{L} + n$$

where m and n are coefficients. He quotes data for various headings and wind-strengths as coefficients for this equation. Two factors contribute to the speed reduction in rough seas; firstly, the waves cause an increase in the hull's resistance, and secondly, the captain may order a reduction in power according to individual subjective criteria concerning seaworthiness. The rough sea resistance is so important that some estimate must be made of its effect. Using Aertssen's data, it is possible to calculate an effective rough water resistance increment by assuming that the speed reduction is entirely due to the first factor discussed. A weather factor, w, can be defined so that;

$$W = \frac{C_{xw}}{C_x + C_{xR}}$$

Its value can be determined from Aertssen's data by equating the power in rough and smooth seas;

$$\tfrac{1}{2}\rho_H \left(\frac{\rho_A}{\rho_H} L^2\right) V_H^3 (C_x + C_{xR}) = \tfrac{1}{2}\rho_H \left(\frac{\rho_A}{\rho_H} L^2\right)(V_H - \Delta V_H)^3 (C_x + C_{xR} + C_{xw})$$

$$\Rightarrow \quad W = \left(\frac{1}{1 - \frac{\Delta V_H}{V_H}}\right)^3 - 1$$

Table A7.2 gives values of w at a range of headings and wind strengths; an interpolation procedure is used for intermediate values.

Force coefficients associated with leeway: the required data is adapted from test data published by Smitt and Chislett (1974). They tested a 6.5 metre model

Mariner class vessel of proportions closely similar to those of the ship being considered here. The tests were carried out to obtain coefficients for manoeuvring simulations. They make no attempt to correct model data for scale effects. They conclude that, "the good correlation between the simulation and full scale trials seems to indicate that no pronounced scale effects are present in this case." There is, however, some dependency of rudder force on propeller speed. The data used here is for a vessel with a propeller speed corresponding to a ship speed of 15 kts. The dimensions of the ship modelled in these tests are;

$$L = 160.93m$$

$$B = 23.17m$$

$$D = 7.47m$$

$$\text{trim} = 1/132 \text{ by stern}$$

$$C_B = 0.6$$

As shown previously, a function is required relating the rudder angle, λ_R, to the leeway, λ_H , and the position of the centre of effort, L_H: so a functional relationship is required of the form;

$$\lambda_R = f_n(L_H, \lambda_H)$$

In this example application the aerodynamic centre of pressure has been assumed constant ($L_A = L/2$) and this implies, for equilibrium of yawing moments, that the resultant hydrodynamic centre of pressure is also constant ($L_H = L/2$). In this case the rudder angle becomes a function only of leeway;

$$\lambda_R = f_n(\lambda_H)$$

This relationship is obtained by considering yawing moments

for hull and rudder and requiring their sum to be zero. Figure A7.4 indicates the graphical procedure to obtain the rudder angle required to maintain a specified leeway (the graphs show moments about the ship's longitudinal centre). The force coefficients obtained from Smitt and Chislett are non dimensionalised by $\frac{1}{2}\rho_H L^2 V_H^2$: they are multiplied by ρ_H/ρ_A to put them in the form used in this performance model. Figure A7.5 consists of graphs showing the forces associated with leeway and the forces associated with rudder angle; figure A7.6 is a graph showing the relationship between the total forces associated with leeway-and-corresponding-rudder-angle and the leeway.

Stability: the following case is considered as an example. The rig is assumed to have a mass of 400 tonnes with the centre of mass 45 metres above the keel. The hull and cargo are assumed to have a mass of 17450 tonnes with the centre of mass 6.5 metres above the keel. Then, using previously derived equations;

$$KG = 7.36m$$

$$KM_o = 10.13m$$

$$GM_o = 2.76m$$

It is unlikely that the centre of mass could be lowered much below the assumed position. The value of GM obtained is thus near the upper limit of possible values for such a ship. GM=2.76m represents excessive stability for a conventional power driven vessel. Even for a sailing vessel a lower value is probably required. This is achieved by raising the centre of gravity. Barnaby (1960) discusses stability for traditional sailing vessels: "The stability

must be suitable for the sail area that is to be carried. An overstiff ship is extremely hard on her masts and gear and this may lead to breakages and even dismasting. An overtender ship will have to reef too early and will not be suitable for heavy weather." Other problems associated with excessive stability include the possibility that jerky sharp rolling will lead to cargo shifting and the possibility of wave synchronism occurring. GM=2m is used for this example application of the performance model.

Effective wind speed: for the multimast rigs tested, typical gaps between sails are small compared with the height of the sails, so the local flow near the sails is likely to be substantially two-dimensional away from the ends. However, such a rig presents a low aspect ratio silhouette to the relative wind, and the overall flow past the ship is sensibly three dimensional. Cermak (1976) discusses the flow over buildings. The mean pressure distribution varies in a complicated way with the building's shape and attitude and the velocity structure of the boundary layer. The flow over low aspect ratio sailing ships is clearly a similarly complex problem. The forces experienced by the ship and sails vary with height; they vary both because of the three dimensional nature of the flow and because of the wind profile in which the ship must operate. To include the effects of the wind profile a significant simplification must be made; this is that the effects of the wind profile can be modelled as being those of an effective wind speed, and that this effective wind speed can be calculated by assuming that the flow past the ship is two-dimensional. Those are poor assumptions,

but some such assumptions must be made to include the effects of the wind profile in the performance model. Wagner (1967) makes these assumptions and defines an effective wind speed related to the wind speed at a reference height. For rectangular sails this effective wind speed is the root-mean-square velocity over the sail's height. An effective wind speed factor, E, is defined as the ratio of the effective wind speed, V_T, to the reference wind speed, V_{10}. Wagner's definition gives;

$$E^2 = \frac{1}{Z_u - Z_l} \int_{Z_l}^{Z_u} \sqrt[5]{Z/Z_{10}}\, dZ$$

So, for the example ship;

$$E = 1.129$$

Wind-twist: As a sailing ship sails in a wind which varies with height, the relative wind changes direction with height. Schenzle (1976) considers the effect of the wind-twist on the inflow angles to the sails. He concludes that "the twist of the inflow is extremely small in the most critical condition sailing close to the wind. It is surely negligible, especially for multimast arrangements, which are not so sensitive to flow separation as single aerofoils. The somewhat larger variation of the inflow angle in the less critical reaching and running condition can be neglected because of larger inflow angles to the sails." This assertion overstates the justification for neglecting the effects of wind-twist when sailing close to

the wind; however, the example cases considered do show that the wind-twist is small (of the order of several degrees) in this case. The effects of wind-twist are ignored in this model.

Vertical centres of pressure: as discussed above, the pressure varies with height over the sails. There appears to be no simple way of predicting the exact height of the centre of pressure which depends on the wind profile and the complicated three dimensional flow past the sailing ship. For a ship with a rectangular silhouette, it is likely to be nearer to the rig's mid height than it would be for a solid bluff body with a similar silhouette; this is because the gaps between aerofoil sails are small compared with the heights of the sails, so the flow can be expected to be substantially two dimensional away from the ends. On the other hand, the position of the centre of pressure will be influenced by the higher wind velocity aloft and the very bluff flow over the hull low down. Without other information taking the mid-height of the ship as the vertical centre of pressure seems a reasonable approximate assumption. This is justified experimentally by Wagner (1967c): "eine Analyse der Rollmomente zeigte, dass man die Seitenkrafte Y für Stabilitätsbetrachtung mit guter Näherung im Segelsschwerpunkt angriefend denken kann". This assumption is the traditional assumption (kemp, 1897); it is made by Wagner (1967a) and Schenzle (1976); and it is made for this performance model.

The depth of the hydrodynamic centre of pressure is more difficult to estimate. However, as the draft is small compared with the sail height, the length of the

heeling arm is comparatively insensitive to this depth. In this model the depth is taken as the mid-draft; this is the assumption made by Wagner (1967a) and Schenzle (1976).

TABLE A7.1

NUMERICAL STEPS TO OBTAIN THE RESISTANCE COEFFICIENTS FOR A HULL OF GIVEN PROPORTIONS AND SIZE

SPEED KTS, 121.92M SHIP		10	11	12	13	14	15	16	17	18	19
FROUDE NUMBER, FN	(1)	.1489	.1638	.1787	.1936	.2085	.2234	.2383	.2532	.2681	.2829
SPEED M/S, 160M SHIP	(2)	5.898	6.488	7.078	7.668	8.258	8.847	9.437	10.027	10.617	11.207
BASIS $\mathbb{C}$	(3)	.634	.634	.638	.660	.663	.660	.666	.703	.834	1.074
B/D CORRECTION	(4)	1.01	1.01	1.01	1.01	1.03	1.05	1.05	1.04	1.01	0.99
$L/\nabla^{\frac{1}{3}}$ CORRECTION	(5)	0.98	0.98	0.98	0.99	0.98	0.98	1.00	0.98	0.98	0.98
LCB CORRECTION	(6)	1.01	1.00	0.99	0.98	0.97	0.97	0.99	0.98	0.97	0.97
CORRECTED $\mathbb{C}$	(7)	.634	.628	.625	.647	.649	.659	.692	.702	.801	1.011
FROUDE FRICTION CORRECTION	(8)	-.017	-.017	-.017	-.017	-.016	-.016	-.016	-.016	-.016	-.016
$\mathbb{C}_{ITTC} - \mathbb{C}_{FROUDE}$	(9)	-.132	-.127	-.123	-.119	-.116	-.113	-.110	-.108	-.106	-.104
$\mathbb{C}_{ITTC}$, 160M SHIP	(10)	.485	.484	.485	.511	.517	.530	.566	.578	.679	.891
C_x	(11)	.272	.271	.272	.287	.290	.297	.318	.324	.381	.500

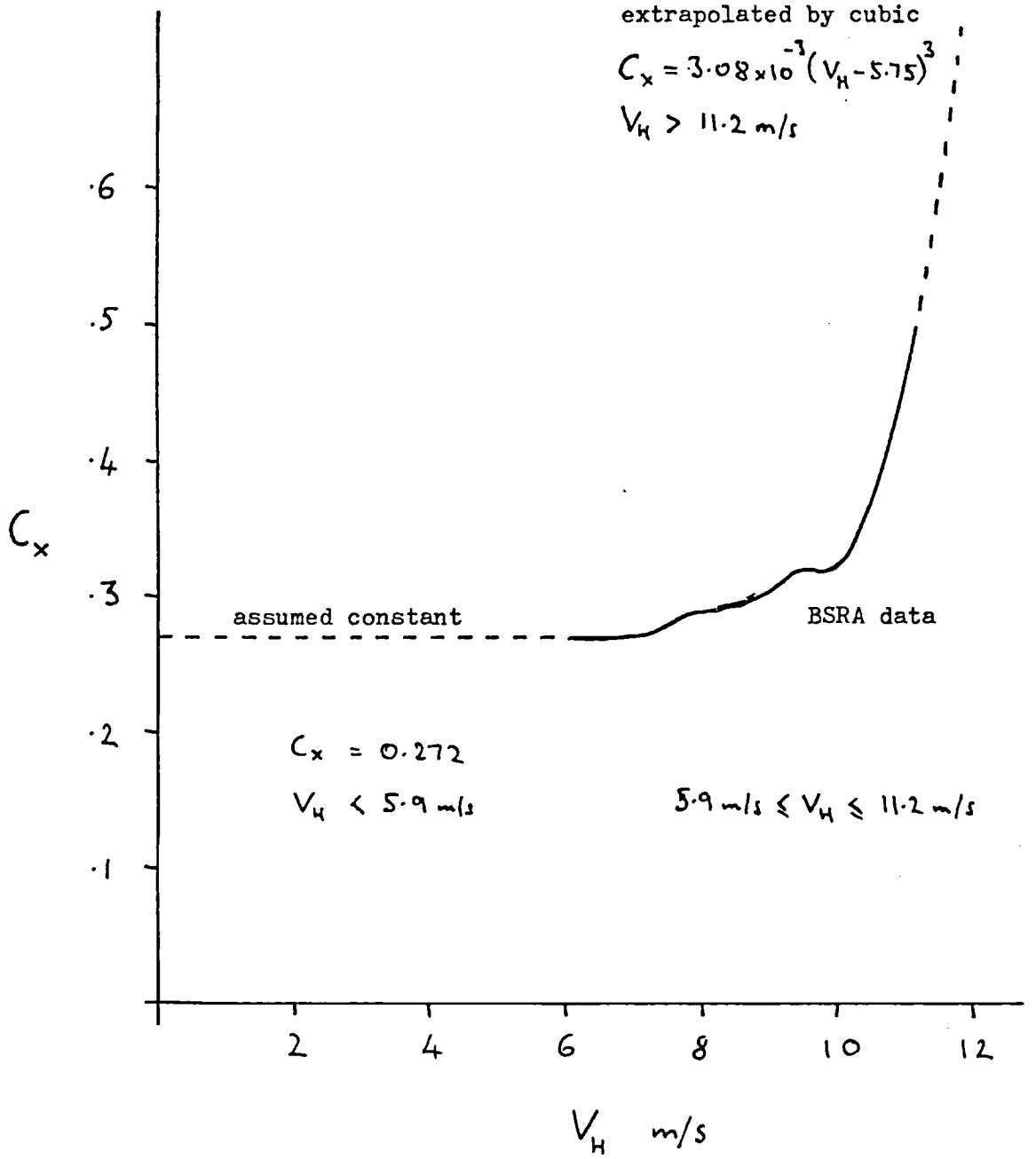

Figure A7.3

Change of "straight line" resistance with velocity

TABLE A7.2

VALUES OF WEATHER FACTOR

COURSE	0°	45°	90°	180°
BEAUFORT WIND FORCE				
0	0	0	0	0
1	0	0	0	0
2	0	0	0	0
3	.031	.031	.031	0
4	.031	.031	.031	0
5	.268	.219	.102	.018
6	.578	.428	.208	.072
7	1.287	.736	.345	.148
8	3.747	1.508	.534	.259
9	14.625	9.974	5.011	.628

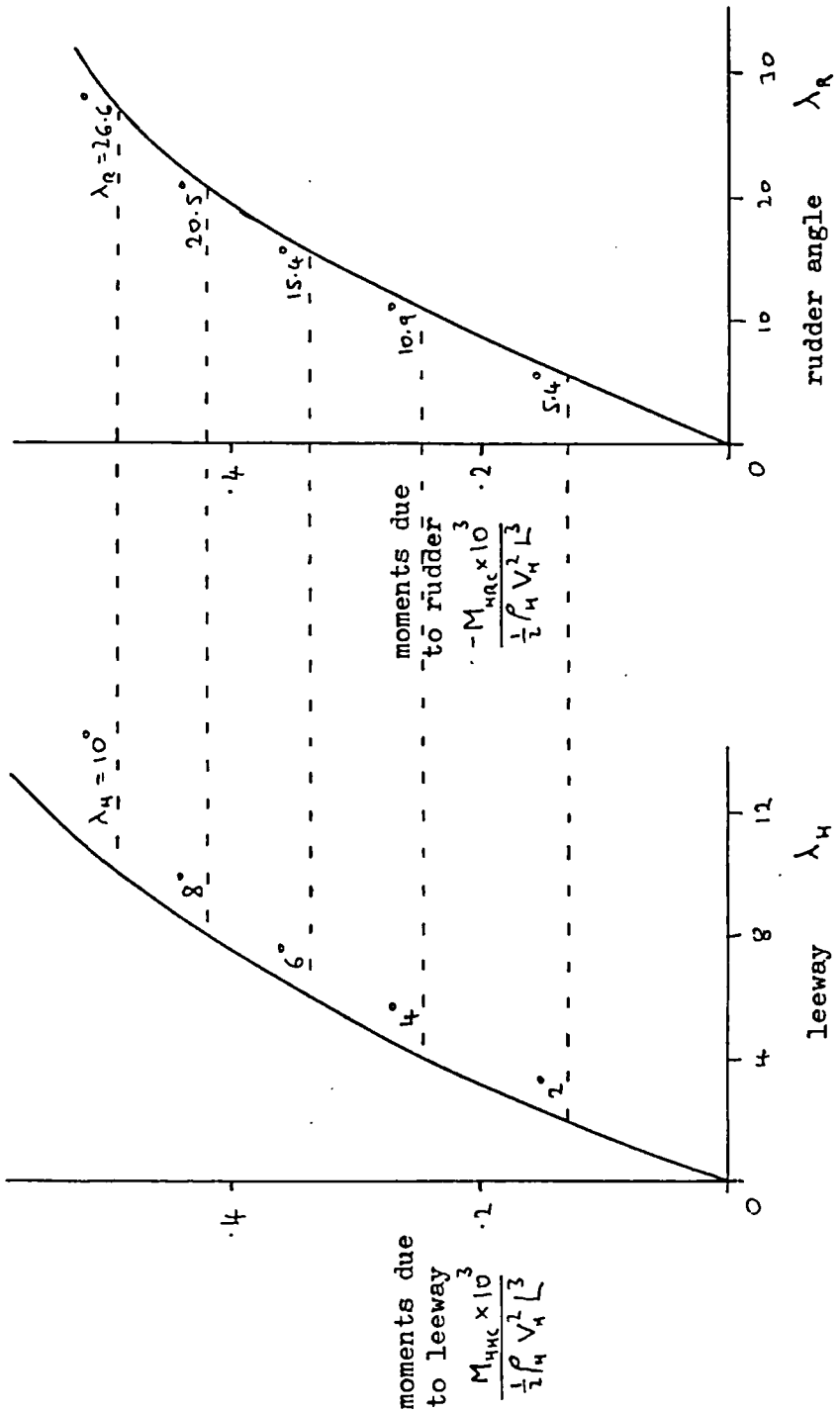

Figure A7.4

Graphical procedure to determine the rudder angle required to maintain a specified leeway

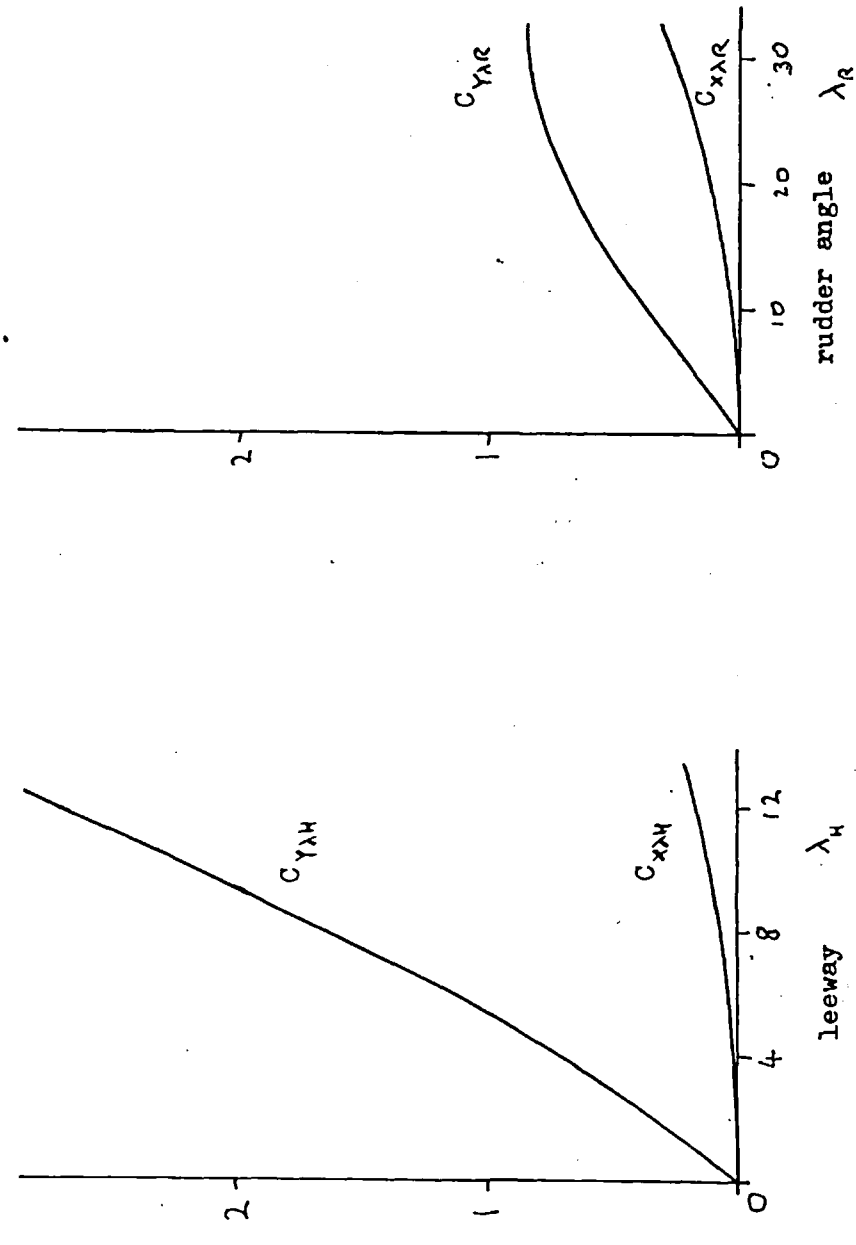

Figure A7.5

Dependence of forces on leeway and rudder angle

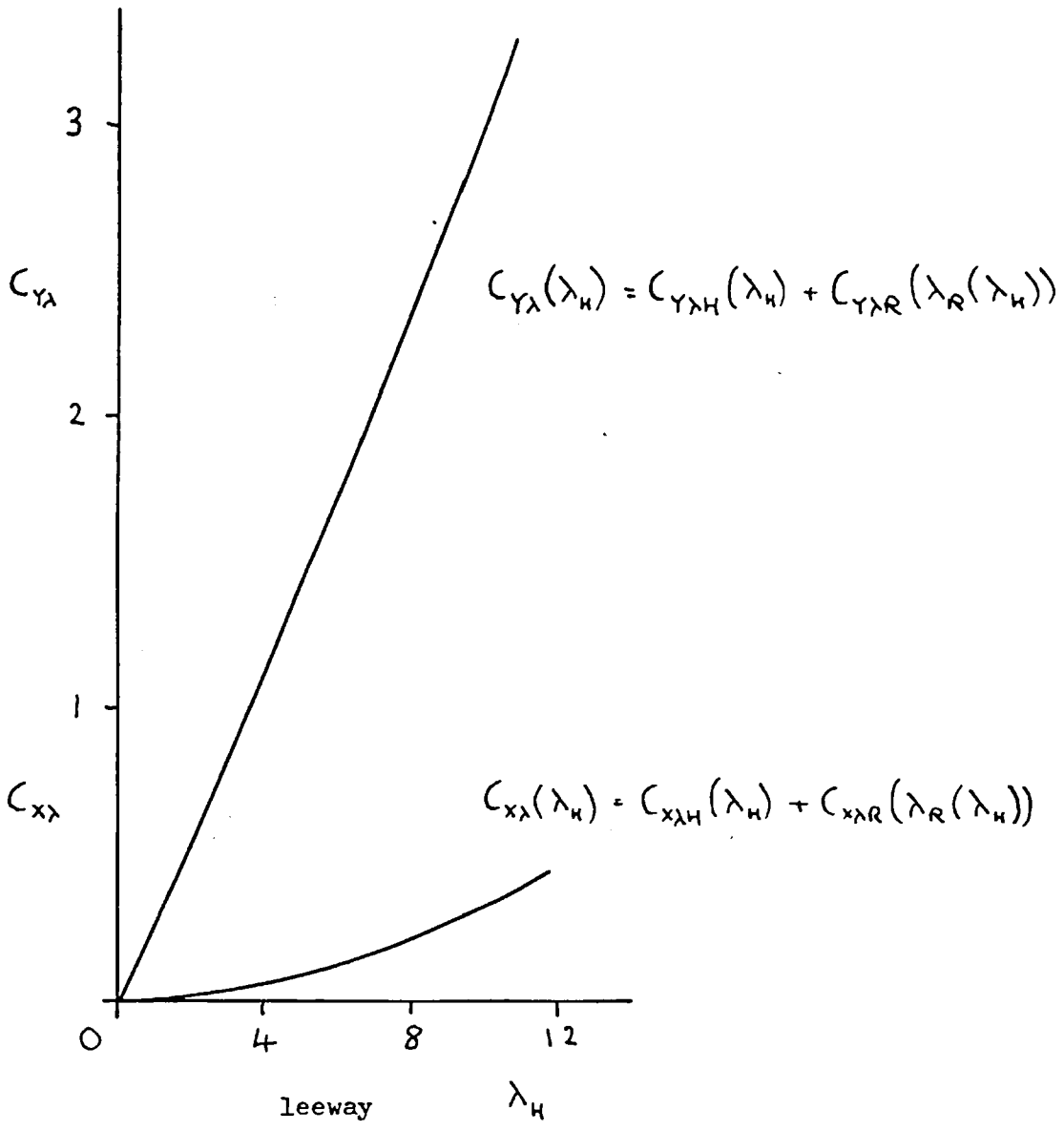

Figure A7.6

Total forces associated with specified leeway

A7.3 Symbols used in the performance analysis

β	angle between relative wind and course
γ	angle between true wind and cource
ε_A	drag angle, air
ε_{Ao}	drag angle, air at zero heel
ε_H	drag angle, water
λ_A	angle of incidence, air relative to heading
λ_{Ao}	angle of incidence, air relative to heading at zero heel
λ_H	angle of incidence, water relative to heading
λ_R	rudder angle
φ	heel angle
B	beam
D	draft
D_{deck}	height of deck above keel
GM	metacentric height
h	height of vessel, keel to masthead
h_A	height of above water ship centre of pressure
h_H	depth of below water ship centre of pressure
KM	height of metacentre above keel
KG	height of centre of gravity above keel
L	length between perpendiculars
L_A	position of centre of effort, air, fraction of length from bow
L_H	position of centre of effort, water, fraction of length from bow
z_o	reference height
z_u	height of sailhead above sea
z_l	height of sail foot above sea

∇ displacement volume

Δ displacement, tonnes of salt water

V_T true wind speed

V_A relative wind speed

V_H relative water speed

V_N component of relative wind in plane parallel to deck plane

V_o wind speed at reference height above sea

V_{10} wind speed 10m above sea

V_S desired service speed

$\underline{F}_G$ gravitational force $\underline{F}_G = (G_X, G_Y, G_Z)$

$\underline{F}_H$ hydrodynamic force $\underline{F}_H = (H_X, H_Y, H_Z)$

$\underline{F}_A$ aerodynamic force $\underline{F}_A = (A_X, A_Y, A_Z)$

H_{YH} side force hull

H_{YR} side force rudder

T_N aerodynamic force in plane parallel to deck plane

T_A component of T_N in a horizontal plane

$\underline{M}_G$ gravitational moment

$\underline{M}_H$ hydrodynamic moment

$\underline{M}_A$ aerodynamic moment

$\underline{M}_H$ yawing moment, total

$\underline{M}_{HH}$ yawing moment, hull

$\underline{M}_{HR}$ yawing moment, rudder

ρ_A density, air

ρ_H density, sea water

g gravitational acceleration

C_{TA} coefficient total force, air

C_{TA0} coefficient total force, air at zero heel

C_{TH} coefficient total force, water

C_{HX} coefficient hydrodynamic force parallel to ship's centreline

C_{HY} coefficient hydrodynamic force perpendicular to ship's centreline

C_X coefficient straight line resistance

C_{XR} coefficient roughness and fouling resistance increment

C_{XW} coefficient rough water resistance increment

$C_{X\varphi}$ coefficient heeling resistance increment

$C_{X\lambda}$ coefficient leeway resistance

$C_{Y\lambda}$ coefficient leeway sideforce

C_{XT} coefficient propeller thrust

C_{FO} Reynolds number dependent part of C_X

© resistance coefficient

C_B box coefficient

Ⓢ wetted surface coefficient

E effective wind factor

P non dimensional power

W weather factor

F_N Froude number

R_e Reynolds number

Note on force coefficients

Aerodynamic forces are non dimensionalised by

$$\tfrac{1}{2}\rho_A (L^2) V_A^2$$

Hydrodynamic forces are non dimensionalised by

$$\tfrac{1}{2}\rho_H \left(\frac{\rho_A}{\rho_H} L^2\right) V_H^2$$

$\left(\frac{\rho_A}{\rho_H} L^2\right)$ is chosen as the hydrodynamic reference area because this simplifies the algebra of sailing ships. This choice is discussed by Hafner (1980).

The following values are assumed:

$\rho_A \approx 1.205 \ kg/m^3$ $\qquad \mu_A = 18.1 \times 10^{-6} \ kg/sm$

$\rho_H \approx 1.026 \times 10^3 \ kg/m^3$ $\qquad \mu_H = 1.002 \times 10^{-3} \ kg/sm$

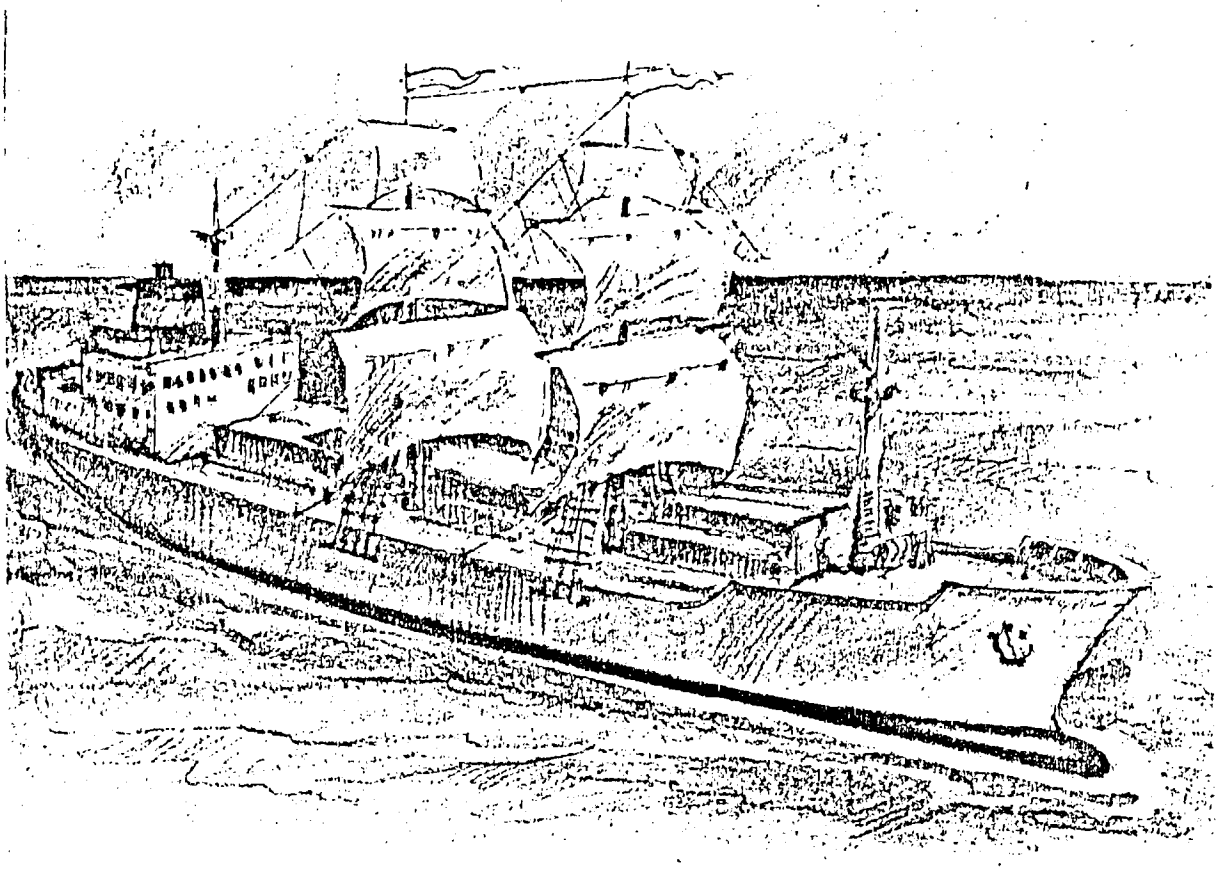

There isn't really an alternative to oil. So why don't you get most out of it.

Look at it this way:
Safe storing of energy is decisive for seaborne transport. Therefore, storing of energy in liquid form, such as oil, is more than a gift of nature. It's an invention in itself. If it didn't exist, it would be invented, indeed!
So why don't you get most out of the oil you use for the propulsion of your ships? Why don't you get most out of the B&W operational economy concept?
The new B&W L-GFC engine series will give you up to 15-17% in fuel savings, thanks to a unique combination of the uniflow scavenge system and the constant pressure turbocharging efficiency.
That's optimal utilization of oil, indeed...
Optimal opportunity for financial stability during today's times of recession...
and optimal opportunities for new prosperity when recession finally, and inevitably, comes to an end.

B&W Operational economy. Designed to propel you - through.

BWE4

Advertisement: THE MOTOR SHIP, January 1980